Effects of strongly quantizing magnetic field on outer crust of cold non-accreting neutron stars

Ioannis Mavroudis

Supervised by: Prof. Charalampos Moustakidis

Master of Science

Subatomic Physics and Technological Applications

School of Physics

Aristotle University of Thessaloniki

Thessaloniki, Greece

A thesis submitted to Aristotle University of Thessaloniki, in partial fulfillment of the requirements of the degree of Master of Science in the program "Graduate Studies in SubAtomic Physics and Technological Applications"

December 19, 2023

Contents

Abstract xvii

Περίληψη (Abstract in Greek) xviii

Acknowledgements xx

List of Tables xxv

List of Figures l

List of Abbreviations and Symbols li

1 Introduction 1
- 1.1 Structure of neutron stars . . . 1
- 1.2 Units and useful constants . . . 4

2 Preliminaries 6
- 2.1 General relativity - TOV equations . . . 6
- 2.2 Thermodynamics . . . 8
- 2.3 Statistical mechanics . . . 10
- 2.4 Critical values for outer crust . . . 12

3 BPS model 18
- 3.1 Absence of magnetic field . . . 18
- 3.2 Presence of magnetic field . . . 23
  - 3.2.1 Magnetic field regimes . . . 23
  - 3.2.2 Strong quantization . . . 26

4 Properties of outer crust 28
- 4.1 EoS - Polytrope fitting . . . 28
- 4.2 Composition . . . 32
- 4.3 Adiabatic index . . . 35

4.4 Speed of sound . . . 35
4.5 Elastic moduli . . . 37
4.6 Mass and Thickness . . . 41

5 Results - Discussion **46**
5.1 Used experimental nuclear masses . . . 46
5.2 Used nuclear mass models . . . 46
5.3 Computational details . . . 50
5.4 Comparison: SEMF vs FRDM2012 . . . 51
5.4.1 Layers properties for $B_\star = 0$ . . . 51
5.4.2 Layers properties for $B_\star = 1500$ . . . 55
5.4.3 Fitting $P = K\epsilon^G$ for $B_\star = 0$ . . . 57
5.4.4 Fitting $P = K\epsilon^G$ for $B_\star = 1500$ . . . 58
5.4.5 P vs ϵ or n_b for different $B_\star$ . . . 60
5.4.6 Γ vs ϵ or n_b for different $B_\star$ . . . 61
5.4.7 c_s vs ϵ or n_b for different $B_\star$ . . . 63
5.4.8 K_{mod} vs ϵ or n_b for different $B_\star$ . . . 64
5.4.9 S_{mod} vs ϵ or n_b for different $B_\star$ . . . 66
5.4.10 S_{mod}/K_{mod} vs ϵ or n_b for different $B_\star$ . . . 67
5.4.11 Z, N, Z/A vs ϵ or n_b for different $B_\star$ . . . 69
5.4.12 M_{cr} for different M and R and various $B_\star$ . . . 72
5.4.13 z_{drip} for different M and R and various $B_\star$ . . . 73
5.5 The surface of outer crust . . . 75
5.6 The bottom of outer crust . . . 76
5.7 P_{drip} vs $B_\star$ . . . 77
5.8 Different models with $B_\star = 0, 1500$ . . . 78
5.8.1 P vs ϵ or n_b . . . 78
5.8.2 Γ vs ϵ or n_b . . . 80
5.8.3 c_s vs ϵ or n_b . . . 81
5.8.4 K_{mod} vs ϵ or n_b . . . 83
5.8.5 S_{mod} vs ϵ or n_b . . . 84
5.8.6 S_{mod}/K_{mod} vs ϵ or n_b . . . 86
5.8.7 Z, N, Z/A vs ϵ or n_b . . . 87
5.8.8 M_{cr} for different M and R . . . 90
5.8.9 z_{drip} for different M and R . . . 91

6 Summary and Conclusions **94**

A Tables for $B_\star = 0$ **96**
A.1 WS4RBF . . . 96
A.2 BSKG3 . . . 97

A.3 HFB31 98
A.4 DDMED 99
A.5 DDPC1 100
A.6 SVMIN 101
A.7 UNEDF0 102

B Tables for $B_\star = 1500$ 103
B.1 WS4RBF 103
B.2 BSKG3 104
B.3 HFB31 105
B.4 DDMED 106
B.5 DDPC1 107
B.6 SVMIN 108
B.7 UNEDF0 109

C Tables for $B_\star = 2000$ 110
C.1 SEMF 110
C.2 FRDM2012 111
C.3 WS4RBF 112
C.4 BSKG3 113
C.5 HFB31 114
C.6 DDMED 115
C.7 DDPC1 116
C.8 SVMIN 117
C.9 UNEDF0 118

D Tables for $B_\star = 2500$ 119
D.1 SEMF 119
D.2 FRDM2012 120
D.3 WS4RBF 121
D.4 BSKG3 122
D.5 HFB31 123
D.6 DDMED 124
D.7 DDPC1 125
D.8 SVMIN 126
D.9 UNEDF0 127

E Figures for $B_\star = 0$ 128
E.1 P vs ϵ or n_b 128
E.1.1 SEMF 128
E.1.2 FRDM2012 129

E.1.3 WS4RBF . . . 129
E.1.4 BSKG3 . . . 130
E.1.5 HFB31 . . . 130
E.1.6 DDMED . . . 131
E.1.7 DDPC1 . . . 131
E.1.8 SVMIN . . . 132
E.1.9 UNEDF0 . . . 132
E.2 Fitting $P = K\epsilon^G$ . . . 133
E.2.1 WS4RBF . . . 133
E.2.2 BSKG3 . . . 133
E.2.3 HFB31 . . . 134
E.2.4 DDMED . . . 134
E.2.5 DDPC1 . . . 135
E.2.6 SVMIN . . . 135
E.2.7 UNEDF0 . . . 136
E.3 Γ vs ϵ or n_b . . . 136
E.3.1 SEMF . . . 136
E.3.2 FRDM2012 . . . 137
E.3.3 WS4RBF . . . 137
E.3.4 BSKG3 . . . 138
E.3.5 HFB31 . . . 138
E.3.6 DDMED . . . 139
E.3.7 DDPC1 . . . 139
E.3.8 SVMIN . . . 140
E.3.9 UNEDF0 . . . 140
E.4 c_s vs ϵ or n_b . . . 141
E.4.1 SEMF . . . 141
E.4.2 FRDM2012 . . . 141
E.4.3 WS4RBF . . . 142
E.4.4 BSKG3 . . . 142
E.4.5 HFB31 . . . 143
E.4.6 DDMED . . . 143
E.4.7 DDPC1 . . . 144
E.4.8 SVMIN . . . 144
E.4.9 UNEDF0 . . . 145
E.5 K_{mod} vs ϵ or n_b . . . 145
E.5.1 SEMF . . . 145
E.5.2 FRDM2012 . . . 146
E.5.3 WS4RBF . . . 146
E.5.4 BSKG3 . . . 147
E.5.5 HFB31 . . . 147

E.5.6 DDMED . . . 148
E.5.7 DDPC1 . . . 148
E.5.8 SVMIN . . . 149
E.5.9 UNEDF0 . . . 149
E.6 S_{mod} vs ϵ or n_b . . . 150
E.6.1 SEMF . . . 150
E.6.2 FRDM2012 . . . 150
E.6.3 WS4RBF . . . 151
E.6.4 BSKG3 . . . 151
E.6.5 HFB31 . . . 152
E.6.6 DDMED . . . 152
E.6.7 DDPC1 . . . 153
E.6.8 SVMIN . . . 153
E.6.9 UNEDF0 . . . 154
E.7 S_{mod}/K_{mod} vs ϵ or n_b . . . 154
E.7.1 SEMF . . . 154
E.7.2 FRDM2012 . . . 155
E.7.3 WS4RBF . . . 155
E.7.4 BSKG3 . . . 156
E.7.5 HFB31 . . . 156
E.7.6 DDMED . . . 157
E.7.7 DDPC1 . . . 157
E.7.8 SVMIN . . . 158
E.7.9 UNEDF0 . . . 158
E.8 Z, N, Z/A vs ϵ or n_b . . . 158
E.8.1 SEMF . . . 159
E.8.2 FRDM2012 . . . 160
E.8.3 WS4RBF . . . 161
E.8.4 BSKG3 . . . 162
E.8.5 HFB31 . . . 163
E.8.6 DDMED . . . 164
E.8.7 DDPC1 . . . 165
E.8.8 SVMIN . . . 166
E.8.9 UNEDF0 . . . 167
E.9 M_{cr} for different M and R . . . 168
E.9.1 SEMF . . . 168
E.9.2 FRDM2012 . . . 169
E.9.3 WS4RBF . . . 169
E.9.4 BSKG3 . . . 170
E.9.5 HFB31 . . . 170
E.9.6 DDMED . . . 171

E.9.7 DDPC1 171
E.9.8 SVMIN 172
E.9.9 UNEDF0 172
E.10 z_{drip} for different M and R 173
E.10.1 SEMF 173
E.10.2 FRDM2012 174
E.10.3 WS4RBF 174
E.10.4 BSKG3 175
E.10.5 HFB31 175
E.10.6 DDMED 176
E.10.7 DDPC1 176
E.10.8 SVMIN 177
E.10.9 UNEDF0 177

F Figures for $B_\star = 1500$ 178
F.1 P vs ϵ or n_b 178
F.1.1 SEMF 178
F.1.2 FRDM2012 179
F.1.3 WS4RBF 179
F.1.4 BSKG3 180
F.1.5 HFB31 180
F.1.6 DDMED 181
F.1.7 DDPC1 181
F.1.8 SVMIN 182
F.1.9 UNEDF0 182
F.2 Fitting $P = K\epsilon^G$ 183
F.2.1 WS4RBF 183
F.2.2 BSKG3 183
F.2.3 HFB31 184
F.2.4 DDMED 184
F.2.5 DDPC1 185
F.2.6 SVMIN 185
F.2.7 UNEDF0 186
F.3 Γ vs ϵ or n_b 186
F.3.1 SEMF 186
F.3.2 FRDM2012 187
F.3.3 WS4RBF 187
F.3.4 BSKG3 188
F.3.5 HFB31 188
F.3.6 DDMED 189
F.3.7 DDPC1 189

F.3.8 SVMIN . . . 190
F.3.9 UNEDF0 . . . 190
F.4 c_s vs ϵ or n_b . . . 191
F.4.1 SEMF . . . 191
F.4.2 FRDM2012 . . . 191
F.4.3 WS4RBF . . . 192
F.4.4 BSKG3 . . . 192
F.4.5 HFB31 . . . 193
F.4.6 DDMED . . . 193
F.4.7 DDPC1 . . . 194
F.4.8 SVMIN . . . 194
F.4.9 UNEDF0 . . . 195
F.5 K_{mod} vs ϵ or n_b . . . 195
F.5.1 SEMF . . . 195
F.5.2 FRDM2012 . . . 196
F.5.3 WS4RBF . . . 196
F.5.4 BSKG3 . . . 197
F.5.5 HFB31 . . . 197
F.5.6 DDMED . . . 198
F.5.7 DDPC1 . . . 198
F.5.8 SVMIN . . . 199
F.5.9 UNEDF0 . . . 199
F.6 S_{mod} vs ϵ or n_b . . . 200
F.6.1 SEMF . . . 200
F.6.2 FRDM2012 . . . 200
F.6.3 WS4RBF . . . 201
F.6.4 BSKG3 . . . 201
F.6.5 HFB31 . . . 202
F.6.6 DDMED . . . 202
F.6.7 DDPC1 . . . 203
F.6.8 SVMIN . . . 203
F.6.9 UNEDF0 . . . 204
F.7 S_{mod}/K_{mod} vs ϵ or n_b . . . 204
F.7.1 SEMF . . . 204
F.7.2 FRDM2012 . . . 205
F.7.3 WS4RBF . . . 205
F.7.4 BSKG3 . . . 206
F.7.5 HFB31 . . . 206
F.7.6 DDMED . . . 207
F.7.7 DDPC1 . . . 207
F.7.8 SVMIN . . . 208

F.7.9 UNEDF0 208
F.8 Z, N, Z/A vs ϵ or n_b 208
F.8.1 SEMF 209
F.8.2 FRDM2012 210
F.8.3 WS4RBF 211
F.8.4 BSKG3 212
F.8.5 HFB31 213
F.8.6 DDMED 214
F.8.7 DDPC1 215
F.8.8 SVMIN 216
F.8.9 UNEDF0 217
F.9 M_{cr} for different M and R 218
F.9.1 SEMF 218
F.9.2 FRDM2012 219
F.9.3 WS4RBF 219
F.9.4 BSKG3 220
F.9.5 HFB31 220
F.9.6 DDMED 221
F.9.7 DDPC1 221
F.9.8 SVMIN 222
F.9.9 UNEDF0 222
F.10 z_{drip} for different M and R 223
F.10.1 SEMF 223
F.10.2 FRDM2012 224
F.10.3 WS4RBF 224
F.10.4 BSKG3 225
F.10.5 HFB31 225
F.10.6 DDMED 226
F.10.7 DDPC1 226
F.10.8 SVMIN 227
F.10.9 UNEDF0 227

G Figures for $B_\star = 2000$ 228
G.1 P vs ϵ or n_b 228
G.1.1 SEMF 228
G.1.2 FRDM2012 229
G.1.3 WS4RBF 229
G.1.4 BSKG3 230
G.1.5 HFB31 230
G.1.6 DDMED 231
G.1.7 DDPC1 231

G.1.8 SVMIN . . . 232
G.1.9 UNEDF0 . . . 232
G.2 Fitting $P = K\epsilon^G$ . . . 233
G.2.1 SEMF . . . 233
G.2.2 FRDM2012 . . . 234
G.2.3 WS4RBF . . . 234
G.2.4 BSKG3 . . . 235
G.2.5 HFB31 . . . 235
G.2.6 DDMED . . . 236
G.2.7 DDPC1 . . . 236
G.2.8 SVMIN . . . 237
G.2.9 UNEDF0 . . . 237
G.3 Γ vs ϵ or n_b . . . 238
G.3.1 SEMF . . . 238
G.3.2 FRDM2012 . . . 238
G.3.3 WS4RBF . . . 239
G.3.4 BSKG3 . . . 239
G.3.5 HFB31 . . . 240
G.3.6 DDMED . . . 240
G.3.7 DDPC1 . . . 241
G.3.8 SVMIN . . . 241
G.3.9 UNEDF0 . . . 242
G.4 c_s vs ϵ or n_b . . . 242
G.4.1 SEMF . . . 242
G.4.2 FRDM2012 . . . 243
G.4.3 WS4RBF . . . 243
G.4.4 BSKG3 . . . 244
G.4.5 HFB31 . . . 244
G.4.6 DDMED . . . 245
G.4.7 DDPC1 . . . 245
G.4.8 SVMIN . . . 246
G.4.9 UNEDF0 . . . 246
G.5 K_{mod} vs ϵ or n_b . . . 247
G.5.1 SEMF . . . 247
G.5.2 FRDM2012 . . . 247
G.5.3 WS4RBF . . . 248
G.5.4 BSKG3 . . . 248
G.5.5 HFB31 . . . 249
G.5.6 DDMED . . . 249
G.5.7 DDPC1 . . . 250
G.5.8 SVMIN . . . 250

G.5.9 UNEDF0 251
G.6 S_{mod} vs ϵ or n_b 251
G.6.1 SEMF 251
G.6.2 FRDM2012 252
G.6.3 WS4RBF 252
G.6.4 BSKG3 253
G.6.5 HFB31 253
G.6.6 DDMED 254
G.6.7 DDPC1 254
G.6.8 SVMIN 255
G.6.9 UNEDF0 255
G.7 S_{mod}/K_{mod} vs ϵ or n_b 256
G.7.1 SEMF 256
G.7.2 FRDM2012 256
G.7.3 WS4RBF 257
G.7.4 BSKG3 257
G.7.5 HFB31 258
G.7.6 DDMED 258
G.7.7 DDPC1 259
G.7.8 SVMIN 259
G.7.9 UNEDF0 260
G.8 Z, N, Z/A vs ϵ or n_b 260
G.8.1 SEMF 261
G.8.2 FRDM2012 262
G.8.3 WS4RBF 263
G.8.4 BSKG3 264
G.8.5 HFB31 265
G.8.6 DDMED 266
G.8.7 DDPC1 267
G.8.8 SVMIN 268
G.8.9 UNEDF0 269
G.9 M_{cr} for different M and R 270
G.9.1 SEMF 270
G.9.2 FRDM2012 271
G.9.3 WS4RBF 271
G.9.4 BSKG3 272
G.9.5 HFB31 272
G.9.6 DDMED 273
G.9.7 DDPC1 273
G.9.8 SVMIN 274
G.9.9 UNEDF0 274

G.10 z_{drip} for different M and R . . . 275
G.10.1 SEMF . . . 275
G.10.2 FRDM2012 . . . 276
G.10.3 WS4RBF . . . 276
G.10.4 BSKG3 . . . 277
G.10.5 HFB31 . . . 277
G.10.6 DDMED . . . 278
G.10.7 DDPC1 . . . 278
G.10.8 SVMIN . . . 279
G.10.9 UNEDF0 . . . 279

H Figures for $B_\star = 2500$ 280
H.1 P vs ϵ or n_b . . . 280
H.1.1 SEMF . . . 280
H.1.2 FRDM2012 . . . 281
H.1.3 WS4RBF . . . 281
H.1.4 BSKG3 . . . 282
H.1.5 HFB31 . . . 282
H.1.6 DDMED . . . 283
H.1.7 DDPC1 . . . 283
H.1.8 SVMIN . . . 284
H.1.9 UNEDF0 . . . 284
H.2 Fitting $P = K\epsilon^G$ . . . 285
H.2.1 SEMF . . . 285
H.2.2 FRDM2012 . . . 286
H.2.3 WS4RBF . . . 286
H.2.4 BSKG3 . . . 287
H.2.5 HFB31 . . . 287
H.2.6 DDMED . . . 288
H.2.7 DDPC1 . . . 288
H.2.8 SVMIN . . . 289
H.2.9 UNEDF0 . . . 289
H.3 Γ vs ϵ or n_b . . . 290
H.3.1 SEMF . . . 290
H.3.2 FRDM2012 . . . 290
H.3.3 WS4RBF . . . 291
H.3.4 BSKG3 . . . 291
H.3.5 HFB31 . . . 292
H.3.6 DDMED . . . 292
H.3.7 DDPC1 . . . 293
H.3.8 SVMIN . . . 293

H.3.9 UNEDF0 . . . 294
H.4 c_s vs ϵ or n_b . . . 294
H.4.1 SEMF . . . 294
H.4.2 FRDM2012 . . . 295
H.4.3 WS4RBF . . . 295
H.4.4 BSKG3 . . . 296
H.4.5 HFB31 . . . 296
H.4.6 DDMED . . . 297
H.4.7 DDPC1 . . . 297
H.4.8 SVMIN . . . 298
H.4.9 UNEDF0 . . . 298
H.5 K_{mod} vs ϵ or n_b . . . 299
H.5.1 SEMF . . . 299
H.5.2 FRDM2012 . . . 299
H.5.3 WS4RBF . . . 300
H.5.4 BSKG3 . . . 300
H.5.5 HFB31 . . . 301
H.5.6 DDMED . . . 301
H.5.7 DDPC1 . . . 302
H.5.8 SVMIN . . . 302
H.5.9 UNEDF0 . . . 303
H.6 S_{mod} vs ϵ or n_b . . . 303
H.6.1 SEMF . . . 303
H.6.2 FRDM2012 . . . 304
H.6.3 WS4RBF . . . 304
H.6.4 BSKG3 . . . 305
H.6.5 HFB31 . . . 305
H.6.6 DDMED . . . 306
H.6.7 DDPC1 . . . 306
H.6.8 SVMIN . . . 307
H.6.9 UNEDF0 . . . 307
H.7 S_{mod}/K_{mod} vs ϵ or n_b . . . 308
H.7.1 SEMF . . . 308
H.7.2 FRDM2012 . . . 308
H.7.3 WS4RBF . . . 309
H.7.4 BSKG3 . . . 309
H.7.5 HFB31 . . . 310
H.7.6 DDMED . . . 310
H.7.7 DDPC1 . . . 311
H.7.8 SVMIN . . . 311
H.7.9 UNEDF0 . . . 312

H.8 Z, N, Z/A vs ϵ or n_b . . . 312
H.8.1 SEMF . . . 313
H.8.2 FRDM2012 . . . 314
H.8.3 WS4RBF . . . 315
H.8.4 BSKG3 . . . 316
H.8.5 HFB31 . . . 317
H.8.6 DDMED . . . 318
H.8.7 DDPC1 . . . 319
H.8.8 SVMIN . . . 320
H.8.9 UNEDF0 . . . 321
H.9 M_{cr} for different M and R . . . 322
H.9.1 SEMF . . . 322
H.9.2 FRDM2012 . . . 323
H.9.3 WS4RBF . . . 323
H.9.4 BSKG3 . . . 324
H.9.5 HFB31 . . . 324
H.9.6 DDMED . . . 325
H.9.7 DDPC1 . . . 325
H.9.8 SVMIN . . . 326
H.9.9 UNEDF0 . . . 326
H.10 z_{drip} for different M and R . . . 327
H.10.1 SEMF . . . 327
H.10.2 FRDM2012 . . . 328
H.10.3 WS4RBF . . . 328
H.10.4 BSKG3 . . . 329
H.10.5 HFB31 . . . 329
H.10.6 DDMED . . . 330
H.10.7 DDPC1 . . . 330
H.10.8 SVMIN . . . 331
H.10.9 UNEDF0 . . . 331

I Figures for mixed plots **332**
I.1 P vs ϵ or n_b . . . 332
I.1.1 WS4RBF . . . 332
I.1.2 BSKG3 . . . 333
I.1.3 HFB31 . . . 333
I.1.4 DDMED . . . 334
I.1.5 DDPC1 . . . 334
I.1.6 SVMIN . . . 335
I.1.7 UNEDF0 . . . 335
I.1.8 $B_\star = 2000$ . . . 336

I.1.9 $B_\star = 2500$ . . . 336
I.2 Γ vs ϵ or n_b . . . 337
I.2.1 WS4RBF . . . 337
I.2.2 BSKG3 . . . 337
I.2.3 HFB31 . . . 338
I.2.4 DDMED . . . 338
I.2.5 DDPC1 . . . 339
I.2.6 SVMIN . . . 339
I.2.7 UNEDF0 . . . 340
I.2.8 $B_\star = 2000$ . . . 340
I.2.9 $B_\star = 2500$ . . . 341
I.3 c_s vs ϵ or n_b . . . 341
I.3.1 WS4RBF . . . 341
I.3.2 BSKG3 . . . 342
I.3.3 HFB31 . . . 342
I.3.4 DDMED . . . 343
I.3.5 DDPC1 . . . 343
I.3.6 SVMIN . . . 344
I.3.7 UNEDF0 . . . 344
I.3.8 $B_\star = 2000$ . . . 345
I.3.9 $B_\star = 2500$ . . . 345
I.4 K_{mod} vs ϵ or n_b . . . 346
I.4.1 WS4RBF . . . 346
I.4.2 BSKG3 . . . 346
I.4.3 HFB31 . . . 347
I.4.4 DDMED . . . 347
I.4.5 DDPC1 . . . 348
I.4.6 SVMIN . . . 348
I.4.7 UNEDF0 . . . 349
I.4.8 $B_\star = 2000$ . . . 349
I.4.9 $B_\star = 2500$ . . . 350
I.5 S_{mod} vs ϵ or n_b . . . 350
I.5.1 WS4RBF . . . 350
I.5.2 BSKG3 . . . 351
I.5.3 HFB31 . . . 351
I.5.4 DDMED . . . 352
I.5.5 DDPC1 . . . 352
I.5.6 SVMIN . . . 353
I.5.7 UNEDF0 . . . 353
I.5.8 $B_\star = 2000$ . . . 354
I.5.9 $B_\star = 2500$ . . . 354

I.6 S_{mod}/K_{mod} vs ϵ or n_b . . . 355
I.6.1 WS4RBF . . . 355
I.6.2 BSKG3 . . . 355
I.6.3 HFB31 . . . 356
I.6.4 DDMED . . . 356
I.6.5 DDPC1 . . . 357
I.6.6 SVMIN . . . 357
I.6.7 UNEDF0 . . . 358
I.6.8 $B_\star = 2000$ . . . 358
I.6.9 $B_\star = 2500$ . . . 359
I.7 Z, N, Z/A vs ϵ or n_b . . . 359
I.7.1 WS4RBF . . . 360
I.7.2 BSKG3 . . . 361
I.7.3 HFB31 . . . 362
I.7.4 DDMED . . . 363
I.7.5 DDPC1 . . . 364
I.7.6 SVMIN . . . 365
I.7.7 UNEDF0 . . . 366
I.7.8 $B_\star = 2000$ . . . 367
I.7.9 $B_\star = 2500$ . . . 368
I.8 M_{cr} for different M and R . . . 369
I.8.1 WS4RBF . . . 369
I.8.2 BSKG3 . . . 370
I.8.3 HFB31 . . . 370
I.8.4 DDMED . . . 371
I.8.5 DDPC1 . . . 371
I.8.6 SVMIN . . . 372
I.8.7 UNEDF0 . . . 372
I.8.8 $B_\star = 2000$ . . . 373
I.8.9 $B_\star = 2500$ . . . 373
I.9 z_{drip} for different M and R . . . 374
I.9.1 WS4RBF . . . 374
I.9.2 BSKG3 . . . 375
I.9.3 HFB31 . . . 375
I.9.4 DDMED . . . 376
I.9.5 DDPC1 . . . 376
I.9.6 SVMIN . . . 377
I.9.7 UNEDF0 . . . 377
I.9.8 $B_\star = 2000$ . . . 378
I.9.9 $B_\star = 2500$ . . . 378

J Code A **379**

K Code B **412**

Bibliography **432**

Abstract

Several fields of physics are involved in the study of the properties of the outer crust of neutron stars, for example, nuclear physics, general relativity, condensed matter physics and theory of elasticity. So, the crust is an astrophysical laboratory with conditions that cannot be achieved in a terrestrial laboratory. Therefore, physical ideas and theories can be applied, but they are simultaneously limited by the astronomical observations.

In the present thesis, the model developed in the classical paper of Baym, Pethick and Sutherland is adopted to study the properties of outer crust of cold non-accreting neutron stars, where each crustal layer consists of a body-centered cubic crystal lattice made of a single nuclear species, embedded in an electron gas, distinguishing two cases: a) absence of magnetic field and b) presence of strongly quantizing magnetic field. In both cases, experimentally measured nuclear masses from AME2020 are used, supplemented with theoretically predicted masses for the experimentally unknown masses, whenever necessary. For this purpose, nine different models are employed, which are: 1) the Semi-Empirical Mass Formula (SEMF) of Bethe and Weizsäcker, 2) the FRDM(2012), 3) the WS4^{RBF}, 4) the BSkG3, 5) the HFB-31, 6) the DD-MEδ, 7) the DD-PC1, 8) the SV-min, and 9) the UNEDF0 nuclear mass model.

Among the properties of outer crust that are investigated for different magnetic field strengths are: 1) the Equation of State (i.e., the pressure as a function of density) for which a polytrope is fitted, 2) the composition (i.e., the stratification of the crust), 3) the adiabatic index, 4) the speed of sound, 5) the compression elastic modulus, the effective shear elastic modulus and the ratio of effective shear modulus to compression modulus as a function of density, 6) the mass and the thickness of outer crust, solving the TOV equations, and 7) the abundances of nuclei present in the crust.

Thus, comparing the results, we can conclude if the above properties are dependent on the magnetic field strength and the nuclear model used for the nuclear masses.

Περίληψη (Abstract in Greek)

Αρκετοί τομείς της φυσικής εμπλέκονται στη μελέτη των ιδιοτήτων του εξωτερικού φλοιού των αστέρων νετρονίων, για παράδειγμα, πυρηνική φυσική, γενική σχετικότητα, φυσική συμπυκνωμένης ύλης και θεωρία ελαστικότητας. Έτσι, ο φλοιός είναι ένα αστροφυσικό εργαστήριο με συνθήκες, οι οποίες δεν μπορούν να επιτευχθούν σε ένα γήινο εργαστήριο. Συνεπώς, ιδέες και θεωρίες της φυσικής μπορούν να εφαρμοστούν, αλλά ταυτόχρονα περιορίζονται από τις αστρονομικές παρατηρήσεις.

Στην παρούσα διπλωματική εργασία, το μοντέλο που αναπτύχθηκε στην κλασσική εργασία των Baym, Pethick και Sutherland υιοθετείται για τη μελέτη των ιδιοτήτων του εξωτερικού φλοιού ψυχρών μη-προσαυξανόμενων αστέρων νετρονίων, όπου κάθε στρώμα του φλοιού αποτελείται από ένα ενδοκεντρωμένο κυβικό κρυσταλλικό πλέγμα δομημένο από ενός είδους νουκλίδιο, εμβαπτισμένο σε ένα αέριο ηλεκτρονίων, διακρίνοντας δύο περιπτώσεις: α) απουσία μαγνητικού πεδίου και β) παρουσία ισχυρά κβαντισμένου μαγνητικού πεδίου. Και στις δύο περιπτώσεις, χρησιμοποιούνται πειραματικά μετρούμενες πυρηνικές μάζες από την AME2020, με τη συμπλήρωση θεωρητικά προβλεπόμενων μαζών για τις πειραματικά άγνωστες μάζες, όποτε αυτό είναι απαραίτητο. Για τον σκοπό αυτό, γίνεται χρήση εννέα διαφορετικών μοντέλων, τα οποία είναι: 1) ο ημιεμπειρικός τύπος μάζας (SEMF) των Bethe και Weizsäcker, 2) το FRDM (2012), 3) το $WS4^{RBF}$, 4) το BSkG3, 5) το HFB-31, 6) το DD-MEδ, 7) το DD-PC1, 8) το SV-min, και 9) το UNEDF0 μοντέλο πυρηνικών μαζών.

Μεταξύ των ιδιοτήτων του εξωτερικού φλοιού που διερευνώνται για διάφορες εντάσεις μαγνητικού πεδίου είναι: 1) η καταστατική εξίσωση (πίεση ως συνάρτηση της πυκνότητας), για την οποία προσαρμόζεται ένα πολύτροπο, 2) η σύσταση (διαστρωμάτωση) του φλοιού, 3) ο αδιαβατικός δείκτης, 4) η ταχύτητα του ήχου, 5) το μέτρο ελαστικότητας συμπίεσης, το δραστικό μέτρο ελαστικότητας διάτμησης και ο λόγος του δραστικού μέτρου διάτμησης προς το μέτρο συμπίεσης ως συνάρτηση της πυκνότητας, 6) η μάζα και το πάχος του εξωτερικού φλοιού, λύνοντας τις εξισώσεις TOV, και 7) η αφθονία των πυρήνων που βρίσκονται στον φλοιό.

Οπότε, συγκρίνοντας τα αποτελέσματα, μπορούμε να συμπεράνουμε εάν οι

παραπάνω ιδιότητες είναι εξαρτόμενες από την ένταση του μαγνητικού πεδίου και από το πυρηνικό μοντέλο που χρησιμοποιείται για τις πυρηνικές μάζες.

Acknowledgements

I would like to express my sincere appreciation to all of those who made this thesis possible with their help. So, I want to thank my supervisor, Prof. Charalampos Moustakidis, for giving me the opportunity to work on neutron stars, and my family for their unconditional support during my studies.

List of Tables

1.1 Useful constants 5

3.1 Madelung constant C_M for different lattices 21

5.1 For each model are listed the rms deviation between experimental data and predictions in MeV (the intrinsic model error in MeV given in parentheses) and, for infinite nuclear matter at saturation, the energy per particle a_V in MeV and the symmetry energy J in MeV 49

5.2 For each layer are listed the minimum (maximum) pressure P_{min} (P_{max}) in MeV/fm^3, the minimum (maximum) energy density ϵ_{min} (ϵ_{max}) in MeV/fm^3, the minimum (maximum) baryon number density $n_{b_{min}}$ ($n_{b_{max}}$) in fm^{-3}, the mass number A, the atomic number Z, the neutron number N, the proton fraction Z/A, the minimum (maximum) baryon chemical potential $\mu_{b_{min}}$ ($\mu_{b_{max}}$) in MeV and the minimum (maximum) electron chemical potential $\mu_{e_{min}}$ ($\mu_{e_{max}}$) in MeV, using the SEMF model with magnetic field strength $B_\star = 0$ 53

5.3 For a typical NS with $M = 1.4M_\odot$ and $R = 12.5km$, are listed the mass of outer crust M_{cr} in $M_\odot$, the fractional mass M_{cr}/M, the coordinate thickness ΔR_{cr} in km, the fractional coordinate thickness $\Delta R_{cr}/R$, the baryonic mass $M_{b_{cr}}$ in $M_\odot$, the relative fraction of outer crust's mass due to gravitational binding energy Δ_{grav}, the proper depth of neutron-drip transition z_{drip} in km and the total number of baryons ΔN of outer crust, using the SEMF model with magnetic field strength $B_\star = 0$ . . 53

5.4 For a typical NS with $M = 1.4M_\odot$ and $R = 12.5km$, are listed the minimum (maximum) radius of the layer r_{min} (r_{max}) in km, the coordinate thickness ΔR_l in km, the fractional coordinate thickness $\Delta R_l/\Delta R_{cr}$, the proper depth z_l in km, the fractional proper depth z_l/z_{drip}, the baryonic mass M_{b_l} in $M_\odot$, the fractional baryonic mass $M_{b_l}/M_{b_{cr}}$, the mass M_l in $M_\odot$, the fractional mass M_l/M_{cr}, the number of baryons ΔN_l and the fractional number of baryons $\Delta N_l/\Delta N$, using the SEMF model with magnetic field strength $B_\star = 0$ 54
5.5 The same as Table 5.2, using the FRDM2012 model with $B_\star = 0$ 54
5.6 The same as Table 5.3, using the FRDM2012 model with $B_\star = 0$ 54
5.7 The same as Table 5.4, using the FRDM2012 model with $B_\star = 0$ 55
5.8 The same as Table 5.2, using the SEMF model with $B_\star = 1500$ 55
5.9 The same as Table 5.3, using the SEMF model with $B_\star = 1500$ 55
5.10 The same as Table 5.4, using the SEMF model with $B_\star = 1500$ 56
5.11 The same as Table 5.2, using the FRDM2012 model with $B_\star = 1500$ 56
5.12 The same as Table 5.3, using the FRDM2012 model with $B_\star = 1500$ 56
5.13 The same as Table 5.4, using the FRDM2012 model with $B_\star = 1500$ 57
5.14 At the surface of outer crust are listed the surface energy density ϵ_{surf} in MeV/fm^3 and the surface baryon number density in fm^{-3}, using different models with various magnetic field strengths $B_\star$ 75
5.15 At the bottom of outer crust are listed the *element*, the pressure P_{drip} in MeV/fm^3, the energy density ϵ_{drip} in MeV/fm^3, the baryon number density $n_{b_{drip}}$ in fm^{-3}, the atomic number Z_{drip}, the neutron number N_{drip}, the baryon chemical potential $\mu_{b_{drip}}$ in MeV and the electron chemical potential $\mu_{e_{drip}}$ in MeV, at the neutron-drip transition, using different models with magnetic field strength $B_\star = 0$ 76
5.16 The same as Table 5.15, using different models with $B_\star = 1500$ 76
5.17 The same as Table 5.15, using different models with $B_\star = 2000$ 77
5.18 The same as Table 5.15, using different models with $B_\star = 2500$ 77

A.1 The same as Table 5.2, using the WS4RBF model with $B_\star = 0$ 96
A.2 The same as Table 5.3, using the WS4RBF model with $B_\star = 0$ 96
A.3 The same as Table 5.4, using the WS4RBF model with $B_\star = 0$ 97
A.4 The same as Table 5.2, using the BSKG3 model with $B_\star = 0$. 97
A.5 The same as Table 5.3, using the BSKG3 model with $B_\star = 0$. 97

A.6 The same as Table 5.4, using the BSKG3 model with $B_\star = 0$. 98
A.7 The same as Table 5.2, using the HFB31 model with $B_\star = 0$. 98
A.8 The same as Table 5.3, using the HFB31 model with $B_\star = 0$. 98
A.9 The same as Table 5.4, using the HFB31 model with $B_\star = 0$. 99
A.10 The same as Table 5.2, using the DDMED model with $B_\star = 0$ 99
A.11 The same as Table 5.3, using the DDMED model with $B_\star = 0$ 99
A.12 The same as Table 5.4, using the DDMED model with $B_\star = 0$ 100
A.13 The same as Table 5.2, using the DDPC1 model with $B_\star = 0$. 100
A.14 The same as Table 5.3, using the DDPC1 model with $B_\star = 0$. 100
A.15 The same as Table 5.4, using the DDPC1 model with $B_\star = 0$. 100
A.16 The same as Table 5.2, using the SVMIN model with $B_\star = 0$. 101
A.17 The same as Table 5.3, using the SVMIN model with $B_\star = 0$. 101
A.18 The same as Table 5.4, using the SVMIN model with $B_\star = 0$. 101
A.19 The same as Table 5.2, using the UNEDF0 model with $B_\star = 0$ 102
A.20 The same as Table 5.3, using the UNEDF0 model with $B_\star = 0$ 102
A.21 The same as Table 5.4, using the UNEDF0 model with $B_\star = 0$ 102

B.1 The same as Table 5.2, using the WS4RBF model with $B_\star =$ 1500 103
B.2 The same as Table 5.3, using the WS4RBF model with $B_\star =$ 1500 103
B.3 The same as Table 5.4, using the WS4RBF model with $B_\star =$ 1500 104
B.4 The same as Table 5.2, using the BSKG3 model with $B_\star = 1500$ 104
B.5 The same as Table 5.3, using the BSKG3 model with $B_\star = 1500$ 104
B.6 The same as Table 5.4, using the BSKG3 model with $B_\star = 1500$ 104
B.7 The same as Table 5.2, using the HFB31 model with $B_\star = 1500$ 105
B.8 The same as Table 5.3, using the HFB31 model with $B_\star = 1500$ 105
B.9 The same as Table 5.4, using the HFB31 model with $B_\star = 1500$ 105
B.10 The same as Table 5.2, using the DDMED model with $B_\star = 1500$ 106
B.11 The same as Table 5.3, using the DDMED model with $B_\star = 1500$ 106
B.12 The same as Table 5.4, using the DDMED model with $B_\star = 1500$ 106
B.13 The same as Table 5.2, using the DDPC1 model with $B_\star = 1500$ 107
B.14 The same as Table 5.3, using the DDPC1 model with $B_\star = 1500$ 107
B.15 The same as Table 5.4, using the DDPC1 model with $B_\star = 1500$ 107
B.16 The same as Table 5.2, using the SVMIN model with $B_\star = 1500$ 108
B.17 The same as Table 5.3, using the SVMIN model with $B_\star = 1500$ 108
B.18 The same as Table 5.4, using the SVMIN model with $B_\star = 1500$ 108
B.19 The same as Table 5.2, using the UNEDF0 model with $B_\star =$ 1500 109

B.20 The same as Table 5.3, using the UNEDF0 model with $B_\star = 1500$ . . . 109
B.21 The same as Table 5.4, using the UNEDF0 model with $B_\star = 1500$ . . . 109

C.1 The same as Table 5.2, using the SEMF model with $B_\star = 2000$ 110
C.2 The same as Table 5.3, using the SEMF model with $B_\star = 2000$ 110
C.3 The same as Table 5.4, using the SEMF model with $B_\star = 2000$ 111
C.4 The same as Table 5.2, using the FRDM2012 model with $B_\star = 2000$ . . . 111
C.5 The same as Table 5.3, using the FRDM2012 model with $B_\star = 2000$ . . . 111
C.6 The same as Table 5.4, using the FRDM2012 model with $B_\star = 2000$ . . . 112
C.7 The same as Table 5.2, using the WS4RBF model with $B_\star = 2000$ . . . 112
C.8 The same as Table 5.3, using the WS4RBF model with $B_\star = 2000$ . . . 112
C.9 The same as Table 5.4, using the WS4RBF model with $B_\star = 2000$ . . . 112
C.10 The same as Table 5.2, using the BSKG3 model with $B_\star = 2000$ 113
C.11 The same as Table 5.3, using the BSKG3 model with $B_\star = 2000$ 113
C.12 The same as Table 5.4, using the BSKG3 model with $B_\star = 2000$ 113
C.13 The same as Table 5.2, using the HFB31 model with $B_\star = 2000$ 114
C.14 The same as Table 5.3, using the HFB31 model with $B_\star = 2000$ 114
C.15 The same as Table 5.4, using the HFB31 model with $B_\star = 2000$ 114
C.16 The same as Table 5.2, using the DDMED model with $B_\star = 2000$ 115
C.17 The same as Table 5.3, using the DDMED model with $B_\star = 2000$ 115
C.18 The same as Table 5.4, using the DDMED model with $B_\star = 2000$ 115
C.19 The same as Table 5.2, using the DDPC1 model with $B_\star = 2000$ 116
C.20 The same as Table 5.3, using the DDPC1 model with $B_\star = 2000$ 116
C.21 The same as Table 5.4, using the DDPC1 model with $B_\star = 2000$ 116
C.22 The same as Table 5.2, using the SVMIN model with $B_\star = 2000$ 117
C.23 The same as Table 5.3, using the SVMIN model with $B_\star = 2000$ 117
C.24 The same as Table 5.4, using the SVMIN model with $B_\star = 2000$ 117
C.25 The same as Table 5.2, using the UNEDF0 model with $B_\star = 2000$ . . . 118
C.26 The same as Table 5.3, using the UNEDF0 model with $B_\star = 2000$ . . . 118
C.27 The same as Table 5.4, using the UNEDF0 model with $B_\star = 2000$ . . . 118

D.1 The same as Table 5.2, using the SEMF model with $B_\star = 2500$ 119
D.2 The same as Table 5.3, using the SEMF model with $B_\star = 2500$ 119
D.3 The same as Table 5.4, using the SEMF model with $B_\star = 2500$ 120
D.4 The same as Table 5.2, using the FRDM2012 model with $B_\star = 2500$ . . . 120
D.5 The same as Table 5.3, using the FRDM2012 model with $B_\star = 2500$ . . . 120
D.6 The same as Table 5.4, using the FRDM2012 model with $B_\star = 2500$ . . . 121
D.7 The same as Table 5.2, using the WS4RBF model with $B_\star = 2500$ . . . 121
D.8 The same as Table 5.3, using the WS4RBF model with $B_\star = 2500$ . . . 121
D.9 The same as Table 5.4, using the WS4RBF model with $B_\star = 2500$ . . . 121
D.10 The same as Table 5.2, using the BSKG3 model with $B_\star = 2500$ 122
D.11 The same as Table 5.3, using the BSKG3 model with $B_\star = 2500$ 122
D.12 The same as Table 5.4, using the BSKG3 model with $B_\star = 2500$ 122
D.13 The same as Table 5.2, using the HFB31 model with $B_\star = 2500$ 123
D.14 The same as Table 5.3, using the HFB31 model with $B_\star = 2500$ 123
D.15 The same as Table 5.4, using the HFB31 model with $B_\star = 2500$ 123
D.16 The same as Table 5.2, using the DDMED model with $B_\star = 2500$ 124
D.17 The same as Table 5.3, using the DDMED model with $B_\star = 2500$ 124
D.18 The same as Table 5.4, using the DDMED model with $B_\star = 2500$ 124
D.19 The same as Table 5.2, using the DDPC1 model with $B_\star = 2500$ 125
D.20 The same as Table 5.3, using the DDPC1 model with $B_\star = 2500$ 125
D.21 The same as Table 5.4, using the DDPC1 model with $B_\star = 2500$ 125
D.22 The same as Table 5.2, using the SVMIN model with $B_\star = 2500$ 126
D.23 The same as Table 5.3, using the SVMIN model with $B_\star = 2500$ 126
D.24 The same as Table 5.4, using the SVMIN model with $B_\star = 2500$ 126
D.25 The same as Table 5.2, using the UNEDF0 model with $B_\star = 2500$ . . . 127
D.26 The same as Table 5.3, using the UNEDF0 model with $B_\star = 2500$ . . . 127
D.27 The same as Table 5.4, using the UNEDF0 model with $B_\star = 2500$ . . . 127

List of Figures

1.1 The structure of a neutron star. Taken from Ref. [2] 2

4.1 Application of the knowledge of nuclei abundances in initially cold outer crust, (a) normalized abundance distributions to the solar system r-abundance distribution before the decompression and (b) after the decompression. Taken from Ref. [18] 43

5.1 A polytropic EoS $P = K\epsilon^G$ for fitting, using the SEMF model with magnetic field strength $B_\star = 0$ 57

5.2 The same as Figure 5.1, using the FRDM2012 model with $B_\star = 0$ 58

5.3 A polytropic EoS $P = K\epsilon^G$ for fitting, using the SEMF model with magnetic field strength $B_\star = 1500$ 59

5.4 The same as Figure 5.3, using the FRDM2012 model with $B_\star = 1500$ 59

5.5 Equation of State, (a) pressure as a function of energy density and (b) pressure as a function of baryon number density, using the SEMF model with different magnetic field strengths $B_\star$ . . 60

5.6 The same as Figure 5.5, using the FRDM2012 model with different magnetic field strengths $B_\star$ 61

5.7 Adiabatic index as a function of (a) energy density and of (b) baryon number density, using the SEMF model with different magnetic field strengths $B_\star$. The horizontal dashed line corresponds to $\Gamma = 4/3$ 62

5.8 The same as Figure 5.7, using the FRDM2012 model with different magnetic field strengths $B_\star$ 62

5.9 Speed of sound as a function of (a) energy density and of (b) baryon number density, using the SEMF model with different magnetic field strengths $B_\star$ 63

5.10 The same as Figure 5.9, using the FRDM2012 model with different magnetic field strengths $B_\star$ 64
5.11 Compression modulus as a function of (a) energy density and of (b) baryon number density, using the SEMF model with different magnetic field strengths $B_\star$ 65
5.12 The same as Figure 5.11, using the FRDM2012 model with different magnetic field strengths $B_\star$ 65
5.13 Effective shear modulus as a function of (a) energy density and of (b) baryon number density, using the SEMF model with different magnetic field strengths $B_\star$ 66
5.14 The same as Figure 5.13, using the FRDM2012 model with different magnetic field strengths $B_\star$ 67
5.15 Effective shear modulus over compression modulus as a function of (a) energy density and of (b) baryon number density, using the SEMF model with different magnetic field strengths $B_\star$ 68
5.16 The same as Figure 5.15, using the FRDM2012 model with different magnetic field strengths $B_\star$ 68
5.17 Atomic number, neutron number and proton fraction as a function of (a) energy density and of (b) baryon number density, using the SEMF model with different magnetic field strengths $B_\star$ 70
5.18 The same as Figure 5.17, using the FRDM2012 model with different magnetic field strengths $B_\star$ 71
5.19 Mass of outer crust for different masses and radii of NS, using the SEMF model with different magnetic field strengths $B_\star$. Clarification: the 2nd line from above (i.e., 1st dark blue line from above) and the 4th line from above (i.e., 1st orange line from above) correspond to ($M = 1.4$, $B_\star = 2500$) and ($M = 1.6$, $B_\star = 2500$), respectively 72
5.20 The same as Figure 5.19, using the FRDM2012 model with different magnetic field strengths $B_\star$ 73
5.21 Proper depth of neutron-drip transition for different masses and radii of NS, using the SEMF model with different magnetic field strengths $B_\star$. Clarification: the dark blue line of the 2nd group of overlapping lines from above and the orange line of the 3rd group of overlapping lines from above correspond to ($M = 1.4$, $B_\star = 2500$) and ($M = 1.6$, $B_\star = 2500$), respectively 74
5.22 The same as Figure 5.21, using the FRDM2012 model with different magnetic field strengths $B_\star$ 75

5.23 Neutron-drip transition pressure as a function of magnetic field strength, using different nuclear mass models 78
5.24 Equation of State, (a) pressure as a function of energy density and (b) pressure as a function of baryon number density, using different models with magnetic field strength $B_\star = 0$ 79
5.25 The same as Figure 5.24, using different models with magnetic field strength $B_\star = 1500$ 79
5.26 Adiabatic index as a function of (a) energy density and of (b) baryon number density, using different models with magnetic field strength $B_\star = 0$. The horizontal dashed line corresponds to $\Gamma = 4/3$ 80
5.27 The same as Figure 5.26, using different models with magnetic field strength $B_\star = 1500$ 81
5.28 Speed of sound as a function of (a) energy density and of (b) baryon number density, using different models with magnetic field strength $B_\star = 0$ 82
5.29 The same as Figure 5.28, using different models with magnetic field strength $B_\star = 1500$ 82
5.30 Compression modulus as a function of (a) energy density and of (b) baryon number density, using different models with magnetic field strength $B_\star = 0$ 83
5.31 The same as Figure 5.30, using different models with magnetic field strength $B_\star = 1500$ 84
5.32 Effective shear modulus as a function of (a) energy density and of (b) baryon number density, using different models with magnetic field strength $B_\star = 0$ 85
5.33 The same as Figure 5.32, using different models with magnetic field strength $B_\star = 1500$ 85
5.34 Effective shear modulus over compression modulus as a function of (a) energy density and of (b) baryon number density, using different models with magnetic field strength $B_\star = 0$ . . 86
5.35 The same as Figure 5.34, using different models with magnetic field strength $B_\star = 1500$ 87
5.36 Atomic number, neutron number and proton fraction as a function of (a) energy density and of (b) baryon number density, using different models with magnetic field strength $B_\star = 0$ 88
5.37 The same as Figure 5.36, using different models with magnetic field strength $B_\star = 1500$ 89

5.38 Mass of outer crust for different masses and radii of NS, using different models with magnetic field strength $B_\star = 0$. Clarification: the dark blue line of the 2nd group of overlapping lines from above and the orange line of the 3rd group of overlapping lines from above correspond to $(M = 1.4, model: SVMIN)$ and $(M = 1.6, model: SVMIN)$, respectively 90
5.39 The same as Figure 5.38, using different models with magnetic field strength $B_\star = 1500$ 91
5.40 Proper depth of neutron-drip transition for different masses and radii of NS, using different models with magnetic field strength $B_\star = 0$. Clarification: the dark blue line of the 2nd group of overlapping lines from above and the orange line of the 3rd group of overlapping lines from above correspond to $(M = 1.4, model: SVMIN)$ and $(M = 1.6, model: SVMIN)$, respectively 92
5.41 The same as Figure 5.40, using different models with magnetic field strength $B_\star = 1500$ 93

E.1 Equation of State, (a) pressure as a function of energy density and (b) pressure as a function of baryon number density, using the SEMF model with magnetic field strength $B_\star = 0$ 128
E.2 The same as Figure E.1, using the FRDM2012 model with $B_\star = 0$ 129
E.3 The same as Figure E.1, using the WS4RBF model with $B_\star = 0$ 129
E.4 The same as Figure E.1, using the BSKG3 model with $B_\star = 0$ 130
E.5 The same as Figure E.1, using the HFB31 model with $B_\star = 0$ 130
E.6 The same as Figure E.1, using the DDMED model with $B_\star = 0$ 131
E.7 The same as Figure E.1, using the DDPC1 model with $B_\star = 0$ 131
E.8 The same as Figure E.1, using the SVMIN model with $B_\star = 0$ 132
E.9 The same as Figure E.1, using the UNEDF0 model with $B_\star = 0$ 132
E.10 The same as Figure 5.1, using the WS4RBF model with $B_\star = 0$ 133
E.11 The same as Figure 5.1, using the BSKG3 model with $B_\star = 0$ 133
E.12 The same as Figure 5.1, using the HFB31 model with $B_\star = 0$. 134
E.13 The same as Figure 5.1, using the DDMED model with $B_\star = 0$ 134
E.14 The same as Figure 5.1, using the DDPC1 model with $B_\star = 0$ 135
E.15 The same as Figure 5.1, using the SVMIN model with $B_\star = 0$ 135
E.16 The same as Figure 5.1, using the UNEDF0 model with $B_\star = 0$ 136
E.17 Adiabatic index as a function of (a) energy density and of (b) baryon number density, using the SEMF model with magnetic field strength $B_\star = 0$. The horizontal dashed line corresponds to $\Gamma = 4/3$ 136

E.18 The same as Figure E.17, using the FRDM2012 model with $B_\star = 0$ 137
E.19 The same as Figure E.17, using the WS4RBF model with $B_\star = 0$ 137
E.20 The same as Figure E.17, using the BSKG3 model with $B_\star = 0$ 138
E.21 The same as Figure E.17, using the HFB31 model with $B_\star = 0$ 138
E.22 The same as Figure E.17, using the DDMED model with $B_\star = 0$ 139
E.23 The same as Figure E.17, using the DDPC1 model with $B_\star = 0$ 139
E.24 The same as Figure E.17, using the SVMIN model with $B_\star = 0$ 140
E.25 The same as Figure E.17, using the UNEDF0 model with $B_\star = 0$ 140
E.26 Speed of sound as a function of (a) energy density and of (b) baryon number density, using the SEMF model with magnetic field strength $B_\star = 0$ 141
E.27 The same as Figure E.26, using the FRDM2012 model with $B_\star = 0$ 141
E.28 The same as Figure E.26, using the WS4RBF model with $B_\star = 0$ 142
E.29 The same as Figure E.26, using the BSKG3 model with $B_\star = 0$ 142
E.30 The same as Figure E.26, using the HFB31 model with $B_\star = 0$ 143
E.31 The same as Figure E.26, using the DDMED model with $B_\star = 0$ 143
E.32 The same as Figure E.26, using the DDPC1 model with $B_\star = 0$ 144
E.33 The same as Figure E.26, using the SVMIN model with $B_\star = 0$ 144
E.34 The same as Figure E.26, using the UNEDF0 model with $B_\star = 0$ 145
E.35 Compression modulus as a function of (a) energy density and of (b) baryon number density, using the SEMF model with magnetic field strength $B_\star = 0$ 145
E.36 The same as Figure E.35, using the FRDM2012 model with $B_\star = 0$ 146
E.37 The same as Figure E.35, using the WS4RBF model with $B_\star = 0$ 146
E.38 The same as Figure E.35, using the BSKG3 model with $B_\star = 0$ 147
E.39 The same as Figure E.35, using the HFB31 model with $B_\star = 0$ 147
E.40 The same as Figure E.35, using the DDMED model with $B_\star = 0$ 148
E.41 The same as Figure E.35, using the DDPC1 model with $B_\star = 0$ 148
E.42 The same as Figure E.35, using the SVMIN model with $B_\star = 0$ 149
E.43 The same as Figure E.35, using the UNEDF0 model with $B_\star = 0$ 149
E.44 Effective shear modulus as a function of (a) energy density and of (b) baryon number density, using the SEMF model with magnetic field strength $B_\star = 0$ 150
E.45 The same as Figure E.44, using the FRDM2012 model with $B_\star = 0$ 150
E.46 The same as Figure E.44, using the WS4RBF model with $B_\star = 0$ 151
E.47 The same as Figure E.44, using the BSKG3 model with $B_\star = 0$ 151
E.48 The same as Figure E.44, using the HFB31 model with $B_\star = 0$ 152

E.49 The same as Figure E.44, using the DDMED model with $B_\star = 0$ 152
E.50 The same as Figure E.44, using the DDPC1 model with $B_\star = 0$ 153
E.51 The same as Figure E.44, using the SVMIN model with $B_\star = 0$ 153
E.52 The same as Figure E.44, using the UNEDF0 model with $B_\star = 0$ 154
E.53 Effective shear modulus over compression modulus as a function of (a) energy density and of (b) baryon number density, using the SEMF model with magnetic field strength $B_\star = 0$ . . 154
E.54 The same as Figure E.53, using the FRDM2012 model with $B_\star = 0$ 155
E.55 The same as Figure E.53, using the WS4RBF model with $B_\star = 0$ 155
E.56 The same as Figure E.53, using the BSKG3 model with $B_\star = 0$ 156
E.57 The same as Figure E.53, using the HFB31 model with $B_\star = 0$ 156
E.58 The same as Figure E.53, using the DDMED model with $B_\star = 0$ 157
E.59 The same as Figure E.53, using the DDPC1 model with $B_\star = 0$ 157
E.60 The same as Figure E.53, using the SVMIN model with $B_\star = 0$ 158
E.61 The same as Figure E.53, using the UNEDF0 model with $B_\star = 0$ 158
E.62 Atomic number, neutron number and proton fraction as a function of (a) energy density and of (b) baryon number density, using the SEMF model with magnetic field strength $B_\star = 0$ 159
E.63 The same as Figure E.62, using the FRDM2012 model with $B_\star = 0$ 160
E.64 The same as Figure E.62, using the WS4RBF model with $B_\star = 0$ 161
E.65 The same as Figure E.62, using the BSKG3 model with $B_\star = 0$ 162
E.66 The same as Figure E.62, using the HFB31 model with $B_\star = 0$ 163
E.67 The same as Figure E.62, using the DDMED model with $B_\star = 0$ 164
E.68 The same as Figure E.62, using the DDPC1 model with $B_\star = 0$ 165
E.69 The same as Figure E.62, using the SVMIN model with $B_\star = 0$ 166
E.70 The same as Figure E.62, using the UNEDF0 model with $B_\star = 0$ 167
E.71 Mass of outer crust for different masses and radii of NS, using the SEMF model with magnetic field strength $B_\star = 0$ 168
E.72 The same as Figure E.71, using the FRDM2012 model with $B_\star = 0$ 169
E.73 The same as Figure E.71, using the WS4RBF model with $B_\star = 0$ 169
E.74 The same as Figure E.71, using the BSKG3 model with $B_\star = 0$ 170
E.75 The same as Figure E.71, using the HFB31 model with $B_\star = 0$ 170
E.76 The same as Figure E.71, using the DDMED model with $B_\star = 0$ 171
E.77 The same as Figure E.71, using the DDPC1 model with $B_\star = 0$ 171
E.78 The same as Figure E.71, using the SVMIN model with $B_\star = 0$ 172
E.79 The same as Figure E.71, using the UNEDF0 model with $B_\star = 0$ 172

E.80 Proper depth of neutron-drip transition for different masses and radii of NS, using the SEMF model with magnetic field strength $B_\star = 0$ . . . 173
E.81 The same as Figure E.80, using the FRDM2012 model with $B_\star = 0$ . . . 174
E.82 The same as Figure E.80, using the WS4RBF model with $B_\star = 0$ 174
E.83 The same as Figure E.80, using the BSKG3 model with $B_\star = 0$ 175
E.84 The same as Figure E.80, using the HFB31 model with $B_\star = 0$ 175
E.85 The same as Figure E.80, using the DDMED model with $B_\star = 0$ 176
E.86 The same as Figure E.80, using the DDPC1 model with $B_\star = 0$ 176
E.87 The same as Figure E.80, using the SVMIN model with $B_\star = 0$ 177
E.88 The same as Figure E.80, using the UNEDF0 model with $B_\star = 0$ 177

F.1 Equation of State, (a) pressure as a function of energy density and (b) pressure as a function of baryon number density, using the SEMF model with magnetic field strength $B_\star = 1500$ . . . 178
F.2 The same as Figure F.1, using the FRDM2012 model with $B_\star = 1500$ . . . 179
F.3 The same as Figure F.1, using the WS4RBF model with $B_\star = 1500$ . . . 179
F.4 The same as Figure F.1, using the BSKG3 model with $B_\star = 1500$ 180
F.5 The same as Figure F.1, using the HFB31 model with $B_\star = 1500$ 180
F.6 The same as Figure F.1, using the DDMED model with $B_\star = 1500$ . . . 181
F.7 The same as Figure F.1, using the DDPC1 model with $B_\star = 1500$ 181
F.8 The same as Figure F.1, using the SVMIN model with $B_\star = 1500$ 182
F.9 The same as Figure F.1, using the UNEDF0 model with $B_\star = 1500$ . . . 182
F.10 The same as Figure 5.3, using the WS4RBF model with $B_\star = 1500$ . . . 183
F.11 The same as Figure 5.3, using the BSKG3 model with $B_\star = 1500$ 183
F.12 The same as Figure 5.3, using the HFB31 model with $B_\star = 1500$ 184
F.13 The same as Figure 5.3, using the DDMED model with $B_\star = 1500$ . . . 184
F.14 The same as Figure 5.3, using the DDPC1 model with $B_\star = 1500$ 185
F.15 The same as Figure 5.3, using the SVMIN model with $B_\star = 1500$ 185
F.16 The same as Figure 5.3, using the UNEDF0 model with $B_\star = 1500$ . . . 186
F.17 Adiabatic index as a function of (a) energy density and of (b) baryon number density, using the SEMF model with magnetic field strength $B_\star = 1500$ . . . 186

F.18 The same as Figure F.17, using the FRDM2012 model with $B_\star = 1500$ . . . 187
F.19 The same as Figure F.17, using the WS4RBF model with $B_\star = 1500$ . . . 187
F.20 The same as Figure F.17, using the BSKG3 model with $B_\star = 1500$ . . . 188
F.21 The same as Figure F.17, using the HFB31 model with $B_\star = 1500$ . . . 188
F.22 The same as Figure F.17, using the DDMED model with $B_\star = 1500$ . . . 189
F.23 The same as Figure F.17, using the DDPC1 model with $B_\star = 1500$ . . . 189
F.24 The same as Figure F.17, using the SVMIN model with $B_\star = 1500$ . . . 190
F.25 The same as Figure F.17, using the UNEDF0 model with $B_\star = 1500$ . . . 190
F.26 Speed of sound as a function of (a) energy density and of (b) baryon number density, using the SEMF model with magnetic field strength $B_\star = 1500$ . . . 191
F.27 The same as Figure F.26, using the FRDM2012 model with $B_\star = 1500$ . . . 191
F.28 The same as Figure F.26, using the WS4RBF model with $B_\star = 1500$ . . . 192
F.29 The same as Figure F.26, using the BSKG3 model with $B_\star = 1500$ . . . 192
F.30 The same as Figure F.26, using the HFB31 model with $B_\star = 1500$ . . . 193
F.31 The same as Figure F.26, using the DDMED model with $B_\star = 1500$ . . . 193
F.32 The same as Figure F.26, using the DDPC1 model with $B_\star = 1500$ . . . 194
F.33 The same as Figure F.26, using the SVMIN model with $B_\star = 1500$ . . . 194
F.34 The same as Figure F.26, using the UNEDF0 model with $B_\star = 1500$ . . . 195
F.35 Compression modulus as a function of (a) energy density and of (b) baryon number density, using the SEMF model with magnetic field strength $B_\star = 1500$ . . . 195
F.36 The same as Figure F.35, using the FRDM2012 model with $B_\star = 1500$ . . . 196

F.37 The same as Figure F.35, using the WS4RBF model with $B_\star = 1500$ . . . 196
F.38 The same as Figure F.35, using the BSKG3 model with $B_\star = 1500$ . . . 197
F.39 The same as Figure F.35, using the HFB31 model with $B_\star = 1500$ . . . 197
F.40 The same as Figure F.35, using the DDMED model with $B_\star = 1500$ . . . 198
F.41 The same as Figure F.35, using the DDPC1 model with $B_\star = 1500$ . . . 198
F.42 The same as Figure F.35, using the SVMIN model with $B_\star = 1500$ . . . 199
F.43 The same as Figure F.35, using the UNEDF0 model with $B_\star = 1500$ . . . 199
F.44 Effective shear modulus as a function of (a) energy density and of (b) baryon number density, using the SEMF model with magnetic field strength $B_\star = 1500$ . . . 200
F.45 The same as Figure F.44, using the FRDM2012 model with $B_\star = 1500$ . . . 200
F.46 The same as Figure F.44, using the WS4RBF model with $B_\star = 1500$ . . . 201
F.47 The same as Figure F.44, using the BSKG3 model with $B_\star = 1500$ . . . 201
F.48 The same as Figure F.44, using the HFB31 model with $B_\star = 1500$ . . . 202
F.49 The same as Figure F.44, using the DDMED model with $B_\star = 1500$ . . . 202
F.50 The same as Figure F.44, using the DDPC1 model with $B_\star = 1500$ . . . 203
F.51 The same as Figure F.44, using the SVMIN model with $B_\star = 1500$ . . . 203
F.52 The same as Figure F.44, using the UNEDF0 model with $B_\star = 1500$ . . . 204
F.53 Effective shear modulus over compression modulus as a function of (a) energy density and of (b) baryon number density, using the SEMF model with magnetic field strength $B_\star = 1500$ 204
F.54 The same as Figure F.53, using the FRDM2012 model with $B_\star = 1500$ . . . 205
F.55 The same as Figure F.53, using the WS4RBF model with $B_\star = 1500$ . . . 205

F.56 The same as Figure F.53, using the BSKG3 model with $B_\star = 1500$ . . . 206
F.57 The same as Figure F.53, using the HFB31 model with $B_\star = 1500$ . . . 206
F.58 The same as Figure F.53, using the DDMED model with $B_\star = 1500$ . . . 207
F.59 The same as Figure F.53, using the DDPC1 model with $B_\star = 1500$ . . . 207
F.60 The same as Figure F.53, using the SVMIN model with $B_\star = 1500$ . . . 208
F.61 The same as Figure F.53, using the UNEDF0 model with $B_\star = 1500$ . . . 208
F.62 Atomic number, neutron number and proton fraction as a function of (a) energy density and of (b) baryon number density, using the SEMF model with magnetic field strength $B_\star = 1500$ . . . 209
F.63 The same as Figure F.62, using the FRDM2012 model with $B_\star = 1500$ . . . 210
F.64 The same as Figure F.62, using the WS4RBF model with $B_\star = 1500$ . . . 211
F.65 The same as Figure F.62, using the BSKG3 model with $B_\star = 1500$ . . . 212
F.66 The same as Figure F.62, using the HFB31 model with $B_\star = 1500$ . . . 213
F.67 The same as Figure F.62, using the DDMED model with $B_\star = 1500$ . . . 214
F.68 The same as Figure F.62, using the DDPC1 model with $B_\star = 1500$ . . . 215
F.69 The same as Figure F.62, using the SVMIN model with $B_\star = 1500$ . . . 216
F.70 The same as Figure F.62, using the UNEDF0 model with $B_\star = 1500$ . . . 217
F.71 Mass of outer crust for different masses and radii of NS, using the SEMF model with magnetic field strength $B_\star = 1500$ . . . 218
F.72 The same as Figure F.71, using the FRDM2012 model with $B_\star = 1500$ . . . 219
F.73 The same as Figure F.71, using the WS4RBF model with $B_\star = 1500$ . . . 219
F.74 The same as Figure F.71, using the BSKG3 model with $B_\star = 1500$ . . . 220

F.75 The same as Figure F.71, using the HFB31 model with $B_\star = 1500$ . . . 220
F.76 The same as Figure F.71, using the DDMED model with $B_\star = 1500$ . . . 221
F.77 The same as Figure F.71, using the DDPC1 model with $B_\star = 1500$ . . . 221
F.78 The same as Figure F.71, using the SVMIN model with $B_\star = 1500$ . . . 222
F.79 The same as Figure F.71, using the UNEDF0 model with $B_\star = 1500$ . . . 222
F.80 Proper depth of neutron-drip transition for different masses and radii of NS, using the SEMF model with magnetic field strength $B_\star = 1500$ . . . 223
F.81 The same as Figure F.80, using the FRDM2012 model with $B_\star = 1500$ . . . 224
F.82 The same as Figure F.80, using the WS4RBF model with $B_\star = 1500$ . . . 224
F.83 The same as Figure F.80, using the BSKG3 model with $B_\star = 1500$ . . . 225
F.84 The same as Figure F.80, using the HFB31 model with $B_\star = 1500$ . . . 225
F.85 The same as Figure F.80, using the DDMED model with $B_\star = 1500$ . . . 226
F.86 The same as Figure F.80, using the DDPC1 model with $B_\star = 1500$ . . . 226
F.87 The same as Figure F.80, using the SVMIN model with $B_\star = 1500$ . . . 227
F.88 The same as Figure F.80, using the UNEDF0 model with $B_\star = 1500$ . . . 227

G.1 Equation of State, (a) pressure as a function of energy density and (b) pressure as a function of baryon number density, using the SEMF model with magnetic field strength $B_\star = 2000$ . . . 228
G.2 The same as Figure G.1, using the FRDM2012 model with $B_\star = 2000$ . . . 229
G.3 The same as Figure G.1, using the WS4RBF model with $B_\star = 2000$ . . . 229
G.4 The same as Figure G.1, using the BSKG3 model with $B_\star = 2000$ 230
G.5 The same as Figure G.1, using the HFB31 model with $B_\star = 2000$ 230
G.6 The same as Figure G.1, using the DDMED model with $B_\star = 2000$ . . . 231

G.7 The same as Figure G.1, using the DDPC1 model with $B_\star = 2000$ . . . 231
G.8 The same as Figure G.1, using the SVMIN model with $B_\star = 2000$ 232
G.9 The same as Figure G.1, using the UNEDF0 model with $B_\star = 2000$ . . . 232
G.10 A polytropic EoS $P = K\epsilon^G$ for fitting, using the SEMF model with magnetic field strength $B_\star = 2000$ . . . 233
G.11 The same as Figure G.10, using the FRDM2012 model with $B_\star = 2000$ . . . 234
G.12 The same as Figure G.10, using the WS4RBF model with $B_\star = 2000$ . . . 234
G.13 The same as Figure G.10, using the BSKG3 model with $B_\star = 2000$ . . . 235
G.14 The same as Figure G.10, using the HFB31 model with $B_\star = 2000$ . . . 235
G.15 The same as Figure G.10, using the DDMED model with $B_\star = 2000$ . . . 236
G.16 The same as Figure G.10, using the DDPC1 model with $B_\star = 2000$ . . . 236
G.17 The same as Figure G.10, using the SVMIN model with $B_\star = 2000$ . . . 237
G.18 The same as Figure G.10, using the UNEDF0 model with $B_\star = 2000$ . . . 237
G.19 Adiabatic index as a function of (a) energy density and of (b) baryon number density, using the SEMF model with magnetic field strength $B_\star = 2000$ . . . 238
G.20 The same as Figure G.19, using the FRDM2012 model with $B_\star = 2000$ . . . 238
G.21 The same as Figure G.19, using the WS4RBF model with $B_\star = 2000$ . . . 239
G.22 The same as Figure G.19, using the BSKG3 model with $B_\star = 2000$ . . . 239
G.23 The same as Figure G.19, using the HFB31 model with $B_\star = 2000$ . . . 240
G.24 The same as Figure G.19, using the DDMED model with $B_\star = 2000$ . . . 240
G.25 The same as Figure G.19, using the DDPC1 model with $B_\star = 2000$ . . . 241
G.26 The same as Figure G.19, using the SVMIN model with $B_\star = 2000$ . . . 241

G.27 The same as Figure G.19, using the UNEDF0 model with $B_\star = 2000$ . . . 242
G.28 Speed of sound as a function of (a) energy density and of (b) baryon number density, using the SEMF model with magnetic field strength $B_\star = 2000$ . . . 242
G.29 The same as Figure G.28, using the FRDM2012 model with $B_\star = 2000$ . . . 243
G.30 The same as Figure G.28, using the WS4RBF model with $B_\star = 2000$ . . . 243
G.31 The same as Figure G.28, using the BSKG3 model with $B_\star = 2000$ . . . 244
G.32 The same as Figure G.28, using the HFB31 model with $B_\star = 2000$ . . . 244
G.33 The same as Figure G.28, using the DDMED model with $B_\star = 2000$ . . . 245
G.34 The same as Figure G.28, using the DDPC1 model with $B_\star = 2000$ . . . 245
G.35 The same as Figure G.28, using the SVMIN model with $B_\star = 2000$ . . . 246
G.36 The same as Figure G.28, using the UNEDF0 model with $B_\star = 2000$ . . . 246
G.37 Compression modulus as a function of (a) energy density and of (b) baryon number density, using the SEMF model with magnetic field strength $B_\star = 2000$ . . . 247
G.38 The same as Figure G.37, using the FRDM2012 model with $B_\star = 2000$ . . . 247
G.39 The same as Figure G.37, using the WS4RBF model with $B_\star = 2000$ . . . 248
G.40 The same as Figure G.37, using the BSKG3 model with $B_\star = 2000$ . . . 248
G.41 The same as Figure G.37, using the HFB31 model with $B_\star = 2000$ . . . 249
G.42 The same as Figure G.37, using the DDMED model with $B_\star = 2000$ . . . 249
G.43 The same as Figure G.37, using the DDPC1 model with $B_\star = 2000$ . . . 250
G.44 The same as Figure G.37, using the SVMIN model with $B_\star = 2000$ . . . 250
G.45 The same as Figure G.37, using the UNEDF0 model with $B_\star = 2000$ . . . 251

G.46 Effective shear modulus as a function of (a) energy density and of (b) baryon number density, using the SEMF model with magnetic field strength $B_\star = 2000$ 251
G.47 The same as Figure G.46, using the FRDM2012 model with $B_\star = 2000$ 252
G.48 The same as Figure G.46, using the WS4RBF model with $B_\star = 2000$ 252
G.49 The same as Figure G.46, using the BSKG3 model with $B_\star = 2000$ 253
G.50 The same as Figure G.46, using the HFB31 model with $B_\star = 2000$ 253
G.51 The same as Figure G.46, using the DDMED model with $B_\star = 2000$ 254
G.52 The same as Figure G.46, using the DDPC1 model with $B_\star = 2000$ 254
G.53 The same as Figure G.46, using the SVMIN model with $B_\star = 2000$ 255
G.54 The same as Figure G.46, using the UNEDF0 model with $B_\star = 2000$ 255
G.55 Effective shear modulus over compression modulus as a function of (a) energy density and of (b) baryon number density, using the SEMF model with magnetic field strength $B_\star = 2000$ 256
G.56 The same as Figure G.55, using the FRDM2012 model with $B_\star = 2000$ 256
G.57 The same as Figure G.55, using the WS4RBF model with $B_\star = 2000$ 257
G.58 The same as Figure G.55, using the BSKG3 model with $B_\star = 2000$ 257
G.59 The same as Figure G.55, using the HFB31 model with $B_\star = 2000$ 258
G.60 The same as Figure G.55, using the DDMED model with $B_\star = 2000$ 258
G.61 The same as Figure G.55, using the DDPC1 model with $B_\star = 2000$ 259
G.62 The same as Figure G.55, using the SVMIN model with $B_\star = 2000$ 259
G.63 The same as Figure G.55, using the UNEDF0 model with $B_\star = 2000$ 260

G.64 Atomic number, neutron number and proton fraction as a function of (a) energy density and of (b) baryon number density, using the SEMF model with magnetic field strength $B_\star = 2000$ . . . 261
G.65 The same as Figure G.64, using the FRDM2012 model with $B_\star = 2000$ . . . 262
G.66 The same as Figure G.64, using the WS4RBF model with $B_\star = 2000$ . . . 263
G.67 The same as Figure G.64, using the BSKG3 model with $B_\star = 2000$ . . . 264
G.68 The same as Figure G.64, using the HFB31 model with $B_\star = 2000$ . . . 265
G.69 The same as Figure G.64, using the DDMED model with $B_\star = 2000$ . . . 266
G.70 The same as Figure G.64, using the DDPC1 model with $B_\star = 2000$ . . . 267
G.71 The same as Figure G.64, using the SVMIN model with $B_\star = 2000$ . . . 268
G.72 The same as Figure G.64, using the UNEDF0 model with $B_\star = 2000$ . . . 269
G.73 Mass of outer crust for different masses and radii of NS, using the SEMF model with magnetic field strength $B_\star = 2000$ . . . 270
G.74 The same as Figure G.73, using the FRDM2012 model with $B_\star = 2000$ . . . 271
G.75 The same as Figure G.73, using the WS4RBF model with $B_\star = 2000$ . . . 271
G.76 The same as Figure G.73, using the BSKG3 model with $B_\star = 2000$ . . . 272
G.77 The same as Figure G.73, using the HFB31 model with $B_\star = 2000$ . . . 272
G.78 The same as Figure G.73, using the DDMED model with $B_\star = 2000$ . . . 273
G.79 The same as Figure G.73, using the DDPC1 model with $B_\star = 2000$ . . . 273
G.80 The same as Figure G.73, using the SVMIN model with $B_\star = 2000$ . . . 274
G.81 The same as Figure G.73, using the UNEDF0 model with $B_\star = 2000$ . . . 274
G.82 Proper depth of neutron-drip transition for different masses and radii of NS, using the SEMF model with magnetic field strength $B_\star = 2000$ . . . 275

G.83 The same as Figure G.82, using the FRDM2012 model with $B_\star = 2000$ . . . 276
G.84 The same as Figure G.82, using the WS4RBF model with $B_\star = 2000$ . . . 276
G.85 The same as Figure G.82, using the BSKG3 model with $B_\star = 2000$ . . . 277
G.86 The same as Figure G.82, using the HFB31 model with $B_\star = 2000$ . . . 277
G.87 The same as Figure G.82, using the DDMED model with $B_\star = 2000$ . . . 278
G.88 The same as Figure G.82, using the DDPC1 model with $B_\star = 2000$ . . . 278
G.89 The same as Figure G.82, using the SVMIN model with $B_\star = 2000$ . . . 279
G.90 The same as Figure G.82, using the UNEDF0 model with $B_\star = 2000$ . . . 279

H.1 Equation of State, (a) pressure as a function of energy density and (b) pressure as a function of baryon number density, using the SEMF model with magnetic field strength $B_\star = 2500$ . . . 280
H.2 The same as Figure H.1, using the FRDM2012 model with $B_\star = 2500$ . . . 281
H.3 The same as Figure H.1, using the WS4RBF model with $B_\star = 2500$ . . . 281
H.4 The same as Figure H.1, using the BSKG3 model with $B_\star = 2500$ 282
H.5 The same as Figure H.1, using the HFB31 model with $B_\star = 2500$ 282
H.6 The same as Figure H.1, using the DDMED model with $B_\star = 2500$ . . . 283
H.7 The same as Figure H.1, using the DDPC1 model with $B_\star = 2500$ . . . 283
H.8 The same as Figure H.1, using the SVMIN model with $B_\star = 2500$ 284
H.9 The same as Figure H.1, using the UNEDF0 model with $B_\star = 2500$ . . . 284
H.10 A polytropic EoS $P = K\epsilon^G$ for fitting, using the SEMF model with magnetic field strength $B_\star = 2500$ . . . 285
H.11 The same as Figure H.10, using the FRDM2012 model with $B_\star = 2500$ . . . 286
H.12 The same as Figure H.10, using the WS4RBF model with $B_\star = 2500$ . . . 286
H.13 The same as Figure H.10, using the BSKG3 model with $B_\star = 2500$ . . . 287

H.14 The same as Figure H.10, using the HFB31 model with $B_\star = 2500$ . . . 287
H.15 The same as Figure H.10, using the DDMED model with $B_\star = 2500$ . . . 288
H.16 The same as Figure H.10, using the DDPC1 model with $B_\star = 2500$ . . . 288
H.17 The same as Figure H.10, using the SVMIN model with $B_\star = 2500$ . . . 289
H.18 The same as Figure H.10, using the UNEDF0 model with $B_\star = 2500$ . . . 289
H.19 Adiabatic index as a function of (a) energy density and of (b) baryon number density, using the SEMF model with magnetic field strength $B_\star = 2500$ . . . 290
H.20 The same as Figure H.19, using the FRDM2012 model with $B_\star = 2500$ . . . 290
H.21 The same as Figure H.19, using the WS4RBF model with $B_\star = 2500$ . . . 291
H.22 The same as Figure H.19, using the BSKG3 model with $B_\star = 2500$ . . . 291
H.23 The same as Figure H.19, using the HFB31 model with $B_\star = 2500$ . . . 292
H.24 The same as Figure H.19, using the DDMED model with $B_\star = 2500$ . . . 292
H.25 The same as Figure H.19, using the DDPC1 model with $B_\star = 2500$ . . . 293
H.26 The same as Figure H.19, using the SVMIN model with $B_\star = 2500$ . . . 293
H.27 The same as Figure H.19, using the UNEDF0 model with $B_\star = 2500$ . . . 294
H.28 Speed of sound as a function of (a) energy density and of (b) baryon number density, using the SEMF model with magnetic field strength $B_\star = 2500$ . . . 294
H.29 The same as Figure H.28, using the FRDM2012 model with $B_\star = 2500$ . . . 295
H.30 The same as Figure H.28, using the WS4RBF model with $B_\star = 2500$ . . . 295
H.31 The same as Figure H.28, using the BSKG3 model with $B_\star = 2500$ . . . 296
H.32 The same as Figure H.28, using the HFB31 model with $B_\star = 2500$ . . . 296

H.33 The same as Figure H.28, using the DDMED model with $B_\star = 2500$ . . . 297
H.34 The same as Figure H.28, using the DDPC1 model with $B_\star = 2500$ . . . 297
H.35 The same as Figure H.28, using the SVMIN model with $B_\star = 2500$ . . . 298
H.36 The same as Figure H.28, using the UNEDF0 model with $B_\star = 2500$ . . . 298
H.37 Compression modulus as a function of (a) energy density and of (b) baryon number density, using the SEMF model with magnetic field strength $B_\star = 2500$ . . . 299
H.38 The same as Figure H.37, using the FRDM2012 model with $B_\star = 2500$ . . . 299
H.39 The same as Figure H.37, using the WS4RBF model with $B_\star = 2500$ . . . 300
H.40 The same as Figure H.37, using the BSKG3 model with $B_\star = 2500$ . . . 300
H.41 The same as Figure H.37, using the HFB31 model with $B_\star = 2500$ . . . 301
H.42 The same as Figure H.37, using the DDMED model with $B_\star = 2500$ . . . 301
H.43 The same as Figure H.37, using the DDPC1 model with $B_\star = 2500$ . . . 302
H.44 The same as Figure H.37, using the SVMIN model with $B_\star = 2500$ . . . 302
H.45 The same as Figure H.37, using the UNEDF0 model with $B_\star = 2500$ . . . 303
H.46 Effective shear modulus as a function of (a) energy density and of (b) baryon number density, using the SEMF model with magnetic field strength $B_\star = 2500$ . . . 303
H.47 The same as Figure H.46, using the FRDM2012 model with $B_\star = 2500$ . . . 304
H.48 The same as Figure H.46, using the WS4RBF model with $B_\star = 2500$ . . . 304
H.49 The same as Figure H.46, using the BSKG3 model with $B_\star = 2500$ . . . 305
H.50 The same as Figure H.46, using the HFB31 model with $B_\star = 2500$ . . . 305
H.51 The same as Figure H.46, using the DDMED model with $B_\star = 2500$ . . . 306

H.52 The same as Figure H.46, using the DDPC1 model with $B_\star = 2500$ . . . 306
H.53 The same as Figure H.46, using the SVMIN model with $B_\star = 2500$ . . . 307
H.54 The same as Figure H.46, using the UNEDF0 model with $B_\star = 2500$ . . . 307
H.55 Effective shear modulus over compression modulus as a function of (a) energy density and of (b) baryon number density, using the SEMF model with magnetic field strength $B_\star = 2500$ 308
H.56 The same as Figure H.55, using the FRDM2012 model with $B_\star = 2500$ . . . 308
H.57 The same as Figure H.55, using the WS4RBF model with $B_\star = 2500$ . . . 309
H.58 The same as Figure H.55, using the BSKG3 model with $B_\star = 2500$ . . . 309
H.59 The same as Figure H.55, using the HFB31 model with $B_\star = 2500$ . . . 310
H.60 The same as Figure H.55, using the DDMED model with $B_\star = 2500$ . . . 310
H.61 The same as Figure H.55, using the DDPC1 model with $B_\star = 2500$ . . . 311
H.62 The same as Figure H.55, using the SVMIN model with $B_\star = 2500$ . . . 311
H.63 The same as Figure H.55, using the UNEDF0 model with $B_\star = 2500$ . . . 312
H.64 Atomic number, neutron number and proton fraction as a function of (a) energy density and of (b) baryon number density, using the SEMF model with magnetic field strength $B_\star = 2500$ . . . 313
H.65 The same as Figure H.64, using the FRDM2012 model with $B_\star = 2500$ . . . 314
H.66 The same as Figure H.64, using the WS4RBF model with $B_\star = 2500$ . . . 315
H.67 The same as Figure H.64, using the BSKG3 model with $B_\star = 2500$ . . . 316
H.68 The same as Figure H.64, using the HFB31 model with $B_\star = 2500$ . . . 317
H.69 The same as Figure H.64, using the DDMED model with $B_\star = 2500$ . . . 318
H.70 The same as Figure H.64, using the DDPC1 model with $B_\star = 2500$ . . . 319

H.71 The same as Figure H.64, using the SVMIN model with $B_\star = 2500$ . . . 320
H.72 The same as Figure H.64, using the UNEDF0 model with $B_\star = 2500$ . . . 321
H.73 Mass of outer crust for different masses and radii of NS, using the SEMF model with magnetic field strength $B_\star = 2500$ . . . 322
H.74 The same as Figure H.73, using the FRDM2012 model with $B_\star = 2500$ . . . 323
H.75 The same as Figure H.73, using the WS4RBF model with $B_\star = 2500$ . . . 323
H.76 The same as Figure H.73, using the BSKG3 model with $B_\star = 2500$ . . . 324
H.77 The same as Figure H.73, using the HFB31 model with $B_\star = 2500$ . . . 324
H.78 The same as Figure H.73, using the DDMED model with $B_\star = 2500$ . . . 325
H.79 The same as Figure H.73, using the DDPC1 model with $B_\star = 2500$ . . . 325
H.80 The same as Figure H.73, using the SVMIN model with $B_\star = 2500$ . . . 326
H.81 The same as Figure H.73, using the UNEDF0 model with $B_\star = 2500$ . . . 326
H.82 Proper depth of neutron-drip transition for different masses and radii of NS, using the SEMF model with magnetic field strength $B_\star = 2500$ . . . 327
H.83 The same as Figure H.82, using the FRDM2012 model with $B_\star = 2500$ . . . 328
H.84 The same as Figure H.82, using the WS4RBF model with $B_\star = 2500$ . . . 328
H.85 The same as Figure H.82, using the BSKG3 model with $B_\star = 2500$ . . . 329
H.86 The same as Figure H.82, using the HFB31 model with $B_\star = 2500$ . . . 329
H.87 The same as Figure H.82, using the DDMED model with $B_\star = 2500$ . . . 330
H.88 The same as Figure H.82, using the DDPC1 model with $B_\star = 2500$ . . . 330
H.89 The same as Figure H.82, using the SVMIN model with $B_\star = 2500$ . . . 331
H.90 The same as Figure H.82, using the UNEDF0 model with $B_\star = 2500$ . . . 331

I.1 The same as Figure 5.5, using the WS4RBF model with different magnetic field strengths $B_\star$ 332
I.2 The same as Figure 5.5, using the BSKG3 model with different magnetic field strengths $B_\star$ 333
I.3 The same as Figure 5.5, using the HFB31 model with different magnetic field strengths $B_\star$ 333
I.4 The same as Figure 5.5, using the DDMED model with different magnetic field strengths $B_\star$ 334
I.5 The same as Figure 5.5, using the DDPC1 model with different magnetic field strengths $B_\star$ 334
I.6 The same as Figure 5.5, using the SVMIN model with different magnetic field strengths $B_\star$ 335
I.7 The same as Figure 5.5, using the UNEDF0 model with different magnetic field strengths $B_\star$ 335
I.8 The same as Figure 5.24, using different models with magnetic field strength $B_\star = 2000$ 336
I.9 The same as Figure 5.24, using different models with magnetic field strength $B_\star = 2500$ 336
I.10 The same as Figure 5.7, using the WS4RBF model with different magnetic field strengths $B_\star$ 337
I.11 The same as Figure 5.7, using the BSKG3 model with different magnetic field strengths $B_\star$ 337
I.12 The same as Figure 5.7, using the HFB31 model with different magnetic field strengths $B_\star$ 338
I.13 The same as Figure 5.7, using the DDMED model with different magnetic field strengths $B_\star$ 338
I.14 The same as Figure 5.7, using the DDPC1 model with different magnetic field strengths $B_\star$ 339
I.15 The same as Figure 5.7, using the SVMIN model with different magnetic field strengths $B_\star$ 339
I.16 The same as Figure 5.7, using the UNEDF0 model with different magnetic field strengths $B_\star$ 340
I.17 The same as Figure 5.26, using different models with magnetic field strength $B_\star = 2000$ 340
I.18 The same as Figure 5.26, using different models with magnetic field strength $B_\star = 2500$ 341
I.19 The same as Figure 5.9, using the WS4RBF model with different magnetic field strengths $B_\star$ 341
I.20 The same as Figure 5.9, using the BSKG3 model with different magnetic field strengths $B_\star$ 342

I.21 The same as Figure 5.9, using the HFB31 model with different magnetic field strengths $B_\star$ . . . 342
I.22 The same as Figure 5.9, using the DDMED model with different magnetic field strengths $B_\star$ . . . 343
I.23 The same as Figure 5.9, using the DDPC1 model with different magnetic field strengths $B_\star$ . . . 343
I.24 The same as Figure 5.9, using the SVMIN model with different magnetic field strengths $B_\star$ . . . 344
I.25 The same as Figure 5.9, using the UNEDF0 model with different magnetic field strengths $B_\star$ . . . 344
I.26 The same as Figure 5.28, using different models with magnetic field strength $B_\star = 2000$ . . . 345
I.27 The same as Figure 5.28, using different models with magnetic field strength $B_\star = 2500$ . . . 345
I.28 The same as Figure 5.11, using the WS4RBF model with different magnetic field strengths $B_\star$ . . . 346
I.29 The same as Figure 5.11, using the BSKG3 model with different magnetic field strengths $B_\star$ . . . 346
I.30 The same as Figure 5.11, using the HFB31 model with different magnetic field strengths $B_\star$ . . . 347
I.31 The same as Figure 5.11, using the DDMED model with different magnetic field strengths $B_\star$ . . . 347
I.32 The same as Figure 5.11, using the DDPC1 model with different magnetic field strengths $B_\star$ . . . 348
I.33 The same as Figure 5.11, using the SVMIN model with different magnetic field strengths $B_\star$ . . . 348
I.34 The same as Figure 5.11, using the UNEDF0 model with different magnetic field strengths $B_\star$ . . . 349
I.35 The same as Figure 5.30, using different models with magnetic field strength $B_\star = 2000$ . . . 349
I.36 The same as Figure 5.30, using different models with magnetic field strength $B_\star = 2500$ . . . 350
I.37 The same as Figure 5.13, using the WS4RBF model with different magnetic field strengths $B_\star$ . . . 350
I.38 The same as Figure 5.13, using the BSKG3 model with different magnetic field strengths $B_\star$ . . . 351
I.39 The same as Figure 5.13, using the HFB31 model with different magnetic field strengths $B_\star$ . . . 351
I.40 The same as Figure 5.13, using the DDMED model with different magnetic field strengths $B_\star$ . . . 352

I.41 The same as Figure 5.13, using the DDPC1 model with different magnetic field strengths $B_\star$ 352
I.42 The same as Figure 5.13, using the SVMIN model with different magnetic field strengths $B_\star$ 353
I.43 The same as Figure 5.13, using the UNEDF0 model with different magnetic field strengths $B_\star$ 353
I.44 The same as Figure 5.32, using different models with magnetic field strength $B_\star = 2000$ 354
I.45 The same as Figure 5.32, using different models with magnetic field strength $B_\star = 2500$ 354
I.46 The same as Figure 5.15, using the WS4RBF model with different magnetic field strengths $B_\star$ 355
I.47 The same as Figure 5.15, using the BSKG3 model with different magnetic field strengths $B_\star$ 355
I.48 The same as Figure 5.15, using the HFB31 model with different magnetic field strengths $B_\star$ 356
I.49 The same as Figure 5.15, using the DDMED model with different magnetic field strengths $B_\star$ 356
I.50 The same as Figure 5.15, using the DDPC1 model with different magnetic field strengths $B_\star$ 357
I.51 The same as Figure 5.15, using the SVMIN model with different magnetic field strengths $B_\star$ 357
I.52 The same as Figure 5.15, using the UNEDF0 model with different magnetic field strengths $B_\star$ 358
I.53 The same as Figure 5.34, using different models with magnetic field strength $B_\star = 2000$ 358
I.54 The same as Figure 5.34, using different models with magnetic field strength $B_\star = 2500$ 359
I.55 The same as Figure 5.17, using the WS4RBF model with different magnetic field strengths $B_\star$ 360
I.56 The same as Figure 5.17, using the BSKG3 model with different magnetic field strengths $B_\star$ 361
I.57 The same as Figure 5.17, using the HFB31 model with different magnetic field strengths $B_\star$ 362
I.58 The same as Figure 5.17, using the DDMED model with different magnetic field strengths $B_\star$ 363
I.59 The same as Figure 5.17, using the DDPC1 model with different magnetic field strengths $B_\star$ 364
I.60 The same as Figure 5.17, using the SVMIN model with different magnetic field strengths $B_\star$ 365

I.61 The same as Figure 5.17, using the UNEDF0 model with different magnetic field strengths $B_\star$ 366
I.62 The same as Figure 5.36, using different models with magnetic field strength $B_\star = 2000$ 367
I.63 The same as Figure 5.36, using different models with magnetic field strength $B_\star = 2500$ 368
I.64 The same as Figure 5.19, using the WS4RBF model with different magnetic field strengths $B_\star$ 369
I.65 The same as Figure 5.19, using the BSKG3 model with different magnetic field strengths $B_\star$ 370
I.66 The same as Figure 5.19, using the HFB31 model with different magnetic field strengths $B_\star$ 370
I.67 The same as Figure 5.19, using the DDMED model with different magnetic field strengths $B_\star$ 371
I.68 The same as Figure 5.19, using the DDPC1 model with different magnetic field strengths $B_\star$ 371
I.69 The same as Figure 5.19, using the SVMIN model with different magnetic field strengths $B_\star$ 372
I.70 The same as Figure 5.19, using the UNEDF0 model with different magnetic field strengths $B_\star$ 372
I.71 The same as Figure 5.38, using different models with magnetic field strength $B_\star = 2000$ 373
I.72 The same as Figure 5.38, using different models with magnetic field strength $B_\star = 2500$ 373
I.73 The same as Figure 5.21, using the WS4RBF model with different magnetic field strengths $B_\star$ 374
I.74 The same as Figure 5.21, using the BSKG3 model with different magnetic field strengths $B_\star$ 375
I.75 The same as Figure 5.21, using the HFB31 model with different magnetic field strengths $B_\star$ 375
I.76 The same as Figure 5.21, using the DDMED model with different magnetic field strengths $B_\star$ 376
I.77 The same as Figure 5.21, using the DDPC1 model with different magnetic field strengths $B_\star$ 376
I.78 The same as Figure 5.21, using the SVMIN model with different magnetic field strengths $B_\star$ 377
I.79 The same as Figure 5.21, using the UNEDF0 model with different magnetic field strengths $B_\star$ 377
I.80 The same as Figure 5.40, using different models with magnetic field strength $B_\star = 2000$ 378

I.81 The same as Figure 5.40, using different models with magnetic field strength $B_\star = 2500$ 378

List of Abbreviations and Symbols

This list is not comprehensive, as several notations are omitted, for instance, some of the following symbols are accompanied by the tilde symbol, when they refer to the presence of a magnetic field (e.g., $\tilde{n}_e$, $\tilde{\epsilon}_e$, $\tilde{P}_e$).

A – mass number
A_{drip} – mass number at neutron-drip transition
α – fine-structure constant
B – magnetic field magnitude
bcc – body-centered cubic
BE_e – binding energy of electrons
BE_N – nuclear binding energy
$B_\star$ – magnetic field strength
c – speed of light in vacuum
C – compactness
C_M – Madelung constant
c_s – speed of sound
Δ_{grav} – relative fraction of mass due to gravitational binding energy
ΔM_{at} – atomic mass excess
ΔN – total number of baryons of outer crust
ΔN_l – number of baryons of a crustal layer
ΔR_{cr} – coordinate thickness of outer crust
ΔR_l – coordinate thickness of a crustal layer
e – elementary electric charge
EoS – Equation of State
ϵ – total energy density
ϵ_{drip} – total energy density at neutron-drip transition
ϵ_e – electron energy density
$E_{F,e}$ – electron Fermi energy
ϵ_L – lattice energy density

ϵ_{surf} – surface total energy density
G – gravitational constant or parameter in polytrope
g – Gibbs free energy per baryon
Γ – adiabatic index
γ_e – dimensionless electron chemical potential
g_s – surface gravity
$\hbar$ – reduced Planck constant
K – parameter in polytrope
k_B – Boltzmann constant
K_{mod} – compression modulus
$\lambda\!\!\!^{-}_e$ – reduced electron Compton wavelength
M – gravitational mass of neutron star
$M_\odot$ – solar mass
M_{at} – atomic mass
$M_{b_{cr}}$ – baryonic mass of outer crust
M_{b_l} – baryonic mass of a crustal layer
M_{cr} – gravitational mass of outer crust
m_e – electron mass
M_l – gravitational mass of a crustal layer
m_n – neutron mass
m_p – proton mass
m_u – atomic mass unit
μ_b – baryon chemical potential
$\mu_{b_{drip}}$ – baryon chemical potential at neutron-drip transition
μ_e – electron chemical potential
$\mu_{e_{drip}}$ – electron chemical potential at neutron-drip transition
n_b – baryon number density
$n_{b_{drip}}$ – baryon number density at neutron-drip transition
$n_{b_{surf}}$ – surface baryon number density
n_e – electron number density
n_N – number density of nuclei
NS – neutron star
P – total pressure
P_{drip} – total pressure at neutron-drip transition
P_e – electron pressure
$p_{F,e}$ – electron Fermi momentum
$\Phi(r)$ – metric function
P_L – lattice pressure
R – radius of neutron star
r – radial coordinate
r_{cell} – radius of the Wigner-Seitz cell

r_g – Schwarzschild radius
S_{mod} – effective shear modulus
T – temperature
TOV – Tolman-Oppenheimer-Volkoff
W_N – energy of the nucleus
x_e – dimensionless electron Fermi momentum
Z – atomic number
z_{drip} – proper thickness of outer crust
Z_{drip} – atomic number at neutron-drip transition
z_l – proper depth of a crustal layer

Chapter 1

Introduction

1.1 Structure of neutron stars

Neutrons stars belong to the category of compact stars, like white dwarfs and black holes. The compact stars have a huge range of densities, involving all four fundamental interactions under extreme conditions, and do not burn nuclear fuel, so they are not supported by thermal pressure against the gravity. The degeneracy pressure of electrons and the repulsive interactions between nucleons support the white dwarfs and neutron stars, respectively, while black holes are completely collapsed objects. Neutrons stars, white dwarfs and black holes are the endpoints of stellar evolution. What of the three types is formed, depends on the initial mass of the star when it reaches stable hydrogen burning (Zero Age Main Sequence - ZAMS) mass. For $M_{ZAMS} = 8 - 25M_{\odot}$, the endpoint is a neutron star [1].

A common perception of the structure of a neutron star is that consists of a uniform layer of neutrons. With densities which can exceed that of saturation nuclear energy density (normal nuclear density), $\epsilon_0 \simeq 150MeV/fm^3$, corresponding to a number density, $n_0 \simeq 0.16fm^{-3}$ [2], but the reality is far different, as shown in Fig. 1.1. A typical neutron star is made of: 1) the atmosphere, 2) the ocean, 3) the outer crust, 4) the inner crust, 5) the mantle, 6) the outer core, and 7) the inner core. With more details, moving into denser regions:

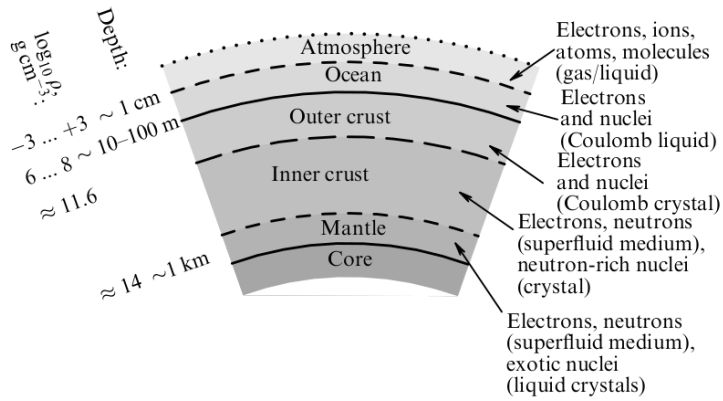

Figure 1.1: The structure of a neutron star. Taken from Ref. [2]

- **Atmosphere**

The atmosphere is the outermost layer of neutron star, consisting of plasma with the composition to depend on the production mechanism of neutron star and the surroundings of neutron star. In this region the thermal electromagnetic radiation spectrum is formed. So, it contains information about the effective surface temperature, the gravitational acceleration, the chemical composition, the magnetic field, the mass and the radius of the star. The thickness varies from a few millimeters to tens of centimeters [1, 2].

- **Ocean**

The ocean is the layer between the atmosphere and the outer crust, and consists of atomic nuclei surrounded by electrons. There is no a clear ocean-atmosphere interface, but the internal boundary coincides with the crystallization point of the Coulomb liquid, depending on temperature. So, the nuclei do not form crystal lattice, but roam freely in the electron gas [1, 2]. Nevertheless, a cold enough neutron star may lose both the atmosphere and the ocean in a superstrong magnetic field, thus the external boundary of the outer crust is the stellar surface [2].

- **Outer crust**

The outer crust, which is the region of interest for this thesis, has similarities to the core of white dwarfs. It is hundreds of meters thick and consists of nuclei (completely ionized atoms) and degenerate free electrons. The nuclei form a Coulomb crystal, with the main contribution to the total pressure to be the pressure of degenerate electrons and the crust is stratified into a succession of layers with different compositions. The Fermi energy of electrons in deeper layers increases, so the nuclei are enriched by neutrons through inverse β-decay (e^-- capture). Finally, one reaches the outer-inner

crust interface, where neutrons are no longer bound to nuclei [1, 2].

- **Inner crust**

The inner crust begins at neutron-drip density, where neutrons drip out of the nuclei, so it is composed of neutron-rich heavy nuclei embedded in a fluid of neutrons and electrons and the pressure is largely created by degenerate neutrons. Like in outer crust, the nuclei form a crystal lattice, while the neutron fluid may be superfluid, because degenerate fermions can form bound pairs (Cooper pairs) if there is an attractive potential between them (one attractive channel of neutron-neutron interaction). The superfluidity of neutrons has consequences for the transport properties of neutron star. The inner crust is $\sim 1-2km$ thick and stops at density $\sim 0.5\epsilon_0$, where the lattice structure disappears, the nuclei are dissolved and form a homogeneous mass, reaching the liquid outer core [1, 2].

- **Mantle (nuclear pasta)**

At the high-density internal boundary of the inner crust is located the mantle, which separates the inner crust from outer core. This layer contains exotic nuclei (nuclear pasta), because at such high densities the spherical shape of the atomic nucleus may no longer be energetically preferable. Therefore, the mantle consists of a few layers containing phases of matter in which nuclei are shaped like: a) cylinder (spaghetti phase), b) plane-parallel plates (lasagna phase), c) inverse phases composed of nuclear phases with entrapped neutron cylinders and bubbles. The Coulomb lattice still exists in all phases and the electrons are uniform in background [1, 2].

- **Outer core**

In outer core the density is so high that localized structures of neutrons and protons are absent. The matter mainly consists of neutrons with a small admixture of protons, electrons and muons ($npe\mu$ matter). The nucleons form a strongly interacting Fermi liquid, whereas leptons form an almost ideal Fermi gas [1, 2].

- **Inner core**

As density increases above the normal nuclear density, the nucleons may be converted into hyperons (i.e., baryons containing one or more strange quarks), leading to hyperonization of matter. In addition, exotic phases of dense matter may be formed: a) condensation of pions (i.e., the lightest mesons), b) condensation of kaons (i.e., the lightest strange mesons), and c) quark matter (i.e., deconfinement of quarks) [2, 3].

1.2 Units and useful constants

In this Section, some useful, for the following Chapters, relationships between the different unit systems, and constants are presented (see, Ref. [4]).

Using the *geometrized (gravitational) units*, the speed of light in vacuum, c, and the gravitational constant, G, are set equal to unity: $c = G = 1$. So[1],

$$\begin{cases} 1 = c = 2.9979 \cdot 10^{10} cmsec^{-1} \\ 1 = G = 6.6720 \cdot 10^{-8} dyncm^2 gr^{-2} \\ 1sec = 2.9979 \cdot 10^{10} cm \\ 1gr = 7.4237 \cdot 10^{-29} cm \\ 1erg = 8.2601 \cdot 10^{-50} cm \\ 1dyn/cm^2 = 8.2601 \cdot 10^{-40} km^{-2} \\ 1gr/cm^3 = 7.4237 \cdot 10^{-19} km^{-2} \end{cases} \tag{1.2.1}$$

and there are no powers of c and G and the expressions are simplified. The last two units of Eq. 1.2.1 are used in astrophysics, the dyn/cm^2 as unit of the pressure and the gr/cm^3 as unit of density.
The solar mass is:

$$M_\odot = 1.989 \cdot 10^{33} gr = 1.4766 km \tag{1.2.2}$$

Hence, solving the TOV equations (see, Section 2.1), is useful to have the quantities pressure and energy density in km^{-2}, because the mass of a typical neutron star is of the order of unity.

In nuclear physics, the energy (or mass, mc^2) is expressed in MeV, having:

$$\begin{aligned} 1MeV &= 1.6022 \cdot 10^{-6} erg \\ &= 1.3234 \cdot 10^{-55} cm \\ &= 1.7827 \cdot 10^{-27} gr \end{aligned} \tag{1.2.3}$$

Also, the length is better to be expressed in fm: $1fm = 10^{-13} cm$ and the reduced Compton wavelength of a particle, $\lambda\!\!\!^{-}$, is defined as:

$$\lambda\!\!\!^{-} = \frac{\hbar}{mc} \tag{1.2.4}$$

[1] $1dyn = 1grcmsec^{-2} (= 10^{-5} N \ in \ SI \ units)$ and $1erg = 1dyncm = 1grcm^2 sec^{-2} (= 10^{-7} J \ in \ SI \ units)$

where $\hbar$ is the reduced Planck constant ($\hbar = \frac{h}{2\pi}$) and m the particle's mass. The elementary electric charge, e, can be expressed as:

$$e = \sqrt{\alpha\hbar c} = \sqrt{\alpha \lambda\!\!\!^{-}_e m_e c^2} \tag{1.2.5}$$

where $\alpha \approx 1/137$ is the fine-structure constant, $\lambda\!\!\!^{-}_e$ the reduced electron Compton wavelength and m_e the electron mass. In Table 1.1 are listed some constants with their values used in this work.

Table 1.1: Useful constants[2]

constant	symbol	value
neutron mass	m_n	939.565421 MeV/c^2
proton mass	m_p	938.272088 MeV/c^2
electron mass	m_e	0.510999 MeV/c^2
atomic mass unit	m_u	931.494102 MeV/c^2
reduced Planck constant times c	$\hbar c$	197.326980 $MeV fm$
fine-structure constant	α	$7.297353 \cdot 10^{-3}$
reduced electron Compton wavelength	$\lambda\!\!\!^{-}_e$	386.159268 fm
Boltzmann constant	k_B	$8.617333 \cdot 10^{-11}$ MeV/K

From Eqs. 1.2.1 and 1.2.3:

$$\begin{aligned} 1MeV/fm^3 &= 1.7827 \cdot 10^{12} gr/cm^3 \\ &= 1.6022 \cdot 10^{33} dyn/cm^2 \end{aligned} \tag{1.2.6}$$

where the unit MeV/fm^3 is used in the present thesis to express the pressure and the energy density, exclusively.

Lastly, in nuclear physics, more frequently, the *natural units* are used, setting: $\hbar = c = 1$. So, some really useful factors for *mixed units* (in stellar calculations) are:

$$\begin{cases} 1MeV/fm^3 = 1.3234 \cdot 10^{-6} km^{-2} \\ 1MeV/c^2 = 8.964992783 \cdot 10^{-61} M_\odot \end{cases} \tag{1.2.7}$$

where km^{-2} is the unit to express the pressure and the energy density, solving the TOV equations. In all the following, the constants $(c, \hbar, G, k_B)$ will be appeared, explicitly.

[2]source: https://physics.nist.gov/cuu/Constants/

Chapter 2

Preliminaries

2.1 General relativity - TOV equations

A typical neutron star has mass, $M = 1 - 2M_{\odot}$, radius, $R = 10 - 15km$, and compactness, $C = 0.1 - 0.3$ [1]. The compactness is defined as the ratio of the gravitational mass to the radius, namely:

$$C = \frac{GM}{Rc^2} \tag{2.1.1}$$

and it is a measure of how close the radius of the star is to the size of a black hole of the same mass. For non-rotating black holes: $C = 0.5$, because $R = r_g$, where:

$$r_g = 2GM/c^2 \tag{2.1.2}$$

is the Schwarzschild radius. So, a neutron star having $C \sim 0.5$ means that it is essential to describe it within general relativity.

The star as a system with many particles can be described as a fluid with macroscopic quantities[1]: the total mass-energy density, ϵ, of the matter, which does not contain any gravitational component, the pressure, P, and the 4-velocity, u^{μ}, of the matter. Also, the fluid is considered a perfect fluid, where there are no effects from dissipation, heat transport, shear or bulk viscosity [1]. For this purpose, a useful quantity in curved spacetime, having a metric tensor $g_{\mu\nu}$, is the energy-momentum tensor, $T^{\mu\nu}$, and can be expressed in a covariant form as:

$$T^{\mu\nu} = (\frac{\epsilon}{c^2} + \frac{P}{c^2})u^{\mu}u^{\nu} + Pg^{\mu\nu} \tag{2.1.3}$$

[1] the thermodynamic quantities (e.g. ϵ, P) are well defined in the rest frame of the matter

Therefore, the Einstein equation:

$$G^{\mu\nu} = \frac{8\pi G}{c^4} T^{\mu\nu} \tag{2.1.4}$$

needs to be solved, where $G^{\mu\nu}$ is the Einstein tensor, which describes the curvature of spacetime. Assuming, a *static spherically symmetric* star with radius $R > r_g$ and the matter as a *perfect fluid*, the solution of Einstein equation is the *Tolman-Oppenheimer-Volkoff (TOV) equations* [5, 6]:

$$\begin{cases} \frac{dm(r)}{dr} = 4\pi r^2 \epsilon(r)/c^2 \\ \frac{dP(r)}{dr} = -\dfrac{G\epsilon(r)m(r)}{c^2 r^2}(1 + \frac{P(r)}{\epsilon(r)})(1 + \frac{4\pi r^3 P(r)}{m(r)c^2})(1 - \frac{2Gm(r)}{c^2 r})^{-1} \end{cases} \tag{2.1.5}$$

where r is the radial coordinate (circumferential radius), i.e., the proper length of the equator of star ($2\pi r$) as measured by a local observer [3]. In the 2nd equation of Eq. 2.1.5, the 1st term on the right-hand side is the Newtonian term of hydrostatic equilibrium and the other three terms come from the general relativity.

To close the system of Eq. 2.1.5, an additional equation is needed, which is the one-parameter relationship between the pressure and the total mass-energy density, the *Equation of State (EoS)*:

$$P = P(\epsilon) \tag{2.1.6}$$

and describes the physics beyond gravitational interaction [1].

• The *gravitational mass*[2] in a shell of inner and outer radii r_1 and r_2, respectively, is:

$$\Delta M = 4\pi \int_{r_1}^{r_2} r^2 \epsilon(r)/c^2 dr \tag{2.1.7}$$

and so the total gravitational mass (i.e., measured by an exterior observer at an asymptotically flat spacetime distance [1]) of the star is given by:

$$M = 4\pi \int_0^R r^2 \epsilon(r)/c^2 dr \tag{2.1.8}$$

• The *baryonic mass*, which involves the proper volume element $dV = 4\pi r^2 \Phi(r) dr$ [3], in this shell is:

$$\Delta M_b = 4\pi \int_{r_1}^{r_2} r^2 \Phi(r) \epsilon(r)/c^2 dr \tag{2.1.9}$$

[2] when only the word mass is used, the gravitational mass is meant

where the metric function $\Phi(r)$ is defined as:

$$\Phi(r) = (1 - \frac{2Gm(r)}{c^2 r})^{-1/2} \tag{2.1.10}$$

Consequently, the total baryonic mass of the star is given by:

$$M_b = 4\pi \int_0^R r^2 \Phi(r) \epsilon(r)/c^2 dr \tag{2.1.11}$$

and as $r > 2Gm(r)/c^2$, always the baryonic mass is greater than the gravitational mass, because of the gravitational binding energy.

• The *relative fraction of mass due to the gravitational binding energy*, in this shell, Δ_{grav}, is calculated by:

$$\Delta_{grav} = \frac{\Delta M_b - \Delta M}{\Delta M} \tag{2.1.12}$$

• Knowing the number density of baryons, $n_b(r)$, the *number of baryons* in this shell is given by:

$$\Delta N = 4\pi \int_{r_1}^{r_2} r^2 \Phi(r) n_b(r) dr \tag{2.1.13}$$

and the total number of baryons in the star is:

$$N_{tot} = 4\pi \int_0^R r^2 \Phi(r) n_b(r) dr \tag{2.1.14}$$

• The proper length element (i.e., the radial distance as measured by a local observer) is $dl = \Phi(r)dr$ [3], so provided that $r > 2Gm(r)/c^2$, always $dl > dr$. And the *depth (proper thickness)*, below the stellar surface is:

$$z(r) = \int_r^R \Phi(r) dr \tag{2.1.15}$$

with the proper thickness, $z(r)$, to be greater than the coordinate thickness, $R - r$.

2.2 Thermodynamics

For a system containing different species of particles (i.e., reactions may occur), from the 1st law of thermodynamics:

$$dE = TdS - PdV + \sum_i \mu_i dN_i \tag{2.2.1}$$

where E is the total energy (including rest-mass energy), T the temperature, S the entropy, P the pressure, V the volume of the system, μ_i the chemical potential (including the rest-mass energy) of i-th species. The total number of particles, $N = \sum_i N_i$, is usually a conserved quantity (e.g., the number of baryons), so it is better to define the quantities on a per baryon basis [7]. So,

$$d(\epsilon/n_b) = Tds - Pd(1/n_b) + \sum_i \mu_i dY_i \tag{2.2.2}$$

where $n_b = N/V$ is the number density of baryons, $\epsilon = E/V$ the total energy density (including rest-mass energy), $\epsilon/n_b = E/N$ the energy per baryon, $s = S/N$ the entropy per baryon, $1/n_b$ the volume per baryon and $Y_i = n_i/n_b$ the concentration of i-th species, with $n_i = N_i/V$ the number density of i-species. So,

$$\begin{cases} P = n_b^2 \frac{\partial(\epsilon/n_b)}{\partial n_b} \\ T = \frac{\partial(\epsilon/n_b)}{\partial s} \\ \mu_i = \frac{\partial \epsilon}{\partial n_i} \end{cases} \tag{2.2.3}$$

In equilibrium, having the system thermally isolated and no work is done, the following relation holds [7]:

$$\sum_i \mu_i dY_i = 0 \tag{2.2.4}$$

In the more general case, where the system is not thermally isolated and work may be done, from 2nd law of thermodynamics:

$$d(\epsilon/n_b) + Pd(1/n_b) \leq Tds \tag{2.2.5}$$

so, if equilibrium is achieved at constant n_b and s:

$$d\epsilon \leq 0 \tag{2.2.6}$$

Thus, the equilibrium corresponds to $d\epsilon = 0$ and is a minimum of ϵ at fixed n_b and s, and again the Eq. 2.2.4 holds.

An other more useful, in our case,[3] thermodynamic potential is the Gibbs free energy, $\mathcal{G}$, given by:

$$\mathcal{G} = E + PV - TS \Rightarrow d\mathcal{G} = VdP - SdT + \sum_i \mu_i dN_i \tag{2.2.7}$$

[3]because as we will see there are phase transitions with discontinuities in n_b, while T and P are continuous variables [7]

Thus, the *Gibbs free energy per baryon*, g, is [7]:

$$g = \mathcal{G}/N = \frac{\epsilon + P}{n_b} - Ts \tag{2.2.8}$$

with

$$dg = \frac{1}{n_b} dP - sdT + \sum_i \mu_i dY_i \tag{2.2.9}$$

If equilibrium achieved at constant T and P:

$$dg \leq 0 \tag{2.2.10}$$

and the equilibrium corresponds to a minimum in g (i.e., $dg = 0$) at fixed T and P, and again the Eq. 2.2.4 holds. Also, an alternative expression for the Gibbs free energy per baryon, requiring all the extensive quantities to scale with volume in the same way, is the following:

$$g = \sum_i \mu_i Y_i \tag{2.2.11}$$

The reactions, in an interacting mixture of baryons and leptons, conserve the total baryon number, N_b, the total lepton number, N_L, and the total electric charge, N_Q. And the corresponding chemical potentials to those conserved quantities are μ_b, μ_L and μ_Q, respectively. So, the chemical potential of i-th species is decomposed, as: $\mu_i = B_i\mu_b + L_i\mu_L + Q_i\mu_Q$, where B_i is the baryon number, L_i the lepton number and Q_i the electric charge of i-th species. Making the assumption of electric charge neutrality (e.g., $N_Q = 0$), which fixes μ_Q, and of cold matter (T=0K), where neutrinos are allowed to escape, means that the whole system is simply described by the baryon chemical potential, μ_b, or, equivalently, the baryon number density, n_b [1, 7].

2.3 Statistical mechanics

The density of states in phase space, for each type of particle, is [7]:

$$\frac{d\mathcal{N}}{d^3x d^3p} = \frac{g_d}{h^3}\psi \tag{2.3.1}$$

where $\psi = \psi(\vec{x}, \vec{p}, t)$ is a dimensionless distribution function and g_d the degeneracy factor ($g_d = 2s + 1$) for spin, e.g., for electrons, which are $s - 1/2$ particles, $g_d = 2$.

The number density, of each particle species, is given by:

$$n = \frac{g_d}{h^3} \int \psi d^3p \tag{2.3.2}$$

with integration over all momenta and if the integrand depends only on the magnitude of the momentum: $\int d^3p = 4\pi \int p^2 dp$.

The energy density (including the rest-mass energy) is:

$$\epsilon = \frac{g_d}{h^3} \int E\psi d^3p \tag{2.3.3}$$

where $E = (p^2c^2 + m^2c^4)^{1/2}$ and m is the rest mass of the particle.

And the pressure, for an isotropic distribution of momenta, is:

$$P = \frac{g_d}{3h^3} \int p\upsilon\psi d^3p = \frac{g_d c^2}{3h^3} \int \frac{p^2}{E}\psi d^3p \tag{2.3.4}$$

where $\upsilon = pc^2/E$ is the velocity.

For an ideal gas:

$$\psi = \psi(E) = [e^{\frac{E-\mu}{k_B T}} \pm 1]^{-1} \tag{2.3.5}$$

where the plus sign is for fermions (Fermi-Dirac statistics) and the minus sign for bosons (Bose-Einstein statistics).

In the limiting case of the *completely degenerate fermions* ($T = 0K$):

$$\psi(E) = \begin{cases} 1, & E \leq E_F \\ 0, & E > E_F \end{cases} \tag{2.3.6}$$

where the chemical potential μ is the Fermi energy E_F, i.e.,

$$\mu = E_F = (p_F^2c^2 + m^2c^4)^{1/2} \tag{2.3.7}$$

with p_F to be the Fermi momentum.
So, for a *degenerate Fermi gas*, the number density is:

$$n = \frac{g_d}{h^3} \int_0^{p_F} 4\pi p^2 dp = \frac{g_d}{6\pi^2 \lambda\!\!\!^{-3}} x^3 \tag{2.3.8}$$

where we define the dimensionless Fermi momentum or relativity parameter, x, as:

$$x = \frac{p_F}{mc} \tag{2.3.9}$$

and the dimensionless Fermi energy or dimensionless chemical potential, γ, as:

$$\gamma = \frac{\mu}{mc^2} = (x^2+1)^{1/2} \tag{2.3.10}$$

In addition, the energy density and the pressure are, respectively:

$$\epsilon = \frac{g_d}{h^3}\int_0^{p_F}(p^2c^2+m^2c^4)^{1/2}4\pi p^2 dp = \frac{mc^2}{\lambda\!\!\!^{-3}}f(x) \tag{2.3.11}$$

and[4]

$$P = \frac{g_d}{3h^3}\int_0^{p_F}\frac{p^2c^2}{(p^2c^2+m^2c^4)^{1/2}}4\pi p^2 dp = \frac{mc^2}{\lambda\!\!\!^{-3}}g(x) \tag{2.3.12}$$

where the functions $f(x)$ and $g(x)$ are:

$$\begin{cases} f(x) = \frac{g_d}{16\pi^2}\{x(1+x^2)^{1/2}(1+2x^2) - ln[x+(x^2+1)^{1/2}]\} \\ \\ g(x) = \frac{g_d}{16\pi^2}\{x(1+x^2)^{1/2}(\frac{2}{3}x^2-1) + ln[x+(x^2+1)^{1/2}]\} \end{cases} \tag{2.3.13}$$

It is mentioned that when the above quantities of this Section refer to electrons, the subscript "e" is used and $g_d = 2$.

2.4 Critical values for outer crust

In this Section, some critical values for the density and the temperature of the matter, which determine the behavior of the electrons and the atomic nuclei, are presented.

Before this, it is stressed that, in outer crust (i.e., subnuclear densities), the total mass-energy density, ϵ, is dominated by the rest-mass energy of nuclei and is related to the baryon number density, n_b, as:

$$\epsilon \approx m_n c^2 n_b \tag{2.4.1}$$

where the average mass per nucleon is approximated here by the neutron mass, m_n. Also, if n_e is the electron number density and n_N the number density of nuclei and assuming electric charge neutrality, the relations that connect the number densities n_b, n_e and n_N, are:

$$\begin{cases} n_e = Zn_N \\ n_b = An_N = \frac{A}{Z}n_e \end{cases} \tag{2.4.2}$$

[4]it is noted that the pressure can also be calculated from (see, Eq. 2.2.3), $P = n^2\frac{\partial(\epsilon/n)}{\partial n} = -\epsilon + n\frac{\partial\epsilon}{\partial n} = -\epsilon + n\mu$

where Z is the atomic number and A the mass number.

- **Completely ionized atoms**

When the electron kinetic energy ($KE_e = E_{F,e} - m_e c^2 \approx \frac{p_{F,e}^2}{2m_e}$, in non-relativistic limit, $x_e = \frac{p_{F,e}}{m_e c} << 1$) equals the binding energy of the last bound electron ($BE_{e,last}(Z) \approx 13.6 \cdot 10^{-6} Z^2 MeV$), all electrons can be stripped from the nucleus and form a Fermi gas [1]. This condition is written as:

$$\frac{p_{F,e}^2}{2m_e} = 13.6 \cdot 10^{-6} Z^2 MeV \tag{2.4.3}$$

and corresponds to a critical energy density, $\epsilon_{c,ion}$, using Eqs. 2.3.8, 2.3.9 and 2.4.1 - 2.4.3:

$$\begin{aligned} \epsilon_{c,ion} &= \frac{4.79107 \cdot 10^{-9} m_n c^2}{\lambda\!\!\!^{-3}_e (m_e c^2)^{3/2}} MeV^{3/2} A Z^2 \\ &\simeq 2.14008 \cdot 10^{-13} A Z^2 MeV/fm^3 \end{aligned} \tag{2.4.4}$$

equivalently, in baryon number density:

$$\begin{aligned} n_{b_{c,ion}} &= \frac{4.79107 \cdot 10^{-9}}{\lambda\!\!\!^{-3}_e (m_e c^2)^{3/2}} MeV^{3/2} A Z^2 \\ &\simeq 2.27773 \cdot 10^{-16} A Z^2 fm^{-3} \end{aligned} \tag{2.4.5}$$

For the nuclide[5] ^{56}Fe (i.e., $Z = 26$, $N = 30$):

$$\begin{cases} \epsilon_{c,ion} \simeq 8.101 \cdot 10^{-9} MeV/fm^3 \\ n_{b_{c,ion}} \simeq 8.623 \cdot 10^{-12} fm^{-3} \end{cases} \tag{2.4.6}$$

So, for $\epsilon > \epsilon_{c,ion}$, the atoms are completely ionized.

- **Relativistic electrons**

For higher densities, the electrons eventually become relativistic, when their Fermi momentum is [1]:

$$p_{F,e} \approx m_e c \tag{2.4.7}$$

corresponding to a critical energy density, $\epsilon_{c,rel}$, using Eqs. 2.3.8, 2.3.9, 2.4.1, 2.4.2 and 2.4.7:

$$\begin{aligned} \epsilon_{c,rel} &= \frac{m_n c^2 A}{3\pi^2 \lambda\!\!\!^{-3}_e Z} \\ &\simeq 5.5107 \cdot 10^{-7} \frac{A}{Z} MeV/fm^3 \end{aligned} \tag{2.4.8}$$

[5] of all nuclides, ^{56}Fe has the lowest total energy per nucleon and is present in the surface layer of outer crust (see, Chapter 5)

equivalently, in baryon number density:

$$\begin{aligned} n_{b_{c,rel}} &= \frac{A}{3\pi^2 \lambda\!\!\!^{-3}_e Z} \\ &\simeq 5.86516 \cdot 10^{-10} \frac{A}{Z} fm^{-3} \end{aligned} \tag{2.4.9}$$

For the nuclide ^{56}Fe:

$$\begin{cases} \epsilon_{c,rel} \simeq 1.187 \cdot 10^{-6} MeV/fm^3 \\ n_{b_{c,rel}} \simeq 1.263 \cdot 10^{-9} fm^{-3} \end{cases} \tag{2.4.10}$$

So, for $\epsilon > \epsilon_{c,rel}$, the electrons are relativistic.

- **Change in composition**

For even higher densities, the neutronization of matter is favored, through $inverse\ \beta-decay$ ($e^- + p^+ \rightarrow n + \nu_e$), while the reaction ($n \rightarrow e^- + p^+ + \bar{\nu}_e$) is blocked if the density of electrons is high enough, so all the available energy levels are occupied [1]. Thus, the nuclei begin to become neutron-rich, if:

$$p_{F,e} \approx (m_n - m_p)c \simeq 1.29 MeV/c \tag{2.4.11}$$

because $E_{F,e} \approx m_e c^2 x_e$, for $x_e >> 1$ (ultra-relativistic limit), with the critical neutronization energy density, $\epsilon_{c,neutr}$, using Eqs. 2.3.8, 2.3.9, 2.4.1, 2.4.2 and 2.4.11, to be:

$$\begin{aligned} \epsilon_{c,neutr} &= \frac{m_n c^2 (m_n - m_p)^3 A}{3\pi^2 \lambda\!\!\!^{-3}_e m_e^3 Z} \\ &\simeq 8.93465 \cdot 10^{-6} \frac{A}{Z} MeV/fm^3 \end{aligned} \tag{2.4.12}$$

equivalently, in baryon number density:

$$\begin{aligned} n_{b_{c,neutr}} &= \frac{(m_n - m_p)^3 A}{3\pi^2 \lambda\!\!\!^{-3}_e m_e^3 Z} \\ &\simeq 9.50934 \cdot 10^{-9} \frac{A}{Z} fm^{-3} \end{aligned} \tag{2.4.13}$$

For the nuclide ^{56}Fe:

$$\begin{cases} \epsilon_{c,neutr} \simeq 1.924 \cdot 10^{-5} MeV/fm^3 \\ n_{b_{c,neutr}} \simeq 2.048 \cdot 10^{-8} fm^{-3} \end{cases} \tag{2.4.14}$$

So, for $\epsilon > \epsilon_{c,neutr}$, the composition begins to change.

• **Nonvanishing temperature - Degeneracy**

For $T > 0K$, the effects for non-zero temperature can be ignored in first approximation. The critical condition for degeneracy is [1]:

$$\frac{p_{F,e}^2}{2m_e} = k_B T \tag{2.4.15}$$

where the term $k_B T$ expresses the thermal energy and $\frac{p_{F,e}^2}{2m_e}$ is the electron kinetic energy in non-relativistic limit. Thus, this condition corresponds to a critical energy density, $\epsilon_{c,deg}^{non-rel}$, using Eqs. 2.3.8, 2.3.9, 2.4.1, 2.4.2 and 2.4.15, is given by:

$$\begin{aligned}\epsilon_{c,deg}^{non-rel} &= \frac{2^{3/2} m_n c^2 (k_B T)^{3/2} A}{3\pi^2 \lambda\!\!\!^{-}_e{}^3 (m_e c^2)^{3/2} Z} \\ &\simeq 3.41335 \cdot 10^{-21} \frac{AT[K]^{3/2}}{Z} MeV/fm^3\end{aligned} \tag{2.4.16}$$

equivalently, in baryon number density:

$$\begin{aligned}n_{b_{c,deg}}^{non-rel} &= \frac{2^{3/2} (k_B T)^{3/2} A}{3\pi^2 \lambda\!\!\!^{-}_e{}^3 (m_e c^2)^{3/2} Z} \\ &\simeq 3.6329 \cdot 10^{-24} \frac{AT[K]^{3/2}}{Z} fm^{-3}\end{aligned} \tag{2.4.17}$$

On the contrary, for ultra-relativistic electrons (i.e., $x_e >> 1 \Rightarrow E_{F,e} \approx p_{F,e} c$), the critical condition is:

$$p_{F,e} c = k_B T \tag{2.4.18}$$

And following similar steps, the critical energy density, $\epsilon_{c,deg}^{ultra-rel}$, is:

$$\begin{aligned}\epsilon_{c,deg}^{ultra-rel} &= \frac{m_n c^2 (k_B T)^3 A}{3\pi^2 \lambda\!\!\!^{-}_e{}^3 (m_e c^2)^3 Z} \\ &\simeq 2.6428 \cdot 10^{-36} \frac{AT[K]^3}{Z} MeV/fm^3\end{aligned} \tag{2.4.19}$$

and the corresponding baryon number density:

$$\begin{aligned}n_{b_{c,deg}}^{ultra-rel} &= \frac{(k_B T)^3 A}{3\pi^2 \lambda\!\!\!^{-}_e{}^3 (m_e c^2)^3 Z} \\ &\simeq 2.8128 \cdot 10^{-39} \frac{AT[K]^3}{Z} fm^{-3}\end{aligned} \tag{2.4.20}$$

Alternatively, the electron Fermi temperature, $T_{F,e}$, is defined as [8]:

$$\begin{aligned} T_{F,e} &= \frac{E_{F,e} - m_e c^2}{k_B} \\ &= \frac{m_e c^2}{k_B}(\gamma_e - 1) \\ &\simeq 5.93 \cdot 10^9 (\gamma_e - 1) K \end{aligned} \tag{2.4.21}$$

So, the electrons are strongly degenerate for: $T << T_{F,e}$. And solving the Eqs. 2.4.16 and 2.4.17 for the temperature, the electron Fermi temperature, $T_{F,e}^{non-rel}$, in the non-relativistic limit, is:

$$\begin{cases} T_{F,e}^{non-rel} = \dfrac{(3\pi^2)^{2/3} \lambda\!\!\!^{-}_e{}^2 m_e c^2 Z^{2/3} \epsilon^{2/3}}{2k_B (m_n c^2)^{2/3} A^{2/3}} \\ \qquad\qquad \simeq 4.41109 \cdot 10^{13} \dfrac{Z^{2/3} \epsilon [MeV fm^{-3}]^{2/3}}{A^{2/3}} K \\ or \\ T_{F,e}^{non-rel} = \dfrac{(3\pi^2)^{2/3} \lambda\!\!\!^{-}_e{}^2 m_e c^2 Z^{2/3} n_b^{2/3}}{2k_B A^{2/3}} \\ \qquad\qquad \simeq 4.23153 \cdot 10^{15} \dfrac{Z^{2/3} n_b [fm^{-3}]^{2/3}}{A^{2/3}} K \end{cases} \tag{2.4.22}$$

and in the ultra-relativistic limit, the electron Fermi temperature, $T_{F,e}^{ultra-rel}$, using Eqs. 2.4.19 and 2.4.20, is given by:

$$\begin{cases} T_{F,e}^{ultra-rel} = \dfrac{(3\pi^2)^{1/3} \lambda\!\!\!^{-}_e m_e c^2 Z^{1/3} \epsilon^{1/3}}{k_B (m_n c^2)^{1/3} A^{1/3}} \\ \qquad\qquad \simeq 7.23289 \cdot 10^{11} \dfrac{Z^{1/3} \epsilon [MeV fm^{-3}]^{1/3}}{A^{1/3}} K \\ or \\ T_{F,e}^{ultra-rel} = \dfrac{(3\pi^2)^{1/3} \lambda\!\!\!^{-}_e m_e c^2 Z^{1/3} n_b^{1/3}}{k_B A^{1/3}} \\ \qquad\qquad \simeq 7.08414 \cdot 10^{12} \dfrac{Z^{1/3} n_b [fm^{-3}]^{1/3}}{A^{1/3}} K \end{cases} \tag{2.4.23}$$

- **Nonvanishing temperature - Coulomb lattice**

The nuclei in outer crust form a Coulomb crystal lattice, but if the thermal energy ($k_B T$) is greater than the binding energy of Coulomb lattice, it will melt (see, *ocean* in Section 1.1). For this reason, the Coulomb interaction parameter is defined as [1]:

$$\Gamma_C = \frac{Coulomb\ energy}{thermal\ energy} = \frac{Z^2 e^2}{r_{cell} k_B T} \tag{2.4.24}$$

where, $r_{cell} = (\frac{4\pi n_N}{3})^{-1/3}$, is the radius of the Wigner-Seitz cell (see, Section 3.1). From simulations at melting, $\Gamma_{C,m} \approx 175$ [3], so the melting temperature, T_m, using the Eqs. 1.2.5, 2.4.1, 2.4.2 and 2.4.24, is given by:

$$\begin{aligned} T_m &= \frac{(4\pi)^{1/3}\alpha \lambda\!\!\!^{-}_e m_e c^2 Z^2 \epsilon^{1/3}}{3^{1/3}\Gamma_{C,m} k_B (m_n c^2)^{1/3} A^{1/3}} \\ &\simeq 1.57155 \cdot 10^7 \frac{Z^2 \epsilon [MeV fm^{-3}]^{1/3}}{A^{1/3}} K \end{aligned} \tag{2.4.25}$$

or in terms of baryon number density:

$$\begin{aligned} T_m &= \frac{(4\pi)^{1/3}\alpha \lambda\!\!\!^{-}_e m_e c^2 Z^2 n_b^{1/3}}{3^{1/3}\Gamma_{C,m} k_B A^{1/3}} \\ &\simeq 1.53923 \cdot 10^8 \frac{Z^2 n_b [fm^{-3}]^{1/3}}{A^{1/3}} K \end{aligned} \tag{2.4.26}$$

So, when $T < T_m$, the nuclei are arranged in a crystal lattice. Also, comparing the Eqs. 2.4.22, 2.4.23, 2.4.25 and 2.4.26, the melting temperature, T_m, is generally much lower than the electron Fermi temperature, $T_{F,e}$, consequently the electrons are highly degenerate.

In any case, the thermal effects can be ignored, because the neutron star is considered cold ($T \to 0K$), in the present work.

Chapter 3

BPS model

In a cold non-accreting neutron star, the *cold catalyzed matter* hypothesis may be applied, which means complete thermodynamic equilibrium with respect to all interactions at T=0K, so the matter is in its ground state with the lowest possible energy [8].

In general lines, in the range of densities of outer crust, the most energetically favorable state for nucleons (i.e., protons and neutrons) is to build individual nuclei and these nuclei form a solid crystal lattice, and the electrons are not bound to nuclei, but form a degenerate Fermi gas, maintaining the electric charge neutrality. In denser regions, the nuclei become more neutron-rich (inverse β-decay), until the neutron-drip energy density, ϵ_{drip} (corresponding to the neutron-drip pressure, P_{drip}), where the ratio Z/A reaches a critical point and neutrons drip for greater densities.

The methodology followed is based on the seminal work by Baym, Pethick and Sutherland [9] (BPS model), as well as more recent Refs. [10, 11], for the case of the absence of magnetic field, and Refs. [12, 13, 14], taking into account the presence of magnetic field.

3.1 Absence of magnetic field

The total energy density, ϵ, of the system before the neutron-drip transition point, is given by:

$$\epsilon = n_N W_N(A, Z) + \epsilon_e + \epsilon_L \tag{3.1.1}$$

where n_N is the number density of nuclei, W_N the energy of the nucleus, having mass number A and atomic number Z, ϵ_e is the electron energy density

and ϵ_L the lattice energy density. With more details for each term:

- **Nucleus contribution**

The energy of the nucleus (i.e., fully ionized atom), W_N, is calculated either by the relation:

$$W_N(A,Z) = \Delta M_{at}(A,Z)c^2 + Am_u c^2 - Zm_e c^2 + BE_e(Z) \tag{3.1.2}$$

if the atomic mass excess, ΔM_{at}, is known, or by the relation:

$$W_N(A,Z) = Zm_p c^2 + (A-Z)m_n c^2 - BE_N(A,Z) \tag{3.1.3}$$

if the nuclear binding energy, BE_N, is known. In Eq. 3.1.2, m_u is the atomic mass unit, m_e the electron mass and BE_e the binding energy of electrons, while in Eq. 3.1.3, m_p is the proton mass and m_n the neutron mass. The atomic mass excess is defined as:

$$\Delta M_{at}(A,Z) = M_{at}(A,Z) - Am_u \tag{3.1.4}$$

where M_{at} is the atomic mass, including the contribution of electrons, for this reason the presence of the last two terms in Eq. 3.1.2 is justified[1]. And the binding energy of electrons is calculated by [15]:

$$BE_e(Z) = 1.44381 \cdot 10^{-5} Z^{2.39} + 1.55468 \cdot 10^{-12} Z^{5.35} MeV \tag{3.1.5}$$

- **Electron contribution**

The quantities related to the electron contribution were calculated in Section 2.3, so the electron energy density, ϵ_e, is given by Eq. 2.3.11:

$$\epsilon_e = \frac{m_e c^2}{\lambda\!\!\!^{-3}_e} f(x_e) \tag{3.1.6}$$

where from Eq. 2.3.13:

$$f(x_e) = \frac{1}{8\pi^2}\{x_e(1+x_e^2)^{1/2}(1+2x_e^2) - ln[x_e + (x_e^2+1)^{1/2}]\} \tag{3.1.7}$$

Also, the electron number density and the electron pressure are given by Eqs. 2.3.8 and 2.3.12, respectively, so:

$$n_e = \frac{x_e^3}{3\pi^2 \lambda\!\!\!^{-3}_e} \tag{3.1.8}$$

[1] in Ref. [9] only the electron rest masses are subtracted, while the binding energy of electrons is kept, because of electron screening effects

$$P_e = \frac{m_e c^2}{\lambda_e^3} g(x_e) \tag{3.1.9}$$

where from Eq. 2.3.13:

$$g(x_e) = \frac{1}{8\pi^2}\{x_e(1+x_e^2)^{1/2}(\frac{2}{3}x_e^2 - 1) + ln[x_e + (x_e^2+1)^{1/2}]\} \tag{3.1.10}$$

And the dimensionless electron chemical potential, from Eq. 2.3.10, is:

$$\gamma_e = \frac{\mu_e}{m_e c^2} = (x_e^2+1)^{1/2} \tag{3.1.11}$$

• **Lattice contribution**

Here the assumption of the *one-component plasma* model [8] is imposed, which means that at given density only one species of nuclei present (i.e., a single nuclear species at lattice sites). Of course, according to Ref. [16], a phase composed of mixed lattices[2] is preferable to a body-centered cubic (bcc) lattice of any single nuclide. This phase appears between almost every pair of phases (single type lattice), over a narrow pressure range, about a hundredth of a percent of the pressure at which the transition from (A, Z) to (A', Z') phase occurs, and phases can change more continuously. Also, the possibility of the existence of compounds in outer crust is examined in Ref. [17].

As said previously, ions of charge Z (i.e., nuclei) are located in a lattice and electrons form a degenerate Fermi gas, considering it to 1st approximation as uniform. According to *Wigner-Seitz approximation*, the gas is divided into neutral spheres of radius, r_{cell}, about each nucleus, which contain the Z electrons closest to the nucleus. So, a spherical cell has volume:

$$\frac{4\pi r_{cell}^3}{3} = \frac{1}{n_N} \tag{3.1.12}$$

The total electrostatic energy of a sphere (lattice energy), E_L, is the sum of the energy due to electron-electron interaction, E_{ee}, and the energy due to electron-ion interaction, E_{ei}, so [7]:

$$E_L = E_{ee} + E_{ei} \tag{3.1.13}$$

The E_{ee} is the energy to assemble a uniform sphere of Z electrons and is given by:

$$E_{ee} = \int_0^{r_{cell}} \frac{qdq}{r} = \frac{3}{5}\frac{Z^2e^2}{r_{cell}} \tag{3.1.14}$$

[2]interpenetrating cubic lattices, i.e., bcc lattices with (Z, A)-nuclei at the corners and (Z', A')-nuclei in the middle

with $q = -Ze\frac{r^3}{r_{cell}^3}$ to be the charge inside radius r. And the E_{ei} is the energy to assemble the electron sphere about the central nucleus of charge Ze, so:

$$E_{ei} = Ze\int_0^{r_{cell}} \frac{dq}{r} = -\frac{3}{2}\frac{Z^2e^2}{r_{cell}} \tag{3.1.15}$$

Therefore, the lattice energy is given by:

$$E_L = -\frac{9}{10}\frac{Z^2e^2}{r_{cell}} \tag{3.1.16}$$

using Eqs. 2.4.2 and 3.1.12 , the E_L is written as:

$$E_L = -\frac{9}{10}(\frac{4\pi}{3})^{1/3}e^2Z^{5/3}n_e^{1/3} \tag{3.1.17}$$

The factor, (9/10), is very close to the Madelung constant, C_M, of different type of lattices, as shown in Table 3.1 and from the listed values the bcc lattice gives the lowest lattice energy, so:

$$E_L = -C_M(\frac{4\pi}{3})^{1/3}e^2Z^{5/3}n_e^{1/3} \tag{3.1.18}$$

where for the C_M is considered the value for the bcc lattice.

Table 3.1: Madelung constant C_M for different lattices [3]

lattice	$\boldsymbol{C_M}$
bcc	0.895929255682
fcc	0.895873615195
hcp	0.895838120459

The lattice energy density, ϵ_L, is given by:

$$\epsilon_L = n_N E_L = -C_M(\frac{4\pi}{3})^{1/3}e^2Z^{2/3}n_e^{4/3} \tag{3.1.19}$$

and the lattice pressure, P_L, is expressed as:

$$P_L = n_e^2\frac{\partial}{\partial n_e}(\frac{\epsilon_L}{n_e}) = -\frac{1}{3}C_M(\frac{4\pi}{3})^{1/3}e^2Z^{2/3}n_e^{4/3} = \frac{1}{3}\epsilon_L \tag{3.1.20}$$

and is negative.

It is worth mentioning that corrections concerning: 1) the screening (or polarization) effect (Thomas-Fermi energy), which describes the deviation

of the electron distribution from uniformity due to the charged ions, 2) the electron exchange effect, which takes into account the fermionic nature of electron-electron interaction, 3) the zero-point motion of the nuclei in the lattice, and others (see, e.g., Ref. [11]) like, 4) the electron correlation energy, 5) the screening of electrons by protons, 6) the finite nuclear size, 7) the screening of protons by electrons and 8) thermal correction, were not included, considering that are negligible.

So, the total energy is a function of x_e, A and Z:

$$\epsilon = \epsilon(x_e, A, Z) = \frac{n_e(x_e)}{Z} W_N(A, Z) + \epsilon_e(x_e) + \epsilon_L(n_e(x_e), Z) \tag{3.1.21}$$

And the total pressure, P, using Eq. 2.2.3, is given by:

$$P = P(x_e, Z) = P_e(x_e) + P_L(n_e(x_e), Z) \tag{3.1.22}$$

The lattice energy is important for the equilibrium composition, although, the lattice pressure is a small correction to electron pressure (see, Section 4.1). The pressure in a star increases continuously with increasing depth. However, an abrupt density discontinuity occurs in a transition phase (i.e., change in equilibrium nucleus), because $P \approx P_e$ (in 1st approximation), n_e is continuous across each transition, but $n_b = An_e/Z$, so for a transition from (A, Z) to (A', Z') nucleus:

$$n_b' - n_b \approx n_e(\frac{A'}{Z'} - \frac{A}{Z}) \tag{3.1.23}$$

and, also, using Eq. 2.4.1, the fractional change in ϵ and n_b is:

$$\frac{\Delta\epsilon}{\epsilon} \approx \frac{\Delta n_b}{n_b} \approx \frac{Z/A}{Z'/A'} - 1 \tag{3.1.24}$$

A method to find the equilibrium nucleus (A and Z), is to minimize the ϵ, for a fixed n_b. But, because of the density discontinuities it is necessary to make a Maxwell equal-area construction in a plot of P vs $1/n_b$ [9], in order to determine the pressure at which the transition occurs. So, it is better to use the Gibbs free energy per baryon, g, which equals the baryon chemical potential, μ_b, and from Eq. 2.2.8 (T=0K), is given by:

$$g = \mu_b = \frac{\epsilon + P}{n_b} = \frac{W_N(A, Z)}{A} + \frac{Z}{A} m_e c^2 (1 + x_e^2)^{1/2} + \frac{4Z}{3An_e(x_e)} \epsilon_L(n_e(x_e), Z) \tag{3.1.25}$$

The method is for a fixed P, a trial pair (A, Z) is selected from a table of nuclides, the Eq. 3.1.22 is numerically solved for the variable x_e, then given x_e the quantity g is calculated from Eq. 3.1.25. This process is repeated for all the available nuclei and the nucleus, which gives the minimum g, is the equilibrium nucleus for this pressure. The procedure continues for the next pressure value, with a quite small pressure step (i.e., a fine pressure grid), so not to miss any layer. The g (or μ_b) is a continuous variable across transition, increases monotonically with density and in equilibrium equals the neutron chemical potential, so the above minimization procedure ends for some pressure P_{drip}, where the condition:

$$g_{min} = m_n c^2, \tag{3.1.26}$$

for an equilibrium nucleus (A_{drip}, Z_{drip}), is satisfied for the first time, and neutron-drip begins, passing into the inner crust.

3.2 Presence of magnetic field

3.2.1 Magnetic field regimes

Neutron stars can have extremely intense magnetic fields, unattainable in terrestrial laboratories. Typical pulsars, which are a type of neutron stars, have a surface magnetic field magnitude[3], $B_{surf} \sim 10^{12}G$, while in some others could reach up to $\sim 10^{15}G$, in comparison the Earth's surface magnetic field is approximately $0.5G$. In the interior of neutron stars, even stronger magnetic fields might exist, the class of magnetars could be a such environment [13, 14]. The theoretical upper limit in the interior magnetic field can be evaluated through the virial theorem [12]:

$$2T_k + W_{grav} + 3\Pi + \mathcal{M} = 0 \tag{3.2.1}$$

where T_k is the total kinetic energy, Π due to internal energy, W_{grav} the gravitational potential energy and $\mathcal{M}$ the magnetic energy. Because $T_k, \Pi > 0$, the maximum $\mathcal{M}$ can never exceed W_{grav} in equilibrium. So, for a neutron star of mass M and radius R:

$$\frac{4\pi R^3}{3}\frac{B_{max}^2}{8\pi} \approx \frac{GM^2}{R} \Rightarrow B_{max} \approx 2 \cdot 10^8 (\frac{M}{M_\odot})(\frac{R}{R_\odot})^{-2} G \tag{3.2.2}$$

Considering $M = 1.4M_\odot$ and $R = 12km$, with $R_\odot \approx 695700km$ the solar radius, the maximum interior field is $B_{max} \sim 10^{18}G$.

[3] $1G = 10^{-4} Tesla$

Let's consider free electrons inside a uniform magnetic field of magnitude, B, along z-axis: $\vec{B} = B\hat{z}$. The motion of electrons perpendicular to the magnetic field is quantized into the Landau levels. For sufficiently high field, the cyclotron energy of electrons:

$$E_{cycl} = \hbar\omega_{cycl} \simeq 11.5 \cdot 10^{-3} \frac{B}{10^{12}G} MeV, \tag{3.2.3}$$

where

$$\omega_{cycl} = \frac{eB}{m_e c} \tag{3.2.4}$$

is the cyclotron angular frequency of electrons, becomes comparable to the electron rest-mass energy, $m_e c^2$. So, from the condition $E_{cycl} = m_e c^2$, the critical magnetic field, B_c, is defined as:

$$B_c = \frac{m_e^2 c^3}{e\hbar} = \sqrt{\frac{m_e c^2}{\alpha \lambda\!\!\!^{-}_e{}^3}} \simeq 4.414 \cdot 10^{13} G \tag{3.2.5}$$

And it is useful to define, the magnetic field strength, $B_\star$, as:

$$B_\star = \frac{B}{B_c} \tag{3.2.6}$$

which is a dimensionless parameter and characterizes the magnetic field. Thus, for $B_\star \gtrsim 1$, the electrons are treated in a relativistic framework and the solution of Dirac equation gives the energy levels:

$$E_{\nu,p_z} = [p_z^2 c^2 + m_e^2 c^4 (1 + 2\nu B_\star)]^{1/2} \tag{3.2.7}$$

where $\nu = 0, 1, 2, ...$ (i.e., a non-negative quantum number) and p_z is the momentum along the magnetic field and is a continuous variable. The ground state Landau level ($\nu = 0$) is non-degenerate, but the levels $\nu \geq 1$ are doubly[4] degenerate.

Three different regimes can be distinguished: a) the strongly quantizing magnetic field, for sufficiently low temperature and density, where all electrons are in the ground state level ($\nu = 0$), b) the weakly quantizing magnetic field, where only a few Landau levels are occupied and the Landau quantization can remain important, and c) the non-quantizing magnetic field, for high temperature or density, where electrons are distributed in many levels.

[4] the anomalous magnetic moment of electron splits the energy levels $\nu \geq 1$ and removes the spin degeneracy, but it is negligible [3]

For this reason, the critical value in electron number density, n_{e_B}, is defined as [3]:

$$n_{e_B} = \frac{1}{\pi^2 \sqrt{2} a_m^3} = \frac{B_\star^{3/2}}{\pi^2 \sqrt{2} \lambda\!\!\!^{-}_e^3} \simeq 1.244 \cdot 10^{-9} B_\star^{3/2} fm^{-3} \tag{3.2.8}$$

where $a_m = \sqrt{\frac{\hbar c}{eB}} = \frac{\lambda\!\!\!^{-}_e}{\sqrt{B_\star}}$ is the characteristic magnetic length, the n_{e_B} corresponds to a critical baryon number density, n_{b_B}, which is given by:

$$n_{b_B} = \frac{A B_\star^{3/2}}{\pi^2 \sqrt{2} \lambda\!\!\!^{-}_e^3 Z} \simeq 1.244 \cdot 10^{-9} \frac{A B_\star^{3/2}}{Z} fm^{-3} \tag{3.2.9}$$

and the corresponding energy density can be easily found from Eq. 2.4.1. Also, the critical value in temperature, T_B, is defined as [3]:

$$T_B = \begin{cases} T_{cycl}, \ for \ n_b < n_{b_B} \\ \frac{T_{cycl}}{\sqrt{1+x_e^2}}, \ for \ n_b > n_{b_B} \end{cases} \tag{3.2.10}$$

where the T_{cycl} is given by:

$$T_{cycl} = \frac{\hbar \omega_{cycl}}{k_B} = \frac{m_e c^2}{k_B} B_\star \simeq 5.930 \cdot 10^9 B_\star K \tag{3.2.11}$$

Therefore, the conditions for each regime are:

- **Strongly quantizing magnetic field**:

$$\begin{cases} n_b < n_{b_B} \\ and \\ T << T_B \end{cases} \tag{3.2.12}$$

- **Weakly quantizing magnetic field**:

$$\begin{cases} n_b > n_{b_B} \\ and \\ T \lesssim T_B \end{cases} \tag{3.2.13}$$

- **Non-quantizing magnetic field**:

$$\begin{cases} n_b >> n_{b_B} \\ or \\ T >> T_B \end{cases} \tag{3.2.14}$$

The present work deals with the strongly quantizing magnetic field regime at T=0K.

3.2.2 Strong quantization

According to *Bohr-van Leeuwen theorem*, the lattice energy density is not affected by the magnetic field. Other indirect effects on lattice configuration are neglected, considering a bcc lattice, like in Section 3.1. Also, the effects of the magnetic field on nuclear masses are ignored, of course, according to Ref. [14], the nuclear binding energy has a parabolic increasing trend with the magnetic field and for nuclei present in outer crust does not increase by more than 10% for $B \sim 10^{17} - 10^{18}G$, in addition, the pairing effects decrease with increasing magnetic field. So, the same mass tables, for the field-free case, are used, having the maximum magnetic field strength $B_\star = 2500$ ($B \simeq 1.10 \cdot 10^{17}G$) in calculations.

Thus, only the effects of magnetic field on the electrons are taken into account, quantizing the electron motion, as said previously. The quantities related to the energy of nucleus and the lattice, are the same as given in Section 3.1, and only the quantities[5] related to the electron contribution (i.e., n_e, ϵ_e and P_e) will change.

The density of states in an interval of longitudinal momentum, Δp_z, for a given ν is [12]: $g_\nu(\frac{eB}{h^2c})\Delta p_z$, where

$$g_\nu = \begin{cases} 1, \ for \ \nu = 0 \\ 2, \ for \ \nu \geq 1 \end{cases} \tag{3.2.15}$$

is the spin degeneracy. So, the quantity, $\frac{2}{h^3}\int d^3p = \frac{1}{\pi^2 \lambda\!\!\!^{-3}_e m_e^3 c^3}\int p^2 dp$ (see, Eq. 2.3.1), must be replaced by: $\frac{eB}{h^2c}\sum_\nu g_\nu \int dp_z = \frac{B_\star}{(2\pi)^2 \lambda\!\!\!^{-3}_e m_e c}\sum_\nu g_\nu \int dp_z$. The dimensionless electron Fermi momentum is written:

$$\tilde{x}_e(\nu) = \frac{\tilde{p}_{F,e}(\nu)}{m_e c} \tag{3.2.16}$$

where $\tilde{p}_{F,e}(\nu) \geq 0$ is the maximum z-momentum, defined by:

$$\tilde{\mu}_e^2 = (m_e c^2)^2 \tilde{\gamma}_e^2 = \tilde{p}_{F,e}(\nu)^2 c^2 + m_e^2 c^4 (1 + 2\nu B_\star) \tag{3.2.17}$$

with $\tilde{\mu}_e$ and $\tilde{\gamma}_e$ to be the electron chemical potential (or electron Fermi energy) and the dimensionless electron chemical potential, respectively. The upper limit ν_{max} of the summation over the index ν is set by the condition: $\tilde{p}_{F,e}(\nu)^2 \geq 0 \ or \ \tilde{\gamma}_e^2 \geq 1 + 2\nu B_\star$.

[5] the tilde symbol, "˜", will be used for the case of the presence of magnetic field, when necessary to avoid any confusion

The electron number density, $\tilde{n}_e$, the electron energy density, $\tilde{\epsilon}_e$, and the electron pressure, $\tilde{P}_e$, are given by:

$$\begin{aligned}\tilde{n}_e &= \frac{B_\star}{(2\pi)^2 \lambda\!\!\!^{-3}_e m_e c} \sum_{\nu=0}^{\nu_{max}} g_\nu \int_{-\tilde{p}_{F,e}(\nu)}^{\tilde{p}_{F,e}(\nu)} dp_z \\ &= \frac{B_\star}{2\pi^2 \lambda\!\!\!^{-3}_e} \sum_{\nu=0}^{\nu_{max}} g_\nu \tilde{x}_e(\nu)\end{aligned} \tag{3.2.18}$$

$$\begin{aligned}\tilde{\epsilon}_e &= \frac{B_\star}{(2\pi)^2 \lambda\!\!\!^{-3}_e m_e c} \sum_{\nu=0}^{\nu_{max}} g_\nu \int_{-\tilde{p}_{F,e}(\nu)}^{\tilde{p}_{F,e}(\nu)} E_{\nu,p_z} dp_z \\ &= \frac{m_e c^2 B_\star}{(2\pi)^2 \lambda\!\!\!^{-3}_e} \sum_{\nu=0}^{\nu_{max}} g_\nu (1+2\nu B_\star) \tilde{f}\left(\frac{\tilde{x}_e(\nu)}{(1+2\nu B_\star)^{1/2}}\right)\end{aligned} \tag{3.2.19}$$

$$\begin{aligned}\tilde{P}_e &= -\tilde{\epsilon}_e + \tilde{n}_e \tilde{\mu}_e \\ &= \frac{m_e c^2 B_\star}{(2\pi)^2 \lambda\!\!\!^{-3}_e} \sum_{\nu=0}^{\nu_{max}} g_\nu (1+2\nu B_\star) \tilde{g}\left(\frac{\tilde{x}_e(\nu)}{(1+2\nu B_\star)^{1/2}}\right)\end{aligned} \tag{3.2.20}$$

where the functions $\tilde{f}(w)$ and $\tilde{g}(w)$ are:

$$\begin{cases}\tilde{f}(w) = w(1+w^2)^{1/2} + ln[w + (w^2+1)^{1/2}] \\ \tilde{g}(w) = w(1+w^2)^{1/2} - ln[w + (w^2+1)^{1/2}]\end{cases} \tag{3.2.21}$$

However, for *strongly quantizing magnetic field*, $\nu_{max} = 0$, the expressions for $\tilde{\mu}_e$ (or $\tilde{\gamma}_e$), $\tilde{n}_e$, $\tilde{\epsilon}_e$ and $\tilde{P}_e$ are simplified and the Eqs. 3.2.17, 3.2.18, 3.2.19 and 3.2.20 are finally written, respectively:

$$\tilde{\mu}_e = m_e c^2 \tilde{\gamma}_e = m_e c^2 (\tilde{x}_e + 1)^{1/2} \tag{3.2.22}$$

$$\tilde{n}_e = \frac{B_\star}{2\pi^2 \lambda\!\!\!^{-3}_e} \tilde{x}_e \tag{3.2.23}$$

$$\tilde{\epsilon}_e = \frac{m_e c^2 B_\star}{(2\pi)^2 \lambda\!\!\!^{-3}_e} \tilde{f}(\tilde{x}_e) \tag{3.2.24}$$

$$\tilde{P}_e = \frac{m_e c^2 B_\star}{(2\pi)^2 \lambda\!\!\!^{-3}_e} \tilde{g}(\tilde{x}_e) \tag{3.2.25}$$

It is noted that, for the case of strongly quantizing magnetic field, in Eqs. 3.1.19 - 3.1.22 and 3.1.25, the quantities n_e, ϵ_e, P_e and x_e are replaced with $\tilde{n}_e$, $\tilde{\epsilon}_e$, $\tilde{P}_e$ and $\tilde{x}_e$, respectively, and the minimization procedure (see, Section 3.1) is the same.

Chapter 4

Properties of outer crust

4.1 EoS - Polytrope fitting

The Equation of State (EoS) is a relation of pressure as a function of energy density (or baryon number density), i.e.,

$$P = P(\epsilon) \; or \; P = P(n_b) \tag{4.1.1}$$

In this EoS, a polytrope (polytropic EoS) can be fitted, which is a power law for the pressure in terms of the energy density, so:

$$P = K\epsilon^G \tag{4.1.2}$$

or

$$P = K' n_b^{G'} \tag{4.1.3}$$

if one considers the baryon number density. K, G, K' and G' are parameters, which are calculated through fitting in the data, the G and G' are dimensionless and the dimensions of K and K' depend on G and G', respectively. From Eq. 2.4.1, the two definitions (see, Eqs. 4.1.2 and 4.1.3) are equivalent, providing that:

$$\begin{cases} G = G' \\ and \\ K = \frac{K'}{(m_n c^2)^{G'}} \end{cases} \tag{4.1.4}$$

Some approximate expressions are introduced in this Chapter, as well as, a toy model for the energy of the nucleus (see, Section 4.2), to explain the essential physics and the results of Chapter 5, where numerical methods and sophisticated mass models are used.

Approximations

• **For $x_e << 1$** (i.e., non-relativistic limit in surface layers) **and $B_\star = 0$** (i.e., absence of magnetic field):
The leading term of functions $f(x_e)$ and $g(x_e)$ is, respectively:

$$f(x_e) \approx \frac{x_e^3}{3\pi^2} \tag{4.1.5}$$

$$g(x_e) \approx \frac{x_e^5}{15\pi^2} \tag{4.1.6}$$

and the Eqs. 3.1.6 and 3.1.9, using Eq. 3.1.8, are approximately:

$$\epsilon_e \approx m_e c^2 n_e \tag{4.1.7}$$

$$P_e \approx \frac{3^{2/3}\pi^{4/3}}{5} m_e c^2 \lambda\!\!\!^{-2}_e n_e^{5/3} \tag{4.1.8}$$

The electron chemical potential (see, Eq. 3.1.11) becomes:

$$\mu_e \approx m_e c^2 + \frac{m_e c^2 x_e^2}{2} \tag{4.1.9}$$

The total pressure (see, Eq. 3.1.22) is now:

$$\begin{aligned} P &= P_e(1 + \frac{P_L}{P_e}) \\ &= \frac{3^{2/3}\pi^{4/3} m_e c^2 \lambda\!\!\!^{-2}_e n_e^{5/3}}{5}(1 - \frac{5 \cdot 2^{2/3} C_M \alpha Z^{2/3}}{9\pi \lambda\!\!\!^{-}_e n_e^{1/3}}) \\ &\simeq 14.586 \cdot 10^4 n_e[fm^{-3}]^{5/3}(1 - 4.753 \cdot 10^{-6} Z^{2/3} n_e[fm^{-3}]^{-1/3}) MeV/fm^3 \end{aligned} \tag{4.1.10}$$

For $P = 0$, the surface baryon number density, $n_{b_{surf}}$, assuming A_{surf} and Z_{surf} the equilibrium nucleus at the surface, is:

$$n_{b_{surf}} = \frac{500\alpha^3 C_M^3 A_{surf} Z_{surf}}{729 \lambda\!\!\!^{-3}_e \pi^3} \simeq 1.0735 \cdot 10^{-16} A_{surf} Z_{surf} fm^{-3} \tag{4.1.11}$$

and for the nuclide ^{56}Fe leads to:

$$n_{b_{surf}}^{^{56}Fe} \simeq 1.563 \cdot 10^{-13} fm^{-3} \tag{4.1.12}$$

• **For $x_e >> 1$** (i.e., ultra-relativistic limit in bottom layers) **and $B_\star = 0$** (i.e., absence of magnetic field):
The leading term of functions $f(x_e)$ and $g(x_e)$ is, respectively:

$$f(x_e) \approx \frac{x_e^4}{4\pi^2} \tag{4.1.13}$$

$$g(x_e) \approx \frac{x_e^4}{12\pi^2} \tag{4.1.14}$$

and the Eqs. 3.1.6 and 3.1.9, using Eq. 3.1.8, are approximately:

$$\epsilon_e \approx \frac{3^{4/3}\pi^{2/3}}{4} m_e c^2 \lambda\!\!\!^{-}_e n_e^{4/3} \tag{4.1.15}$$

$$P_e \approx \frac{3^{1/3}\pi^{2/3}}{4} m_e c^2 \lambda\!\!\!^{-}_e n_e^{4/3} \tag{4.1.16}$$

The electron chemical potential (see, Eq. 3.1.11) becomes:

$$\mu_e \approx m_e c^2 x_e \tag{4.1.17}$$

The total pressure (see, Eq. 3.1.22) is now:

$$\begin{aligned} P &= P_e(1 + \frac{P_L}{P_e}) \\ &= \frac{3^{1/3}\pi^{2/3} m_e c^2 \lambda\!\!\!^{-}_e n_e^{4/3}}{4}(1 - \frac{2^{8/3}\alpha C_M Z^{2/3}}{3^{5/3}\pi^{1/3}}) \\ &\simeq 152.616 n_e[fm^{-3}]^{4/3}(1 - 4.54221 \cdot 10^{-3} Z^{2/3}) MeV/fm^3 \end{aligned} \tag{4.1.18}$$

The second term in parentheses is negligible (i.e., the lattice pressure), so $P \approx P_e$.

• **For $\tilde{x}_e << 1$** (i.e., non-relativistic limit in surface layers) **and $B_\star \neq 0$** (i.e., presence of magnetic field):
The leading term of functions $\tilde{f}(\tilde{x}_e)$ and $\tilde{g}(\tilde{x}_e)$ is, respectively:

$$\tilde{f}(\tilde{x}_e) \approx 2\tilde{x}_e \tag{4.1.19}$$

$$\tilde{g}(\tilde{x}_e) \approx \frac{2\tilde{x}_e^3}{3} \tag{4.1.20}$$

and the Eqs. 3.2.24 and 3.2.25, using Eq. 3.2.23, are approximately:

$$\tilde{\epsilon}_e \approx m_e c^2 \tilde{n}_e \tag{4.1.21}$$

$$\tilde{P}_e \approx \frac{4\pi^4 m_e c^2 \lambda\!\!\!^{-}_e{}^6 \tilde{n}_e^3}{3B_\star^2} \tag{4.1.22}$$

The electron chemical potential (see, Eq. 3.2.22) becomes:

$$\tilde{\mu}_e \approx m_e c^2 + \frac{m_e c^2 \tilde{x}_e^2}{2} \tag{4.1.23}$$

The total pressure (see, Eq. 3.1.22) is now:

$$\begin{aligned}\tilde{P} &= \tilde{P}_e(1+\frac{\tilde{P}_L}{\tilde{P}_e}) \\ &= \frac{4\pi^4 m_e c^2 \lambda\!\!\!^{-}_e{}^6 \tilde{n}_e^3}{3B_\star^2}(1-\frac{\alpha C_M B_\star^2 Z^{2/3}}{2\cdot 6^{1/3}\pi^{11/3}\lambda\!\!\!^{-}_e{}^5 \tilde{n}_e^{5/3}}) \\ &\simeq 2.2007\cdot 10^{17}\frac{\tilde{n}_e[fm^{-3}]^3}{B_\star^2}(1-3.15\cdot 10^{-18}B_\star^2 Z^{2/3}\tilde{n}_e[fm^{-3}]^{-5/3})MeV/fm^3\end{aligned} \tag{4.1.24}$$

For $\tilde{P}=0$, the surface baryon number density, $\tilde{n}_{b_{surf}}$, assuming A_{surf} and Z_{surf} the equilibrium nucleus at the surface, is:

$$\tilde{n}_{b_{surf}} = (\frac{\alpha^3 C_M^3}{3\cdot 2^4\pi^{11}})^{1/5}\frac{B_\star^{6/5}A_{surf}}{\lambda\!\!\!^{-}_e{}^3 Z_{surf}^{3/5}} \simeq 3.1549\cdot 10^{-11}\frac{B_\star^{6/5}A_{surf}}{Z_{surf}^{3/5}}fm^{-3} \tag{4.1.25}$$

and for the nuclide ^{56}Fe leads to:

$$\tilde{n}_{b_{surf}}^{^{56}Fe} \simeq 2.501\cdot 10^{-10}B_\star^{6/5}fm^{-3} \tag{4.1.26}$$

The Eq. 4.1.26 shows that as the $B_\star$ increases, the surface density also increases ($\propto B_\star^{6/5}$). And comparing with Eq. 4.1.12, the field-free case has lower surface density. It is noted that the condition $\tilde{x}_e << 1$, using Eqs. 3.2.23 and 4.1.25, gives an upper limit for $B_\star$:

$$B_\star << \frac{3\pi}{2\alpha^3 C_M^3 Z_{surf}^2} \simeq 2.494\cdot 10^4,\ for\ Z_{surf}=26 \tag{4.1.27}$$

• **For $\tilde{x}_e >> 1$** (i.e., ultra-relativistic limit in bottom layers) **and $B_\star \neq 0$** (i.e., presence of magnetic field):
The leading term of functions $\tilde{f}(\tilde{x}_e)$ and $\tilde{g}(\tilde{x}_e)$ is, respectively:

$$\tilde{f}(\tilde{x}_e) \approx \tilde{x}_e^2 \tag{4.1.28}$$

$$\tilde{g}(\tilde{x}_e) \approx \tilde{x}_e^2 \tag{4.1.29}$$

and the Eqs. 3.2.24 and 3.2.25, using Eq. 3.2.23, are approximately:

$$\tilde{\epsilon}_e \approx \frac{\pi^2 m_e c^2 \lambda\!\!\!^{-}_e{}^3 \tilde{n}_e^2}{B_\star} \tag{4.1.30}$$

$$\tilde{P}_e \approx \frac{\pi^2 m_e c^2 \lambda\!\!\!^{-}_e{}^3 \tilde{n}_e^2}{B_\star} \tag{4.1.31}$$

The electron chemical potential (see, Eq. 3.2.22) becomes:

$$\tilde{\mu}_e \approx m_e c^2 \tilde{x}_e \tag{4.1.32}$$

The total pressure (see, Eq. 3.1.22) is now:

$$\begin{aligned}\tilde{P} &= \tilde{P}_e(1+\frac{\tilde{P}_L}{\tilde{P}_e}) \\ &= \frac{\pi^2 m_e c^2 \lambda\!\!\!^{-}_e{}^3 \tilde{n}_e^2}{B_\star}(1-\frac{2^{2/3}\alpha C_M B_\star Z^{2/3}}{3^{4/3}\pi^{5/3}\lambda\!\!\!^{-}_e{}^2 \tilde{n}_e^{2/3}}) \\ &\simeq 2.904\cdot 10^8 \frac{\tilde{n}_e[fm^{-3}]^2}{B_\star}(1-2.387\cdot 10^{-9} B_\star Z^{2/3}\tilde{n}_e[fm^{-3}]^{-2/3}) MeV/fm^3\end{aligned} \tag{4.1.33}$$

The second term in parentheses is negligible (i.e., the lattice pressure), so $\tilde{P} \approx \tilde{P}_e$. The condition for the baryon number density of Eq. 3.2.12 gives an upper limit for the pressure, using the Eqs. 3.2.9 and 4.1.31, and given that $\tilde{P} \approx \tilde{P}_e$, is:

$$\tilde{P} < \frac{m_e c^2 B_\star^2}{2\pi^2 \lambda\!\!\!^{-}_e{}^3} \simeq 4.496\cdot 10^{-10} B_\star^2 MeV/fm^3 \tag{4.1.34}$$

Returning to Eq. 4.1.2, in the denser regions, where electrons are ultra-relativistic (i.e., $P \approx P_e$), using Eqs. 2.4.1, 2.4.2 and 4.1.16, the parameters K and G for the field-free case, are approximately:

$$\begin{cases} K = \frac{3^{1/3}\pi^{2/3} m_e c^2 \lambda\!\!\!^{-}_e}{4(m_n c^2)^{4/3}}(\frac{Z}{A})^{4/3} \simeq 0.0166(\frac{Z}{A})^{4/3},\ \epsilon\ and\ P\ in\ MeV/fm^3 \\ G = 4/3 \end{cases} \tag{4.1.35}$$

Respectively, for strongly quantizing field, from Eq. 4.1.31, are:

$$\begin{cases} \tilde{K} = \frac{\pi^2 m_e c^2 \lambda\!\!\!^{-}_e{}^3}{B_\star (m_n c^2)^2}(\frac{Z}{A})^2 \simeq \frac{328.977}{B_\star}(\frac{Z}{A})^2,\ \tilde{\epsilon}\ and\ \tilde{P}\ in\ MeV/fm^3 \\ \tilde{G} = 2 \end{cases} \tag{4.1.36}$$

4.2 Composition

A toy model for the energy of nucleus is the following (see, Ref. [13]):

$$W_N(A,Z) = Am_n c^2 + Aa_V + AJ(1-2\frac{Z}{A})^2 \tag{4.2.1}$$

where a_V is the energy per particle of symmetric nuclear matter at saturation, J the symmetry energy and Z/A the proton fraction. The terms for Coulomb,

surface and pairing effects are neglected, and, also, the difference between the mass of protons and neutrons is ignored. Typical values for a_V and J can be found in Table 5.1. So, the Eq. 3.1.25, neglecting the lattice contribution, is written[1]:

$$\begin{aligned}\tilde{g} &\approx \frac{W_N(A,Z)}{A} + \frac{Z}{A} m_e c^2 (1+\tilde{x}_e^2)^{1/2} \\ &= m_n c^2 + a_V + J(1-2\frac{Z}{A})^2 + \frac{Z}{A}\tilde{\mu}_e\end{aligned} \tag{4.2.2}$$

Considering the Z/A as a continuous variable, at the minimum of $\tilde{g}$, $\tilde{g}_{min}$, (i.e., $\frac{\partial \tilde{g}}{\partial (Z/A)} = 0$), with fixed $\tilde{\mu}_e$, the proton fraction is:

$$\frac{Z}{A} = \frac{1}{2} - \frac{\tilde{\mu}_e}{8J} \tag{4.2.3}$$

But, at neutron-drip transition, $\tilde{g}_{min} = m_n c^2$, so substituting the $\tilde{\mu}_e$ of Eq. 4.2.3 into Eq. 4.2.2, the proton fraction, $\frac{Z_{drip}}{A_{drip}}$, is given by:

$$\frac{Z_{drip}}{A_{drip}} \approx \frac{1}{2}\sqrt{1+\frac{a_V}{J}} \tag{4.2.4}$$

And from Eqs. 4.2.3 and 4.2.4, the electron chemical potential at neutron-drip is:

$$\tilde{\mu}_{e_{drip}} \approx 4J(1-\sqrt{1+\frac{a_V}{J}}) \tag{4.2.5}$$

From Eqs. 4.2.4 and 4.2.5, the equilibrium nucleus and the electron chemical potential, at neutron-drip point, are *independent* of the magnetic field and determined by the mass model, hence: $\tilde{\mu}_{e_{drip}} = \mu_{e_{drip}}$.

In the absence of magnetic field, the neutron-drip pressure and the baryon number density ($x_e >> 1 \rightarrow P \approx P_e$), using Eqs. 3.1.8, 4.1.16 and 4.1.17, are approximately:

$$\begin{aligned}P_{drip} &\approx \frac{\mu_{e_{drip}}^4}{12\pi^2 \lambda\!\!\!^{-3}_e (m_e c^2)^3} \\ &\simeq 1.0989 \cdot 10^{-9} \mu_{e_{drip}} [MeV]^4 MeV/fm^3\end{aligned} \tag{4.2.6}$$

$$\begin{aligned}n_{b_{drip}} &\approx \frac{A_{drip}\mu_{e_{drip}}^3}{Z_{drip} 3\pi^2 \lambda\!\!\!^{-3}_e (m_e c^2)^3} \\ &\simeq 4.3956 \cdot 10^{-9} \frac{A_{drip}}{Z_{drip}} \mu_{e_{drip}} [MeV]^3 fm^{-3}\end{aligned} \tag{4.2.7}$$

[1] has the same form, like the field-free case, because: $\frac{Z}{An_e}(\epsilon_e + P_e) = \frac{Z}{A} m_e c^2 (1+x_e^2)^{1/2}$ and $\frac{Z}{A\tilde{n}_e}(\tilde{\epsilon}_e + \tilde{P}_e) = \frac{Z}{A} m_e c^2 (1+\tilde{x}_e^2)^{1/2}$

Respectively, for strongly quantizing field, using Eqs. 3.2.23, 4.1.31 and 4.1.32, are:

$$\begin{aligned}\tilde{P}_{drip} &\approx \frac{\mu_{e_{drip}}^2 B_\star}{4\pi^2 \lambda\!\!\!^{-}_e{}^3 m_e c^2} \\ &\simeq 8.6084 \cdot 10^{-10} B_\star \mu_{e_{drip}} [MeV]^2 MeV/fm^3\end{aligned} \tag{4.2.8}$$

$$\begin{aligned}\tilde{n}_{b_{drip}} &\approx \frac{A_{drip}\mu_{e_{drip}} B_\star}{Z_{drip} 2\pi^2 \lambda\!\!\!^{-}_e{}^3 m_e c^2} \\ &\simeq 1.7217 \cdot 10^{-9} \frac{A_{drip}}{Z_{drip}} B_\star \mu_{e_{drip}} [MeV] fm^{-3}\end{aligned} \tag{4.2.9}$$

From Eqs. 4.2.8 and 4.2.9, the neutron-drip pressure and the baryon number density increase linearly with the magnetic field strength.

From the condition of Eq. 4.1.34 and given that the maximum pressure coincides with the neutron-drip pressure of Eq. 4.2.8, means that $\tilde{P}_{drip} < \frac{m_e c^2 B_\star^2}{2\pi^2 \lambda\!\!\!^{-}_e{}^3}$, and imposes a lower limit for the magnetic field strength:

$$B_\star > \frac{\mu_{e_{drip}}^2}{2(m_e c^2)^2} \simeq 1.9148 \mu_{e_{drip}} [MeV]^2 \tag{4.2.10}$$

Approximately, $\mu_{e_{drip}} \approx 26 MeV$ (see, Table 5.15), so $B_\star > 1294$ to have strong quantization. According to Ref. [13], the condition is $B_\star > 1304$.

The ratio of P_{drip} to $\tilde{P}_{drip}$, using the Eqs. 4.2.6 and 4.2.8, is:

$$\begin{aligned}\frac{P_{drip}}{\tilde{P}_{drip}} &= \frac{\mu_{e_{drip}}^2}{3(m_e c^2)^2 B_\star} \\ &\simeq 1.2766 \frac{\mu_{e_{drip}} [MeV]^2}{B_\star}\end{aligned} \tag{4.2.11}$$

and, respectively, the ratio of $n_{b_{drip}}$ to $\tilde{n}_{b_{drip}}$, using the Eqs. 4.2.7 and 4.2.9, is:

$$\begin{aligned}\frac{n_{b_{drip}}}{\tilde{n}_{b_{drip}}} &= \frac{2\mu_{e_{drip}}^2}{3(m_e c^2)^2 B_\star} \\ &\simeq 2.5531 \frac{\mu_{e_{drip}} [MeV]^2}{B_\star}\end{aligned} \tag{4.2.12}$$

But, because of Eq. 4.2.10,

$$\begin{cases} \frac{P_{drip}}{\tilde{P}_{drip}} < \frac{2}{3} \approx 0.67 \\ \\ \frac{n_{b_{drip}}}{\tilde{n}_{b_{drip}}} < \frac{4}{3} \approx 1.33 \end{cases} \tag{4.2.13}$$

Therefore, for strongly quantizing field, the neutron-drip pressure is greater than the respective pressure for the field-free case, while from the second relation of Eq. 4.2.13 is not clear if always $n_{b_{drip}} < \tilde{n}_{b_{drip}}$.

4.3 Adiabatic index

The adiabatic index, Γ, is defined as:

$$\Gamma = \frac{\partial lnP}{\partial lnn_b} = \frac{n_b}{P}\frac{\partial P}{\partial n_b} \tag{4.3.1}$$

At high densities (i.e., $x_e >> 1$) and without magnetic field, using Eqs. 2.4.2 and 4.1.16:

$$\begin{cases} P \approx P_e \propto n_b^{4/3} \\ \Rightarrow \Gamma = 4/3 \end{cases} \tag{4.3.2}$$

Respectively, with the presence of magnetic field, using Eqs. 2.4.2 and 4.1.31:

$$\begin{cases} \tilde{P} \approx \tilde{P}_e \propto \tilde{n}_b^2 \\ \Rightarrow \tilde{\Gamma} = 2 \end{cases} \tag{4.3.3}$$

Thus, the adiabatic index is expected to approach the value 4/3, for the field-free case, and the value 2, for strongly quantizing field, at the bottom layers of outer crust.

4.4 Speed of sound

The speed of sound, c_s, in units of speed of light, is defined as:

$$\frac{c_s}{c} = \sqrt{\frac{dP}{d\epsilon}} \tag{4.4.1}$$

The c_s is an important quantity for the causality (principle of relativity). According to the causal limit, the speed of sound in the medium must be smaller than or equal to the speed of light.

Approximations at high densities (i.e., $x_e >> 1$ and $P \approx P_e$)

- ***Absence of magnetic field***

Using Eqs. 2.4.1, 2.4.2 and 4.1.16, the pressure is expressed as a function of ϵ, so from the definition of Eq. 4.4.1, the speed of sound is approximately:

$$\begin{aligned}\frac{c_s}{c} &\approx \frac{\pi^{1/3}(m_e c^2)^{1/2}\lambda\!\!\!^{-}_e{}^{1/2}}{3^{1/3}(m_n c^2)^{2/3}}(\frac{Z}{A})^{2/3}\epsilon^{1/6} \\ &\simeq 0.14870(\frac{Z}{A})^{2/3}\epsilon[MeV fm^{-3}]^{1/6}\end{aligned} \tag{4.4.2}$$

Also, at neutron-drip transition, from Eq. 4.2.7, the speed of sound is:

$$\begin{aligned}\frac{c_{s_{drip}}}{c} &\approx (\frac{\mu_{e_{drip}} Z_{drip}}{3 m_n c^2 A_{drip}})^{1/2} \\ &\simeq 0.01884(\frac{Z_{drip}}{A_{drip}})^{1/2}\mu_{e_{drip}}[MeV]^{1/2}\end{aligned} \tag{4.4.3}$$

- ***Presence of magnetic field***

Respectively, using Eqs. 2.4.1, 2.4.2 and 4.1.31 and the definition of sound speed, for strongly quantizing field:

$$\begin{aligned}\frac{\tilde{c}_s}{c} &\approx \frac{2^{1/2}\pi(m_e c^2)^{1/2}\lambda\!\!\!^{-}_e{}^{3/2}}{m_n c^2}(\frac{Z}{A})\frac{\tilde{\epsilon}^{1/2}}{B_\star^{1/2}} \\ &\simeq 25.6506(\frac{Z}{A})\frac{\tilde{\epsilon}[MeV fm^{-3}]^{1/2}}{B_\star^{1/2}}\end{aligned} \tag{4.4.4}$$

And, at neutron-drip transition, from Eq. 4.2.9, the speed of sound is:

$$\begin{aligned}\frac{\tilde{c}_{s_{drip}}}{c} &\approx (\frac{Z_{drip}\mu_{e_{drip}}}{A_{drip} m_n c^2})^{1/2} \\ &\simeq 0.03262(\frac{Z_{drip}}{A_{drip}})^{1/2}\mu_{e_{drip}}[MeV]^{1/2}\end{aligned} \tag{4.4.5}$$

From the above relation, the $\tilde{c}_{s_{drip}}$ is independent of the magnetic field strength.

The ratio of $c_{s_{drip}}/c$ to $\tilde{c}_{s_{drip}}/c$, using Eqs. 4.4.3 and 4.4.5, is:

$$\frac{c_{s_{drip}}/c}{\tilde{c}_{s_{drip}}/c} = 3^{-1/2} \approx 0.577 \tag{4.4.6}$$

So, for strongly quantizing field the speed of sound, at neutron-drip point, is greater than the respective speed for the field-free case.

4.5 Elastic moduli

The elastic properties of the solid outer crust are described within the framework of Newtonian approximation at T=0K, according to Ref. [3].

At the equilibrium, the positions of the nuclei (i.e., the lattice sites) are denoted by the vectors $\vec{r}$. But, during a deformation, there is a displacement, $\vec{u}(\vec{r})$, from the equilibrium, so the new position of the nuclei is, $\vec{r}' = \vec{r} + \vec{u}(\vec{r})$. A small deformation is described by the strain tensor, u_{ik}, which is:

$$u_{ik} = \frac{1}{2}(\frac{\partial u_i}{\partial x_k} + \frac{\partial u_k}{\partial x_i}) \tag{4.5.1}$$

where $i, k = 1, 2, 3$. The deformation can be decomposed into two components, the compression and the shear part:

$$u_{ik} = u_{ik}^{compr} + u_{ik}^{shear} \tag{4.5.2}$$

The deformation energy, ϵ_{def}, is written:

$$\epsilon_{def} = \frac{1}{2}\lambda_{iklm} u_{ik} u_{lm} \tag{4.5.3}$$

and the stress tensor, σ_{ik}, is:

$$\sigma_{ik} = \frac{\partial \epsilon_{def}}{\partial u_{ik}} \tag{4.5.4}$$

The tensor λ_{iklm} has 81 components, however, because of symmetry, only 21 are independent and are called elastic moduli. With the existence of more symmetries the number of elastic moduli decreases even more. For example, in a cubic crystal, there are three moduli and in an isotropic solid only two moduli.

For simplicity, the crust is considered as an isotropic solid (a bcc lattice polycrystal). The two elastic moduli are the *compression modulus*, K_{mod}, and the *effective shear modulus*, S_{mod}. For a pure uniform compression (does not affect the shape), the K_{mod} is given by [3]:

$$K_{mod} = n_b \frac{\partial P}{\partial n_b} = \Gamma \cdot P \tag{4.5.5}$$

where Γ is the adiabatic index, from Eq. 4.3.1. And, for a pure shear deformation (keeps the volume constant), the S_{mod} is [3]:

$$S_{mod} = 0.1194 \frac{n_N Z^2 e^2}{r_{cell}} \tag{4.5.6}$$

where the n_N and r_{cell} are given by Eqs. 2.4.2 and 3.1.12, respectively.

K_{mod} - Approximations at high densities (i.e., $x_e >> 1$ and $P \approx P_e$)

- ***Absence of magnetic field***

Using Eqs. 4.3.2, 4.1.16 and 2.4.2, the K_{mod} is approximately:

$$\begin{aligned} K_{mod} &\approx (\frac{\pi}{3})^{2/3} m_e c^2 \lambda\!\!\!^{-}_e (\frac{Z}{A})^{4/3} n_b^{4/3} \\ &\simeq 203.488 (\frac{Z}{A})^{4/3} n_b [fm^{-3}]^{4/3} MeV/fm^3 \end{aligned} \tag{4.5.7}$$

And, at neutron-drip transition, from Eq. 4.2.7, the compression modulus is:

$$\begin{aligned} K_{mod,drip} &\approx \frac{\mu_{e_{drip}}^4}{9\pi^2 \lambda\!\!\!^{-}_e{}^3 (m_e c^2)^3} \\ &\simeq 1.4652 \cdot 10^{-9} \mu_{e_{drip}} [MeV]^4 MeV/fm^3 \end{aligned} \tag{4.5.8}$$

- ***Presence of magnetic field***

Respectively, using Eqs. 4.3.3, 4.1.31 and 2.4.2, the $\tilde{K}_{mod}$, for strongly quantizing field, is:

$$\begin{aligned} \tilde{K}_{mod} &\approx \frac{2\pi^2 m_e c^2 \lambda\!\!\!^{-}_e{}^3}{B_\star} (\frac{Z}{A})^2 \tilde{n}_b^2 \\ &\simeq 5.8083 \cdot 10^8 (\frac{Z}{A})^2 \frac{\tilde{n}_b [fm^{-3}]^2}{B_\star} MeV/fm^3 \end{aligned} \tag{4.5.9}$$

And, at neutron-drip transition, from Eq. 4.2.9, the compression modulus is:

$$\begin{aligned} \tilde{K}_{mod,drip} &\approx \frac{\mu_{e_{drip}}^2 B_\star}{2\pi^2 \lambda\!\!\!^{-}_e{}^3 m_e c^2} \\ &\simeq 1.7217 \cdot 10^{-9} B_\star \mu_{e_{drip}} [MeV]^2 MeV/fm^3 \end{aligned} \tag{4.5.10}$$

The ratio of $K_{mod,drip}$ to $\tilde{K}_{mod,drip}$, using Eqs. 4.5.8 and 4.5.10, is:

$$\begin{aligned} \frac{K_{mod,drip}}{\tilde{K}_{mod,drip}} &= \frac{2\mu_{e_{drip}}^2}{9(m_e c^2)^2 B_\star} \\ &\simeq 0.8510 \frac{\mu_{e_{drip}} [MeV]^2}{B_\star} \end{aligned} \tag{4.5.11}$$

But, from Eq. 4.2.10, the following inequality holds:

$$\frac{K_{mod,drip}}{\tilde{K}_{mod,drip}} < \frac{4}{9} \approx 0.44 \tag{4.5.12}$$

S_{mod} - Approximations at high densities (i.e., $x_e >> 1$ and $P \approx P_e$)

- ***Absence of magnetic field***

Using Eqs. 2.4.2 and 3.1.12, the S_{mod} is approximately:

$$\begin{aligned} S_{mod} &\approx 0.1194 \cdot (\frac{4\pi}{3})^{1/3} \alpha \lambda\!\!\!^{-}_e m_e c^2 \frac{Z^2}{A^{4/3}} n_b^{4/3} \\ &\simeq 0.2772 \frac{Z^2}{A^{4/3}} n_b [fm^{-3}]^{4/3} MeV/fm^3 \end{aligned} \tag{4.5.13}$$

And, at neutron-drip transition, from Eq. 4.2.7, the effective shear modulus is:

$$\begin{aligned} S_{mod,drip} &\approx \frac{0.1194 \cdot 4^{1/3}}{3^{5/3}\pi^{7/3}} \alpha Z_{drip}^{2/3} \frac{\mu_{e_{drip}}^4}{\lambda\!\!\!^{-}_e{}^3 (m_e c^2)^3} \\ &\simeq 1.9956 \cdot 10^{-12} Z_{drip}^{2/3} \mu_{e_{drip}} [MeV]^4 MeV/fm^3 \end{aligned} \tag{4.5.14}$$

- ***Presence of magnetic field***

The $\tilde{S}_{mod}$ is given by Eq. 4.5.13 and, at neutron-drip transition, the $\tilde{S}_{mod,drip}$, from Eq. 4.2.9, is:

$$\begin{aligned} \tilde{S}_{mod,drip} &\approx \frac{0.1194}{3^{1/3} \cdot 2^{2/3} \cdot \pi^{7/3}} \alpha Z_{drip}^{2/3} \frac{\mu_{e_{drip}}^{4/3} B_\star^{4/3}}{\lambda\!\!\!^{-}_e{}^3 (m_e c^2)^{1/3}} \\ &\simeq 5.719 \cdot 10^{-13} Z_{drip}^{2/3} B_\star^{4/3} \mu_{e_{drip}} [MeV]^{4/3} MeV/fm^3 \end{aligned} \tag{4.5.15}$$

The ratio of $S_{mod,drip}$ to $\tilde{S}_{mod,drip}$, using Eqs. 4.5.14 and 4.5.15, is:

$$\begin{aligned} \frac{S_{mod,drip}}{\tilde{S}_{mod,drip}} &= [\frac{2\mu_{e_{drip}}^2}{3B_\star (m_e c^2)^2}]^{4/3} \\ &\simeq 3.4895 \cdot \frac{\mu_{e_{drip}} [MeV]^{8/3}}{B_\star^{4/3}} \end{aligned} \tag{4.5.16}$$

But, from Eq. 4.2.10, the following inequality holds:

$$\frac{S_{mod,drip}}{\tilde{S}_{mod,drip}} < (\frac{4}{3})^{4/3} \approx 1.47 \tag{4.5.17}$$

$\frac{S_{mod}}{K_{mod}}$ - Approximations at high densities (i.e., $x_e >> 1$ and $P \approx P_e$)

The compression modulus and the effective shear modulus have the same units, MeV/fm^3, and it is useful to calculate the ratio $\frac{S_{mod}}{K_{mod}}$ to see if the

outer crust is more susceptible to compression deformation or to shear deformation, because a high elastic modulus means that a material is very stiff or rigid and it does not deform much when a stress is applied to it.

- ***Absence of magnetic field***

Using Eqs. 4.5.7 and 4.5.13, the $\frac{S_{mod}}{K_{mod}}$ is approximately:

$$\begin{aligned}\frac{S_{mod}}{K_{mod}} &\approx 0.1194 \cdot 2^{2/3} \cdot 3^{1/3}\pi^{-1/3}\alpha Z^{2/3} \\ &\simeq 1.3620 \cdot 10^{-3} Z^{2/3}\end{aligned} \tag{4.5.18}$$

and the respective ratio, at neutron-drip transition, is obviously:

$$\begin{aligned}\frac{S_{mod,drip}}{K_{mod,drip}} &\approx 0.1194 \cdot 2^{2/3} \cdot 3^{1/3}\pi^{-1/3}\alpha Z_{drip}^{2/3} \\ &\simeq 1.3620 \cdot 10^{-3} Z_{drip}^{2/3}\end{aligned} \tag{4.5.19}$$

- ***Presence of magnetic field***

Respectively, using Eqs. 4.5.9 and 4.5.13, the $\frac{\tilde{S}_{mod}}{\tilde{K}_{mod}}$, for strongly quantizing field, is:

$$\begin{aligned}\frac{\tilde{S}_{mod}}{\tilde{K}_{mod}} &\approx \frac{0.1194 \cdot \alpha}{2^{1/3} \cdot 3^{1/3}\pi^{5/3}\lambda\!\!\!^{-}_{e}^{2}} \cdot \frac{B_\star A^{2/3}}{\tilde{n}_b^{2/3}} \\ &\simeq 4.7717 \cdot 10^{-10} \frac{B_\star A^{2/3}}{\tilde{n}_b[fm^{-3}]^{2/3}}\end{aligned} \tag{4.5.20}$$

And, at neutron-drip transition, from Eq. 4.2.9, the ratio is:

$$\begin{aligned}\frac{\tilde{S}_{mod,drip}}{\tilde{K}_{mod,drip}} &\approx \frac{0.1194 \cdot 2^{1/3} \cdot \alpha (m_e c^2)^{2/3}}{(3\pi)^{1/3}} \cdot \frac{B_\star^{1/3} Z_{drip}^{2/3}}{\mu_{e_{drip}}^{2/3}} \\ &\simeq 3.3218 \cdot 10^{-4} \frac{B_\star^{1/3} Z_{drip}^{2/3}}{\mu_{e_{drip}}[MeV]^{2/3}}\end{aligned} \tag{4.5.21}$$

The ratio of $\frac{S_{mod,drip}}{K_{mod,drip}}$ to $\frac{\tilde{S}_{mod,drip}}{\tilde{K}_{mod,drip}}$, using Eqs. 4.5.19 and 4.5.21, is:

$$\begin{aligned}\frac{S_{mod,drip}/K_{mod,drip}}{\tilde{S}_{mod,drip}/\tilde{K}_{mod,drip}} &= [\frac{18\mu_{e_{drip}}^2}{(m_e c^2)^2 B_\star}]^{1/3} \\ &\simeq 4.1003 \cdot \frac{\mu_{e_{drip}}[MeV]^{2/3}}{B_\star^{1/3}}\end{aligned} \tag{4.5.22}$$

But, from Eq. 4.2.10, the following inequality holds:

$$\frac{S_{mod,drip}/K_{mod,drip}}{\tilde{S}_{mod,drip}/\tilde{K}_{mod,drip}} < (36)^{1/3} \approx 3.30 \tag{4.5.23}$$

4.6 Mass and Thickness

Traditionally, the numerical solution of TOV equations (see, Eq. 2.1.5), proceeds by integrating from the center up to the stellar surface. But, in this work, only the outer crust is examined, so the TOV equations are integrated inward from the surface, where $P = 0$, down to the bottom of the outer crust (i.e., the neutron-drip transition), without any assumptions for the deeper layers of the neutron star. The initial conditions, which incorporate the unknown deeper layers, are the gravitational mass, M, and the radius, R, of the star (i.e., $P(r = R) \approx 0$ and $m(r = R) = M$), making the assumption that the outer crust is the outermost layer of the star (i.e., absence of ocean and atmosphere).

The radius, r_{drip}, where the numerical integration terminates, is defined by the condition:

$$P(r_{drip}) = P_{drip}, \tag{4.6.1}$$

corresponding to a mass M_{drip}. So, the mass of outer crust, M_{cr}, is:

$$M_{cr} = M - M_{drip} \tag{4.6.2}$$

and the coordinate thickness, ΔR_{cr}, is:

$$\Delta R_{cr} = R - r_{drip} \tag{4.6.3}$$

These give a fractional mass, M_{cr}/M, and a fractional coordinate thickness, $\Delta R_{cr}/R$.

With the TOV equations solved, the functions $\epsilon(r)$ and $m(r)$ are now known, so the baryonic mass, $M_{b_{cr}}$, and the proper thickness, z_{drip}, of outer crust, can be numerically computed by (see, Eqs. 2.1.9 and 2.1.15):

$$M_{b_{cr}} = 4\pi \int_{r_{drip}}^{R} r^2 \Phi(r) \epsilon(r)/c^2 dr \tag{4.6.4}$$

$$z_{drip} = \int_{r_{drip}}^{R} \Phi(r) dr \tag{4.6.5}$$

Also, the relative fraction of mass of outer crust due to the gravitational binding energy, Δ_{grav}, is given by (see, Eq. 2.1.12):

$$\Delta_{grav} = \frac{M_{b_{cr}} - M_{cr}}{M_{cr}} \tag{4.6.6}$$

and the total number of baryons of outer crust, ΔN, from Eqs. 2.1.13 and 2.4.1, is:

$$\Delta N = \frac{M_{b_{cr}}}{m_n} \tag{4.6.7}$$

Furthermore, for each crustal layer, knowing the minimum energy density, ϵ_{min}, and the maximum energy density, ϵ_{max}, easily the corresponding radii r_{min} and r_{max} can be calculated through interpolation. Thus, for a layer, are calculated:
1) the coordinate thickness, $\Delta R_l = r_{max} - r_{min}$,
2) the fractional coordinate thickness, $\Delta R_l/\Delta R_{cr}$,
3) the proper depth, $z_l = \int_{r_{min}}^{R} \Phi(r)dr$,
4) the fractional proper depth, z_l/z_{drip},
5) the baryonic mass, $M_{b_l} = 4\pi \int_{r_{min}}^{r_{max}} r^2\Phi(r)\epsilon(r)/c^2 dr$,
6) the fractional baryonic mass, $M_{b_l}/M_{b_{cr}}$,
7) the mass, $M_l = m(r = r_{max}) - m(r = r_{min})$,
8) the fractional mass, M_l/M_{cr},
9) the number of baryons, $\Delta N_l = M_{b_l}/m_n$, and
10) the fractional number of baryons, $\Delta N_l/\Delta N$.

It is noted that the fractional number of baryons, $\Delta N_l/\Delta N$, corresponds to the *abundance* of each nuclide in outer crust. According to Ref. [18], the abundances provide the initial conditions for the rapid neutron-capture process (r-process nucleosynthesis), which explains the production of stable and some long-lived radioactive neutron-rich nuclides that are heavier than iron and observed in the solar system. For an initially cold outer crust, after the decompression the distribution of nuclear abundances is far from the distribution of the solar system, but appears as a potential site for producing the $115 \lesssim A \lesssim 124$ r-nuclei, as shown in Fig. 4.1, whereas for an initially outer crust at $T \sim 10^{10}K$, there is a much better agreement with the solar distribution.

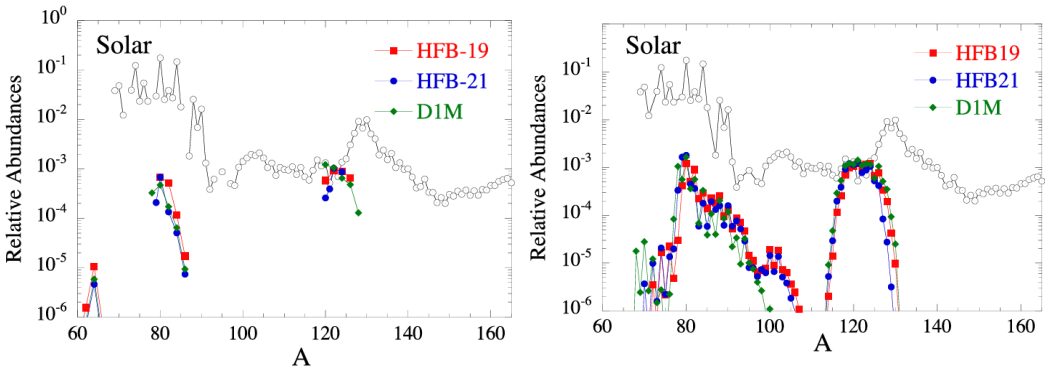

(a) (b)

Figure 4.1: Application of the knowledge of nuclei abundances in initially cold outer crust, (a) normalized abundance distributions to the solar system r-abundance distribution before the decompression and (b) after the decompression. Taken from Ref. [18]

Approximations for mass and thickness of outer crust

Within the light and thin crust approximation [8], the mass and the thickness of outer crust are very small, comparing with the total mass and the radius of the star, respectively (i.e., $M_{cr}/M << 1$ and $\Delta R_{cr}/R << 1$). For the TOV equations, one may assume that $m \approx M$, $\frac{P}{\epsilon} << 1$, $\frac{4\pi r^3 P}{Mc^2} << 1$, and, also, $dz \approx -(1-\frac{r_g}{R})^{-1/2}dr$, where r_g is the Schwarzschild radius, given by Eq. 2.1.2. Then, TOV equations (see, Eq. 2.1.5) are written:

$$\begin{cases} \frac{dm}{dz} = -4\pi G M g_s^{-1} \frac{\epsilon}{c^2} \\ \frac{dP}{dz} = g_s \frac{\epsilon}{c^2} \end{cases} \tag{4.6.8}$$

where

$$g_s = \frac{GM}{R^2\sqrt{1-\frac{r_g}{R}}} \tag{4.6.9}$$

is the surface gravity.
From Eq. 4.6.8:

$$\begin{cases} dm = -4\pi G M g_s^{-2} dP \\ \Rightarrow M - m = 4\pi G M g_s^{-2} P, \ for\ P = 0: \ m = M \end{cases} \tag{4.6.10}$$

So, at neutron-drip point, where $P = P_{drip}$ and $m = M_{drip}$, using Eq. 4.6.2, the M_{cr} is approximately:

$$M_{cr} \approx 4\pi G M g_s^{-2} P_{drip} = \frac{8\pi P_{drip} R^3}{c^2}(\frac{R}{r_g} - 1) \tag{4.6.11}$$

In addition, the baryonic mass of outer crust is approximately:

$$M_{b_{cr}} \approx (1 - \frac{r_g}{R})^{-1/2} M_{cr} \tag{4.6.12}$$

and because $r_g < R$, the baryonic mass is greater by a factor of $(1 - \frac{r_g}{R})^{-1/2}$.

- ***Absence of magnetic field***

Using Eqs. 4.6.11 and 4.2.6, the mass of outer crust, in the absence of magnetic field, is:

$$M_{cr} \approx \frac{2\mu_{e_{drip}}^4 R^3}{3\pi c^2 \lambda\!\!\!^{-}_e{}^3 (m_e c^2)^3} (\frac{R}{r_g} - 1) \tag{4.6.13}$$

- ***Presence of magnetic field***

While, using Eqs. 4.6.11 and 4.2.8, the mass of outer crust, in the presence of strongly quantizing magnetic field, is:

$$\tilde{M}_{cr} \approx \frac{2\mu_{e_{drip}}^2 B_\star R^3}{\pi c^2 \lambda\!\!\!^{-}_e{}^3 m_e c^2} (\frac{R}{r_g} - 1) \tag{4.6.14}$$

The ratio of M_{cr} to $\tilde{M}_{cr}$, using Eqs. 4.6.13 and 4.6.14 and for the same M and R, is:

$$\begin{aligned} \frac{M_{cr}}{\tilde{M}_{cr}} &= \frac{\mu_{e_{drip}}^2}{3(m_e c^2)^2 B_\star} \\ &\simeq 1.2766 \frac{\mu_{e_{drip}} [MeV]^2}{B_\star} \end{aligned} \tag{4.6.15}$$

But, from Eq. 4.2.10, the following inequality holds:

$$\frac{M_{cr}}{\tilde{M}_{cr}} < \frac{2}{3} \approx 0.67 \tag{4.6.16}$$

Now, assuming that the main contribution to EoS is from ultra-relativistic electrons (i.e., $P \approx P_e$) [11], an approximate expression for the proper depth, z_{drip}, can be obtained.

- ***Absence of magnetic field***

From Eqs. 2.4.1, 2.4.2 and 4.1.16, the pressure is expressed as:

$$P \approx P_e \approx \mathcal{C} \epsilon^{4/3}, \tag{4.6.17}$$

with $\mathcal{C} = \frac{3^{1/3} \pi^{2/3} m_e c^2 \lambda\!\!\!^{-}_e Z^{4/3}}{4 (m_n c^2)^{4/3} A^{4/3}}$. So, from the second relation of Eq. 4.6.8,

$$\begin{cases} \frac{4}{3} \mathcal{C} \epsilon^{1/3} d\epsilon = \frac{g_s}{c^2} \epsilon dz \\ \Rightarrow 4 \mathcal{C} \epsilon^{1/3} = g_s z / c^2, \ for \ z = 0: \ \epsilon \approx 0 \\ \Rightarrow 4 \frac{P}{\epsilon} = g_s z / c^2 \end{cases} \tag{4.6.18}$$

Thus, at the neutron-drip transition, where $P = P_{drip}$ and $\epsilon = \epsilon_{drip}$, the z_{drip} is given by:

$$z_{drip} \approx \frac{4P_{drip}c^2}{\epsilon_{drip}g_s} = \frac{8P_{drip}R}{\epsilon_{drip}}\sqrt{\frac{R}{r_g}(\frac{R}{r_g}-1)} \tag{4.6.19}$$

or, using the Eqs. 2.4.1, 4.2.6 and 4.2.7:

$$z_{drip} \approx \frac{2Z_{drip}\mu_{e_{drip}}R}{A_{drip}m_nc^2}\sqrt{\frac{R}{r_g}(\frac{R}{r_g}-1)} \tag{4.6.20}$$

- ***Presence of magnetic field***

Respectively, in the presence of strongly quantizing magnetic field, from Eqs. 2.4.1, 2.4.2 and 4.1.31, the pressure is expressed as:

$$\tilde{P} \approx \tilde{P}_e \approx \tilde{\mathcal{C}}\tilde{\epsilon}^2, \tag{4.6.21}$$

with $\tilde{\mathcal{C}} = \frac{\pi^2 m_e c^2 \lambda\!\!\!^{-3}_e Z^2}{B_\star (m_n c^2)^2 A^2}$. So, from the second relation of Eq. 4.6.8,

$$\begin{cases} 2\tilde{\mathcal{C}}\tilde{\epsilon}d\tilde{\epsilon} = \frac{g_s}{c^2}\tilde{\epsilon}d\tilde{z} \\ \Rightarrow 2\tilde{\mathcal{C}}\tilde{\epsilon} = g_s\tilde{z}/c^2, \ for\ \tilde{z}=0: \ \tilde{\epsilon}\approx 0 \\ \Rightarrow 2\frac{\tilde{P}}{\tilde{\epsilon}} = g_s\tilde{z}/c^2 \end{cases} \tag{4.6.22}$$

And, at the neutron-drip transition, where $\tilde{P} = \tilde{P}_{drip}$ and $\tilde{\epsilon} = \tilde{\epsilon}_{drip}$, the $\tilde{z}_{drip}$ is given by:

$$\tilde{z}_{drip} \approx \frac{2\tilde{P}_{drip}c^2}{\tilde{\epsilon}_{drip}g_s} = \frac{4\tilde{P}_{drip}R}{\tilde{\epsilon}_{drip}}\sqrt{\frac{R}{r_g}(\frac{R}{r_g}-1)} \tag{4.6.23}$$

or, using the Eqs. 2.4.1, 4.2.8 and 4.2.9:

$$\tilde{z}_{drip} \approx \frac{2Z_{drip}\mu_{e_{drip}}R}{A_{drip}m_nc^2}\sqrt{\frac{R}{r_g}(\frac{R}{r_g}-1)} \tag{4.6.24}$$

Comparing the Eqs. 4.6.20 and 4.6.24, the proper depth does not depend on the magnetic field strength,

$$z_{drip} = \tilde{z}_{drip}, \tag{4.6.25}$$

for the same M and R.

Chapter 5

Results - Discussion

5.1 Used experimental nuclear masses

In this work, the results of the atomic mass evaluation **AME2020** [19, 20] are used, and, more specifically, the tabulated atomic mass excesses, available on the website [21]. Totally, there are 3558 masses for the ground state, from which 2550 values are derived from experimental results (i.e., experimental masses) and the rest 1008 values are estimated, based on the trends from the mass surface (TMS) , which is a method to obtain unknown, poorly known, or questionable masses by extrapolation from the well-known values in the neighborhood (i.e., estimated masses). It is noted that, here, only the experimental masses were used.

Among the 2550 experimental masses, 122 nuclides have precision better than 0.1keV, 402 better than 1keV, 1532 better than 10keV, 2407 better than 100keV, and 143 have uncertainties $\geq$ 100keV. In comparison with AME2016, the mass precision has been improved for 427 nuclides and masses of 74 nuclides, which were experimentally unknown, are measured and included [19].

5.2 Used nuclear mass models

The experimental atomic mass data from AME2020 are supplemented with masses evaluated using a nuclear mass model, for experimentally unknown values. Here, nine different models are used, which are the **Semi-Empirical Mass Formula of Bethe and Weizsäcker** (hereafter SEMF), and other more sophisticated models, which are macro-micro models taking into account microscopic effects and others, which based on Density Functional

Theory (DFT), either relativistic or non-relativistic. These models are: the $\boldsymbol{FRDM(2012)}$, the $\boldsymbol{WS4^{RBF}}$, the $\boldsymbol{BSkG3}$, the $\boldsymbol{HFB-31}$, the $\boldsymbol{DD-ME\delta}$ (hereafter DDMED), the $\boldsymbol{DD-PC1}$, the $\boldsymbol{SV-min}$ (hereafter SVMIV), and the $\boldsymbol{UNEDF0}$.

According to SEMF model, the nucleus is considered as an incompressible droplet and all nuclei have the same density, but this model cannot describe any microscopic effect, such as shell effects and effects from the deformation of nuclei. And it gives the binding energy of nuclei, better for medium and heavy nuclei than light nuclei. The nuclear binding energy[1], $BE_N(A,Z)$, is given by the Bethe - Weizsäcker mass formula:

$$BE_N(A,Z) = a_v A - a_s A^{2/3} - a_C \frac{Z(Z-1)}{A^{1/3}} - a_{sym}\frac{(A-2Z)^2}{A} + \delta \quad (5.2.1)$$

with

$$\delta = \begin{cases} a_p A^{-1/2}, \ for\ even\ Z - even\ N \\ -a_p A^{-1/2}, \ for\ odd\ Z - odd\ N \\ 0, \ for\ odd\ A \end{cases} \quad (5.2.2)$$

where the A is the mass number, Z the atomic number, N the neutron number, and the coefficients a_v, a_s, a_C, a_{sym} and a_p are, respectively, the volume, surface, Coulomb, asymmetry and pairing energy term, which are determined by least square fitting to observed mass excesses, minimizing either the mean square deviation, $\sigma^2 = \frac{1}{N}\sum_i^N(\Delta M_{at,th} - \Delta M_{at,exp})^2$ or the $\chi^2/N = \frac{1}{N}\sum_i^N[\frac{\Delta M_{at,th}-\Delta M_{at,exp}}{\Delta M_{at,exp}}]^2$ where N is the number of data points, $\Delta M_{at,th}$ the theoretical atomic mass excess and $\Delta M_{at,exp}$ the experimental atomic mass excess. χ^2/N is a measure of relative error, while σ^2 a measure of absolute error, but they cannot be minimized simultaneously [22]. In this work, the values of energy coefficients (i.e., a_v, a_s, a_C, a_{sym} and a_p) are taken from the χ^2/N minimization, using only the 2228 experimental masses from AME2003, and their values in MeV are [22]:

$$\begin{cases} a_v = 15.777 \\ a_s = 18.341 \\ a_C = 0.710 \\ a_{sym} = 23.211 \\ a_p = 11.996 \end{cases} \quad (5.2.3)$$

The nuclei can be either bound or unbound, so the limits of nuclear chart (i.e., considering bound nuclei) define the nucleon drip lines, where there is

[1] as a positive number

no longer enough binding energy to prevent the last nucleons from escaping the nucleus. For this reason, apart from $BE_N > 0$, the four quantities: one-proton separation energy, S_p, the one-neutron separation energy, S_n, the two-proton separation energy, S_{2p}, and the two-neutron separation energy, S_{2n}, defined as:

$$\begin{cases} S_p = BE_N(A,Z) - BE_N(A-1,Z-1) \\ S_n = BE_N(A,Z) - BE_N(A-1,Z) \\ S_{2p} = BE_N(A,Z) - BE_N(A-2,Z-2) \\ S_{2n} = BE_N(A,Z) - BE_N(A-2,Z) \end{cases} \tag{5.2.4}$$

must be positive.

The FRDM2012 mass model [23] gives the atomic mass excesses of 9318 nuclei ranging from ^{16}O to A=339. It is a macro-micro model, based on the finite-range droplet macroscopic and the folded-Yukawa single-particle microscopic nuclear structure models. The mass table, which contains atomic mass excesses, was taken from [24].

The WS4 model [25], includes the nuclear surface diffuseness effect in Weizsäcker-Skyrme (WS) formula, which is a macro-micro mass formula where the axially deformed Woods-Saxon potential, as a phenomenological mean-field, is adopted to obtain the single-particle levels of nuclei. The combination of WS4 with radial basis function (RBF) improves the accuracy of the mass formula, as shown in Table 5.1. The WS4RBF mass table, which contains atomic mass excesses, was taken from [26].

The BSKG3 model [27] is the latest entry in the Brussels-Skyrme-on-a-grid series of large-scale models of nuclear structure based on an energy density functional of Skyrme type and has the best mass accuracy among the $BSkG1$ and $BSkG2$ models. The HFB31 model [28] belongs to the family of the three Hartree-Fock-Bogoliubov (HFB) mass models: $HFB-30$, $HFB-31$, $HFB-32$, along with their underlying Skyrme type interactions BSk30, BSk31 and BSk32, respectively, where the HFB31 has the lowest mass error. The BSKG3 and HFB31 mass tables, which contain atomic mass excesses, were taken from [29].

The DDMED [30] and DDPC1 [31] mass models come from covariant energy density functionals. Covariant density functional models can be divided into three groups: a) the nonlinear meson-nucleon coupling models (e.g., NL3*), b) the density dependent meson exchange models (e.g., DDMED)

and c) the density dependent point coupling models (e.g., DDPC1). The main differences between them are the range of the interaction and the density dependence. DDMED has finite range interaction determined by the mass of mesons (Yukawa type), while DDPC1 has δ-forces (0th order expansion of meson propagator). Both DDMED and DDPC1 have explicit density dependence of coupling constants [32]. The SVMIN [33] and UNEDF0 [34] models are based on Skyrme type energy density functionals. The DDMED and DDPC1 mass tables [32, 35, 36] and the respective of SVMIN and UNEDF0 models [37],which contain the binding energy of even-even nuclei, were taken from [38].

Table 5.1: For each model are listed the rms deviation between experimental data and predictions in MeV (the intrinsic model error in MeV given in parentheses) and, for infinite nuclear matter at saturation, the energy per particle a_V in MeV and the symmetry energy J in MeV

model	**rms deviation (model error)**	$\boldsymbol{a_V}$	$\boldsymbol{J}$
SEMF[2]	3.426 (-)	-15.41	22.44
FRDM2012	- (0.5595)	-16.19	32.30
WS4	0.298 (-)	-15.52	30.16
WS4RBF	0.170 (-)	-	-
BSKG3	0.631 (0.627)	-16.08	31.00
HFB31	0.571 (0.561)	-16.11	31.00
DDMED	2.29 (-)	-16.12	32.35
DDPC1	2.01 (-)	-16.06	33.00
SVMIN	0.62 (-)	-15.91	30.66
UNEDF0	1.45 (-)	-16.06	30.54

It is noted that the ideal case would be if all models used the same experimental data for parameter adjustment, but such mass tables were not available. For example, the SEMF model uses 2228 experimentally measured nuclei from AME2003 [22], the FRDM2012 2149 experimentally measured nuclei with $Z \geq 8$ and $N \geq 8$ from AME2003 [23], the WS4/WS4RBF 2353 experimentally measured nuclei with $Z \geq 8$ and $N \geq 8$ from AME2012 [25], the BSKG3 2457 experimentally measured nuclei with $Z \geq 8$ and $N \geq 8$ from AME2020 [27] and the HFB31 2353 experimentally measured nuclei with $Z \geq 8$ and $N \geq 8$ from AME2012 [28].

[2]for SEMF model are listed the values, for the minimization of the mean square deviation (σ^2), using only the experimentally measured masses, considering the coefficient a_{sym} as the J (see, Ref. [22])

The root mean square deviation (σ), between theoretically calculated values and experimental values, in which both theoretical and experimental errors contribute (i.e., overestimates the intrinsic model error), and the model error (see, Ref. [23]), if it is available, are listed in Table[3] 5.1 . Generally, the error is not uniform over all mass range, and predictions are very divergent for the lighter nuclei and for heavy neutron-rich nuclei. Also, for infinite nuclear matter, the energy per particle of symmetric matter at saturation, a_V, and the symmetry energy, J, are listed in the same Table.

5.3 Computational details

For the computational procedure (see, Appendix J), the region of interest[4] for the nuclei was restricted in the values: $24 \leq Z \leq 56$, for the number of protons and $24 \leq N \leq 132$, for the number of neutrons. Those limits in Z and N were imposed to reduce the computation time and the choice was based on previous results of similar works (see, e.g., Refs. [9, 10, 11, 12, 13, 14]) for the equilibrium nuclei present in outer crust, keeping in mind that nuclei with magic numbers[5] (2, 8, 20, 28, 50, 82, 126, ...) for protons or neutrons, are expected to appear. So, the values N=28, 50, 82, 126 and Z=28, 50 were included, extending the upper limits of these values to $Z_{max} = 56$ and $N_{max} = 132$ to be less biased decision. While, for the lower limits, having in the mind that ^{56}Fe (Z=26, N=30) is the equilibrium nucleus on the surface of outer crust, it was reasonable to choose $Z_{min} = 24$ and $N_{min} = 24$, to be again less biased, including also the magic number 28. As mentioned earlier, extrapolated nuclear masses from models were only used if experimental values in the above region of interest were not available.

Then, for the minimization process to find the optimal nucleus for each pressure, a pressure grid of 18000 values, evenly spaced on a logarithmic scale, was used, from $P_{min} = 6.082 \cdot 10^{-15}\ MeV/fm^3$, which coincides with the value in Ref. [9], to $P_{max} = 20.0 \cdot 10^{-4}\ MeV/fm^3$, having the upper pressure limit greater than the neutron-drip pressure ($P_{max} > P_{drip}$), keeping in mind, the neutron-drip pressure increases with the magnetic field strength, $B_\star$.

[3] for the models SEMF, FRDM2012, WS4/WS4RBF, BSKG3 and HFB31 errors concern the atomic mass excess, while for DDMED, DDPC1, SVMIV and UNEDF0 errors concern the binding energy for even-even nuclei

[4] in Ref. [9] only 130 nuclei were used in minimization and they were all even-even

[5] are particularly stable compared to nuclei in the neighborhood of nuclear chart, because of the shell effects

Finally, the Runge-Kutta 4th order method (RK4) was applied to solve the TOV equations, where for a system of two coupled ordinary differential equations given by:

$$\frac{dy_i(x)}{dx} = f_i(x, y_1, y_2) \tag{5.3.1}$$

where $i = 1, 2$ with initial conditions $y_i(x_0) = y_{i0}$, can be numerically solved by the following steps:

$$\begin{cases} y_{i,n+1} = y_{i,n} + \frac{1}{6}(k_i + 2s_i + 2l_i + p_i) \\ x_{n+1} = x_n + h \end{cases} \tag{5.3.2}$$

where

$$\begin{cases} k_i = hf_i(x_n, y_{1,n}, y_{2,n}) \\ s_i = hf_i(x_n + h/2, y_{1,n} + k_1/2, y_{2,n} + k_2/2) \\ l_i = hf_i(x_n + h/2, y_{1,n} + s_1/2, y_{2,n} + s_2/2) \\ p_i = hf_i(x_n + h, y_{1,n} + l_1, y_{2,n} + l_2) \end{cases} \tag{5.3.3}$$

and $n = 0, 1, 2, ...$, given a step size h. In our case $y_1 = m(r)$, $y_2 = P(r)$ and $h = -2 \cdot 10^{-6}\ km$.

5.4 Comparison: SEMF vs FRDM2012

The aim is twofold, firstly, to determine the properties of outer crust, which were discussed in Chapter 4, for different magnetic field strengths, more specifically, $B_\star = 0$ (i.e., the field-free case), $B_\star = 1500$ (or $B = 6.62 \cdot 10^{16} G$), $B_\star = 2000$ (or $B = 8.83 \cdot 10^{16} G$) and $B_\star = 2500$ (or $B = 1.10 \cdot 10^{17} G$). Secondly, to conclude if there is any model dependency on those properties, for this reason, nine different models used (see, Section 5.2). The data (e.g., mass tables), the code (see, Appendices J and K) and the results (e.g., tabulated EoS) of this work are publicly available online via GitHub[6].

5.4.1 Layers properties for $B_\star = 0$

Using[7] the SEMF and FRDM2012 for $B_\star = 0$, at the top layers of outer crust, where the density is low, the composition is well established, because the masses are experimentally known (i.e., come from AME2020) and the

[6] https://github.com/johnmavr/master-thesis

[7] the composition and the results from TOV equations, for the other models and magnetic field strengths, are presented in Appendices A, B, C and D

primary contribution is from Fe and Ni isotopes[8], as shown in Tables 5.2 and 5.5. While, at the bottom layers, the masses of neutron-rich nuclei are extrapolated by theoretical mass models, so there is model dependency. Also, the magic neutron numbers (50 and 82) dominate, which shows the crucial role of shell effects, but they are not included in SEMF model. Moreover, all nuclei, present in outer crust, are even-even, because of the pairing effect in both models. During the phase-transition, the pressure remains constant within the limits from a finite pressure grid, but the discontinuities in density (see, Eq. 3.1.24) are irreducible, even with a very fine pressure grid, because of the one-component plasma model assumption. The values of μ_b and μ_e rise, as the density increases, and eventually are equal to $m_n c^2$ and $\sim 26MeV$, respectively, as shown in the last row of Table.

For a typical neutron star with $M = 1.4M_\odot$ and $R = 12.5km$, the results of the solution of TOV equations are listed in Tables 5.3 and 5.6, for the two models. The coordinate thickness, ΔR_{cr}, is smaller than the proper thickness, z_{drip}, as well as, the gravitational mass, M_{cr}, compared to the baryonic mass, $M_{b_{cr}}$, of outer crust (see, Eqs. 2.1.15 and 4.6.12), with the relative fraction of mass of outer crust due to the gravitational binding energy to be ~ 0.23, for both models. The mass of outer crust represents a very small fraction of the total mass $\sim 2.5 \cdot 10^{-5}$, for SEMF, and $\sim 2.7 \cdot 10^{-5}$, for FRDM2012, while the fractional coordinate thickness is ~ 0.038, for both models. And, the total number of baryons is $\sim 5.1 \cdot 10^{52}$, for SEMF, and $\sim 5.5 \cdot 10^{52}$, for FRDM2012 model.

At the same time, for the same typical star, the most of crustal mass is concentrated in the deepest layers (i.e, there the nuclides have greater abundances), while the surface layers have negligible contribution to the total crustal mass as shown in Tables 5.4 and 5.7, because the density is low.

[8]it is noted that the ^{62}Ni has the highest binding energy per nucleon, but a higher neutron to proton ratio than ^{56}Fe, which lifts its total energy

SEMF model

Table 5.2: For each layer are listed the minimum (maximum) pressure P_{min} (P_{max}) in MeV/fm^3, the minimum (maximum) energy density ϵ_{min} (ϵ_{max}) in MeV/fm^3, the minimum (maximum) baryon number density $n_{b_{min}}$ ($n_{b_{max}}$) in fm^{-3}, the mass number A, the atomic number Z, the neutron number N, the proton fraction Z/A, the minimum (maximum) baryon chemical potential $\mu_{b_{min}}$ ($\mu_{b_{max}}$) in MeV and the minimum (maximum) electron chemical potential $\mu_{e_{min}}$ ($\mu_{e_{max}}$) in MeV, using the SEMF model with magnetic field strength $B_\star = 0$

№	P_{min}	P_{max}	ϵ_{min}	ϵ_{max}	$n_{b_{min}}$	$n_{b_{max}}$	A	Z	N	Z/A	$\mu_{b_{min}}$	$\mu_{b_{max}}$	$\mu_{e_{min}}$	$\mu_{e_{max}}$
1	6.082E-15	3.388E-10	5.857E-09	4.615E-06	6.295E-12	4.960E-09	56	26	30	0.464	930.414	930.603	0.518	0.954
2	3.393E-10	4.160E-08	4.758E-06	1.470E-04	5.113E-09	1.579E-07	62	28	34	0.452	930.604	931.306	0.955	2.583
3	4.166E-08	4.393E-08	1.480E-04	1.539E-04	1.590E-07	1.653E-07	58	26	32	0.448	931.306	931.320	2.582	2.615
4	4.400E-08	3.565E-07	1.582E-04	7.466E-04	1.699E-07	8.015E-07	64	28	36	0.438	931.321	932.040	2.617	4.335
5	3.570E-07	4.137E-07	7.708E-04	8.603E-04	8.274E-07	9.234E-07	66	28	38	0.424	932.041	932.106	4.337	4.496
6	4.143E-07	1.028E-06	8.782E-04	1.731E-03	9.426E-07	1.857E-06	86	36	50	0.419	932.107	932.556	4.507	5.637
7	1.030E-06	5.572E-06	1.790E-03	6.332E-03	1.920E-06	6.788E-06	84	34	50	0.405	932.557	933.686	5.636	8.565
8	5.581E-06	1.766E-05	6.566E-03	1.557E-02	7.038E-06	1.668E-05	82	32	50	0.390	933.687	934.747	8.564	11.410
9	1.769E-05	5.809E-05	1.620E-02	3.954E-02	1.735E-05	4.230E-05	80	30	50	0.375	934.748	936.160	11.408	15.347
10	5.817E-05	1.939E-04	4.057E-02	1.002E-01	4.340E-05	1.070E-04	82	30	52	0.366	936.162	938.045	15.352	20.735
11	1.941E-04	2.320E-04	1.022E-01	1.169E-01	1.092E-04	1.248E-04	132	48	84	0.364	938.048	938.372	20.831	21.779
12	2.324E-04	2.542E-04	1.273E-01	1.362E-01	1.359E-04	1.454E-04	132	44	88	0.333	938.375	938.530	21.768	22.262
13	2.546E-04	2.968E-04	1.385E-01	1.554E-01	1.478E-04	1.658E-04	140	46	94	0.329	938.533	938.802	22.280	23.150
14	2.972E-04	3.354E-04	1.578E-01	1.728E-01	1.684E-04	1.844E-04	142	46	96	0.324	938.804	939.021	23.158	23.868
15	3.359E-04	3.807E-04	1.754E-01	1.927E-01	1.871E-04	2.055E-04	150	48	102	0.320	939.023	939.252	23.887	24.646
16	3.812E-04	4.220E-04	1.954E-01	2.110E-01	2.085E-04	2.250E-04	152	48	104	0.316	939.254	939.443	24.656	25.290
17	4.226E-04	4.503E-04	2.137E-01	2.241E-01	2.279E-04	2.390E-04	160	50	110	0.312	939.445	939.564	25.310	25.714

Table 5.3: For a typical NS with $M = 1.4M_\odot$ and $R = 12.5km$, are listed the mass of outer crust M_{cr} in $M_\odot$, the fractional mass M_{cr}/M, the coordinate thickness ΔR_{cr} in km, the fractional coordinate thickness $\Delta R_{cr}/R$, the baryonic mass $M_{b_{cr}}$ in $M_\odot$, the relative fraction of outer crust's mass due to gravitational binding energy Δ_{grav}, the proper depth of neutron-drip transition z_{drip} in km and the total number of baryons ΔN of outer crust, using the SEMF model with magnetic field strength $B_\star = 0$

M_{cr}	M_{cr}/M	ΔR_{cr}	$\Delta R_{cr}/R$	$M_{b_{cr}}$	Δ_{grav}	z_{drip}	ΔN
3.471E-05	2.479E-05	4.717E-01	3.774E-02	4.276E-05	2.322E-01	5.794E-01	5.077E+52

Table 5.4: For a typical NS with $M = 1.4M_{\odot}$ and $R = 12.5km$, are listed the minimum (maximum) radius of the layer r_{min} (r_{max}) in km, the coordinate thickness ΔR_l in km, the fractional coordinate thickness $\Delta R_l/\Delta R_{cr}$, the proper depth z_l in km, the fractional proper depth z_l/z_{drip}, the baryonic mass M_{b_l} in $M_{\odot}$, the fractional baryonic mass $M_{b_l}/M_{b_{cr}}$, the mass M_l in $M_{\odot}$, the fractional mass M_l/M_{cr}, the number of baryons ΔN_l and the fractional number of baryons $\Delta N_l/\Delta N$, using the SEMF model with magnetic field strength $B_{\star} = 0$

№	r_{min}	r_{max}	ΔR_l	$\Delta R_l/\Delta R_{cr}$	z_l	z_l/z_{drip}	M_{b_l}	$M_{b_l}/M_{b_{cr}}$	M_l	M_l/M_{cr}	ΔN_l	$\Delta N_l/\Delta N$
1	12.490	12.500	1.027E-02	2.177E-02	0.013	2.167E-02	3.676E-11	8.595E-07	3.006E-11	8.660E-07	4.364E+46	8.595E-07
2	12.452	12.490	3.794E-02	8.044E-02	0.059	1.018E-01	4.432E-09	1.036E-04	3.623E-09	1.044E-04	5.262E+48	1.036E-04
3	12.451	12.452	7.507E-04	1.591E-03	0.060	1.034E-01	2.421E-10	5.662E-06	1.979E-10	5.702E-06	2.875E+47	5.662E-06
4	12.412	12.451	3.854E-02	8.172E-02	0.107	1.849E-01	3.315E-08	7.752E-04	2.708E-08	7.803E-04	3.936E+49	7.752E-04
5	12.409	12.412	3.452E-03	7.318E-03	0.111	1.923E-01	5.977E-09	1.398E-04	4.881E-09	1.406E-04	7.096E+48	1.398E-04
6	12.385	12.409	2.389E-02	5.064E-02	0.141	2.428E-01	6.443E-08	1.507E-03	5.260E-08	1.516E-03	7.649E+49	1.507E-03
7	12.326	12.385	5.945E-02	1.260E-01	0.214	3.687E-01	4.691E-07	1.097E-02	3.826E-07	1.102E-02	5.569E+50	1.097E-02
8	12.270	12.325	5.507E-02	1.168E-01	0.281	4.855E-01	1.224E-06	2.862E-02	9.970E-07	2.873E-02	1.453E+51	2.862E-02
9	12.198	12.270	7.236E-02	1.534E-01	0.370	6.392E-01	3.999E-06	9.351E-02	3.254E-06	9.375E-02	4.748E+51	9.351E-02
10	12.103	12.198	9.466E-02	2.007E-01	0.487	8.406E-01	1.303E-05	3.047E-01	1.058E-05	3.050E-01	1.547E+52	3.047E-01
11	12.087	12.103	1.609E-02	3.412E-02	0.507	8.751E-01	3.576E-06	8.363E-02	2.901E-06	8.360E-02	4.246E+51	8.363E-02
12	12.079	12.087	7.692E-03	1.631E-02	0.517	8.917E-01	2.054E-06	4.803E-02	1.666E-06	4.800E-02	2.438E+51	4.803E-02
13	12.066	12.079	1.328E-02	2.816E-02	0.533	9.203E-01	3.948E-06	9.232E-02	3.201E-06	9.224E-02	4.687E+51	9.232E-02
14	12.055	12.066	1.066E-02	2.260E-02	0.547	9.433E-01	3.558E-06	8.321E-02	2.885E-06	8.312E-02	4.225E+51	8.321E-02
15	12.044	12.055	1.122E-02	2.378E-02	0.561	9.674E-01	4.162E-06	9.732E-02	3.373E-06	9.719E-02	4.941E+51	9.732E-02
16	12.034	12.043	9.224E-03	1.956E-02	0.572	9.874E-01	3.775E-06	8.827E-02	3.059E-06	8.813E-02	4.481E+51	8.827E-02
17	12.028	12.034	5.794E-03	1.228E-02	0.579	1.000E+00	2.552E-06	5.967E-02	2.067E-06	5.957E-02	3.030E+51	5.967E-02

FRDM2012 model

Table 5.5: The same as Table 5.2, using the FRDM2012 model with $B_{\star} = 0$

№	P_{min}	P_{max}	ϵ_{min}	ϵ_{max}	$n_{b_{min}}$	$n_{b_{max}}$	A	Z	N	Z/A	$\mu_{b_{min}}$	$\mu_{b_{max}}$	$\mu_{e_{min}}$	$\mu_{e_{max}}$
1	6.082E-15	3.388E-10	5.857E-09	4.615E-06	6.295E-12	4.960E-09	56	26	30	0.464	930.414	930.603	0.518	0.954
2	3.393E-10	4.160E-08	4.758E-06	1.470E-04	5.113E-09	1.579E-07	62	28	34	0.452	930.604	931.306	0.955	2.583
3	4.166E-08	4.393E-08	1.480E-04	1.539E-04	1.590E-07	1.653E-07	58	26	32	0.448	931.306	931.320	2.582	2.615
4	4.400E-08	3.565E-07	1.582E-04	7.466E-04	1.699E-07	8.015E-07	64	28	36	0.438	931.321	932.040	2.617	4.335
5	3.570E-07	4.137E-07	7.708E-04	8.603E-04	8.274E-07	9.234E-07	66	28	38	0.424	932.041	932.106	4.337	4.496
6	4.143E-07	1.028E-06	8.782E-04	1.731E-03	9.426E-07	1.857E-06	86	36	50	0.419	932.107	932.556	4.507	5.637
7	1.030E-06	5.572E-06	1.790E-03	6.332E-03	1.920E-06	6.788E-06	84	34	50	0.405	932.557	933.686	5.636	8.565
8	5.581E-06	1.766E-05	6.566E-03	1.557E-02	7.038E-06	1.668E-05	82	32	50	0.390	933.687	934.747	8.564	11.410
9	1.769E-05	3.583E-05	1.620E-02	2.751E-02	1.735E-05	2.944E-05	80	30	50	0.375	934.748	935.535	11.408	13.603
10	3.588E-05	1.099E-04	2.873E-02	6.658E-02	3.074E-05	7.117E-05	78	28	50	0.359	935.537	937.045	13.601	17.987
11	1.101E-04	1.168E-04	6.932E-02	7.246E-02	7.410E-05	7.744E-05	126	44	82	0.349	937.047	937.136	18.063	18.331
12	1.170E-04	1.828E-04	7.469E-02	1.044E-01	7.982E-05	1.116E-04	124	42	82	0.339	937.138	937.830	18.329	20.491
13	1.830E-04	2.810E-04	1.079E-01	1.488E-01	1.152E-04	1.589E-04	122	40	82	0.328	937.832	938.551	20.489	22.805
14	2.814E-04	4.276E-04	1.541E-01	2.110E-01	1.645E-04	2.251E-04	120	38	82	0.317	938.554	939.309	22.803	25.316
15	4.283E-04	4.905E-04	2.189E-01	2.424E-01	2.335E-04	2.585E-04	118	36	82	0.305	939.312	939.564	25.313	26.185

Table 5.6: The same as Table 5.3, using the FRDM2012 model with $B_{\star} = 0$

M_{cr}	M_{cr}/M	ΔR_{cr}	$\Delta R_{cr}/R$	$M_{b_{cr}}$	Δ_{grav}	z_{drip}	ΔN
3.778E-05	2.699E-05	4.717E-01	3.774E-02	4.655E-05	2.322E-01	5.794E-01	5.527E+52

Table 5.7: The same as Table 5.4, using the FRDM2012 model with $B_\star = 0$

№	r_{min}	r_{max}	ΔR_l	$\Delta R_l/\Delta R_{cr}$	z_l	z_l/z_{drip}	M_{b_l}	$M_{b_l}/M_{b_{cr}}$	M_l	M_l/M_{cr}	ΔN_l	$\Delta N_l/\Delta N$
1	12.490	12.500	1.027E-02	2.177E-02	0.013	2.167E-02	3.676E-11	7.895E-07	3.006E-11	7.956E-07	4.364E+46	7.895E-07
2	12.452	12.490	3.794E-02	8.043E-02	0.059	1.018E-01	4.432E-09	9.520E-05	3.623E-09	9.590E-05	5.262E+48	9.520E-05
3	12.451	12.452	7.507E-04	1.591E-03	0.060	1.034E-01	2.421E-10	5.201E-06	1.979E-10	5.238E-06	2.875E+47	5.201E-06
4	12.412	12.451	3.854E-02	8.171E-02	0.107	1.849E-01	3.315E-08	7.121E-04	2.708E-08	7.168E-04	3.936E+49	7.121E-04
5	12.409	12.412	3.452E-03	7.318E-03	0.111	1.923E-01	5.977E-09	1.284E-04	4.881E-09	1.292E-04	7.096E+48	1.284E-04
6	12.385	12.409	2.389E-02	5.064E-02	0.141	2.428E-01	6.443E-08	1.384E-03	5.260E-08	1.392E-03	7.649E+49	1.384E-03
7	12.326	12.385	5.945E-02	1.260E-01	0.214	3.687E-01	4.691E-07	1.008E-02	3.826E-07	1.013E-02	5.569E+50	1.008E-02
8	12.270	12.325	5.507E-02	1.168E-01	0.281	4.855E-01	1.224E-06	2.629E-02	9.970E-07	2.639E-02	1.453E+51	2.629E-02
9	12.230	12.270	4.047E-02	8.580E-02	0.331	5.715E-01	1.808E-06	3.883E-02	1.471E-06	3.894E-02	2.146E+51	3.883E-02
10	12.153	12.230	7.654E-02	1.623E-01	0.425	7.342E-01	7.222E-06	1.551E-01	5.870E-06	1.554E-01	8.574E+51	1.551E-01
11	12.149	12.153	4.434E-03	9.400E-03	0.431	7.439E-01	6.434E-07	1.382E-02	5.226E-07	1.383E-02	7.639E+50	1.382E-02
12	12.114	12.149	3.464E-02	7.343E-02	0.474	8.177E-01	6.292E-06	1.351E-01	5.108E-06	1.352E-01	7.470E+51	1.351E-01
13	12.078	12.114	3.570E-02	7.568E-02	0.518	8.939E-01	9.251E-06	1.987E-01	7.505E-06	1.986E-01	1.098E+52	1.987E-01
14	12.041	12.078	3.717E-02	7.879E-02	0.564	9.733E-01	1.363E-05	2.927E-01	1.105E-05	2.924E-01	1.618E+52	2.927E-01
15	12.028	12.041	1.238E-02	2.624E-02	0.579	1.000E+00	5.745E-06	1.234E-01	4.655E-06	1.232E-01	6.820E+51	1.234E-01

5.4.2 Layers properties for $B_\star = 1500$

Respectively, for $B_\star = 1500$, the composition of outer crust is presented in Tables 5.8 and 5.11, the results from TOV equations, for the whole outer crust in Tables 5.9 and 5.12, and for each crustal layer in Tables 5.10 and 5.13, with the same M and R as previously. The differences will be discussed and made more understandable below.

SEMF model

Table 5.8: The same as Table 5.2, using the SEMF model with $B_\star = 1500$

№	P_{min}	P_{max}	ϵ_{min}	ϵ_{max}	$n_{b_{min}}$	$n_{b_{max}}$	A	Z	N	Z/A	$\mu_{b_{min}}$	$\mu_{b_{max}}$	$\mu_{e_{min}}$	$\mu_{e_{max}}$
1	6.082E-15	2.628E-07	1.597E-03	3.584E-03	1.717E-06	3.852E-06	56	26	30	0.464	930.348	930.438	0.597	0.861
2	2.632E-07	9.711E-06	3.717E-03	1.577E-02	3.995E-06	1.694E-05	62	28	34	0.452	930.438	931.318	0.866	3.007
3	9.725E-06	1.081E-05	1.629E-02	1.711E-02	1.750E-05	1.838E-05	64	28	36	0.438	931.319	931.379	3.009	3.156
4	1.083E-05	1.885E-05	1.752E-02	2.268E-02	1.882E-05	2.436E-05	88	38	50	0.432	931.380	931.751	3.189	4.105
5	1.887E-05	5.072E-05	2.337E-02	3.747E-02	2.510E-05	4.023E-05	86	36	50	0.419	931.752	932.727	4.101	6.541
6	5.080E-05	1.063E-04	3.874E-02	5.548E-02	4.159E-05	5.952E-05	84	34	50	0.405	932.728	933.825	6.538	9.343
7	1.064E-04	1.790E-04	5.753E-02	7.427E-02	6.172E-05	7.964E-05	82	32	50	0.390	933.828	934.855	9.341	12.045
8	1.793E-04	3.029E-04	7.729E-02	1.001E-01	8.287E-05	1.073E-04	80	30	50	0.375	934.858	936.159	12.044	15.587
9	3.034E-04	4.165E-04	1.027E-01	1.202E-01	1.100E-04	1.287E-04	82	30	52	0.366	936.163	937.110	15.598	18.237
10	4.171E-04	5.984E-04	1.216E-01	1.454E-01	1.302E-04	1.556E-04	132	48	84	0.364	937.115	938.384	18.341	21.911
11	5.993E-04	6.199E-04	1.587E-01	1.614E-01	1.698E-04	1.726E-04	138	46	92	0.333	938.389	938.510	21.917	22.287
12	6.208E-04	6.713E-04	1.639E-01	1.703E-01	1.753E-04	1.821E-04	140	46	94	0.329	938.515	938.797	22.303	23.179
13	6.722E-04	7.110E-04	1.729E-01	1.778E-01	1.849E-04	1.901E-04	142	46	96	0.324	938.803	939.009	23.196	23.847
14	7.120E-04	7.586E-04	1.802E-01	1.859E-01	1.926E-04	1.988E-04	150	48	102	0.320	939.015	939.253	23.874	24.633
15	7.597E-04	8.023E-04	1.885E-01	1.937E-01	2.016E-04	2.071E-04	152	48	104	0.316	939.258	939.467	24.651	25.324
16	8.034E-04	8.226E-04	1.960E-01	1.983E-01	2.095E-04	2.119E-04	160	50	110	0.312	939.472	939.563	25.353	25.650

Table 5.9: The same as Table 5.3, using the SEMF model with $B_\star = 1500$

M_{cr}	M_{cr}/M	ΔR_{cr}	$\Delta R_{cr}/R$	$M_{b_{cr}}$	Δ_{grav}	z_{drip}	ΔN
6.479E-05	4.628E-05	4.750E-01	3.800E-02	7.972E-05	2.306E-01	5.834E-01	9.465E+52

Table 5.10: The same as Table 5.4, using the SEMF model with $B_\star = 1500$

№	r_{min}	r_{max}	ΔR_l	$\Delta R_l/\Delta R_{cr}$	z_l	z_l/z_{drip}	M_{b_l}	$M_{b_l}/M_{b_{cr}}$	M_l	M_l/M_{cr}	ΔN_l	$\Delta N_l/\Delta N$
1	12.495	12.500	4.892E-03	1.030E-02	0.006	1.025E-02	2.855E-08	3.582E-04	2.336E-08	3.605E-04	3.390E+49	3.582E-04
2	12.448	12.495	4.755E-02	1.001E-01	0.064	1.099E-01	1.016E-06	1.274E-02	8.306E-07	1.282E-02	1.206E+51	1.274E-02
3	12.444	12.448	3.257E-03	6.858E-03	0.068	1.169E-01	1.161E-07	1.457E-03	9.490E-08	1.465E-03	1.379E+50	1.457E-03
4	12.424	12.444	1.989E-02	4.187E-02	0.093	1.587E-01	8.521E-07	1.069E-02	6.962E-07	1.075E-02	1.012E+51	1.069E-02
5	12.372	12.424	5.179E-02	1.090E-01	0.156	2.676E-01	3.341E-06	4.191E-02	2.728E-06	4.210E-02	3.967E+51	4.191E-02
6	12.315	12.372	5.761E-02	1.213E-01	0.227	3.889E-01	5.709E-06	7.161E-02	4.655E-06	7.186E-02	6.778E+51	7.161E-02
7	12.261	12.315	5.328E-02	1.122E-01	0.292	5.013E-01	7.327E-06	9.191E-02	5.969E-06	9.213E-02	8.699E+51	9.191E-02
8	12.195	12.261	6.654E-02	1.401E-01	0.374	6.418E-01	1.221E-05	1.532E-01	9.936E-06	1.534E-01	1.450E+52	1.532E-01
9	12.147	12.194	4.784E-02	1.007E-01	0.434	7.432E-01	1.094E-05	1.373E-01	8.893E-06	1.373E-01	1.299E+52	1.373E-01
10	12.083	12.146	6.328E-02	1.332E-01	0.512	8.773E-01	1.720E-05	2.157E-01	1.396E-05	2.155E-01	2.042E+52	2.157E-01
11	12.077	12.083	5.968E-03	1.257E-02	0.520	8.905E-01	1.936E-06	2.428E-02	1.570E-06	2.423E-02	2.298E+51	2.428E-02
12	12.063	12.077	1.393E-02	2.932E-02	0.537	9.205E-01	4.708E-06	5.905E-02	3.817E-06	5.892E-02	5.589E+51	5.905E-02
13	12.052	12.062	1.016E-02	2.140E-02	0.550	9.426E-01	3.599E-06	4.514E-02	2.917E-06	4.503E-02	4.272E+51	4.514E-02
14	12.040	12.052	1.168E-02	2.459E-02	0.565	9.678E-01	4.312E-06	5.408E-02	3.494E-06	5.394E-02	5.119E+51	5.408E-02
15	12.030	12.040	1.020E-02	2.147E-02	0.578	9.900E-01	3.925E-06	4.923E-02	3.180E-06	4.908E-02	4.659E+51	4.923E-02
16	12.025	12.029	4.446E-03	9.361E-03	0.583	1.000E+00	1.763E-06	2.211E-02	1.428E-06	2.204E-02	2.093E+51	2.211E-02

FRDM2012 model

Table 5.11: The same as Table 5.2, using the FRDM2012 model with $B_\star = 1500$

№	P_{min}	P_{max}	ϵ_{min}	ϵ_{max}	$n_{b_{min}}$	$n_{b_{max}}$	A	Z	N	Z/A	$\mu_{b_{min}}$	$\mu_{b_{max}}$	$\mu_{e_{min}}$	$\mu_{e_{max}}$
1	6.082E-15	2.628E-07	1.597E-03	3.584E-03	1.717E-06	3.852E-06	56	26	30	0.464	930.348	930.438	0.597	0.861
2	2.632E-07	9.711E-06	3.717E-03	1.577E-02	3.995E-06	1.694E-05	62	28	34	0.452	930.438	931.318	0.866	3.007
3	9.725E-06	1.081E-05	1.629E-02	1.711E-02	1.750E-05	1.838E-05	64	28	36	0.438	931.319	931.379	3.009	3.156
4	1.083E-05	1.885E-05	1.752E-02	2.268E-02	1.882E-05	2.436E-05	88	38	50	0.432	931.380	931.751	3.189	4.105
5	1.887E-05	5.072E-05	2.337E-02	3.747E-02	2.510E-05	4.023E-05	86	36	50	0.419	931.752	932.727	4.101	6.541
6	5.080E-05	1.063E-04	3.874E-02	5.548E-02	4.159E-05	5.952E-05	84	34	50	0.405	932.728	933.825	6.538	9.343
7	1.064E-04	1.790E-04	5.753E-02	7.427E-02	6.172E-05	7.964E-05	82	32	50	0.390	933.828	934.855	9.341	12.045
8	1.793E-04	2.476E-04	7.729E-02	9.062E-02	8.287E-05	9.712E-05	80	30	50	0.375	934.858	935.617	12.044	14.113
9	2.479E-04	3.521E-04	9.468E-02	1.126E-01	1.015E-04	1.206E-04	78	28	50	0.359	935.621	936.558	14.113	16.775
10	3.526E-04	4.353E-04	1.164E-01	1.292E-01	1.247E-04	1.383E-04	126	44	82	0.349	936.562	937.191	16.868	18.711
11	4.359E-04	5.366E-04	1.332E-01	1.477E-01	1.426E-04	1.580E-04	124	42	82	0.339	937.196	937.865	18.715	20.734
12	5.374E-04	6.566E-04	1.526E-01	1.686E-01	1.633E-04	1.803E-04	122	40	82	0.328	937.870	938.564	20.739	22.896
13	6.576E-04	8.011E-04	1.746E-01	1.926E-01	1.867E-04	2.059E-04	120	38	82	0.317	938.569	939.300	22.902	25.251
14	8.023E-04	8.585E-04	2.000E-01	2.068E-01	2.138E-04	2.211E-04	118	36	82	0.305	939.306	939.565	25.259	26.120

Table 5.12: The same as Table 5.3, using the FRDM2012 model with $B_\star = 1500$

M_{cr}	M_{cr}/M	ΔR_{cr}	$\Delta R_{cr}/R$	$M_{b_{cr}}$	Δ_{grav}	z_{drip}	ΔN
6.755E-05	4.825E-05	4.751E-01	3.800E-02	8.313E-05	2.306E-01	5.835E-01	9.869E+52

Table 5.13: The same as Table 5.4, using the FRDM2012 model with $B_\star = 1500$

№	r_{min}	r_{max}	ΔR_l	$\Delta R_l/\Delta R_{cr}$	z_l	z_l/z_{drip}	M_{b_l}	$M_{b_l}/M_{b_{cr}}$	M_l	M_l/M_{cr}	ΔN_l	$\Delta N_l/\Delta N$
1	12.495	12.500	4.892E-03	1.030E-02	0.006	1.025E-02	2.855E-08	3.435E-04	2.336E-08	3.458E-04	3.390E+49	3.435E-04
2	12.448	12.495	4.755E-02	1.001E-01	0.064	1.099E-01	1.016E-06	1.222E-02	8.306E-07	1.230E-02	1.206E+51	1.222E-02
3	12.444	12.448	3.257E-03	6.856E-03	0.068	1.169E-01	1.161E-07	1.397E-03	9.490E-08	1.405E-03	1.379E+50	1.397E-03
4	12.424	12.444	1.989E-02	4.187E-02	0.093	1.587E-01	8.521E-07	1.025E-02	6.962E-07	1.031E-02	1.012E+51	1.025E-02
5	12.372	12.424	5.179E-02	1.090E-01	0.156	2.675E-01	3.341E-06	4.019E-02	2.728E-06	4.038E-02	3.967E+51	4.019E-02
6	12.315	12.372	5.761E-02	1.213E-01	0.227	3.888E-01	5.709E-06	6.867E-02	4.655E-06	6.892E-02	6.778E+51	6.867E-02
7	12.261	12.315	5.328E-02	1.121E-01	0.292	5.012E-01	7.327E-06	8.814E-02	5.969E-06	8.836E-02	8.699E+51	8.814E-02
8	12.222	12.261	3.894E-02	8.197E-02	0.340	5.835E-01	6.780E-06	8.156E-02	5.517E-06	8.167E-02	8.049E+51	8.156E-02
9	12.174	12.222	4.766E-02	1.003E-01	0.399	6.844E-01	1.018E-05	1.225E-01	8.277E-06	1.225E-01	1.209E+52	1.225E-01
10	12.142	12.174	3.167E-02	6.667E-02	0.439	7.517E-01	7.971E-06	9.589E-02	6.475E-06	9.586E-02	9.463E+51	9.589E-02
11	12.109	12.142	3.347E-02	7.046E-02	0.480	8.228E-01	9.589E-06	1.154E-01	7.784E-06	1.152E-01	1.138E+52	1.154E-01
12	12.074	12.109	3.442E-02	7.246E-02	0.523	8.960E-01	1.122E-05	1.350E-01	9.101E-06	1.347E-01	1.332E+52	1.350E-01
13	12.038	12.074	3.597E-02	7.572E-02	0.568	9.726E-01	1.333E-05	1.604E-01	1.081E-05	1.600E-01	1.583E+52	1.604E-01
14	12.025	12.038	1.266E-02	2.665E-02	0.584	1.000E+00	5.181E-06	6.233E-02	4.198E-06	6.214E-02	6.151E+51	6.233E-02

5.4.3 Fitting $P = K\epsilon^G$ for $B_\star = 0$

A polytropic EoS[9] is not a good function to be fitted in the EoS of outer crust, especially in the low density region, as shown in Figs. 5.1 and 5.2, for the SEMF and the FRDM2012 model, respectively, also, are listed the values for the parameters K and G. At higher densities, according to Eq. 4.1.35, $K_{approx} \approx 0.0035$ (for $Z/A \approx 0.31$) and $G_{approx} = 4/3 \approx 1.33$.

SEMF model

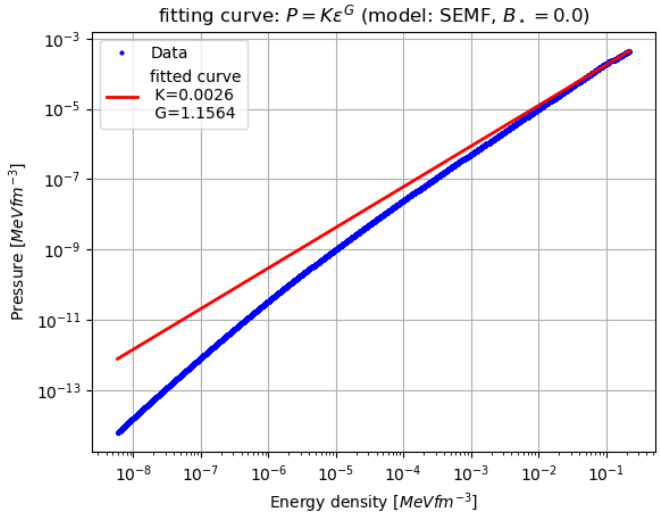

Figure 5.1: A polytropic EoS $P = K\epsilon^G$ for fitting, using the SEMF model with magnetic field strength $B_\star = 0$

[9] for the other models and magnetic field strengths, see Appendices E, F, G and H

FRDM2012 model

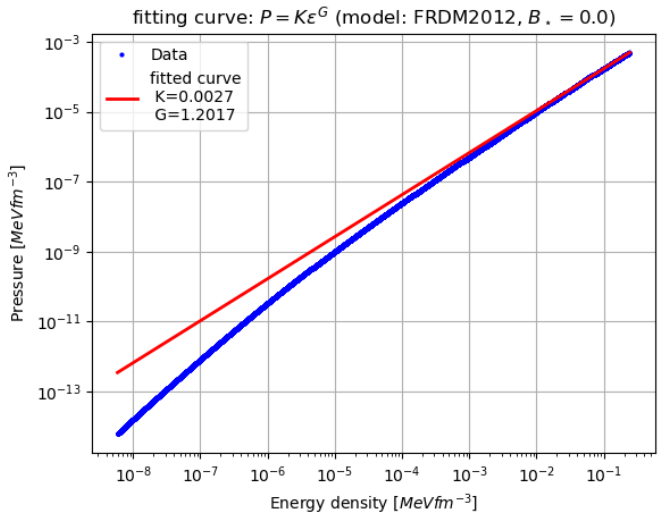

Figure 5.2: The same as Figure 5.1, using the FRDM2012 model with $B_\star = 0$

5.4.4 Fitting $P = K\epsilon^G$ for $B_\star = 1500$

Again, for strongly quantizing field with $B_\star = 1500$, a polytrope is not a good choice to fit the EoS, as shown in Figs. 5.3 and 5.4, for the SEMF and the FRDM2012 model, respectively. At higher densities, from Eq. 4.1.36, $\tilde{K}_{approx} \approx 0.0211$ (for $Z/A \approx 0.31$) and $\tilde{G}_{approx} = 2$.

SEMF model

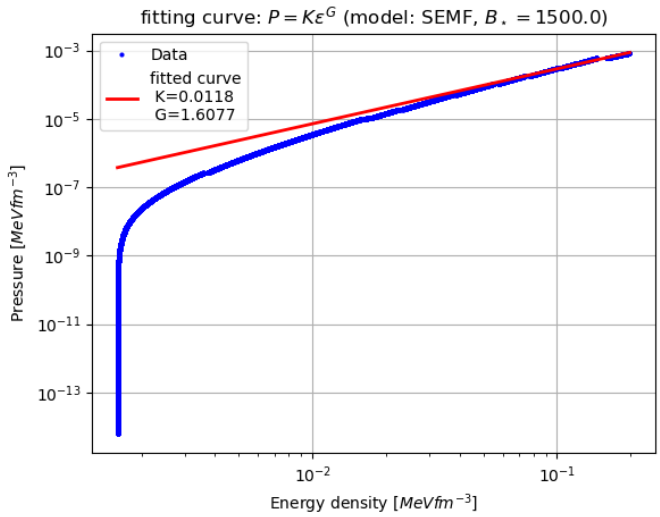

Figure 5.3: A polytropic EoS $P = K\epsilon^G$ for fitting, using the SEMF model with magnetic field strength $B_\star = 1500$

FRDM2012 model

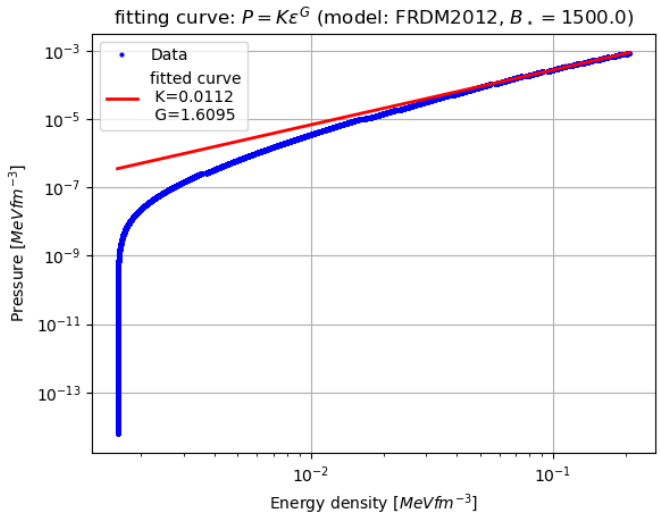

Figure 5.4: The same as Figure 5.3, using the FRDM2012 model with $B_\star = 1500$

5.4.5 P vs ϵ or n_b for different $B_\star$

At low densities, the quantization of electron motion leads to an almost incompressible matter, i.e., a strong stiffening of EoS[10], as shown in Figs. 5.5 and 5.6, for the SEMF and the FRDM2012 model, respectively. Also, at high densities, from Eqs. 4.1.35 and 4.1.36, $P \approx P_e \propto \epsilon^{4/3}$ and $\tilde{P} \approx \tilde{P}_e \propto \tilde{\epsilon}^2, \frac{1}{B_\star}$, so, according to the last relation, the pressure is higher, for smaller magnetic field strength, at the same density. At the neutron-drip transition, $\tilde{P}_{drip} \propto B_\star$ (see, Eq. 4.2.8), giving a higher neutron-drip pressure for greater $B_\star$. In addition, the first inequality of Eq. 4.2.13 is verified, because $P_{drip} < \tilde{P}_{drip}$. Furthermore, in all cases, the pressure increases with increasing density, as it was expected, and there are steps, which correspond to the phase transition.

SEMF model

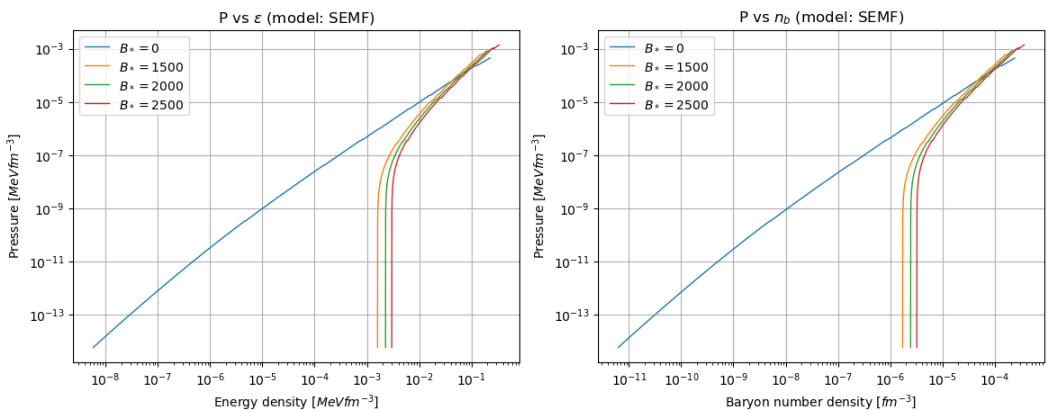

(a) (b)

Figure 5.5: Equation of State, (a) pressure as a function of energy density and (b) pressure as a function of baryon number density, using the SEMF model with different magnetic field strengths $B_\star$

[10]for the other models, see Appendix I

FRDM2012 model

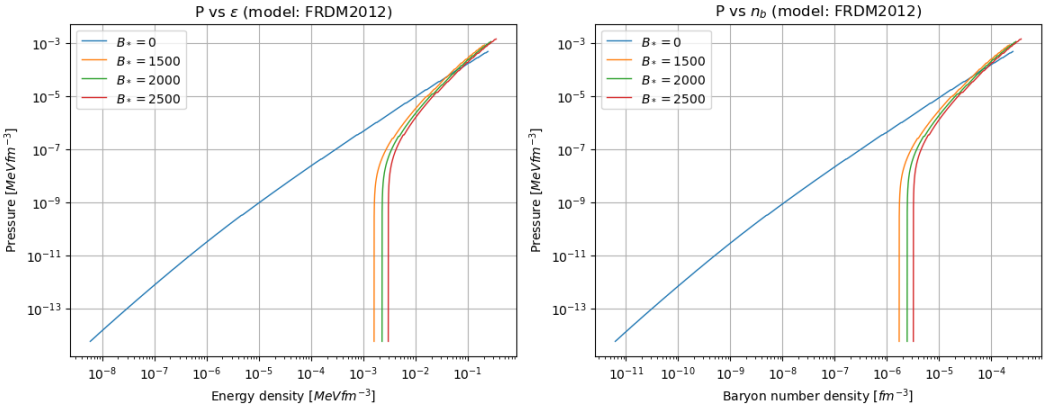

(a) (b)

Figure 5.6: The same as Figure 5.5, using the FRDM2012 model with different magnetic field strengths $B_\star$

5.4.6 Γ vs ϵ or n_b for different $B_\star$

There are differences between the magnetic field-free case and the strong quantization regime, as far as, the adiabatic index[11], as shown in Figs. 5.7 and 5.8, for the SEMF and the FRDM2012 model, respectively. At the transition points from one equilibrium nucleus to the other, the value of the adiabatic index jumps to zero, because the pressure in both phases is equal. And, at high densities, the adiabatic index approaches asymptotically the value 4/3, for the field-free case, and the value 2, for strongly quantizing magnetic field (see, Eqs. 4.3.2 and 4.3.3).

[11] for the other models, see Appendix I

SEMF model

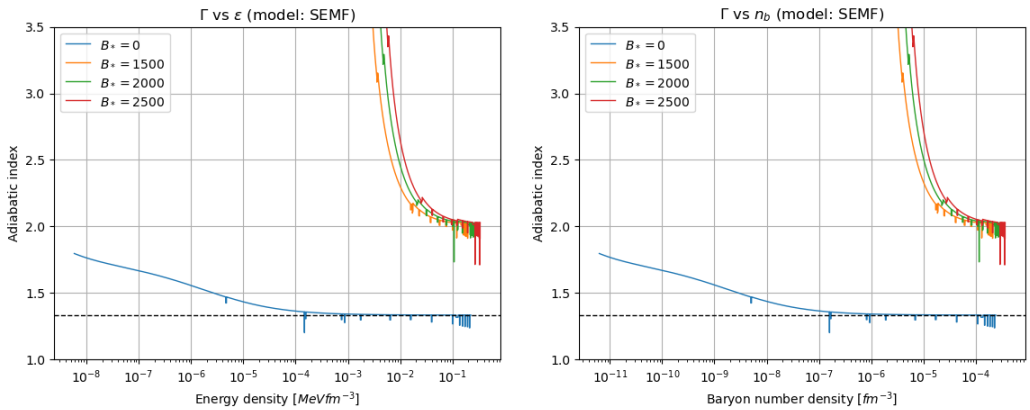

(a) (b)

Figure 5.7: Adiabatic index as a function of (a) energy density and of (b) baryon number density, using the SEMF model with different magnetic field strengths $B_\star$. The horizontal dashed line corresponds to $\Gamma = 4/3$

FRDM2012 model

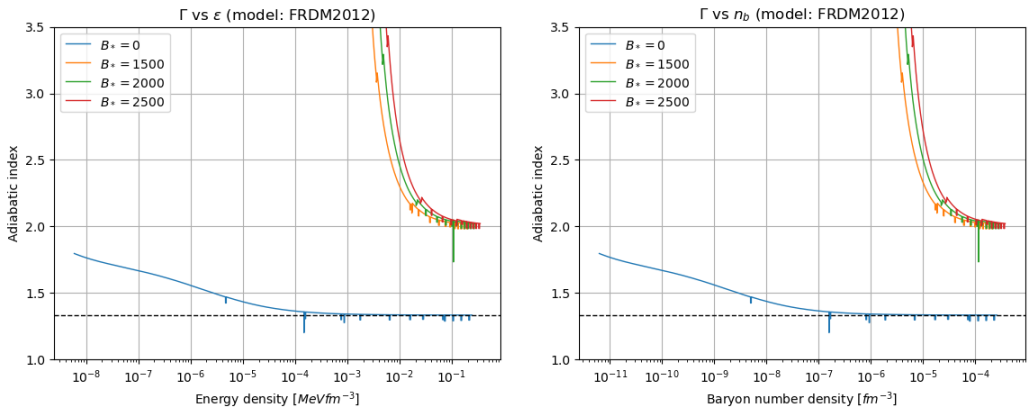

(a) (b)

Figure 5.8: The same as Figure 5.7, using the FRDM2012 model with different magnetic field strengths $B_\star$

5.4.7 c_s vs ϵ or n_b for different $B_\star$

The speed of sound[12] as a function of density, for the SEMF and FRDM2012 model, and different magnetic field strengths, is shown in Figs. 5.9 and 5.10, respectively. At high densities, according to Eqs. 4.4.2 and 4.4.4, $c_s/c \propto \epsilon^{1/6}$ and $\tilde{c}_s/c \propto \tilde{\epsilon}^{1/2}, B_\star^{-1/2}$, so a low $B_\star$ means a higher speed of sound at the same density, during the presence of a strongly quantizing magnetic field. At the neutron-drip transition, the speed of sound is independent of the magnetic field (see, Eq. 4.4.5), also, the $c_{s_{drip}}$ is almost half of the $\tilde{c}_{s_{drip}}$ (see, Eq. 4.4.6). Furthermore, in all cases, the speed of sound has a relative small value, in units of speed of light, but increases with the density.

SEMF model

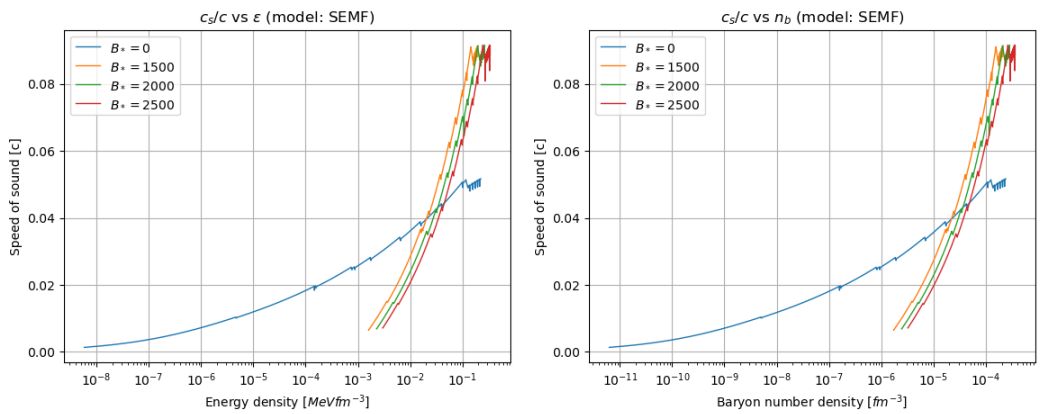

(a) (b)

Figure 5.9: Speed of sound as a function of (a) energy density and of (b) baryon number density, using the SEMF model with different magnetic field strengths $B_\star$

[12]for the other models, see Appendix I

FRDM2012 model

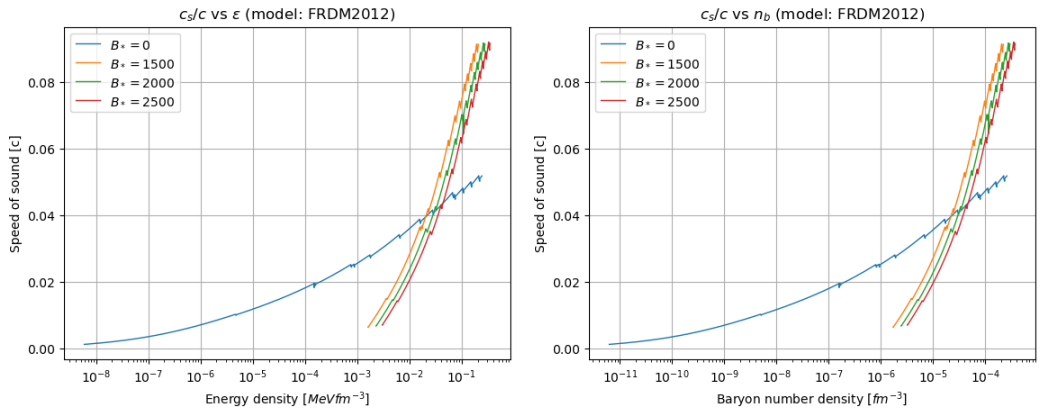

(a) (b)

Figure 5.10: The same as Figure 5.9, using the FRDM2012 model with different magnetic field strengths $B_\star$

5.4.8 K_{mod} vs ϵ or n_b for different $B_\star$

The compression modulus[13] as a function of density, for the SEMF and FRDM2012 model, and different magnetic field strengths, is shown in Figs. 5.11 and 5.12, respectively. At high densities, from Eqs. 4.5.7 and 4.5.9, $K_{mod} \propto n_b^{4/3}$ and $\tilde{K}_{mod} \propto \tilde{n}_b^2, \frac{1}{B_\star}$. So, at the same density and in the strongly quantizing regime, the greatest $B_\star$ has the smallest compression modulus. Moreover, at the neutron-drip transition, $\tilde{K}_{mod} \propto B_\star$ (see, Eq. 4.5.10), which leads to a greater compression modulus for the highest $B_\star$, also, from the inequality of Eq. 4.5.12, the neutron-drip compression modulus, in the absence of magnetic field, is always smaller than the respective compression modulus, in the presence of a strongly quantizing magnetic field. Furthermore, in all cases, the compression modulus increases with the density.

[13]for the other models, see Appendix I

SEMF model

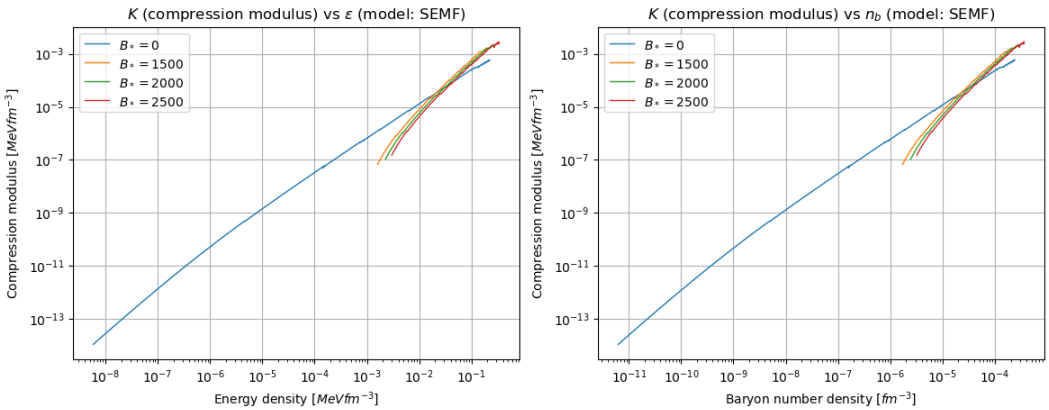

(a) (b)

Figure 5.11: Compression modulus as a function of (a) energy density and of (b) baryon number density, using the SEMF model with different magnetic field strengths $B_\star$

FRDM2012 model

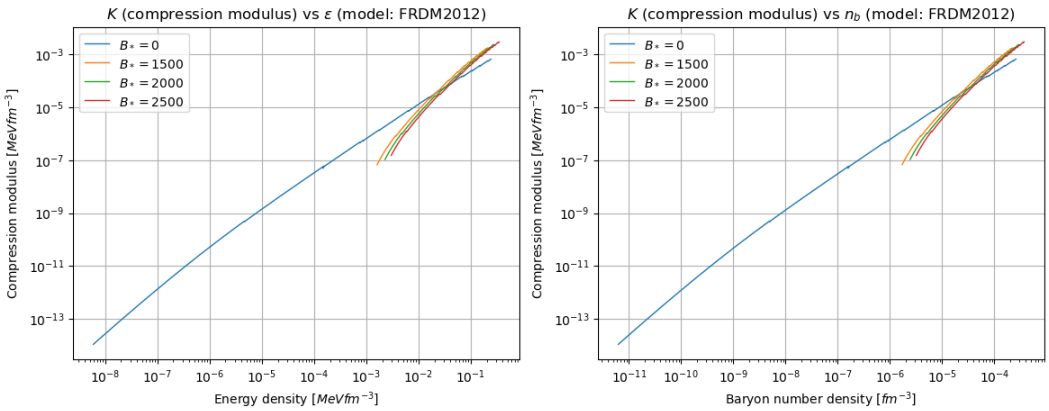

(a) (b)

Figure 5.12: The same as Figure 5.11, using the FRDM2012 model with different magnetic field strengths $B_\star$

5.4.9 S_{mod} vs ϵ or n_b for different $B_\star$

The effective shear modulus[14] as a function of density, for the SEMF and FRDM2012 model, and different magnetic field strengths, is shown in Figs. 5.13 and 5.14, respectively. At high densities, from Eq. 4.5.13, $S_{mod} \propto n_b^{4/3}$ and $\tilde{S}_{mod} \propto \tilde{n}_b^{4/3}$, which is independent of the magnetic field strength, for this reason, there are not many differences. At the neutron-drip transition, $\tilde{S}_{mod,drip} \propto B_\star^{4/3}$ (see, Eq. 4.5.15), so, in the strong quantization regime, the neutron-drip effective shear modulus increases with the magnetic field strength. Also, from the inequality of Eq. 4.5.17, it is not clear if always $S_{mod.drip} < \tilde{S}_{mod,drip}$. Furthermore, in all cases, the effective shear modulus increases with the density.

SEMF model

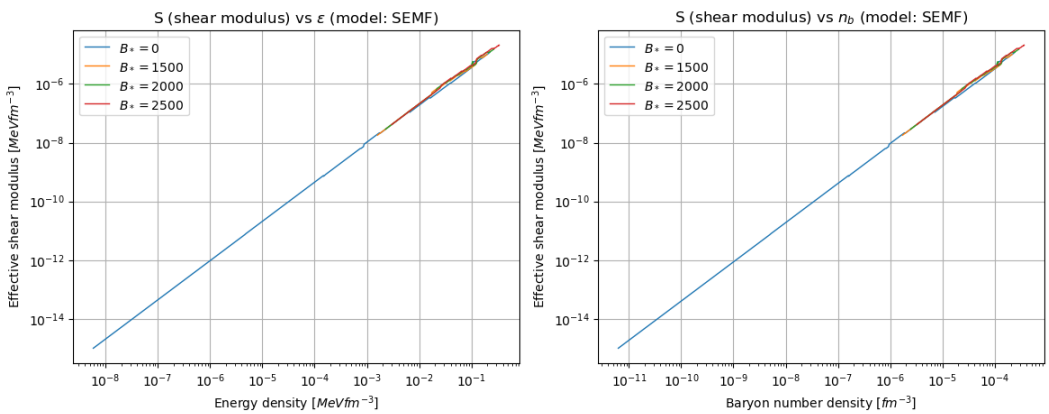

(a) (b)

Figure 5.13: Effective shear modulus as a function of (a) energy density and of (b) baryon number density, using the SEMF model with different magnetic field strengths $B_\star$

[14]for the other models, see Appendix I

FRDM2012 model

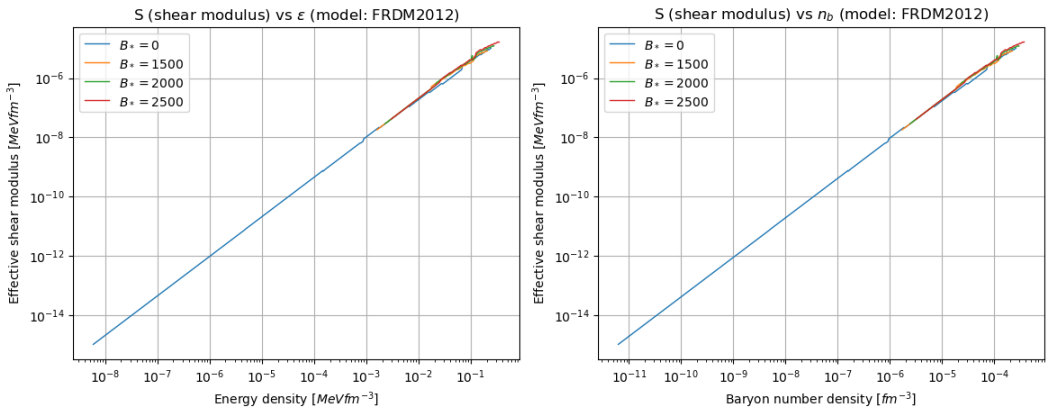

(a) (b)

Figure 5.14: The same as Figure 5.13, using the FRDM2012 model with different magnetic field strengths $B_\star$

5.4.10 S_{mod}/K_{mod} vs ϵ or n_b for different $B_\star$

The ratio of the effective shear modulus to the compression modulus[15] as a function of density, for the SEMF and FRDM2012 model, and different magnetic field strengths, is shown in Figs. 5.15 and 5.16, respectively. At high densities, from Eq. 4.5.18, the S_{mod}/K_{mod} is independent of the density, which explains the flatness of the curve, in the field-free case, while, from Eq. 4.5.20, $\tilde{S}_{mod}/\tilde{K}_{mod} \propto \tilde{n}_b^{-2/3}, B_\star$, which means that the ratio decreases with the density, and, at the same density, the ratio has greater value for the strongest field. At the neutron-drip transition, $\tilde{S}_{mod,drip}/\tilde{K}_{mod,drip} \propto B_\star^{1/3}$ (see, Eq. 4.5.21), so, in the strong quantization regime, the ratio slightly increases with the magnetic field strength. Also, from the inequality of Eq. 4.5.23, it is not clear if always $S_{mod,drip}/K_{mod,drip} < \tilde{S}_{mod,drip}/\tilde{K}_{mod,drip}$, here, in all cases, $S_{mod,drip}/K_{mod,drip} > \tilde{S}_{mod,drip}/\tilde{K}_{mod,drip}$. Furthermore, because the ratio is smaller than one, in all cases, the outer crust is more susceptible to shear than to compression deformation.

[15] for the other models, see Appendix I

SEMF model

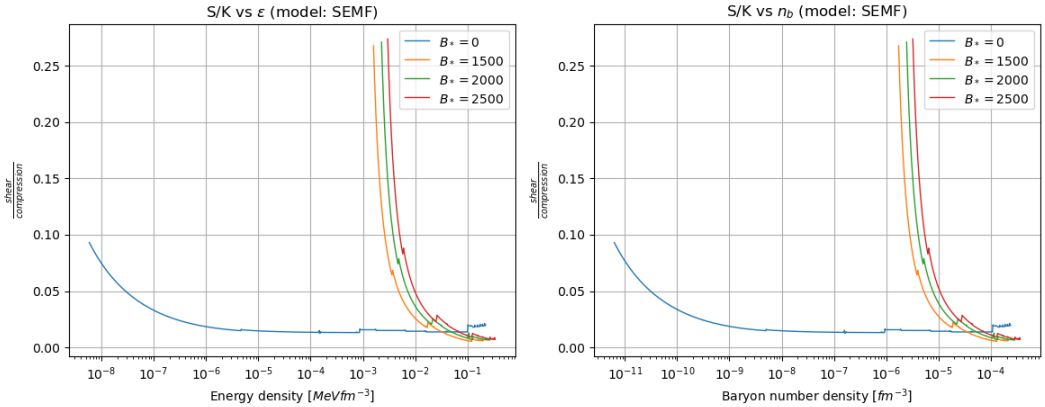

(a) (b)

Figure 5.15: Effective shear modulus over compression modulus as a function of (a) energy density and of (b) baryon number density, using the SEMF model with different magnetic field strengths $B_\star$

FRDM2012 model

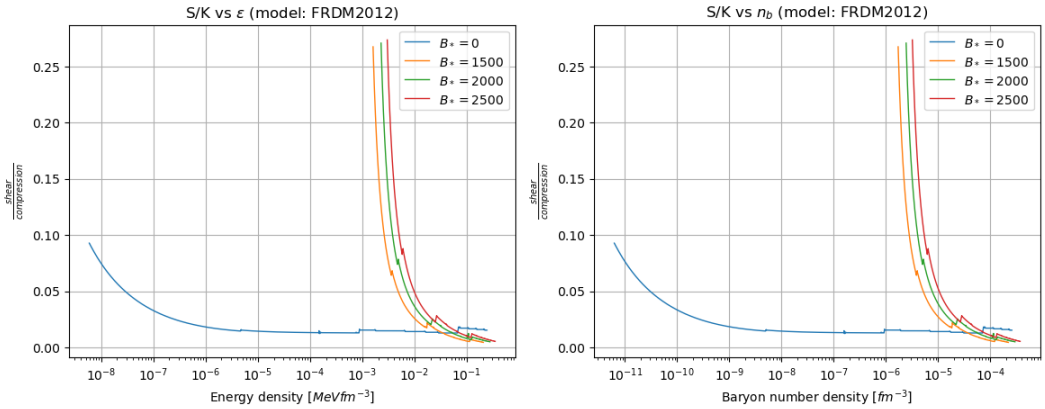

(a) (b)

Figure 5.16: The same as Figure 5.15, using the FRDM2012 model with different magnetic field strengths $B_\star$

5.4.11 Z, N, Z/A vs ϵ or n_b for different $B_\star$

The atomic number, Z, the neutron number, N, and the proton fraction, Z/A, as a function of density[16], for the SEMF and FRDM2012 model, and different magnetic field strengths, are shown in Figs. 5.17 and 5.18, respectively. With increasing density, the nuclei become more neutron-rich, because of the inverse $\beta-decay$ and the proton fraction decreases. Also, with a strong magnetic field, there is a delay in the appearance of a new phase and the transitions occur at higher densities. Moreover, the nuclei at a high $B_\star$ are more symmetric (i.e., the value of Z/A is closer to 0.5) at the same density and, in all cases, the range of $Z/A \approx 0.30 - 0.45$.

[16]for the other models, see Appendix I

SEMF model

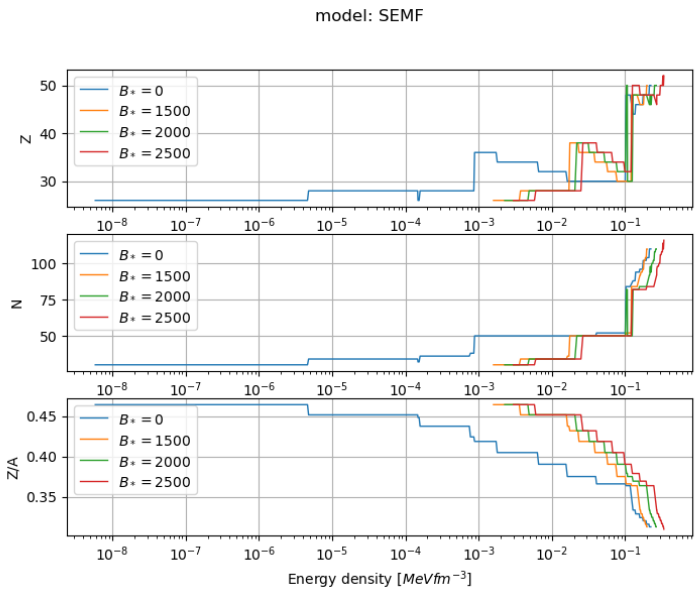

(a)

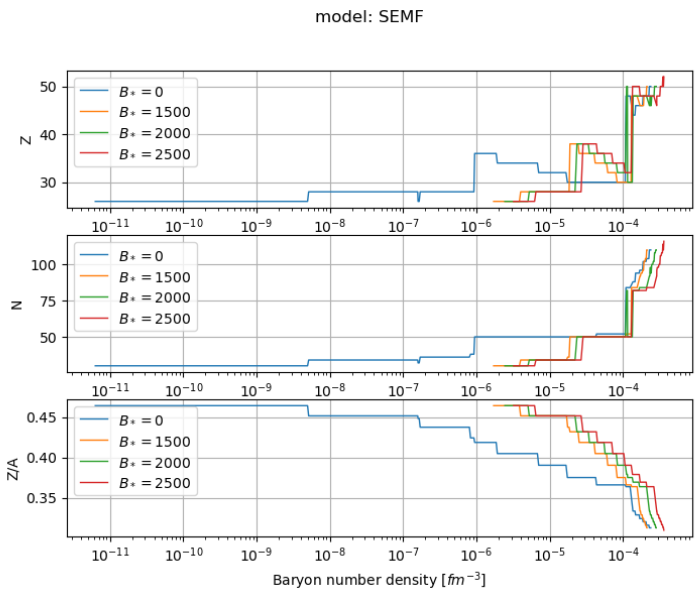

(b)

Figure 5.17: Atomic number, neutron number and proton fraction as a function of (a) energy density and of (b) baryon number density, using the SEMF model with different magnetic field strengths $B_\star$

FRDM2012 model

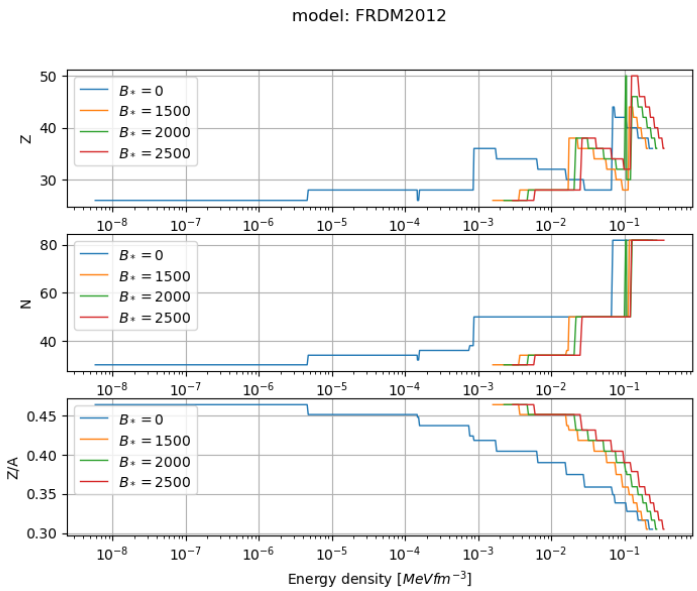

(a)

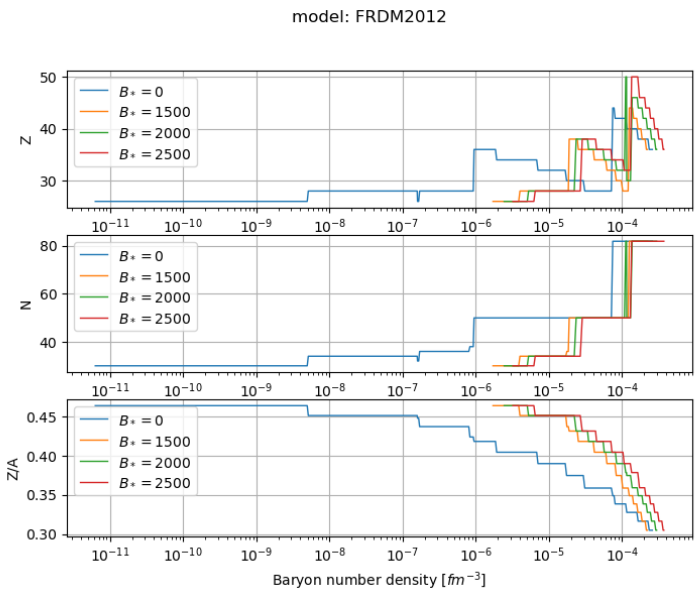

(b)

Figure 5.18: The same as Figure 5.17, using the FRDM2012 model with different magnetic field strengths $B_\star$

5.4.12 M_{cr} for different M and R and various $B_\star$

The gravitational mass[17], in solar mass units, of outer crust, for various combinations of gravitational mass M and radius R of a neutron star, using the SEMF and FRDM2012 model, and different magnetic field strengths, is shown in Figs. 5.19 and 5.20, respectively. For the same M and R, from the inequality of Eq. 4.6.16, the mass of outer crust, in the absence of magnetic field, is always smaller than the respective mass, in a strongly quantizing magnetic field, also, from Eq. 4.6.14, $\tilde{M}_{cr} \propto B_\star$, so, the mass of outer crust increases with the magnetic field strength, in the strong quantization regime. Furthermore, M_{cr} *and* $\tilde{M}_{cr} \propto R^3(\frac{Rc^2}{2GM} - 1)$ (see, Eqs. 4.6.13 and 4.6.14), so, the mass of outer crust increases with the radius R and decreases with the mass M.

SEMF model

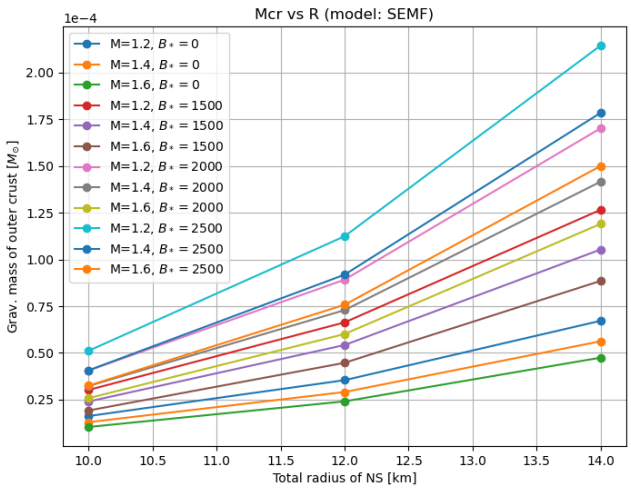

Figure 5.19: Mass of outer crust for different masses and radii of NS, using the SEMF model with different magnetic field strengths $B_\star$. Clarification: the 2nd line from above (i.e., 1st dark blue line from above) and the 4th line from above (i.e., 1st orange line from above) correspond to ($M = 1.4$, $B_\star = 2500$) and ($M = 1.6$, $B_\star = 2500$), respectively

[17]for the other models, see Appendix I

FRDM2012 model

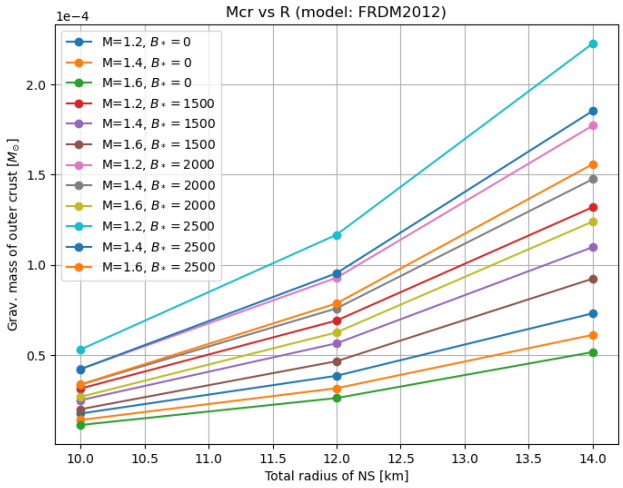

Figure 5.20: The same as Figure 5.19, using the FRDM2012 model with different magnetic field strengths $B_\star$

5.4.13 z_{drip} for different M and R and various $B_\star$

The proper thickness[18], in km, of outer crust, for various combinations of gravitational mass M and radius R of a neutron star, using the SEMF and FRDM2012 model, and different magnetic field strengths, is shown in Figs. 5.21 and 5.22, respectively. For the same M and R, from Eq. 4.6.25, the proper thickness does not depend on the magnetic field strength and the thickness of the field-free case is equal to the respective thickness of the strongly quantizing magnetic field. In addition, z_{drip} *and* $\tilde{z}_{drip} \propto R\sqrt{\frac{Rc^2}{2GM}(\frac{Rc^2}{2GM}-1)}$ (see, Eqs. 4.6.20 and 4.6.24), so, the thickness of outer crust increases with the radius R and decreases with the mass M.

[18]for the other models, see Appendix I

SEMF model

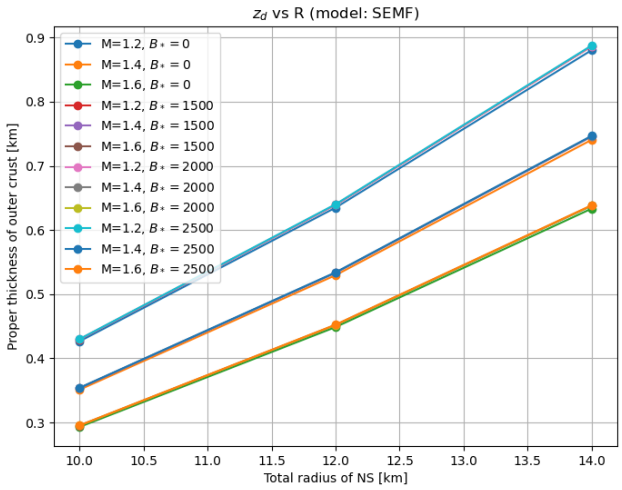

Figure 5.21: Proper depth of neutron-drip transition for different masses and radii of NS, using the SEMF model with different magnetic field strengths $B_\star$. Clarification: the dark blue line of the 2nd group of overlapping lines from above and the orange line of the 3rd group of overlapping lines from above correspond to ($M = 1.4$, $B_\star = 2500$) and ($M = 1.6$, $B_\star = 2500$), respectively

FRDM2012 model

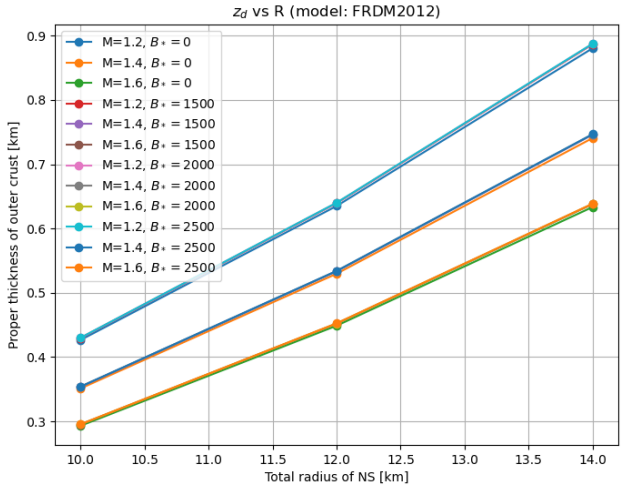

Figure 5.22: The same as Figure 5.21, using the FRDM2012 model with different magnetic field strengths $B_\star$

5.5 The surface of outer crust

The surface density, in the case of a strongly quantizing field, is much higher than the respective density for the field-free case, as shown in Table 5.14 (see, also, Eqs. 4.1.12 and 4.1.26). In addition, in the strong quantization regime, $\tilde{n}_{b_{surf}} \propto B_\star^{6/5}$, so, the surface density increases with the magnetic field strength. Moreover, the value of surface density does not depend on the mass model, because the equilibrium nucleus, at the surface layer, is ^{56}Fe.

Table 5.14: At the surface of outer crust are listed the surface energy density ϵ_{surf} in MeV/fm^3 and the surface baryon number density in fm^{-3}, using different models with various magnetic field strengths $B_\star$

$B_\star$	0		1500		2000		2500	
model	ϵ_{surf}	$n_{b_{surf}}$	ϵ_{surf}	$n_{b_{surf}}$	ϵ_{surf}	$n_{b_{surf}}$	ϵ_{surf}	$n_{b_{surf}}$
SEMF	5.857E-09	6.295E-12	1.597E-03	1.717E-06	2.271E-03	2.441E-06	2.986E-03	3.210E-06
FRDM2012	5.857E-09	6.295E-12	1.597E-03	1.717E-06	2.271E-03	2.441E-06	2.986E-03	3.210E-06
WS4RBF	5.857E-09	6.295E-12	1.597E-03	1.717E-06	2.271E-03	2.441E-06	2.986E-03	3.210E-06
BSKG3	5.857E-09	6.295E-12	1.597E-03	1.717E-06	2.271E-03	2.441E-06	2.986E-03	3.210E-06
HFB31	5.857E-09	6.295E-12	1.597E-03	1.717E-06	2.271E-03	2.441E-06	2.986E-03	3.210E-06
DDMED	5.857E-09	6.295E-12	1.597E-03	1.717E-06	2.271E-03	2.441E-06	2.986E-03	3.210E-06
DDPC1	5.857E-09	6.295E-12	1.597E-03	1.717E-06	2.271E-03	2.441E-06	2.986E-03	3.210E-06
SVMIN	5.857E-09	6.295E-12	1.597E-03	1.717E-06	2.271E-03	2.441E-06	2.986E-03	3.210E-06
UNEDF0	5.857E-09	6.295E-12	1.597E-03	1.717E-06	2.271E-03	2.441E-06	2.986E-03	3.210E-06

5.6 The bottom of outer crust

The properties of the bottom layer of outer crust, for different models and magnetic field strengths, are listed in Tables 5.15, 5.16, 5.17 and 5.18. The nuclide present in the bottom layer (i.e., Z_{drip} and A_{drip}) depends on the mass model, but remains the same for all $B_\star$ (see, Eq. 4.2.4), with some exceptions, as regard, the SEMF and UNEDF0 model. Also, the electron chemical potential is approximately $26MeV$, in all cases, and, obviously, the baryon chemical potential is equal to the neutron mass. In addition, for strongly quantizing magnetic field, the pressure and the density increase with the magnetic field strength, with some small differences among the models (see, Eqs. 4.2.8 and 4.2.9), and, also, the inequalities of Eq. 4.2.13 hold.

Table 5.15: At the bottom of outer crust are listed the *element*, the pressure P_{drip} in MeV/fm^3, the energy density ϵ_{drip} in MeV/fm^3, the baryon number density $n_{b_{drip}}$ in fm^{-3}, the atomic number Z_{drip}, the neutron number N_{drip}, the baryon chemical potential $\mu_{b_{drip}}$ in MeV and the electron chemical potential $\mu_{e_{drip}}$ in MeV, at the neutron-drip transition, using different models with magnetic field strength $B_\star = 0$

model	element	P_{drip}	ϵ_{drip}	$n_{b_{drip}}$	Z_{drip}	N_{drip}	$\mu_{b_{drip}}$	$\mu_{e_{drip}}$
SEMF	^{160}Sn	4.503E-04	2.241E-01	2.390E-04	50	110	939.564	25.714
FRDM2012	^{118}Kr	4.905E-04	2.424E-01	2.585E-04	36	82	939.564	26.185
WS4RBF	^{120}Sr	4.699E-04	2.265E-01	2.416E-04	38	82	939.563	25.919
BSKG3	^{124}Sr	4.861E-04	2.401E-01	2.560E-04	38	86	939.565	26.140
HFB31	^{122}Sr	4.876E-04	2.367E-01	2.525E-04	38	84	939.564	26.159
DDMED	^{118}Kr	4.876E-04	2.413E-01	2.574E-04	36	82	939.564	26.146
DDPC1	^{118}Kr	5.044E-04	2.475E-01	2.640E-04	36	82	939.564	26.369
SVMIN	^{126}Sr	4.912E-04	2.459E-01	2.622E-04	38	88	939.565	26.207
UNEDF0	^{174}Sn	4.955E-04	2.619E-01	2.793E-04	50	124	939.564	26.337

Table 5.16: The same as Table 5.15, using different models with $B_\star = 1500$

model	element	P_{drip}	ϵ_{drip}	$n_{b_{drip}}$	Z_{drip}	N_{drip}	$\mu_{b_{drip}}$	$\mu_{e_{drip}}$
SEMF	^{160}Sn	8.226E-04	1.983E-01	2.119E-04	50	110	939.563	25.650
FRDM2012	^{118}Kr	8.585E-04	2.068E-01	2.211E-04	36	82	939.565	26.120
WS4RBF	^{120}Sr	8.410E-04	1.973E-01	2.109E-04	38	82	939.565	25.866
BSKG3	^{124}Sr	8.547E-04	2.056E-01	2.197E-04	38	86	939.565	26.075
HFB31	^{122}Sr	8.560E-04	2.024E-01	2.163E-04	38	84	939.564	26.094
DDMED	^{118}Kr	8.560E-04	2.065E-01	2.207E-04	36	82	939.565	26.082
DDPC1	^{118}Kr	8.700E-04	2.082E-01	2.225E-04	36	82	939.563	26.292
SVMIN	^{126}Sr	8.585E-04	2.093E-01	2.237E-04	38	88	939.563	26.132
UNEDF0	^{136}Zr	8.623E-04	2.152E-01	2.300E-04	40	96	939.564	26.200

Table 5.17: The same as Table 5.15, using different models with $B_\star = 2000$

model	element	P_{drip}	ϵ_{drip}	$n_{b_{drip}}$	Z_{drip}	N_{drip}	$\mu_{b_{drip}}$	$\mu_{e_{drip}}$
SEMF	^{160}Sn	1.106E-03	2.659E-01	2.842E-04	50	110	939.560	25.796
FRDM2012	^{118}Kr	1.153E-03	2.771E-01	2.961E-04	36	82	939.564	26.242
WS4RBF	^{120}Sr	1.129E-03	2.643E-01	2.825E-04	38	82	939.563	25.989
BSKG3	^{124}Sr	1.148E-03	2.754E-01	2.943E-04	38	86	939.563	26.198
HFB31	^{122}Sr	1.149E-03	2.711E-01	2.898E-04	38	84	939.562	26.217
DDMED	^{118}Kr	1.149E-03	2.767E-01	2.957E-04	36	82	939.563	26.204
DDPC1	^{118}Kr	1.168E-03	2.789E-01	2.981E-04	36	82	939.562	26.415
SVMIN	^{126}Sr	1.153E-03	2.804E-01	2.997E-04	38	88	939.561	26.255
UNEDF0	^{174}Sn	1.160E-03	2.961E-01	3.163E-04	50	124	939.563	26.404

Table 5.18: The same as Table 5.15, using different models with $B_\star = 2500$

model	element	P_{drip}	ϵ_{drip}	$n_{b_{drip}}$	Z_{drip}	N_{drip}	$\mu_{b_{drip}}$	$\mu_{e_{drip}}$
SEMF	^{168}Te	1.394E-03	3.375E-01	3.607E-04	52	116	939.561	25.946
FRDM2012	^{118}Kr	1.448E-03	3.476E-01	3.715E-04	36	82	939.560	26.337
WS4RBF	^{120}Sr	1.421E-03	3.319E-01	3.547E-04	38	82	939.564	26.102
BSKG3	^{124}Sr	1.444E-03	3.457E-01	3.695E-04	38	86	939.564	26.312
HFB31	^{122}Sr	1.446E-03	3.404E-01	3.638E-04	38	84	939.563	26.332
DDMED	^{118}Kr	1.444E-03	3.471E-01	3.710E-04	36	82	939.560	26.299
DDPC1	^{118}Kr	1.470E-03	3.501E-01	3.742E-04	36	82	939.564	26.530
SVMIN	^{126}Sr	1.451E-03	3.521E-01	3.763E-04	38	88	939.562	26.370
UNEDF0	^{174}Sn	1.461E-03	3.720E-01	3.975E-04	50	124	939.565	26.544

5.7 P_{drip} vs $B_\star$

The neutron-drip pressure as a function of the magnetic field strength increases linearly (see, Eq. 4.2.8), in the strong quantization regime (i.e., for $B_\star \gtrsim 1300$, from Eq. 4.2.10), as shown in Fig. 5.23. Also, the small differences in the value of P_{drip}, which was listed in the Tables of Section 5.6, among the models, are observed.

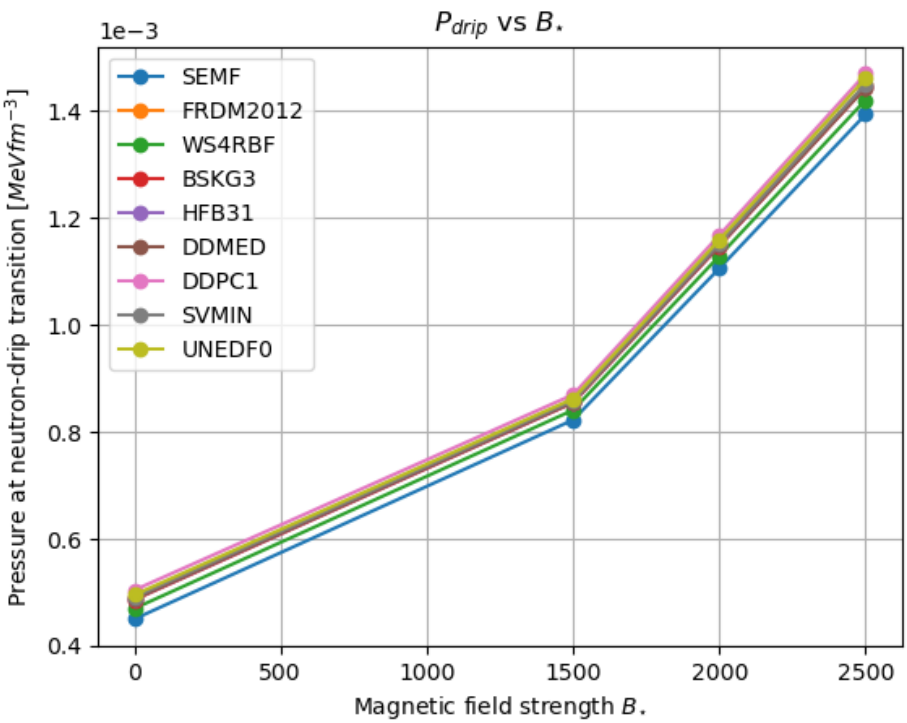

Figure 5.23: Neutron-drip transition pressure as a function of magnetic field strength, using different nuclear mass models

5.8 Different models with $B_\star = 0, 1500$

The last part of this work is to put the graphs of the different models in the same plot (see, Appendix K), in order to ascertain if there is a dependence on the model used, in the above properties.

5.8.1 P vs ϵ or n_b

The EoS[19], for $B_\star = 0, 1500$, using various mass models, is shown in Figs. 5.24 and 5.25, respectively. The EoS is substantially the same for all models, because the main contribution to the total pressure is from the electron pressure.

[19]for the other magnetic field strengths (i.e., $B_\star = 2000, 2500$), see Appendix I

$B_\star = 0$

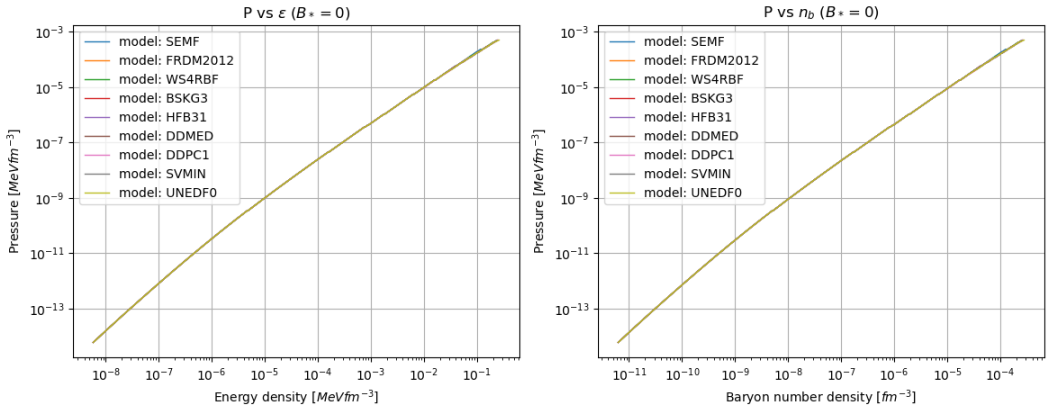

(a) (b)

Figure 5.24: Equation of State, (a) pressure as a function of energy density and (b) pressure as a function of baryon number density, using different models with magnetic field strength $B_\star = 0$

$B_\star = 1500$

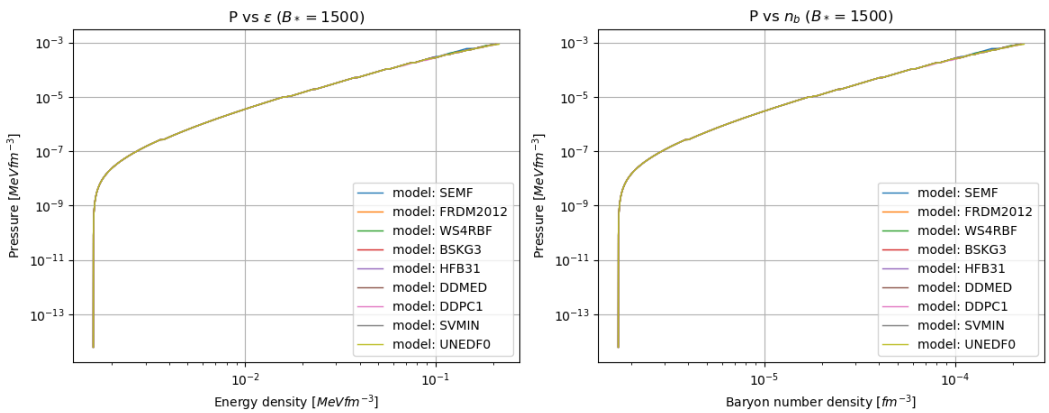

(a) (b)

Figure 5.25: The same as Figure 5.24, using different models with magnetic field strength $B_\star = 1500$

5.8.2 Γ vs ϵ or n_b

The adiabatic index[20], for $B_\star = 0, 1500$, using various mass models, is shown in Figs. 5.26 and 5.27, respectively. The adiabatic index as a function of density does not present any noticeable difference, for the different models, apart from the jumps, corresponding to phase transition.

$B_\star = 0$

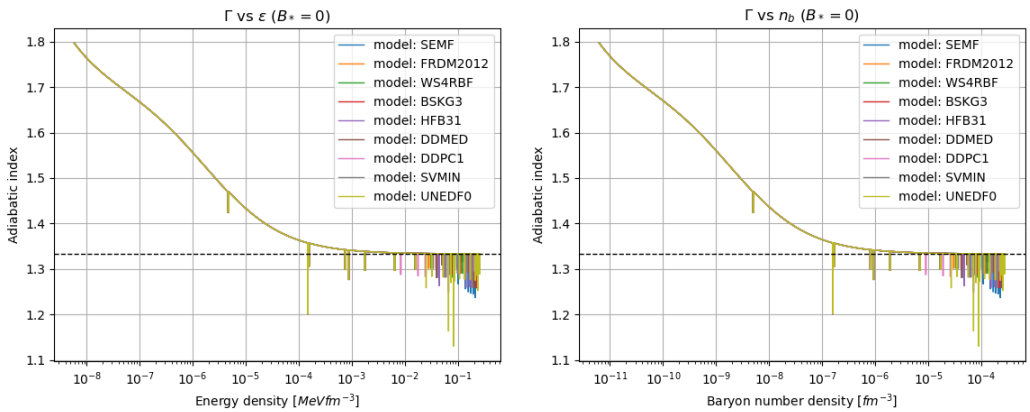

(a) (b)

Figure 5.26: Adiabatic index as a function of (a) energy density and of (b) baryon number density, using different models with magnetic field strength $B_\star = 0$. The horizontal dashed line corresponds to $\Gamma = 4/3$

[20]for the other magnetic field strengths (i.e., $B_\star = 2000, 2500$), see Appendix I

$B_\star = 1500$

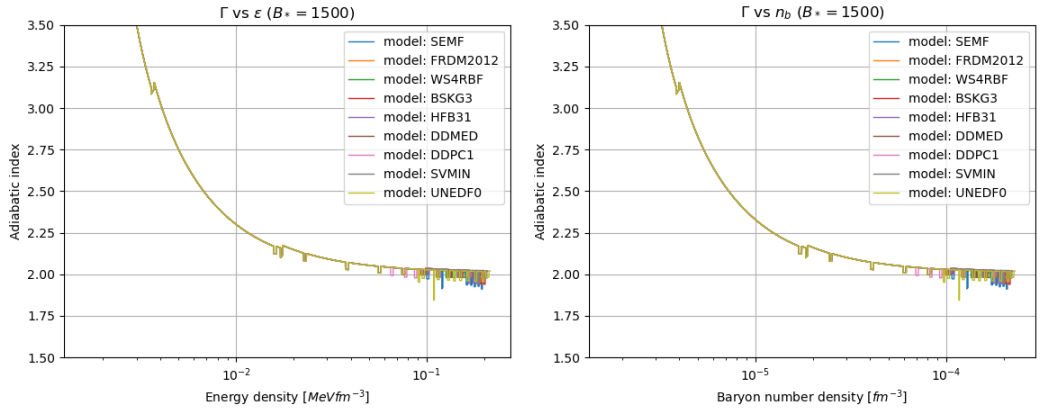

(a) (b)

Figure 5.27: The same as Figure 5.26, using different models with magnetic field strength $B_\star = 1500$

5.8.3 c_s vs ϵ or n_b

The speed of sound[21] as a function of density, for $B_\star = 0, 1500$, using various mass models, is shown in Figs. 5.28 and 5.29, respectively. Some deviations are observed at high densities, where the composition varies from one model to the other.

[21] for the other magnetic field strengths (i.e., $B_\star = 2000, 2500$), see Appendix I

$B_\star = 0$

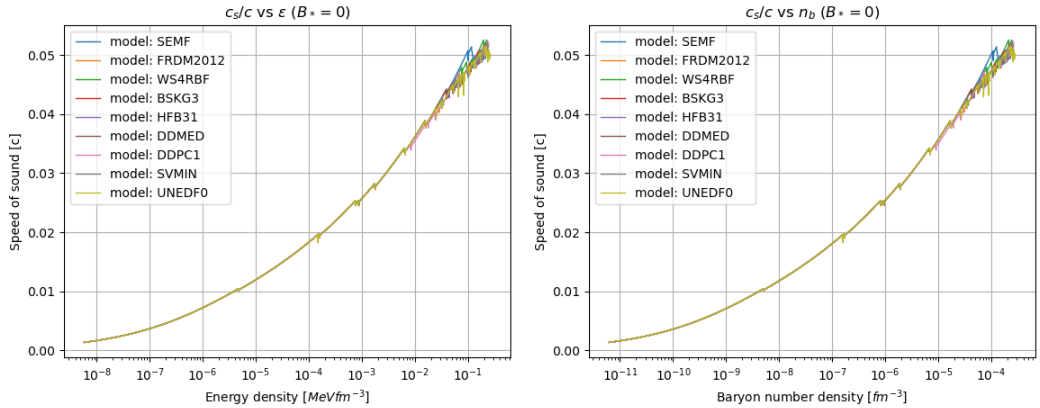

(a) (b)

Figure 5.28: Speed of sound as a function of (a) energy density and of (b) baryon number density, using different models with magnetic field strength $B_\star = 0$

$B_\star = 1500$

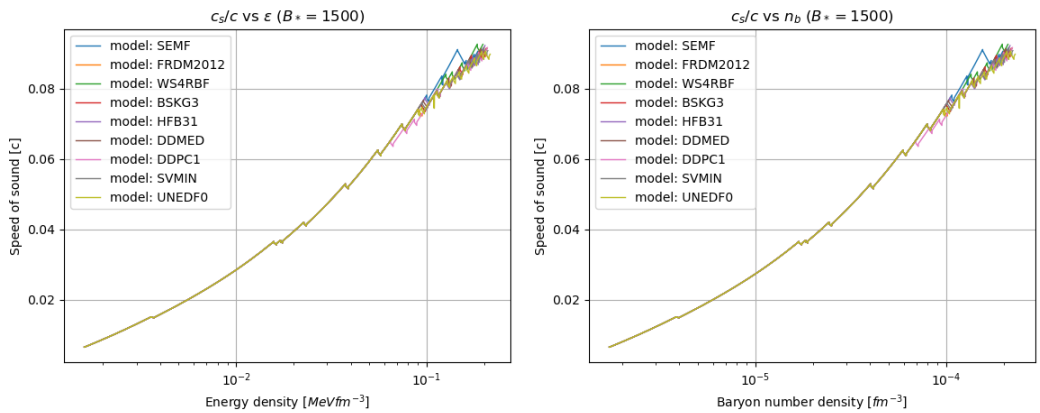

(a) (b)

Figure 5.29: The same as Figure 5.28, using different models with magnetic field strength $B_\star = 1500$

5.8.4 K_{mod} vs ϵ or n_b

The compression modulus[22] as a function of density, for $B_\star = 0, 1500$, using various mass models, is shown in Figs. 5.30 and 5.31, respectively. The compression modulus does not present important differences among the mass models.

$B_\star = 0$

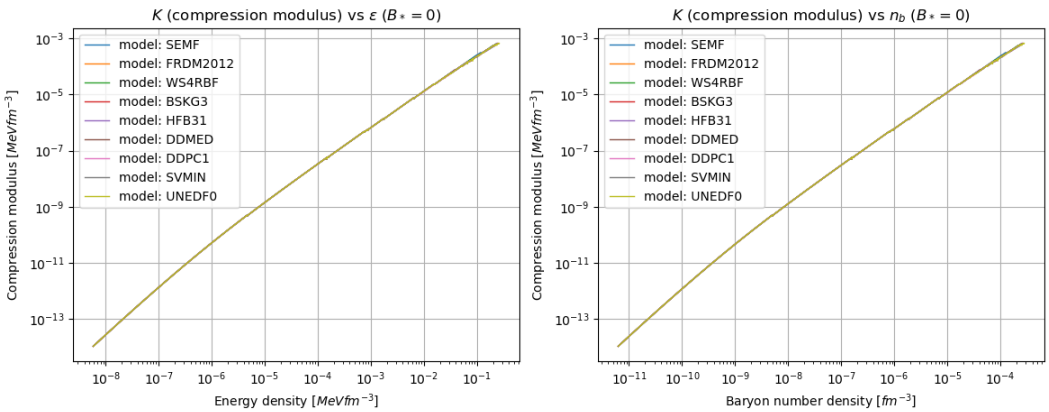

(a) (b)

Figure 5.30: Compression modulus as a function of (a) energy density and of (b) baryon number density, using different models with magnetic field strength $B_\star = 0$

[22] for the other magnetic field strengths (i.e., $B_\star = 2000, 2500$), see Appendix I

$B_\star = 1500$

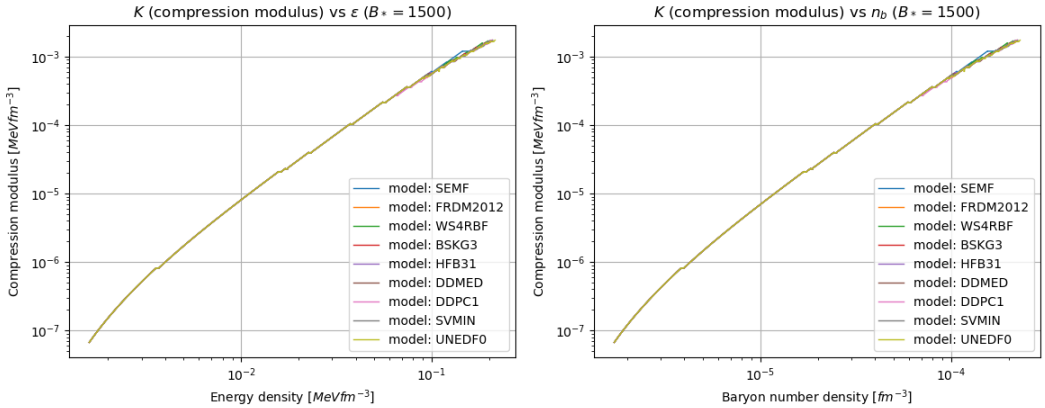

(a) (b)

Figure 5.31: The same as Figure 5.30, using different models with magnetic field strength $B_\star = 1500$

5.8.5 S_{mod} vs ϵ or n_b

The effective shear modulus[23] as a function of density, for $B_\star = 0, 1500$, using various mass models, is shown in Figs. 5.32 and 5.33, respectively. At the high densities, the effective shear modulus presents some noticeable differences, especially, for the case of a strongly quantizing magnetic field, where the values of the modulus have a smaller range.

[23] for the other magnetic field strengths (i.e., $B_\star = 2000, 2500$), see Appendix I

$B_\star = 0$

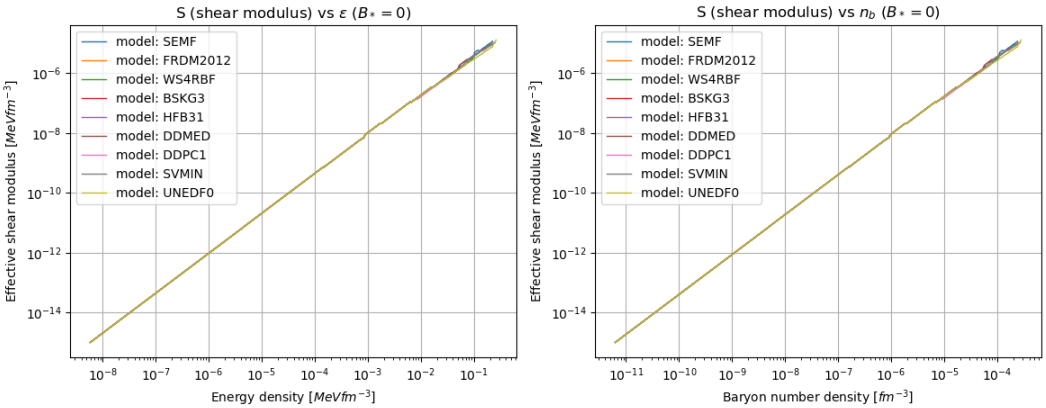

(a) (b)

Figure 5.32: Effective shear modulus as a function of (a) energy density and of (b) baryon number density, using different models with magnetic field strength $B_\star = 0$

$B_\star = 1500$

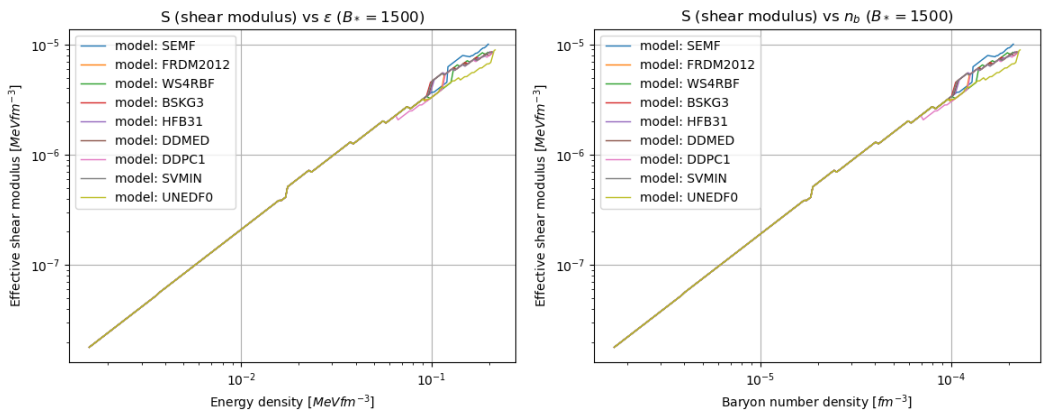

(a) (b)

Figure 5.33: The same as Figure 5.32, using different models with magnetic field strength $B_\star = 1500$

5.8.6 S_{mod}/K_{mod} vs ϵ or n_b

The ratio of the effective shear modulus to the compression modulus[24] as a function of density, for $B_\star = 0, 1500$, using various mass models, is shown in Figs. 5.34 and 5.35, respectively. At the region of high densities, some deviations are observed, for the field-free case, where the ratio has a smaller range of values.

$B_\star = 0$

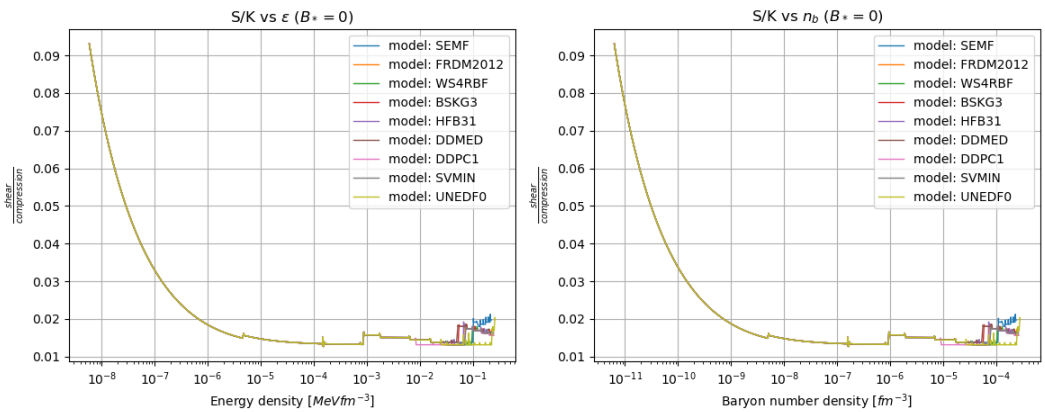

(a) (b)

Figure 5.34: Effective shear modulus over compression modulus as a function of (a) energy density and of (b) baryon number density, using different models with magnetic field strength $B_\star = 0$

[24] for the other magnetic field strengths (i.e., $B_\star = 2000, 2500$), see Appendix I

$B_\star = 1500$

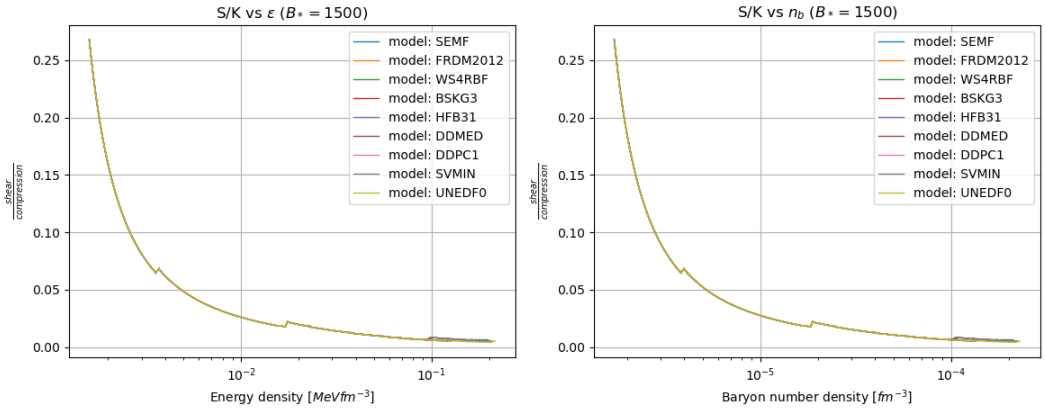

(a) (b)

Figure 5.35: The same as Figure 5.34, using different models with magnetic field strength $B_\star = 1500$

5.8.7 Z, N, Z/A vs ϵ or n_b

The atomic number, Z, the neutron number, N, and the proton fraction, Z/A,[25] as a function of density, for $B_\star = 0, 1500$, using some of the available models, are shown in Figs. 5.36 and 5.37, respectively. In the region of high densities, there are some differences, because the predictions for the composition depend on the mass model.

[25] for the other magnetic field strengths (i.e., $B_\star = 2000, 2500$), see Appendix I

$B_\star = 0$

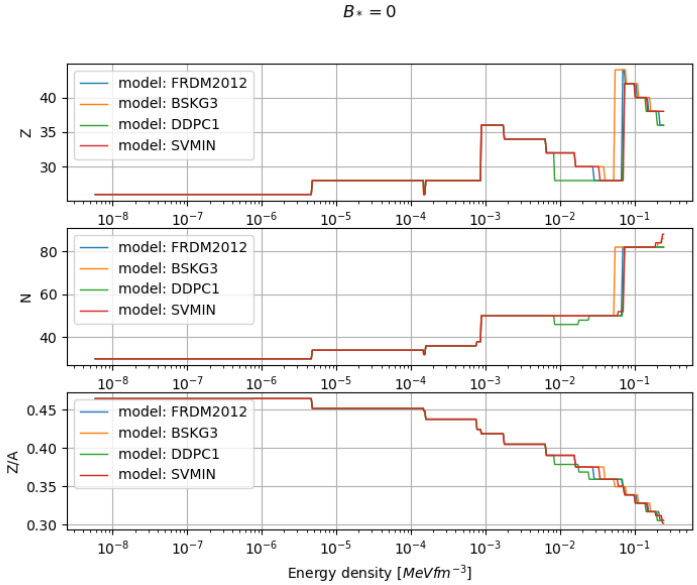

(a)

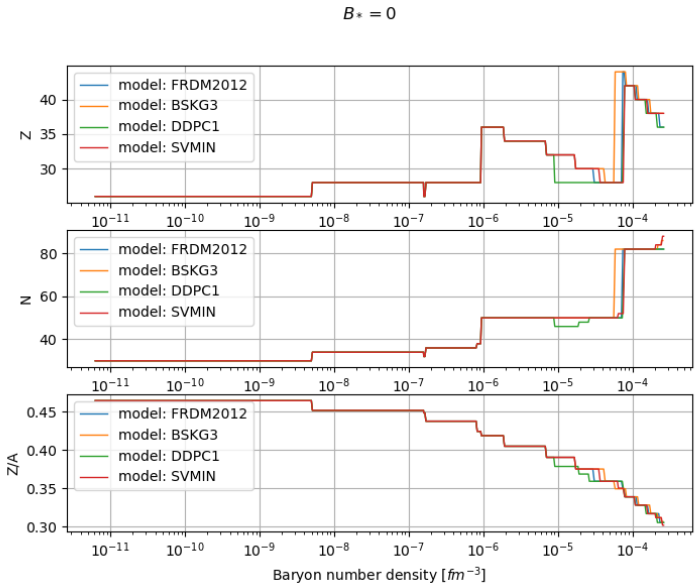

(b)

Figure 5.36: Atomic number, neutron number and proton fraction as a function of (a) energy density and of (b) baryon number density, using different models with magnetic field strength $B_\star = 0$

$B_\star = 1500$

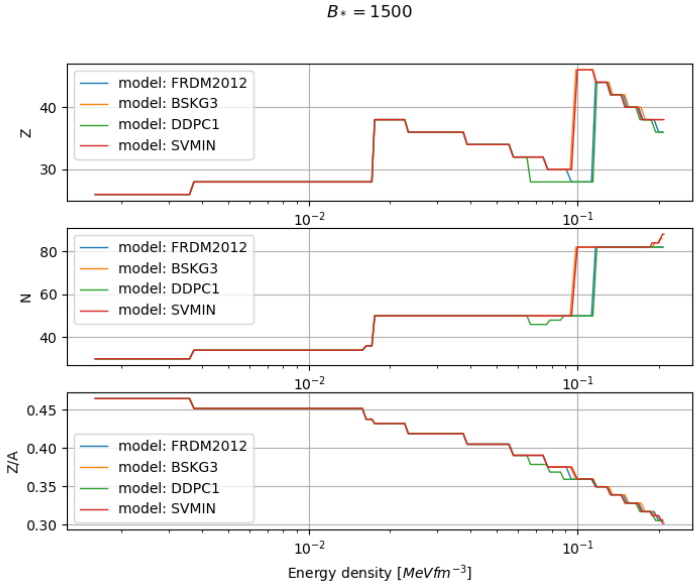

(a)

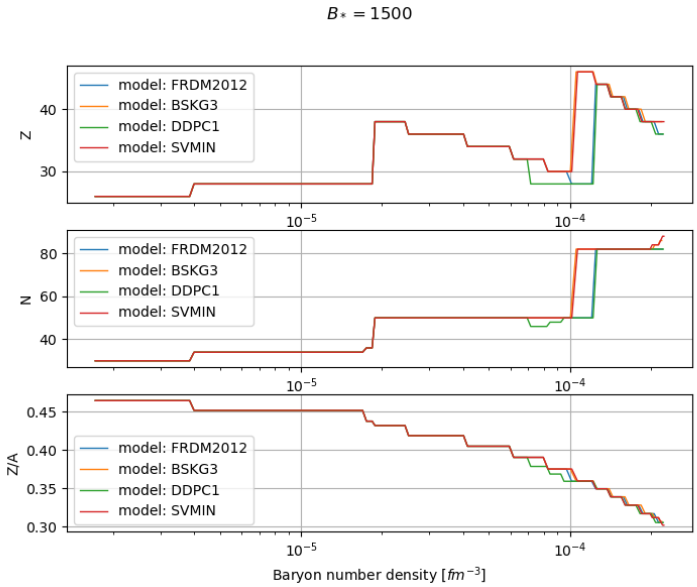

(b)

Figure 5.37: The same as Figure 5.36, using different models with magnetic field strength $B_\star = 1500$

5.8.8 M_{cr} for different M and R

The gravitational mass[26], in solar mass units, of outer crust, for various combinations of gravitational mass M and radius R of a neutron star, with $B_\star = 0, 1500$ and using some of the available models, is shown in Figs. 5.38 and 5.39, respectively. The mass of outer crust is slightly model-dependent, of course, the neutron-drip pressure is approximately the same for all models (see, Tables of Section 5.6), a quantity from which the mass of outer crust depends linearly (see, Eq. 4.6.11).

$B_\star = 0$

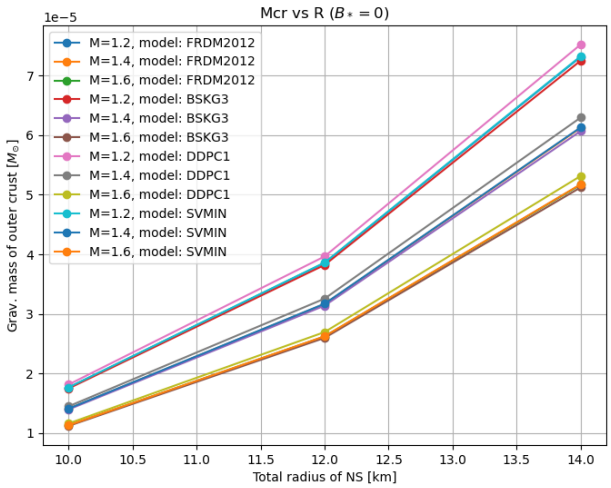

Figure 5.38: Mass of outer crust for different masses and radii of NS, using different models with magnetic field strength $B_\star = 0$. Clarification: the dark blue line of the 2nd group of overlapping lines from above and the orange line of the 3rd group of overlapping lines from above correspond to ($M = 1.4$, $model: SVMIN$) and ($M = 1.6$, $model: SVMIN$), respectively

[26]for the other magnetic field strengths (i.e., $B_\star = 2000, 2500$), see Appendix I

$B_\star = 1500$

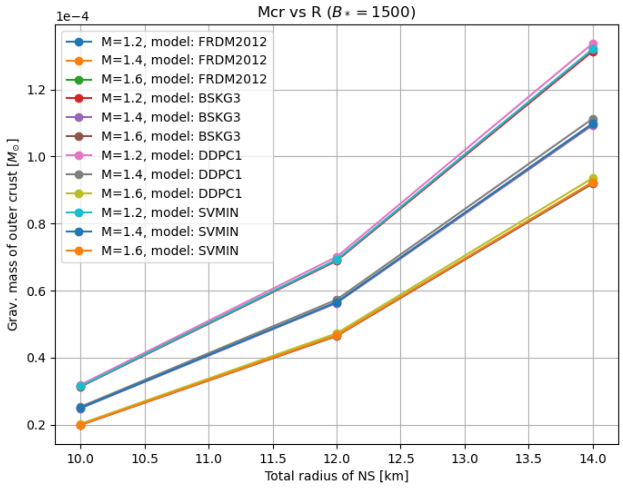

Figure 5.39: The same as Figure 5.38, using different models with magnetic field strength $B_\star = 1500$

5.8.9 z_{drip} for different M and R

The proper thickness[27], in km, of outer crust, for various combinations of gravitational mass M and radius R of a neutron star, with $B_\star = 0, 1500$ and using some of the available models, is shown in Figs. 5.40 and 5.41, respectively. The proper thickness is essentially the same for all models, because depends on the ratio of neutron-drip pressure to neutron-drip energy density (see, Eqs. 4.6.19 and 4.6.23), quantities that are approximately the same for all models (see, Tables of Section 5.6).

[27]for the other magnetic field strengths (i.e., $B_\star = 2000, 2500$), see Appendix I

$B_\star = 0$

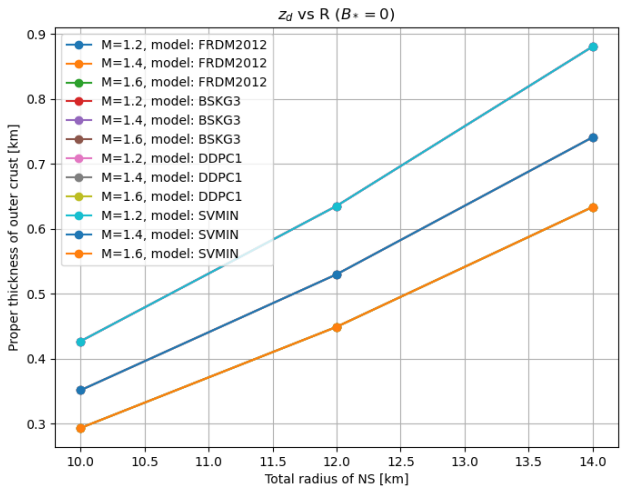

Figure 5.40: Proper depth of neutron-drip transition for different masses and radii of NS, using different models with magnetic field strength $B_\star = 0$. Clarification: the dark blue line of the 2nd group of overlapping lines from above and the orange line of the 3rd group of overlapping lines from above correspond to ($M = 1.4$, $model: SVMIN$) and ($M = 1.6$, $model: SVMIN$), respectively

$B_\star = 1500$

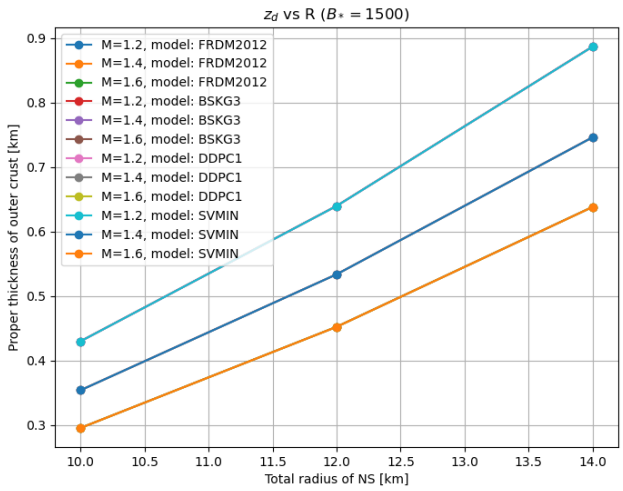

Figure 5.41: The same as Figure 5.40, using different models with magnetic field strength $B_\star = 1500$

Chapter 6

Summary and Conclusions

The aim of this work was to study the properties of the outer crust of cold non-accreting neutron stars, firstly, in the absence of a magnetic field, and, then, in the presence of a strongly quantizing magnetic field, using a theoretical mass model for the experimentally unknown nuclear masses. Thus, some conclusions were drawn on how the magnetic field and the choice of a mass model affect these properties. More specifically:

The Equation of State presents a strong stiffness for the case of a strongly quantizing field, at surface layers, and a much higher surface density, which increases with the magnetic field strength. Also, the neutron-drip pressure and density increase with the magnetic field and, generally, the EoS is substantially the same for all models. However, a polytrope is not a good choice to fit the EoS on the whole range of densities, because of its too simple form.

The composition is well established at the top layers, because the masses of the nuclei are derived from experimental data, while, at the bottom layers, there are some uncertainties, since the predictions are model-dependent. Future experiments are expected to find the properties of neutron-rich nuclei near the neutron-drip line, reducing these uncertainties. In addition, the pairing and shell effects play a crucial role, due to the presence of even-even nuclei and nuclei with magic numbers. With increasing density, the nuclei become more neutron-rich and the proton fraction decreases. Also, in the presence of a strongly quantizing magnetic field, there is a delay in the appearance of a new phase and the phase transitions occur at higher densities, with the nuclei to be more symmetric, at the same density.

The adiabatic index approaches asymptotically, at the high densities, the value 4/3, for the field-free case, and the value 2, for the strongly quantizing

magnetic field, but, does not present any noticeable difference among the different models used.

The speed of sound increases with the density, having a relative small value, in units of speed of light. At the neutron-drip transition, the speed of sound is almost twice, in the presence of a strongly quantizing magnetic field, comparing with the respective speed of the field-free case. In addition, some deviations are observed at high densities, where the composition varies from one model to the other.

The outer crust is more susceptible to shear than to compression deformation, as the ratio of the effective shear modulus to the compression modulus is smaller than one. Both the compression and the effective shear modulus increase with the density. At the neutron-drip transition, the compression modulus, in the absence of a magnetic field, is always smaller than the respective compression modulus, in the presence of a strongly quantizing field, and, also, does not present important differences among the mass models. On the contrary, for the effective shear modulus, at the neutron-drip transition, it is not clear if always it is smaller, without magnetic field, but in the presence of a strong field, increases with the magnetic field strength, and there is a model-dependency at high densities.

Finally, the presence of a strongly quantizing magnetic field increases the gravitational mass of outer crust, while the proper thickness does not depend on the magnetic field strength. But, both quantities increase with the radius and decrease with the mass of the neutron star, and, also, they are quite model-independent, especially the thickness.

Appendix A

Tables for $B_\star = 0$

Below are the Tables, like those in Subsections 5.4.1 - 5.4.2, for the models: WS4RBF, BSKG3, HFB31, DDMED, DDPC1, SVMIN and UNEDF0, with magnetic field strength $B_\star = 0$.

A.1 WS4RBF

Table A.1: The same as Table 5.2, using the WS4RBF model with $B_\star = 0$

№	P_{min}	P_{max}	ϵ_{min}	ϵ_{max}	$n_{b_{min}}$	$n_{b_{max}}$	A	Z	N	Z/A	$\mu_{b_{min}}$	$\mu_{b_{max}}$	$\mu_{e_{min}}$	$\mu_{e_{max}}$
1	6.082E-15	3.388E-10	5.857E-09	4.615E-06	6.295E-12	4.960E-09	56	26	30	0.464	930.414	930.603	0.518	0.954
2	3.393E-10	4.160E-08	4.758E-06	1.470E-04	5.113E-09	1.579E-07	62	28	34	0.452	930.604	931.306	0.955	2.583
3	4.166E-08	4.393E-08	1.480E-04	1.539E-04	1.590E-07	1.653E-07	58	26	32	0.448	931.306	931.320	2.582	2.615
4	4.400E-08	3.565E-07	1.582E-04	7.466E-04	1.699E-07	8.015E-07	64	28	36	0.438	931.321	932.040	2.617	4.335
5	3.570E-07	4.137E-07	7.708E-04	8.603E-04	8.274E-07	9.234E-07	66	28	38	0.424	932.041	932.106	4.337	4.496
6	4.143E-07	1.028E-06	8.782E-04	1.731E-03	9.426E-07	1.857E-06	86	36	50	0.419	932.107	932.556	4.507	5.637
7	1.030E-06	5.572E-06	1.790E-03	6.332E-03	1.920E-06	6.788E-06	84	34	50	0.405	932.557	933.686	5.636	8.565
8	5.581E-06	1.766E-05	6.566E-03	1.557E-02	7.038E-06	1.668E-05	82	32	50	0.390	933.687	934.747	8.564	11.410
9	1.769E-05	4.182E-05	1.620E-02	3.090E-02	1.735E-05	3.306E-05	80	30	50	0.375	934.748	935.727	11.408	14.139
10	4.188E-05	1.316E-04	3.226E-02	7.620E-02	3.452E-05	8.144E-05	78	28	50	0.359	935.729	937.337	14.136	18.813
11	1.318E-04	1.688E-04	7.825E-02	9.423E-02	8.362E-05	1.007E-04	80	28	52	0.350	937.340	937.742	18.819	20.020
12	1.690E-04	2.175E-04	9.849E-02	1.190E-01	1.052E-04	1.271E-04	124	42	82	0.339	937.744	938.162	20.095	21.401
13	2.178E-04	4.122E-04	1.229E-01	1.985E-01	1.312E-04	2.118E-04	122	40	82	0.328	938.165	939.312	21.399	25.096
14	4.128E-04	4.699E-04	2.055E-01	2.265E-01	2.192E-04	2.416E-04	120	38	82	0.317	939.315	939.563	25.093	25.919

Table A.2: The same as Table 5.3, using the WS4RBF model with $B_\star = 0$

M_{cr}	M_{cr}/M	ΔR_{cr}	$\Delta R_{cr}/R$	$M_{b_{cr}}$	Δ_{grav}	z_{drip}	ΔN
3.622E-05	2.587E-05	4.717E-01	3.773E-02	4.462E-05	2.320E-01	5.794E-01	5.297E+52

Table A.3: The same as Table 5.4, using the WS4RBF model with $B_\star = 0$

№	r_{min}	r_{max}	ΔR_l	$\Delta R_l/\Delta R_{cr}$	z_l	z_l/z_{drip}	M_{b_l}	$M_{b_l}/M_{b_{cr}}$	M_l	M_l/M_{cr}	ΔN_l	$\Delta N_l/\Delta N$
1	12.490	12.500	1.027E-02	2.177E-02	0.013	2.167E-02	3.676E-11	8.238E-07	3.006E-11	8.299E-07	4.364E+46	8.238E-07
2	12.452	12.490	3.794E-02	8.044E-02	0.059	1.018E-01	4.432E-09	9.933E-05	3.623E-09	1.000E-04	5.262E+48	9.933E-05
3	12.451	12.452	7.507E-04	1.591E-03	0.060	1.034E-01	2.421E-10	5.427E-06	1.979E-10	5.464E-06	2.875E+47	5.427E-06
4	12.412	12.451	3.854E-02	8.172E-02	0.107	1.849E-01	3.315E-08	7.430E-04	2.708E-08	7.477E-04	3.936E+49	7.430E-04
5	12.409	12.412	3.452E-03	7.319E-03	0.111	1.923E-01	5.977E-09	1.339E-04	4.881E-09	1.348E-04	7.096E+48	1.339E-04
6	12.385	12.409	2.389E-02	5.064E-02	0.141	2.429E-01	6.443E-08	1.444E-03	5.260E-08	1.452E-03	7.649E+49	1.444E-03
7	12.326	12.385	5.945E-02	1.260E-01	0.214	3.687E-01	4.691E-07	1.051E-02	3.826E-07	1.056E-02	5.569E+50	1.051E-02
8	12.270	12.325	5.507E-02	1.168E-01	0.281	4.856E-01	1.224E-06	2.743E-02	9.970E-07	2.753E-02	1.453E+51	2.743E-02
9	12.220	12.270	5.029E-02	1.066E-01	0.343	5.924E-01	2.400E-06	5.379E-02	1.953E-06	5.393E-02	2.850E+51	5.379E-02
10	12.139	12.220	8.139E-02	1.726E-01	0.443	7.654E-01	8.708E-06	1.952E-01	7.077E-06	1.954E-01	1.034E+52	1.952E-01
11	12.118	12.138	2.013E-02	4.268E-02	0.468	8.085E-01	3.535E-06	7.923E-02	2.870E-06	7.924E-02	4.197E+51	7.923E-02
12	12.097	12.118	2.080E-02	4.410E-02	0.494	8.530E-01	4.593E-06	1.029E-01	3.727E-06	1.029E-01	5.452E+51	1.029E-01
13	12.041	12.097	5.664E-02	1.201E-01	0.564	9.738E-01	1.817E-05	4.072E-01	1.473E-05	4.067E-01	2.157E+52	4.072E-01
14	12.028	12.040	1.215E-02	2.576E-02	0.579	1.000E+00	5.280E-06	1.183E-01	4.278E-06	1.181E-01	6.268E+51	1.183E-01

A.2 BSKG3

Table A.4: The same as Table 5.2, using the BSKG3 model with $B_\star = 0$

№	P_{min}	P_{max}	ϵ_{min}	ϵ_{max}	$n_{b_{min}}$	$n_{b_{max}}$	A	Z	N	Z/A	$\mu_{b_{min}}$	$\mu_{b_{max}}$	$\mu_{e_{min}}$	$\mu_{e_{max}}$
1	6.082E-15	3.388E-10	5.857E-09	4.615E-06	6.295E-12	4.960E-09	56	26	30	0.464	930.414	930.603	0.518	0.954
2	3.393E-10	4.160E-08	4.758E-06	1.470E-04	5.113E-09	1.579E-07	62	28	34	0.452	930.604	931.306	0.955	2.583
3	4.166E-08	4.393E-08	1.480E-04	1.539E-04	1.590E-07	1.653E-07	58	26	32	0.448	931.306	931.320	2.582	2.615
4	4.400E-08	3.565E-07	1.582E-04	7.466E-04	1.699E-07	8.015E-07	64	28	36	0.438	931.321	932.040	2.617	4.335
5	3.570E-07	4.137E-07	7.708E-04	8.603E-04	8.274E-07	9.234E-07	66	28	38	0.424	932.041	932.106	4.337	4.496
6	4.143E-07	1.028E-06	8.782E-04	1.731E-03	9.426E-07	1.857E-06	86	36	50	0.419	932.107	932.556	4.507	5.637
7	1.030E-06	5.572E-06	1.790E-03	6.332E-03	1.920E-06	6.788E-06	84	34	50	0.405	932.557	933.686	5.636	8.565
8	5.581E-06	1.766E-05	6.566E-03	1.557E-02	7.038E-06	1.668E-05	82	32	50	0.390	933.687	934.747	8.564	11.410
9	1.769E-05	5.598E-05	1.620E-02	3.846E-02	1.735E-05	4.114E-05	80	30	50	0.375	934.748	936.110	11.408	15.206
10	5.607E-05	8.020E-05	4.016E-02	5.255E-02	4.296E-05	5.619E-05	78	28	50	0.359	936.112	936.601	15.204	16.625
11	8.032E-05	1.228E-04	5.471E-02	7.524E-02	5.850E-05	8.041E-05	126	44	82	0.349	936.603	937.217	16.696	18.562
12	1.230E-04	1.947E-04	7.755E-02	1.095E-01	8.288E-05	1.170E-04	124	42	82	0.339	937.220	937.942	18.560	20.818
13	1.950E-04	3.070E-04	1.131E-01	1.591E-01	1.208E-04	1.698E-04	122	40	82	0.328	937.945	938.720	20.816	23.314
14	3.074E-04	4.032E-04	1.647E-01	2.018E-01	1.757E-04	2.153E-04	120	38	82	0.317	938.723	939.214	23.312	24.946
15	4.038E-04	4.583E-04	2.054E-01	2.260E-01	2.192E-04	2.410E-04	122	38	84	0.311	939.217	939.454	24.955	25.757
16	4.590E-04	4.861E-04	2.299E-01	2.401E-01	2.452E-04	2.560E-04	124	38	86	0.306	939.456	939.565	25.767	26.140

Table A.5: The same as Table 5.3, using the BSKG3 model with $B_\star = 0$

M_{cr}	M_{cr}/M	ΔR_{cr}	$\Delta R_{cr}/R$	$M_{b_{cr}}$	Δ_{grav}	z_{drip}	ΔN
3.745E-05	2.675E-05	4.717E-01	3.774E-02	4.614E-05	2.321E-01	5.794E-01	5.478E+52

Table A.6: The same as Table 5.4, using the BSKG3 model with $B_\star = 0$

№	r_{min}	r_{max}	ΔR_l	$\Delta R_l/\Delta R_{cr}$	z_l	z_l/z_{drip}	M_{b_l}	$M_{b_l}/M_{b_{cr}}$	M_l	M_l/M_{cr}	ΔN_l	$\Delta N_l/\Delta N$
1	12.490	12.500	1.027E-02	2.177E-02	0.013	2.167E-02	3.676E-11	7.966E-07	3.006E-11	8.026E-07	4.364E+46	7.966E-07
2	12.452	12.490	3.794E-02	8.043E-02	0.059	1.018E-01	4.432E-09	9.605E-05	3.623E-09	9.675E-05	5.262E+48	9.605E-05
3	12.451	12.452	7.507E-04	1.591E-03	0.060	1.034E-01	2.421E-10	5.248E-06	1.979E-10	5.284E-06	2.875E+47	5.248E-06
4	12.412	12.451	3.854E-02	8.171E-02	0.107	1.849E-01	3.315E-08	7.185E-04	2.708E-08	7.231E-04	3.936E+49	7.185E-04
5	12.409	12.412	3.452E-03	7.318E-03	0.111	1.922E-01	5.977E-09	1.295E-04	4.881E-09	1.303E-04	7.096E+48	1.295E-04
6	12.385	12.409	2.389E-02	5.063E-02	0.141	2.428E-01	6.443E-08	1.396E-03	5.260E-08	1.405E-03	7.649E+49	1.396E-03
7	12.326	12.385	5.945E-02	1.260E-01	0.214	3.687E-01	4.691E-07	1.017E-02	3.826E-07	1.022E-02	5.569E+50	1.017E-02
8	12.270	12.325	5.507E-02	1.167E-01	0.281	4.855E-01	1.224E-06	2.652E-02	9.970E-07	2.662E-02	1.453E+51	2.652E-02
9	12.201	12.270	6.980E-02	1.480E-01	0.367	6.337E-01	3.793E-06	8.221E-02	3.086E-06	8.241E-02	4.503E+51	8.221E-02
10	12.176	12.200	2.479E-02	5.254E-02	0.398	6.865E-01	2.355E-06	5.103E-02	1.914E-06	5.111E-02	2.796E+51	5.103E-02
11	12.145	12.176	3.097E-02	6.565E-02	0.436	7.525E-01	4.101E-06	8.887E-02	3.331E-06	8.895E-02	4.868E+51	8.887E-02
12	12.108	12.144	3.614E-02	7.661E-02	0.481	8.296E-01	6.848E-06	1.484E-01	5.559E-06	1.484E-01	8.130E+51	1.484E-01
13	12.070	12.108	3.845E-02	8.151E-02	0.528	9.117E-01	1.055E-05	2.286E-01	8.555E-06	2.284E-01	1.252E+52	2.286E-01
14	12.045	12.070	2.415E-02	5.119E-02	0.558	9.634E-01	8.918E-06	1.933E-01	7.229E-06	1.930E-01	1.059E+52	1.933E-01
15	12.034	12.045	1.162E-02	2.464E-02	0.573	9.884E-01	5.048E-06	1.094E-01	4.091E-06	1.092E-01	5.993E+51	1.094E-01
16	12.028	12.034	5.298E-03	1.123E-02	0.579	1.000E+00	2.505E-06	5.429E-02	2.030E-06	5.419E-02	2.974E+51	5.429E-02

A.3 HFB31

Table A.7: The same as Table 5.2, using the HFB31 model with $B_\star = 0$

№	P_{min}	P_{max}	ϵ_{min}	ϵ_{max}	$n_{b_{min}}$	$n_{b_{max}}$	A	Z	N	Z/A	$\mu_{b_{min}}$	$\mu_{b_{max}}$	$\mu_{e_{min}}$	$\mu_{e_{max}}$
1	6.082E-15	3.388E-10	5.857E-09	4.615E-06	6.295E-12	4.960E-09	56	26	30	0.464	930.414	930.603	0.518	0.954
2	3.393E-10	4.160E-08	4.758E-06	1.470E-04	5.113E-09	1.579E-07	62	28	34	0.452	930.604	931.306	0.955	2.583
3	4.166E-08	4.393E-08	1.480E-04	1.539E-04	1.590E-07	1.653E-07	58	26	32	0.448	931.306	931.320	2.582	2.615
4	4.400E-08	3.565E-07	1.582E-04	7.466E-04	1.699E-07	8.015E-07	64	28	36	0.438	931.321	932.040	2.617	4.335
5	3.570E-07	4.137E-07	7.708E-04	8.603E-04	8.274E-07	9.234E-07	66	28	38	0.424	932.041	932.106	4.337	4.496
6	4.143E-07	1.028E-06	8.782E-04	1.731E-03	9.426E-07	1.857E-06	86	36	50	0.419	932.107	932.556	4.507	5.637
7	1.030E-06	5.572E-06	1.790E-03	6.332E-03	1.920E-06	6.788E-06	84	34	50	0.405	932.557	933.686	5.636	8.565
8	5.581E-06	1.766E-05	6.566E-03	1.557E-02	7.038E-06	1.668E-05	82	32	50	0.390	933.687	934.747	8.564	11.410
9	1.769E-05	5.809E-05	1.620E-02	3.954E-02	1.735E-05	4.230E-05	80	30	50	0.375	934.748	936.160	11.408	15.347
10	5.817E-05	6.478E-05	4.057E-02	4.398E-02	4.340E-05	4.705E-05	82	30	52	0.366	936.162	936.308	15.352	15.770
11	6.487E-05	8.583E-05	4.481E-02	5.529E-02	4.793E-05	5.912E-05	78	28	50	0.359	936.310	936.703	15.768	16.909
12	8.596E-05	1.049E-04	5.677E-02	6.592E-02	6.070E-05	7.046E-05	80	28	52	0.350	936.705	936.994	16.915	17.776
13	1.050E-04	1.109E-04	6.691E-02	6.971E-02	7.152E-05	7.451E-05	126	44	82	0.349	936.996	937.077	17.852	18.096
14	1.111E-04	1.668E-04	7.185E-02	9.751E-02	7.680E-05	1.042E-04	124	42	82	0.339	937.079	937.698	18.095	20.029
15	1.671E-04	2.599E-04	1.007E-01	1.404E-01	1.076E-04	1.499E-04	122	40	82	0.328	937.700	938.426	20.027	22.365
16	2.603E-04	3.111E-04	1.428E-01	1.633E-01	1.525E-04	1.743E-04	121	39	82	0.322	938.428	938.740	22.368	23.386
17	3.115E-04	3.469E-04	1.663E-01	1.803E-01	1.775E-04	1.924E-04	120	38	82	0.317	938.742	938.934	23.389	24.026
18	3.474E-04	4.876E-04	1.835E-01	2.367E-01	1.958E-04	2.525E-04	122	38	84	0.311	938.936	939.564	24.035	26.159

Table A.8: The same as Table 5.3, using the HFB31 model with $B_\star = 0$

M_{cr}	M_{cr}/M	ΔR_{cr}	$\Delta R_{cr}/R$	$M_{b_{cr}}$	Δ_{grav}	z_{drip}	ΔN
3.756E-05	2.683E-05	4.717E-01	3.774E-02	4.628E-05	2.322E-01	5.794E-01	5.494E+52

Table A.9: The same as Table 5.4, using the HFB31 model with $B_\star = 0$

№	r_{min}	r_{max}	ΔR_l	$\Delta R_l/\Delta R_{cr}$	z_l	z_l/z_{drip}	M_{b_l}	$M_{b_l}/M_{b_{cr}}$	M_l	M_l/M_{cr}	ΔN_l	$\Delta N_l/\Delta N$
1	12.490	12.500	1.027E-02	2.177E-02	0.013	2.167E-02	3.676E-11	7.942E-07	3.006E-11	8.003E-07	4.364E+46	7.942E-07
2	12.452	12.490	3.794E-02	8.044E-02	0.059	1.018E-01	4.432E-09	9.577E-05	3.623E-09	9.647E-05	5.262E+48	9.577E-05
3	12.451	12.452	7.507E-04	1.591E-03	0.060	1.034E-01	2.421E-10	5.232E-06	1.979E-10	5.269E-06	2.875E+47	5.232E-06
4	12.412	12.451	3.854E-02	8.172E-02	0.107	1.849E-01	3.315E-08	7.164E-04	2.708E-08	7.211E-04	3.936E+49	7.164E-04
5	12.409	12.412	3.452E-03	7.319E-03	0.111	1.923E-01	5.977E-09	1.291E-04	4.881E-09	1.300E-04	7.096E+48	1.291E-04
6	12.385	12.409	2.389E-02	5.064E-02	0.141	2.428E-01	6.443E-08	1.392E-03	5.260E-08	1.400E-03	7.649E+49	1.392E-03
7	12.326	12.385	5.945E-02	1.260E-01	0.214	3.687E-01	4.691E-07	1.014E-02	3.826E-07	1.019E-02	5.569E+50	1.014E-02
8	12.270	12.325	5.507E-02	1.168E-01	0.281	4.855E-01	1.224E-06	2.644E-02	9.970E-07	2.655E-02	1.453E+51	2.644E-02
9	12.198	12.270	7.236E-02	1.534E-01	0.370	6.392E-01	3.999E-06	8.641E-02	3.254E-06	8.663E-02	4.748E+51	8.641E-02
10	12.190	12.198	7.418E-03	1.573E-02	0.380	6.552E-01	6.458E-07	1.395E-02	5.250E-07	1.398E-02	7.667E+50	1.395E-02
11	12.170	12.190	1.987E-02	4.212E-02	0.404	6.976E-01	2.039E-06	4.406E-02	1.657E-06	4.413E-02	2.421E+51	4.406E-02
12	12.156	12.170	1.456E-02	3.087E-02	0.422	7.288E-01	1.829E-06	3.953E-02	1.486E-06	3.957E-02	2.172E+51	3.953E-02
13	12.152	12.156	4.054E-03	8.595E-03	0.427	7.376E-01	5.671E-07	1.225E-02	4.607E-07	1.227E-02	6.733E+50	1.225E-02
14	12.120	12.152	3.102E-02	6.577E-02	0.466	8.038E-01	5.338E-06	1.153E-01	4.334E-06	1.154E-01	6.337E+51	1.153E-01
15	12.084	12.120	3.609E-02	7.650E-02	0.510	8.808E-01	8.786E-06	1.899E-01	7.129E-06	1.898E-01	1.043E+52	1.899E-01
16	12.069	12.084	1.538E-02	3.261E-02	0.529	9.138E-01	4.764E-06	1.029E-01	3.863E-06	1.029E-01	5.656E+51	1.029E-01
17	12.059	12.069	9.431E-03	1.999E-02	0.541	9.342E-01	3.303E-06	7.137E-02	2.678E-06	7.130E-02	3.921E+51	7.137E-02
18	12.028	12.059	3.078E-02	6.526E-02	0.579	1.000E+00	1.299E-05	2.807E-01	1.053E-05	2.803E-01	1.542E+52	2.807E-01

A.4 DDMED

Table A.10: The same as Table 5.2, using the DDMED model with $B_\star = 0$

№	P_{min}	P_{max}	ϵ_{min}	ϵ_{max}	$n_{b_{min}}$	$n_{b_{max}}$	A	Z	N	Z/A	$\mu_{b_{min}}$	$\mu_{b_{max}}$	$\mu_{e_{min}}$	$\mu_{e_{max}}$
1	6.082E-15	3.388E-10	5.857E-09	4.615E-06	6.295E-12	4.960E-09	56	26	30	0.464	930.414	930.603	0.518	0.954
2	3.393E-10	4.160E-08	4.758E-06	1.470E-04	5.113E-09	1.579E-07	62	28	34	0.452	930.604	931.306	0.955	2.583
3	4.166E-08	4.393E-08	1.480E-04	1.539E-04	1.590E-07	1.653E-07	58	26	32	0.448	931.306	931.320	2.582	2.615
4	4.400E-08	3.565E-07	1.582E-04	7.466E-04	1.699E-07	8.015E-07	64	28	36	0.438	931.321	932.040	2.617	4.335
5	3.570E-07	4.137E-07	7.708E-04	8.603E-04	8.274E-07	9.234E-07	66	28	38	0.424	932.041	932.106	4.337	4.496
6	4.143E-07	1.028E-06	8.782E-04	1.731E-03	9.426E-07	1.857E-06	86	36	50	0.419	932.107	932.556	4.507	5.637
7	1.030E-06	5.572E-06	1.790E-03	6.332E-03	1.920E-06	6.788E-06	84	34	50	0.405	932.557	933.686	5.636	8.565
8	5.581E-06	1.766E-05	6.566E-03	1.557E-02	7.038E-06	1.668E-05	82	32	50	0.390	933.687	934.747	8.564	11.410
9	1.769E-05	5.809E-05	1.620E-02	3.954E-02	1.735E-05	4.230E-05	80	30	50	0.375	934.748	936.160	11.408	15.347
10	5.817E-05	7.550E-05	4.057E-02	4.935E-02	4.340E-05	5.277E-05	82	30	52	0.366	936.162	936.523	15.352	16.385
11	7.561E-05	1.203E-04	5.228E-02	7.408E-02	5.591E-05	7.917E-05	126	44	82	0.349	936.525	937.191	16.446	18.466
12	1.204E-04	1.849E-04	7.636E-02	1.054E-01	8.161E-05	1.125E-04	124	42	82	0.339	937.193	937.861	18.465	20.552
13	1.852E-04	2.794E-04	1.088E-01	1.482E-01	1.162E-04	1.582E-04	122	40	82	0.328	937.864	938.553	20.550	22.772
14	2.798E-04	4.220E-04	1.534E-01	2.089E-01	1.637E-04	2.228E-04	120	38	82	0.317	938.556	939.296	22.769	25.232
15	4.226E-04	4.876E-04	2.168E-01	2.413E-01	2.312E-04	2.574E-04	118	36	82	0.305	939.299	939.564	25.229	26.146

Table A.11: The same as Table 5.3, using the DDMED model with $B_\star = 0$

M_{cr}	M_{cr}/M	ΔR_{cr}	$\Delta R_{cr}/R$	$M_{b_{cr}}$	Δ_{grav}	z_{drip}	ΔN
3.756E-05	2.683E-05	4.717E-01	3.774E-02	4.628E-05	2.322E-01	5.794E-01	5.494E+52

Table A.12: The same as Table 5.4, using the DDMED model with $B_\star = 0$

№	r_{min}	r_{max}	ΔR_l	$\Delta R_l/\Delta R_{cr}$	z_l	z_l/z_{drip}	M_{b_l}	$M_{b_l}/M_{b_{cr}}$	M_l	M_l/M_{cr}	ΔN_l	$\Delta N_l/\Delta N$
1	12.490	12.500	1.027E-02	2.177E-02	0.013	2.167E-02	3.676E-11	7.942E-07	3.006E-11	8.003E-07	4.364E+46	7.942E-07
2	12.452	12.490	3.794E-02	8.043E-02	0.059	1.018E-01	4.432E-09	9.577E-05	3.623E-09	9.647E-05	5.262E+48	9.577E-05
3	12.451	12.452	7.507E-04	1.591E-03	0.060	1.034E-01	2.421E-10	5.232E-06	1.979E-10	5.269E-06	2.875E+47	5.232E-06
4	12.412	12.451	3.854E-02	8.171E-02	0.107	1.849E-01	3.315E-08	7.164E-04	2.708E-08	7.211E-04	3.936E+49	7.164E-04
5	12.409	12.412	3.452E-03	7.318E-03	0.111	1.923E-01	5.977E-09	1.291E-04	4.881E-09	1.300E-04	7.096E+48	1.291E-04
6	12.385	12.409	2.389E-02	5.064E-02	0.141	2.428E-01	6.443E-08	1.392E-03	5.260E-08	1.400E-03	7.649E+49	1.392E-03
7	12.326	12.385	5.945E-02	1.260E-01	0.214	3.687E-01	4.691E-07	1.014E-02	3.826E-07	1.019E-02	5.569E+50	1.014E-02
8	12.270	12.325	5.507E-02	1.167E-01	0.281	4.855E-01	1.224E-06	2.644E-02	9.970E-07	2.655E-02	1.453E+51	2.644E-02
9	12.198	12.270	7.236E-02	1.534E-01	0.370	6.391E-01	3.999E-06	8.641E-02	3.254E-06	8.663E-02	4.748E+51	8.641E-02
10	12.180	12.198	1.832E-02	3.883E-02	0.393	6.783E-01	1.691E-06	3.655E-02	1.375E-06	3.661E-02	2.008E+51	3.655E-02
11	12.146	12.179	3.356E-02	7.113E-02	0.434	7.498E-01	4.317E-06	9.329E-02	3.507E-06	9.339E-02	5.125E+51	9.329E-02
12	12.112	12.146	3.342E-02	7.085E-02	0.476	8.210E-01	6.160E-06	1.331E-01	5.001E-06	1.332E-01	7.313E+51	1.331E-01
13	12.078	12.112	3.424E-02	7.259E-02	0.518	8.942E-01	8.888E-06	1.920E-01	7.210E-06	1.920E-01	1.055E+52	1.920E-01
14	12.041	12.078	3.642E-02	7.721E-02	0.563	9.720E-01	1.326E-05	2.865E-01	1.075E-05	2.861E-01	1.574E+52	2.865E-01
15	12.028	12.041	1.302E-02	2.760E-02	0.579	1.000E+00	6.000E-06	1.297E-01	4.862E-06	1.294E-01	7.124E+51	1.297E-01

A.5 DDPC1

Table A.13: The same as Table 5.2, using the DDPC1 model with $B_\star = 0$

№	P_{min}	P_{max}	ϵ_{min}	ϵ_{max}	$n_{b_{min}}$	$n_{b_{max}}$	A	Z	N	Z/A	$\mu_{b_{min}}$	$\mu_{b_{max}}$	$\mu_{e_{min}}$	$\mu_{e_{max}}$
1	6.082E-15	3.388E-10	5.857E-09	4.615E-06	6.295E-12	4.960E-09	56	26	30	0.464	930.414	930.603	0.518	0.954
2	3.393E-10	4.160E-08	4.758E-06	1.470E-04	5.113E-09	1.579E-07	62	28	34	0.452	930.604	931.306	0.955	2.583
3	4.166E-08	4.393E-08	1.480E-04	1.539E-04	1.590E-07	1.653E-07	58	26	32	0.448	931.306	931.320	2.582	2.615
4	4.400E-08	3.565E-07	1.582E-04	7.466E-04	1.699E-07	8.015E-07	64	28	36	0.438	931.321	932.040	2.617	4.335
5	3.570E-07	4.137E-07	7.708E-04	8.603E-04	8.274E-07	9.234E-07	66	28	38	0.424	932.041	932.106	4.337	4.496
6	4.143E-07	1.028E-06	8.782E-04	1.731E-03	9.426E-07	1.857E-06	86	36	50	0.419	932.107	932.556	4.507	5.637
7	1.030E-06	5.572E-06	1.790E-03	6.332E-03	1.920E-06	6.788E-06	84	34	50	0.405	932.557	933.686	5.636	8.565
8	5.581E-06	7.548E-06	6.566E-03	8.233E-03	7.038E-06	8.824E-06	82	32	50	0.390	933.687	933.936	8.564	9.233
9	7.559E-06	1.978E-05	8.475E-03	1.744E-02	9.083E-06	1.867E-05	74	28	46	0.378	933.937	934.843	9.227	11.725
10	1.981E-05	2.923E-05	1.793E-02	2.400E-02	1.920E-05	2.569E-05	76	28	48	0.368	934.844	935.266	11.729	12.924
11	2.928E-05	1.139E-04	2.466E-02	6.837E-02	2.640E-05	7.308E-05	78	28	50	0.359	935.268	937.062	12.929	18.146
12	1.141E-04	1.703E-04	7.329E-02	9.903E-02	7.834E-05	1.058E-04	124	42	82	0.339	937.064	937.678	18.215	20.132
13	1.705E-04	2.538E-04	1.023E-01	1.379E-01	1.093E-04	1.472E-04	122	40	82	0.328	937.680	938.333	20.130	22.233
14	2.542E-04	3.840E-04	1.427E-01	1.946E-01	1.524E-04	2.076E-04	120	38	82	0.317	938.336	939.061	22.231	24.644
15	3.846E-04	5.044E-04	2.019E-01	2.475E-01	2.154E-04	2.640E-04	118	36	82	0.305	939.064	939.564	24.642	26.369

Table A.14: The same as Table 5.3, using the DDPC1 model with $B_\star = 0$

M_{cr}	M_{cr}/M	ΔR_{cr}	$\Delta R_{cr}/R$	$M_{b_{cr}}$	Δ_{grav}	z_{drip}	ΔN
3.885E-05	2.775E-05	4.717E-01	3.774E-02	4.787E-05	2.322E-01	5.794E-01	5.684E+52

Table A.15: The same as Table 5.4, using the DDPC1 model with $B_\star = 0$

№	r_{min}	r_{max}	ΔR_l	$\Delta R_l/\Delta R_{cr}$	z_l	z_l/z_{drip}	M_{b_l}	$M_{b_l}/M_{b_{cr}}$	M_l	M_l/M_{cr}	ΔN_l	$\Delta N_l/\Delta N$
1	12.490	12.500	1.027E-02	2.177E-02	0.013	2.167E-02	3.676E-11	7.678E-07	3.006E-11	7.736E-07	4.364E+46	7.678E-07
2	12.452	12.490	3.794E-02	8.043E-02	0.059	1.018E-01	4.432E-09	9.258E-05	3.623E-09	9.326E-05	5.262E+48	9.258E-05
3	12.451	12.452	7.507E-04	1.591E-03	0.060	1.034E-01	2.421E-10	5.058E-06	1.979E-10	5.094E-06	2.875E+47	5.058E-06
4	12.412	12.451	3.854E-02	8.171E-02	0.107	1.849E-01	3.315E-08	6.925E-04	2.708E-08	6.971E-04	3.936E+49	6.925E-04
5	12.409	12.412	3.452E-03	7.318E-03	0.111	1.923E-01	5.977E-09	1.248E-04	4.881E-09	1.256E-04	7.096E+48	1.248E-04
6	12.385	12.409	2.389E-02	5.064E-02	0.141	2.428E-01	6.443E-08	1.346E-03	5.260E-08	1.354E-03	7.649E+49	1.346E-03
7	12.326	12.385	5.945E-02	1.260E-01	0.214	3.687E-01	4.691E-07	9.798E-03	3.826E-07	9.847E-03	5.569E+50	9.798E-03
8	12.312	12.325	1.299E-02	2.755E-02	0.230	3.964E-01	2.010E-07	4.199E-03	1.639E-07	4.217E-03	2.387E+50	4.199E-03
9	12.265	12.312	4.699E-02	9.961E-02	0.287	4.960E-01	1.235E-06	2.579E-02	1.006E-06	2.589E-02	1.466E+51	2.579E-02
10	12.244	12.265	2.170E-02	4.601E-02	0.314	5.422E-01	9.408E-07	1.965E-02	7.658E-07	1.971E-02	1.117E+51	1.965E-02
11	12.152	12.244	9.120E-02	1.933E-01	0.426	7.360E-01	8.263E-06	1.726E-01	6.718E-06	1.729E-01	9.810E+51	1.726E-01
12	12.121	12.152	3.076E-02	6.521E-02	0.464	8.016E-01	5.386E-06	1.125E-01	4.374E-06	1.126E-01	6.395E+51	1.125E-01
13	12.089	12.121	3.248E-02	6.886E-02	0.505	8.710E-01	7.892E-06	1.649E-01	6.404E-06	1.648E-01	9.370E+51	1.649E-01
14	12.053	12.089	3.579E-02	7.587E-02	0.549	9.474E-01	1.215E-05	2.537E-01	9.850E-06	2.535E-01	1.442E+52	2.537E-01
15	12.028	12.053	2.455E-02	5.204E-02	0.579	1.000E+00	1.109E-05	2.317E-01	8.987E-06	2.313E-01	1.317E+52	2.317E-01

A.6 SVMIN

Table A.16: The same as Table 5.2, using the SVMIN model with $B_\star = 0$

№	P_{min}	P_{max}	ϵ_{min}	ϵ_{max}	$n_{b_{min}}$	$n_{b_{max}}$	A	Z	N	Z/A	$\mu_{b_{min}}$	$\mu_{b_{max}}$	$\mu_{e_{min}}$	$\mu_{e_{max}}$
1	6.082E-15	3.388E-10	5.857E-09	4.615E-06	6.295E-12	4.960E-09	56	26	30	0.464	930.414	930.603	0.518	0.954
2	3.393E-10	4.160E-08	4.758E-06	1.470E-04	5.113E-09	1.579E-07	62	28	34	0.452	930.604	931.306	0.955	2.583
3	4.166E-08	4.393E-08	1.480E-04	1.539E-04	1.590E-07	1.653E-07	58	26	32	0.448	931.306	931.320	2.582	2.615
4	4.400E-08	3.565E-07	1.582E-04	7.466E-04	1.699E-07	8.015E-07	64	28	36	0.438	931.321	932.040	2.617	4.335
5	3.570E-07	4.137E-07	7.708E-04	8.603E-04	8.274E-07	9.234E-07	66	28	38	0.424	932.041	932.106	4.337	4.496
6	4.143E-07	1.028E-06	8.782E-04	1.731E-03	9.426E-07	1.857E-06	86	36	50	0.419	932.107	932.556	4.507	5.637
7	1.030E-06	5.572E-06	1.790E-03	6.332E-03	1.920E-06	6.788E-06	84	34	50	0.405	932.557	933.686	5.636	8.565
8	5.581E-06	1.766E-05	6.566E-03	1.557E-02	7.038E-06	1.668E-05	82	32	50	0.390	933.687	934.747	8.564	11.410
9	1.769E-05	4.562E-05	1.620E-02	3.298E-02	1.735E-05	3.529E-05	80	30	50	0.375	934.748	935.838	11.408	14.449
10	4.568E-05	9.321E-05	3.444E-02	5.882E-02	3.685E-05	6.289E-05	78	28	50	0.359	935.840	936.808	14.446	17.261
11	9.335E-05	1.144E-04	6.040E-02	7.036E-02	6.457E-05	7.520E-05	80	28	52	0.350	936.810	937.112	17.267	18.166
12	1.146E-04	1.690E-04	7.354E-02	9.849E-02	7.860E-05	1.052E-04	124	42	82	0.339	937.114	937.709	18.235	20.095
13	1.693E-04	2.701E-04	1.017E-01	1.445E-01	1.087E-04	1.542E-04	122	40	82	0.328	937.712	938.484	20.093	22.580
14	2.705E-04	3.685E-04	1.495E-01	1.887E-01	1.596E-04	2.013E-04	120	38	82	0.317	938.486	939.031	22.577	24.392
15	3.691E-04	4.665E-04	1.920E-01	2.290E-01	2.049E-04	2.442E-04	122	38	84	0.311	939.034	939.468	24.401	25.872
16	4.672E-04	4.912E-04	2.368E-01	2.459E-01	2.525E-04	2.622E-04	126	38	88	0.302	939.471	939.565	25.881	26.207

Table A.17: The same as Table 5.3, using the SVMIN model with $B_\star = 0$

M_{cr}	M_{cr}/M	ΔR_{cr}	$\Delta R_{cr}/R$	$M_{b_{cr}}$	Δ_{grav}	z_{drip}	ΔN
3.783E-05	2.702E-05	4.717E-01	3.774E-02	4.662E-05	2.322E-01	5.794E-01	5.535E+52

Table A.18: The same as Table 5.4, using the SVMIN model with $B_\star = 0$

№	r_{min}	r_{max}	ΔR_l	$\Delta R_l/\Delta R_{cr}$	z_l	z_l/z_{drip}	M_{b_l}	$M_{b_l}/M_{b_{cr}}$	M_l	M_l/M_{cr}	ΔN_l	$\Delta N_l/\Delta N$
1	12.490	12.500	1.027E-02	2.177E-02	0.013	2.167E-02	3.676E-11	7.884E-07	3.006E-11	7.945E-07	4.364E+46	7.884E-07
2	12.452	12.490	3.794E-02	8.043E-02	0.059	1.018E-01	4.432E-09	9.507E-05	3.623E-09	9.577E-05	5.262E+48	9.507E-05
3	12.451	12.452	7.507E-04	1.591E-03	0.060	1.034E-01	2.421E-10	5.194E-06	1.979E-10	5.231E-06	2.875E+47	5.194E-06
4	12.412	12.451	3.854E-02	8.171E-02	0.107	1.849E-01	3.315E-08	7.111E-04	2.708E-08	7.158E-04	3.936E+49	7.111E-04
5	12.409	12.412	3.452E-03	7.318E-03	0.111	1.923E-01	5.977E-09	1.282E-04	4.881E-09	1.290E-04	7.096E+48	1.282E-04
6	12.385	12.409	2.389E-02	5.064E-02	0.141	2.428E-01	6.443E-08	1.382E-03	5.260E-08	1.390E-03	7.649E+49	1.382E-03
7	12.326	12.385	5.945E-02	1.260E-01	0.214	3.687E-01	4.691E-07	1.006E-02	3.826E-07	1.011E-02	5.569E+50	1.006E-02
8	12.270	12.325	5.507E-02	1.167E-01	0.281	4.855E-01	1.224E-06	2.625E-02	9.970E-07	2.635E-02	1.453E+51	2.625E-02
9	12.214	12.270	5.596E-02	1.186E-01	0.350	6.044E-01	2.775E-06	5.952E-02	2.258E-06	5.968E-02	3.294E+51	5.952E-02
10	12.165	12.214	4.910E-02	1.041E-01	0.411	7.088E-01	4.637E-06	9.946E-02	3.769E-06	9.962E-02	5.505E+51	9.946E-02
11	12.150	12.165	1.518E-02	3.219E-02	0.430	7.413E-01	2.031E-06	4.357E-02	1.650E-06	4.362E-02	2.412E+51	4.357E-02
12	12.120	12.150	2.983E-02	6.324E-02	0.466	8.049E-01	5.215E-06	1.119E-01	4.234E-06	1.119E-01	6.191E+51	1.119E-01
13	12.081	12.120	3.837E-02	8.133E-02	0.514	8.868E-01	9.530E-06	2.044E-01	7.732E-06	2.044E-01	1.131E+52	2.044E-01
14	12.054	12.081	2.689E-02	5.700E-02	0.547	9.443E-01	9.169E-06	1.967E-01	7.434E-06	1.965E-01	1.088E+52	1.967E-01
15	12.033	12.054	2.132E-02	4.520E-02	0.574	9.900E-01	9.031E-06	1.937E-01	7.318E-06	1.934E-01	1.072E+52	1.937E-01
16	12.028	12.033	4.562E-03	9.671E-03	0.579	1.000E+00	2.215E-06	4.751E-02	1.794E-06	4.743E-02	2.629E+51	4.751E-02

A.7 UNEDF0

Table A.19: The same as Table 5.2, using the UNEDF0 model with $B_\star = 0$

№	P_{min}	P_{max}	ϵ_{min}	ϵ_{max}	$n_{b_{min}}$	$n_{b_{max}}$	A	Z	N	Z/A	$\mu_{b_{min}}$	$\mu_{b_{max}}$	$\mu_{e_{min}}$	$\mu_{e_{max}}$
1	6.082E-15	3.388E-10	5.857E-09	4.615E-06	6.295E-12	4.960E-09	56	26	30	0.464	930.414	930.603	0.518	0.954
2	3.393E-10	4.160E-08	4.758E-06	1.470E-04	5.113E-09	1.579E-07	62	28	34	0.452	930.604	931.306	0.955	2.583
3	4.166E-08	4.393E-08	1.480E-04	1.539E-04	1.590E-07	1.653E-07	58	26	32	0.448	931.306	931.320	2.582	2.615
4	4.400E-08	3.565E-07	1.582E-04	7.466E-04	1.699E-07	8.015E-07	64	28	36	0.438	931.321	932.040	2.617	4.335
5	3.570E-07	4.137E-07	7.708E-04	8.603E-04	8.274E-07	9.234E-07	66	28	38	0.424	932.041	932.106	4.337	4.496
6	4.143E-07	1.028E-06	8.782E-04	1.731E-03	9.426E-07	1.857E-06	86	36	50	0.419	932.107	932.556	4.507	5.637
7	1.030E-06	5.572E-06	1.790E-03	6.332E-03	1.920E-06	6.788E-06	84	34	50	0.405	932.557	933.686	5.636	8.565
8	5.581E-06	1.766E-05	6.566E-03	1.557E-02	7.038E-06	1.668E-05	82	32	50	0.390	933.687	934.747	8.564	11.410
9	1.769E-05	3.142E-05	1.620E-02	2.493E-02	1.735E-05	2.669E-05	80	30	50	0.375	934.748	935.378	11.408	13.165
10	3.147E-05	4.282E-05	2.537E-02	3.196E-02	2.715E-05	3.420E-05	76	28	48	0.368	935.380	935.751	13.164	14.215
11	4.288E-05	7.892E-05	3.284E-02	5.191E-02	3.514E-05	5.551E-05	78	28	50	0.359	935.753	936.557	14.220	16.558
12	7.903E-05	1.055E-04	5.330E-02	6.621E-02	5.700E-05	7.077E-05	80	28	52	0.350	936.559	936.974	16.564	17.802
13	1.056E-04	1.189E-04	6.660E-02	7.277E-02	7.120E-05	7.777E-05	86	30	56	0.349	936.976	937.154	17.818	18.350
14	1.190E-04	1.365E-04	7.431E-02	8.236E-02	7.942E-05	8.801E-05	82	28	54	0.341	937.156	937.365	18.348	18.986
15	1.367E-04	1.416E-04	8.271E-02	8.494E-02	8.839E-05	9.076E-05	88	30	58	0.341	937.367	937.422	19.003	19.172
16	1.418E-04	1.847E-04	8.684E-02	1.059E-01	9.278E-05	1.131E-04	84	28	56	0.333	937.425	937.841	19.169	20.474
17	1.849E-04	2.404E-04	1.085E-01	1.321E-01	1.159E-04	1.411E-04	86	28	58	0.326	937.844	938.276	20.482	21.868
18	2.407E-04	3.242E-04	1.354E-01	1.693E-01	1.445E-04	1.806E-04	88	28	60	0.318	938.279	938.793	21.876	23.565
19	3.247E-04	4.214E-04	1.733E-01	2.108E-01	1.850E-04	2.249E-04	90	28	62	0.311	938.796	939.269	23.573	25.160
20	4.220E-04	4.463E-04	2.157E-01	2.250E-01	2.301E-04	2.400E-04	92	28	64	0.304	939.272	939.375	25.169	25.524
21	4.470E-04	4.536E-04	2.317E-01	2.343E-01	2.472E-04	2.499E-04	134	40	94	0.299	939.378	939.405	25.609	25.703
22	4.543E-04	4.897E-04	2.381E-01	2.519E-01	2.539E-04	2.686E-04	136	40	96	0.294	939.407	939.543	25.713	26.200
23	4.905E-04	4.955E-04	2.599E-01	2.619E-01	2.771E-04	2.793E-04	174	50	124	0.287	939.546	939.564	26.269	26.337

Table A.20: The same as Table 5.3, using the UNEDF0 model with $B_\star = 0$

M_{cr}	M_{cr}/M	ΔR_{cr}	$\Delta R_{cr}/R$	$M_{b_{cr}}$	Δ_{grav}	z_{drip}	ΔN
3.817E-05	2.726E-05	4.717E-01	3.774E-02	4.703E-05	2.322E-01	5.794E-01	5.583E+52

Table A.21: The same as Table 5.4, using the UNEDF0 model with $B_\star = 0$

№	r_{min}	r_{max}	ΔR_l	$\Delta R_l/\Delta R_{cr}$	z_l	z_l/z_{drip}	M_{b_l}	$M_{b_l}/M_{b_{cr}}$	M_l	M_l/M_{cr}	ΔN_l	$\Delta N_l/\Delta N$
1	12.490	12.500	1.027E-02	2.177E-02	0.013	2.167E-02	3.676E-11	7.815E-07	3.006E-11	7.875E-07	4.364E+46	7.815E-07
2	12.452	12.490	3.794E-02	8.043E-02	0.059	1.018E-01	4.432E-09	9.424E-05	3.623E-09	9.493E-05	5.262E+48	9.424E-05
3	12.451	12.452	7.507E-04	1.591E-03	0.060	1.034E-01	2.421E-10	5.149E-06	1.979E-10	5.185E-06	2.875E+47	5.149E-06
4	12.412	12.451	3.854E-02	8.171E-02	0.107	1.849E-01	3.315E-08	7.049E-04	2.708E-08	7.096E-04	3.936E+49	7.049E-04
5	12.409	12.412	3.452E-03	7.318E-03	0.111	1.923E-01	5.977E-09	1.271E-04	4.881E-09	1.279E-04	7.096E+48	1.271E-04
6	12.385	12.409	2.389E-02	5.064E-02	0.141	2.428E-01	6.443E-08	1.370E-03	5.260E-08	1.378E-03	7.649E+49	1.370E-03
7	12.326	12.385	5.945E-02	1.260E-01	0.214	3.687E-01	4.691E-07	9.974E-03	3.826E-07	1.002E-02	5.569E+50	9.974E-03
8	12.270	12.325	5.507E-02	1.168E-01	0.281	4.855E-01	1.224E-06	2.602E-02	9.970E-07	2.612E-02	1.453E+51	2.602E-02
9	12.238	12.270	3.243E-02	6.875E-02	0.321	5.545E-01	1.371E-06	2.915E-02	1.116E-06	2.924E-02	1.628E+51	2.915E-02
10	12.219	12.238	1.898E-02	4.025E-02	0.345	5.949E-01	1.123E-06	2.388E-02	9.136E-07	2.394E-02	1.333E+51	2.388E-02
11	12.178	12.219	4.087E-02	8.665E-02	0.395	6.819E-01	3.527E-06	7.500E-02	2.868E-06	7.513E-02	4.187E+51	7.500E-02
12	12.157	12.178	2.096E-02	4.443E-02	0.421	7.266E-01	2.563E-06	5.449E-02	2.082E-06	5.456E-02	3.042E+51	5.449E-02
13	12.148	12.157	8.927E-03	1.892E-02	0.432	7.458E-01	1.273E-06	2.707E-02	1.034E-06	2.710E-02	1.512E+51	2.707E-02
14	12.137	12.148	1.048E-02	2.223E-02	0.445	7.684E-01	1.678E-06	3.569E-02	1.363E-06	3.571E-02	1.992E+51	3.569E-02
15	12.134	12.137	2.751E-03	5.832E-03	0.449	7.745E-01	4.711E-07	1.002E-02	3.825E-07	1.002E-02	5.592E+50	1.002E-02
16	12.113	12.134	2.083E-02	4.415E-02	0.475	8.190E-01	4.083E-06	8.681E-02	3.314E-06	8.684E-02	4.847E+51	8.681E-02
17	12.092	12.113	2.151E-02	4.559E-02	0.501	8.650E-01	5.249E-06	1.116E-01	4.259E-06	1.116E-01	6.231E+51	1.116E-01
18	12.066	12.092	2.546E-02	5.397E-02	0.533	9.194E-01	7.832E-06	1.665E-01	6.352E-06	1.664E-01	9.299E+51	1.665E-01
19	12.043	12.066	2.326E-02	4.932E-02	0.562	9.692E-01	9.001E-06	1.914E-01	7.296E-06	1.912E-01	1.069E+52	1.914E-01
20	12.038	12.043	5.066E-03	1.074E-02	0.568	9.803E-01	2.249E-06	4.783E-02	1.823E-06	4.776E-02	2.670E+51	4.783E-02
21	12.036	12.037	1.306E-03	2.769E-03	0.570	9.834E-01	6.129E-07	1.303E-02	4.966E-07	1.301E-02	7.277E+50	1.303E-02
22	12.029	12.036	6.639E-03	1.407E-02	0.578	9.978E-01	3.273E-06	6.959E-02	2.652E-06	6.947E-02	3.885E+51	6.959E-02
23	12.028	12.029	8.941E-04	1.896E-03	0.579	1.000E+00	4.693E-07	9.978E-03	3.802E-07	9.960E-03	5.571E+50	9.978E-03

Appendix B

Tables for $B_\star = 1500$

Below are the Tables, like those in Subsections 5.4.1 - 5.4.2, for the models: WS4RBF, BSKG3, HFB31, DDMED, DDPC1, SVMIN and UNEDF0, with magnetic field strength $B_\star = 1500$.

B.1 WS4RBF

Table B.1: The same as Table 5.2, using the WS4RBF model with $B_\star = 1500$

№	P_{min}	P_{max}	ϵ_{min}	ϵ_{max}	$n_{b_{min}}$	$n_{b_{max}}$	A	Z	N	Z/A	$\mu_{b_{min}}$	$\mu_{b_{max}}$	$\mu_{e_{min}}$	$\mu_{e_{max}}$
1	6.082E-15	2.628E-07	1.597E-03	3.584E-03	1.717E-06	3.852E-06	56	26	30	0.464	930.348	930.438	0.597	0.861
2	2.632E-07	9.711E-06	3.717E-03	1.577E-02	3.995E-06	1.694E-05	62	28	34	0.452	930.438	931.318	0.866	3.007
3	9.725E-06	1.081E-05	1.629E-02	1.711E-02	1.750E-05	1.838E-05	64	28	36	0.438	931.319	931.379	3.009	3.156
4	1.083E-05	1.885E-05	1.752E-02	2.268E-02	1.882E-05	2.436E-05	88	38	50	0.432	931.380	931.751	3.189	4.105
5	1.887E-05	5.072E-05	2.337E-02	3.747E-02	2.510E-05	4.023E-05	86	36	50	0.419	931.752	932.727	4.101	6.541
6	5.080E-05	1.063E-04	3.874E-02	5.548E-02	4.159E-05	5.952E-05	84	34	50	0.405	932.728	933.825	6.538	9.343
7	1.064E-04	1.790E-04	5.753E-02	7.427E-02	6.172E-05	7.964E-05	82	32	50	0.390	933.828	934.855	9.341	12.045
8	1.793E-04	2.661E-04	7.729E-02	9.392E-02	8.287E-05	1.006E-04	80	30	50	0.375	934.858	935.804	12.044	14.623
9	2.665E-04	4.437E-04	9.812E-02	1.263E-01	1.051E-04	1.352E-04	78	28	50	0.359	935.808	937.282	14.623	18.805
10	4.443E-04	4.854E-04	1.305E-01	1.364E-01	1.397E-04	1.460E-04	126	44	82	0.349	937.287	937.575	18.903	19.744
11	4.861E-04	5.819E-04	1.406E-01	1.537E-01	1.505E-04	1.645E-04	124	42	82	0.339	937.580	938.187	19.749	21.580
12	5.827E-04	7.870E-04	1.589E-01	1.845E-01	1.700E-04	1.972E-04	122	40	82	0.328	938.192	939.305	21.586	25.043
13	7.882E-04	8.410E-04	1.911E-01	1.973E-01	2.042E-04	2.109E-04	120	38	82	0.317	939.311	939.565	25.050	25.866

Table B.2: The same as Table 5.3, using the WS4RBF model with $B_\star = 1500$

M_{cr}	M_{cr}/M	ΔR_{cr}	$\Delta R_{cr}/R$	$M_{b_{cr}}$	Δ_{grav}	z_{drip}	ΔN
6.621E-05	4.729E-05	4.751E-01	3.801E-02	8.147E-05	2.306E-01	5.835E-01	9.672E+52

Table B.3: The same as Table 5.4, using the WS4RBF model with $B_\star = 1500$

№	r_{min}	r_{max}	ΔR_l	$\Delta R_l/\Delta R_{cr}$	z_l	z_l/z_{drip}	M_{b_l}	$M_{b_l}/M_{b_{cr}}$	M_l	M_l/M_{cr}	ΔN_l	$\Delta N_l/\Delta N$
1	12.495	12.500	4.892E-03	1.030E-02	0.006	1.025E-02	2.855E-08	3.505E-04	2.336E-08	3.528E-04	3.390E+49	3.505E-04
2	12.448	12.495	4.755E-02	1.001E-01	0.064	1.099E-01	1.016E-06	1.247E-02	8.306E-07	1.255E-02	1.206E+51	1.247E-02
3	12.444	12.448	3.257E-03	6.856E-03	0.068	1.168E-01	1.161E-07	1.425E-03	9.490E-08	1.433E-03	1.379E+50	1.425E-03
4	12.424	12.444	1.989E-02	4.186E-02	0.093	1.587E-01	8.521E-07	1.046E-02	6.962E-07	1.051E-02	1.012E+51	1.046E-02
5	12.372	12.424	5.179E-02	1.090E-01	0.156	2.675E-01	3.341E-06	4.101E-02	2.728E-06	4.120E-02	3.967E+51	4.101E-02
6	12.315	12.372	5.761E-02	1.213E-01	0.227	3.888E-01	5.709E-06	7.007E-02	4.655E-06	7.032E-02	6.778E+51	7.007E-02
7	12.261	12.315	5.328E-02	1.121E-01	0.292	5.011E-01	7.327E-06	8.994E-02	5.969E-06	9.015E-02	8.699E+51	8.994E-02
8	12.213	12.261	4.851E-02	1.021E-01	0.352	6.037E-01	8.605E-06	1.056E-01	7.002E-06	1.058E-01	1.022E+52	1.056E-01
9	12.138	12.212	7.454E-02	1.569E-01	0.444	7.613E-01	1.718E-05	2.108E-01	1.396E-05	2.108E-01	2.039E+52	2.108E-01
10	12.123	12.138	1.439E-02	3.029E-02	0.462	7.921E-01	3.919E-06	4.811E-02	3.182E-06	4.806E-02	4.653E+51	4.811E-02
11	12.093	12.123	3.026E-02	6.370E-02	0.500	8.566E-01	9.062E-06	1.112E-01	7.354E-06	1.111E-01	1.076E+52	1.112E-01
12	12.038	12.093	5.487E-02	1.155E-01	0.568	9.731E-01	1.904E-05	2.337E-01	1.544E-05	2.332E-01	2.261E+52	2.337E-01
13	12.025	12.037	1.244E-02	2.619E-02	0.584	1.000E+00	4.862E-06	5.967E-02	3.939E-06	5.949E-02	5.772E+51	5.967E-02

B.2 BSKG3

Table B.4: The same as Table 5.2, using the BSKG3 model with $B_\star = 1500$

№	P_{min}	P_{max}	ϵ_{min}	ϵ_{max}	$n_{b_{min}}$	$n_{b_{max}}$	A	Z	N	Z/A	$\mu_{b_{min}}$	$\mu_{b_{max}}$	$\mu_{e_{min}}$	$\mu_{e_{max}}$
1	6.082E-15	2.628E-07	1.597E-03	3.584E-03	1.717E-06	3.852E-06	56	26	30	0.464	930.348	930.438	0.597	0.861
2	2.632E-07	9.711E-06	3.717E-03	1.577E-02	3.995E-06	1.694E-05	62	28	34	0.452	930.438	931.318	0.866	3.007
3	9.725E-06	1.081E-05	1.629E-02	1.711E-02	1.750E-05	1.838E-05	64	28	36	0.438	931.319	931.379	3.009	3.156
4	1.083E-05	1.885E-05	1.752E-02	2.268E-02	1.882E-05	2.436E-05	88	38	50	0.432	931.380	931.751	3.189	4.105
5	1.887E-05	5.072E-05	2.337E-02	3.747E-02	2.510E-05	4.023E-05	86	36	50	0.419	931.752	932.727	4.101	6.541
6	5.080E-05	1.063E-04	3.874E-02	5.548E-02	4.159E-05	5.952E-05	84	34	50	0.405	932.728	933.825	6.538	9.343
7	1.064E-04	1.790E-04	5.753E-02	7.427E-02	6.172E-05	7.964E-05	82	32	50	0.390	933.828	934.855	9.341	12.045
8	1.793E-04	2.653E-04	7.729E-02	9.378E-02	8.287E-05	1.005E-04	80	30	50	0.375	934.858	935.797	12.044	14.602
9	2.657E-04	3.583E-04	9.845E-02	1.141E-01	1.055E-04	1.222E-04	128	46	82	0.359	935.800	936.614	14.688	17.012
10	3.589E-04	4.457E-04	1.174E-01	1.307E-01	1.258E-04	1.399E-04	126	44	82	0.349	936.618	937.272	17.015	18.930
11	4.463E-04	5.518E-04	1.348E-01	1.497E-01	1.443E-04	1.602E-04	124	42	82	0.339	937.276	937.969	18.934	21.023
12	5.526E-04	6.842E-04	1.548E-01	1.721E-01	1.656E-04	1.840E-04	122	40	82	0.328	937.974	938.727	21.028	23.368
13	6.852E-04	7.790E-04	1.782E-01	1.899E-01	1.906E-04	2.031E-04	120	38	82	0.317	938.732	939.209	23.374	24.904
14	7.801E-04	8.299E-04	1.933E-01	1.993E-01	2.066E-04	2.130E-04	122	38	84	0.311	939.214	939.452	24.922	25.697
15	8.311E-04	8.547E-04	2.027E-01	2.056E-01	2.167E-04	2.197E-04	124	38	86	0.306	939.457	939.565	25.716	26.075

Table B.5: The same as Table 5.3, using the BSKG3 model with $B_\star = 1500$

M_{cr}	M_{cr}/M	ΔR_{cr}	$\Delta R_{cr}/R$	$M_{b_{cr}}$	Δ_{grav}	z_{drip}	ΔN
6.726E-05	4.804E-05	4.751E-01	3.800E-02	8.277E-05	2.306E-01	5.835E-01	9.826E+52

Table B.6: The same as Table 5.4, using the BSKG3 model with $B_\star = 1500$

№	r_{min}	r_{max}	ΔR_l	$\Delta R_l/\Delta R_{cr}$	z_l	z_l/z_{drip}	M_{b_l}	$M_{b_l}/M_{b_{cr}}$	M_l	M_l/M_{cr}	ΔN_l	$\Delta N_l/\Delta N$
1	12.495	12.500	4.892E-03	1.030E-02	0.006	1.025E-02	2.855E-08	3.450E-04	2.336E-08	3.473E-04	3.390E+49	3.450E-04
2	12.448	12.495	4.755E-02	1.001E-01	0.064	1.099E-01	1.016E-06	1.228E-02	8.306E-07	1.235E-02	1.206E+51	1.228E-02
3	12.444	12.448	3.257E-03	6.856E-03	0.068	1.168E-01	1.161E-07	1.403E-03	9.490E-08	1.411E-03	1.379E+50	1.403E-03
4	12.424	12.444	1.989E-02	4.186E-02	0.093	1.587E-01	8.521E-07	1.029E-02	6.962E-07	1.035E-02	1.012E+51	1.029E-02
5	12.372	12.424	5.179E-02	1.090E-01	0.156	2.675E-01	3.341E-06	4.037E-02	2.728E-06	4.056E-02	3.967E+51	4.037E-02
6	12.315	12.372	5.761E-02	1.213E-01	0.227	3.888E-01	5.709E-06	6.897E-02	4.655E-06	6.922E-02	6.778E+51	6.897E-02
7	12.261	12.315	5.328E-02	1.121E-01	0.292	5.012E-01	7.327E-06	8.853E-02	5.969E-06	8.874E-02	8.699E+51	8.853E-02
8	12.213	12.261	4.811E-02	1.013E-01	0.352	6.028E-01	8.528E-06	1.030E-01	6.939E-06	1.032E-01	1.012E+52	1.030E-01
9	12.172	12.213	4.130E-02	8.694E-02	0.403	6.903E-01	9.038E-06	1.092E-01	7.347E-06	1.092E-01	1.073E+52	1.092E-01
10	12.138	12.171	3.287E-02	6.920E-02	0.444	7.601E-01	8.355E-06	1.009E-01	6.787E-06	1.009E-01	9.919E+51	1.009E-01
11	12.104	12.138	3.460E-02	7.282E-02	0.486	8.337E-01	1.003E-05	1.212E-01	8.144E-06	1.211E-01	1.191E+52	1.212E-01
12	12.066	12.103	3.729E-02	7.850E-02	0.533	9.130E-01	1.236E-05	1.493E-01	1.002E-05	1.490E-01	1.467E+52	1.493E-01
13	12.042	12.066	2.342E-02	4.929E-02	0.562	9.631E-01	8.702E-06	1.051E-01	7.053E-06	1.049E-01	1.033E+52	1.051E-01
14	12.031	12.042	1.163E-02	2.447E-02	0.577	9.882E-01	4.595E-06	5.551E-02	3.723E-06	5.535E-02	5.455E+51	5.551E-02
15	12.025	12.030	5.286E-03	1.113E-02	0.584	1.000E+00	2.170E-06	2.622E-02	1.758E-06	2.614E-02	2.577E+51	2.622E-02

B.3 HFB31

Table B.7: The same as Table 5.2, using the HFB31 model with $B_\star = 1500$

№	P_{min}	P_{max}	ϵ_{min}	ϵ_{max}	$n_{b_{min}}$	$n_{b_{max}}$	A	Z	N	Z/A	$\mu_{b_{min}}$	$\mu_{b_{max}}$	$\mu_{e_{min}}$	$\mu_{e_{max}}$
1	6.082E-15	2.628E-07	1.597E-03	3.584E-03	1.717E-06	3.852E-06	56	26	30	0.464	930.348	930.438	0.597	0.861
2	2.632E-07	9.711E-06	3.717E-03	1.577E-02	3.995E-06	1.694E-05	62	28	34	0.452	930.438	931.318	0.866	3.007
3	9.725E-06	1.081E-05	1.629E-02	1.711E-02	1.750E-05	1.838E-05	64	28	36	0.438	931.319	931.379	3.009	3.156
4	1.083E-05	1.885E-05	1.752E-02	2.268E-02	1.882E-05	2.436E-05	88	38	50	0.432	931.380	931.751	3.189	4.105
5	1.887E-05	5.072E-05	2.337E-02	3.747E-02	2.510E-05	4.023E-05	86	36	50	0.419	931.752	932.727	4.101	6.541
6	5.080E-05	1.063E-04	3.874E-02	5.548E-02	4.159E-05	5.952E-05	84	34	50	0.405	932.728	933.825	6.538	9.343
7	1.064E-04	1.790E-04	5.753E-02	7.427E-02	6.172E-05	7.964E-05	82	32	50	0.390	933.828	934.855	9.341	12.045
8	1.793E-04	2.916E-04	7.729E-02	9.825E-02	8.287E-05	1.053E-04	80	30	50	0.375	934.858	936.052	12.044	15.296
9	2.920E-04	3.610E-04	1.031E-01	1.145E-01	1.105E-04	1.226E-04	128	46	82	0.359	936.056	936.648	15.384	17.074
10	3.615E-04	4.251E-04	1.179E-01	1.277E-01	1.262E-04	1.367E-04	126	44	82	0.349	936.652	937.136	17.077	18.495
11	4.258E-04	5.134E-04	1.317E-01	1.445E-01	1.410E-04	1.546E-04	124	42	82	0.339	937.140	937.733	18.499	20.287
12	5.141E-04	6.328E-04	1.493E-01	1.655E-01	1.598E-04	1.770E-04	122	40	82	0.328	937.738	938.443	20.291	22.484
13	6.338E-04	6.883E-04	1.685E-01	1.755E-01	1.802E-04	1.877E-04	121	39	82	0.322	938.448	938.744	22.495	23.431
14	6.893E-04	7.247E-04	1.787E-01	1.832E-01	1.911E-04	1.959E-04	120	38	82	0.317	938.749	938.932	23.442	24.030
15	7.258E-04	8.560E-04	1.864E-01	2.024E-01	1.993E-04	2.163E-04	122	38	84	0.311	938.938	939.564	24.048	26.094

Table B.8: The same as Table 5.3, using the HFB31 model with $B_\star = 1500$

M_{cr}	M_{cr}/M	ΔR_{cr}	$\Delta R_{cr}/R$	$M_{b_{cr}}$	Δ_{grav}	z_{drip}	ΔN
6.735E-05	4.811E-05	4.750E-01	3.800E-02	8.288E-05	2.306E-01	5.835E-01	9.840E+52

Table B.9: The same as Table 5.4, using the HFB31 model with $B_\star = 1500$

№	r_{min}	r_{max}	ΔR_l	$\Delta R_l/\Delta R_{cr}$	z_l	z_l/z_{drip}	M_{b_l}	$M_{b_l}/M_{b_{cr}}$	M_l	M_l/M_{cr}	ΔN_l	$\Delta N_l/\Delta N$
1	12.495	12.500	4.892E-03	1.030E-02	0.006	1.025E-02	2.855E-08	3.445E-04	2.336E-08	3.468E-04	3.390E+49	3.445E-04
2	12.448	12.495	4.755E-02	1.001E-01	0.064	1.099E-01	1.016E-06	1.226E-02	8.306E-07	1.233E-02	1.206E+51	1.226E-02
3	12.444	12.448	3.257E-03	6.857E-03	0.068	1.169E-01	1.161E-07	1.401E-03	9.490E-08	1.409E-03	1.379E+50	1.401E-03
4	12.424	12.444	1.989E-02	4.187E-02	0.093	1.587E-01	8.521E-07	1.028E-02	6.962E-07	1.034E-02	1.012E+51	1.028E-02
5	12.372	12.424	5.179E-02	1.090E-01	0.156	2.675E-01	3.341E-06	4.031E-02	2.728E-06	4.050E-02	3.967E+51	4.031E-02
6	12.315	12.372	5.761E-02	1.213E-01	0.227	3.888E-01	5.709E-06	6.888E-02	4.655E-06	6.912E-02	6.778E+51	6.888E-02
7	12.261	12.315	5.328E-02	1.122E-01	0.292	5.012E-01	7.327E-06	8.841E-02	5.969E-06	8.862E-02	8.699E+51	8.841E-02
8	12.200	12.261	6.110E-02	1.286E-01	0.368	6.303E-01	1.110E-05	1.339E-01	9.031E-06	1.341E-01	1.318E+52	1.339E-01
9	12.170	12.200	3.000E-02	6.316E-02	0.405	6.939E-01	6.716E-06	8.103E-02	5.459E-06	8.105E-02	7.973E+51	8.103E-02
10	12.145	12.170	2.436E-02	5.129E-02	0.435	7.458E-01	6.130E-06	7.396E-02	4.980E-06	7.393E-02	7.277E+51	7.396E-02
11	12.115	12.145	2.966E-02	6.244E-02	0.472	8.089E-01	8.360E-06	1.009E-01	6.788E-06	1.008E-01	9.926E+51	1.009E-01
12	12.080	12.115	3.502E-02	7.371E-02	0.515	8.834E-01	1.120E-05	1.351E-01	9.085E-06	1.349E-01	1.329E+52	1.351E-01
13	12.065	12.080	1.464E-02	3.081E-02	0.534	9.149E-01	5.095E-06	6.148E-02	4.132E-06	6.135E-02	6.049E+51	6.148E-02
14	12.056	12.065	9.011E-03	1.897E-02	0.545	9.345E-01	3.296E-06	3.976E-02	2.672E-06	3.967E-02	3.912E+51	3.976E-02
15	12.025	12.056	3.072E-02	6.466E-02	0.583	1.000E+00	1.203E-05	1.452E-01	9.749E-06	1.448E-01	1.428E+52	1.452E-01

B.4 DDMED

Table B.10: The same as Table 5.2, using the DDMED model with $B_\star = 1500$

№	P_{min}	P_{max}	ϵ_{min}	ϵ_{max}	$n_{b_{min}}$	$n_{b_{max}}$	A	Z	N	Z/A	$\mu_{b_{min}}$	$\mu_{b_{max}}$	$\mu_{e_{min}}$	$\mu_{e_{max}}$
1	6.082E-15	2.628E-07	1.597E-03	3.584E-03	1.717E-06	3.852E-06	56	26	30	0.464	930.348	930.438	0.597	0.861
2	2.632E-07	9.711E-06	3.717E-03	1.577E-02	3.995E-06	1.694E-05	62	28	34	0.452	930.438	931.318	0.866	3.007
3	9.725E-06	1.081E-05	1.629E-02	1.711E-02	1.750E-05	1.838E-05	64	28	36	0.438	931.319	931.379	3.009	3.156
4	1.083E-05	1.885E-05	1.752E-02	2.268E-02	1.882E-05	2.436E-05	88	38	50	0.432	931.380	931.751	3.189	4.105
5	1.887E-05	5.072E-05	2.337E-02	3.747E-02	2.510E-05	4.023E-05	86	36	50	0.419	931.752	932.727	4.101	6.541
6	5.080E-05	1.063E-04	3.874E-02	5.548E-02	4.159E-05	5.952E-05	84	34	50	0.405	932.728	933.825	6.538	9.343
7	1.064E-04	1.790E-04	5.753E-02	7.427E-02	6.172E-05	7.964E-05	82	32	50	0.390	933.828	934.855	9.341	12.045
8	1.793E-04	2.806E-04	7.729E-02	9.641E-02	8.287E-05	1.033E-04	80	30	50	0.375	934.858	935.946	12.044	15.010
9	2.810E-04	3.510E-04	1.012E-01	1.129E-01	1.084E-04	1.210E-04	128	46	82	0.359	935.950	936.561	15.097	16.841
10	3.515E-04	4.411E-04	1.163E-01	1.301E-01	1.245E-04	1.392E-04	126	44	82	0.349	936.565	937.244	16.844	18.834
11	4.417E-04	5.389E-04	1.341E-01	1.480E-01	1.436E-04	1.584E-04	124	42	82	0.339	937.249	937.892	18.838	20.779
12	5.397E-04	6.547E-04	1.530E-01	1.683E-01	1.637E-04	1.800E-04	122	40	82	0.328	937.897	938.566	20.784	22.863
13	6.556E-04	7.952E-04	1.743E-01	1.919E-01	1.865E-04	2.051E-04	120	38	82	0.317	938.571	939.284	22.869	25.160
14	7.964E-04	8.560E-04	1.993E-01	2.065E-01	2.130E-04	2.207E-04	118	36	82	0.305	939.290	939.565	25.167	26.082

Table B.11: The same as Table 5.3, using the DDMED model with $B_\star = 1500$

M_{cr}	M_{cr}/M	ΔR_{cr}	$\Delta R_{cr}/R$	$M_{b_{cr}}$	Δ_{grav}	z_{drip}	ΔN
6.735E-05	4.811E-05	4.750E-01	3.800E-02	8.288E-05	2.306E-01	5.835E-01	9.840E+52

Table B.12: The same as Table 5.4, using the DDMED model with $B_\star = 1500$

№	r_{min}	r_{max}	ΔR_l	$\Delta R_l/\Delta R_{cr}$	z_l	z_l/z_{drip}	M_{b_l}	$M_{b_l}/M_{b_{cr}}$	M_l	M_l/M_{cr}	ΔN_l	$\Delta N_l/\Delta N$
1	12.495	12.500	4.892E-03	1.030E-02	0.006	1.025E-02	2.855E-08	3.445E-04	2.336E-08	3.468E-04	3.390E+49	3.445E-04
2	12.448	12.495	4.755E-02	1.001E-01	0.064	1.099E-01	1.016E-06	1.226E-02	8.306E-07	1.233E-02	1.206E+51	1.226E-02
3	12.444	12.448	3.257E-03	6.857E-03	0.068	1.169E-01	1.161E-07	1.401E-03	9.490E-08	1.409E-03	1.379E+50	1.401E-03
4	12.424	12.444	1.989E-02	4.187E-02	0.093	1.587E-01	8.521E-07	1.028E-02	6.962E-07	1.034E-02	1.012E+51	1.028E-02
5	12.372	12.424	5.179E-02	1.090E-01	0.156	2.675E-01	3.341E-06	4.031E-02	2.728E-06	4.050E-02	3.967E+51	4.031E-02
6	12.315	12.372	5.761E-02	1.213E-01	0.227	3.888E-01	5.709E-06	6.888E-02	4.655E-06	6.912E-02	6.778E+51	6.888E-02
7	12.261	12.315	5.328E-02	1.122E-01	0.292	5.012E-01	7.327E-06	8.840E-02	5.969E-06	8.862E-02	8.699E+51	8.840E-02
8	12.205	12.261	5.575E-02	1.174E-01	0.361	6.190E-01	1.003E-05	1.210E-01	8.159E-06	1.211E-01	1.190E+52	1.210E-01
9	12.174	12.205	3.097E-02	6.519E-02	0.400	6.847E-01	6.825E-06	8.235E-02	5.548E-06	8.238E-02	8.103E+51	8.235E-02
10	12.140	12.174	3.419E-02	7.197E-02	0.442	7.573E-01	8.626E-06	1.041E-01	7.008E-06	1.040E-01	1.024E+52	1.041E-01
11	12.107	12.140	3.217E-02	6.773E-02	0.482	8.257E-01	9.254E-06	1.117E-01	7.512E-06	1.115E-01	1.099E+52	1.117E-01
12	12.074	12.107	3.316E-02	6.981E-02	0.523	8.962E-01	1.081E-05	1.304E-01	8.770E-06	1.302E-01	1.283E+52	1.304E-01
13	12.039	12.074	3.508E-02	7.384E-02	0.567	9.710E-01	1.297E-05	1.565E-01	1.051E-05	1.561E-01	1.540E+52	1.565E-01
14	12.025	12.038	1.345E-02	2.832E-02	0.584	1.000E+00	5.493E-06	6.627E-02	4.450E-06	6.607E-02	6.521E+51	6.627E-02

B.5 DDPC1

Table B.13: The same as Table 5.2, using the DDPC1 model with $B_\star = 1500$

№	P_{min}	P_{max}	ϵ_{min}	ϵ_{max}	$n_{b_{min}}$	$n_{b_{max}}$	A	Z	N	Z/A	$\mu_{b_{min}}$	$\mu_{b_{max}}$	$\mu_{e_{min}}$	$\mu_{e_{max}}$
1	6.082E-15	2.628E-07	1.597E-03	3.584E-03	1.717E-06	3.852E-06	56	26	30	0.464	930.348	930.438	0.597	0.861
2	2.632E-07	9.711E-06	3.717E-03	1.577E-02	3.995E-06	1.694E-05	62	28	34	0.452	930.438	931.318	0.866	3.007
3	9.725E-06	1.081E-05	1.629E-02	1.711E-02	1.750E-05	1.838E-05	64	28	36	0.438	931.319	931.379	3.009	3.156
4	1.083E-05	1.885E-05	1.752E-02	2.268E-02	1.882E-05	2.436E-05	88	38	50	0.432	931.380	931.751	3.189	4.105
5	1.887E-05	5.072E-05	2.337E-02	3.747E-02	2.510E-05	4.023E-05	86	36	50	0.419	931.752	932.727	4.101	6.541
6	5.080E-05	1.063E-04	3.874E-02	5.548E-02	4.159E-05	5.952E-05	84	34	50	0.405	932.728	933.825	6.538	9.343
7	1.064E-04	1.351E-04	5.753E-02	6.467E-02	6.172E-05	6.937E-05	82	32	50	0.390	933.828	934.266	9.341	10.495
8	1.353E-04	1.793E-04	6.664E-02	7.653E-02	7.147E-05	8.206E-05	74	28	46	0.378	934.269	934.841	10.484	12.034
9	1.796E-04	2.168E-04	7.867E-02	8.633E-02	8.434E-05	9.254E-05	76	28	48	0.368	934.845	935.266	12.043	13.212
10	2.171E-04	3.605E-04	8.868E-02	1.139E-01	9.505E-05	1.220E-04	78	28	50	0.359	935.269	936.590	13.221	16.971
11	3.610E-04	4.295E-04	1.178E-01	1.284E-01	1.261E-04	1.374E-04	126	44	82	0.349	936.594	937.114	17.065	18.590
12	4.302E-04	5.187E-04	1.324E-01	1.452E-01	1.417E-04	1.554E-04	124	42	82	0.339	937.119	937.714	18.593	20.390
13	5.195E-04	6.254E-04	1.501E-01	1.645E-01	1.606E-04	1.760E-04	122	40	82	0.328	937.719	938.349	20.395	22.353
14	6.263E-04	7.608E-04	1.704E-01	1.877E-01	1.823E-04	2.007E-04	120	38	82	0.317	938.354	939.056	22.359	24.615
15	7.619E-04	8.700E-04	1.949E-01	2.082E-01	2.084E-04	2.225E-04	118	36	82	0.305	939.062	939.563	24.622	26.292

Table B.14: The same as Table 5.3, using the DDPC1 model with $B_\star = 1500$

M_{cr}	M_{cr}/M	ΔR_{cr}	$\Delta R_{cr}/R$	$M_{b_{cr}}$	Δ_{grav}	z_{drip}	ΔN
6.845E-05	4.889E-05	4.750E-01	3.800E-02	8.423E-05	2.306E-01	5.834E-01	1.000E+53

Table B.15: The same as Table 5.4, using the DDPC1 model with $B_\star = 1500$

№	r_{min}	r_{max}	ΔR_l	$\Delta R_l/\Delta R_{cr}$	z_l	z_l/z_{drip}	M_{b_l}	$M_{b_l}/M_{b_{cr}}$	M_l	M_l/M_{cr}	ΔN_l	$\Delta N_l/\Delta N$
1	12.495	12.500	4.892E-03	1.030E-02	0.006	1.025E-02	2.855E-08	3.390E-04	2.336E-08	3.413E-04	3.390E+49	3.390E-04
2	12.448	12.495	4.755E-02	1.001E-01	0.064	1.099E-01	1.016E-06	1.206E-02	8.306E-07	1.214E-02	1.206E+51	1.206E-02
3	12.444	12.448	3.257E-03	6.858E-03	0.068	1.169E-01	1.161E-07	1.379E-03	9.490E-08	1.386E-03	1.379E+50	1.379E-03
4	12.424	12.444	1.989E-02	4.187E-02	0.093	1.587E-01	8.521E-07	1.012E-02	6.962E-07	1.017E-02	1.012E+51	1.012E-02
5	12.372	12.424	5.179E-02	1.090E-01	0.156	2.676E-01	3.341E-06	3.967E-02	2.728E-06	3.985E-02	3.967E+51	3.967E-02
6	12.315	12.372	5.761E-02	1.213E-01	0.227	3.889E-01	5.709E-06	6.778E-02	4.655E-06	6.802E-02	6.778E+51	6.778E-02
7	12.292	12.315	2.278E-02	4.796E-02	0.255	4.371E-01	2.912E-06	3.457E-02	2.373E-06	3.467E-02	3.457E+51	3.457E-02
8	12.262	12.292	2.964E-02	6.241E-02	0.292	4.998E-01	4.422E-06	5.250E-02	3.601E-06	5.262E-02	5.250E+51	5.250E-02
9	12.240	12.262	2.167E-02	4.563E-02	0.318	5.458E-01	3.713E-06	4.408E-02	3.022E-06	4.416E-02	4.408E+51	4.408E-02
10	12.173	12.240	6.724E-02	1.416E-01	0.401	6.879E-01	1.405E-05	1.668E-01	1.142E-05	1.669E-01	1.668E+52	1.668E-01
11	12.146	12.173	2.621E-02	5.518E-02	0.434	7.436E-01	6.610E-06	7.848E-02	5.370E-06	7.846E-02	7.848E+51	7.848E-02
12	12.116	12.146	2.982E-02	6.279E-02	0.471	8.071E-01	8.450E-06	1.003E-01	6.861E-06	1.002E-01	1.003E+52	1.003E-01
13	12.085	12.116	3.129E-02	6.589E-02	0.510	8.737E-01	1.000E-05	1.188E-01	8.117E-06	1.186E-01	1.188E+52	1.188E-01
14	12.050	12.085	3.464E-02	7.293E-02	0.553	9.475E-01	1.254E-05	1.489E-01	1.017E-05	1.486E-01	1.489E+52	1.489E-01
15	12.025	12.050	2.457E-02	5.173E-02	0.583	1.000E+00	9.973E-06	1.184E-01	8.081E-06	1.181E-01	1.184E+52	1.184E-01

B.6 SVMIN

Table B.16: The same as Table 5.2, using the SVMIN model with $B_\star = 1500$

№	P_{min}	P_{max}	ϵ_{min}	ϵ_{max}	$n_{b_{min}}$	$n_{b_{max}}$	A	Z	N	Z/A	$\mu_{b_{min}}$	$\mu_{b_{max}}$	$\mu_{e_{min}}$	$\mu_{e_{max}}$
1	6.082E-15	2.628E-07	1.597E-03	3.584E-03	1.717E-06	3.852E-06	56	26	30	0.464	930.348	930.438	0.597	0.861
2	2.632E-07	9.711E-06	3.717E-03	1.577E-02	3.995E-06	1.694E-05	62	28	34	0.452	930.438	931.318	0.866	3.007
3	9.725E-06	1.081E-05	1.629E-02	1.711E-02	1.750E-05	1.838E-05	64	28	36	0.438	931.319	931.379	3.009	3.156
4	1.083E-05	1.885E-05	1.752E-02	2.268E-02	1.882E-05	2.436E-05	88	38	50	0.432	931.380	931.751	3.189	4.105
5	1.887E-05	5.072E-05	2.337E-02	3.747E-02	2.510E-05	4.023E-05	86	36	50	0.419	931.752	932.727	4.101	6.541
6	5.080E-05	1.063E-04	3.874E-02	5.548E-02	4.159E-05	5.952E-05	84	34	50	0.405	932.728	933.825	6.538	9.343
7	1.064E-04	1.790E-04	5.753E-02	7.427E-02	6.172E-05	7.964E-05	82	32	50	0.390	933.828	934.855	9.341	12.045
8	1.793E-04	2.716E-04	7.729E-02	9.488E-02	8.287E-05	1.017E-04	80	30	50	0.375	934.858	935.859	12.044	14.772
9	2.721E-04	3.541E-04	9.960E-02	1.134E-01	1.067E-04	1.215E-04	128	46	82	0.359	935.863	936.582	14.859	16.914
10	3.547E-04	4.295E-04	1.168E-01	1.284E-01	1.251E-04	1.374E-04	126	44	82	0.349	936.587	937.157	16.917	18.590
11	4.302E-04	5.172E-04	1.324E-01	1.450E-01	1.417E-04	1.552E-04	124	42	82	0.339	937.162	937.748	18.593	20.361
12	5.179E-04	6.441E-04	1.499E-01	1.670E-01	1.604E-04	1.786E-04	122	40	82	0.328	937.752	938.497	20.365	22.681
13	6.451E-04	7.464E-04	1.729E-01	1.859E-01	1.850E-04	1.988E-04	120	38	82	0.317	938.502	939.030	22.687	24.383
14	7.475E-04	8.373E-04	1.892E-01	2.002E-01	2.023E-04	2.140E-04	122	38	84	0.311	939.036	939.467	24.401	25.810
15	8.385E-04	8.585E-04	2.069E-01	2.093E-01	2.211E-04	2.237E-04	126	38	88	0.302	939.473	939.563	25.829	26.132

Table B.17: The same as Table 5.3, using the SVMIN model with $B_\star = 1500$

M_{cr}	M_{cr}/M	ΔR_{cr}	$\Delta R_{cr}/R$	$M_{b_{cr}}$	Δ_{grav}	z_{drip}	ΔN
6.755E-05	4.825E-05	4.750E-01	3.800E-02	8.313E-05	2.306E-01	5.834E-01	9.869E+52

Table B.18: The same as Table 5.4, using the SVMIN model with $B_\star = 1500$

№	r_{min}	r_{max}	ΔR_l	$\Delta R_l/\Delta R_{cr}$	z_l	z_l/z_{drip}	M_{b_l}	$M_{b_l}/M_{b_{cr}}$	M_l	M_l/M_{cr}	ΔN_l	$\Delta N_l/\Delta N$
1	12.495	12.500	4.892E-03	1.030E-02	0.006	1.025E-02	2.855E-08	3.435E-04	2.336E-08	3.458E-04	3.390E+49	3.435E-04
2	12.448	12.495	4.755E-02	1.001E-01	0.064	1.099E-01	1.016E-06	1.222E-02	8.306E-07	1.230E-02	1.206E+51	1.222E-02
3	12.444	12.448	3.257E-03	6.858E-03	0.068	1.169E-01	1.161E-07	1.397E-03	9.490E-08	1.405E-03	1.379E+50	1.397E-03
4	12.424	12.444	1.989E-02	4.187E-02	0.093	1.587E-01	8.521E-07	1.025E-02	6.962E-07	1.031E-02	1.012E+51	1.025E-02
5	12.372	12.424	5.179E-02	1.090E-01	0.156	2.676E-01	3.341E-06	4.020E-02	2.728E-06	4.038E-02	3.967E+51	4.020E-02
6	12.315	12.372	5.761E-02	1.213E-01	0.227	3.889E-01	5.709E-06	6.868E-02	4.655E-06	6.892E-02	6.778E+51	6.868E-02
7	12.261	12.315	5.328E-02	1.122E-01	0.292	5.013E-01	7.327E-06	8.815E-02	5.969E-06	8.836E-02	8.699E+51	8.815E-02
8	12.210	12.261	5.131E-02	1.080E-01	0.356	6.097E-01	9.149E-06	1.101E-01	7.445E-06	1.102E-01	1.086E+52	1.101E-01
9	12.173	12.210	3.651E-02	7.688E-02	0.401	6.871E-01	8.008E-06	9.633E-02	6.510E-06	9.637E-02	9.507E+51	9.633E-02
10	12.144	12.173	2.874E-02	6.051E-02	0.436	7.482E-01	7.218E-06	8.683E-02	5.864E-06	8.681E-02	8.569E+51	8.683E-02
11	12.115	12.144	2.932E-02	6.173E-02	0.473	8.106E-01	8.299E-06	9.983E-02	6.738E-06	9.974E-02	9.852E+51	9.983E-02
12	12.077	12.114	3.697E-02	7.785E-02	0.519	8.892E-01	1.190E-05	1.431E-01	9.651E-06	1.429E-01	1.412E+52	1.431E-01
13	12.051	12.077	2.602E-02	5.479E-02	0.551	9.448E-01	9.441E-06	1.136E-01	7.654E-06	1.133E-01	1.121E+52	1.136E-01
14	12.030	12.051	2.115E-02	4.454E-02	0.578	9.901E-01	8.297E-06	9.981E-02	6.723E-06	9.953E-02	9.850E+51	9.981E-02
15	12.025	12.029	4.394E-03	9.252E-03	0.583	1.000E+00	1.839E-06	2.213E-02	1.490E-06	2.206E-02	2.184E+51	2.213E-02

B.7 UNEDF0

Table B.19: The same as Table 5.2, using the UNEDF0 model with $B_\star = 1500$

№	P_{min}	P_{max}	ϵ_{min}	ϵ_{max}	$n_{b_{min}}$	$n_{b_{max}}$	A	Z	N	Z/A	$\mu_{b_{min}}$	$\mu_{b_{max}}$	$\mu_{e_{min}}$	$\mu_{e_{max}}$
1	6.082E-15	2.628E-07	1.597E-03	3.584E-03	1.717E-06	3.852E-06	56	26	30	0.464	930.348	930.438	0.597	0.861
2	2.632E-07	9.711E-06	3.717E-03	1.577E-02	3.995E-06	1.694E-05	62	28	34	0.452	930.438	931.318	0.866	3.007
3	9.725E-06	1.081E-05	1.629E-02	1.711E-02	1.750E-05	1.838E-05	64	28	36	0.438	931.319	931.379	3.009	3.156
4	1.083E-05	1.885E-05	1.752E-02	2.268E-02	1.882E-05	2.436E-05	88	38	50	0.432	931.380	931.751	3.189	4.105
5	1.887E-05	5.072E-05	2.337E-02	3.747E-02	2.510E-05	4.023E-05	86	36	50	0.419	931.752	932.727	4.101	6.541
6	5.080E-05	1.063E-04	3.874E-02	5.548E-02	4.159E-05	5.952E-05	84	34	50	0.405	932.728	933.825	6.538	9.343
7	1.064E-04	1.790E-04	5.753E-02	7.427E-02	6.172E-05	7.964E-05	82	32	50	0.390	933.828	934.855	9.341	12.045
8	1.793E-04	2.454E-04	7.729E-02	9.023E-02	8.287E-05	9.670E-05	80	30	50	0.375	934.858	935.594	12.044	14.051
9	2.458E-04	2.611E-04	9.185E-02	9.463E-02	9.843E-05	1.014E-04	76	28	48	0.368	935.598	935.751	14.051	14.475
10	2.614E-04	3.295E-04	9.720E-02	1.090E-01	1.041E-04	1.167E-04	78	28	50	0.359	935.755	936.371	14.486	16.235
11	3.300E-04	3.541E-04	1.097E-01	1.136E-01	1.175E-04	1.217E-04	84	30	54	0.357	936.375	936.577	16.258	16.835
12	3.547E-04	4.334E-04	1.164E-01	1.286E-01	1.247E-04	1.376E-04	86	30	56	0.349	936.582	937.182	16.847	18.599
13	4.340E-04	4.790E-04	1.317E-01	1.383E-01	1.409E-04	1.480E-04	88	30	58	0.341	937.186	937.498	18.612	19.542
14	4.797E-04	5.318E-04	1.414E-01	1.489E-01	1.514E-04	1.593E-04	84	28	56	0.333	937.503	937.838	19.545	20.568
15	5.326E-04	6.055E-04	1.525E-01	1.626E-01	1.632E-04	1.739E-04	86	28	58	0.326	937.843	938.275	20.583	21.931
16	6.064E-04	7.006E-04	1.665E-01	1.789E-01	1.781E-04	1.913E-04	88	28	60	0.318	938.280	938.790	21.947	23.573
17	7.016E-04	7.964E-04	1.831E-01	1.950E-01	1.958E-04	2.085E-04	90	28	62	0.311	938.796	939.265	23.591	25.119
18	7.975E-04	8.360E-04	1.995E-01	2.042E-01	2.133E-04	2.183E-04	92	28	64	0.304	939.270	939.449	25.137	25.732
19	8.373E-04	8.623E-04	2.121E-01	2.152E-01	2.267E-04	2.300E-04	136	40	96	0.294	939.454	939.564	25.821	26.200

Table B.20: The same as Table 5.3, using the UNEDF0 model with $B_\star = 1500$

M_{cr}	M_{cr}/M	ΔR_{cr}	$\Delta R_{cr}/R$	$M_{b_{cr}}$	Δ_{grav}	z_{drip}	ΔN
6.784E-05	4.846E-05	4.750E-01	3.800E-02	8.348E-05	2.306E-01	5.834E-01	9.911E+52

Table B.21: The same as Table 5.4, using the UNEDF0 model with $B_\star = 1500$

№	r_{min}	r_{max}	ΔR_l	$\Delta R_l/\Delta R_{cr}$	z_l	z_l/z_{drip}	M_{b_l}	$M_{b_l}/M_{b_{cr}}$	M_l	M_l/M_{cr}	ΔN_l	$\Delta N_l/\Delta N$
1	12.495	12.500	4.892E-03	1.030E-02	0.006	1.025E-02	2.855E-08	3.420E-04	2.336E-08	3.443E-04	3.390E+49	3.420E-04
2	12.448	12.495	4.755E-02	1.001E-01	0.064	1.099E-01	1.016E-06	1.217E-02	8.306E-07	1.224E-02	1.206E+51	1.217E-02
3	12.444	12.448	3.257E-03	6.857E-03	0.068	1.169E-01	1.161E-07	1.391E-03	9.490E-08	1.399E-03	1.379E+50	1.391E-03
4	12.424	12.444	1.989E-02	4.187E-02	0.093	1.587E-01	8.521E-07	1.021E-02	6.962E-07	1.026E-02	1.012E+51	1.021E-02
5	12.372	12.424	5.179E-02	1.090E-01	0.156	2.675E-01	3.341E-06	4.002E-02	2.728E-06	4.021E-02	3.967E+51	4.002E-02
6	12.315	12.372	5.761E-02	1.213E-01	0.227	3.888E-01	5.709E-06	6.838E-02	4.655E-06	6.863E-02	6.778E+51	6.838E-02
7	12.261	12.315	5.328E-02	1.122E-01	0.292	5.012E-01	7.327E-06	8.777E-02	5.969E-06	8.798E-02	8.699E+51	8.777E-02
8	12.223	12.261	3.779E-02	7.956E-02	0.339	5.812E-01	6.565E-06	7.864E-02	5.342E-06	7.875E-02	7.794E+51	7.864E-02
9	12.215	12.223	7.820E-03	1.646E-02	0.349	5.981E-01	1.507E-06	1.806E-02	1.226E-06	1.807E-02	1.790E+51	1.806E-02
10	12.184	12.215	3.132E-02	6.594E-02	0.388	6.645E-01	6.656E-06	7.973E-02	5.412E-06	7.978E-02	7.902E+51	7.973E-02
11	12.173	12.184	1.023E-02	2.154E-02	0.401	6.865E-01	2.348E-06	2.812E-02	1.908E-06	2.813E-02	2.787E+51	2.812E-02
12	12.143	12.173	3.022E-02	6.362E-02	0.438	7.507E-01	7.585E-06	9.085E-02	6.162E-06	9.083E-02	9.005E+51	9.085E-02
13	12.127	12.143	1.561E-02	3.287E-02	0.458	7.842E-01	4.304E-06	5.156E-02	3.495E-06	5.152E-02	5.110E+51	5.156E-02
14	12.110	12.127	1.675E-02	3.526E-02	0.478	8.200E-01	4.953E-06	5.933E-02	4.020E-06	5.926E-02	5.880E+51	5.933E-02
15	12.088	12.110	2.147E-02	4.521E-02	0.505	8.659E-01	6.875E-06	8.235E-02	5.578E-06	8.222E-02	8.162E+51	8.235E-02
16	12.063	12.088	2.521E-02	5.307E-02	0.537	9.197E-01	8.814E-06	1.056E-01	7.148E-06	1.054E-01	1.046E+52	1.056E-01
17	12.040	12.063	2.304E-02	4.852E-02	0.565	9.690E-01	8.791E-06	1.053E-01	7.126E-06	1.050E-01	1.044E+52	1.053E-01
18	12.031	12.039	8.736E-03	1.839E-02	0.576	9.881E-01	3.551E-06	4.253E-02	2.877E-06	4.241E-02	4.215E+51	4.253E-02
19	12.025	12.030	5.360E-03	1.128E-02	0.583	1.000E+00	2.304E-06	2.759E-02	1.866E-06	2.751E-02	2.735E+51	2.759E-02

Appendix C

Tables for $B_\star = 2000$

Below are the Tables, like those in Subsections 5.4.1 - 5.4.2, for the models: SEMF, FRDM2012, WS4RBF, BSKG3, HFB31, DDMED, DDPC1, SVMIN and UNEDF0, with magnetic field strength $B_\star = 2000$.

C.1 SEMF

Table C.1: The same as Table 5.2, using the SEMF model with $B_\star = 2000$

№	P_{min}	P_{max}	ϵ_{min}	ϵ_{max}	$n_{b_{min}}$	$n_{b_{max}}$	A	Z	N	Z/A	$\mu_{b_{min}}$	$\mu_{b_{max}}$	$\mu_{e_{min}}$	$\mu_{e_{max}}$
1	6.082E-15	3.136E-07	2.271E-03	4.693E-03	2.441E-06	5.044E-06	56	26	30	0.464	930.340	930.420	0.608	0.851
2	3.141E-07	1.227E-05	4.872E-03	2.061E-02	5.237E-06	2.215E-05	62	28	34	0.452	930.420	931.271	0.856	2.949
3	1.229E-05	2.680E-05	2.182E-02	3.130E-02	2.345E-05	3.362E-05	88	38	50	0.432	931.271	931.779	2.985	4.248
4	2.684E-05	7.056E-05	3.226E-02	5.115E-02	3.465E-05	5.492E-05	86	36	50	0.419	931.781	932.756	4.243	6.696
5	7.066E-05	1.461E-04	5.288E-02	7.526E-02	5.676E-05	8.074E-05	84	34	50	0.405	932.758	933.855	6.692	9.505
6	1.463E-04	2.436E-04	7.804E-02	1.002E-01	8.372E-05	1.074E-04	82	32	50	0.390	933.857	934.875	9.502	12.188
7	2.439E-04	2.580E-04	1.041E-01	1.069E-01	1.116E-04	1.147E-04	132	50	82	0.379	934.878	935.002	12.283	12.623
8	2.584E-04	3.505E-04	1.073E-01	1.247E-01	1.150E-04	1.336E-04	80	30	50	0.375	935.006	935.747	12.534	14.559
9	3.510E-04	5.119E-04	1.275E-01	1.536E-01	1.367E-04	1.645E-04	130	48	82	0.369	935.751	936.819	14.663	17.642
10	5.126E-04	8.082E-04	1.560E-01	1.954E-01	1.671E-04	2.091E-04	132	48	84	0.364	936.823	938.395	17.655	22.087
11	8.094E-04	8.348E-04	2.133E-01	2.166E-01	2.282E-04	2.317E-04	138	46	92	0.333	938.400	938.511	22.092	22.432
12	8.360E-04	8.422E-04	2.199E-01	2.207E-01	2.352E-04	2.360E-04	146	48	98	0.329	938.516	938.542	22.459	22.541
13	8.435E-04	8.868E-04	2.209E-01	2.264E-01	2.362E-04	2.421E-04	140	46	94	0.329	938.548	938.729	22.546	23.110
14	8.881E-04	9.532E-04	2.297E-01	2.378E-01	2.456E-04	2.543E-04	148	48	100	0.324	938.734	938.995	23.138	23.959
15	9.546E-04	1.008E-03	2.413E-01	2.479E-01	2.579E-04	2.650E-04	150	48	102	0.320	939.000	939.205	23.977	24.630
16	1.010E-03	1.061E-03	2.509E-01	2.573E-01	2.683E-04	2.750E-04	158	50	108	0.316	939.210	939.401	24.660	25.277
17	1.063E-03	1.106E-03	2.607E-01	2.659E-01	2.787E-04	2.842E-04	160	50	110	0.312	939.407	939.560	25.295	25.796

Table C.2: The same as Table 5.3, using the SEMF model with $B_\star = 2000$

M_{cr}	M_{cr}/M	ΔR_{cr}	$\Delta R_{cr}/R$	$M_{b_{cr}}$	Δ_{grav}	z_{drip}	ΔN
8.711E-05	6.222E-05	4.752E-01	3.802E-02	1.072E-04	2.305E-01	5.837E-01	1.273E+53

Table C.3: The same as Table 5.4, using the SEMF model with $B_\star = 2000$

№	r_{min}	r_{max}	ΔR_l	$\Delta R_l/\Delta R_{cr}$	z_l	z_l/z_{drip}	M_{b_l}	$M_{b_l}/M_{b_{cr}}$	M_l	M_l/M_{cr}	ΔN_l	$\Delta N_l/\Delta N$
1	12.496	12.500	4.374E-03	9.205E-03	0.005	9.160E-03	3.409E-08	3.180E-04	2.788E-08	3.201E-04	4.047E+49	3.180E-04
2	12.450	12.496	4.596E-02	9.671E-02	0.062	1.055E-01	1.287E-06	1.200E-02	1.052E-06	1.208E-02	1.528E+51	1.200E-02
3	12.422	12.450	2.723E-02	5.731E-02	0.095	1.627E-01	1.543E-06	1.439E-02	1.261E-06	1.447E-02	1.832E+51	1.439E-02
4	12.370	12.422	5.183E-02	1.091E-01	0.159	2.716E-01	4.583E-06	4.275E-02	3.742E-06	4.295E-02	5.441E+51	4.275E-02
5	12.313	12.370	5.758E-02	1.212E-01	0.229	3.927E-01	7.757E-06	7.236E-02	6.326E-06	7.261E-02	9.209E+51	7.236E-02
6	12.260	12.313	5.277E-02	1.110E-01	0.294	5.040E-01	9.812E-06	9.153E-02	7.992E-06	9.174E-02	1.165E+52	9.153E-02
7	12.253	12.260	6.395E-03	1.346E-02	0.302	5.178E-01	1.402E-06	1.308E-02	1.141E-06	1.310E-02	1.665E+51	1.308E-02
8	12.215	12.253	3.799E-02	7.994E-02	0.349	5.982E-01	9.125E-06	8.512E-02	7.424E-06	8.523E-02	1.083E+52	8.512E-02
9	12.161	12.215	5.417E-02	1.140E-01	0.416	7.128E-01	1.566E-05	1.461E-01	1.273E-05	1.462E-01	1.860E+52	1.461E-01
10	12.082	12.161	7.848E-02	1.652E-01	0.513	8.789E-01	2.810E-05	2.621E-01	2.281E-05	2.618E-01	3.336E+52	2.621E-01
11	12.076	12.082	5.470E-03	1.151E-02	0.520	8.910E-01	2.382E-06	2.222E-02	1.932E-06	2.218E-02	2.828E+51	2.222E-02
12	12.075	12.076	1.297E-03	2.729E-03	0.522	8.943E-01	5.785E-07	5.396E-03	4.691E-07	5.385E-03	6.868E+50	5.396E-03
13	12.066	12.075	8.942E-03	1.882E-02	0.533	9.137E-01	4.047E-06	3.775E-02	3.281E-06	3.767E-02	4.804E+51	3.775E-02
14	12.053	12.065	1.282E-02	2.697E-02	0.549	9.414E-01	6.054E-06	5.647E-02	4.907E-06	5.633E-02	7.187E+51	5.647E-02
15	12.042	12.052	1.004E-02	2.113E-02	0.562	9.632E-01	4.953E-06	4.621E-02	4.015E-06	4.608E-02	5.881E+51	4.621E-02
16	12.033	12.042	9.352E-03	1.968E-02	0.574	9.836E-01	4.786E-06	4.465E-02	3.878E-06	4.452E-02	5.682E+51	4.465E-02
17	12.025	12.032	7.495E-03	1.577E-02	0.584	1.000E+00	3.969E-06	3.703E-02	3.216E-06	3.691E-02	4.713E+51	3.703E-02

C.2 FRDM2012

Table C.4: The same as Table 5.2, using the FRDM2012 model with $B_\star = 2000$

№	P_{min}	P_{max}	ϵ_{min}	ϵ_{max}	$n_{b_{min}}$	$n_{b_{max}}$	A	Z	N	Z/A	$\mu_{b_{min}}$	$\mu_{b_{max}}$	$\mu_{e_{min}}$	$\mu_{e_{max}}$
1	6.082E-15	3.136E-07	2.271E-03	4.693E-03	2.441E-06	5.044E-06	56	26	30	0.464	930.340	930.420	0.608	0.851
2	3.141E-07	1.227E-05	4.872E-03	2.061E-02	5.237E-06	2.215E-05	62	28	34	0.452	930.420	931.271	0.856	2.949
3	1.229E-05	2.680E-05	2.182E-02	3.130E-02	2.345E-05	3.362E-05	88	38	50	0.432	931.271	931.779	2.985	4.248
4	2.684E-05	7.056E-05	3.226E-02	5.115E-02	3.465E-05	5.492E-05	86	36	50	0.419	931.781	932.756	4.243	6.696
5	7.066E-05	1.461E-04	5.288E-02	7.526E-02	5.676E-05	8.074E-05	84	34	50	0.405	932.758	933.855	6.692	9.505
6	1.463E-04	2.436E-04	7.804E-02	1.002E-01	8.372E-05	1.074E-04	82	32	50	0.390	933.857	934.875	9.502	12.188
7	2.439E-04	2.580E-04	1.041E-01	1.069E-01	1.116E-04	1.147E-04	132	50	82	0.379	934.878	935.002	12.283	12.623
8	2.584E-04	3.314E-04	1.073E-01	1.213E-01	1.150E-04	1.300E-04	80	30	50	0.375	935.006	935.602	12.534	14.163
9	3.319E-04	4.624E-04	1.274E-01	1.500E-01	1.365E-04	1.606E-04	128	46	82	0.359	935.606	936.484	14.257	16.773
10	4.631E-04	5.931E-04	1.544E-01	1.744E-01	1.653E-04	1.867E-04	126	44	82	0.349	936.488	937.227	16.774	18.945
11	5.940E-04	7.290E-04	1.799E-01	1.991E-01	1.926E-04	2.130E-04	124	42	82	0.339	937.231	937.897	18.948	20.960
12	7.301E-04	8.907E-04	2.057E-01	2.270E-01	2.201E-04	2.428E-04	122	40	82	0.328	937.902	938.596	20.964	23.126
13	8.920E-04	1.084E-03	2.351E-01	2.590E-01	2.515E-04	2.768E-04	120	38	82	0.317	938.601	939.326	23.130	25.464
14	1.085E-03	1.153E-03	2.689E-01	2.771E-01	2.874E-04	2.961E-04	118	36	82	0.305	939.332	939.564	25.470	26.242

Table C.5: The same as Table 5.3, using the FRDM2012 model with $B_\star = 2000$

M_{cr}	M_{cr}/M	ΔR_{cr}	$\Delta R_{cr}/R$	$M_{b_{cr}}$	Δ_{grav}	z_{drip}	ΔN
9.070E-05	6.479E-05	4.754E-01	3.803E-02	1.116E-04	2.306E-01	5.839E-01	1.325E+53

Table C.6: The same as Table 5.4, using the FRDM2012 model with $B_\star = 2000$

№	r_{min}	r_{max}	ΔR_l	$\Delta R_l/\Delta R_{cr}$	z_l	z_l/z_{drip}	M_{b_l}	$M_{b_l}/M_{b_{cr}}$	M_l	M_l/M_{cr}	ΔN_l	$\Delta N_l/\Delta N$
1	12.496	12.500	4.374E-03	9.201E-03	0.005	9.157E-03	3.409E-08	3.054E-04	2.788E-08	3.074E-04	4.047E+49	3.054E-04
2	12.450	12.496	4.596E-02	9.667E-02	0.062	1.054E-01	1.287E-06	1.153E-02	1.052E-06	1.160E-02	1.528E+51	1.153E-02
3	12.422	12.450	2.723E-02	5.728E-02	0.095	1.626E-01	1.543E-06	1.382E-02	1.261E-06	1.390E-02	1.832E+51	1.382E-02
4	12.370	12.422	5.183E-02	1.090E-01	0.159	2.715E-01	4.583E-06	4.106E-02	3.742E-06	4.125E-02	5.441E+51	4.106E-02
5	12.313	12.370	5.758E-02	1.211E-01	0.229	3.926E-01	7.757E-06	6.950E-02	6.326E-06	6.974E-02	9.209E+51	6.950E-02
6	12.260	12.313	5.277E-02	1.110E-01	0.294	5.038E-01	9.812E-06	8.791E-02	7.992E-06	8.812E-02	1.165E+52	8.791E-02
7	12.253	12.260	6.395E-03	1.345E-02	0.302	5.176E-01	1.402E-06	1.256E-02	1.141E-06	1.258E-02	1.665E+51	1.256E-02
8	12.223	12.253	3.059E-02	6.435E-02	0.340	5.824E-01	7.245E-06	6.491E-02	5.895E-06	6.500E-02	8.601E+51	6.491E-02
9	12.178	12.222	4.465E-02	9.392E-02	0.395	6.768E-01	1.276E-05	1.144E-01	1.038E-05	1.144E-01	1.515E+52	1.144E-01
10	12.140	12.178	3.722E-02	7.829E-02	0.441	7.557E-01	1.254E-05	1.123E-01	1.019E-05	1.123E-01	1.489E+52	1.123E-01
11	12.107	12.140	3.327E-02	6.998E-02	0.483	8.264E-01	1.285E-05	1.151E-01	1.043E-05	1.150E-01	1.526E+52	1.151E-01
12	12.072	12.107	3.442E-02	7.240E-02	0.525	8.996E-01	1.511E-05	1.354E-01	1.226E-05	1.351E-01	1.794E+52	1.354E-01
13	12.036	12.072	3.566E-02	7.500E-02	0.570	9.755E-01	1.778E-05	1.593E-01	1.441E-05	1.589E-01	2.111E+52	1.593E-01
14	12.025	12.036	1.133E-02	2.383E-02	0.584	1.000E+00	6.222E-06	5.574E-02	5.041E-06	5.557E-02	7.386E+51	5.574E-02

C.3 WS4RBF

Table C.7: The same as Table 5.2, using the WS4RBF model with $B_\star = 2000$

№	P_{min}	P_{max}	ϵ_{min}	ϵ_{max}	$n_{b_{min}}$	$n_{b_{max}}$	A	Z	N	Z/A	$\mu_{b_{min}}$	$\mu_{b_{max}}$	$\mu_{e_{min}}$	$\mu_{e_{max}}$
1	6.082E-15	3.136E-07	2.271E-03	4.693E-03	2.441E-06	5.044E-06	56	26	30	0.464	930.340	930.420	0.608	0.851
2	3.141E-07	1.227E-05	4.872E-03	2.061E-02	5.237E-06	2.215E-05	62	28	34	0.452	930.420	931.271	0.856	2.949
3	1.229E-05	2.680E-05	2.182E-02	3.130E-02	2.345E-05	3.362E-05	88	38	50	0.432	931.271	931.779	2.985	4.248
4	2.684E-05	7.056E-05	3.226E-02	5.115E-02	3.465E-05	5.492E-05	86	36	50	0.419	931.781	932.756	4.243	6.696
5	7.066E-05	1.461E-04	5.288E-02	7.526E-02	5.676E-05	8.074E-05	84	34	50	0.405	932.758	933.855	6.692	9.505
6	1.463E-04	2.436E-04	7.804E-02	1.002E-01	8.372E-05	1.074E-04	82	32	50	0.390	933.857	934.875	9.502	12.188
7	2.439E-04	2.580E-04	1.041E-01	1.069E-01	1.116E-04	1.147E-04	132	50	82	0.379	934.878	935.002	12.283	12.623
8	2.584E-04	3.505E-04	1.073E-01	1.247E-01	1.150E-04	1.336E-04	80	30	50	0.375	935.006	935.747	12.534	14.559
9	3.510E-04	3.745E-04	1.275E-01	1.317E-01	1.367E-04	1.411E-04	130	48	82	0.369	935.751	935.920	14.663	15.136
10	3.751E-04	5.478E-04	1.346E-01	1.623E-01	1.442E-04	1.738E-04	78	28	50	0.359	935.924	937.010	15.041	18.127
11	5.486E-04	6.605E-04	1.678E-01	1.840E-01	1.797E-04	1.969E-04	126	44	82	0.349	937.014	937.608	18.231	19.976
12	6.614E-04	7.905E-04	1.897E-01	2.072E-01	2.030E-04	2.217E-04	124	42	82	0.339	937.613	938.221	19.979	21.814
13	7.917E-04	1.066E-03	2.141E-01	2.482E-01	2.291E-04	2.654E-04	122	40	82	0.328	938.226	939.336	21.819	25.273
14	1.068E-03	1.129E-03	2.571E-01	2.643E-01	2.748E-04	2.825E-04	120	38	82	0.317	939.342	939.563	25.279	25.989

Table C.8: The same as Table 5.3, using the WS4RBF model with $B_\star = 2000$

M_{cr}	M_{cr}/M	ΔR_{cr}	$\Delta R_{cr}/R$	$M_{b_{cr}}$	Δ_{grav}	z_{drip}	ΔN
8.890E-05	6.350E-05	4.753E-01	3.803E-02	1.094E-04	2.306E-01	5.839E-01	1.299E+53

Table C.9: The same as Table 5.4, using the WS4RBF model with $B_\star = 2000$

№	r_{min}	r_{max}	ΔR_l	$\Delta R_l/\Delta R_{cr}$	z_l	z_l/z_{drip}	M_{b_l}	$M_{b_l}/M_{b_{cr}}$	M_l	M_l/M_{cr}	ΔN_l	$\Delta N_l/\Delta N$
1	12.496	12.500	4.374E-03	9.202E-03	0.005	9.158E-03	3.409E-08	3.116E-04	2.788E-08	3.137E-04	4.047E+49	3.116E-04
2	12.450	12.496	4.596E-02	9.668E-02	0.062	1.054E-01	1.287E-06	1.176E-02	1.052E-06	1.183E-02	1.528E+51	1.176E-02
3	12.422	12.450	2.723E-02	5.729E-02	0.095	1.626E-01	1.543E-06	1.410E-02	1.261E-06	1.418E-02	1.832E+51	1.410E-02
4	12.370	12.422	5.183E-02	1.090E-01	0.159	2.715E-01	4.583E-06	4.190E-02	3.742E-06	4.209E-02	5.441E+51	4.190E-02
5	12.313	12.370	5.758E-02	1.211E-01	0.229	3.926E-01	7.757E-06	7.091E-02	6.326E-06	7.116E-02	9.209E+51	7.091E-02
6	12.260	12.313	5.277E-02	1.110E-01	0.294	5.039E-01	9.812E-06	8.970E-02	7.992E-06	8.991E-02	1.165E+52	8.970E-02
7	12.253	12.260	6.395E-03	1.345E-02	0.302	5.177E-01	1.402E-06	1.282E-02	1.141E-06	1.284E-02	1.665E+51	1.282E-02
8	12.215	12.253	3.799E-02	7.991E-02	0.349	5.980E-01	9.125E-06	8.341E-02	7.424E-06	8.352E-02	1.083E+52	8.341E-02
9	12.206	12.215	8.628E-03	1.815E-02	0.360	6.166E-01	2.309E-06	2.111E-02	1.878E-06	2.112E-02	2.741E+51	2.111E-02
10	12.151	12.206	5.495E-02	1.156E-01	0.428	7.328E-01	1.676E-05	1.532E-01	1.362E-05	1.532E-01	1.990E+52	1.532E-01
11	12.121	12.151	2.978E-02	6.265E-02	0.465	7.961E-01	1.070E-05	9.782E-02	8.689E-06	9.774E-02	1.270E+52	9.782E-02
12	12.091	12.121	3.025E-02	6.364E-02	0.502	8.605E-01	1.221E-05	1.116E-01	9.909E-06	1.115E-01	1.450E+52	1.116E-01
13	12.036	12.090	5.471E-02	1.151E-01	0.570	9.766E-01	2.556E-05	2.337E-01	2.072E-05	2.331E-01	3.034E+52	2.337E-01
14	12.025	12.035	1.079E-02	2.270E-02	0.584	1.000E+00	5.660E-06	5.174E-02	4.585E-06	5.158E-02	6.719E+51	5.174E-02

C.4 BSKG3

Table C.10: The same as Table 5.2, using the BSKG3 model with $B_\star = 2000$

№	P_{min}	P_{max}	ϵ_{min}	ϵ_{max}	$n_{b_{min}}$	$n_{b_{max}}$	A	Z	N	Z/A	$\mu_{b_{min}}$	$\mu_{b_{max}}$	$\mu_{e_{min}}$	$\mu_{e_{max}}$
1	6.082E-15	3.136E-07	2.271E-03	4.693E-03	2.441E-06	5.044E-06	56	26	30	0.464	930.340	930.420	0.608	0.851
2	3.141E-07	1.227E-05	4.872E-03	2.061E-02	5.237E-06	2.215E-05	62	28	34	0.452	930.420	931.271	0.856	2.949
3	1.229E-05	2.680E-05	2.182E-02	3.130E-02	2.345E-05	3.362E-05	88	38	50	0.432	931.271	931.779	2.985	4.248
4	2.684E-05	7.056E-05	3.226E-02	5.115E-02	3.465E-05	5.492E-05	86	36	50	0.419	931.781	932.756	4.243	6.696
5	7.066E-05	1.461E-04	5.288E-02	7.526E-02	5.676E-05	8.074E-05	84	34	50	0.405	932.758	933.855	6.692	9.505
6	1.463E-04	2.436E-04	7.804E-02	1.002E-01	8.372E-05	1.074E-04	82	32	50	0.390	933.857	934.875	9.502	12.188
7	2.439E-04	2.580E-04	1.041E-01	1.069E-01	1.116E-04	1.147E-04	132	50	82	0.379	934.878	935.002	12.283	12.623
8	2.584E-04	3.344E-04	1.073E-01	1.218E-01	1.150E-04	1.305E-04	80	30	50	0.375	935.006	935.625	12.534	14.225
9	3.349E-04	4.897E-04	1.279E-01	1.543E-01	1.371E-04	1.652E-04	128	46	82	0.359	935.628	936.653	14.318	17.253
10	4.905E-04	6.064E-04	1.588E-01	1.763E-01	1.701E-04	1.888E-04	126	44	82	0.349	936.657	937.303	17.255	19.153
11	6.073E-04	7.508E-04	1.819E-01	2.020E-01	1.947E-04	2.161E-04	124	42	82	0.339	937.308	938.006	19.156	21.267
12	7.519E-04	9.282E-04	2.087E-01	2.317E-01	2.233E-04	2.478E-04	122	40	82	0.328	938.011	938.760	21.271	23.602
13	9.296E-04	1.047E-03	2.400E-01	2.546E-01	2.566E-04	2.722E-04	120	38	82	0.317	938.765	939.211	23.607	25.041
14	1.049E-03	1.114E-03	2.591E-01	2.670E-01	2.770E-04	2.854E-04	122	38	84	0.311	939.217	939.449	25.059	25.819
15	1.116E-03	1.148E-03	2.716E-01	2.754E-01	2.903E-04	2.943E-04	124	38	86	0.306	939.455	939.563	25.838	26.198

Table C.11: The same as Table 5.3, using the BSKG3 model with $B_\star = 2000$

M_{cr}	M_{cr}/M	ΔR_{cr}	$\Delta R_{cr}/R$	$M_{b_{cr}}$	Δ_{grav}	z_{drip}	ΔN
9.031E-05	6.451E-05	4.754E-01	3.803E-02	1.111E-04	2.306E-01	5.839E-01	1.319E+53

Table C.12: The same as Table 5.4, using the BSKG3 model with $B_\star = 2000$

№	r_{min}	r_{max}	ΔR_l	$\Delta R_l/\Delta R_{cr}$	z_l	z_l/z_{drip}	M_{b_l}	$M_{b_l}/M_{b_{cr}}$	M_l	M_l/M_{cr}	ΔN_l	$\Delta N_l/\Delta N$
1	12.496	12.500	4.374E-03	9.202E-03	0.005	9.157E-03	3.409E-08	3.067E-04	2.788E-08	3.087E-04	4.047E+49	3.067E-04
2	12.450	12.496	4.596E-02	9.668E-02	0.062	1.054E-01	1.287E-06	1.158E-02	1.052E-06	1.165E-02	1.528E+51	1.158E-02
3	12.422	12.450	2.723E-02	5.729E-02	0.095	1.626E-01	1.543E-06	1.388E-02	1.261E-06	1.396E-02	1.832E+51	1.388E-02
4	12.370	12.422	5.183E-02	1.090E-01	0.159	2.715E-01	4.583E-06	4.124E-02	3.742E-06	4.143E-02	5.441E+51	4.124E-02
5	12.313	12.370	5.758E-02	1.211E-01	0.229	3.926E-01	7.757E-06	6.980E-02	6.326E-06	7.004E-02	9.209E+51	6.980E-02
6	12.260	12.313	5.277E-02	1.110E-01	0.294	5.038E-01	9.812E-06	8.829E-02	7.992E-06	8.850E-02	1.165E+52	8.829E-02
7	12.253	12.260	6.395E-03	1.345E-02	0.302	5.177E-01	1.402E-06	1.262E-02	1.141E-06	1.264E-02	1.665E+51	1.262E-02
8	12.221	12.253	3.174E-02	6.678E-02	0.341	5.848E-01	7.535E-06	6.780E-02	6.131E-06	6.789E-02	8.945E+51	6.780E-02
9	12.169	12.221	5.203E-02	1.095E-01	0.406	6.948E-01	1.512E-05	1.361E-01	1.230E-05	1.361E-01	1.795E+52	1.361E-01
10	12.136	12.169	3.250E-02	6.837E-02	0.446	7.638E-01	1.115E-05	1.003E-01	9.058E-06	1.003E-01	1.324E+52	1.003E-01
11	12.101	12.136	3.488E-02	7.338E-02	0.489	8.379E-01	1.364E-05	1.227E-01	1.107E-05	1.226E-01	1.619E+52	1.227E-01
12	12.064	12.101	3.706E-02	7.796E-02	0.535	9.167E-01	1.654E-05	1.488E-01	1.342E-05	1.486E-01	1.964E+52	1.488E-01
13	12.042	12.064	2.191E-02	4.609E-02	0.563	9.636E-01	1.094E-05	9.841E-02	8.864E-06	9.815E-02	1.298E+52	9.841E-02
14	12.030	12.042	1.138E-02	2.393E-02	0.577	9.882E-01	6.026E-06	5.422E-02	4.882E-06	5.406E-02	7.154E+51	5.422E-02
15	12.025	12.030	5.298E-03	1.115E-02	0.584	1.000E+00	2.914E-06	2.622E-02	2.360E-06	2.614E-02	3.459E+51	2.622E-02

C.5 HFB31

Table C.13: The same as Table 5.2, using the HFB31 model with $B_\star = 2000$

№	P_{min}	P_{max}	ϵ_{min}	ϵ_{max}	$n_{b_{min}}$	$n_{b_{max}}$	A	Z	N	Z/A	$\mu_{b_{min}}$	$\mu_{b_{max}}$	$\mu_{e_{min}}$	$\mu_{e_{max}}$
1	6.082E-15	3.136E-07	2.271E-03	4.693E-03	2.441E-06	5.044E-06	56	26	30	0.464	930.340	930.420	0.608	0.851
2	3.141E-07	1.227E-05	4.872E-03	2.061E-02	5.237E-06	2.215E-05	62	28	34	0.452	930.420	931.271	0.856	2.949
3	1.229E-05	2.680E-05	2.182E-02	3.130E-02	2.345E-05	3.362E-05	88	38	50	0.432	931.271	931.779	2.985	4.248
4	2.684E-05	7.056E-05	3.226E-02	5.115E-02	3.465E-05	5.492E-05	86	36	50	0.419	931.781	932.756	4.243	6.696
5	7.066E-05	1.461E-04	5.288E-02	7.526E-02	5.676E-05	8.074E-05	84	34	50	0.405	932.758	933.855	6.692	9.505
6	1.463E-04	2.436E-04	7.804E-02	1.002E-01	8.372E-05	1.074E-04	82	32	50	0.390	933.857	934.875	9.502	12.188
7	2.439E-04	2.580E-04	1.041E-01	1.069E-01	1.116E-04	1.147E-04	132	50	82	0.379	934.878	935.002	12.283	12.623
8	2.584E-04	3.505E-04	1.073E-01	1.247E-01	1.150E-04	1.336E-04	80	30	50	0.375	935.006	935.747	12.534	14.559
9	3.510E-04	3.829E-04	1.275E-01	1.331E-01	1.367E-04	1.426E-04	130	48	82	0.369	935.751	935.979	14.663	15.300
10	3.835E-04	4.934E-04	1.368E-01	1.548E-01	1.465E-04	1.658E-04	128	46	82	0.359	935.983	936.686	15.302	17.315
11	4.941E-04	5.793E-04	1.594E-01	1.724E-01	1.707E-04	1.846E-04	126	44	82	0.349	936.691	937.170	17.317	18.727
12	5.802E-04	6.985E-04	1.778E-01	1.949E-01	1.903E-04	2.086E-04	124	42	82	0.339	937.175	937.768	18.730	20.523
13	6.995E-04	8.585E-04	2.014E-01	2.229E-01	2.155E-04	2.384E-04	122	40	82	0.328	937.773	938.473	20.527	22.709
14	8.598E-04	9.337E-04	2.269E-01	2.363E-01	2.427E-04	2.528E-04	121	39	82	0.322	938.479	938.777	22.719	23.664
15	9.351E-04	9.745E-04	2.407E-01	2.457E-01	2.574E-04	2.627E-04	120	38	82	0.317	938.783	938.934	23.676	24.163
16	9.759E-04	1.149E-03	2.500E-01	2.711E-01	2.673E-04	2.898E-04	122	38	84	0.311	938.939	939.562	24.181	26.217

Table C.14: The same as Table 5.3, using the HFB31 model with $B_\star = 2000$

M_{cr}	M_{cr}/M	ΔR_{cr}	$\Delta R_{cr}/R$	$M_{b_{cr}}$	Δ_{grav}	z_{drip}	ΔN
9.043E-05	6.460E-05	4.753E-01	3.803E-02	1.113E-04	2.306E-01	5.838E-01	1.321E+53

Table C.15: The same as Table 5.4, using the HFB31 model with $B_\star = 2000$

№	r_{min}	r_{max}	ΔR_l	$\Delta R_l/\Delta R_{cr}$	z_l	z_l/z_{drip}	M_{b_l}	$M_{b_l}/M_{b_{cr}}$	M_l	M_l/M_{cr}	ΔN_l	$\Delta N_l/\Delta N$
1	12.496	12.500	4.374E-03	9.202E-03	0.005	9.158E-03	3.409E-08	3.063E-04	2.788E-08	3.083E-04	4.047E+49	3.063E-04
2	12.450	12.496	4.596E-02	9.668E-02	0.062	1.054E-01	1.287E-06	1.156E-02	1.052E-06	1.163E-02	1.528E+51	1.156E-02
3	12.422	12.450	2.723E-02	5.729E-02	0.095	1.626E-01	1.543E-06	1.386E-02	1.261E-06	1.394E-02	1.832E+51	1.386E-02
4	12.370	12.422	5.183E-02	1.091E-01	0.159	2.715E-01	4.583E-06	4.118E-02	3.742E-06	4.137E-02	5.441E+51	4.118E-02
5	12.313	12.370	5.758E-02	1.211E-01	0.229	3.926E-01	7.757E-06	6.970E-02	6.326E-06	6.995E-02	9.209E+51	6.970E-02
6	12.260	12.313	5.277E-02	1.110E-01	0.294	5.039E-01	9.812E-06	8.817E-02	7.992E-06	8.838E-02	1.165E+52	8.817E-02
7	12.253	12.260	6.395E-03	1.345E-02	0.302	5.177E-01	1.402E-06	1.260E-02	1.141E-06	1.262E-02	1.665E+51	1.260E-02
8	12.215	12.253	3.799E-02	7.992E-02	0.349	5.980E-01	9.125E-06	8.199E-02	7.424E-06	8.210E-02	1.083E+52	8.199E-02
9	12.203	12.215	1.163E-02	2.447E-02	0.364	6.229E-01	3.129E-06	2.812E-02	2.545E-06	2.814E-02	3.715E+51	2.812E-02
10	12.167	12.203	3.565E-02	7.501E-02	0.408	6.985E-01	1.069E-05	9.609E-02	8.692E-06	9.612E-02	1.270E+52	9.609E-02
11	12.143	12.167	2.415E-02	5.080E-02	0.438	7.499E-01	8.206E-06	7.374E-02	6.666E-06	7.371E-02	9.742E+51	7.374E-02
12	12.113	12.143	2.968E-02	6.244E-02	0.475	8.130E-01	1.128E-05	1.014E-01	9.162E-06	1.013E-01	1.340E+52	1.014E-01
13	12.078	12.113	3.478E-02	7.317E-02	0.518	8.869E-01	1.498E-05	1.346E-01	1.216E-05	1.344E-01	1.779E+52	1.346E-01
14	12.063	12.078	1.474E-02	3.100E-02	0.536	9.186E-01	6.907E-06	6.207E-02	5.601E-06	6.193E-02	8.200E+51	6.207E-02
15	12.055	12.063	7.456E-03	1.569E-02	0.546	9.349E-01	3.663E-06	3.292E-02	2.970E-06	3.284E-02	4.349E+51	3.292E-02
16	12.025	12.055	3.052E-02	6.421E-02	0.584	1.000E+00	1.602E-05	1.440E-01	1.298E-05	1.435E-01	1.902E+52	1.440E-01

C.6 DDMED

Table C.16: The same as Table 5.2, using the DDMED model with $B_\star = 2000$

№	P_{min}	P_{max}	ϵ_{min}	ϵ_{max}	$n_{b_{min}}$	$n_{b_{max}}$	A	Z	N	Z/A	$\mu_{b_{min}}$	$\mu_{b_{max}}$	$\mu_{e_{min}}$	$\mu_{e_{max}}$
1	6.082E-15	3.136E-07	2.271E-03	4.693E-03	2.441E-06	5.044E-06	56	26	30	0.464	930.340	930.420	0.608	0.851
2	3.141E-07	1.227E-05	4.872E-03	2.061E-02	5.237E-06	2.215E-05	62	28	34	0.452	930.420	931.271	0.856	2.949
3	1.229E-05	2.680E-05	2.182E-02	3.130E-02	2.345E-05	3.362E-05	88	38	50	0.432	931.271	931.779	2.985	4.248
4	2.684E-05	7.056E-05	3.226E-02	5.115E-02	3.465E-05	5.492E-05	86	36	50	0.419	931.781	932.756	4.243	6.696
5	7.066E-05	1.461E-04	5.288E-02	7.526E-02	5.676E-05	8.074E-05	84	34	50	0.405	932.758	933.855	6.692	9.505
6	1.463E-04	2.436E-04	7.804E-02	1.002E-01	8.372E-05	1.074E-04	82	32	50	0.390	933.857	934.875	9.502	12.188
7	2.439E-04	2.580E-04	1.041E-01	1.069E-01	1.116E-04	1.147E-04	132	50	82	0.379	934.878	935.002	12.283	12.623
8	2.584E-04	3.505E-04	1.073E-01	1.247E-01	1.150E-04	1.336E-04	80	30	50	0.375	935.006	935.747	12.534	14.559
9	3.510E-04	3.562E-04	1.275E-01	1.285E-01	1.367E-04	1.376E-04	130	48	82	0.369	935.751	935.789	14.663	14.769
10	3.568E-04	4.790E-04	1.320E-01	1.526E-01	1.414E-04	1.634E-04	128	46	82	0.359	935.792	936.594	14.770	17.066
11	4.797E-04	6.010E-04	1.571E-01	1.756E-01	1.682E-04	1.880E-04	126	44	82	0.349	936.599	937.280	17.068	19.069
12	6.019E-04	7.322E-04	1.811E-01	1.995E-01	1.938E-04	2.135E-04	124	42	82	0.339	937.284	937.924	19.072	21.006
13	7.333E-04	8.881E-04	2.062E-01	2.267E-01	2.206E-04	2.425E-04	122	40	82	0.328	937.929	938.598	21.009	23.092
14	8.894E-04	1.077E-03	2.348E-01	2.582E-01	2.511E-04	2.760E-04	120	38	82	0.317	938.603	939.315	23.097	25.390
15	1.079E-03	1.149E-03	2.681E-01	2.767E-01	2.866E-04	2.957E-04	118	36	82	0.305	939.321	939.563	25.396	26.204

Table C.17: The same as Table 5.3, using the DDMED model with $B_\star = 2000$

M_{cr}	M_{cr}/M	ΔR_{cr}	$\Delta R_{cr}/R$	$M_{b_{cr}}$	Δ_{grav}	z_{drip}	ΔN
9.044E-05	6.460E-05	4.754E-01	3.803E-02	1.113E-04	2.306E-01	5.839E-01	1.321E+53

Table C.18: The same as Table 5.4, using the DDMED model with $B_\star = 2000$

№	r_{min}	r_{max}	ΔR_l	$\Delta R_l/\Delta R_{cr}$	z_l	z_l/z_{drip}	M_{b_l}	$M_{b_l}/M_{b_{cr}}$	M_l	M_l/M_{cr}	ΔN_l	$\Delta N_l/\Delta N$
1	12.496	12.500	4.374E-03	9.201E-03	0.005	9.157E-03	3.409E-08	3.063E-04	2.788E-08	3.083E-04	4.047E+49	3.063E-04
2	12.450	12.496	4.596E-02	9.667E-02	0.062	1.054E-01	1.287E-06	1.156E-02	1.052E-06	1.163E-02	1.528E+51	1.156E-02
3	12.422	12.450	2.723E-02	5.729E-02	0.095	1.626E-01	1.543E-06	1.386E-02	1.261E-06	1.394E-02	1.832E+51	1.386E-02
4	12.370	12.422	5.183E-02	1.090E-01	0.159	2.715E-01	4.583E-06	4.118E-02	3.742E-06	4.137E-02	5.441E+51	4.118E-02
5	12.313	12.370	5.758E-02	1.211E-01	0.229	3.926E-01	7.757E-06	6.970E-02	6.326E-06	6.995E-02	9.209E+51	6.970E-02
6	12.260	12.313	5.277E-02	1.110E-01	0.294	5.038E-01	9.812E-06	8.817E-02	7.992E-06	8.838E-02	1.165E+52	8.817E-02
7	12.253	12.260	6.395E-03	1.345E-02	0.302	5.176E-01	1.402E-06	1.260E-02	1.141E-06	1.262E-02	1.665E+51	1.260E-02
8	12.215	12.253	3.799E-02	7.991E-02	0.349	5.980E-01	9.125E-06	8.199E-02	7.424E-06	8.210E-02	1.083E+52	8.199E-02
9	12.213	12.215	1.936E-03	4.073E-03	0.352	6.024E-01	5.120E-07	4.601E-03	4.164E-07	4.605E-03	6.078E+50	4.601E-03
10	12.172	12.213	4.071E-02	8.564E-02	0.402	6.886E-01	1.193E-05	1.072E-01	9.698E-06	1.072E-01	1.416E+52	1.072E-01
11	12.138	12.172	3.428E-02	7.211E-02	0.445	7.613E-01	1.168E-05	1.049E-01	9.486E-06	1.049E-01	1.386E+52	1.049E-01
12	12.105	12.137	3.196E-02	6.722E-02	0.484	8.293E-01	1.239E-05	1.114E-01	1.006E-05	1.113E-01	1.472E+52	1.114E-01
13	12.072	12.105	3.315E-02	6.973E-02	0.525	8.998E-01	1.455E-05	1.308E-01	1.181E-05	1.305E-01	1.728E+52	1.308E-01
14	12.037	12.072	3.504E-02	7.371E-02	0.569	9.744E-01	1.744E-05	1.567E-01	1.413E-05	1.563E-01	2.070E+52	1.567E-01
15	12.025	12.036	1.185E-02	2.494E-02	0.584	1.000E+00	6.497E-06	5.838E-02	5.263E-06	5.820E-02	7.713E+51	5.838E-02

C.7 DDPC1

Table C.19: The same as Table 5.2, using the DDPC1 model with $B_\star = 2000$

№	P_{min}	P_{max}	ϵ_{min}	ϵ_{max}	$n_{b_{min}}$	$n_{b_{max}}$	A	Z	N	Z/A	$\mu_{b_{min}}$	$\mu_{b_{max}}$	$\mu_{e_{min}}$	$\mu_{e_{max}}$
1	6.082E-15	3.136E-07	2.271E-03	4.693E-03	2.441E-06	5.044E-06	56	26	30	0.464	930.340	930.420	0.608	0.851
2	3.141E-07	1.227E-05	4.872E-03	2.061E-02	5.237E-06	2.215E-05	62	28	34	0.452	930.420	931.271	0.856	2.949
3	1.229E-05	2.680E-05	2.182E-02	3.130E-02	2.345E-05	3.362E-05	88	38	50	0.432	931.271	931.779	2.985	4.248
4	2.684E-05	7.056E-05	3.226E-02	5.115E-02	3.465E-05	5.492E-05	86	36	50	0.419	931.781	932.756	4.243	6.696
5	7.066E-05	1.461E-04	5.288E-02	7.526E-02	5.676E-05	8.074E-05	84	34	50	0.405	932.758	933.855	6.692	9.505
6	1.463E-04	1.893E-04	7.804E-02	8.854E-02	8.372E-05	9.497E-05	82	32	50	0.390	933.857	934.339	9.502	10.775
7	1.896E-04	2.418E-04	9.122E-02	1.028E-01	9.783E-05	1.102E-04	74	28	46	0.378	934.342	934.843	10.762	12.122
8	2.422E-04	2.920E-04	1.057E-01	1.159E-01	1.133E-04	1.242E-04	76	28	48	0.368	934.847	935.266	12.131	13.298
9	2.924E-04	4.755E-04	1.197E-01	1.520E-01	1.283E-04	1.629E-04	128	46	82	0.359	935.270	936.527	13.400	17.005
10	4.762E-04	5.844E-04	1.565E-01	1.732E-01	1.676E-04	1.854E-04	126	44	82	0.349	936.531	937.145	17.007	18.808
11	5.853E-04	7.047E-04	1.786E-01	1.957E-01	1.912E-04	2.095E-04	124	42	82	0.339	937.149	937.745	18.811	20.613
12	7.057E-04	8.485E-04	2.023E-01	2.216E-01	2.164E-04	2.370E-04	122	40	82	0.328	937.750	938.379	20.616	22.577
13	8.497E-04	1.031E-03	2.295E-01	2.526E-01	2.455E-04	2.701E-04	120	38	82	0.317	938.385	939.086	22.582	24.841
14	1.032E-03	1.168E-03	2.623E-01	2.789E-01	2.804E-04	2.981E-04	118	36	82	0.305	939.092	939.562	24.847	26.415

Table C.20: The same as Table 5.3, using the DDPC1 model with $B_\star = 2000$

M_{cr}	M_{cr}/M	ΔR_{cr}	$\Delta R_{cr}/R$	$M_{b_{cr}}$	Δ_{grav}	z_{drip}	ΔN
9.190E-05	6.564E-05	4.753E-01	3.802E-02	1.131E-04	2.306E-01	5.838E-01	1.343E+53

Table C.21: The same as Table 5.4, using the DDPC1 model with $B_\star = 2000$

№	r_{min}	r_{max}	ΔR_l	$\Delta R_l/\Delta R_{cr}$	z_l	z_l/z_{drip}	M_{b_l}	$M_{b_l}/M_{b_{cr}}$	M_l	M_l/M_{cr}	ΔN_l	$\Delta N_l/\Delta N$
1	12.496	12.500	4.374E-03	9.203E-03	0.005	9.158E-03	3.409E-08	3.014E-04	2.788E-08	3.034E-04	4.047E+49	3.014E-04
2	12.450	12.496	4.596E-02	9.669E-02	0.062	1.054E-01	1.287E-06	1.138E-02	1.052E-06	1.145E-02	1.528E+51	1.138E-02
3	12.422	12.450	2.723E-02	5.729E-02	0.095	1.626E-01	1.543E-06	1.364E-02	1.261E-06	1.372E-02	1.832E+51	1.364E-02
4	12.370	12.422	5.183E-02	1.091E-01	0.159	2.715E-01	4.583E-06	4.053E-02	3.742E-06	4.071E-02	5.441E+51	4.053E-02
5	12.313	12.370	5.758E-02	1.211E-01	0.229	3.927E-01	7.757E-06	6.859E-02	6.326E-06	6.883E-02	9.209E+51	6.859E-02
6	12.288	12.313	2.505E-02	5.270E-02	0.260	4.456E-01	4.363E-06	3.858E-02	3.555E-06	3.868E-02	5.180E+51	3.858E-02
7	12.262	12.287	2.594E-02	5.458E-02	0.292	5.005E-01	5.243E-06	4.636E-02	4.270E-06	4.646E-02	6.224E+51	4.636E-02
8	12.240	12.261	2.158E-02	4.541E-02	0.319	5.463E-01	4.964E-06	4.389E-02	4.041E-06	4.397E-02	5.893E+51	4.389E-02
9	12.176	12.240	6.406E-02	1.348E-01	0.398	6.816E-01	1.796E-05	1.588E-01	1.460E-05	1.589E-01	2.132E+52	1.588E-01
10	12.144	12.175	3.090E-02	6.501E-02	0.436	7.472E-01	1.044E-05	9.230E-02	8.481E-06	9.228E-02	1.239E+52	9.230E-02
11	12.114	12.144	2.982E-02	6.275E-02	0.473	8.106E-01	1.139E-05	1.007E-01	9.248E-06	1.006E-01	1.352E+52	1.007E-01
12	12.083	12.114	3.127E-02	6.579E-02	0.512	8.771E-01	1.347E-05	1.191E-01	1.092E-05	1.189E-01	1.599E+52	1.191E-01
13	12.048	12.083	3.460E-02	7.280E-02	0.555	9.507E-01	1.686E-05	1.491E-01	1.367E-05	1.488E-01	2.002E+52	1.491E-01
14	12.025	12.048	2.303E-02	4.845E-02	0.584	1.000E+00	1.255E-05	1.109E-01	1.017E-05	1.106E-01	1.490E+52	1.109E-01

C.8 SVMIN

Table C.22: The same as Table 5.2, using the SVMIN model with $B_\star = 2000$

№	P_{min}	P_{max}	ϵ_{min}	ϵ_{max}	$n_{b_{min}}$	$n_{b_{max}}$	A	Z	N	Z/A	$\mu_{b_{min}}$	$\mu_{b_{max}}$	$\mu_{e_{min}}$	$\mu_{e_{max}}$
1	6.082E-15	3.136E-07	2.271E-03	4.693E-03	2.441E-06	5.044E-06	56	26	30	0.464	930.340	930.420	0.608	0.851
2	3.141E-07	1.227E-05	4.872E-03	2.061E-02	5.237E-06	2.215E-05	62	28	34	0.452	930.420	931.271	0.856	2.949
3	1.229E-05	2.680E-05	2.182E-02	3.130E-02	2.345E-05	3.362E-05	88	38	50	0.432	931.271	931.779	2.985	4.248
4	2.684E-05	7.056E-05	3.226E-02	5.115E-02	3.465E-05	5.492E-05	86	36	50	0.419	931.781	932.756	4.243	6.696
5	7.066E-05	1.461E-04	5.288E-02	7.526E-02	5.676E-05	8.074E-05	84	34	50	0.405	932.758	933.855	6.692	9.505
6	1.463E-04	2.436E-04	7.804E-02	1.002E-01	8.372E-05	1.074E-04	82	32	50	0.390	933.857	934.875	9.502	12.188
7	2.439E-04	2.580E-04	1.041E-01	1.069E-01	1.116E-04	1.147E-04	132	50	82	0.379	934.878	935.002	12.283	12.623
8	2.584E-04	3.423E-04	1.073E-01	1.232E-01	1.150E-04	1.321E-04	80	30	50	0.375	935.006	935.685	12.534	14.391
9	3.429E-04	4.833E-04	1.294E-01	1.533E-01	1.387E-04	1.642E-04	128	46	82	0.359	935.689	936.616	14.485	17.141
10	4.840E-04	5.844E-04	1.578E-01	1.732E-01	1.690E-04	1.854E-04	126	44	82	0.349	936.621	937.188	17.143	18.808
11	5.853E-04	7.026E-04	1.786E-01	1.955E-01	1.912E-04	2.092E-04	124	42	82	0.339	937.192	937.778	18.811	20.583
12	7.037E-04	8.738E-04	2.020E-01	2.249E-01	2.161E-04	2.405E-04	122	40	82	0.328	937.783	938.528	20.586	22.908
13	8.751E-04	1.004E-03	2.329E-01	2.493E-01	2.491E-04	2.665E-04	120	38	82	0.317	938.534	939.032	22.913	24.518
14	1.005E-03	1.126E-03	2.536E-01	2.683E-01	2.712E-04	2.868E-04	122	38	84	0.311	939.038	939.470	24.535	25.951
15	1.128E-03	1.153E-03	2.774E-01	2.804E-01	2.964E-04	2.997E-04	126	38	88	0.302	939.476	939.561	25.970	26.255

Table C.23: The same as Table 5.3, using the SVMIN model with $B_\star = 2000$

M_{cr}	M_{cr}/M	ΔR_{cr}	$\Delta R_{cr}/R$	$M_{b_{cr}}$	Δ_{grav}	z_{drip}	ΔN
9.070E-05	6.478E-05	4.752E-01	3.802E-02	1.116E-04	2.306E-01	5.837E-01	1.325E+53

Table C.24: The same as Table 5.4, using the SVMIN model with $B_\star = 2000$

№	r_{min}	r_{max}	ΔR_l	$\Delta R_l/\Delta R_{cr}$	z_l	z_l/z_{drip}	M_{b_l}	$M_{b_l}/M_{b_{cr}}$	M_l	M_l/M_{cr}	ΔN_l	$\Delta N_l/\Delta N$
1	12.496	12.500	4.374E-03	9.204E-03	0.005	9.160E-03	3.409E-08	3.054E-04	2.788E-08	3.074E-04	4.047E+49	3.054E-04
2	12.450	12.496	4.596E-02	9.670E-02	0.062	1.055E-01	1.287E-06	1.153E-02	1.052E-06	1.160E-02	1.528E+51	1.153E-02
3	12.422	12.450	2.723E-02	5.730E-02	0.095	1.626E-01	1.543E-06	1.382E-02	1.261E-06	1.390E-02	1.832E+51	1.382E-02
4	12.370	12.422	5.183E-02	1.091E-01	0.159	2.715E-01	4.583E-06	4.106E-02	3.742E-06	4.125E-02	5.441E+51	4.106E-02
5	12.313	12.370	5.758E-02	1.212E-01	0.229	3.927E-01	7.757E-06	6.950E-02	6.326E-06	6.974E-02	9.209E+51	6.950E-02
6	12.260	12.313	5.277E-02	1.110E-01	0.294	5.040E-01	9.812E-06	8.791E-02	7.992E-06	8.812E-02	1.165E+52	8.791E-02
7	12.253	12.260	6.395E-03	1.346E-02	0.302	5.178E-01	1.402E-06	1.256E-02	1.141E-06	1.258E-02	1.665E+51	1.256E-02
8	12.218	12.253	3.485E-02	7.333E-02	0.345	5.915E-01	8.321E-06	7.455E-02	6.771E-06	7.465E-02	9.879E+51	7.455E-02
9	12.171	12.218	4.710E-02	9.910E-02	0.403	6.912E-01	1.371E-05	1.228E-01	1.115E-05	1.229E-01	1.628E+52	1.228E-01
10	12.142	12.171	2.854E-02	6.006E-02	0.439	7.518E-01	9.676E-06	8.670E-02	7.861E-06	8.667E-02	1.149E+52	8.670E-02
11	12.113	12.142	2.931E-02	6.168E-02	0.475	8.142E-01	1.118E-05	1.002E-01	9.080E-06	1.001E-01	1.328E+52	1.002E-01
12	12.075	12.112	3.699E-02	7.784E-02	0.521	8.928E-01	1.603E-05	1.436E-01	1.300E-05	1.434E-01	1.903E+52	1.436E-01
13	12.051	12.075	2.457E-02	5.169E-02	0.552	9.453E-01	1.197E-05	1.073E-01	9.706E-06	1.070E-01	1.421E+52	1.073E-01
14	12.029	12.050	2.121E-02	4.464E-02	0.578	9.907E-01	1.115E-05	9.994E-02	9.039E-06	9.966E-02	1.324E+52	9.994E-02
15	12.025	12.029	4.130E-03	8.691E-03	0.584	1.000E+00	2.316E-06	2.075E-02	1.877E-06	2.069E-02	2.750E+51	2.075E-02

C.9 UNEDF0

Table C.25: The same as Table 5.2, using the UNEDF0 model with $B_\star = 2000$

№	P_{min}	P_{max}	ϵ_{min}	ϵ_{max}	$n_{b_{min}}$	$n_{b_{max}}$	A	Z	N	Z/A	$\mu_{b_{min}}$	$\mu_{b_{max}}$	$\mu_{e_{min}}$	$\mu_{e_{max}}$
1	6.082E-15	3.136E-07	2.271E-03	4.693E-03	2.441E-06	5.044E-06	56	26	30	0.464	930.340	930.420	0.608	0.851
2	3.141E-07	1.227E-05	4.872E-03	2.061E-02	5.237E-06	2.215E-05	62	28	34	0.452	930.420	931.271	0.856	2.949
3	1.229E-05	2.680E-05	2.182E-02	3.130E-02	2.345E-05	3.362E-05	88	38	50	0.432	931.271	931.779	2.985	4.248
4	2.684E-05	7.056E-05	3.226E-02	5.115E-02	3.465E-05	5.492E-05	86	36	50	0.419	931.781	932.756	4.243	6.696
5	7.066E-05	1.461E-04	5.288E-02	7.526E-02	5.676E-05	8.074E-05	84	34	50	0.405	932.758	933.855	6.692	9.505
6	1.463E-04	2.436E-04	7.804E-02	1.002E-01	8.372E-05	1.074E-04	82	32	50	0.390	933.857	934.875	9.502	12.188
7	2.439E-04	2.580E-04	1.041E-01	1.069E-01	1.116E-04	1.147E-04	132	50	82	0.379	934.878	935.002	12.283	12.623
8	2.584E-04	3.393E-04	1.073E-01	1.227E-01	1.150E-04	1.315E-04	80	30	50	0.375	935.006	935.663	12.534	14.329
9	3.398E-04	3.510E-04	1.249E-01	1.269E-01	1.338E-04	1.360E-04	76	28	48	0.368	935.666	935.749	14.328	14.558
10	3.515E-04	3.531E-04	1.303E-01	1.306E-01	1.397E-04	1.400E-04	78	28	50	0.359	935.753	935.764	14.568	14.600
11	3.536E-04	4.883E-04	1.314E-01	1.541E-01	1.408E-04	1.650E-04	128	46	82	0.359	935.768	936.649	14.706	17.228
12	4.890E-04	5.827E-04	1.580E-01	1.724E-01	1.692E-04	1.845E-04	86	30	56	0.349	936.653	937.183	17.152	18.701
13	5.836E-04	6.537E-04	1.765E-01	1.867E-01	1.890E-04	1.999E-04	88	30	58	0.341	937.187	937.548	18.715	19.793
14	6.547E-04	7.141E-04	1.910E-01	1.994E-01	2.044E-04	2.134E-04	84	28	56	0.333	937.553	937.837	19.795	20.664
15	7.152E-04	8.130E-04	2.043E-01	2.178E-01	2.186E-04	2.329E-04	86	28	58	0.326	937.842	938.275	20.679	22.032
16	8.142E-04	9.406E-04	2.230E-01	2.396E-01	2.385E-04	2.562E-04	88	28	60	0.318	938.280	938.792	22.048	23.681
17	9.420E-04	1.058E-03	2.452E-01	2.598E-01	2.622E-04	2.778E-04	90	28	62	0.311	938.797	939.228	23.698	25.104
18	1.060E-03	1.109E-03	2.719E-01	2.781E-01	2.906E-04	2.973E-04	134	40	94	0.299	939.233	939.402	25.199	25.775
19	1.111E-03	1.114E-03	2.825E-01	2.829E-01	3.019E-04	3.024E-04	136	40	96	0.294	939.407	939.418	25.794	25.831
20	1.116E-03	1.139E-03	2.871E-01	2.901E-01	3.068E-04	3.100E-04	172	50	122	0.291	939.423	939.499	25.909	26.174
21	1.141E-03	1.160E-03	2.937E-01	2.961E-01	3.138E-04	3.163E-04	174	50	124	0.287	939.504	939.563	26.193	26.404

Table C.26: The same as Table 5.3, using the UNEDF0 model with $B_\star = 2000$

M_{cr}	M_{cr}/M	ΔR_{cr}	$\Delta R_{cr}/R$	$M_{b_{cr}}$	Δ_{grav}	z_{drip}	ΔN
9.121E-05	6.515E-05	4.754E-01	3.803E-02	1.122E-04	2.306E-01	5.839E-01	1.333E+53

Table C.27: The same as Table 5.4, using the UNEDF0 model with $B_\star = 2000$

№	r_{min}	r_{max}	ΔR_l	$\Delta R_l/\Delta R_{cr}$	z_l	z_l/z_{drip}	M_{b_l}	$M_{b_l}/M_{b_{cr}}$	M_l	M_l/M_{cr}	ΔN_l	$\Delta N_l/\Delta N$
1	12.496	12.500	4.374E-03	9.201E-03	0.005	9.157E-03	3.409E-08	3.037E-04	2.788E-08	3.057E-04	4.047E+49	3.037E-04
2	12.450	12.496	4.596E-02	9.668E-02	0.062	1.054E-01	1.287E-06	1.146E-02	1.052E-06	1.153E-02	1.528E+51	1.146E-02
3	12.422	12.450	2.723E-02	5.729E-02	0.095	1.626E-01	1.543E-06	1.375E-02	1.261E-06	1.382E-02	1.832E+51	1.375E-02
4	12.370	12.422	5.183E-02	1.090E-01	0.159	2.715E-01	4.583E-06	4.083E-02	3.742E-06	4.102E-02	5.441E+51	4.083E-02
5	12.313	12.370	5.758E-02	1.211E-01	0.229	3.926E-01	7.757E-06	6.911E-02	6.326E-06	6.935E-02	9.209E+51	6.911E-02
6	12.260	12.313	5.277E-02	1.110E-01	0.294	5.038E-01	9.812E-06	8.742E-02	7.992E-06	8.763E-02	1.165E+52	8.742E-02
7	12.253	12.260	6.395E-03	1.345E-02	0.302	5.177E-01	1.402E-06	1.249E-02	1.141E-06	1.251E-02	1.665E+51	1.249E-02
8	12.219	12.253	3.368E-02	7.085E-02	0.344	5.889E-01	8.024E-06	7.149E-02	6.529E-06	7.159E-02	9.526E+51	7.149E-02
9	12.215	12.219	4.236E-03	8.911E-03	0.349	5.982E-01	1.102E-06	9.819E-03	8.964E-07	9.828E-03	1.308E+51	9.819E-03
10	12.214	12.215	5.667E-04	1.192E-03	0.350	5.998E-01	1.528E-07	1.361E-03	1.242E-07	1.362E-03	1.814E+50	1.361E-03
11	12.169	12.214	4.470E-02	9.403E-02	0.405	6.944E-01	1.314E-05	1.170E-01	1.068E-05	1.171E-01	1.559E+52	1.170E-01
12	12.143	12.169	2.667E-02	5.610E-02	0.439	7.511E-01	9.025E-06	8.041E-02	7.331E-06	8.038E-02	1.071E+52	8.041E-02
13	12.124	12.142	1.806E-02	3.799E-02	0.461	7.897E-01	6.698E-06	5.967E-02	5.438E-06	5.962E-02	7.952E+51	5.967E-02
14	12.110	12.124	1.420E-02	2.987E-02	0.479	8.201E-01	5.647E-06	5.031E-02	4.583E-06	5.025E-02	6.704E+51	5.031E-02
15	12.088	12.110	2.152E-02	4.528E-02	0.506	8.661E-01	9.230E-06	8.223E-02	7.489E-06	8.210E-02	1.096E+52	8.223E-02
16	12.062	12.088	2.526E-02	5.315E-02	0.537	9.200E-01	1.183E-05	1.054E-01	9.596E-06	1.052E-01	1.405E+52	1.054E-01
17	12.041	12.062	2.117E-02	4.453E-02	0.564	9.653E-01	1.079E-05	9.612E-02	8.744E-06	9.587E-02	1.281E+52	9.612E-02
18	12.033	12.041	8.254E-03	1.736E-02	0.574	9.833E-01	4.571E-06	4.073E-02	3.704E-06	4.061E-02	5.427E+51	4.073E-02
19	12.032	12.032	5.301E-04	1.115E-03	0.575	9.850E-01	3.016E-07	2.687E-03	2.443E-07	2.679E-03	3.580E+50	2.687E-03
20	12.028	12.031	3.687E-03	7.755E-03	0.580	9.933E-01	2.141E-06	1.907E-02	1.734E-06	1.901E-02	2.541E+51	1.907E-02
21	12.025	12.028	2.892E-03	6.084E-03	0.584	1.000E+00	1.715E-06	1.528E-02	1.389E-06	1.523E-02	2.036E+51	1.528E-02

Appendix D

Tables for $B_\star = 2500$

Below are the Tables, like those in Subsections 5.4.1 - 5.4.2, for the models: SEMF, FRDM2012, WS4RBF, BSKG3, HFB31, DDMED, DDPC1, SVMIN and UNEDF0, with magnetic field strength $B_\star = 2500$.

D.1 SEMF

Table D.1: The same as Table 5.2, using the SEMF model with $B_\star = 2500$

№	P_{min}	P_{max}	ϵ_{min}	ϵ_{max}	$n_{b_{min}}$	$n_{b_{max}}$	A	Z	N	Z/A	$\mu_{b_{min}}$	$\mu_{b_{max}}$	$\mu_{e_{min}}$	$\mu_{e_{max}}$
1	6.082E-15	3.549E-07	2.986E-03	5.776E-03	3.210E-06	6.209E-06	56	26	30	0.464	930.333	930.406	0.617	0.842
2	3.554E-07	1.412E-05	6.004E-03	2.490E-02	6.453E-06	2.676E-05	62	28	34	0.452	930.406	931.211	0.848	2.854
3	1.414E-05	3.535E-05	2.640E-02	4.028E-02	2.837E-05	4.327E-05	88	38	50	0.432	931.212	931.804	2.892	4.371
4	3.541E-05	9.131E-05	4.151E-02	6.519E-02	4.458E-05	6.998E-05	86	36	50	0.419	931.805	932.780	4.366	6.825
5	9.144E-05	1.874E-04	6.738E-02	9.545E-02	7.233E-05	1.024E-04	84	34	50	0.405	932.782	933.880	6.821	9.644
6	1.877E-04	2.802E-04	9.897E-02	1.204E-01	1.062E-04	1.291E-04	82	32	50	0.390	933.882	934.669	9.640	11.720
7	2.806E-04	4.353E-04	1.252E-01	1.552E-01	1.342E-04	1.663E-04	132	50	82	0.379	934.672	935.701	11.822	14.642
8	4.359E-04	6.460E-04	1.592E-01	1.932E-01	1.706E-04	2.069E-04	130	48	82	0.369	935.705	936.818	14.643	17.754
9	6.470E-04	1.022E-03	1.963E-01	2.459E-01	2.102E-04	2.632E-04	132	48	84	0.364	936.823	938.405	17.767	22.239
10	1.023E-03	1.032E-03	2.684E-01	2.696E-01	2.871E-04	2.884E-04	138	46	92	0.333	938.411	938.442	22.243	22.340
11	1.034E-03	1.035E-03	2.700E-01	2.702E-01	2.888E-04	2.890E-04	144	48	96	0.333	938.448	938.453	22.369	22.385
12	1.037E-03	1.118E-03	2.741E-01	2.845E-01	2.932E-04	3.043E-04	146	48	98	0.329	938.458	938.729	22.401	23.246
13	1.119E-03	1.187E-03	2.886E-01	2.972E-01	3.086E-04	3.177E-04	148	48	100	0.324	938.734	938.951	23.263	23.948
14	1.189E-03	1.257E-03	3.011E-01	3.095E-01	3.219E-04	3.309E-04	156	50	106	0.321	938.957	939.166	23.978	24.648
15	1.259E-03	1.332E-03	3.138E-01	3.226E-01	3.354E-04	3.448E-04	158	50	108	0.316	939.172	939.385	24.666	25.356
16	1.334E-03	1.368E-03	3.263E-01	3.304E-01	3.488E-04	3.531E-04	166	52	114	0.313	939.391	939.487	25.387	25.702
17	1.370E-03	1.388E-03	3.312E-01	3.334E-01	3.540E-04	3.564E-04	160	50	110	0.312	939.493	939.544	25.709	25.877
18	1.390E-03	1.394E-03	3.370E-01	3.375E-01	3.602E-04	3.607E-04	168	52	116	0.310	939.550	939.561	25.909	25.946

Table D.2: The same as Table 5.3, using the SEMF model with $B_\star = 2500$

M_{cr}	M_{cr}/M	ΔR_{cr}	$\Delta R_{cr}/R$	$M_{b_{cr}}$	Δ_{grav}	z_{drip}	ΔN
1.098E-04	7.842E-05	4.756E-01	3.805E-02	1.351E-04	2.305E-01	5.842E-01	1.604E+53

Table D.3: The same as Table 5.4, using the SEMF model with $B_\star = 2500$

№	r_{min}	r_{max}	ΔR_l	$\Delta R_l/\Delta R_{cr}$	z_l	z_l/z_{drip}	M_{b_l}	$M_{b_l}/M_{b_{cr}}$	M_l	M_l/M_{cr}	ΔN_l	$\Delta N_l/\Delta N$
1	12.496	12.500	3.955E-03	8.315E-03	0.005	8.275E-03	3.857E-08	2.855E-04	3.155E-08	2.874E-04	4.579E+49	2.855E-04
2	12.452	12.496	4.355E-02	9.158E-02	0.058	9.947E-02	1.482E-06	1.097E-02	1.211E-06	1.104E-02	1.759E+51	1.097E-02
3	12.421	12.452	3.172E-02	6.669E-02	0.097	1.660E-01	2.256E-06	1.670E-02	1.843E-06	1.679E-02	2.679E+51	1.670E-02
4	12.369	12.421	5.180E-02	1.089E-01	0.161	2.748E-01	5.857E-06	4.336E-02	4.781E-06	4.355E-02	6.954E+51	4.336E-02
5	12.311	12.369	5.762E-02	1.211E-01	0.231	3.959E-01	9.862E-06	7.300E-02	8.042E-06	7.325E-02	1.171E+52	7.300E-02
6	12.270	12.311	4.080E-02	8.580E-02	0.282	4.820E-01	9.347E-06	6.919E-02	7.614E-06	6.936E-02	1.110E+52	6.919E-02
7	12.217	12.270	5.287E-02	1.112E-01	0.347	5.935E-01	1.537E-05	1.138E-01	1.251E-05	1.139E-01	1.824E+52	1.138E-01
8	12.161	12.217	5.646E-02	1.187E-01	0.416	7.128E-01	2.047E-05	1.515E-01	1.664E-05	1.516E-01	2.430E+52	1.515E-01
9	12.081	12.160	7.902E-02	1.662E-01	0.514	8.799E-01	3.560E-05	2.635E-01	2.890E-05	2.632E-01	4.226E+52	2.635E-01
10	12.079	12.081	1.561E-03	3.282E-03	0.516	8.838E-01	8.509E-07	6.299E-03	6.901E-07	6.286E-03	1.010E+51	6.299E-03
11	12.079	12.079	2.601E-04	5.469E-04	0.517	8.849E-01	1.423E-07	1.054E-03	1.154E-07	1.051E-03	1.690E+50	1.054E-03
12	12.065	12.079	1.337E-02	2.812E-02	0.534	9.137E-01	7.560E-06	5.596E-02	6.130E-06	5.584E-02	8.975E+51	5.596E-02
13	12.054	12.065	1.068E-02	2.246E-02	0.547	9.368E-01	6.322E-06	4.680E-02	5.125E-06	4.668E-02	7.505E+51	4.680E-02
14	12.044	12.054	1.030E-02	2.166E-02	0.560	9.591E-01	6.345E-06	4.697E-02	5.143E-06	4.685E-02	7.533E+51	4.697E-02
15	12.033	12.043	1.045E-02	2.197E-02	0.574	9.818E-01	6.696E-06	4.957E-02	5.426E-06	4.942E-02	7.949E+51	4.957E-02
16	12.028	12.033	4.714E-03	9.912E-03	0.580	9.923E-01	3.114E-06	2.305E-02	2.523E-06	2.298E-02	3.697E+51	2.305E-02
17	12.025	12.028	2.514E-03	5.286E-03	0.583	9.982E-01	1.680E-06	1.244E-02	1.361E-06	1.240E-02	1.995E+51	1.244E-02
18	12.024	12.025	5.547E-04	1.166E-03	0.584	1.000E+00	3.761E-07	2.784E-03	3.047E-07	2.775E-03	4.466E+50	2.784E-03

D.2 FRDM2012

Table D.4: The same as Table 5.2, using the FRDM2012 model with $B_\star = 2500$

№	P_{min}	P_{max}	ϵ_{min}	ϵ_{max}	$n_{b_{min}}$	$n_{b_{max}}$	A	Z	N	Z/A	$\mu_{b_{min}}$	$\mu_{b_{max}}$	$\mu_{e_{min}}$	$\mu_{e_{max}}$
1	6.082E-15	3.549E-07	2.986E-03	5.776E-03	3.210E-06	6.209E-06	56	26	30	0.464	930.333	930.406	0.617	0.842
2	3.554E-07	1.412E-05	6.004E-03	2.490E-02	6.453E-06	2.676E-05	62	28	34	0.452	930.406	931.211	0.848	2.854
3	1.414E-05	3.535E-05	2.640E-02	4.028E-02	2.837E-05	4.327E-05	88	38	50	0.432	931.212	931.804	2.892	4.371
4	3.541E-05	9.131E-05	4.151E-02	6.519E-02	4.458E-05	6.998E-05	86	36	50	0.419	931.805	932.780	4.366	6.825
5	9.144E-05	1.874E-04	6.738E-02	9.545E-02	7.233E-05	1.024E-04	84	34	50	0.405	932.782	933.880	6.821	9.644
6	1.877E-04	2.802E-04	9.897E-02	1.204E-01	1.062E-04	1.291E-04	82	32	50	0.390	933.882	934.669	9.640	11.720
7	2.806E-04	4.189E-04	1.252E-01	1.523E-01	1.342E-04	1.632E-04	132	50	82	0.379	934.672	935.602	11.822	14.371
8	4.195E-04	5.896E-04	1.604E-01	1.896E-01	1.719E-04	2.031E-04	128	46	82	0.359	935.606	936.513	14.361	16.965
9	5.905E-04	7.541E-04	1.952E-01	2.202E-01	2.090E-04	2.357E-04	126	44	82	0.349	936.517	937.253	16.966	19.132
10	7.552E-04	9.255E-04	2.271E-01	2.511E-01	2.431E-04	2.687E-04	124	42	82	0.339	937.257	937.923	19.134	21.149
11	9.269E-04	1.129E-03	2.594E-01	2.861E-01	2.776E-04	3.060E-04	122	40	82	0.328	937.928	938.621	21.152	23.314
12	1.131E-03	1.374E-03	2.963E-01	3.263E-01	3.169E-04	3.488E-04	120	38	82	0.317	938.627	939.356	23.318	25.669
13	1.376E-03	1.448E-03	3.388E-01	3.476E-01	3.621E-04	3.715E-04	118	36	82	0.305	939.362	939.560	25.674	26.337

Table D.5: The same as Table 5.3, using the FRDM2012 model with $B_\star = 2500$

M_{cr}	M_{cr}/M	ΔR_{cr}	$\Delta R_{cr}/R$	$M_{b_{cr}}$	Δ_{grav}	z_{drip}	ΔN
1.140E-04	8.141E-05	4.755E-01	3.804E-02	1.403E-04	2.306E-01	5.841E-01	1.665E+53

Table D.6: The same as Table 5.4, using the FRDM2012 model with $B_\star = 2500$

№	r_{min}	r_{max}	ΔR_l	$\Delta R_l/\Delta R_{cr}$	z_l	z_l/z_{drip}	M_{b_l}	$M_{b_l}/M_{b_{cr}}$	M_l	M_l/M_{cr}	ΔN_l	$\Delta N_l/\Delta N$
1	12.496	12.500	3.955E-03	8.316E-03	0.005	8.276E-03	3.857E-08	2.750E-04	3.155E-08	2.768E-04	4.579E+49	2.750E-04
2	12.452	12.496	4.355E-02	9.159E-02	0.058	9.948E-02	1.482E-06	1.056E-02	1.211E-06	1.063E-02	1.759E+51	1.056E-02
3	12.421	12.452	3.172E-02	6.670E-02	0.097	1.660E-01	2.256E-06	1.609E-02	1.843E-06	1.617E-02	2.679E+51	1.609E-02
4	12.369	12.421	5.180E-02	1.089E-01	0.161	2.748E-01	5.857E-06	4.176E-02	4.781E-06	4.195E-02	6.954E+51	4.176E-02
5	12.311	12.369	5.762E-02	1.212E-01	0.231	3.960E-01	9.862E-06	7.031E-02	8.042E-06	7.055E-02	1.171E+52	7.031E-02
6	12.270	12.311	4.080E-02	8.581E-02	0.282	4.820E-01	9.347E-06	6.664E-02	7.614E-06	6.680E-02	1.110E+52	6.664E-02
7	12.222	12.270	4.779E-02	1.005E-01	0.340	5.829E-01	1.376E-05	9.807E-02	1.120E-05	9.822E-02	1.633E+52	9.807E-02
8	12.176	12.222	4.612E-02	9.698E-02	0.397	6.804E-01	1.663E-05	1.186E-01	1.352E-05	1.187E-01	1.975E+52	1.186E-01
9	12.139	12.176	3.705E-02	7.791E-02	0.443	7.589E-01	1.576E-05	1.124E-01	1.281E-05	1.124E-01	1.872E+52	1.124E-01
10	12.105	12.138	3.324E-02	6.991E-02	0.485	8.295E-01	1.620E-05	1.155E-01	1.315E-05	1.154E-01	1.923E+52	1.155E-01
11	12.071	12.105	3.436E-02	7.226E-02	0.527	9.026E-01	1.901E-05	1.356E-01	1.542E-05	1.353E-01	2.257E+52	1.356E-01
12	12.034	12.070	3.586E-02	7.540E-02	0.572	9.789E-01	2.253E-05	1.606E-01	1.826E-05	1.602E-01	2.675E+52	1.606E-01
13	12.024	12.034	9.706E-03	2.041E-02	0.584	1.000E+00	6.701E-06	4.778E-02	5.429E-06	4.763E-02	7.956E+51	4.778E-02

D.3 WS4RBF

Table D.7: The same as Table 5.2, using the WS4RBF model with $B_\star = 2500$

№	P_{min}	P_{max}	ϵ_{min}	ϵ_{max}	$n_{b_{min}}$	$n_{b_{max}}$	A	Z	N	Z/A	$\mu_{b_{min}}$	$\mu_{b_{max}}$	$\mu_{e_{min}}$	$\mu_{e_{max}}$
1	6.082E-15	3.549E-07	2.986E-03	5.776E-03	3.210E-06	6.209E-06	56	26	30	0.464	930.333	930.406	0.617	0.842
2	3.554E-07	1.412E-05	6.004E-03	2.490E-02	6.453E-06	2.676E-05	62	28	34	0.452	930.406	931.211	0.848	2.854
3	1.414E-05	3.535E-05	2.640E-02	4.028E-02	2.837E-05	4.327E-05	88	38	50	0.432	931.212	931.804	2.892	4.371
4	3.541E-05	9.131E-05	4.151E-02	6.519E-02	4.458E-05	6.998E-05	86	36	50	0.419	931.805	932.780	4.366	6.825
5	9.144E-05	1.874E-04	6.738E-02	9.545E-02	7.233E-05	1.024E-04	84	34	50	0.405	932.782	933.880	6.821	9.644
6	1.877E-04	2.802E-04	9.897E-02	1.204E-01	1.062E-04	1.291E-04	82	32	50	0.390	933.882	934.669	9.640	11.720
7	2.806E-04	4.353E-04	1.252E-01	1.552E-01	1.342E-04	1.663E-04	132	50	82	0.379	934.672	935.701	11.822	14.642
8	4.359E-04	5.241E-04	1.592E-01	1.743E-01	1.706E-04	1.867E-04	130	48	82	0.369	935.705	936.198	14.643	16.024
9	5.248E-04	6.883E-04	1.791E-01	2.046E-01	1.918E-04	2.191E-04	128	46	82	0.359	936.202	936.998	16.024	18.304
10	6.893E-04	8.397E-04	2.106E-01	2.322E-01	2.255E-04	2.485E-04	126	44	82	0.349	937.002	937.637	18.305	20.172
11	8.410E-04	1.004E-03	2.395E-01	2.613E-01	2.563E-04	2.796E-04	124	42	82	0.339	937.642	938.249	20.174	22.010
12	1.005E-03	1.352E-03	2.701E-01	3.128E-01	2.889E-04	3.344E-04	122	40	82	0.328	938.254	939.366	22.014	25.478
13	1.354E-03	1.421E-03	3.239E-01	3.319E-01	3.463E-04	3.547E-04	120	38	82	0.317	939.371	939.564	25.483	26.102

Table D.8: The same as Table 5.3, using the WS4RBF model with $B_\star = 2500$

M_{cr}	M_{cr}/M	ΔR_{cr}	$\Delta R_{cr}/R$	$M_{b_{cr}}$	Δ_{grav}	z_{drip}	ΔN
1.119E-04	7.990E-05	4.757E-01	3.806E-02	1.377E-04	2.306E-01	5.844E-01	1.634E+53

Table D.9: The same as Table 5.4, using the WS4RBF model with $B_\star = 2500$

№	r_{min}	r_{max}	ΔR_l	$\Delta R_l/\Delta R_{cr}$	z_l	z_l/z_{drip}	M_{b_l}	$M_{b_l}/M_{b_{cr}}$	M_l	M_l/M_{cr}	ΔN_l	$\Delta N_l/\Delta N$
1	12.496	12.500	3.955E-03	8.312E-03	0.005	8.273E-03	3.857E-08	2.802E-04	3.155E-08	2.821E-04	4.579E+49	2.802E-04
2	12.452	12.496	4.355E-02	9.155E-02	0.058	9.944E-02	1.482E-06	1.076E-02	1.211E-06	1.083E-02	1.759E+51	1.076E-02
3	12.421	12.452	3.172E-02	6.667E-02	0.097	1.660E-01	2.256E-06	1.639E-02	1.843E-06	1.648E-02	2.679E+51	1.639E-02
4	12.369	12.421	5.180E-02	1.089E-01	0.161	2.747E-01	5.857E-06	4.255E-02	4.781E-06	4.274E-02	6.954E+51	4.255E-02
5	12.311	12.369	5.762E-02	1.211E-01	0.231	3.958E-01	9.862E-06	7.164E-02	8.042E-06	7.189E-02	1.171E+52	7.164E-02
6	12.270	12.311	4.080E-02	8.577E-02	0.282	4.818E-01	9.347E-06	6.790E-02	7.614E-06	6.806E-02	1.110E+52	6.790E-02
7	12.217	12.270	5.287E-02	1.111E-01	0.347	5.933E-01	1.537E-05	1.116E-01	1.251E-05	1.118E-01	1.824E+52	1.116E-01
8	12.192	12.217	2.512E-02	5.279E-02	0.378	6.466E-01	8.638E-06	6.275E-02	7.024E-06	6.279E-02	1.026E+52	6.275E-02
9	12.151	12.192	4.019E-02	8.447E-02	0.428	7.317E-01	1.583E-05	1.150E-01	1.286E-05	1.150E-01	1.879E+52	1.150E-01
10	12.119	12.151	3.180E-02	6.685E-02	0.467	7.992E-01	1.438E-05	1.045E-01	1.168E-05	1.044E-01	1.708E+52	1.045E-01
11	12.089	12.119	3.020E-02	6.348E-02	0.505	8.634E-01	1.538E-05	1.117E-01	1.248E-05	1.115E-01	1.825E+52	1.117E-01
12	12.034	12.089	5.476E-02	1.151E-01	0.572	9.795E-01	3.224E-05	2.342E-01	2.614E-05	2.337E-01	3.828E+52	2.342E-01
13	12.024	12.034	9.408E-03	1.978E-02	0.584	1.000E+00	6.206E-06	4.508E-02	5.027E-06	4.494E-02	7.367E+51	4.508E-02

D.4 BSKG3

Table D.10: The same as Table 5.2, using the BSKG3 model with $B_\star = 2500$

№	P_{min}	P_{max}	ϵ_{min}	ϵ_{max}	$n_{b_{min}}$	$n_{b_{max}}$	A	Z	N	Z/A	$\mu_{b_{min}}$	$\mu_{b_{max}}$	$\mu_{e_{min}}$	$\mu_{e_{max}}$
1	6.082E-15	3.549E-07	2.986E-03	5.776E-03	3.210E-06	6.209E-06	56	26	30	0.464	930.333	930.406	0.617	0.842
2	3.554E-07	1.412E-05	6.004E-03	2.490E-02	6.453E-06	2.676E-05	62	28	34	0.452	930.406	931.211	0.848	2.854
3	1.414E-05	3.535E-05	2.640E-02	4.028E-02	2.837E-05	4.327E-05	88	38	50	0.432	931.212	931.804	2.892	4.371
4	3.541E-05	9.131E-05	4.151E-02	6.519E-02	4.458E-05	6.998E-05	86	36	50	0.419	931.805	932.780	4.366	6.825
5	9.144E-05	1.874E-04	6.738E-02	9.545E-02	7.233E-05	1.024E-04	84	34	50	0.405	932.782	933.880	6.821	9.644
6	1.877E-04	2.802E-04	9.897E-02	1.204E-01	1.062E-04	1.291E-04	82	32	50	0.390	933.882	934.669	9.640	11.720
7	2.806E-04	4.226E-04	1.252E-01	1.529E-01	1.342E-04	1.639E-04	132	50	82	0.379	934.672	935.625	11.822	14.433
8	4.233E-04	6.245E-04	1.611E-01	1.951E-01	1.726E-04	2.089E-04	128	46	82	0.359	935.628	936.683	14.423	17.450
9	6.254E-04	7.721E-04	2.008E-01	2.228E-01	2.150E-04	2.385E-04	126	44	82	0.349	936.687	937.334	17.452	19.355
10	7.732E-04	9.532E-04	2.297E-01	2.548E-01	2.459E-04	2.726E-04	124	42	82	0.339	937.339	938.033	19.358	21.458
11	9.546E-04	1.177E-03	2.632E-01	2.920E-01	2.817E-04	3.123E-04	122	40	82	0.328	938.038	938.786	21.461	23.794
12	1.178E-03	1.318E-03	3.024E-01	3.197E-01	3.234E-04	3.418E-04	120	38	82	0.317	938.792	939.211	23.798	25.151
13	1.320E-03	1.402E-03	3.253E-01	3.352E-01	3.477E-04	3.583E-04	122	38	84	0.311	939.217	939.450	25.169	25.932
14	1.404E-03	1.444E-03	3.409E-01	3.457E-01	3.644E-04	3.695E-04	124	38	86	0.306	939.456	939.564	25.951	26.312

Table D.11: The same as Table 5.3, using the BSKG3 model with $B_\star = 2500$

M_{cr}	M_{cr}/M	ΔR_{cr}	$\Delta R_{cr}/R$	$M_{b_{cr}}$	Δ_{grav}	z_{drip}	ΔN
1.136E-04	8.118E-05	4.758E-01	3.806E-02	1.399E-04	2.306E-01	5.844E-01	1.660E+53

Table D.12: The same as Table 5.4, using the BSKG3 model with $B_\star = 2500$

№	r_{min}	r_{max}	ΔR_l	$\Delta R_l/\Delta R_{cr}$	z_l	z_l/z_{drip}	M_{b_l}	$M_{b_l}/M_{b_{cr}}$	M_l	M_l/M_{cr}	ΔN_l	$\Delta N_l/\Delta N$
1	12.496	12.500	3.955E-03	8.312E-03	0.005	8.272E-03	3.857E-08	2.758E-04	3.155E-08	2.776E-04	4.579E+49	2.758E-04
2	12.452	12.496	4.355E-02	9.155E-02	0.058	9.944E-02	1.482E-06	1.060E-02	1.211E-06	1.066E-02	1.759E+51	1.060E-02
3	12.421	12.452	3.172E-02	6.667E-02	0.097	1.660E-01	2.256E-06	1.613E-02	1.843E-06	1.622E-02	2.679E+51	1.613E-02
4	12.369	12.421	5.180E-02	1.089E-01	0.161	2.747E-01	5.857E-06	4.188E-02	4.781E-06	4.207E-02	6.954E+51	4.188E-02
5	12.311	12.369	5.762E-02	1.211E-01	0.231	3.958E-01	9.862E-06	7.052E-02	8.042E-06	7.076E-02	1.171E+52	7.052E-02
6	12.270	12.311	4.080E-02	8.577E-02	0.282	4.818E-01	9.347E-06	6.683E-02	7.614E-06	6.700E-02	1.110E+52	6.683E-02
7	12.221	12.270	4.896E-02	1.029E-01	0.342	5.851E-01	1.412E-05	1.010E-01	1.149E-05	1.011E-01	1.677E+52	1.010E-01
8	12.167	12.221	5.357E-02	1.126E-01	0.408	6.982E-01	1.964E-05	1.405E-01	1.597E-05	1.405E-01	2.332E+52	1.405E-01
9	12.135	12.167	3.253E-02	6.838E-02	0.448	7.672E-01	1.410E-05	1.008E-01	1.145E-05	1.008E-01	1.674E+52	1.008E-01
10	12.100	12.134	3.463E-02	7.280E-02	0.491	8.407E-01	1.709E-05	1.222E-01	1.387E-05	1.221E-01	2.029E+52	1.222E-01
11	12.062	12.099	3.702E-02	7.781E-02	0.537	9.194E-01	2.083E-05	1.489E-01	1.689E-05	1.486E-01	2.473E+52	1.489E-01
12	12.042	12.062	2.064E-02	4.338E-02	0.563	9.635E-01	1.296E-05	9.264E-02	1.050E-05	9.240E-02	1.538E+52	9.264E-02
13	12.030	12.041	1.140E-02	2.397E-02	0.577	9.882E-01	7.581E-06	5.421E-02	6.143E-06	5.405E-02	9.001E+51	5.421E-02
14	12.024	12.030	5.310E-03	1.116E-02	0.584	1.000E+00	3.666E-06	2.622E-02	2.970E-06	2.613E-02	4.353E+51	2.622E-02

D.5 HFB31

Table D.13: The same as Table 5.2, using the HFB31 model with $B_\star = 2500$

№	P_{min}	P_{max}	ϵ_{min}	ϵ_{max}	$n_{b_{min}}$	$n_{b_{max}}$	A	Z	N	Z/A	$\mu_{b_{min}}$	$\mu_{b_{max}}$	$\mu_{e_{min}}$	$\mu_{e_{max}}$
1	6.082E-15	3.549E-07	2.986E-03	5.776E-03	3.210E-06	6.209E-06	56	26	30	0.464	930.333	930.406	0.617	0.842
2	3.554E-07	1.412E-05	6.004E-03	2.490E-02	6.453E-06	2.676E-05	62	28	34	0.452	930.406	931.211	0.848	2.854
3	1.414E-05	3.535E-05	2.640E-02	4.028E-02	2.837E-05	4.327E-05	88	38	50	0.432	931.212	931.804	2.892	4.371
4	3.541E-05	9.131E-05	4.151E-02	6.519E-02	4.458E-05	6.998E-05	86	36	50	0.419	931.805	932.780	4.366	6.825
5	9.144E-05	1.874E-04	6.738E-02	9.545E-02	7.233E-05	1.024E-04	84	34	50	0.405	932.782	933.880	6.821	9.644
6	1.877E-04	2.802E-04	9.897E-02	1.204E-01	1.062E-04	1.291E-04	82	32	50	0.390	933.882	934.669	9.640	11.720
7	2.806E-04	4.353E-04	1.252E-01	1.552E-01	1.342E-04	1.663E-04	132	50	82	0.379	934.672	935.701	11.822	14.642
8	4.359E-04	4.897E-04	1.592E-01	1.685E-01	1.706E-04	1.806E-04	130	48	82	0.369	935.705	936.011	14.643	15.501
9	4.905E-04	6.291E-04	1.732E-01	1.958E-01	1.856E-04	2.097E-04	128	46	82	0.359	936.015	936.717	15.501	17.514
10	6.300E-04	7.365E-04	2.015E-01	2.176E-01	2.158E-04	2.330E-04	126	44	82	0.349	936.721	937.196	17.515	18.912
11	7.376E-04	8.868E-04	2.244E-01	2.458E-01	2.403E-04	2.631E-04	124	42	82	0.339	937.201	937.793	18.914	20.708
12	8.881E-04	1.088E-03	2.540E-01	2.809E-01	2.718E-04	3.005E-04	122	40	82	0.328	937.798	938.498	20.711	22.895
13	1.090E-03	1.184E-03	2.859E-01	2.978E-01	3.058E-04	3.185E-04	121	39	82	0.322	938.503	938.804	22.905	23.857
14	1.185E-03	1.226E-03	3.033E-01	3.084E-01	3.243E-04	3.298E-04	120	38	82	0.317	938.809	938.934	23.867	24.270
15	1.228E-03	1.446E-03	3.138E-01	3.404E-01	3.356E-04	3.638E-04	122	38	84	0.311	938.939	939.563	24.288	26.332

Table D.14: The same as Table 5.3, using the HFB31 model with $B_\star = 2500$

M_{cr}	M_{cr}/M	ΔR_{cr}	$\Delta R_{cr}/R$	$M_{b_{cr}}$	Δ_{grav}	z_{drip}	ΔN
1.138E-04	8.129E-05	4.757E-01	3.806E-02	1.400E-04	2.306E-01	5.843E-01	1.663E+53

Table D.15: The same as Table 5.4, using the HFB31 model with $B_\star = 2500$

№	r_{min}	r_{max}	ΔR_l	$\Delta R_l/\Delta R_{cr}$	z_l	z_l/z_{drip}	M_{b_l}	$M_{b_l}/M_{b_{cr}}$	M_l	M_l/M_{cr}	ΔN_l	$\Delta N_l/\Delta N$
1	12.496	12.500	3.955E-03	8.313E-03	0.005	8.273E-03	3.857E-08	2.754E-04	3.155E-08	2.773E-04	4.579E+49	2.754E-04
2	12.452	12.496	4.355E-02	9.156E-02	0.058	9.945E-02	1.482E-06	1.058E-02	1.211E-06	1.065E-02	1.759E+51	1.058E-02
3	12.421	12.452	3.172E-02	6.668E-02	0.097	1.660E-01	2.256E-06	1.611E-02	1.843E-06	1.620E-02	2.679E+51	1.611E-02
4	12.369	12.421	5.180E-02	1.089E-01	0.161	2.747E-01	5.857E-06	4.183E-02	4.781E-06	4.202E-02	6.954E+51	4.183E-02
5	12.311	12.369	5.762E-02	1.211E-01	0.231	3.958E-01	9.862E-06	7.042E-02	8.042E-06	7.066E-02	1.171E+52	7.042E-02
6	12.270	12.311	4.080E-02	8.578E-02	0.282	4.819E-01	9.347E-06	6.674E-02	7.614E-06	6.691E-02	1.110E+52	6.674E-02
7	12.217	12.270	5.287E-02	1.111E-01	0.347	5.934E-01	1.537E-05	1.097E-01	1.251E-05	1.099E-01	1.824E+52	1.097E-01
8	12.201	12.217	1.561E-02	3.282E-02	0.366	6.266E-01	5.282E-06	3.772E-02	4.295E-06	3.774E-02	6.271E+51	3.772E-02
9	12.166	12.201	3.555E-02	7.473E-02	0.410	7.019E-01	1.349E-05	9.630E-02	1.096E-05	9.633E-02	1.601E+52	9.630E-02
10	12.141	12.165	2.388E-02	5.019E-02	0.440	7.527E-01	1.025E-05	7.318E-02	8.324E-06	7.315E-02	1.217E+52	7.318E-02
11	12.112	12.141	2.964E-02	6.230E-02	0.477	8.157E-01	1.422E-05	1.015E-01	1.154E-05	1.014E-01	1.688E+52	1.015E-01
12	12.077	12.111	3.473E-02	7.302E-02	0.520	8.894E-01	1.886E-05	1.347E-01	1.530E-05	1.345E-01	2.239E+52	1.347E-01
13	12.062	12.076	1.482E-02	3.115E-02	0.538	9.213E-01	8.751E-06	6.249E-02	7.096E-06	6.235E-02	1.039E+52	6.249E-02
14	12.055	12.061	6.149E-03	1.293E-02	0.546	9.348E-01	3.799E-06	2.713E-02	3.080E-06	2.706E-02	4.511E+51	2.713E-02
15	12.024	12.055	3.059E-02	6.430E-02	0.584	1.000E+00	2.016E-05	1.439E-01	1.633E-05	1.435E-01	2.393E+52	1.439E-01

D.6 DDMED

Table D.16: The same as Table 5.2, using the DDMED model with $B_\star = 2500$

№	P_{min}	P_{max}	ϵ_{min}	ϵ_{max}	$n_{b_{min}}$	$n_{b_{max}}$	A	Z	N	Z/A	$\mu_{b_{min}}$	$\mu_{b_{max}}$	$\mu_{e_{min}}$	$\mu_{e_{max}}$
1	6.082E-15	3.549E-07	2.986E-03	5.776E-03	3.210E-06	6.209E-06	56	26	30	0.464	930.333	930.406	0.617	0.842
2	3.554E-07	1.412E-05	6.004E-03	2.490E-02	6.453E-06	2.676E-05	62	28	34	0.452	930.406	931.211	0.848	2.854
3	1.414E-05	3.535E-05	2.640E-02	4.028E-02	2.837E-05	4.327E-05	88	38	50	0.432	931.212	931.804	2.892	4.371
4	3.541E-05	9.131E-05	4.151E-02	6.519E-02	4.458E-05	6.998E-05	86	36	50	0.419	931.805	932.780	4.366	6.825
5	9.144E-05	1.874E-04	6.738E-02	9.545E-02	7.233E-05	1.024E-04	84	34	50	0.405	932.782	933.880	6.821	9.644
6	1.877E-04	2.802E-04	9.897E-02	1.204E-01	1.062E-04	1.291E-04	82	32	50	0.390	933.882	934.669	9.640	11.720
7	2.806E-04	4.353E-04	1.252E-01	1.552E-01	1.342E-04	1.663E-04	132	50	82	0.379	934.672	935.701	11.822	14.642
8	4.359E-04	4.556E-04	1.592E-01	1.627E-01	1.706E-04	1.743E-04	130	48	82	0.369	935.705	935.819	14.643	14.963
9	4.563E-04	6.109E-04	1.672E-01	1.929E-01	1.791E-04	2.067E-04	128	46	82	0.359	935.823	936.624	14.963	17.262
10	6.118E-04	7.642E-04	1.986E-01	2.216E-01	2.127E-04	2.373E-04	126	44	82	0.349	936.629	937.306	17.263	19.257
11	7.653E-04	9.296E-04	2.286E-01	2.516E-01	2.447E-04	2.693E-04	124	42	82	0.339	937.311	937.950	19.260	21.195
12	9.310E-04	1.126E-03	2.600E-01	2.857E-01	2.782E-04	3.055E-04	122	40	82	0.328	937.955	938.623	21.198	23.280
13	1.128E-03	1.364E-03	2.959E-01	3.251E-01	3.164E-04	3.476E-04	120	38	82	0.317	938.628	939.339	23.284	25.576
14	1.366E-03	1.444E-03	3.376E-01	3.471E-01	3.608E-04	3.710E-04	118	36	82	0.305	939.345	939.560	25.581	26.299

Table D.17: The same as Table 5.3, using the DDMED model with $B_\star = 2500$

M_{cr}	M_{cr}/M	ΔR_{cr}	$\Delta R_{cr}/R$	$M_{b_{cr}}$	Δ_{grav}	z_{drip}	ΔN
1.136E-04	8.118E-05	4.755E-01	3.804E-02	1.399E-04	2.306E-01	5.841E-01	1.660E+53

Table D.18: The same as Table 5.4, using the DDMED model with $B_\star = 2500$

№	r_{min}	r_{max}	ΔR_l	$\Delta R_l/\Delta R_{cr}$	z_l	z_l/z_{drip}	M_{b_l}	$M_{b_l}/M_{b_{cr}}$	M_l	M_l/M_{cr}	ΔN_l	$\Delta N_l/\Delta N$
1	12.496	12.500	3.955E-03	8.316E-03	0.005	8.276E-03	3.857E-08	2.758E-04	3.155E-08	2.776E-04	4.579E+49	2.758E-04
2	12.452	12.496	4.355E-02	9.159E-02	0.058	9.949E-02	1.482E-06	1.060E-02	1.211E-06	1.066E-02	1.759E+51	1.060E-02
3	12.421	12.452	3.172E-02	6.670E-02	0.097	1.660E-01	2.256E-06	1.613E-02	1.843E-06	1.622E-02	2.679E+51	1.613E-02
4	12.369	12.421	5.180E-02	1.089E-01	0.161	2.748E-01	5.857E-06	4.188E-02	4.781E-06	4.207E-02	6.954E+51	4.188E-02
5	12.311	12.369	5.762E-02	1.212E-01	0.231	3.960E-01	9.862E-06	7.052E-02	8.042E-06	7.076E-02	1.171E+52	7.052E-02
6	12.270	12.311	4.080E-02	8.581E-02	0.282	4.820E-01	9.347E-06	6.683E-02	7.614E-06	6.700E-02	1.110E+52	6.683E-02
7	12.217	12.270	5.287E-02	1.112E-01	0.347	5.936E-01	1.537E-05	1.099E-01	1.251E-05	1.100E-01	1.824E+52	1.099E-01
8	12.211	12.217	5.826E-03	1.225E-02	0.354	6.063E-01	1.937E-06	1.385E-02	1.575E-06	1.386E-02	2.299E+51	1.385E-02
9	12.170	12.211	4.066E-02	8.550E-02	0.404	6.923E-01	1.507E-05	1.078E-01	1.225E-05	1.078E-01	1.789E+52	1.078E-01
10	12.136	12.170	3.408E-02	7.168E-02	0.447	7.646E-01	1.466E-05	1.049E-01	1.191E-05	1.048E-01	1.741E+52	1.049E-01
11	12.104	12.136	3.193E-02	6.714E-02	0.486	8.324E-01	1.562E-05	1.117E-01	1.268E-05	1.116E-01	1.854E+52	1.117E-01
12	12.070	12.104	3.309E-02	6.958E-02	0.527	9.028E-01	1.831E-05	1.309E-01	1.485E-05	1.307E-01	2.174E+52	1.309E-01
13	12.035	12.070	3.495E-02	7.351E-02	0.571	9.772E-01	2.190E-05	1.566E-01	1.775E-05	1.562E-01	2.600E+52	1.566E-01
14	12.024	12.035	1.051E-02	2.211E-02	0.584	1.000E+00	7.240E-06	5.177E-02	5.865E-06	5.161E-02	8.595E+51	5.177E-02

D.7 DDPC1

Table D.19: The same as Table 5.2, using the DDPC1 model with $B_\star = 2500$

№	P_{min}	P_{max}	ϵ_{min}	ϵ_{max}	$n_{b_{min}}$	$n_{b_{max}}$	A	Z	N	Z/A	$\mu_{b_{min}}$	$\mu_{b_{max}}$	$\mu_{e_{min}}$	$\mu_{e_{max}}$
1	6.082E-15	3.549E-07	2.986E-03	5.776E-03	3.210E-06	6.209E-06	56	26	30	0.464	930.333	930.406	0.617	0.842
2	3.554E-07	1.412E-05	6.004E-03	2.490E-02	6.453E-06	2.676E-05	62	28	34	0.452	930.406	931.211	0.848	2.854
3	1.414E-05	3.535E-05	2.640E-02	4.028E-02	2.837E-05	4.327E-05	88	38	50	0.432	931.212	931.804	2.892	4.371
4	3.541E-05	9.131E-05	4.151E-02	6.519E-02	4.458E-05	6.998E-05	86	36	50	0.419	931.805	932.780	4.366	6.825
5	9.144E-05	1.874E-04	6.738E-02	9.545E-02	7.233E-05	1.024E-04	84	34	50	0.405	932.782	933.880	6.821	9.644
6	1.877E-04	2.468E-04	9.897E-02	1.132E-01	1.062E-04	1.214E-04	82	32	50	0.390	933.882	934.402	9.640	11.017
7	2.472E-04	3.047E-04	1.166E-01	1.292E-01	1.250E-04	1.385E-04	74	28	46	0.378	934.405	934.842	11.003	12.189
8	3.052E-04	3.314E-04	1.328E-01	1.383E-01	1.424E-04	1.483E-04	76	28	48	0.368	934.845	935.026	12.197	12.701
9	3.319E-04	6.064E-04	1.430E-01	1.922E-01	1.533E-04	2.059E-04	128	46	82	0.359	935.029	936.557	12.808	17.200
10	6.073E-04	7.442E-04	1.979E-01	2.187E-01	2.119E-04	2.342E-04	126	44	82	0.349	936.561	937.175	17.201	19.008
11	7.453E-04	8.960E-04	2.256E-01	2.471E-01	2.415E-04	2.644E-04	124	42	82	0.339	937.180	937.775	19.010	20.814
12	8.973E-04	1.076E-03	2.553E-01	2.793E-01	2.732E-04	2.987E-04	122	40	82	0.328	937.780	938.404	20.816	22.762
13	1.077E-03	1.305E-03	2.892E-01	3.180E-01	3.094E-04	3.401E-04	120	38	82	0.317	938.409	939.109	22.766	25.023
14	1.306E-03	1.470E-03	3.302E-01	3.501E-01	3.530E-04	3.742E-04	118	36	82	0.305	939.115	939.564	25.028	26.530

Table D.20: The same as Table 5.3, using the DDPC1 model with $B_\star = 2500$

M_{cr}	M_{cr}/M	ΔR_{cr}	$\Delta R_{cr}/R$	$M_{b_{cr}}$	Δ_{grav}	z_{drip}	ΔN
1.156E-04	8.261E-05	4.758E-01	3.806E-02	1.423E-04	2.306E-01	5.844E-01	1.690E+53

Table D.21: The same as Table 5.4, using the DDPC1 model with $B_\star = 2500$

№	r_{min}	r_{max}	ΔR_l	$\Delta R_l/\Delta R_{cr}$	z_l	z_l/z_{drip}	M_{b_l}	$M_{b_l}/M_{b_{cr}}$	M_l	M_l/M_{cr}	ΔN_l	$\Delta N_l/\Delta N$
1	12.496	12.500	3.955E-03	8.312E-03	0.005	8.272E-03	3.857E-08	2.710E-04	3.155E-08	2.728E-04	4.579E+49	2.710E-04
2	12.452	12.496	4.355E-02	9.155E-02	0.058	9.944E-02	1.482E-06	1.041E-02	1.211E-06	1.048E-02	1.759E+51	1.041E-02
3	12.421	12.452	3.172E-02	6.667E-02	0.097	1.660E-01	2.256E-06	1.585E-02	1.843E-06	1.594E-02	2.679E+51	1.585E-02
4	12.369	12.421	5.180E-02	1.089E-01	0.161	2.747E-01	5.857E-06	4.116E-02	4.781E-06	4.135E-02	6.954E+51	4.116E-02
5	12.311	12.369	5.762E-02	1.211E-01	0.231	3.958E-01	9.862E-06	6.930E-02	8.042E-06	6.954E-02	1.171E+52	6.930E-02
6	12.284	12.311	2.703E-02	5.682E-02	0.265	4.529E-01	5.993E-06	4.211E-02	4.883E-06	4.222E-02	7.115E+51	4.211E-02
7	12.261	12.284	2.256E-02	4.743E-02	0.293	5.006E-01	5.776E-06	4.058E-02	4.703E-06	4.067E-02	6.857E+51	4.058E-02
8	12.252	12.261	9.302E-03	1.955E-02	0.304	5.205E-01	2.620E-06	1.841E-02	2.133E-06	1.845E-02	3.111E+51	1.841E-02
9	12.174	12.252	7.792E-02	1.638E-01	0.400	6.848E-01	2.696E-05	1.894E-01	2.193E-05	1.896E-01	3.201E+52	1.894E-01
10	12.143	12.173	3.092E-02	6.499E-02	0.439	7.504E-01	1.320E-05	9.273E-02	1.072E-05	9.270E-02	1.567E+52	9.273E-02
11	12.113	12.142	2.980E-02	6.264E-02	0.476	8.137E-01	1.437E-05	1.010E-01	1.166E-05	1.009E-01	1.706E+52	1.010E-01
12	12.081	12.112	3.096E-02	6.508E-02	0.514	8.795E-01	1.681E-05	1.181E-01	1.364E-05	1.179E-01	1.996E+52	1.181E-01
13	12.047	12.081	3.452E-02	7.256E-02	0.557	9.529E-01	2.119E-05	1.489E-01	1.718E-05	1.485E-01	2.516E+52	1.489E-01
14	12.024	12.046	2.201E-02	4.627E-02	0.584	1.000E+00	1.508E-05	1.059E-01	1.222E-05	1.056E-01	1.790E+52	1.059E-01

D.8 SVMIN

Table D.22: The same as Table 5.2, using the SVMIN model with $B_\star = 2500$

№	P_{min}	P_{max}	ϵ_{min}	ϵ_{max}	$n_{b_{min}}$	$n_{b_{max}}$	A	Z	N	Z/A	$\mu_{b_{min}}$	$\mu_{b_{max}}$	$\mu_{e_{min}}$	$\mu_{e_{max}}$
1	6.082E-15	3.549E-07	2.986E-03	5.776E-03	3.210E-06	6.209E-06	56	26	30	0.464	930.333	930.406	0.617	0.842
2	3.554E-07	1.412E-05	6.004E-03	2.490E-02	6.453E-06	2.676E-05	62	28	34	0.452	930.406	931.211	0.848	2.854
3	1.414E-05	3.535E-05	2.640E-02	4.028E-02	2.837E-05	4.327E-05	88	38	50	0.432	931.212	931.804	2.892	4.371
4	3.541E-05	9.131E-05	4.151E-02	6.519E-02	4.458E-05	6.998E-05	86	36	50	0.419	931.805	932.780	4.366	6.825
5	9.144E-05	1.874E-04	6.738E-02	9.545E-02	7.233E-05	1.024E-04	84	34	50	0.405	932.782	933.880	6.821	9.644
6	1.877E-04	2.802E-04	9.897E-02	1.204E-01	1.062E-04	1.291E-04	82	32	50	0.390	933.882	934.669	9.640	11.720
7	2.806E-04	4.321E-04	1.252E-01	1.546E-01	1.342E-04	1.657E-04	132	50	82	0.379	934.672	935.682	11.822	14.590
8	4.327E-04	6.163E-04	1.629E-01	1.938E-01	1.745E-04	2.076E-04	128	46	82	0.359	935.686	936.646	14.579	17.337
9	6.172E-04	7.442E-04	1.995E-01	2.188E-01	2.136E-04	2.342E-04	126	44	82	0.349	936.651	937.218	17.338	19.008
10	7.453E-04	8.920E-04	2.256E-01	2.465E-01	2.415E-04	2.638E-04	124	42	82	0.339	937.223	937.803	19.010	20.768
11	8.934E-04	1.106E-03	2.548E-01	2.832E-01	2.726E-04	3.029E-04	122	40	82	0.328	937.808	938.548	20.771	23.078
12	1.108E-03	1.109E-03	2.880E-01	2.883E-01	3.081E-04	3.083E-04	124	40	84	0.323	938.553	938.558	23.095	23.112
13	1.111E-03	1.263E-03	2.937E-01	3.130E-01	3.141E-04	3.346E-04	120	38	82	0.317	938.564	939.032	23.116	24.626
14	1.265E-03	1.415E-03	3.185E-01	3.366E-01	3.405E-04	3.598E-04	122	38	84	0.311	939.038	939.466	24.644	26.046
15	1.417E-03	1.451E-03	3.480E-01	3.521E-01	3.719E-04	3.763E-04	126	38	88	0.302	939.471	939.562	26.064	26.370

Table D.23: The same as Table 5.3, using the SVMIN model with $B_\star = 2500$

M_{cr}	M_{cr}/M	ΔR_{cr}	$\Delta R_{cr}/R$	$M_{b_{cr}}$	Δ_{grav}	z_{drip}	ΔN
1.141E-04	8.152E-05	4.756E-01	3.805E-02	1.405E-04	2.306E-01	5.842E-01	1.667E+53

Table D.24: The same as Table 5.4, using the SVMIN model with $B_\star = 2500$

№	r_{min}	r_{max}	ΔR_l	$\Delta R_l/\Delta R_{cr}$	z_l	z_l/z_{drip}	M_{b_l}	$M_{b_l}/M_{b_{cr}}$	M_l	M_l/M_{cr}	ΔN_l	$\Delta N_l/\Delta N$
1	12.496	12.500	3.955E-03	8.314E-03	0.005	8.275E-03	3.857E-08	2.746E-04	3.155E-08	2.765E-04	4.579E+49	2.746E-04
2	12.452	12.496	4.355E-02	9.157E-02	0.058	9.947E-02	1.482E-06	1.055E-02	1.211E-06	1.061E-02	1.759E+51	1.055E-02
3	12.421	12.452	3.172E-02	6.669E-02	0.097	1.660E-01	2.256E-06	1.606E-02	1.843E-06	1.615E-02	2.679E+51	1.606E-02
4	12.369	12.421	5.180E-02	1.089E-01	0.161	2.748E-01	5.857E-06	4.170E-02	4.781E-06	4.189E-02	6.954E+51	4.170E-02
5	12.311	12.369	5.762E-02	1.211E-01	0.231	3.959E-01	9.862E-06	7.022E-02	8.042E-06	7.046E-02	1.171E+52	7.022E-02
6	12.270	12.311	4.080E-02	8.579E-02	0.282	4.819E-01	9.347E-06	6.655E-02	7.614E-06	6.671E-02	1.110E+52	6.655E-02
7	12.218	12.270	5.188E-02	1.091E-01	0.346	5.914E-01	1.505E-05	1.072E-01	1.225E-05	1.073E-01	1.787E+52	1.072E-01
8	12.169	12.218	4.879E-02	1.026E-01	0.406	6.945E-01	1.792E-05	1.276E-01	1.457E-05	1.276E-01	2.127E+52	1.276E-01
9	12.140	12.169	2.854E-02	6.001E-02	0.441	7.551E-01	1.223E-05	8.704E-02	9.931E-06	8.701E-02	1.451E+52	8.704E-02
10	12.111	12.140	2.904E-02	6.106E-02	0.477	8.169E-01	1.398E-05	9.955E-02	1.135E-05	9.945E-02	1.660E+52	9.955E-02
11	12.074	12.111	3.669E-02	7.715E-02	0.523	8.948E-01	2.003E-05	1.426E-01	1.625E-05	1.424E-01	2.378E+52	1.426E-01
12	12.074	12.074	2.606E-04	5.478E-04	0.523	8.959E-01	1.520E-07	1.082E-03	1.233E-07	1.080E-03	1.805E+50	1.082E-03
13	12.050	12.073	2.308E-02	4.852E-02	0.552	9.452E-01	1.415E-05	1.007E-01	1.147E-05	1.005E-01	1.680E+52	1.007E-01
14	12.029	12.050	2.098E-02	4.411E-02	0.578	9.901E-01	1.384E-05	9.856E-02	1.122E-05	9.828E-02	1.643E+52	9.856E-02
15	12.024	12.029	4.415E-03	9.282E-03	0.584	1.000E+00	3.108E-06	2.212E-02	2.517E-06	2.206E-02	3.689E+51	2.212E-02

D.9 UNEDF0

Table D.25: The same as Table 5.2, using the UNEDF0 model with $B_\star = 2500$

№	P_{min}	P_{max}	ϵ_{min}	ϵ_{max}	$n_{b_{min}}$	$n_{b_{max}}$	A	Z	N	Z/A	$\mu_{b_{min}}$	$\mu_{b_{max}}$	$\mu_{e_{min}}$	$\mu_{e_{max}}$
1	6.082E-15	3.549E-07	2.986E-03	5.776E-03	3.210E-06	6.209E-06	56	26	30	0.464	930.333	930.406	0.617	0.842
2	3.554E-07	1.412E-05	6.004E-03	2.490E-02	6.453E-06	2.676E-05	62	28	34	0.452	930.406	931.211	0.848	2.854
3	1.414E-05	3.535E-05	2.640E-02	4.028E-02	2.837E-05	4.327E-05	88	38	50	0.432	931.212	931.804	2.892	4.371
4	3.541E-05	9.131E-05	4.151E-02	6.519E-02	4.458E-05	6.998E-05	86	36	50	0.419	931.805	932.780	4.366	6.825
5	9.144E-05	1.874E-04	6.738E-02	9.545E-02	7.233E-05	1.024E-04	84	34	50	0.405	932.782	933.880	6.821	9.644
6	1.877E-04	2.802E-04	9.897E-02	1.204E-01	1.062E-04	1.291E-04	82	32	50	0.390	933.882	934.669	9.640	11.720
7	2.806E-04	4.353E-04	1.252E-01	1.552E-01	1.342E-04	1.663E-04	132	50	82	0.379	934.672	935.701	11.822	14.642
8	4.359E-04	4.411E-04	1.592E-01	1.601E-01	1.706E-04	1.716E-04	130	48	82	0.369	935.705	935.735	14.643	14.727
9	4.417E-04	6.498E-04	1.645E-01	1.989E-01	1.763E-04	2.130E-04	128	46	82	0.359	935.739	936.808	14.727	17.794
10	6.508E-04	7.755E-04	2.048E-01	2.233E-01	2.193E-04	2.390E-04	126	44	82	0.349	936.812	937.357	17.796	19.397
11	7.767E-04	7.824E-04	2.270E-01	2.278E-01	2.430E-04	2.439E-04	128	44	84	0.344	937.361	937.385	19.412	19.482
12	7.836E-04	8.947E-04	2.312E-01	2.469E-01	2.475E-04	2.642E-04	124	42	82	0.339	937.390	937.824	19.484	20.799
13	8.960E-04	9.066E-04	2.511E-01	2.525E-01	2.687E-04	2.702E-04	126	42	84	0.333	937.829	937.868	20.814	20.935
14	9.079E-04	1.022E-03	2.576E-01	2.732E-01	2.757E-04	2.922E-04	86	28	58	0.326	937.873	938.273	20.859	22.110
15	1.023E-03	1.182E-03	2.797E-01	3.005E-01	2.992E-04	3.214E-04	88	28	60	0.318	938.278	938.790	22.126	23.764
16	1.184E-03	1.285E-03	3.076E-01	3.205E-01	3.289E-04	3.426E-04	90	28	62	0.311	938.796	939.099	23.781	24.772
17	1.287E-03	1.293E-03	3.304E-01	3.311E-01	3.532E-04	3.540E-04	132	40	92	0.303	939.104	939.121	24.873	24.928
18	1.295E-03	1.342E-03	3.364E-01	3.424E-01	3.596E-04	3.660E-04	134	40	94	0.299	939.126	939.254	24.946	25.385
19	1.344E-03	1.356E-03	3.486E-01	3.502E-01	3.726E-04	3.742E-04	170	50	120	0.294	939.260	939.292	25.467	25.578
20	1.358E-03	1.436E-03	3.546E-01	3.645E-01	3.789E-04	3.895E-04	172	50	122	0.291	939.297	939.500	25.597	26.314
21	1.438E-03	1.461E-03	3.691E-01	3.720E-01	3.944E-04	3.975E-04	174	50	124	0.287	939.506	939.565	26.333	26.544

Table D.26: The same as Table 5.3, using the UNEDF0 model with $B_\star = 2500$

M_{cr}	M_{cr}/M	ΔR_{cr}	$\Delta R_{cr}/R$	$M_{b_{cr}}$	Δ_{grav}	z_{drip}	ΔN
1.149E-04	8.209E-05	4.758E-01	3.806E-02	1.414E-04	2.305E-01	5.844E-01	1.679E+53

Table D.27: The same as Table 5.4, using the UNEDF0 model with $B_\star = 2500$

№	r_{min}	r_{max}	ΔR_l	$\Delta R_l/\Delta R_{cr}$	z_l	z_l/z_{drip}	M_{b_l}	$M_{b_l}/M_{b_{cr}}$	M_l	M_l/M_{cr}	ΔN_l	$\Delta N_l/\Delta N$
1	12.496	12.500	3.955E-03	8.311E-03	0.005	8.272E-03	3.857E-08	2.727E-04	3.155E-08	2.745E-04	4.579E+49	2.727E-04
2	12.452	12.496	4.355E-02	9.154E-02	0.058	9.943E-02	1.482E-06	1.048E-02	1.211E-06	1.054E-02	1.759E+51	1.048E-02
3	12.421	12.452	3.172E-02	6.666E-02	0.097	1.659E-01	2.256E-06	1.595E-02	1.843E-06	1.604E-02	2.679E+51	1.595E-02
4	12.369	12.421	5.180E-02	1.089E-01	0.161	2.747E-01	5.857E-06	4.142E-02	4.781E-06	4.160E-02	6.954E+51	4.142E-02
5	12.311	12.369	5.762E-02	1.211E-01	0.231	3.958E-01	9.862E-06	6.973E-02	8.042E-06	6.997E-02	1.171E+52	6.973E-02
6	12.270	12.311	4.080E-02	8.576E-02	0.282	4.818E-01	9.347E-06	6.609E-02	7.614E-06	6.625E-02	1.110E+52	6.609E-02
7	12.217	12.270	5.287E-02	1.111E-01	0.347	5.933E-01	1.537E-05	1.087E-01	1.251E-05	1.088E-01	1.824E+52	1.087E-01
8	12.215	12.217	1.540E-03	3.237E-03	0.349	5.969E-01	5.081E-07	3.592E-03	4.133E-07	3.596E-03	6.032E+50	3.592E-03
9	12.161	12.215	5.422E-02	1.139E-01	0.416	7.114E-01	2.027E-05	1.433E-01	1.648E-05	1.434E-01	2.407E+52	1.433E-01
10	12.133	12.161	2.735E-02	5.748E-02	0.450	7.695E-01	1.197E-05	8.467E-02	9.725E-06	8.462E-02	1.422E+52	8.467E-02
11	12.132	12.133	1.180E-03	2.481E-03	0.451	7.725E-01	5.480E-07	3.875E-03	4.449E-07	3.871E-03	6.506E+50	3.875E-03
12	12.110	12.132	2.169E-02	4.558E-02	0.478	8.187E-01	1.057E-05	7.472E-02	8.578E-06	7.464E-02	1.255E+52	7.472E-02
13	12.108	12.110	1.962E-03	4.124E-03	0.481	8.234E-01	1.005E-06	7.109E-03	8.159E-07	7.099E-03	1.194E+51	7.109E-03
14	12.088	12.108	1.987E-02	4.176E-02	0.506	8.658E-01	1.071E-05	7.575E-02	8.692E-06	7.563E-02	1.272E+52	7.575E-02
15	12.062	12.088	2.531E-02	5.319E-02	0.538	9.197E-01	1.487E-05	1.051E-01	1.206E-05	1.049E-01	1.765E+52	1.051E-01
16	12.047	12.062	1.491E-02	3.134E-02	0.556	9.518E-01	9.455E-06	6.686E-02	7.664E-06	6.669E-02	1.123E+52	6.686E-02
17	12.046	12.047	7.904E-04	1.661E-03	0.558	9.540E-01	5.273E-07	3.728E-03	4.273E-07	3.718E-03	6.260E+50	3.728E-03
18	12.039	12.046	6.300E-03	1.324E-02	0.566	9.679E-01	4.310E-06	3.048E-02	3.493E-06	3.039E-02	5.117E+51	3.048E-02
19	12.038	12.039	1.564E-03	3.288E-03	0.568	9.717E-01	1.101E-06	7.784E-03	8.921E-07	7.762E-03	1.307E+51	7.784E-03
20	12.027	12.037	9.956E-03	2.092E-02	0.581	9.933E-01	7.204E-06	5.094E-02	5.837E-06	5.079E-02	8.553E+51	5.094E-02
21	12.024	12.027	2.899E-03	6.093E-03	0.584	1.000E+00	2.160E-06	1.527E-02	1.750E-06	1.522E-02	2.564E+51	1.527E-02

Appendix E

Figures for $B_\star = 0$

Below are the Figures, like those in Subsections 5.4.3 - 5.4.13, for the models: SEMF, FRDM2012, WS4RBF, BSKG3, HFB31, DDMED, DDPC1, SVMIN and UNEDF0, individually, with magnetic field strength $B_\star = 0$.

E.1 P vs ϵ or n_b

E.1.1 SEMF

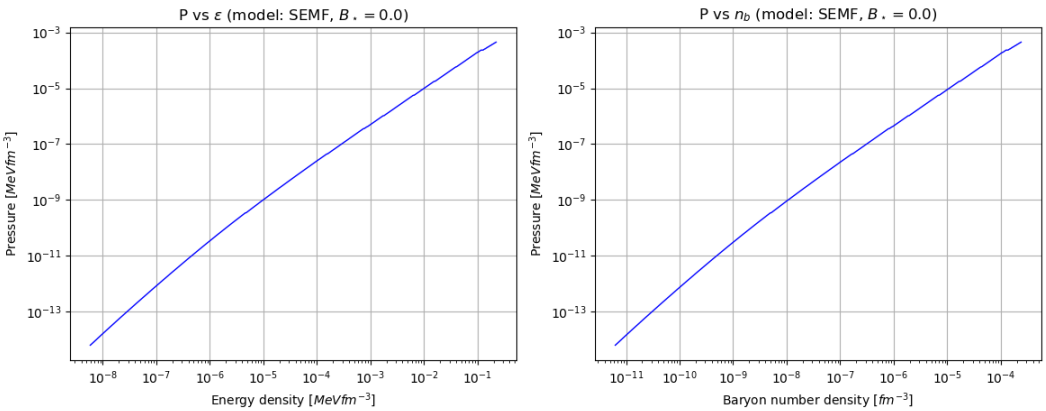

(a) (b)

Figure E.1: Equation of State, (a) pressure as a function of energy density and (b) pressure as a function of baryon number density, using the SEMF model with magnetic field strength $B_\star = 0$

E.1.2 FRDM2012

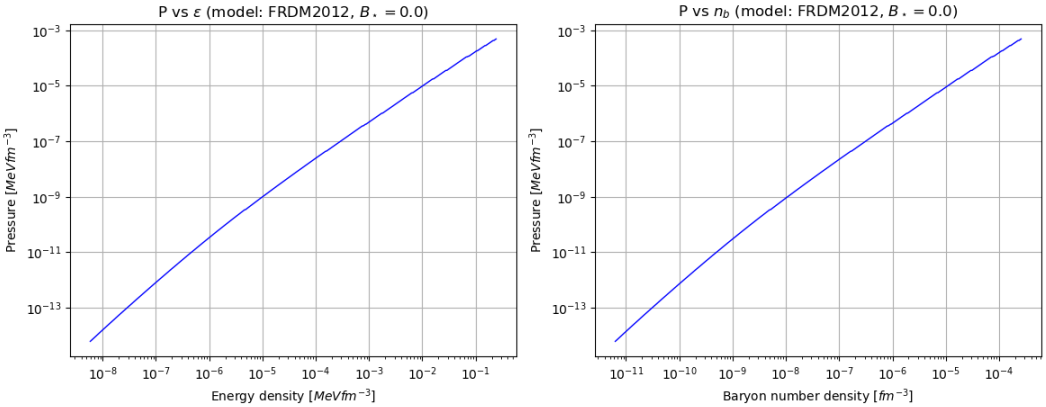

(a) (b)

Figure E.2: The same as Figure E.1, using the FRDM2012 model with $B_\star = 0$

E.1.3 WS4RBF

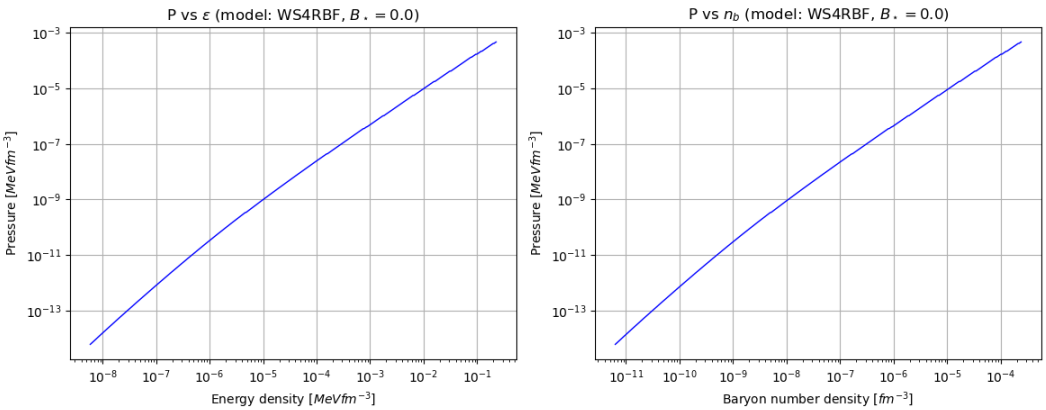

(a) (b)

Figure E.3: The same as Figure E.1, using the WS4RBF model with $B_\star = 0$

E.1.4 BSKG3

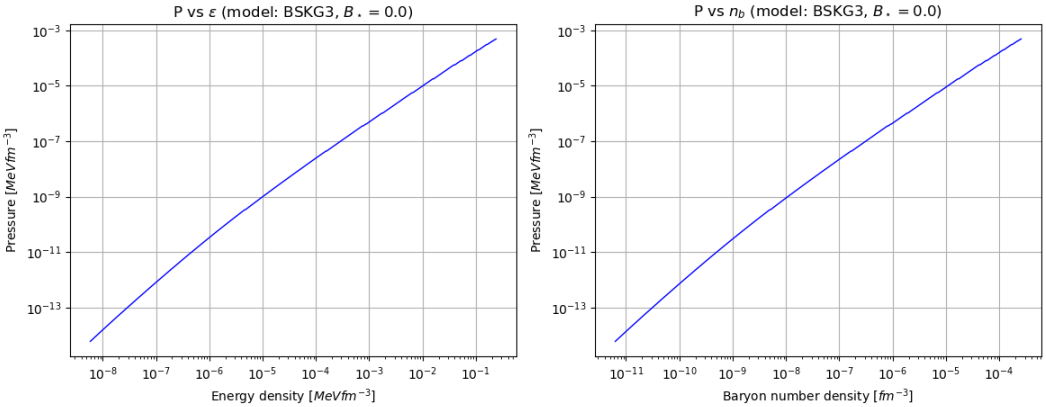

(a) (b)

Figure E.4: The same as Figure E.1, using the BSKG3 model with $B_\star = 0$

E.1.5 HFB31

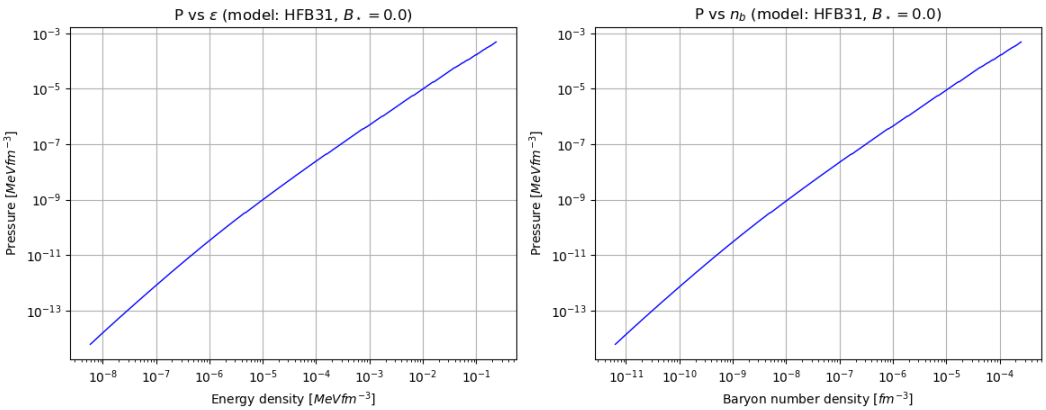

(a) (b)

Figure E.5: The same as Figure E.1, using the HFB31 model with $B_\star = 0$

E.1.6 DDMED

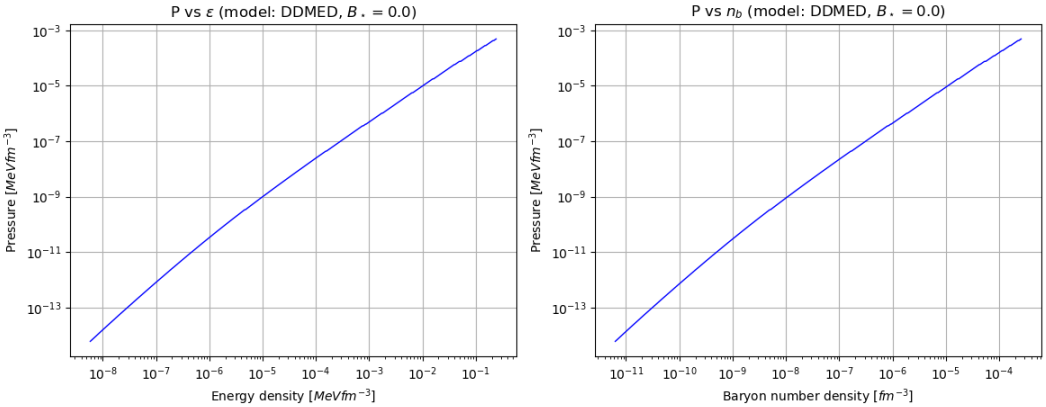

(a) (b)

Figure E.6: The same as Figure E.1, using the DDMED model with $B_\star = 0$

E.1.7 DDPC1

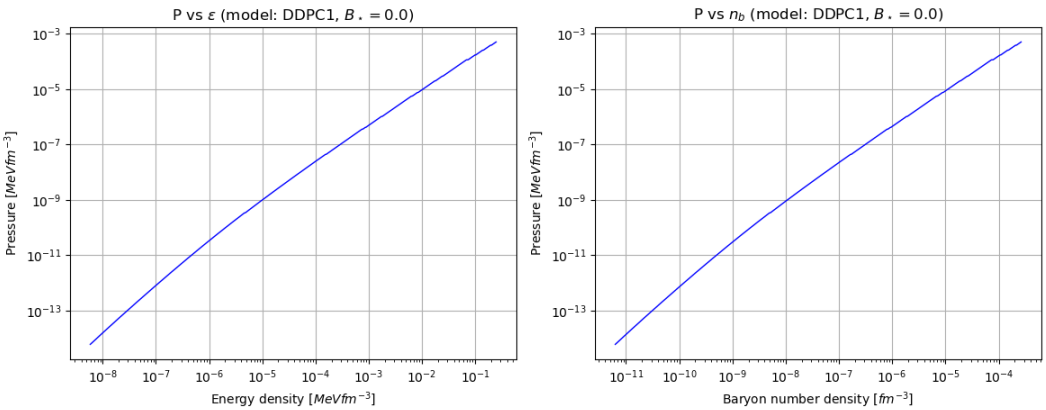

(a) (b)

Figure E.7: The same as Figure E.1, using the DDPC1 model with $B_\star = 0$

E.1.8 SVMIN

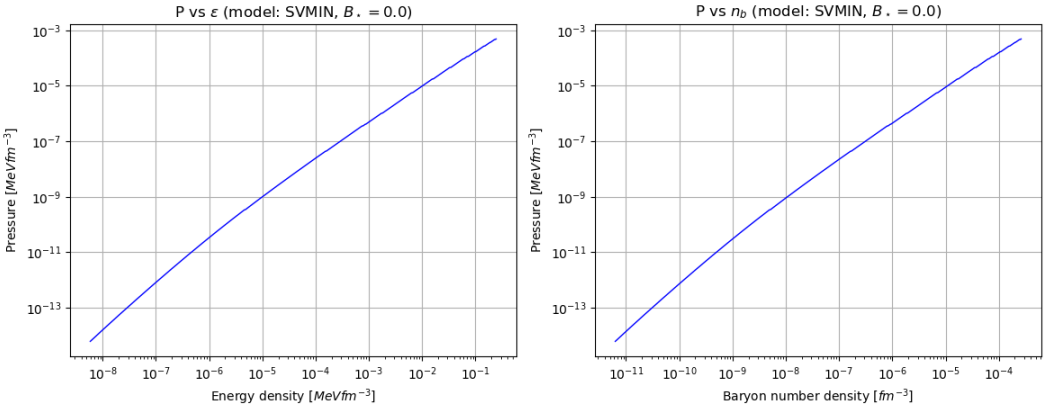

(a) (b)

Figure E.8: The same as Figure E.1, using the SVMIN model with $B_\star = 0$

E.1.9 UNEDF0

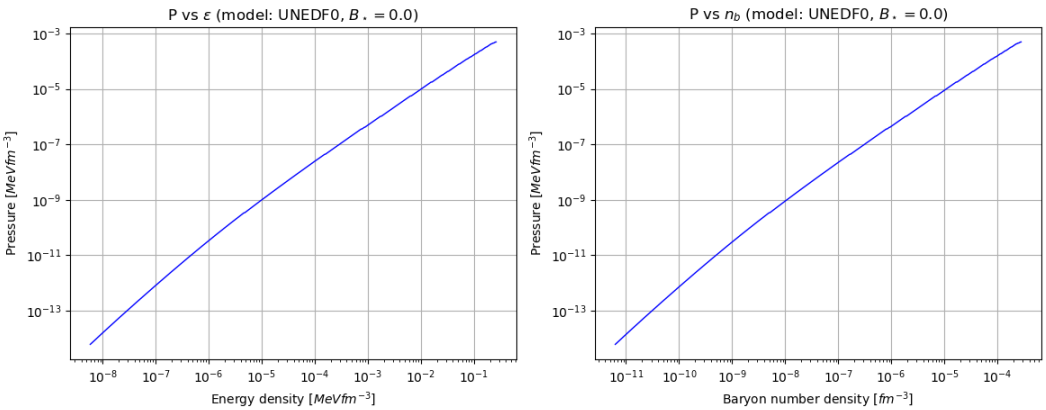

(a) (b)

Figure E.9: The same as Figure E.1, using the UNEDF0 model with $B_\star = 0$

E.2 Fitting $P = K\epsilon^G$

E.2.1 WS4RBF

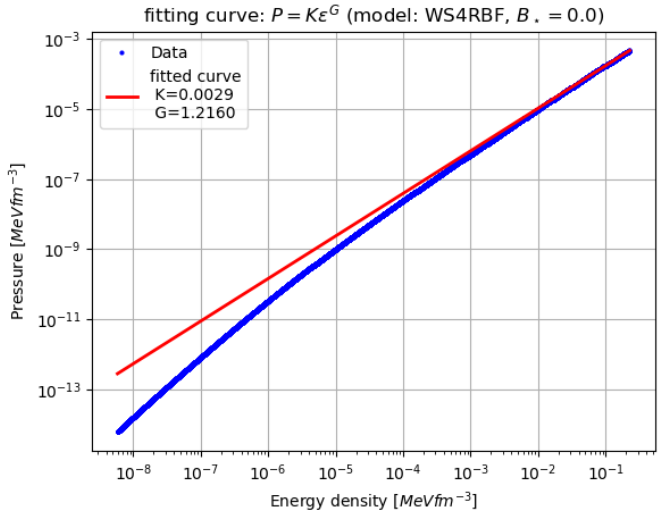

Figure E.10: The same as Figure 5.1, using the WS4RBF model with $B_\star = 0$

E.2.2 BSKG3

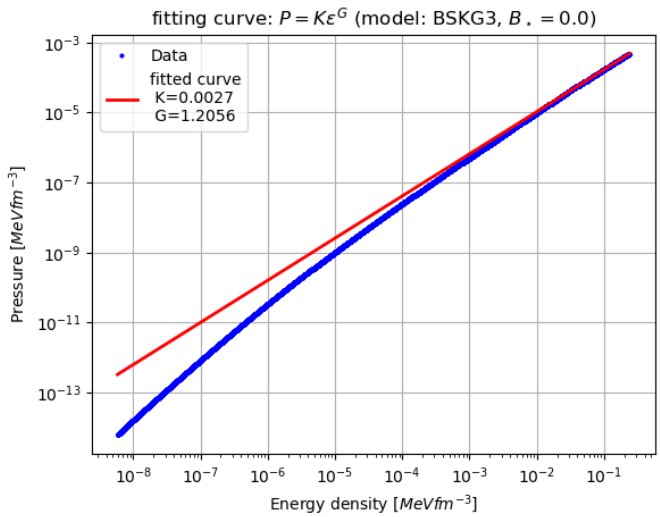

Figure E.11: The same as Figure 5.1, using the BSKG3 model with $B_\star = 0$

E.2.3 HFB31

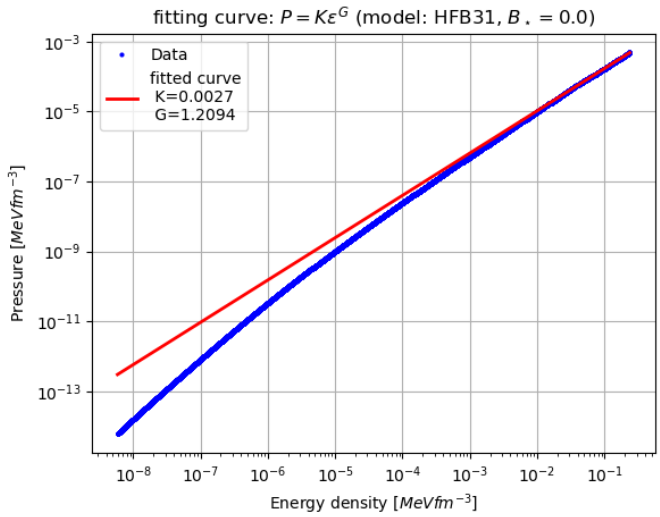

Figure E.12: The same as Figure 5.1, using the HFB31 model with $B_\star = 0$

E.2.4 DDMED

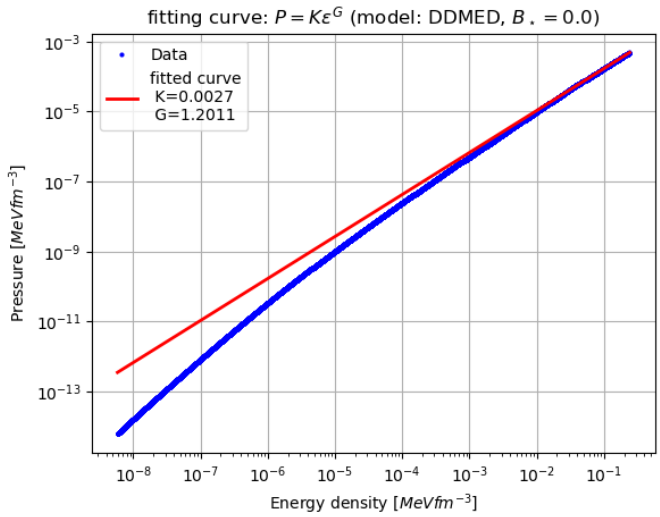

Figure E.13: The same as Figure 5.1, using the DDMED model with $B_\star = 0$

E.2.5 DDPC1

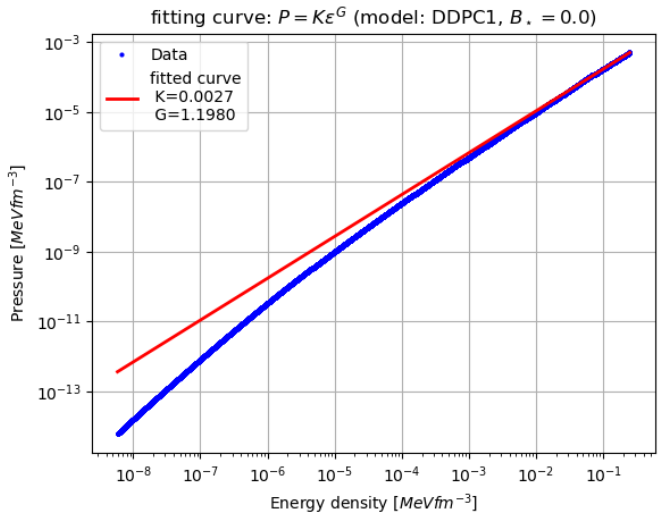

Figure E.14: The same as Figure 5.1, using the DDPC1 model with $B_\star = 0$

E.2.6 SVMIN

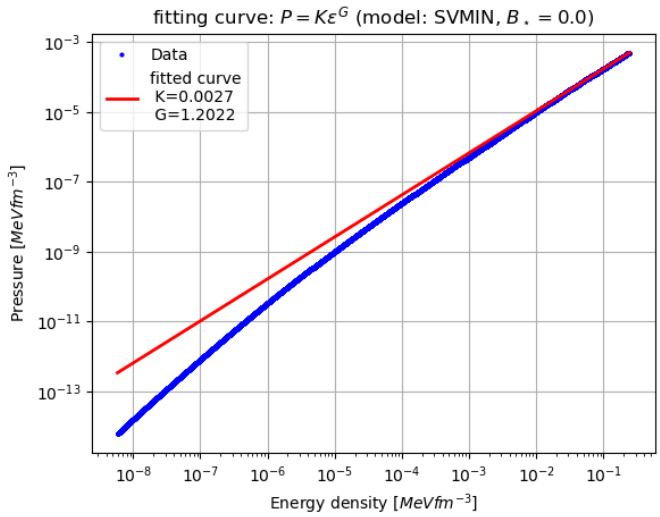

Figure E.15: The same as Figure 5.1, using the SVMIN model with $B_\star = 0$

E.2.7 UNEDF0

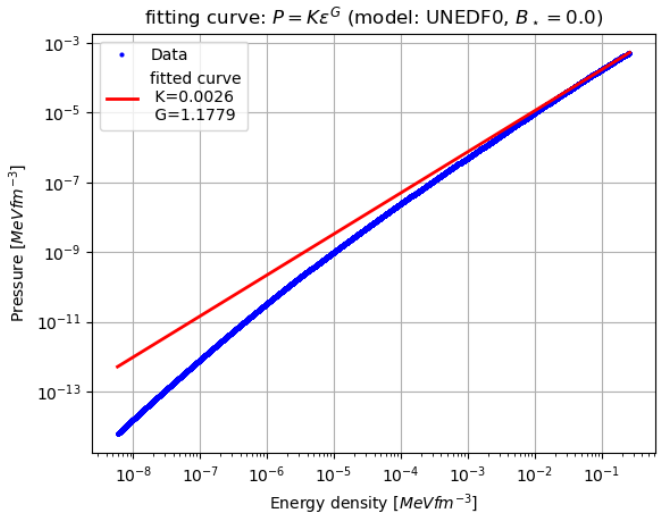

Figure E.16: The same as Figure 5.1, using the UNEDF0 model with $B_\star = 0$

E.3 Γ vs ϵ or n_b

E.3.1 SEMF

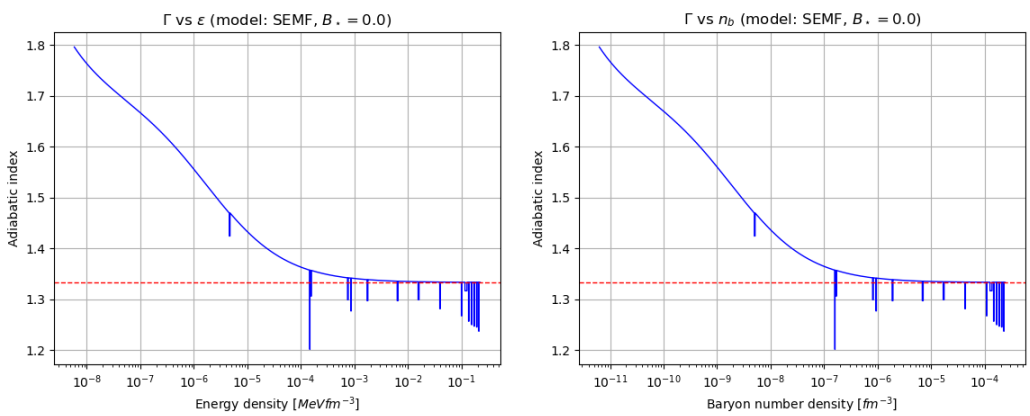

(a) (b)

Figure E.17: Adiabatic index as a function of (a) energy density and of (b) baryon number density, using the SEMF model with magnetic field strength $B_\star = 0$. The horizontal dashed line corresponds to $\Gamma = 4/3$

E.3.2 FRDM2012

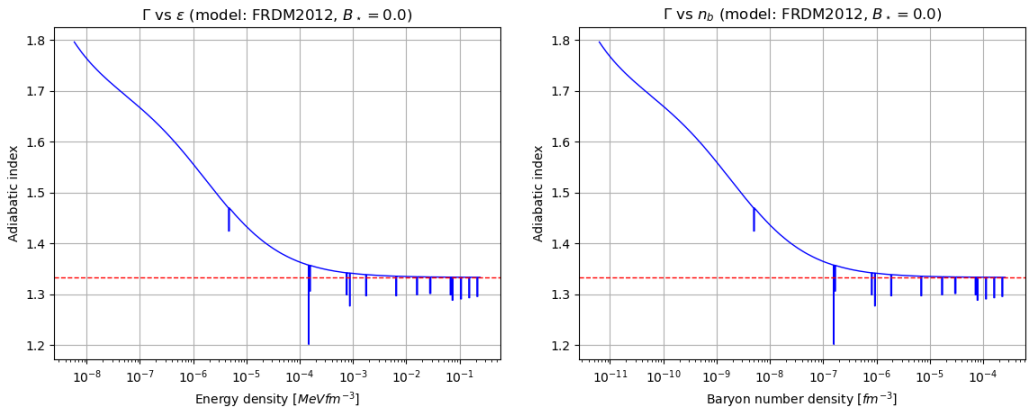

(a) (b)

Figure E.18: The same as Figure E.17, using the FRDM2012 model with $B_\star = 0$

E.3.3 WS4RBF

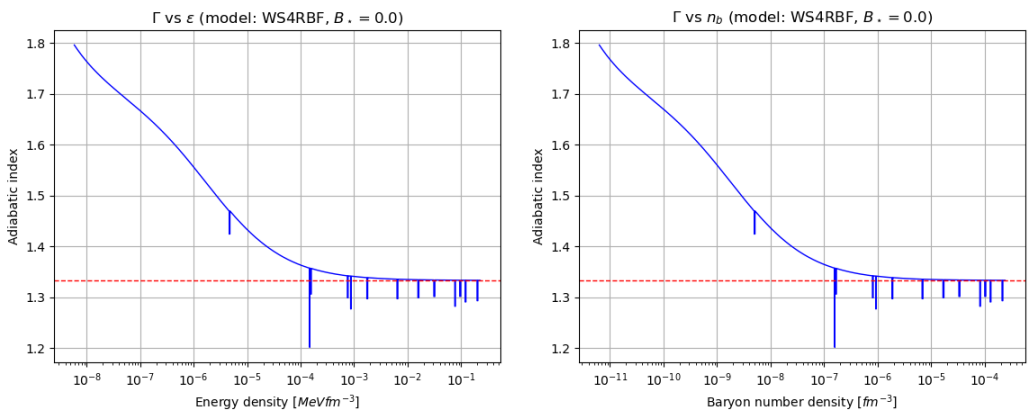

(a) (b)

Figure E.19: The same as Figure E.17, using the WS4RBF model with $B_\star = 0$

E.3.4 BSKG3

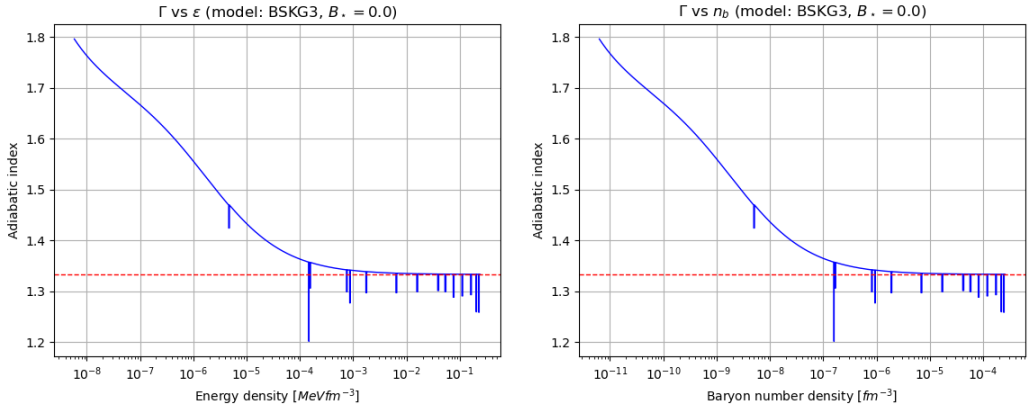

(a) (b)

Figure E.20: The same as Figure E.17, using the BSKG3 model with $B_\star = 0$

E.3.5 HFB31

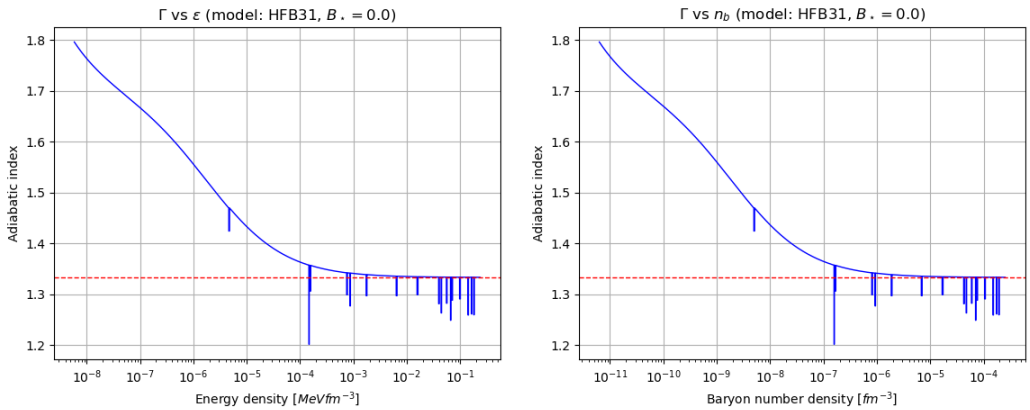

(a) (b)

Figure E.21: The same as Figure E.17, using the HFB31 model with $B_\star = 0$

E.3.6 DDMED

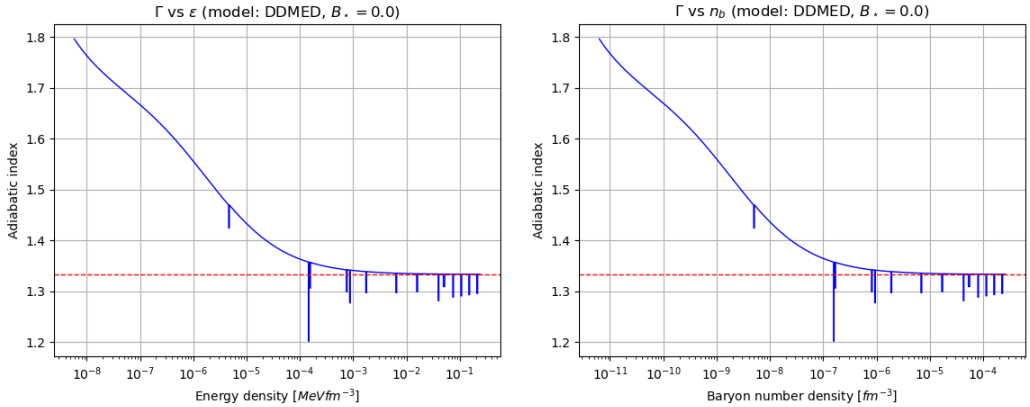

(a) (b)

Figure E.22: The same as Figure E.17, using the DDMED model with $B_\star = 0$

E.3.7 DDPC1

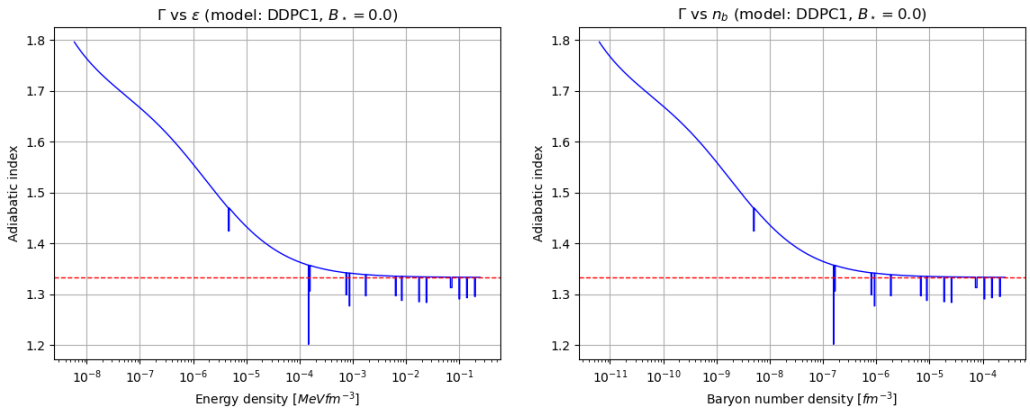

(a) (b)

Figure E.23: The same as Figure E.17, using the DDPC1 model with $B_\star = 0$

E.3.8 SVMIN

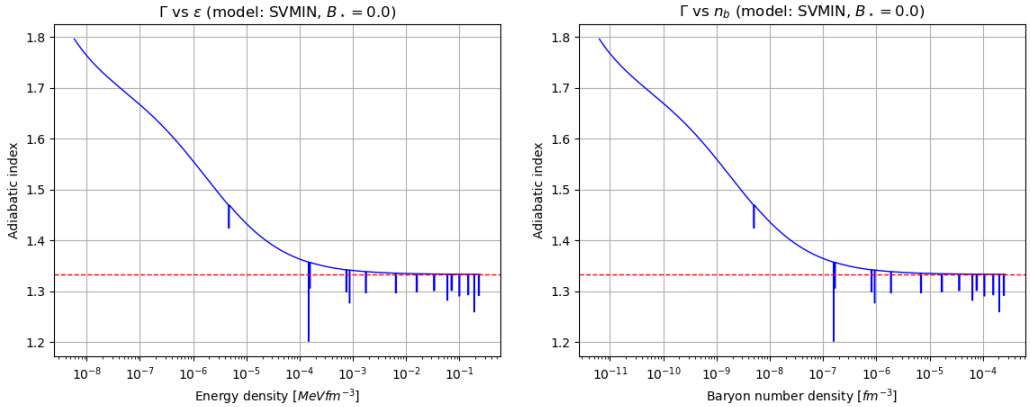

(a) (b)

Figure E.24: The same as Figure E.17, using the SVMIN model with $B_\star = 0$

E.3.9 UNEDF0

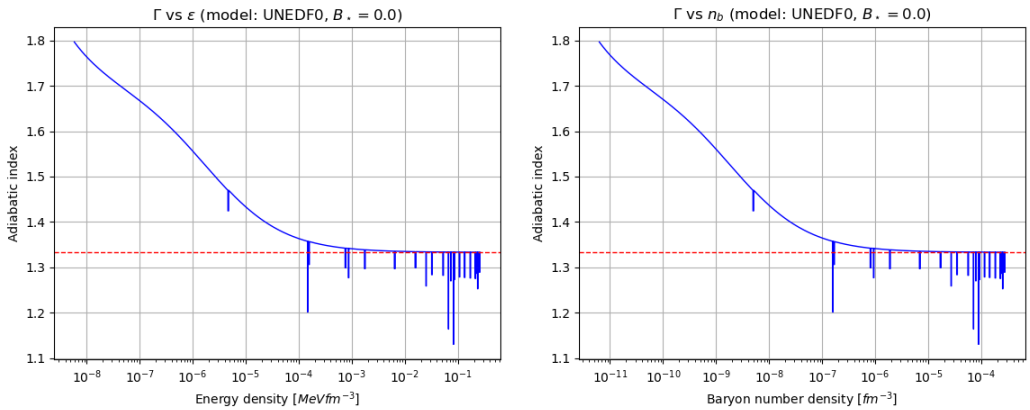

(a) (b)

Figure E.25: The same as Figure E.17, using the UNEDF0 model with $B_\star = 0$

E.4 c_s vs ϵ or n_b

E.4.1 SEMF

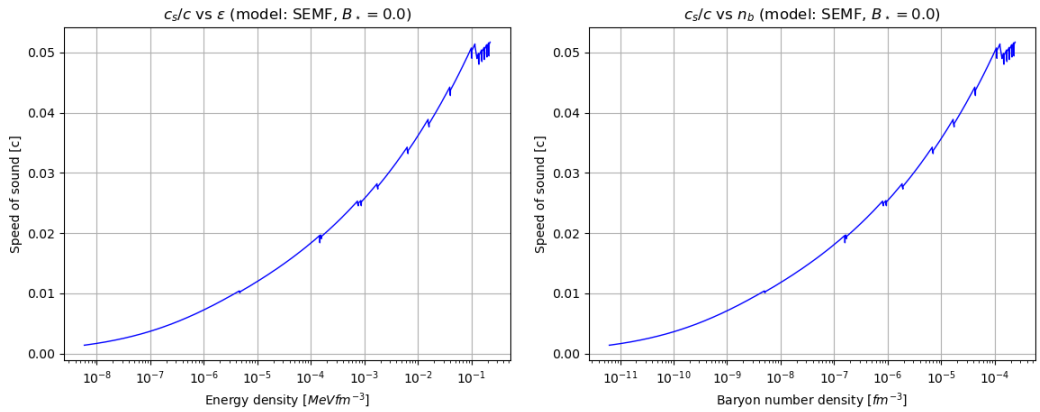

(a) (b)

Figure E.26: Speed of sound as a function of (a) energy density and of (b) baryon number density, using the SEMF model with magnetic field strength $B_\star = 0$

E.4.2 FRDM2012

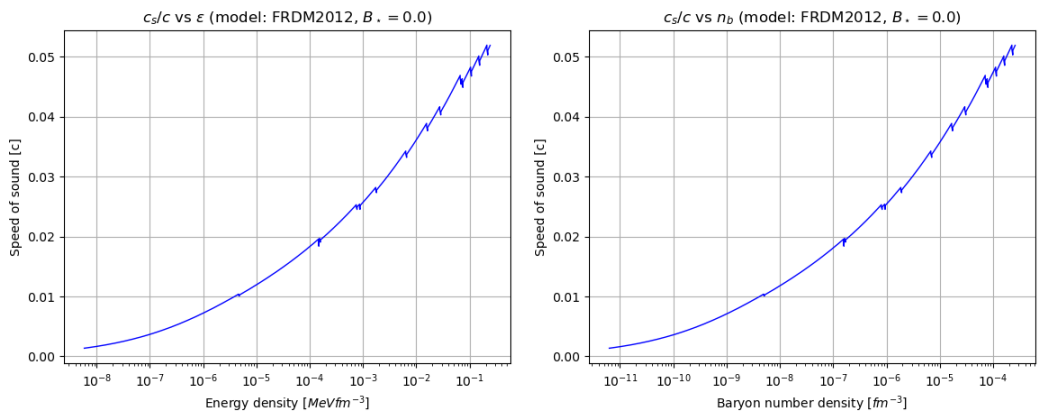

(a) (b)

Figure E.27: The same as Figure E.26, using the FRDM2012 model with $B_\star = 0$

E.4.3 WS4RBF

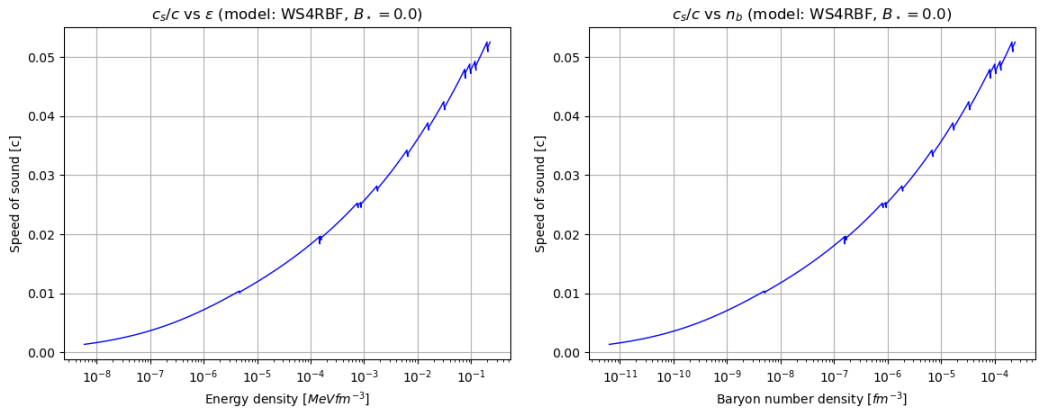

(a) (b)

Figure E.28: The same as Figure E.26, using the WS4RBF model with $B_\star = 0$

E.4.4 BSKG3

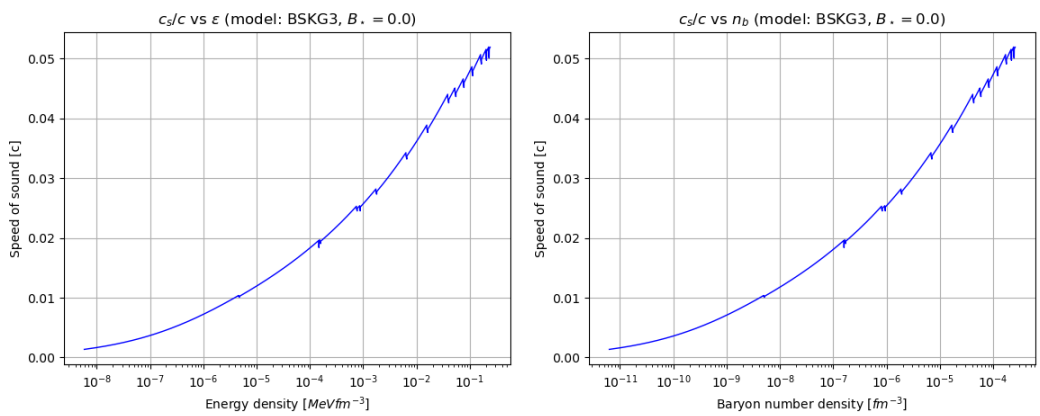

(a) (b)

Figure E.29: The same as Figure E.26, using the BSKG3 model with $B_\star = 0$

E.4.5 HFB31

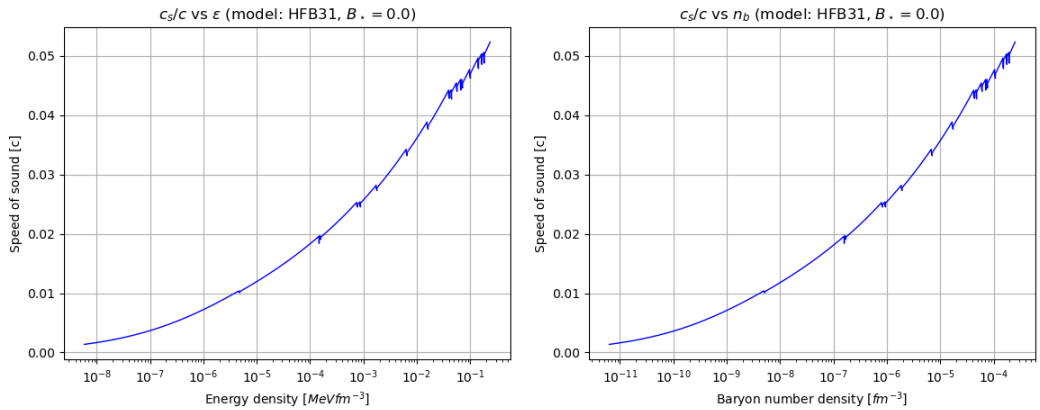

(a) (b)

Figure E.30: The same as Figure E.26, using the HFB31 model with $B_\star = 0$

E.4.6 DDMED

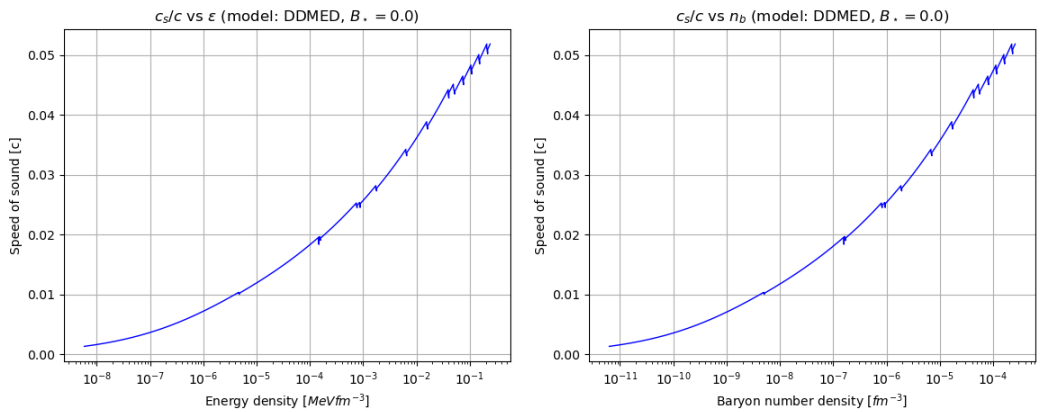

(a) (b)

Figure E.31: The same as Figure E.26, using the DDMED model with $B_\star = 0$

E.4.7 DDPC1

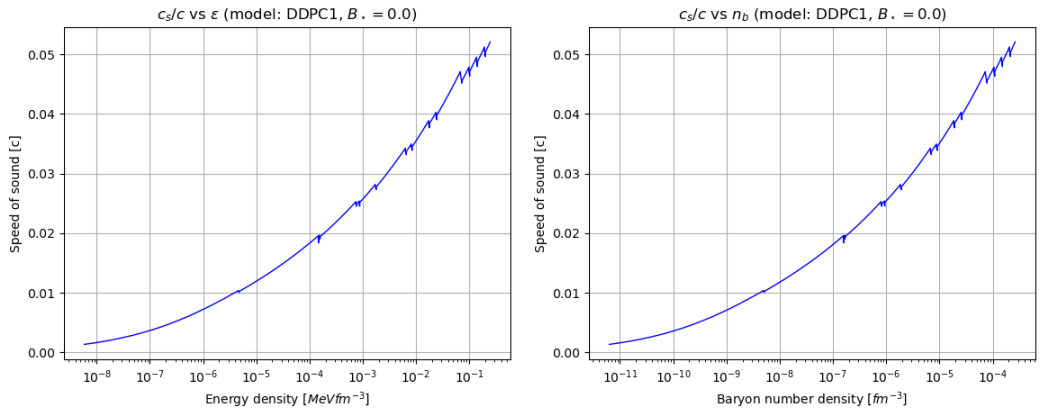

(a) (b)

Figure E.32: The same as Figure E.26, using the DDPC1 model with $B_\star = 0$

E.4.8 SVMIN

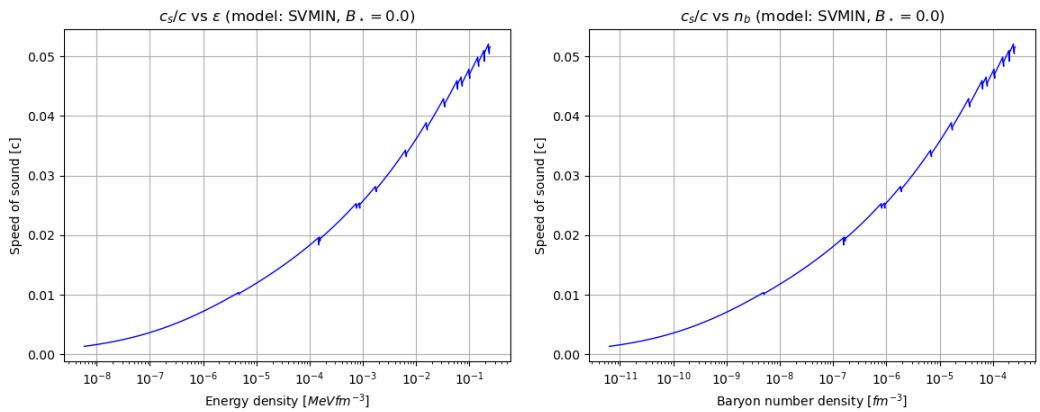

(a) (b)

Figure E.33: The same as Figure E.26, using the SVMIN model with $B_\star = 0$

E.4.9 UNEDF0

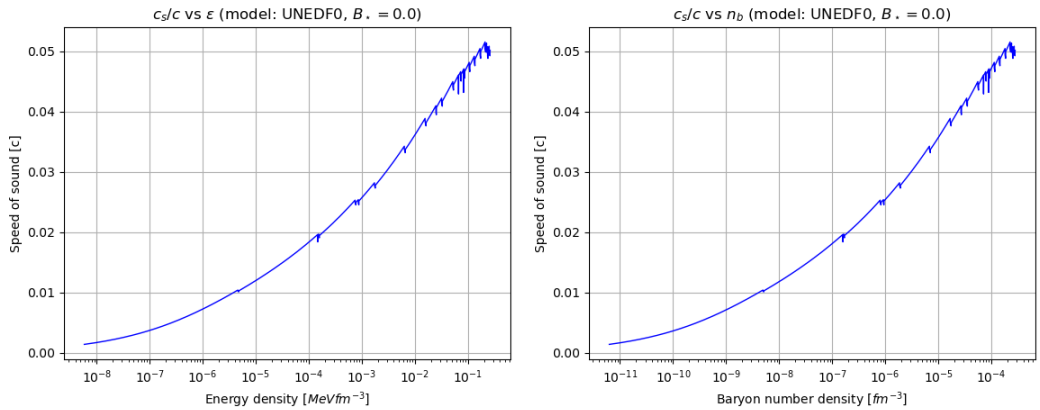

(a) (b)

Figure E.34: The same as Figure E.26, using the UNEDF0 model with $B_\star = 0$

E.5 K_{mod} vs ϵ or n_b

E.5.1 SEMF

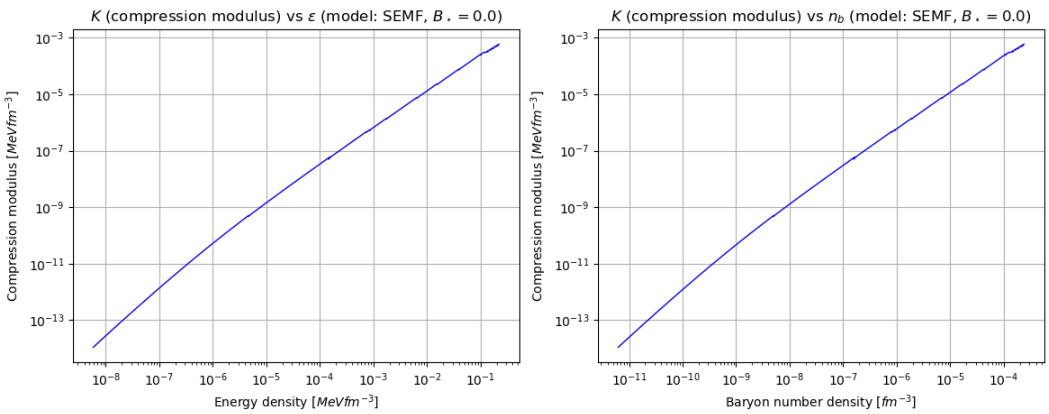

(a) (b)

Figure E.35: Compression modulus as a function of (a) energy density and of (b) baryon number density, using the SEMF model with magnetic field strength $B_\star = 0$

E.5.2 FRDM2012

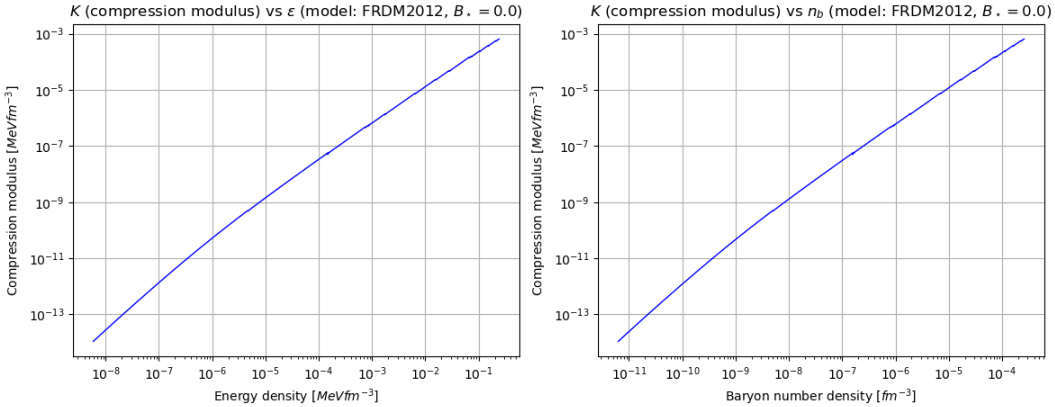

(a) (b)

Figure E.36: The same as Figure E.35, using the FRDM2012 model with $B_\star = 0$

E.5.3 WS4RBF

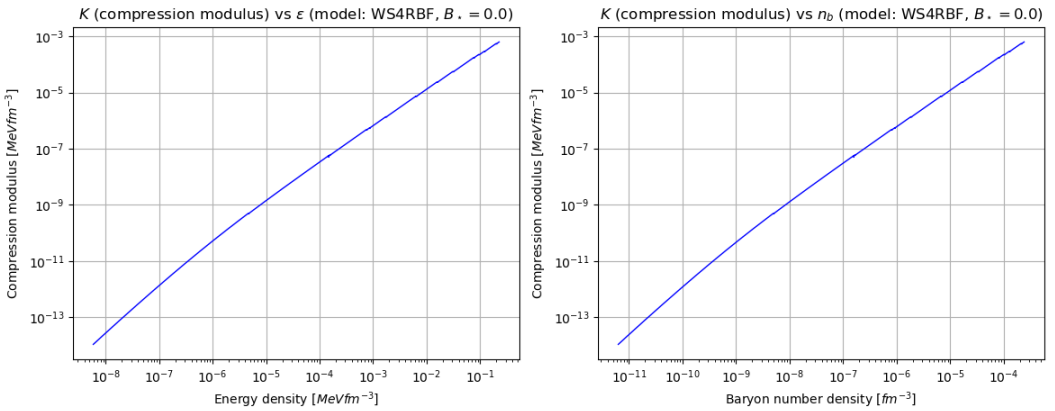

(a) (b)

Figure E.37: The same as Figure E.35, using the WS4RBF model with $B_\star = 0$

E.5.4 BSKG3

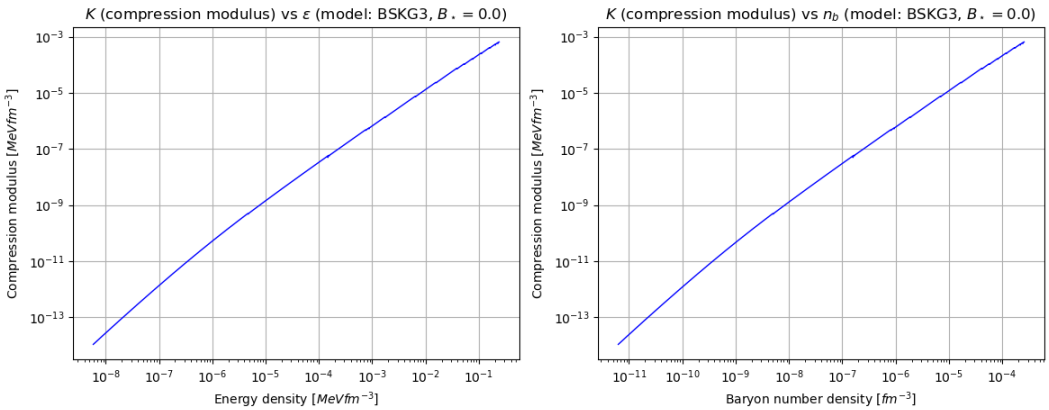

(a) (b)

Figure E.38: The same as Figure E.35, using the BSKG3 model with $B_\star = 0$

E.5.5 HFB31

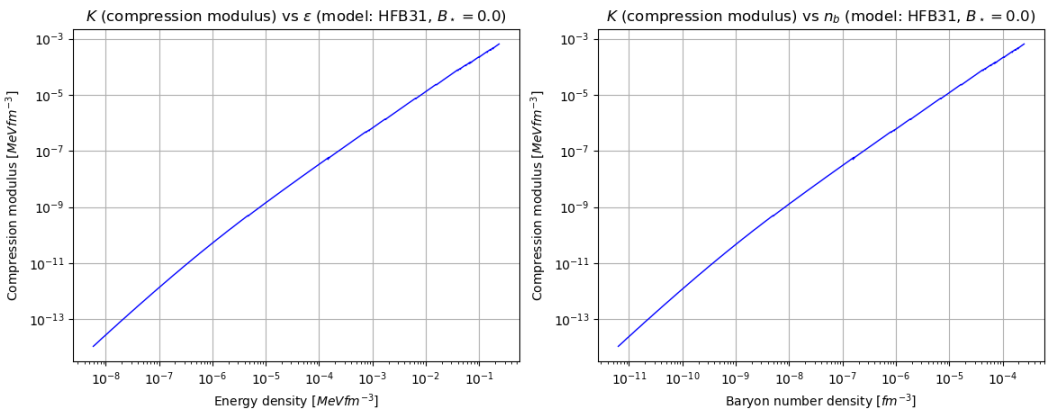

(a) (b)

Figure E.39: The same as Figure E.35, using the HFB31 model with $B_\star = 0$

E.5.6 DDMED

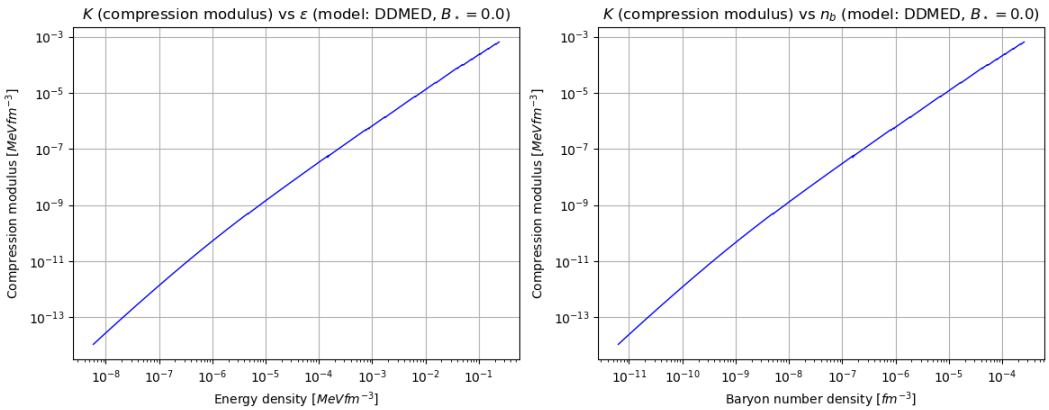

(a) (b)

Figure E.40: The same as Figure E.35, using the DDMED model with $B_\star = 0$

E.5.7 DDPC1

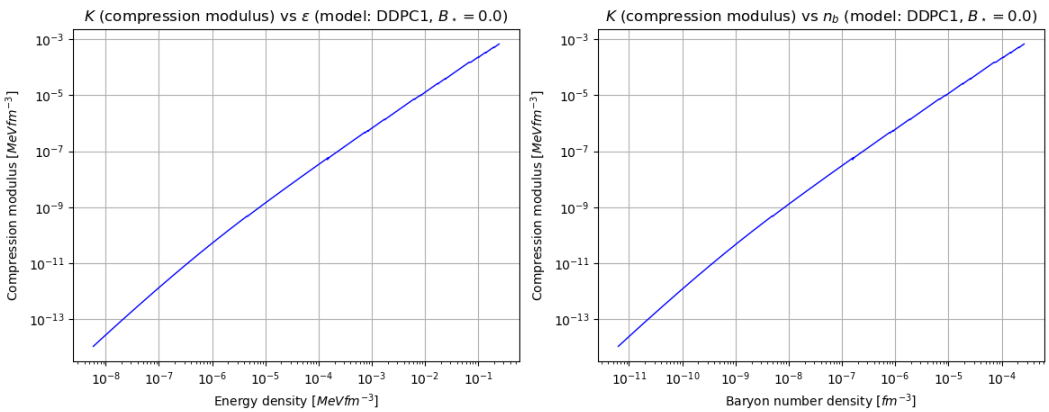

(a) (b)

Figure E.41: The same as Figure E.35, using the DDPC1 model with $B_\star = 0$

E.5.8 SVMIN

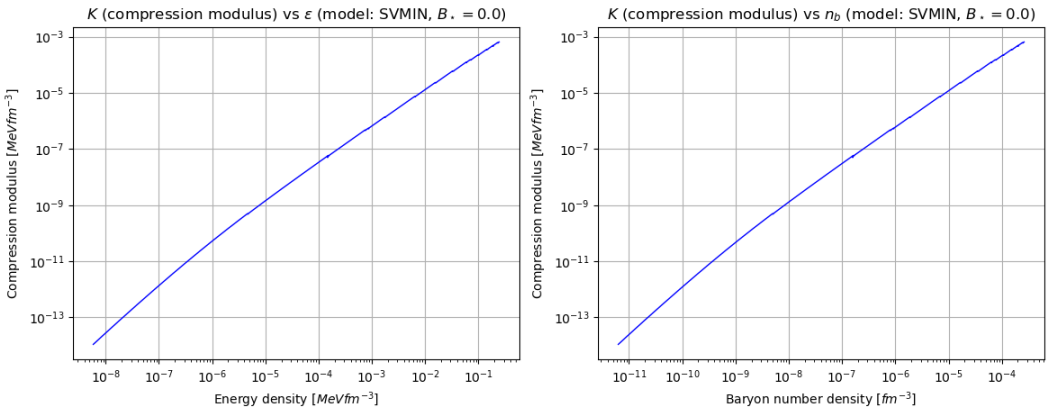

(a) (b)

Figure E.42: The same as Figure E.35, using the SVMIN model with $B_\star = 0$

E.5.9 UNEDF0

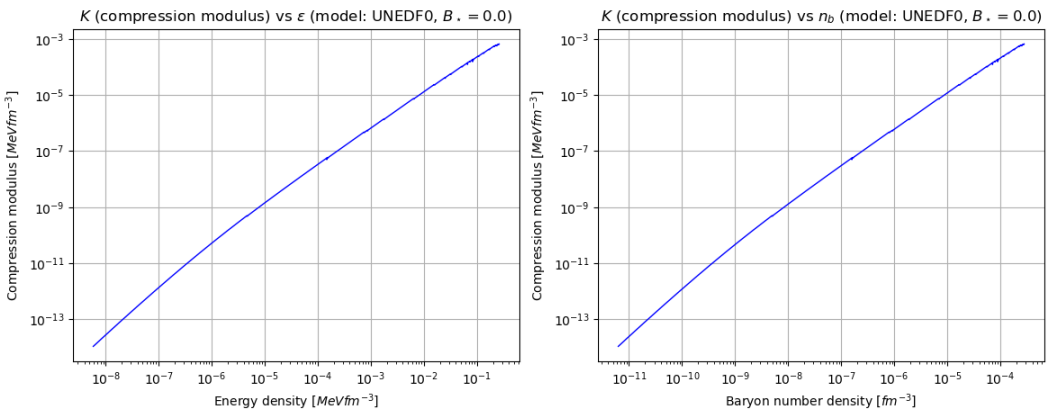

(a) (b)

Figure E.43: The same as Figure E.35, using the UNEDF0 model with $B_\star = 0$

E.6 S_{mod} vs ϵ or n_b

E.6.1 SEMF

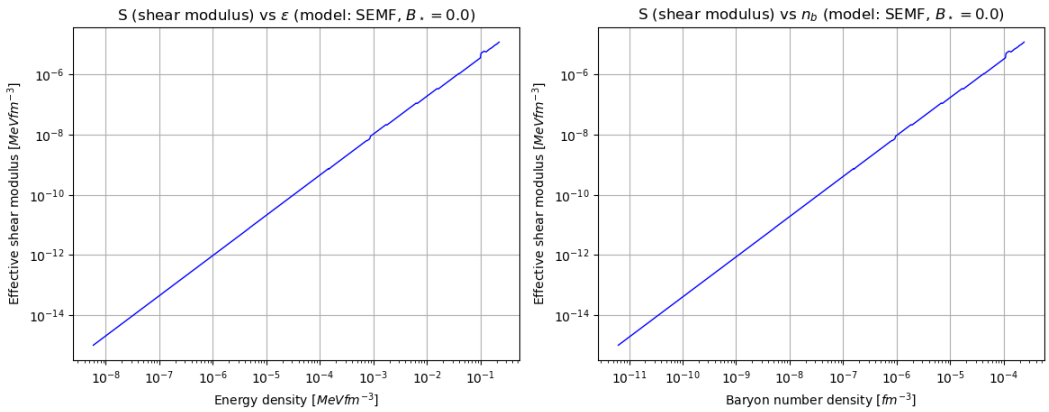

(a) (b)

Figure E.44: Effective shear modulus as a function of (a) energy density and of (b) baryon number density, using the SEMF model with magnetic field strength $B_\star = 0$

E.6.2 FRDM2012

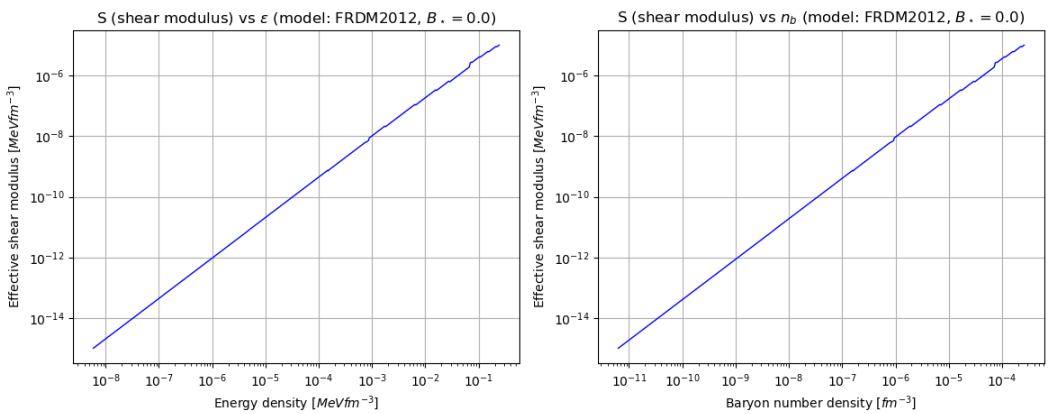

(a) (b)

Figure E.45: The same as Figure E.44, using the FRDM2012 model with $B_\star = 0$

E.6.3 WS4RBF

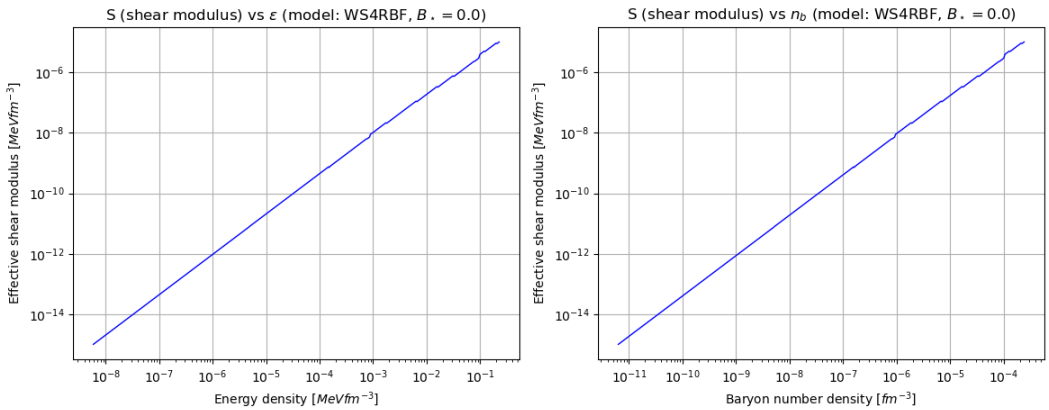

(a) (b)

Figure E.46: The same as Figure E.44, using the WS4RBF model with $B_\star = 0$

E.6.4 BSKG3

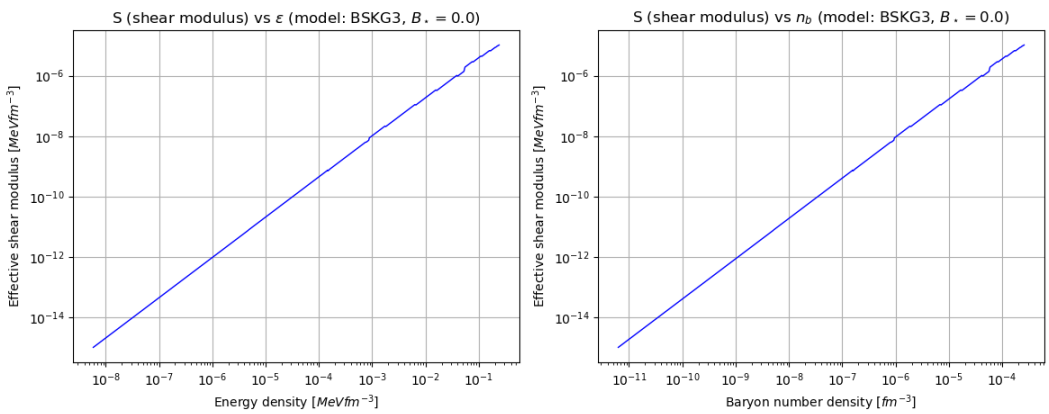

(a) (b)

Figure E.47: The same as Figure E.44, using the BSKG3 model with $B_\star = 0$

E.6.5 HFB31

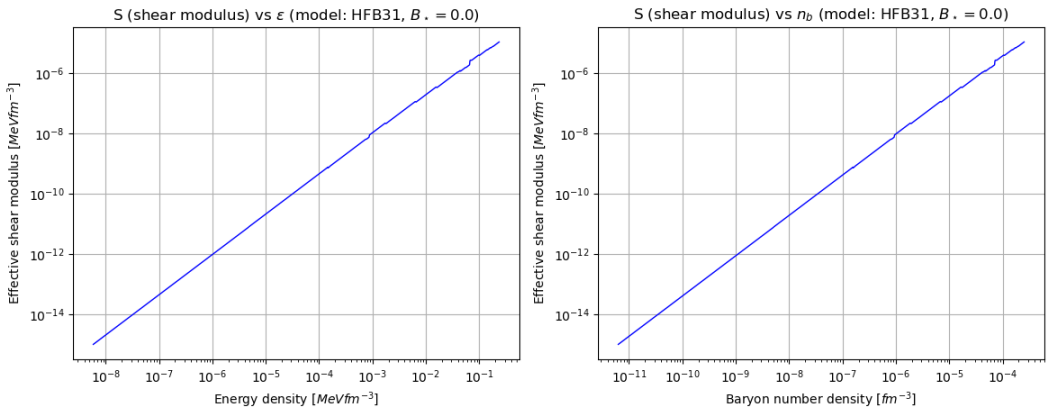

(a) (b)

Figure E.48: The same as Figure E.44, using the HFB31 model with $B_\star = 0$

E.6.6 DDMED

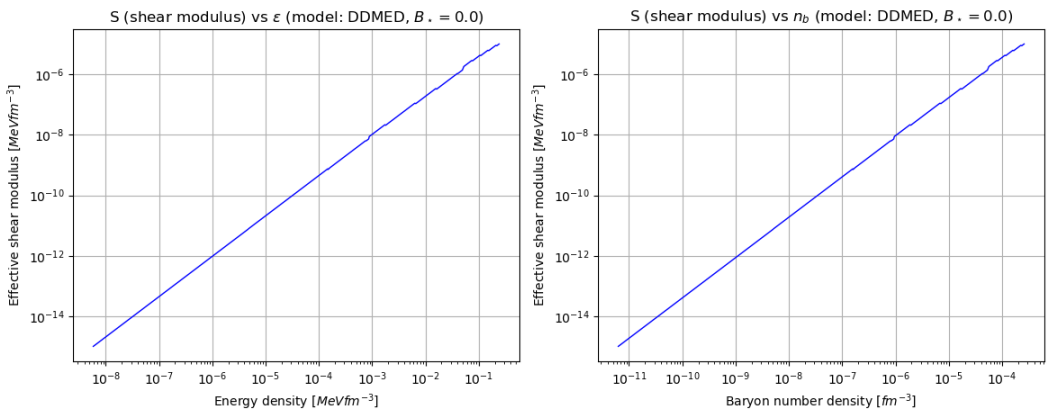

(a) (b)

Figure E.49: The same as Figure E.44, using the DDMED model with $B_\star = 0$

E.6.7 DDPC1

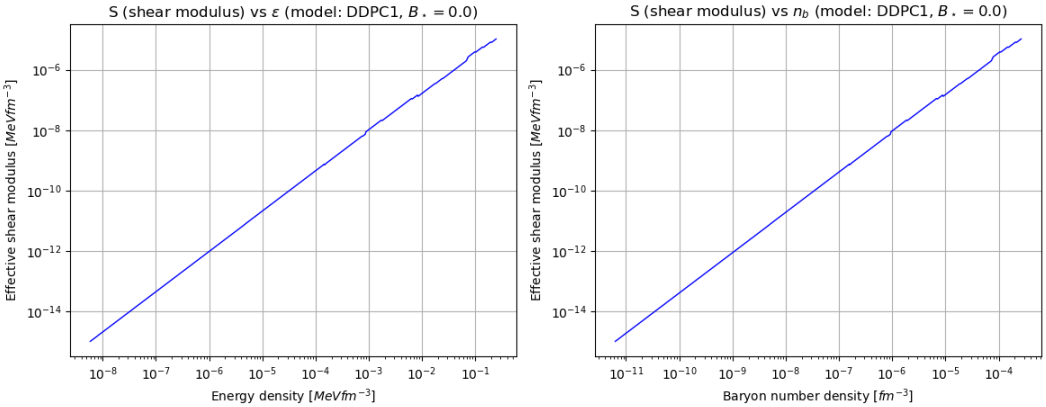

(a) (b)

Figure E.50: The same as Figure E.44, using the DDPC1 model with $B_\star = 0$

E.6.8 SVMIN

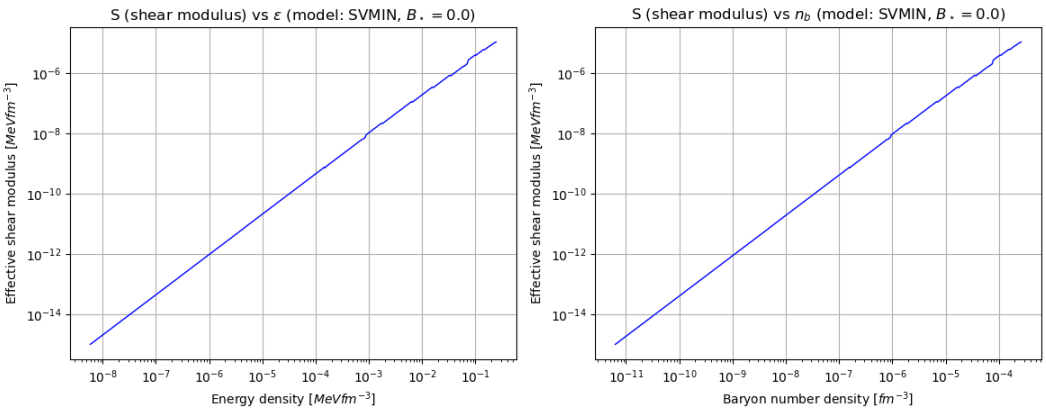

(a) (b)

Figure E.51: The same as Figure E.44, using the SVMIN model with $B_\star = 0$

E.6.9 UNEDF0

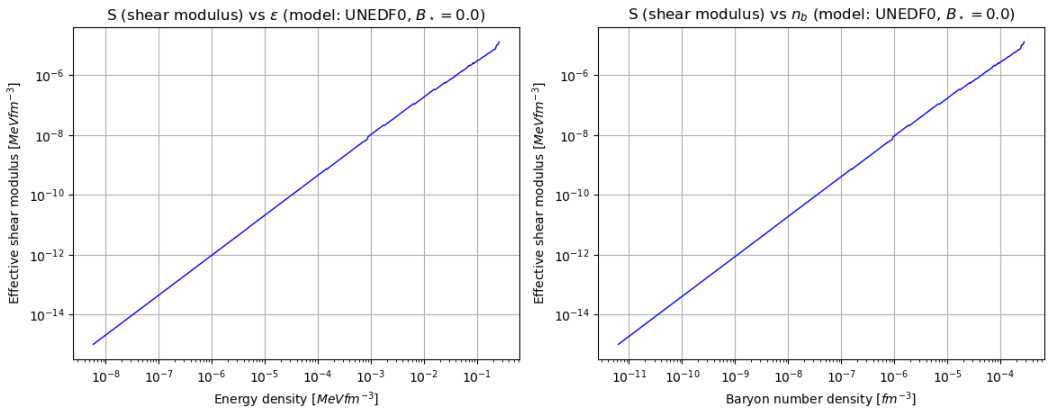

(a) (b)

Figure E.52: The same as Figure E.44, using the UNEDF0 model with $B_\star = 0$

E.7 S_{mod}/K_{mod} vs ϵ or n_b

E.7.1 SEMF

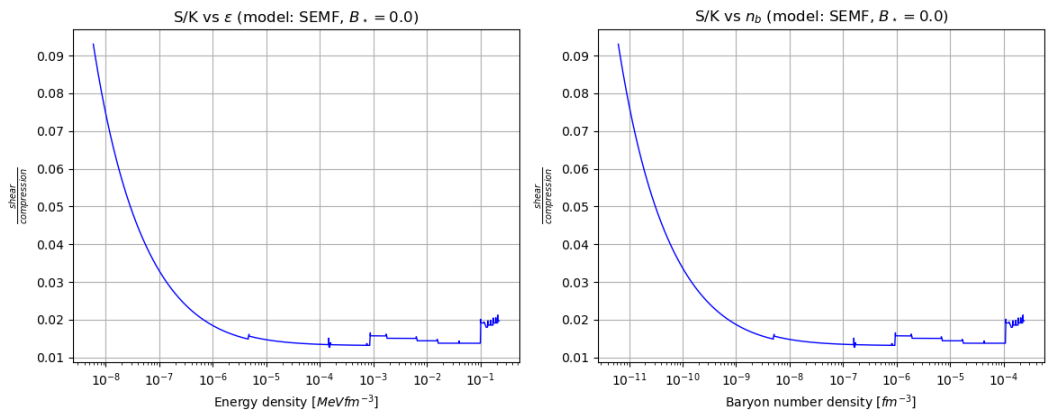

(a) (b)

Figure E.53: Effective shear modulus over compression modulus as a function of (a) energy density and of (b) baryon number density, using the SEMF model with magnetic field strength $B_\star = 0$

E.7.2 FRDM2012

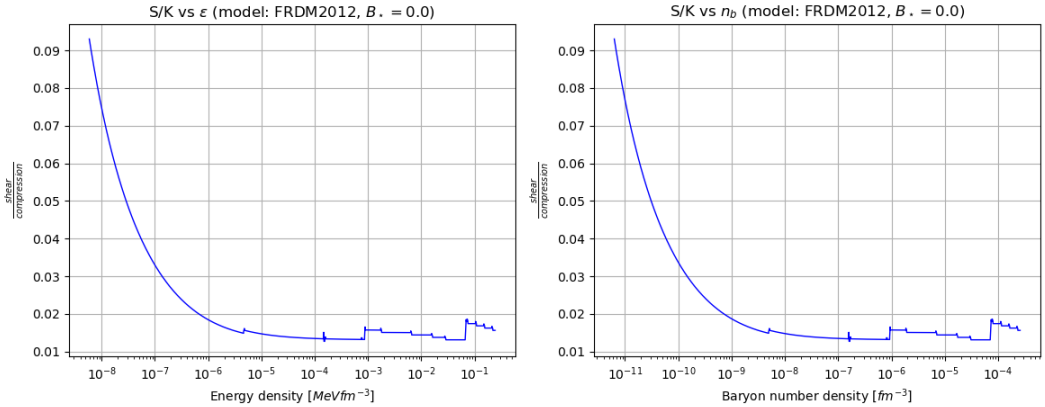

(a) (b)

Figure E.54: The same as Figure E.53, using the FRDM2012 model with $B_\star = 0$

E.7.3 WS4RBF

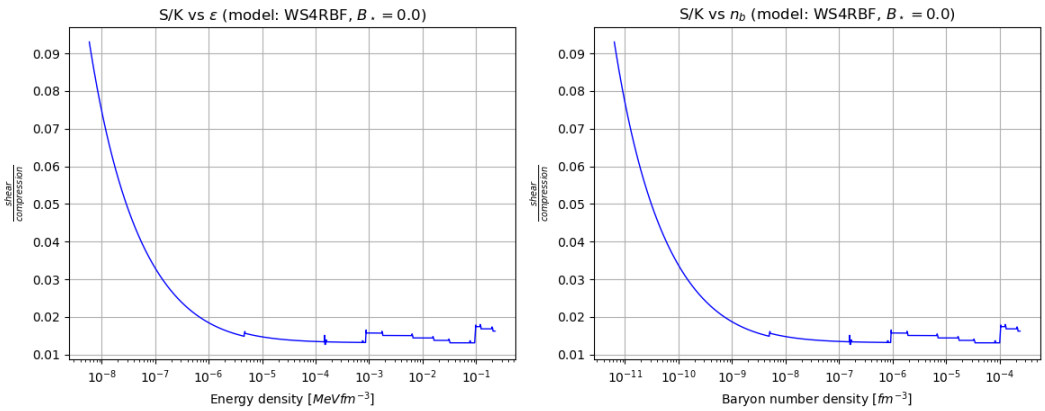

(a) (b)

Figure E.55: The same as Figure E.53, using the WS4RBF model with $B_\star = 0$

E.7.4 BSKG3

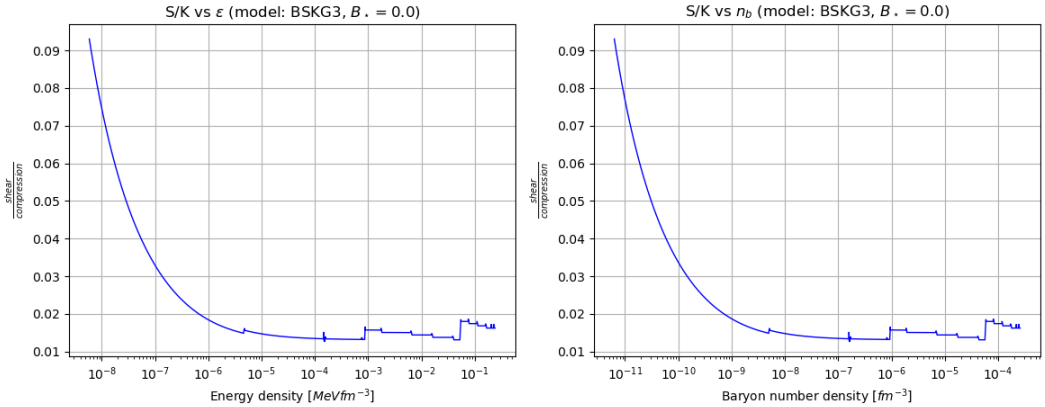

(a) (b)

Figure E.56: The same as Figure E.53, using the BSKG3 model with $B_\star = 0$

E.7.5 HFB31

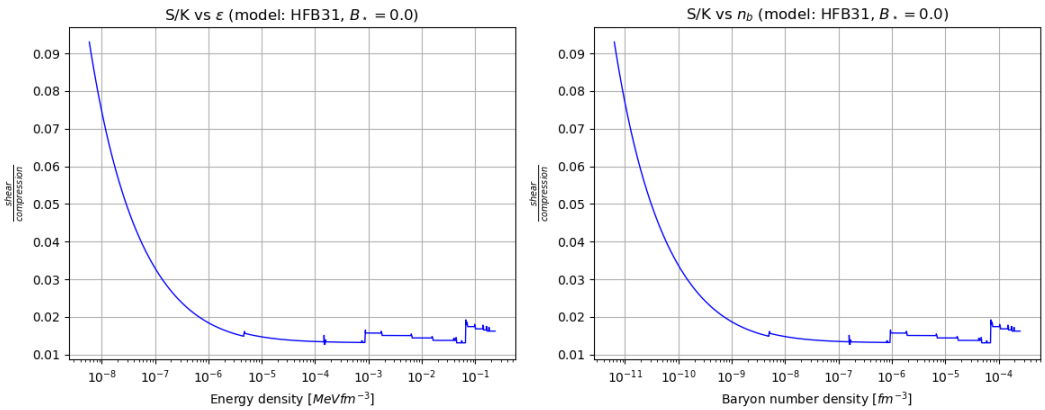

(a) (b)

Figure E.57: The same as Figure E.53, using the HFB31 model with $B_\star = 0$

E.7.6 DDMED

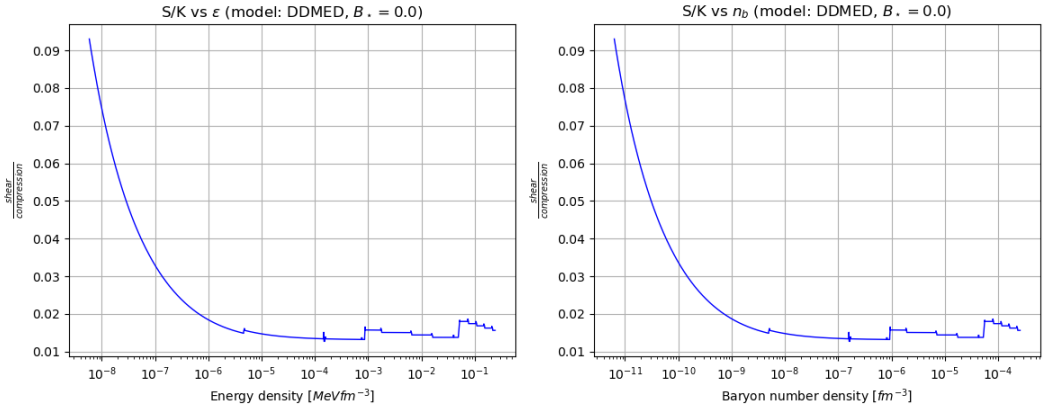

(a) (b)

Figure E.58: The same as Figure E.53, using the DDMED model with $B_\star = 0$

E.7.7 DDPC1

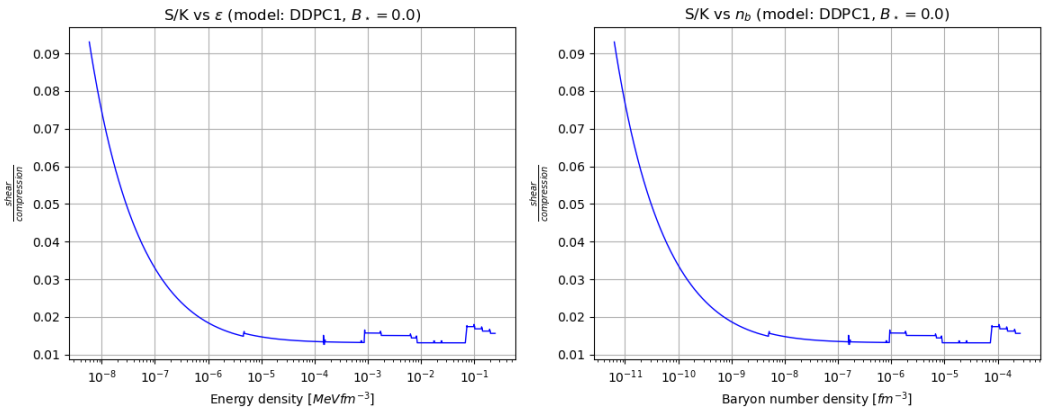

(a) (b)

Figure E.59: The same as Figure E.53, using the DDPC1 model with $B_\star = 0$

E.7.8 SVMIN

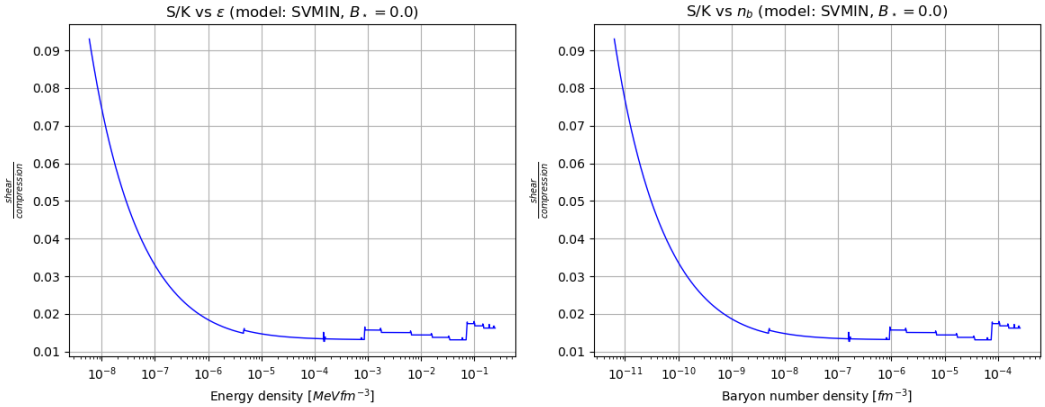

(a) (b)

Figure E.60: The same as Figure E.53, using the SVMIN model with $B_\star = 0$

E.7.9 UNEDF0

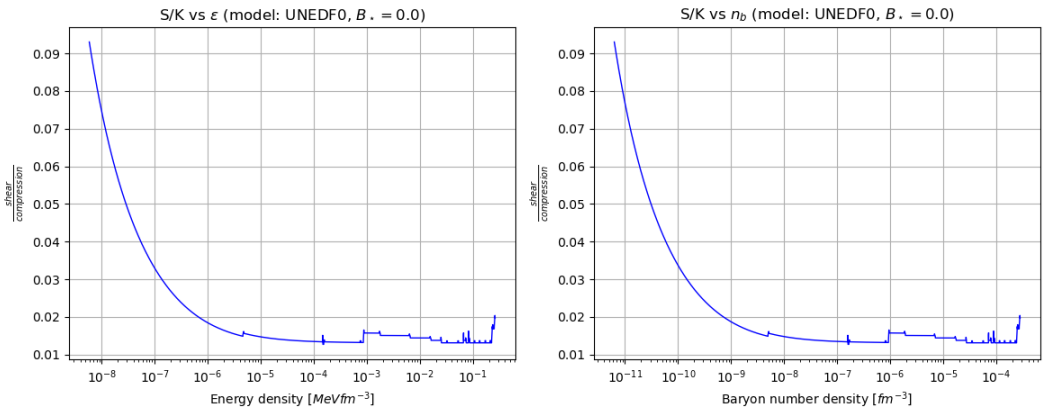

(a) (b)

Figure E.61: The same as Figure E.53, using the UNEDF0 model with $B_\star = 0$

E.8 Z, N, Z/A vs ϵ or n_b

E.8.1 SEMF

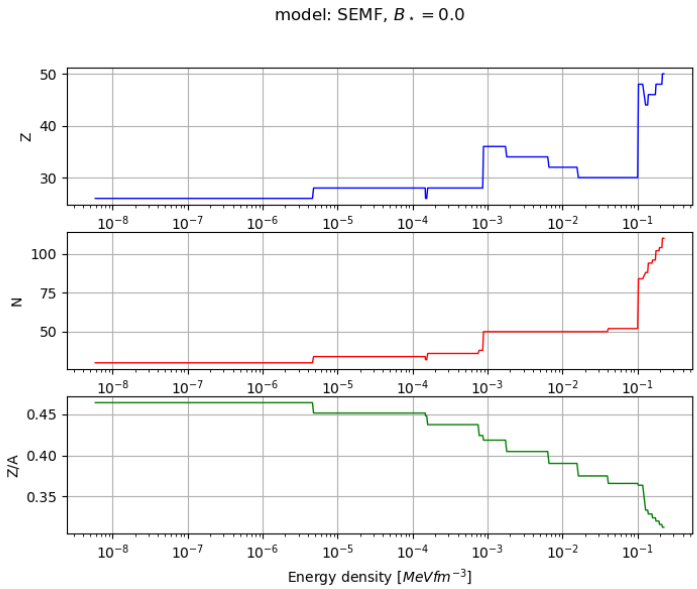

(a)

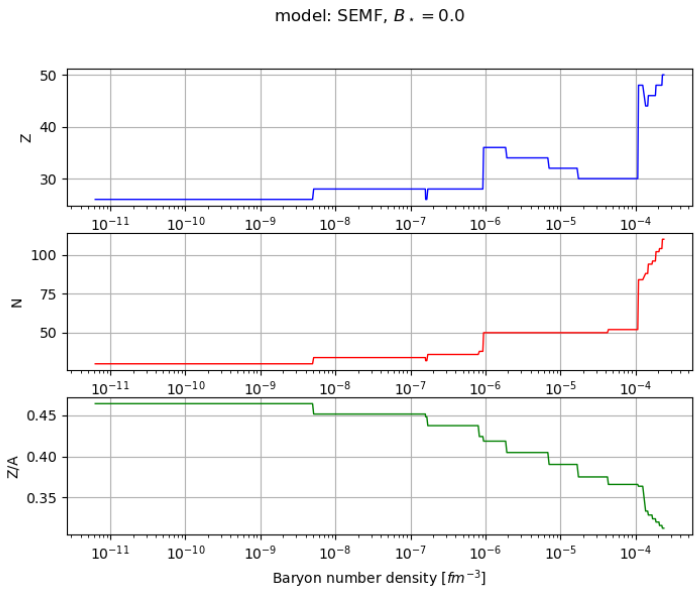

(b)

Figure E.62: Atomic number, neutron number and proton fraction as a function of (a) energy density and of (b) baryon number density, using the SEMF model with magnetic field strength $B_\star = 0$

E.8.2 FRDM2012

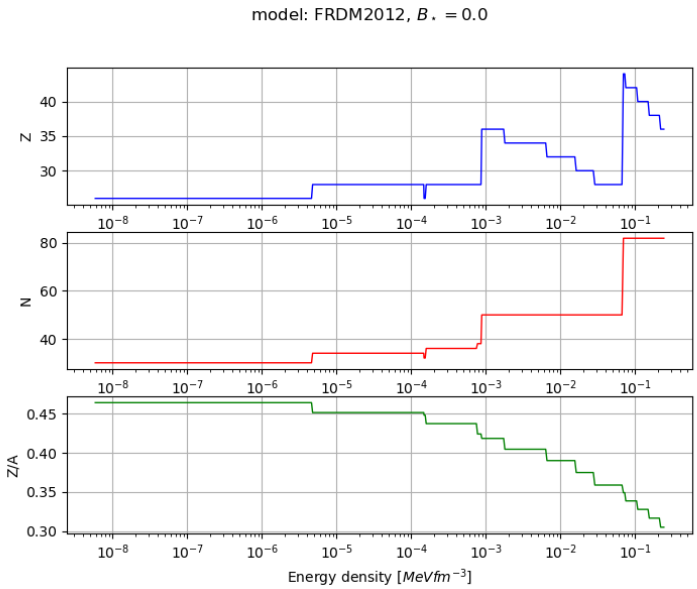

(a)

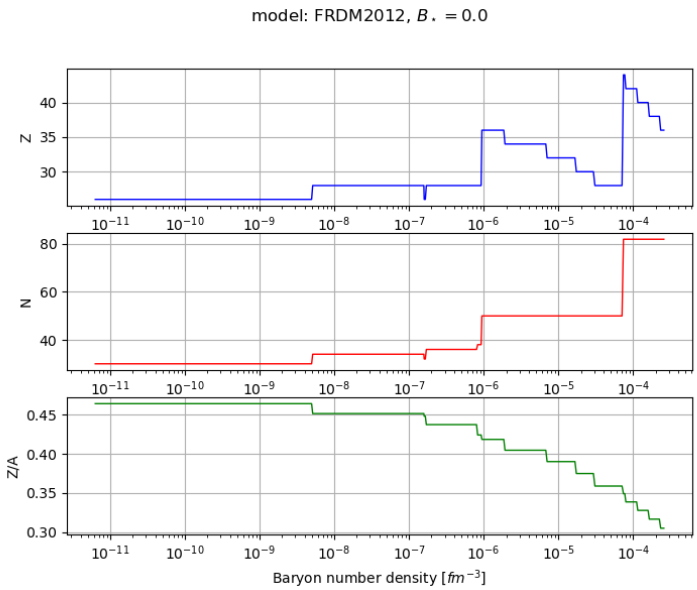

(b)

Figure E.63: The same as Figure E.62, using the FRDM2012 model with $B_\star = 0$

E.8.3 WS4RBF

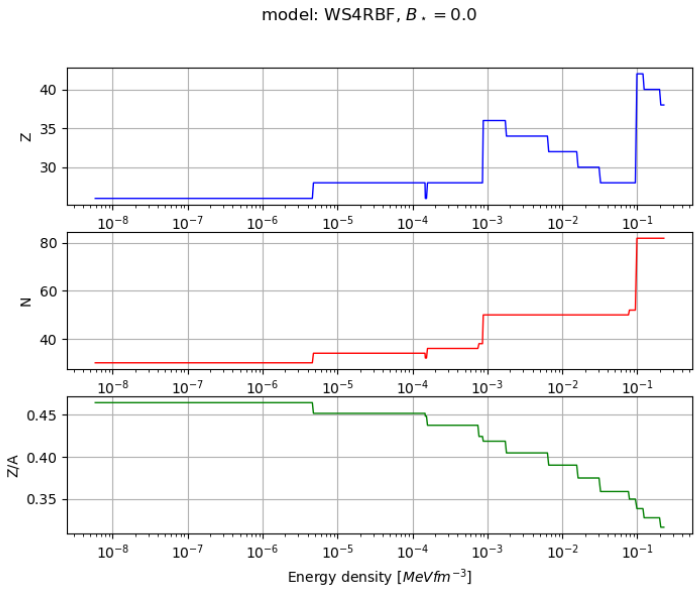

(a)

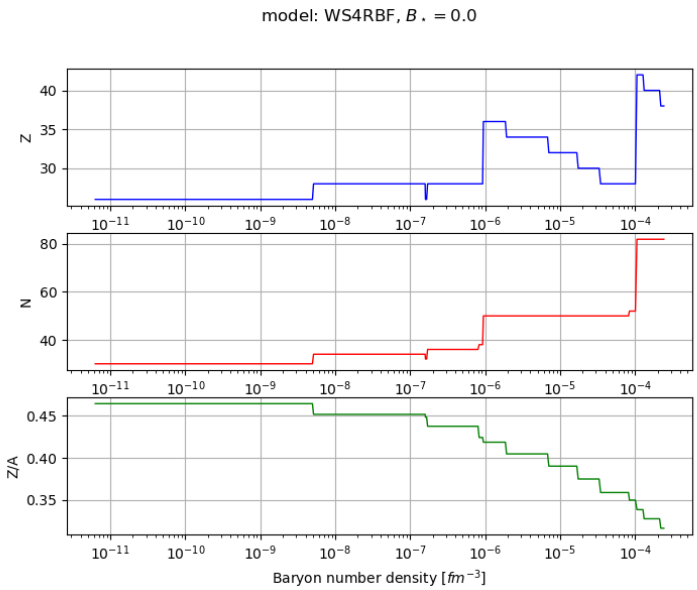

(b)

Figure E.64: The same as Figure E.62, using the WS4RBF model with $B_\star = 0$

E.8.4 BSKG3

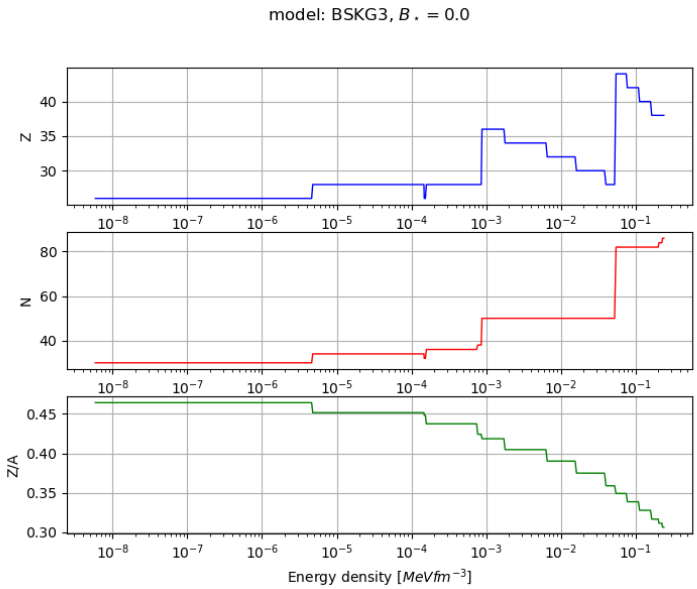

(a)

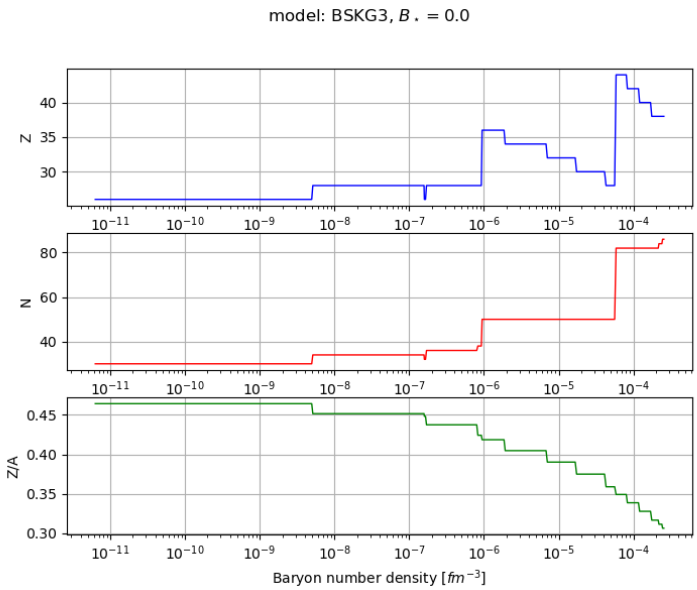

(b)

Figure E.65: The same as Figure E.62, using the BSKG3 model with $B_\star = 0$

E.8.5 HFB31

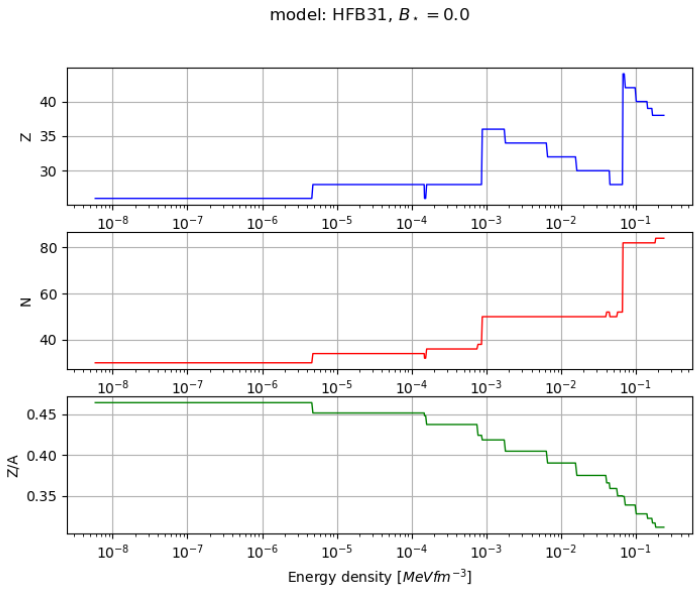

(a)

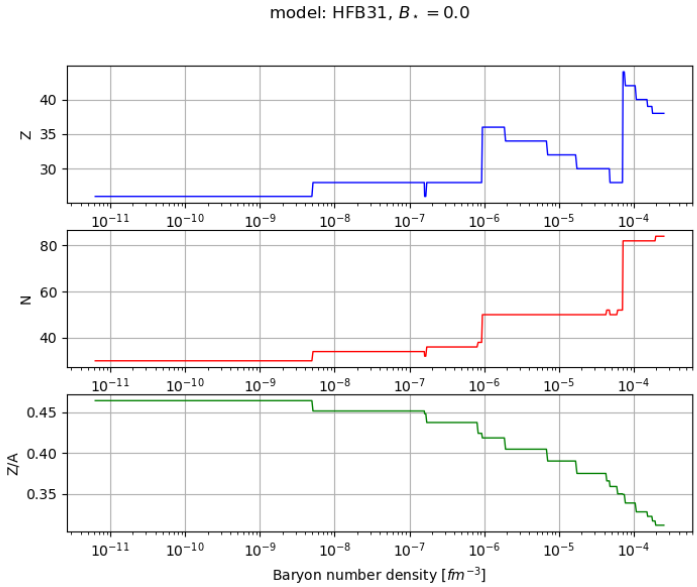

(b)

Figure E.66: The same as Figure E.62, using the HFB31 model with $B_\star = 0$

E.8.6 DDMED

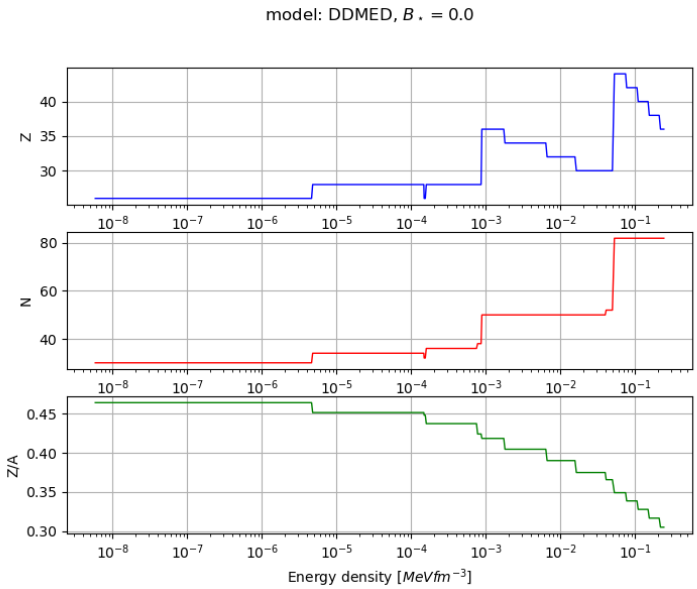

(a)

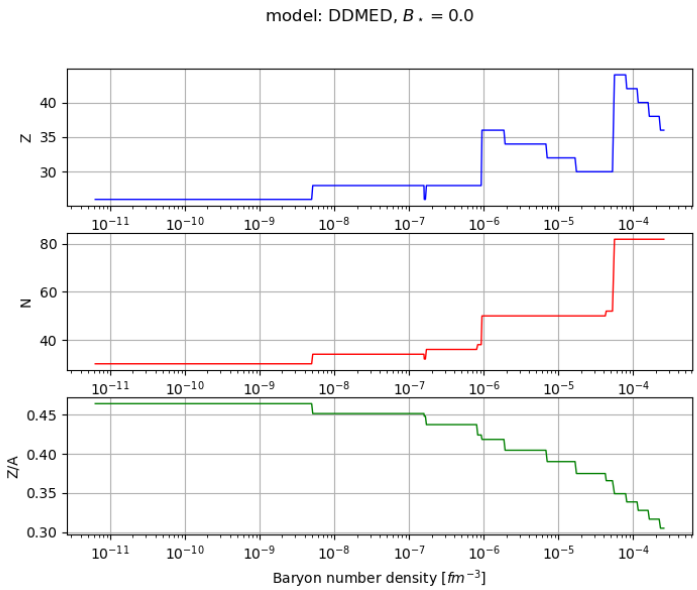

(b)

Figure E.67: The same as Figure E.62, using the DDMED model with $B_\star = 0$

E.8.7 DDPC1

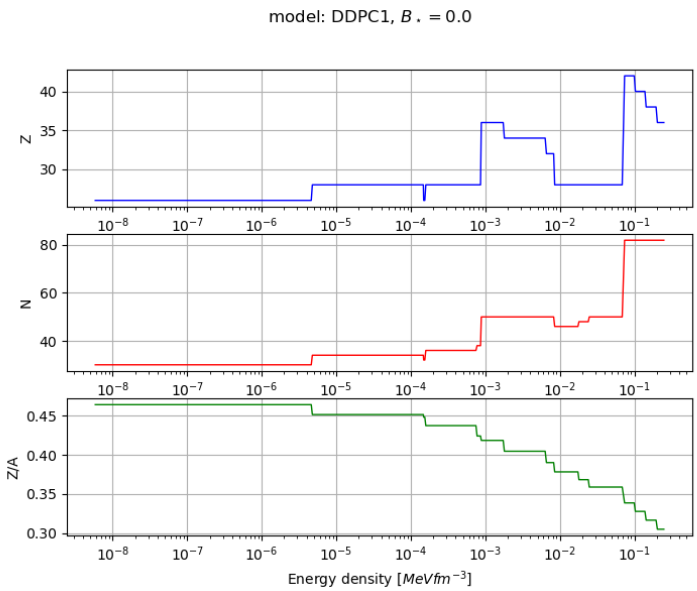

(a)

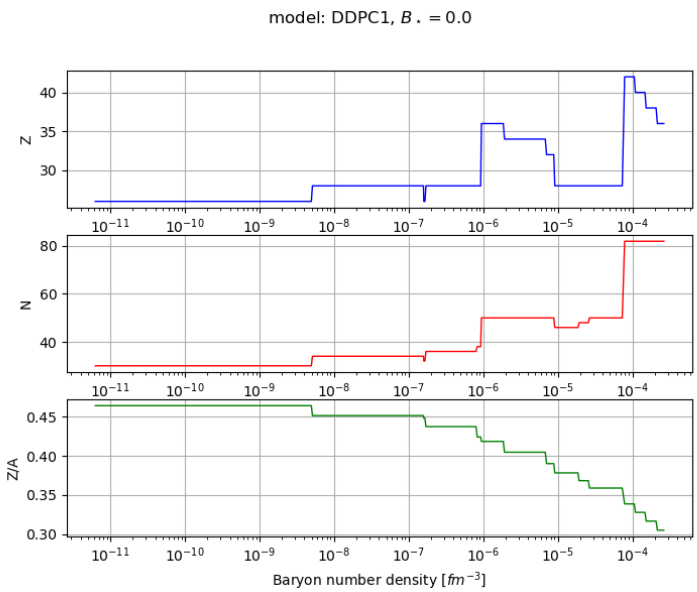

(b)

Figure E.68: The same as Figure E.62, using the DDPC1 model with $B_\star = 0$

E.8.8 SVMIN

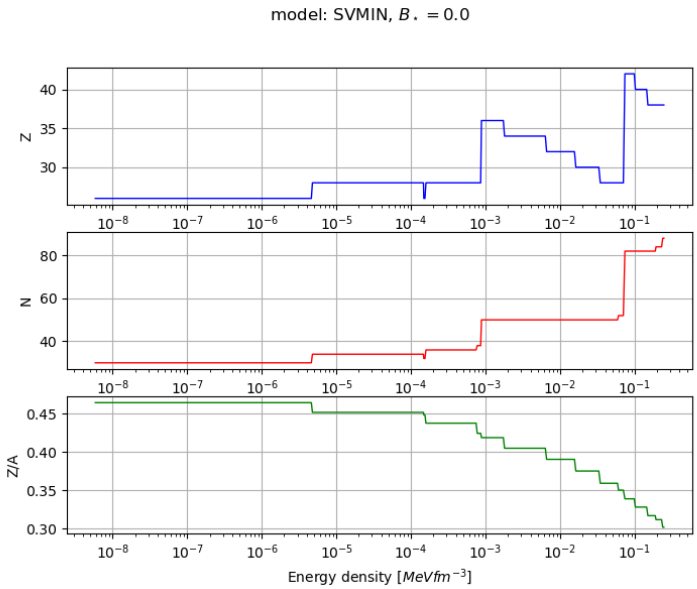

(a)

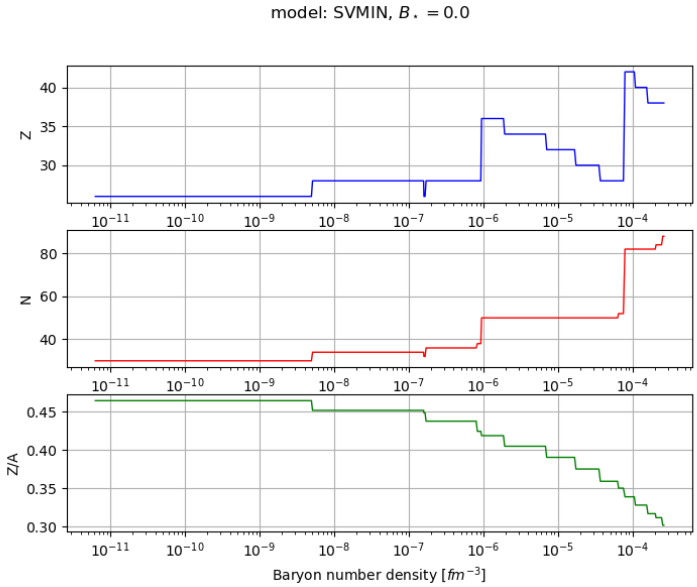

(b)

Figure E.69: The same as Figure E.62, using the SVMIN model with $B_\star = 0$

E.8.9 UNEDF0

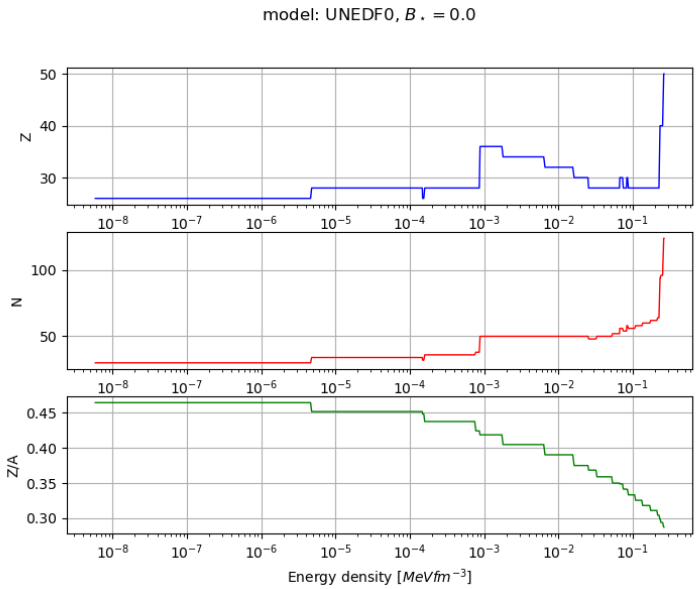

(a)

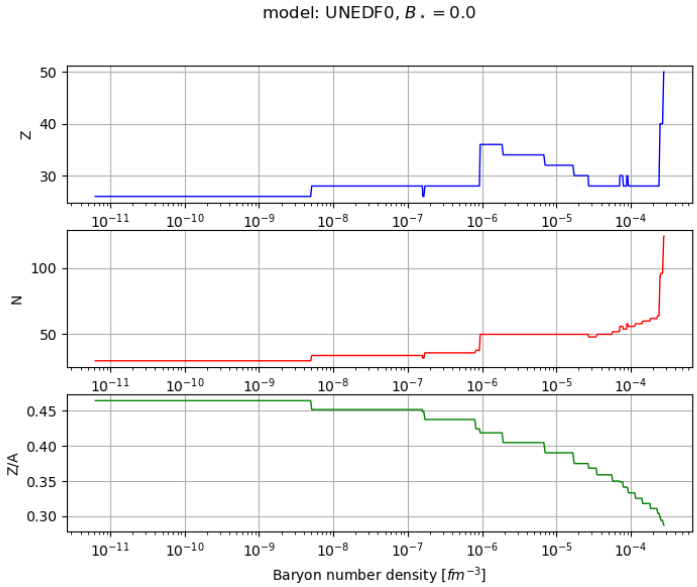

(b)

Figure E.70: The same as Figure E.62, using the UNEDF0 model with $B_\star = 0$

E.9 M_{cr} for different M and R

E.9.1 SEMF

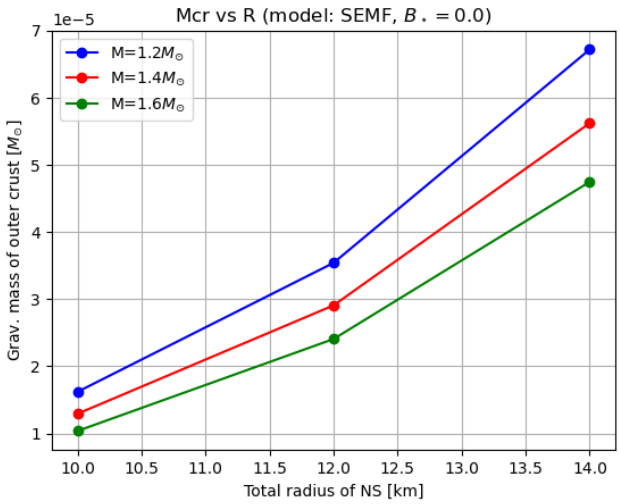

Figure E.71: Mass of outer crust for different masses and radii of NS, using the SEMF model with magnetic field strength $B_\star = 0$

E.9.2 FRDM2012

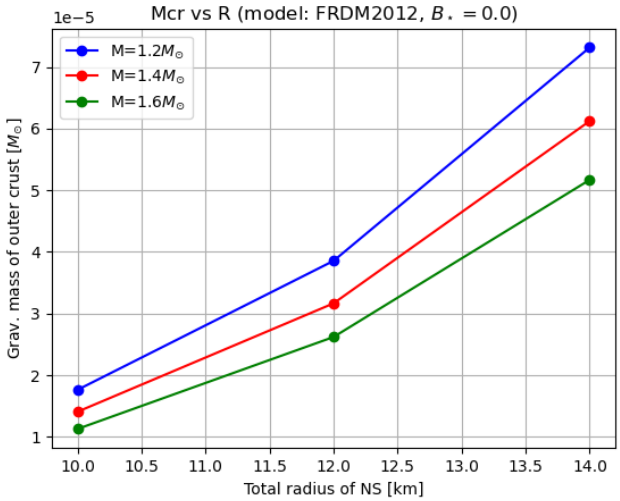

Figure E.72: The same as Figure E.71, using the FRDM2012 model with $B_\star = 0$

E.9.3 WS4RBF

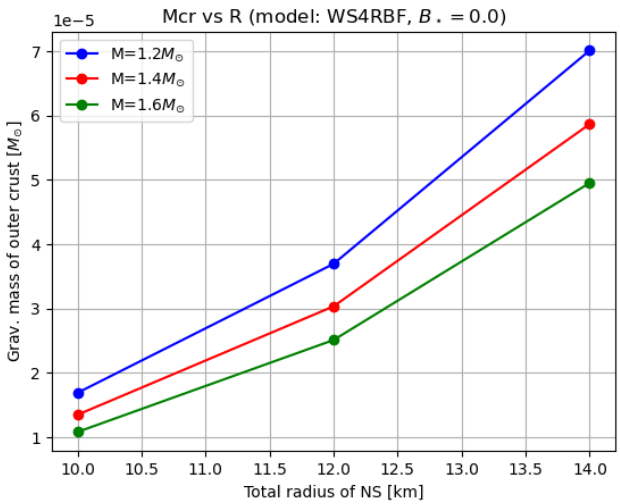

Figure E.73: The same as Figure E.71, using the WS4RBF model with $B_\star = 0$

E.9.4 BSKG3

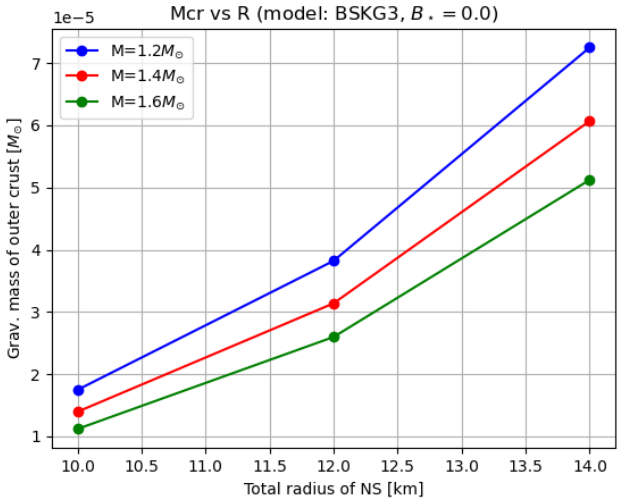

Figure E.74: The same as Figure E.71, using the BSKG3 model with $B_\star = 0$

E.9.5 HFB31

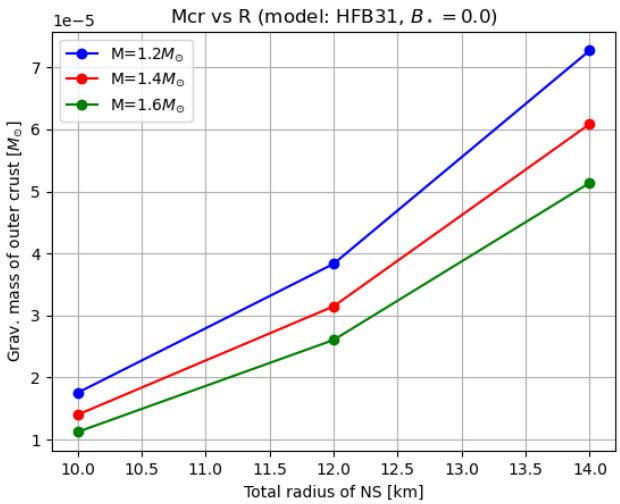

Figure E.75: The same as Figure E.71, using the HFB31 model with $B_\star = 0$

E.9.6 DDMED

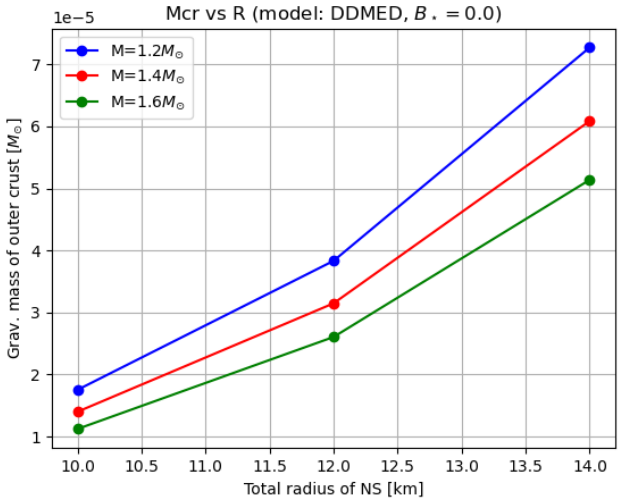

Figure E.76: The same as Figure E.71, using the DDMED model with $B_\star = 0$

E.9.7 DDPC1

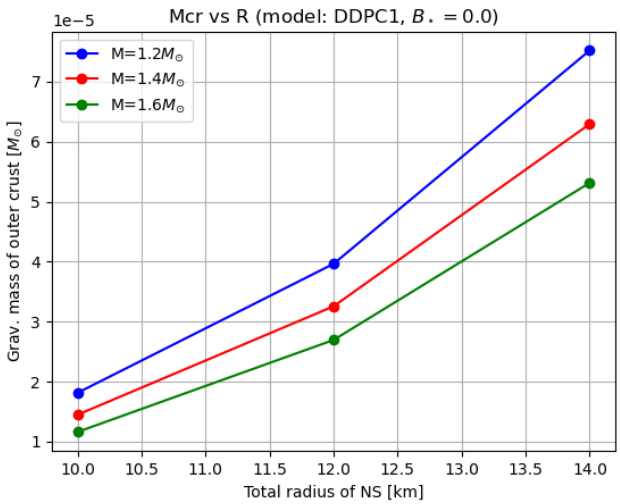

Figure E.77: The same as Figure E.71, using the DDPC1 model with $B_\star = 0$

E.9.8 SVMIN

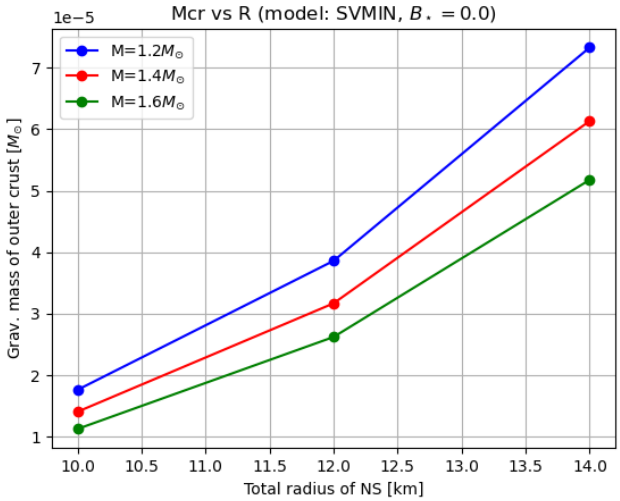

Figure E.78: The same as Figure E.71, using the SVMIN model with $B_\star = 0$

E.9.9 UNEDF0

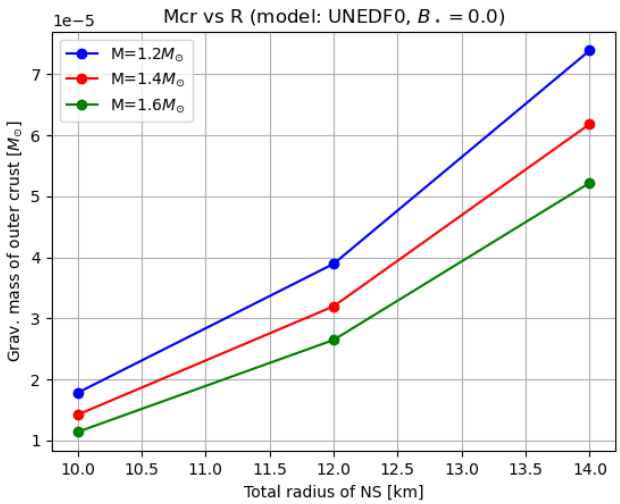

Figure E.79: The same as Figure E.71, using the UNEDF0 model with $B_\star = 0$

E.10 z_{drip} for different M and R

E.10.1 SEMF

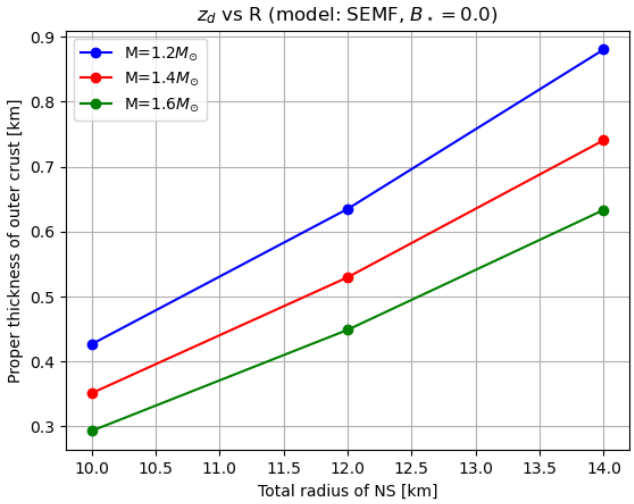

Figure E.80: Proper depth of neutron-drip transition for different masses and radii of NS, using the SEMF model with magnetic field strength $B_\star = 0$

E.10.2 FRDM2012

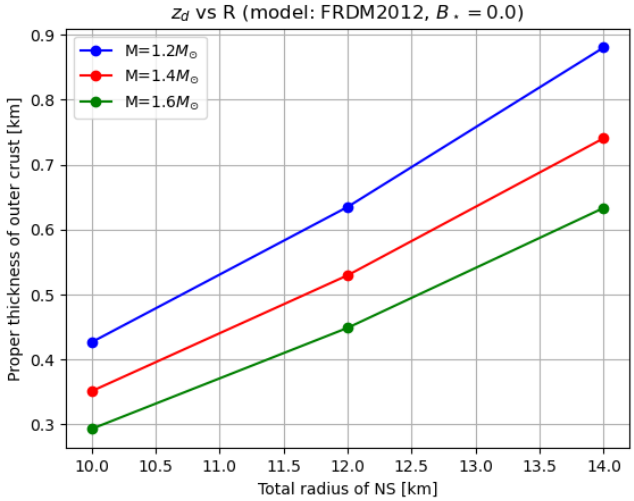

Figure E.81: The same as Figure E.80, using the FRDM2012 model with $B_\star = 0$

E.10.3 WS4RBF

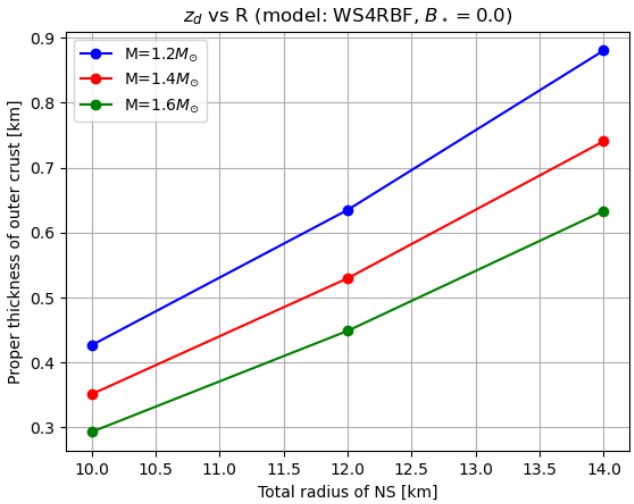

Figure E.82: The same as Figure E.80, using the WS4RBF model with $B_\star = 0$

E.10.4 BSKG3

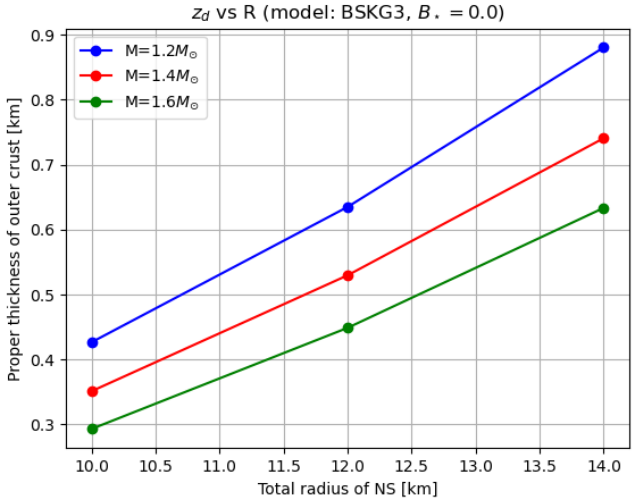

Figure E.83: The same as Figure E.80, using the BSKG3 model with $B_\star = 0$

E.10.5 HFB31

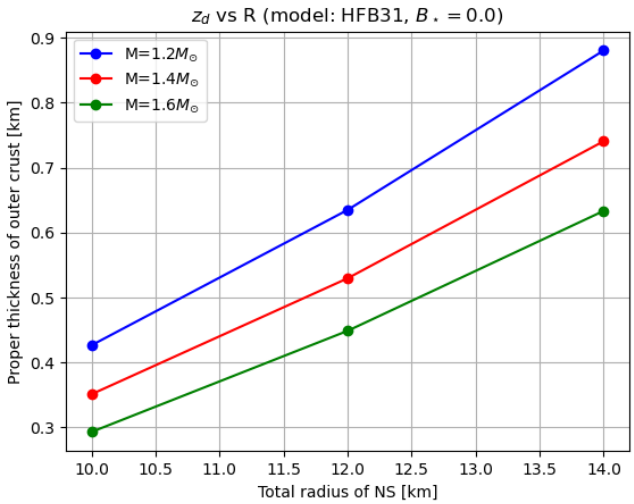

Figure E.84: The same as Figure E.80, using the HFB31 model with $B_\star = 0$

E.10.6 DDMED

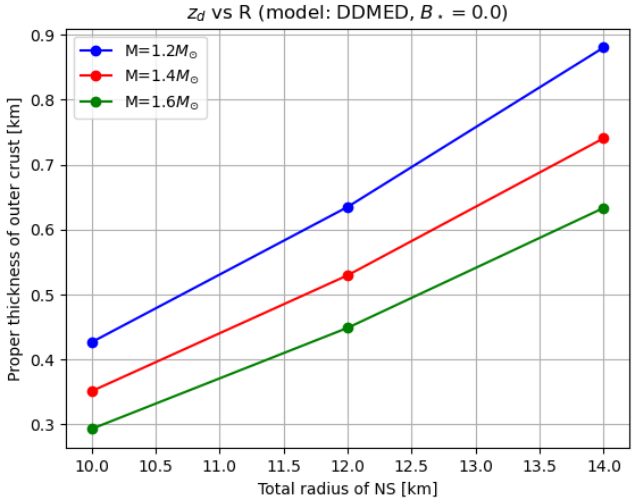

Figure E.85: The same as Figure E.80, using the DDMED model with $B_\star = 0$

E.10.7 DDPC1

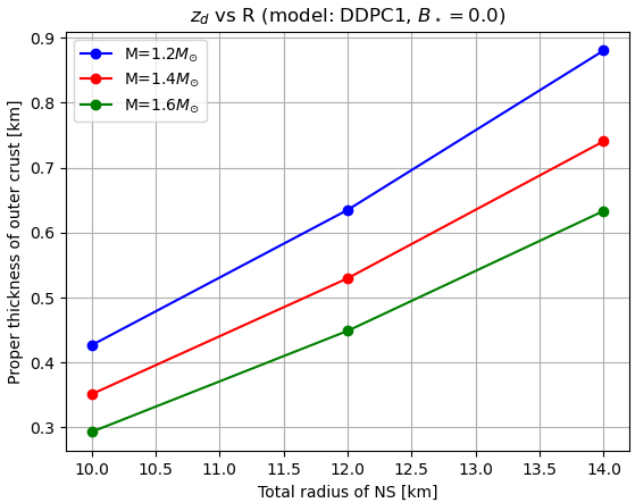

Figure E.86: The same as Figure E.80, using the DDPC1 model with $B_\star = 0$

E.10.8 SVMIN

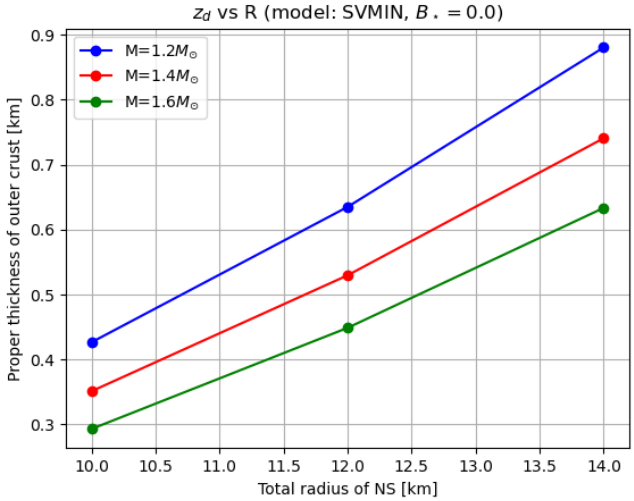

Figure E.87: The same as Figure E.80, using the SVMIN model with $B_\star = 0$

E.10.9 UNEDF0

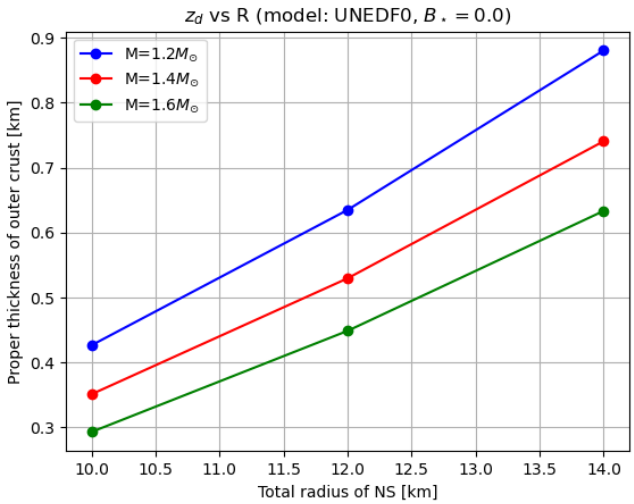

Figure E.88: The same as Figure E.80, using the UNEDF0 model with $B_\star = 0$

Appendix F

Figures for $B_\star = 1500$

Below are the Figures, like those in Subsections 5.4.3 - 5.4.13, for the models: SEMF, FRDM2012, WS4RBF, BSKG3, HFB31, DDMED, DDPC1, SVMIN and UNEDF0, individually, with magnetic field strength $B_\star = 1500$.

F.1 P vs ϵ or n_b

F.1.1 SEMF

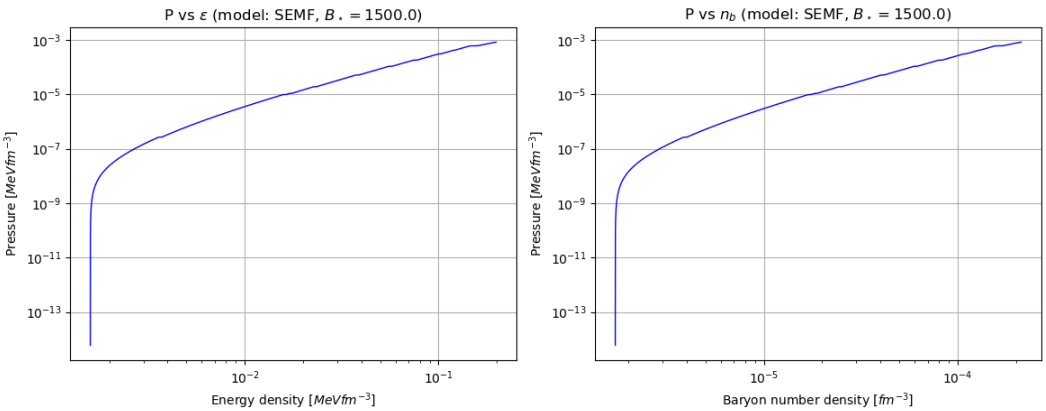

(a) (b)

Figure F.1: Equation of State, (a) pressure as a function of energy density and (b) pressure as a function of baryon number density, using the SEMF model with magnetic field strength $B_\star = 1500$

F.1.2 FRDM2012

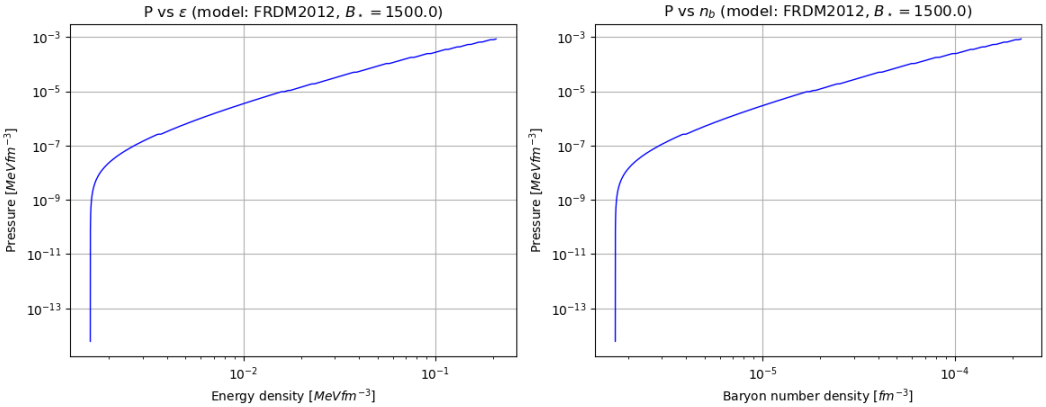

(a) (b)

Figure F.2: The same as Figure F.1, using the FRDM2012 model with $B_\star = 1500$

F.1.3 WS4RBF

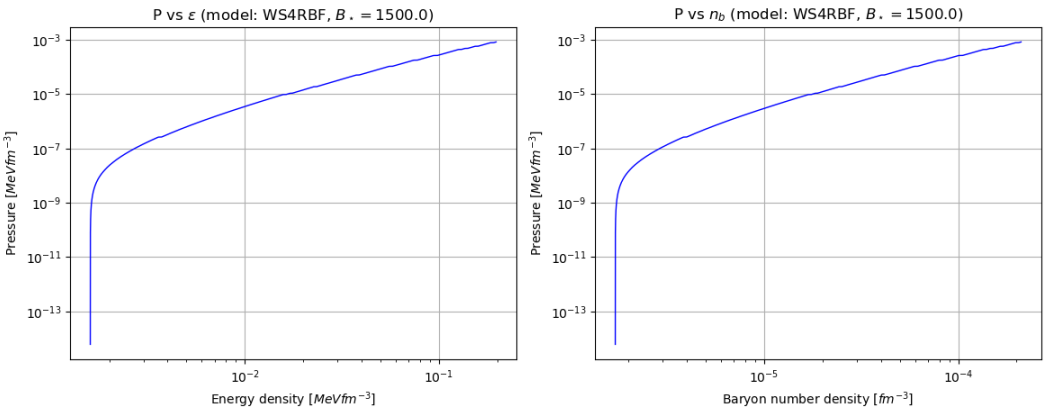

(a) (b)

Figure F.3: The same as Figure F.1, using the WS4RBF model with $B_\star = 1500$

F.1.4 BSKG3

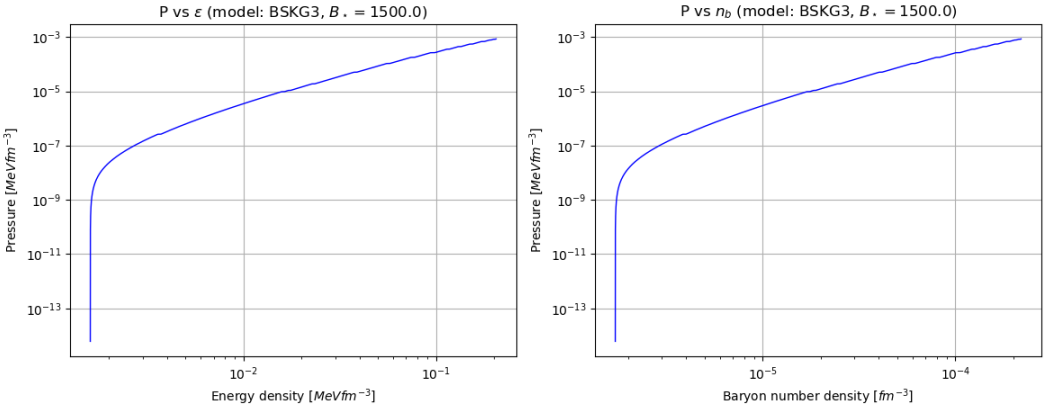

(a) (b)

Figure F.4: The same as Figure F.1, using the BSKG3 model with $B_\star = 1500$

F.1.5 HFB31

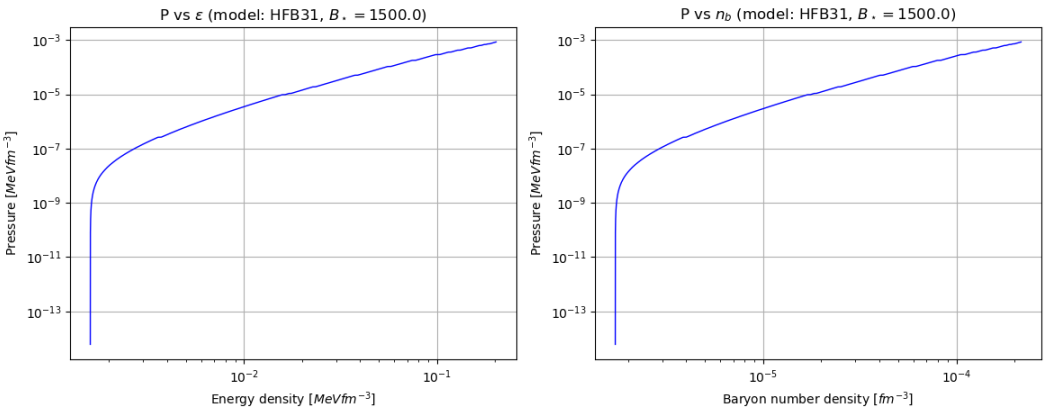

(a) (b)

Figure F.5: The same as Figure F.1, using the HFB31 model with $B_\star = 1500$

F.1.6 DDMED

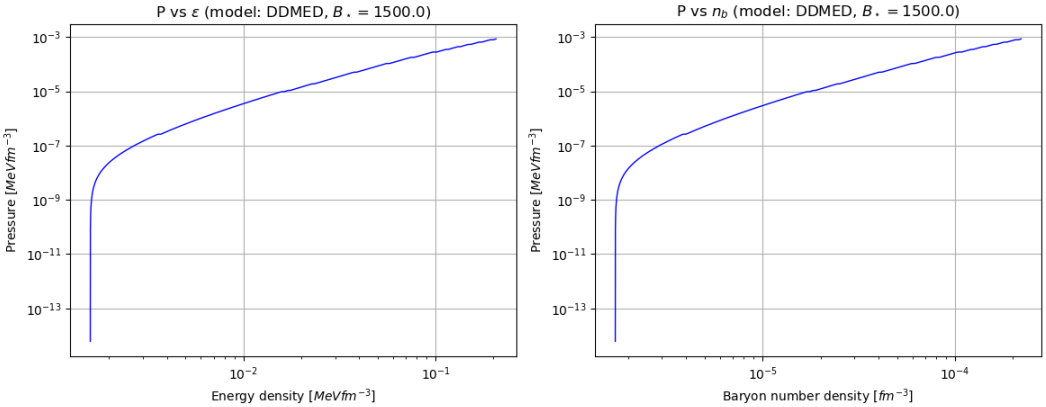

(a) (b)

Figure F.6: The same as Figure F.1, using the DDMED model with $B_\star = 1500$

F.1.7 DDPC1

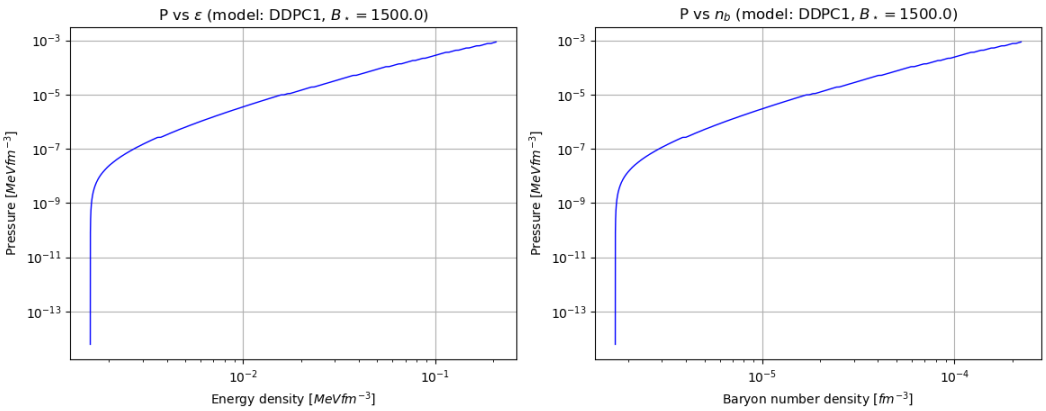

(a) (b)

Figure F.7: The same as Figure F.1, using the DDPC1 model with $B_\star = 1500$

F.1.8 SVMIN

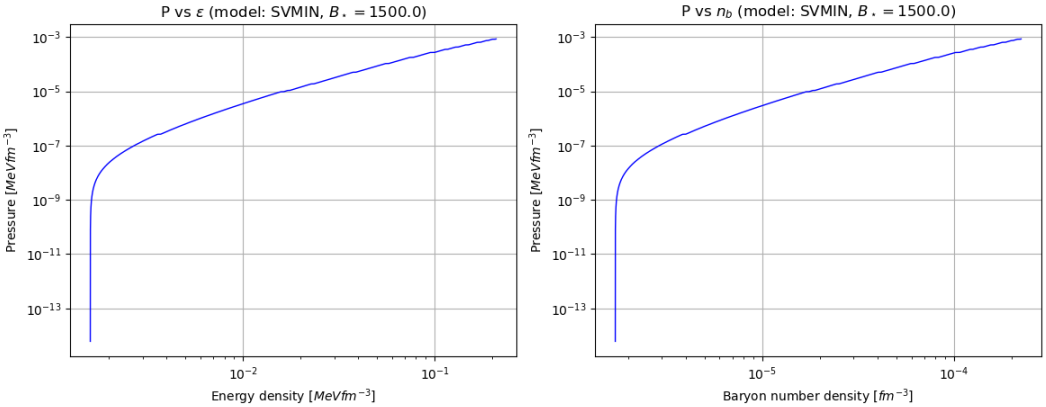

(a) (b)

Figure F.8: The same as Figure F.1, using the SVMIN model with $B_\star = 1500$

F.1.9 UNEDF0

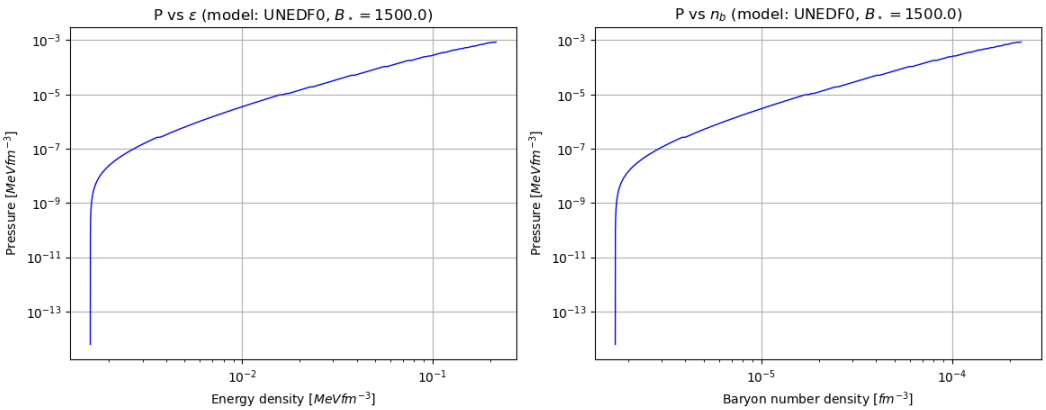

(a) (b)

Figure F.9: The same as Figure F.1, using the UNEDF0 model with $B_\star = 1500$

F.2 Fitting $P = K\epsilon^G$

F.2.1 WS4RBF

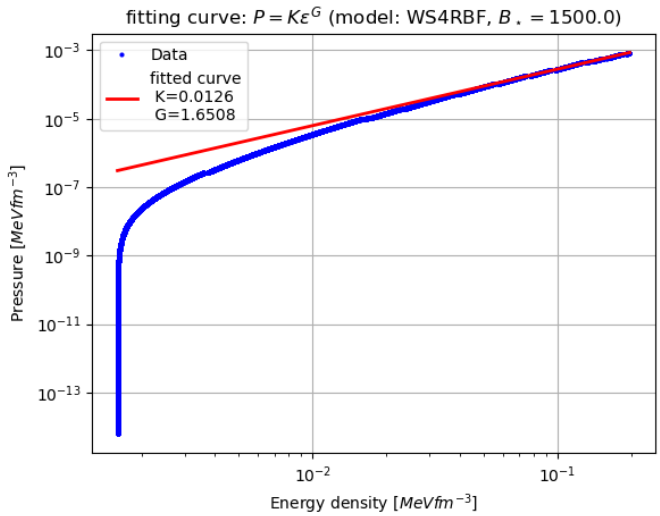

Figure F.10: The same as Figure 5.3, using the WS4RBF model with $B_\star = 1500$

F.2.2 BSKG3

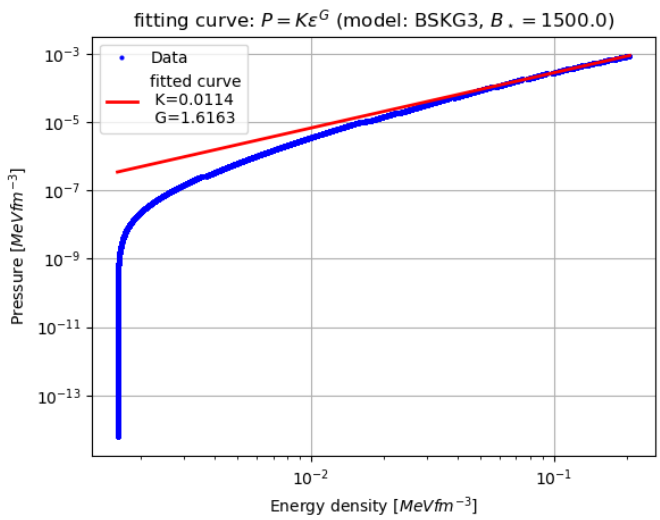

Figure F.11: The same as Figure 5.3, using the BSKG3 model with $B_\star = 1500$

F.2.3 HFB31

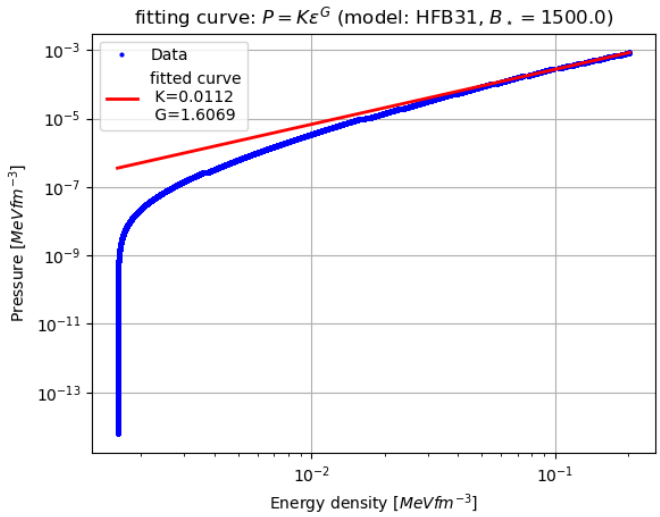

Figure F.12: The same as Figure 5.3, using the HFB31 model with $B_\star = 1500$

F.2.4 DDMED

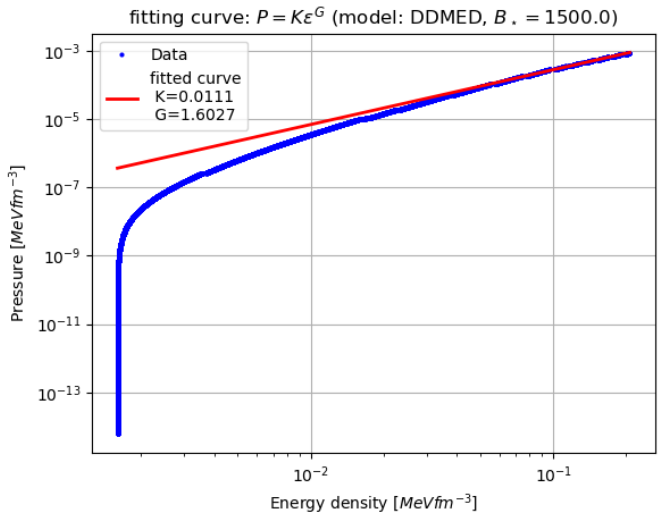

Figure F.13: The same as Figure 5.3, using the DDMED model with $B_\star = 1500$

F.2.5 DDPC1

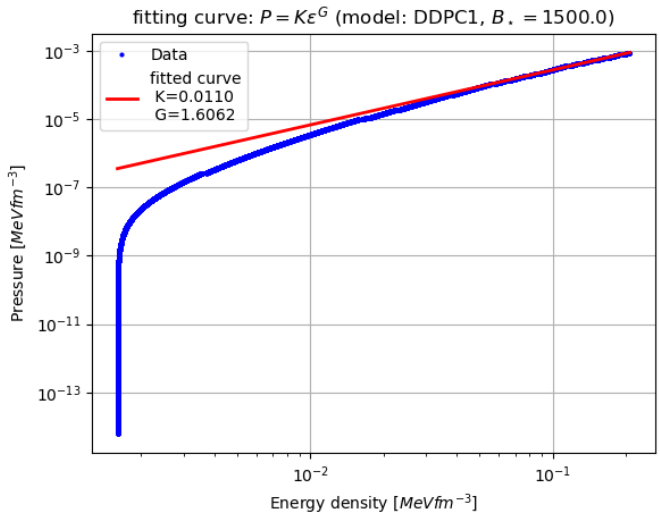

Figure F.14: The same as Figure 5.3, using the DDPC1 model with $B_\star = 1500$

F.2.6 SVMIN

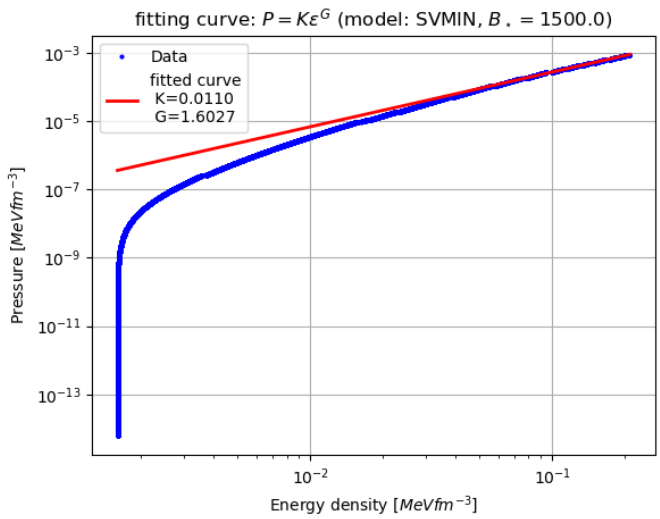

Figure F.15: The same as Figure 5.3, using the SVMIN model with $B_\star = 1500$

F.2.7 UNEDF0

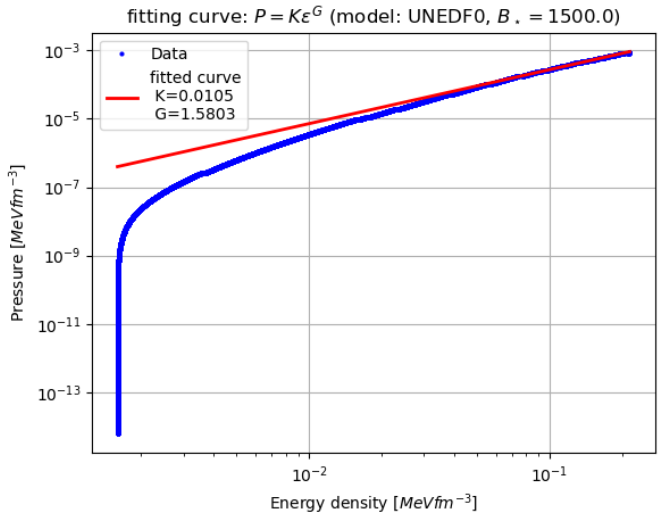

Figure F.16: The same as Figure 5.3, using the UNEDF0 model with $B_\star = 1500$

F.3 Γ vs ϵ or n_b

F.3.1 SEMF

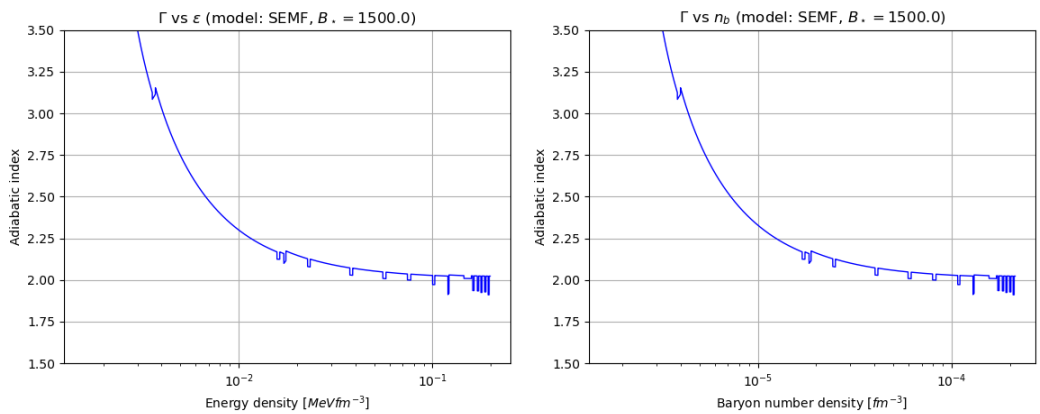

(a) (b)

Figure F.17: Adiabatic index as a function of (a) energy density and of (b) baryon number density, using the SEMF model with magnetic field strength $B_\star = 1500$

F.3.2 FRDM2012

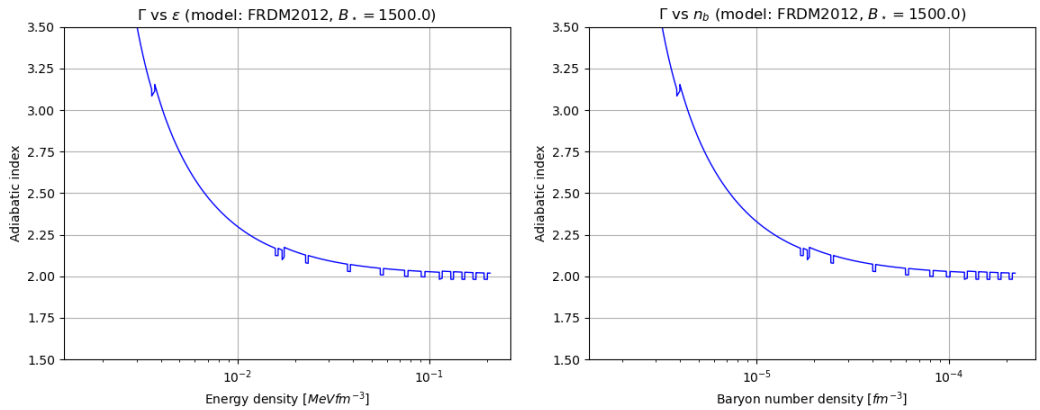

(a) (b)

Figure F.18: The same as Figure F.17, using the FRDM2012 model with $B_\star = 1500$

F.3.3 WS4RBF

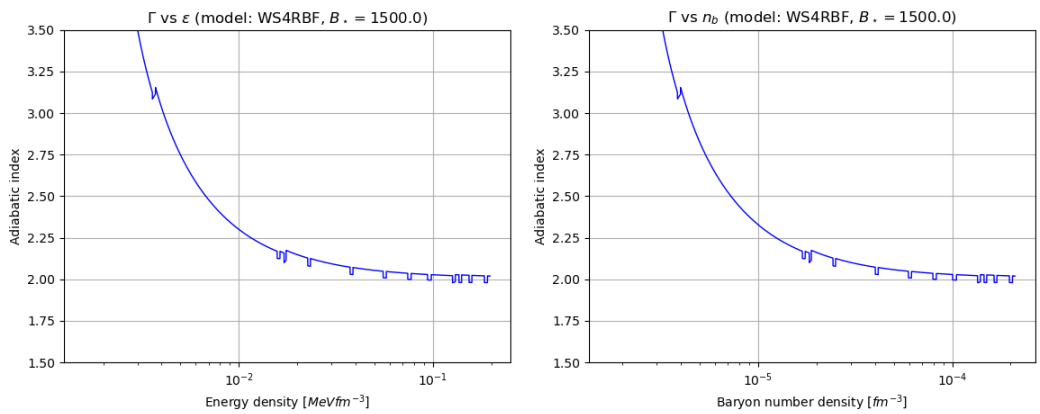

(a) (b)

Figure F.19: The same as Figure F.17, using the WS4RBF model with $B_\star = 1500$

F.3.4 BSKG3

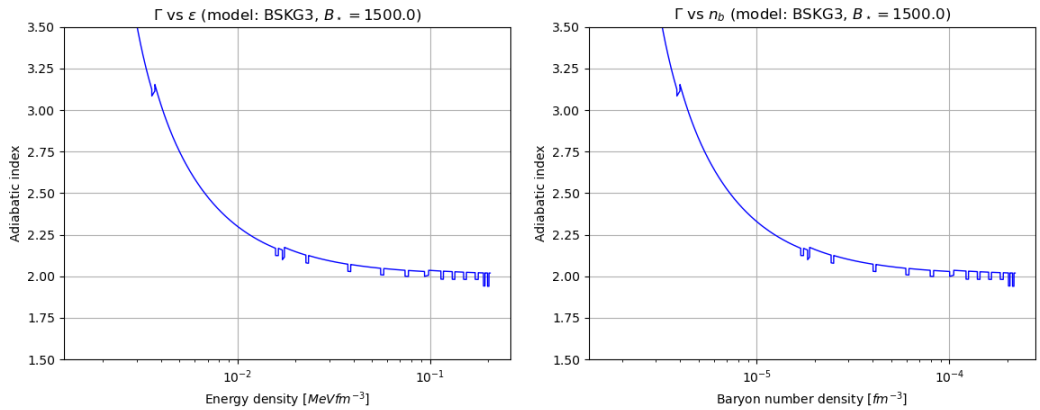

(a) (b)

Figure F.20: The same as Figure F.17, using the BSKG3 model with $B_\star = 1500$

F.3.5 HFB31

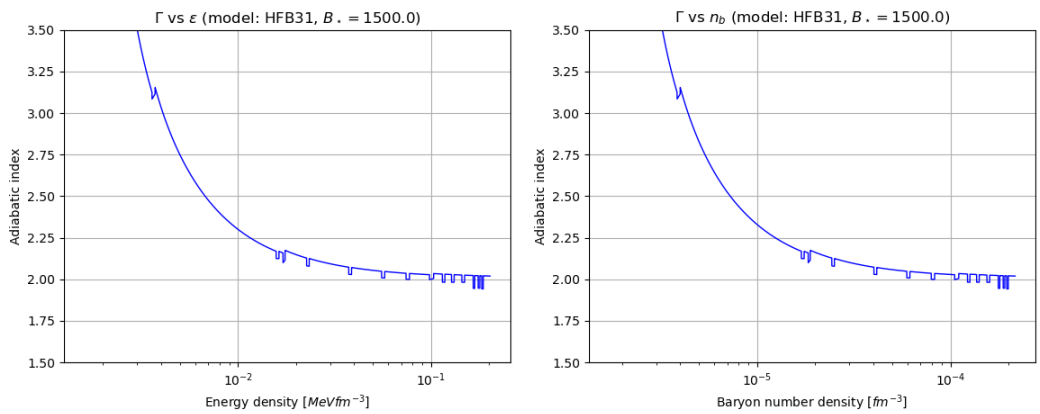

(a) (b)

Figure F.21: The same as Figure F.17, using the HFB31 model with $B_\star = 1500$

F.3.6 DDMED

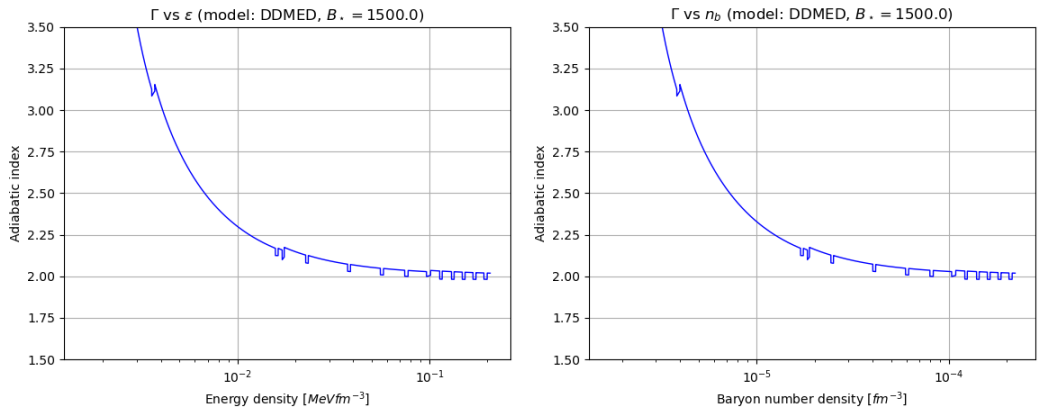

(a) (b)

Figure F.22: The same as Figure F.17, using the DDMED model with $B_\star = 1500$

F.3.7 DDPC1

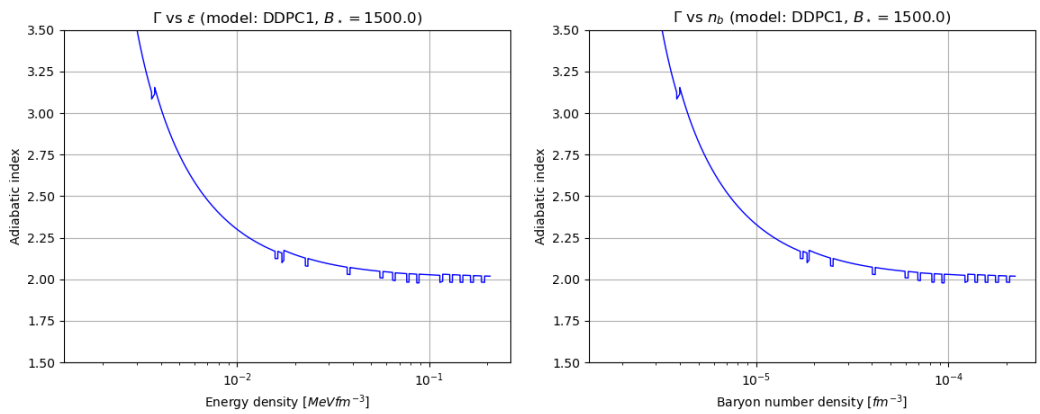

(a) (b)

Figure F.23: The same as Figure F.17, using the DDPC1 model with $B_\star = 1500$

F.3.8 SVMIN

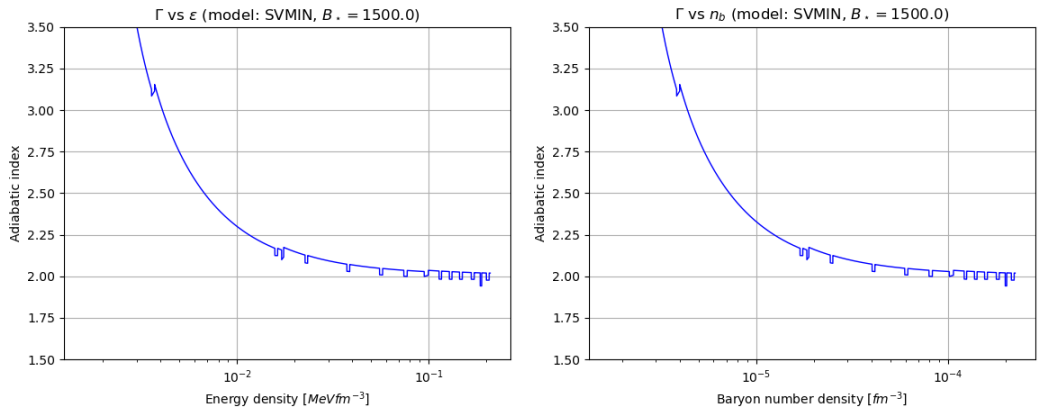

(a) (b)

Figure F.24: The same as Figure F.17, using the SVMIN model with $B_\star = 1500$

F.3.9 UNEDF0

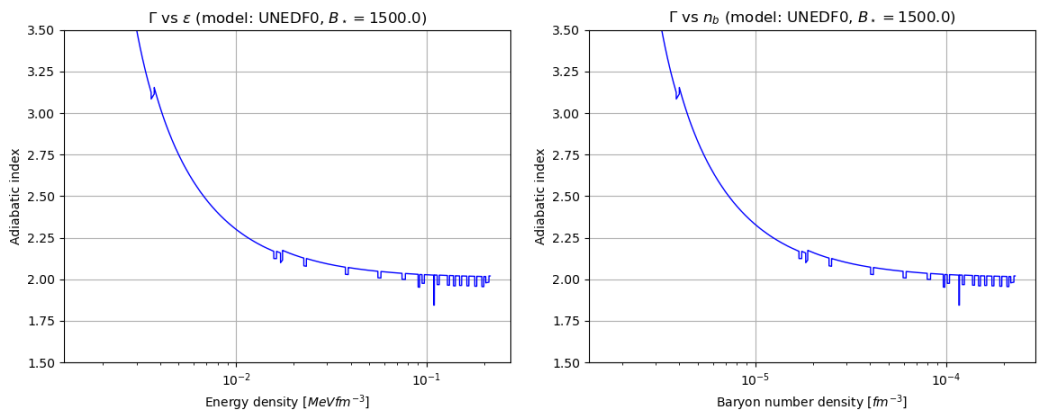

(a) (b)

Figure F.25: The same as Figure F.17, using the UNEDF0 model with $B_\star = 1500$

F.4 c_s vs ϵ or n_b

F.4.1 SEMF

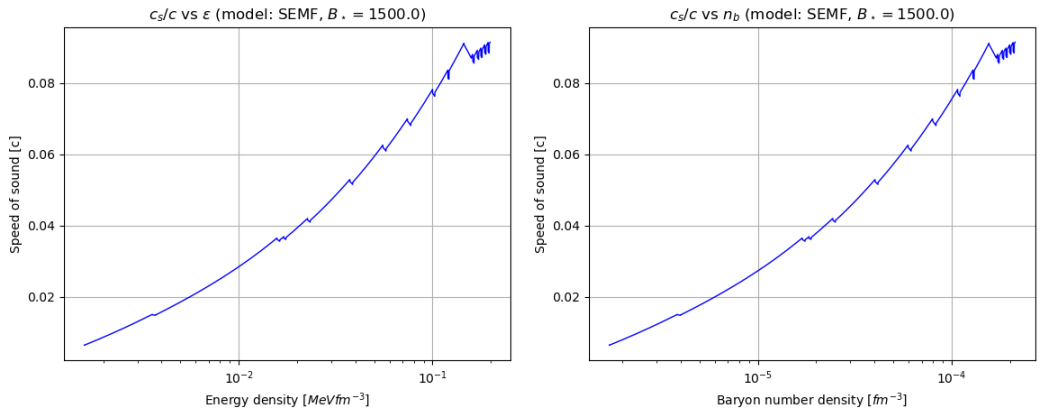

(a) (b)

Figure F.26: Speed of sound as a function of (a) energy density and of (b) baryon number density, using the SEMF model with magnetic field strength $B_\star = 1500$

F.4.2 FRDM2012

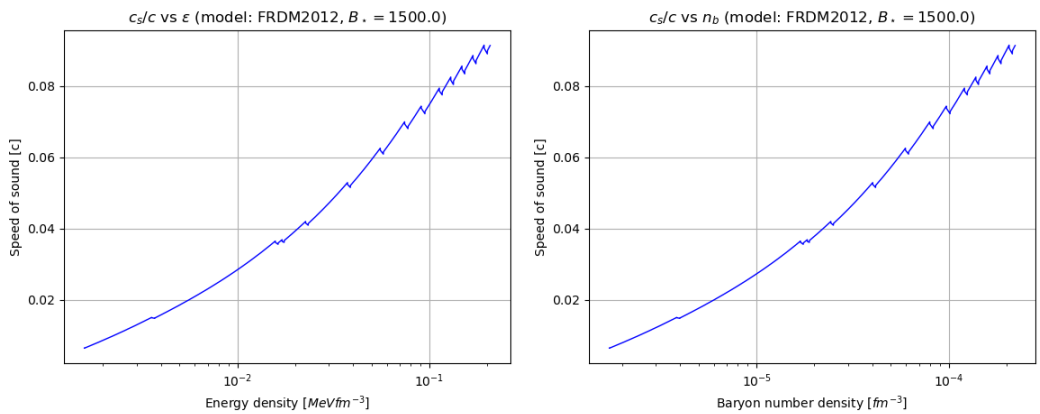

(a) (b)

Figure F.27: The same as Figure F.26, using the FRDM2012 model with $B_\star = 1500$

F.4.3 WS4RBF

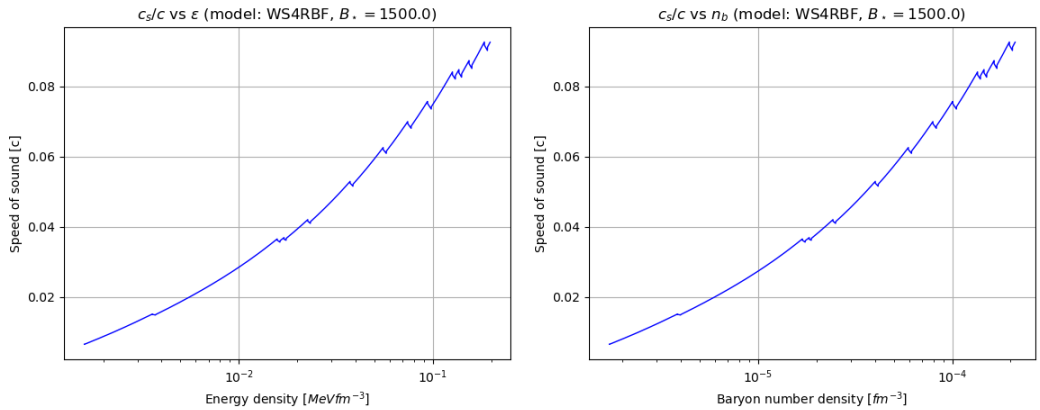

(a) (b)

Figure F.28: The same as Figure F.26, using the WS4RBF model with $B_\star = 1500$

F.4.4 BSKG3

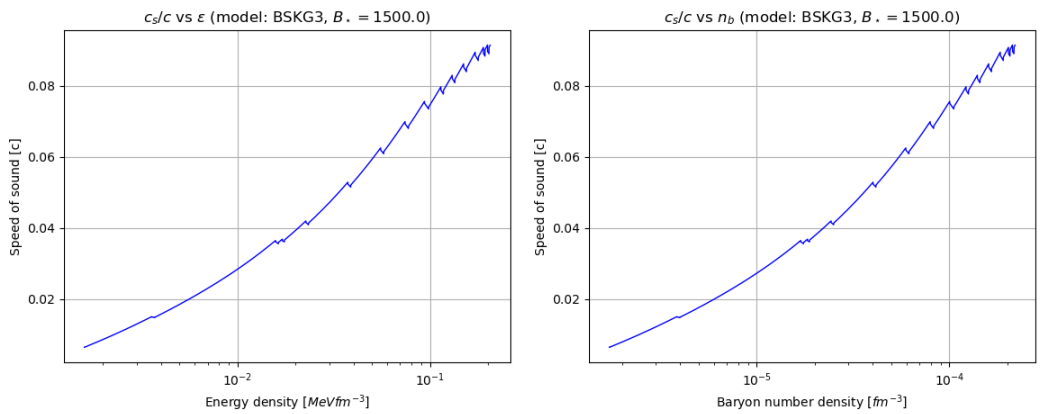

(a) (b)

Figure F.29: The same as Figure F.26, using the BSKG3 model with $B_\star = 1500$

F.4.5 HFB31

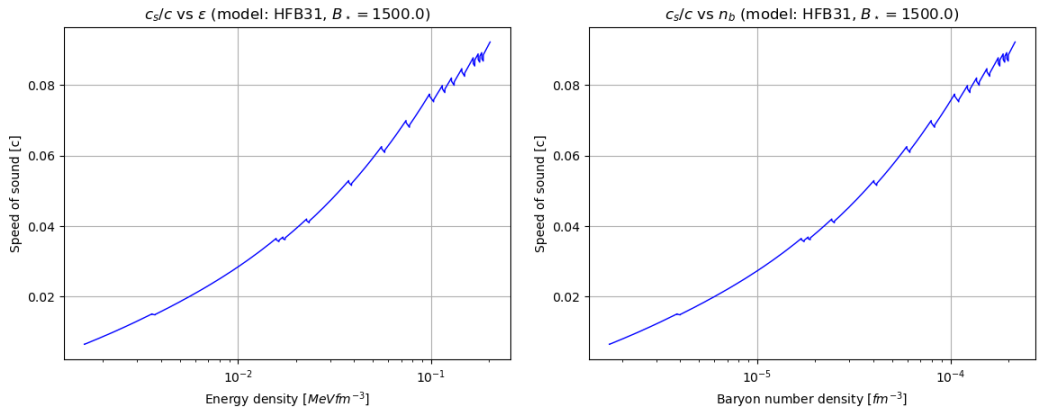

(a) (b)

Figure F.30: The same as Figure F.26, using the HFB31 model with $B_\star = 1500$

F.4.6 DDMED

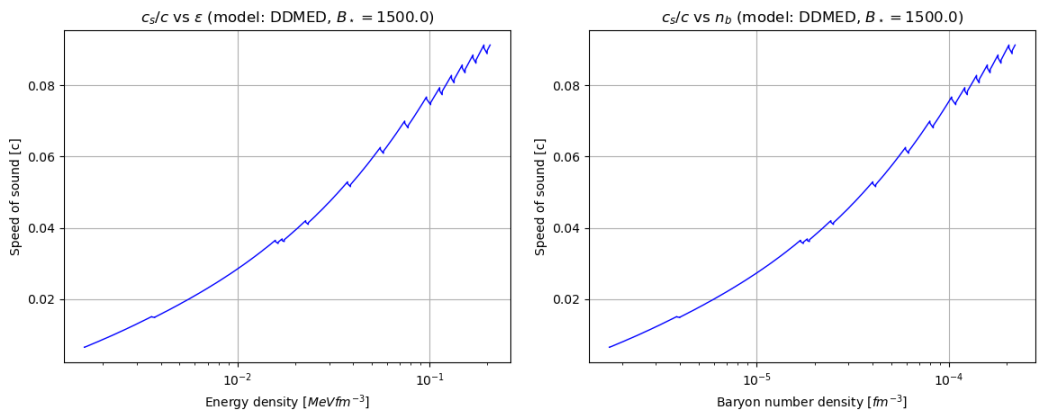

(a) (b)

Figure F.31: The same as Figure F.26, using the DDMED model with $B_\star = 1500$

F.4.7 DDPC1

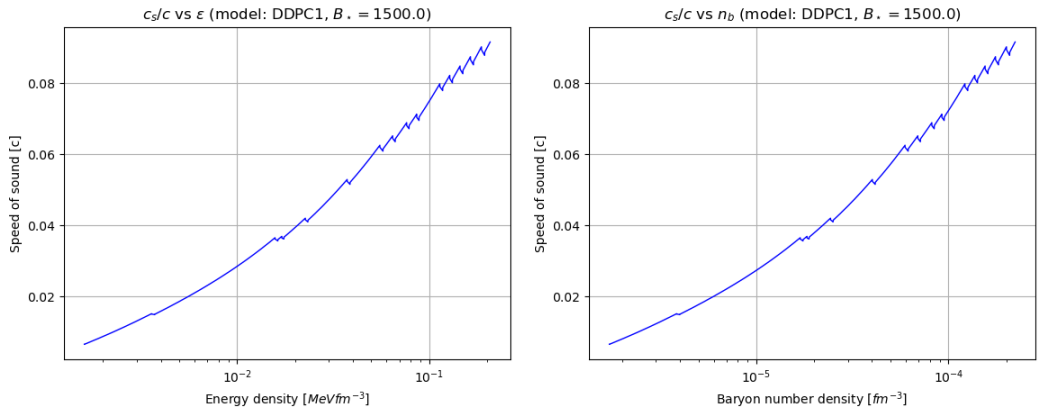

(a) (b)

Figure F.32: The same as Figure F.26, using the DDPC1 model with $B_\star = 1500$

F.4.8 SVMIN

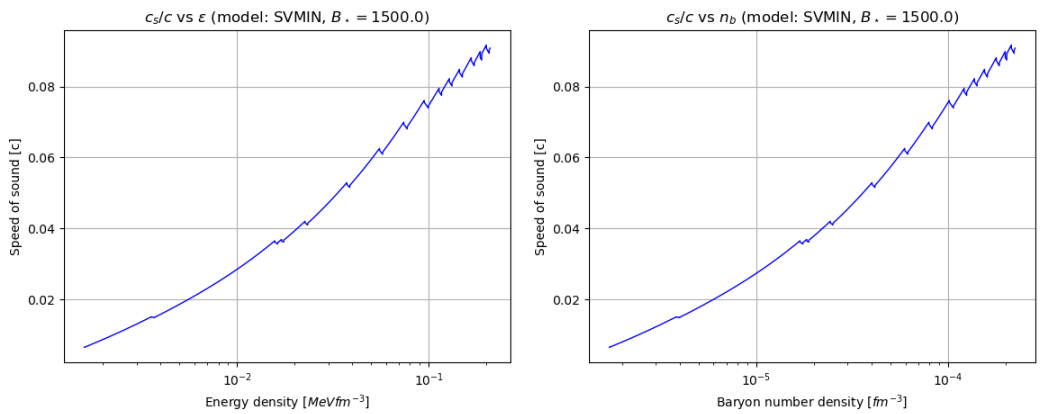

(a) (b)

Figure F.33: The same as Figure F.26, using the SVMIN model with $B_\star = 1500$

F.4.9 UNEDF0

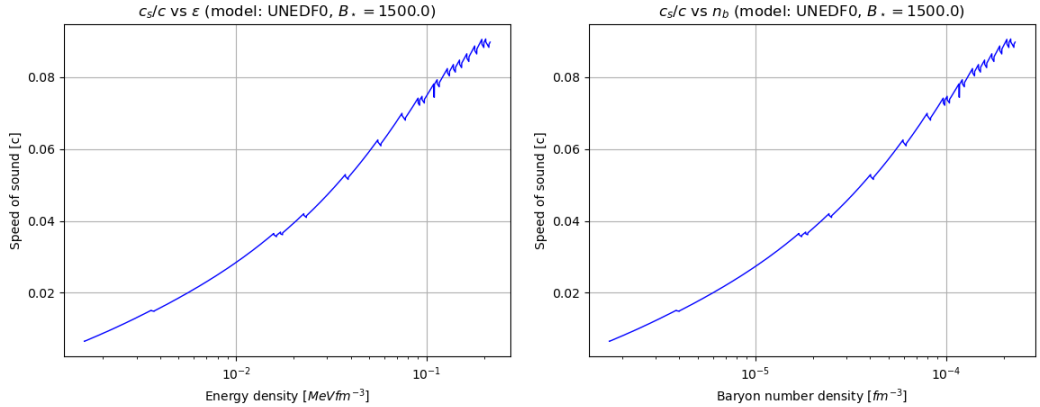

(a) (b)

Figure F.34: The same as Figure F.26, using the UNEDF0 model with $B_\star = 1500$

F.5 K_{mod} vs ϵ or n_b

F.5.1 SEMF

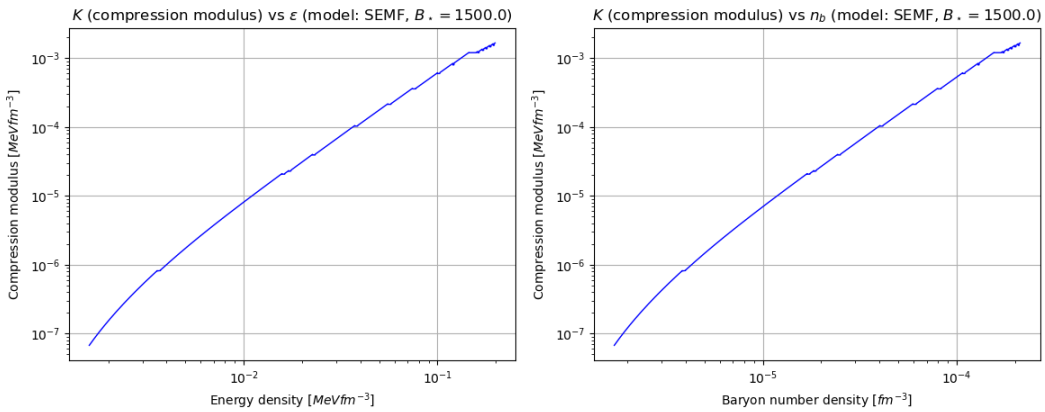

(a) (b)

Figure F.35: Compression modulus as a function of (a) energy density and of (b) baryon number density, using the SEMF model with magnetic field strength $B_\star = 1500$

F.5.2 FRDM2012

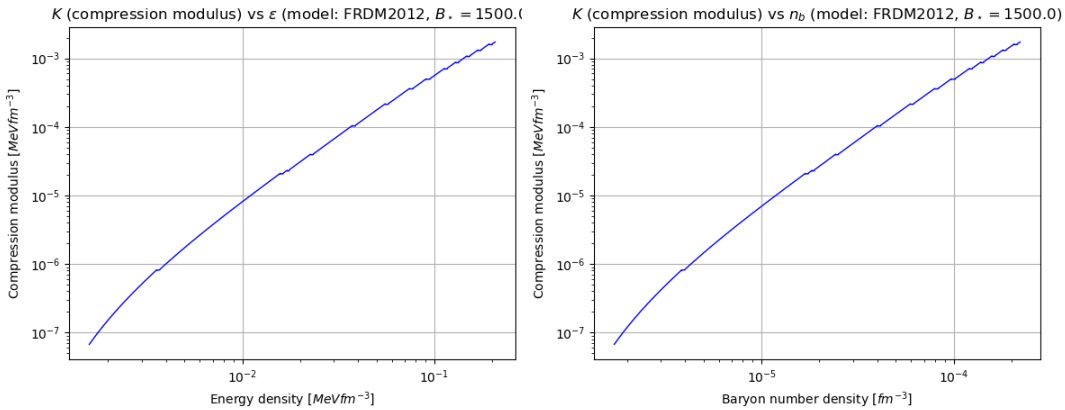

(a) (b)

Figure F.36: The same as Figure F.35, using the FRDM2012 model with $B_\star = 1500$

F.5.3 WS4RBF

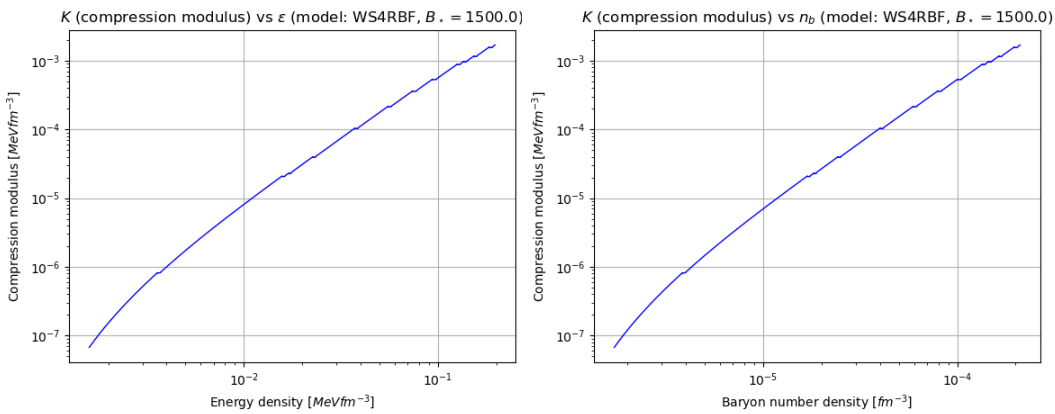

(a) (b)

Figure F.37: The same as Figure F.35, using the WS4RBF model with $B_\star = 1500$

F.5.4 BSKG3

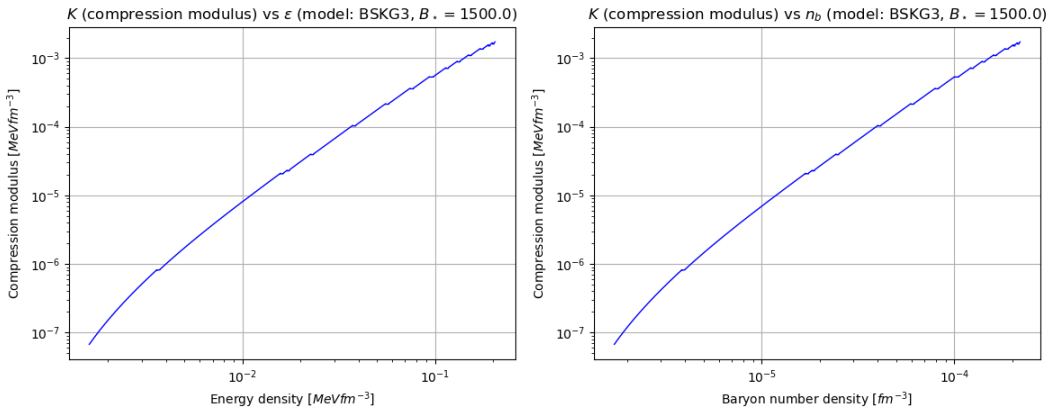

(a) (b)

Figure F.38: The same as Figure F.35, using the BSKG3 model with $B_\star = 1500$

F.5.5 HFB31

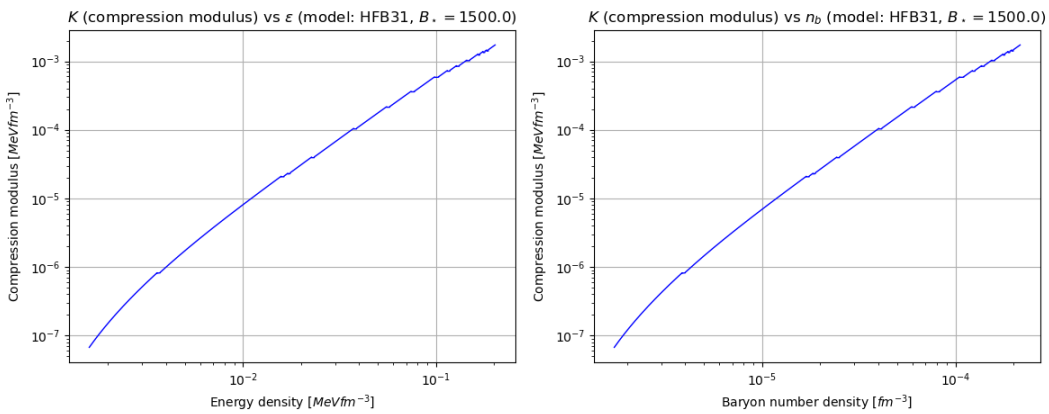

(a) (b)

Figure F.39: The same as Figure F.35, using the HFB31 model with $B_\star = 1500$

F.5.6 DDMED

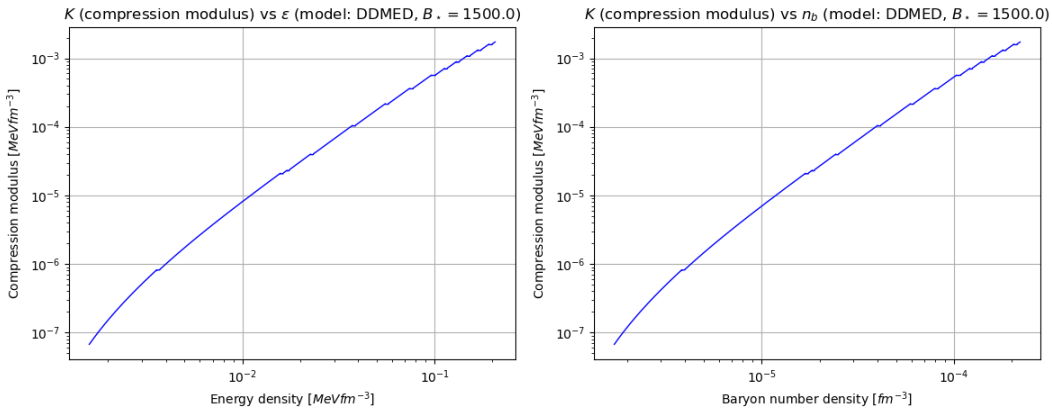

(a) (b)

Figure F.40: The same as Figure F.35, using the DDMED model with $B_\star = 1500$

F.5.7 DDPC1

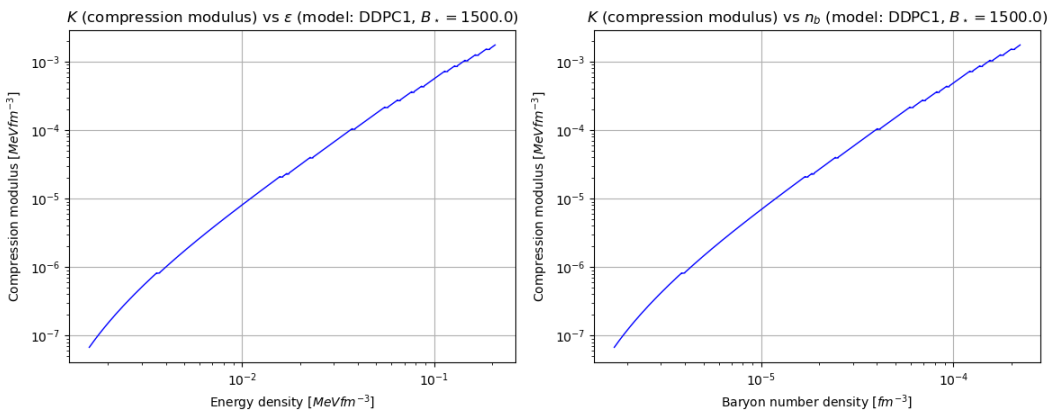

(a) (b)

Figure F.41: The same as Figure F.35, using the DDPC1 model with $B_\star = 1500$

F.5.8 SVMIN

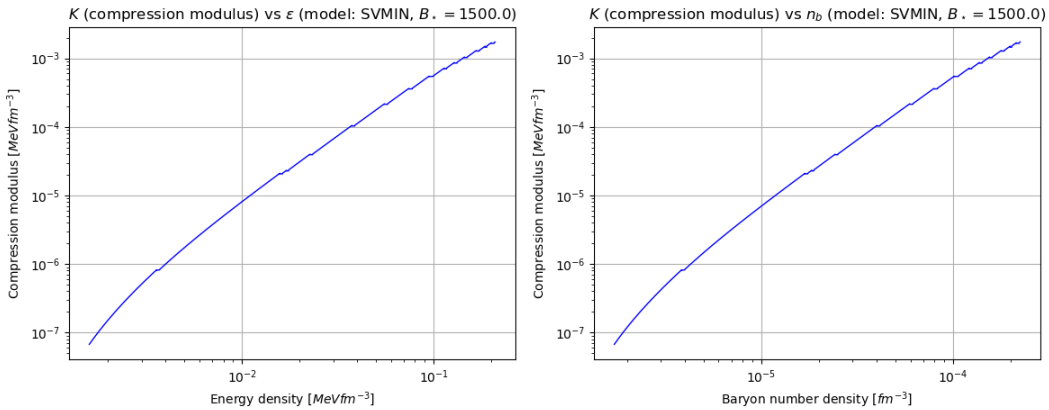

(a) (b)

Figure F.42: The same as Figure F.35, using the SVMIN model with $B_\star = 1500$

F.5.9 UNEDF0

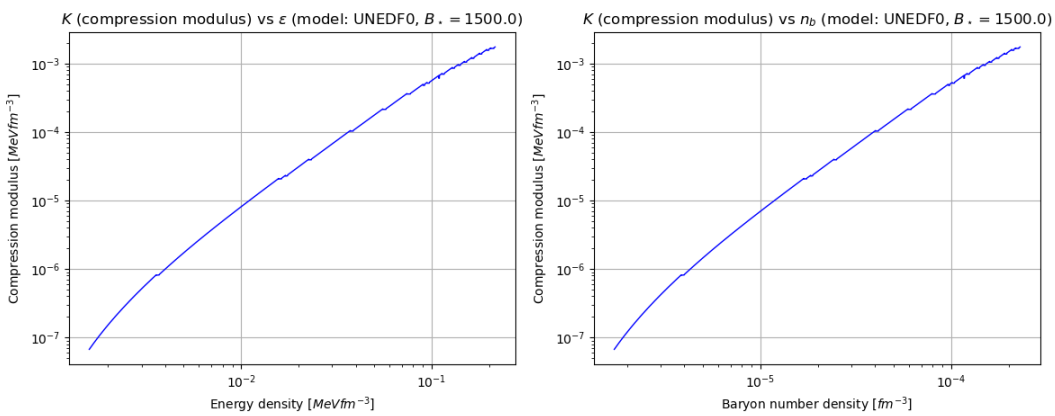

(a) (b)

Figure F.43: The same as Figure F.35, using the UNEDF0 model with $B_\star = 1500$

F.6 S_{mod} vs ϵ or n_b

F.6.1 SEMF

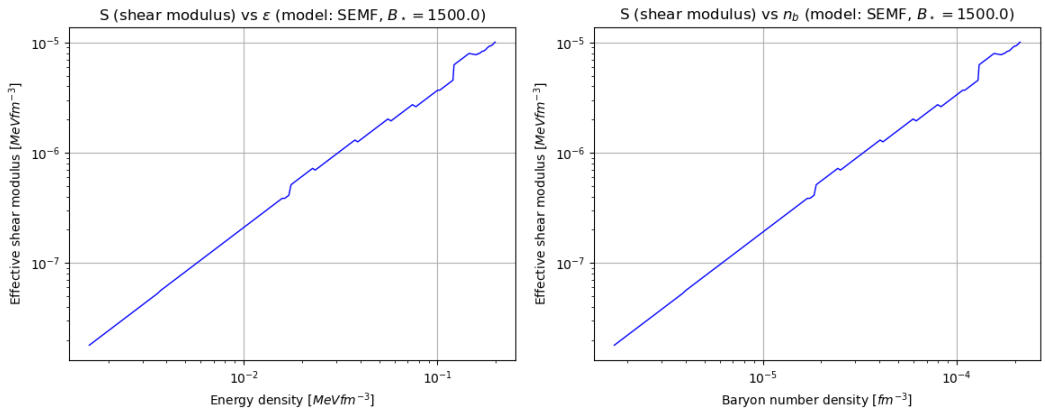

(a) (b)

Figure F.44: Effective shear modulus as a function of (a) energy density and of (b) baryon number density, using the SEMF model with magnetic field strength $B_\star = 1500$

F.6.2 FRDM2012

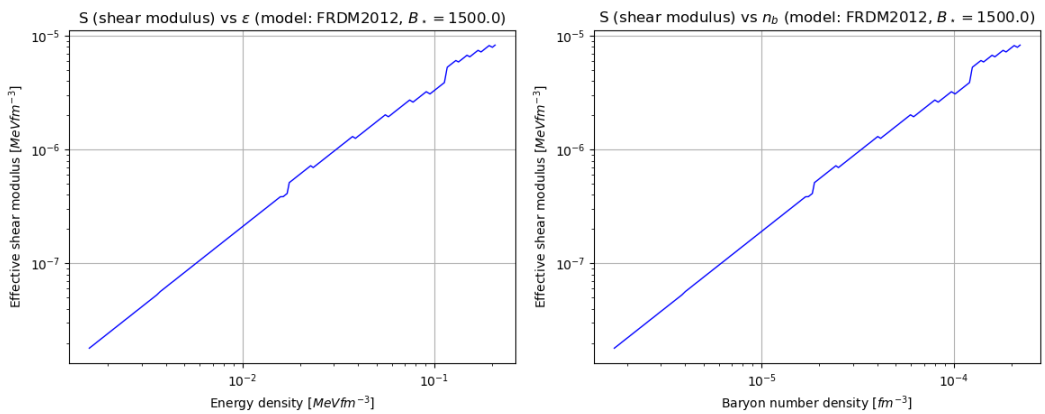

(a) (b)

Figure F.45: The same as Figure F.44, using the FRDM2012 model with $B_\star = 1500$

F.6.3 WS4RBF

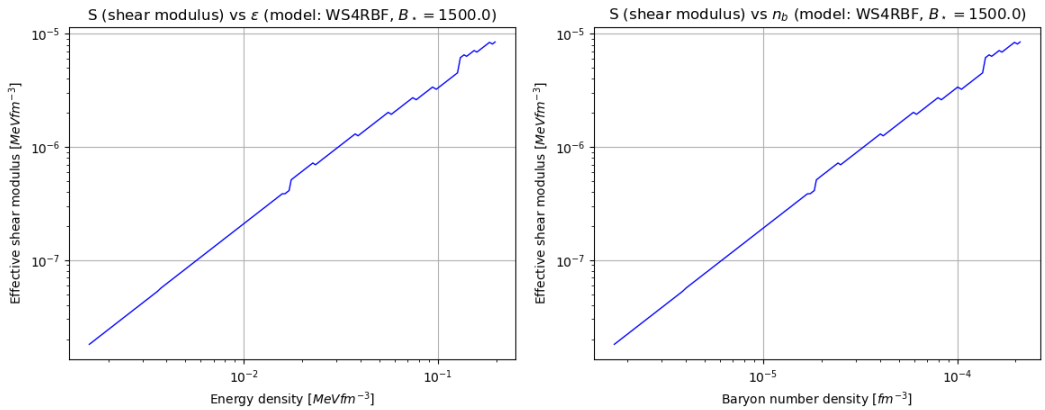

(a) (b)

Figure F.46: The same as Figure F.44, using the WS4RBF model with $B_\star = 1500$

F.6.4 BSKG3

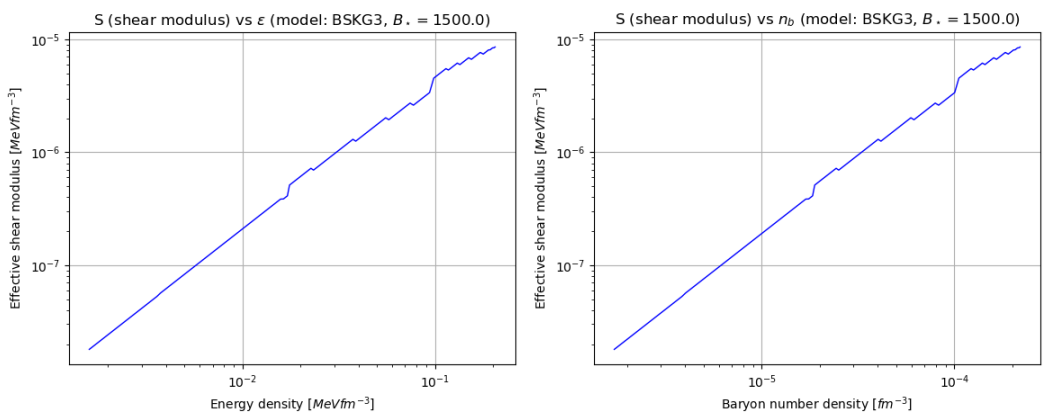

(a) (b)

Figure F.47: The same as Figure F.44, using the BSKG3 model with $B_\star = 1500$

F.6.5 HFB31

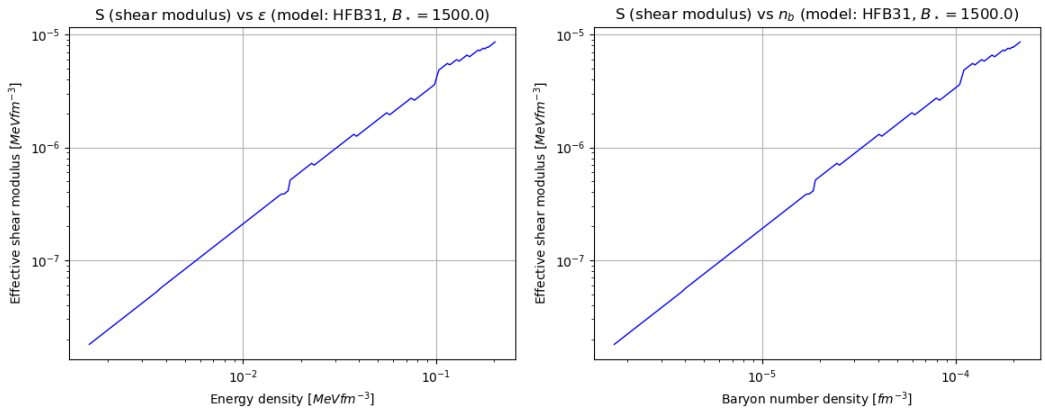

(a) (b)

Figure F.48: The same as Figure F.44, using the HFB31 model with $B_\star = 1500$

F.6.6 DDMED

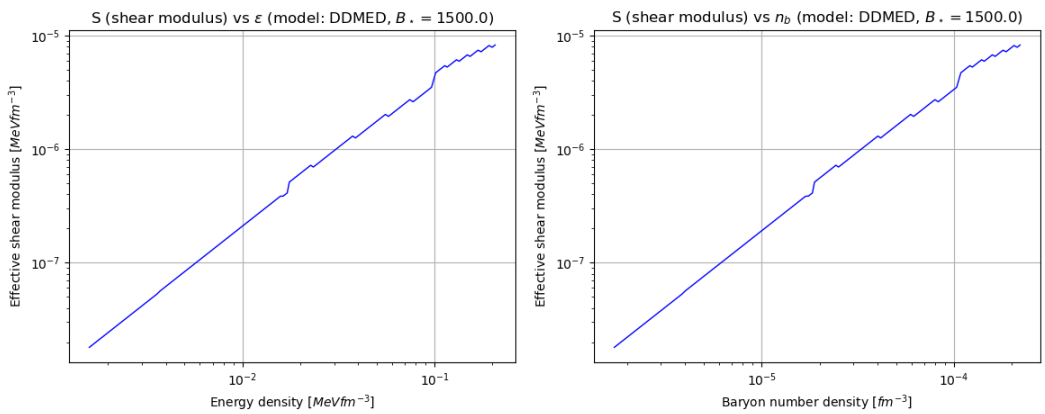

(a) (b)

Figure F.49: The same as Figure F.44, using the DDMED model with $B_\star = 1500$

F.6.7 DDPC1

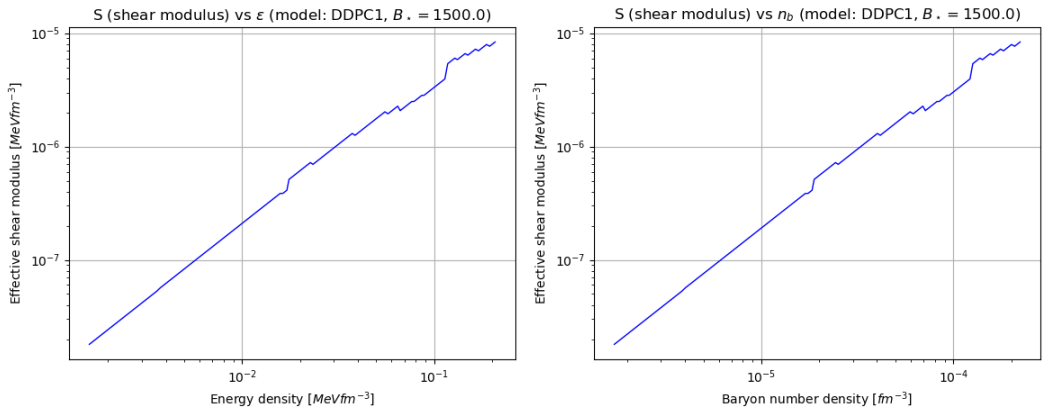

(a) (b)

Figure F.50: The same as Figure F.44, using the DDPC1 model with $B_\star = 1500$

F.6.8 SVMIN

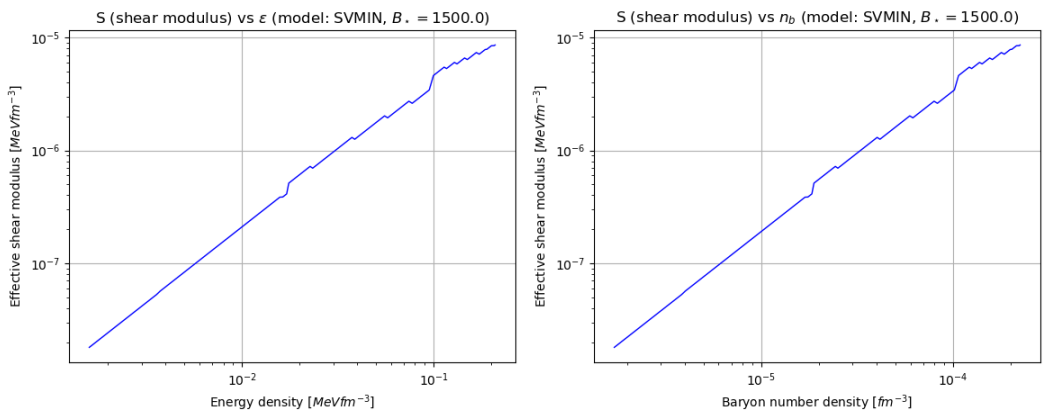

(a) (b)

Figure F.51: The same as Figure F.44, using the SVMIN model with $B_\star = 1500$

F.6.9 UNEDF0

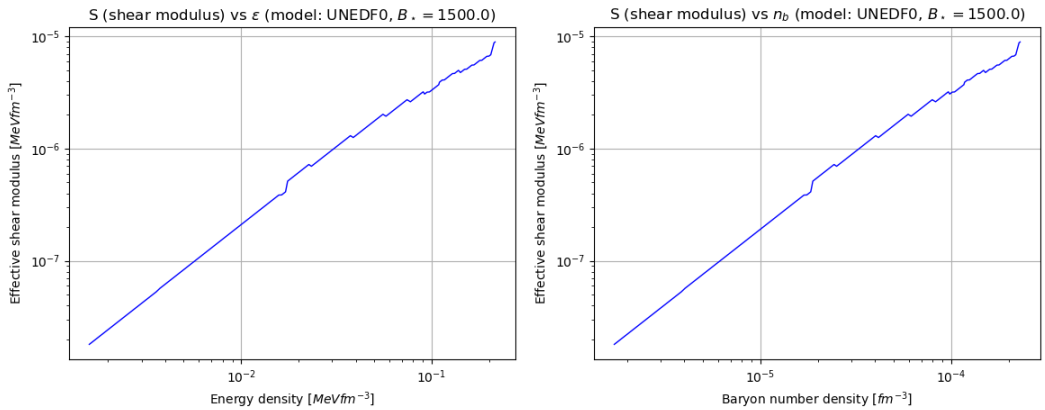

(a) (b)

Figure F.52: The same as Figure F.44, using the UNEDF0 model with $B_\star = 1500$

F.7 S_{mod}/K_{mod} vs ϵ or n_b

F.7.1 SEMF

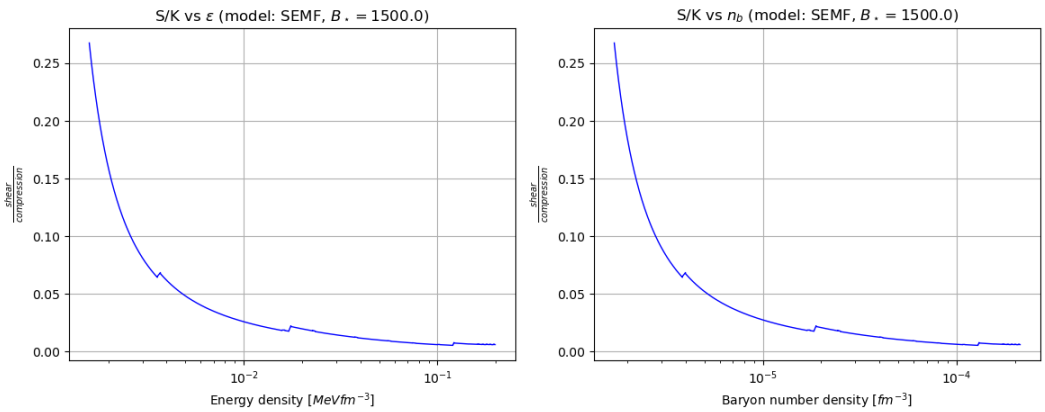

(a) (b)

Figure F.53: Effective shear modulus over compression modulus as a function of (a) energy density and of (b) baryon number density, using the SEMF model with magnetic field strength $B_\star = 1500$

F.7.2 FRDM2012

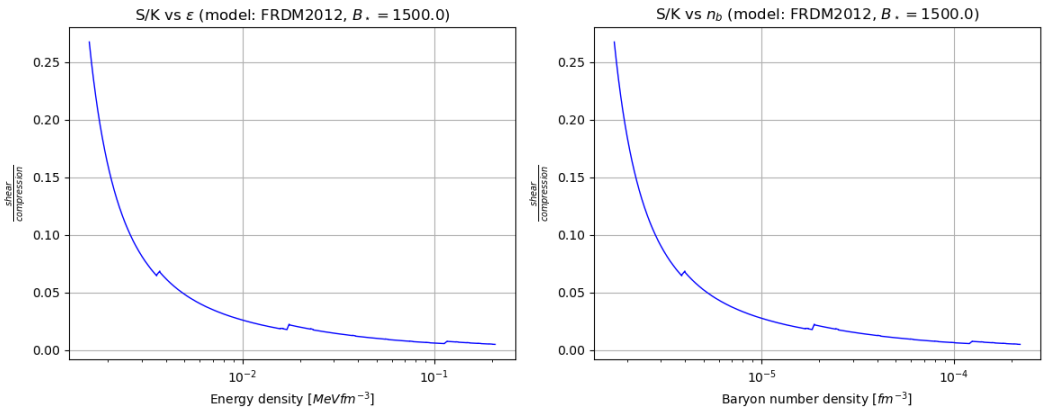

(a) (b)

Figure F.54: The same as Figure F.53, using the FRDM2012 model with $B_\star = 1500$

F.7.3 WS4RBF

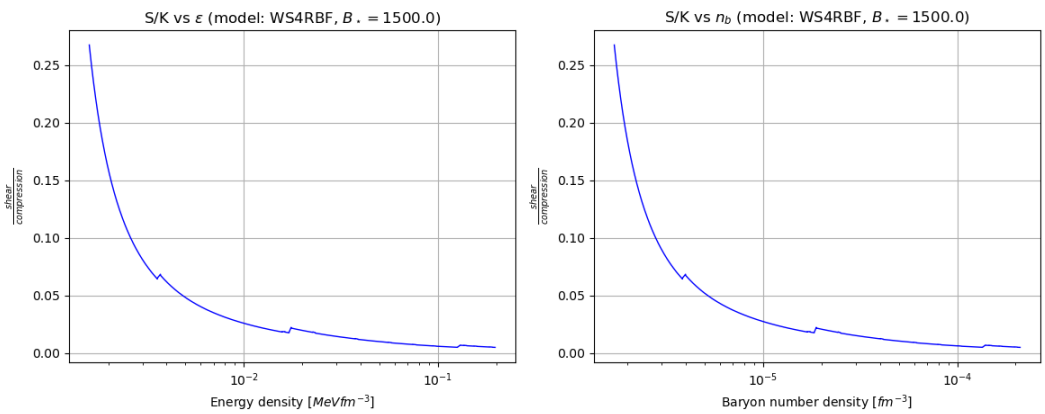

(a) (b)

Figure F.55: The same as Figure F.53, using the WS4RBF model with $B_\star = 1500$

F.7.4 BSKG3

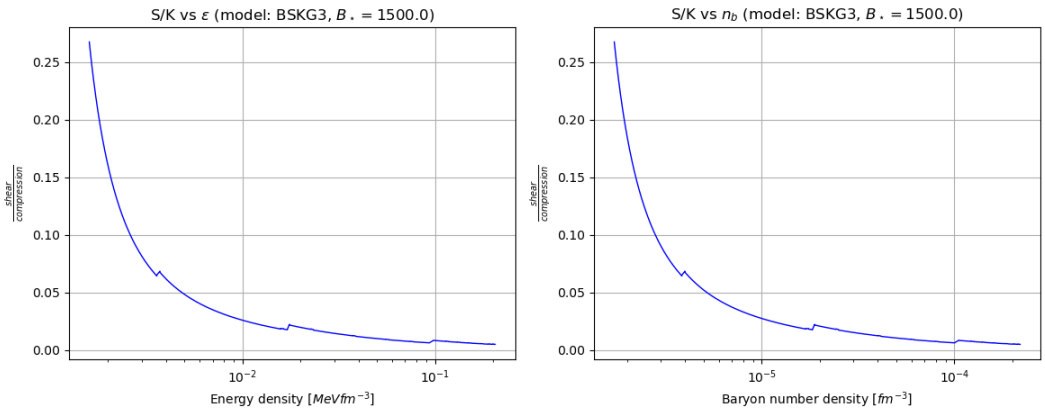

(a) (b)

Figure F.56: The same as Figure F.53, using the BSKG3 model with $B_\star = 1500$

F.7.5 HFB31

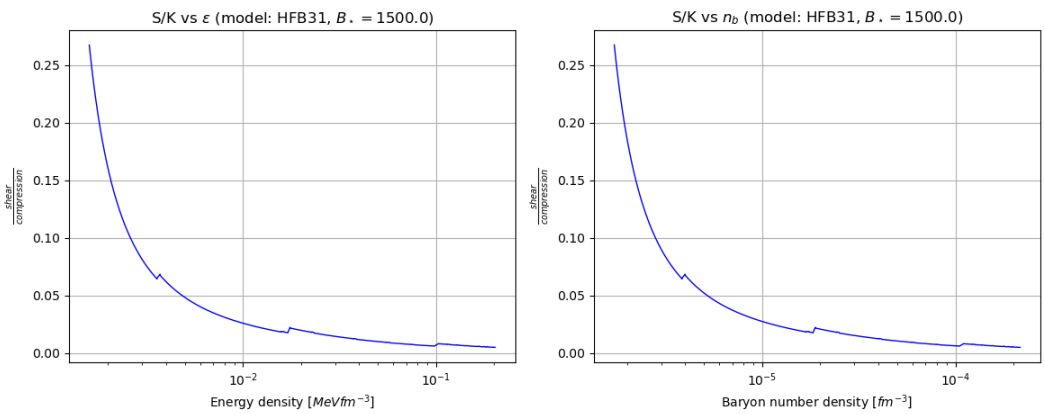

(a) (b)

Figure F.57: The same as Figure F.53, using the HFB31 model with $B_\star = 1500$

F.7.6 DDMED

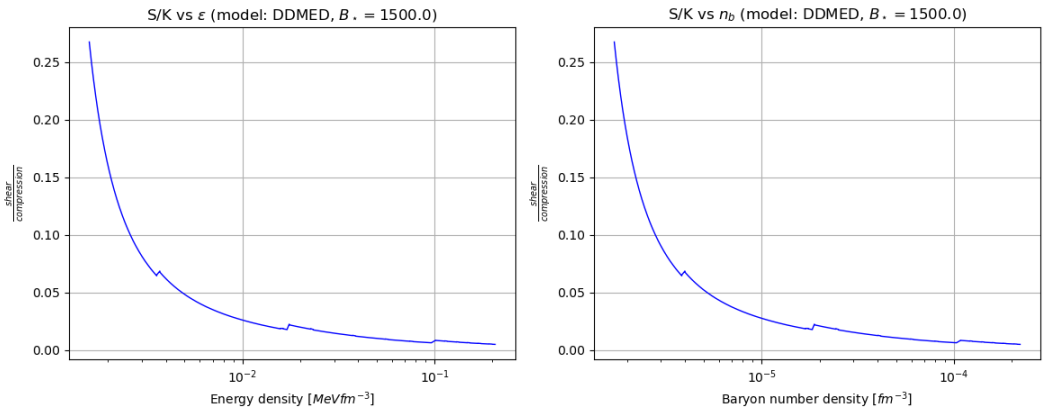

(a) (b)

Figure F.58: The same as Figure F.53, using the DDMED model with $B_\star = 1500$

F.7.7 DDPC1

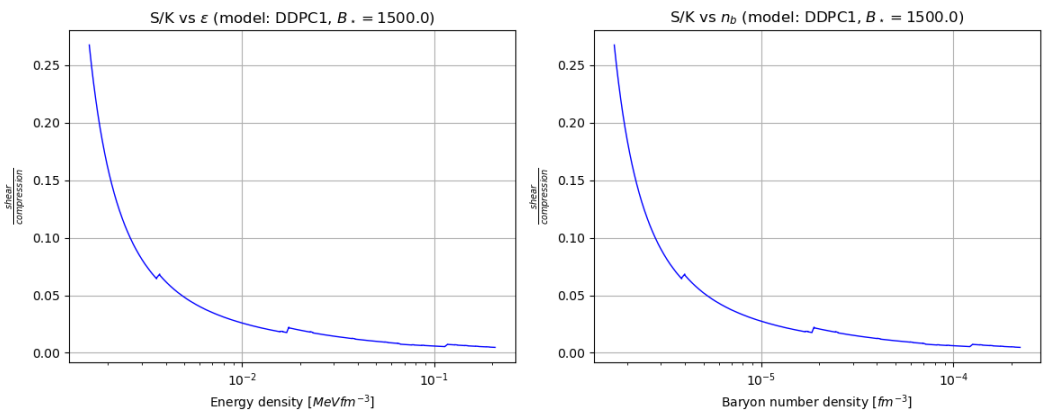

(a) (b)

Figure F.59: The same as Figure F.53, using the DDPC1 model with $B_\star = 1500$

F.7.8 SVMIN

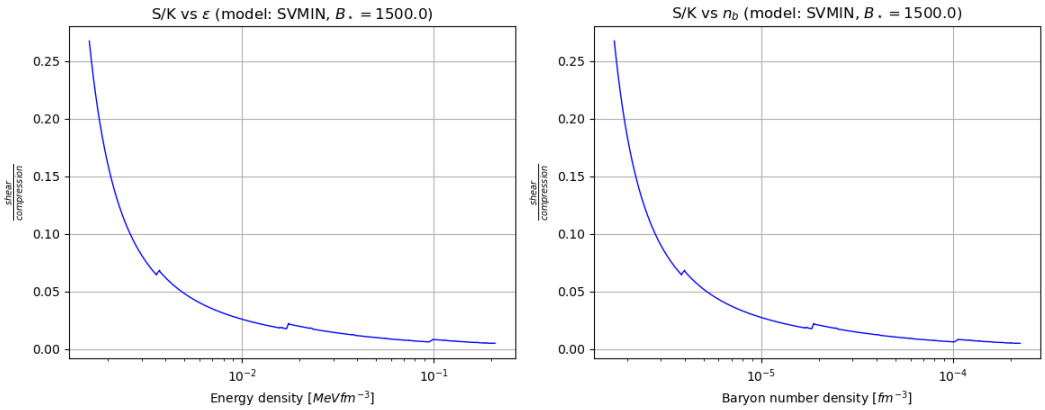

(a) (b)

Figure F.60: The same as Figure F.53, using the SVMIN model with $B_\star = 1500$

F.7.9 UNEDF0

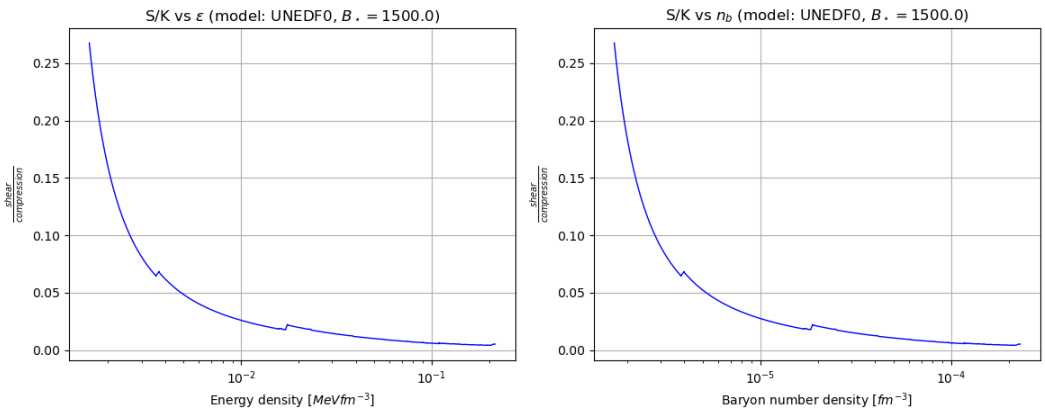

(a) (b)

Figure F.61: The same as Figure F.53, using the UNEDF0 model with $B_\star = 1500$

F.8 Z, N, Z/A vs ϵ or n_b

F.8.1 SEMF

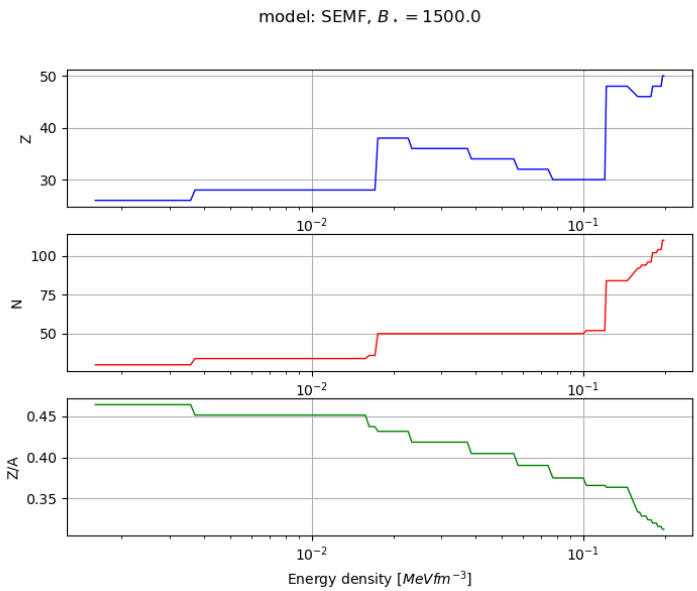

(a)

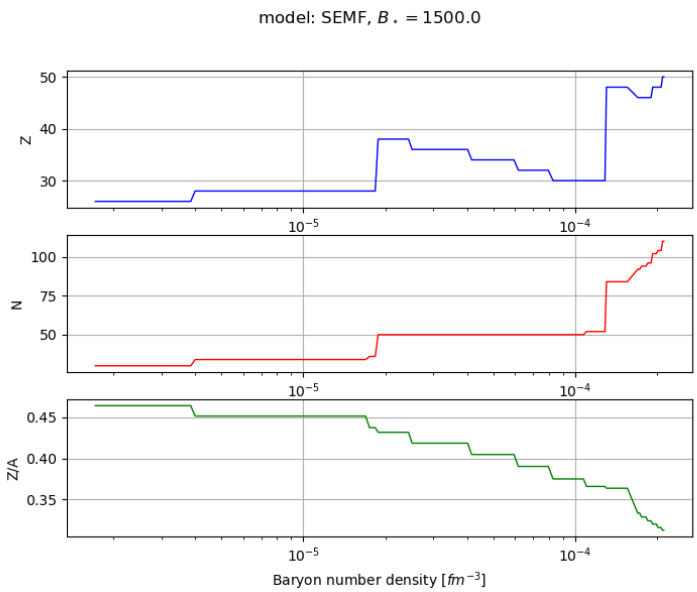

(b)

Figure F.62: Atomic number, neutron number and proton fraction as a function of (a) energy density and of (b) baryon number density, using the SEMF model with magnetic field strength $B_\star = 1500$

F.8.2 FRDM2012

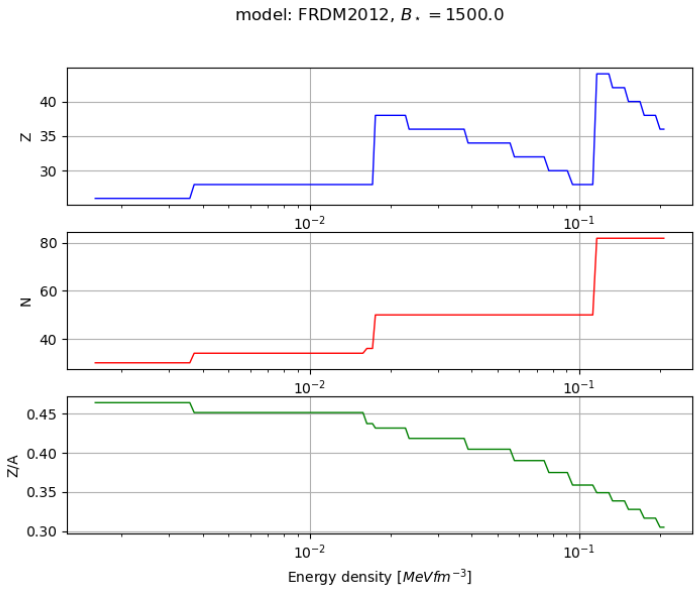

(a)

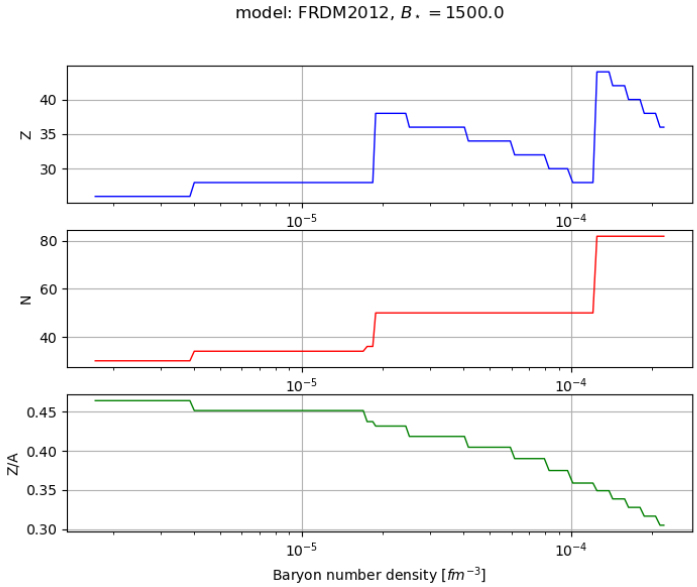

(b)

Figure F.63: The same as Figure F.62, using the FRDM2012 model with $B_\star = 1500$

F.8.3 WS4RBF

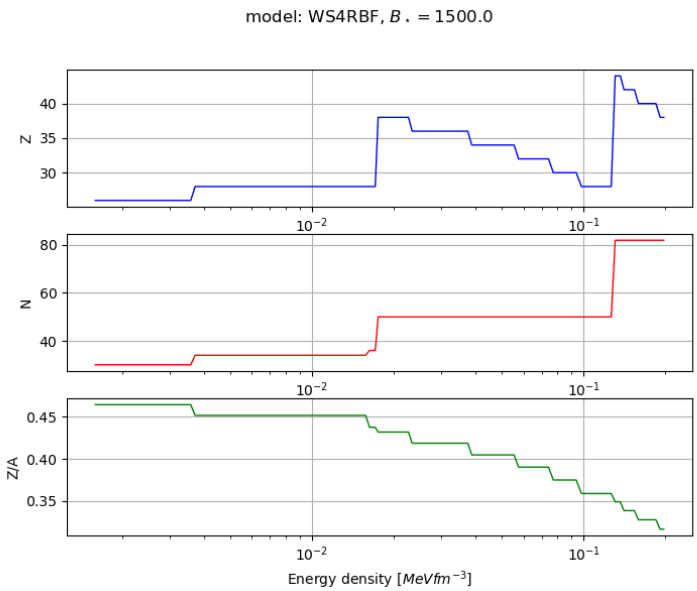

(a)

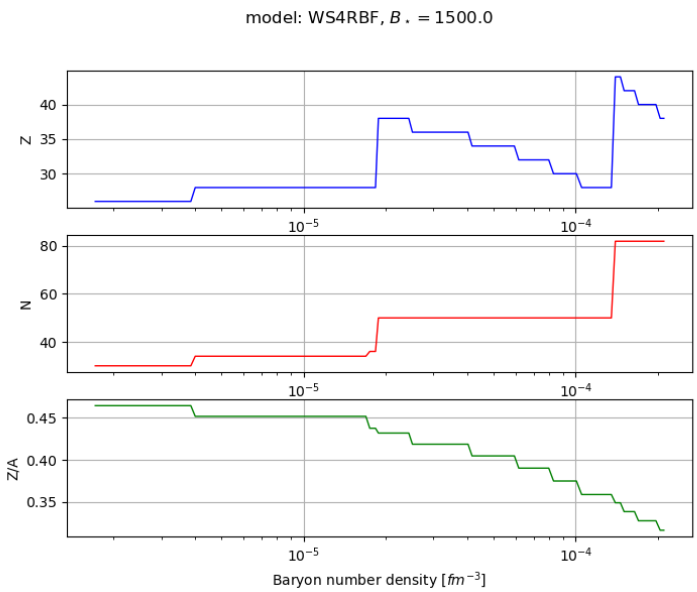

(b)

Figure F.64: The same as Figure F.62, using the WS4RBF model with $B_\star = 1500$

F.8.4 BSKG3

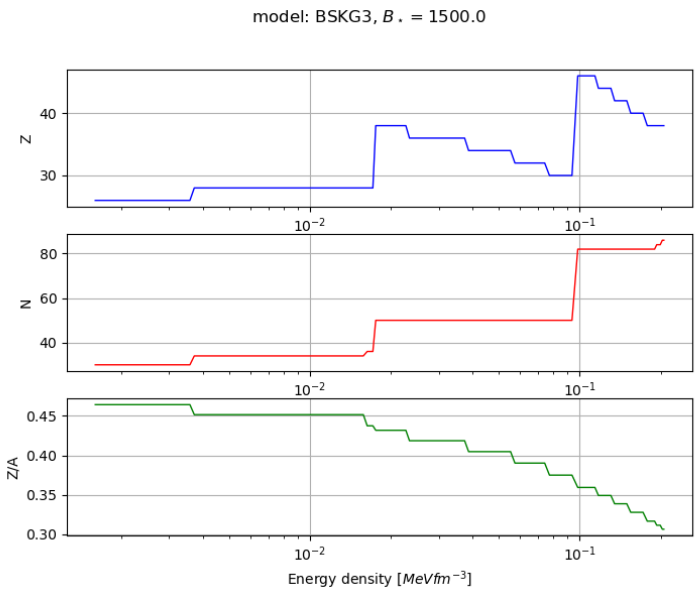

(a)

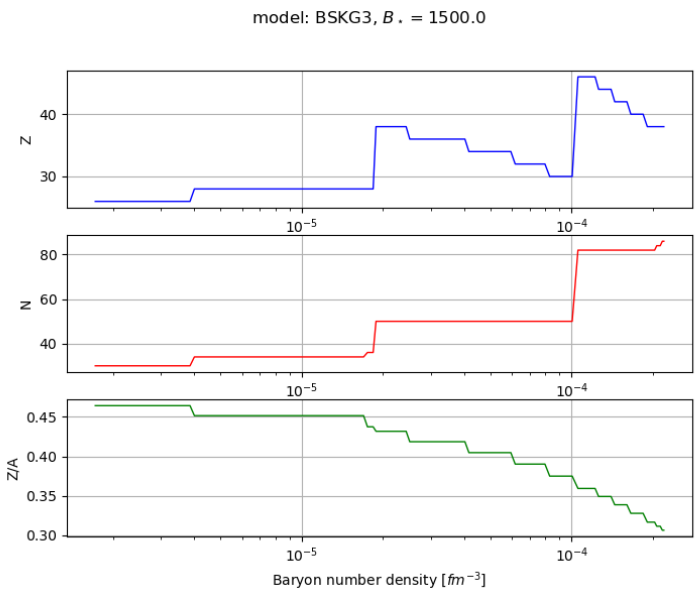

(b)

Figure F.65: The same as Figure F.62, using the BSKG3 model with $B_\star = 1500$

F.8.5 HFB31

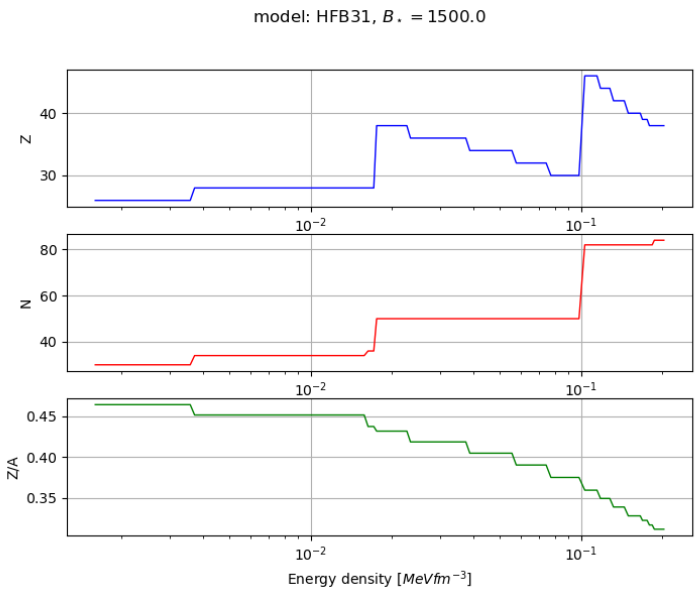

(a)

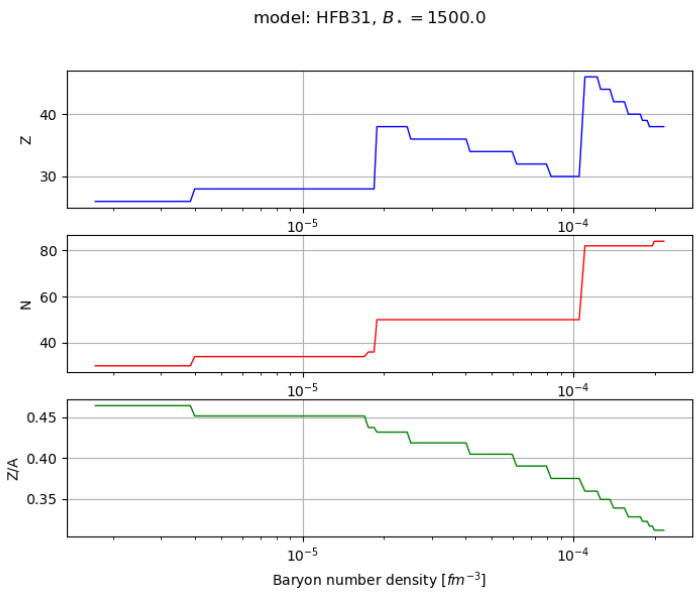

(b)

Figure F.66: The same as Figure F.62, using the HFB31 model with $B_\star = 1500$

F.8.6 DDMED

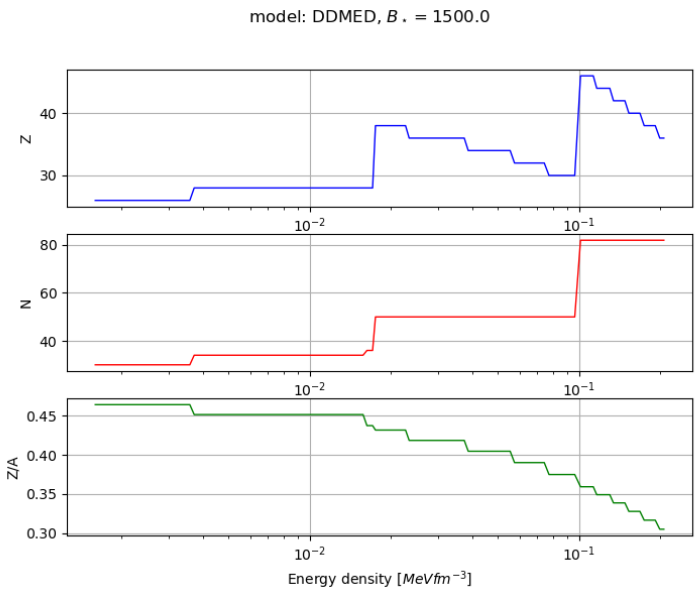

(a)

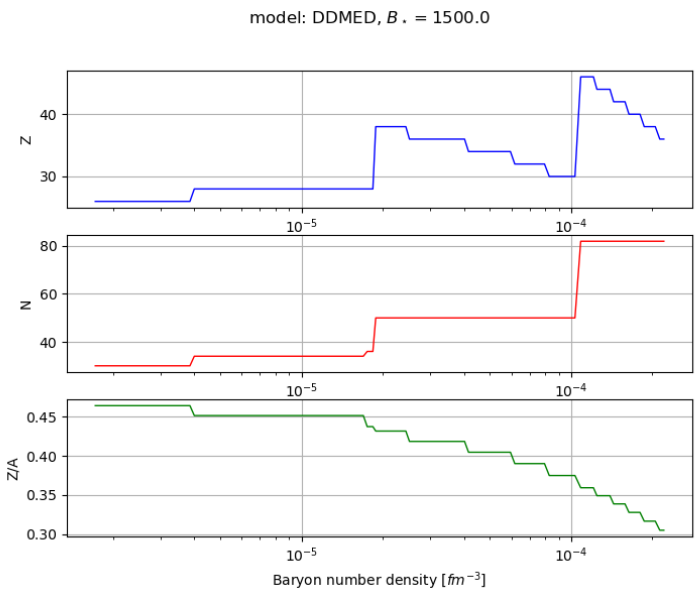

(b)

Figure F.67: The same as Figure F.62, using the DDMED model with $B_\star = 1500$

F.8.7 DDPC1

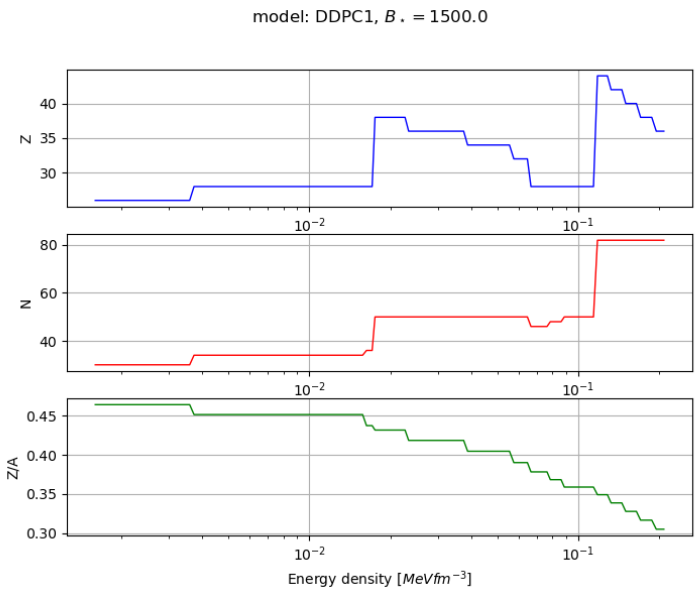

(a)

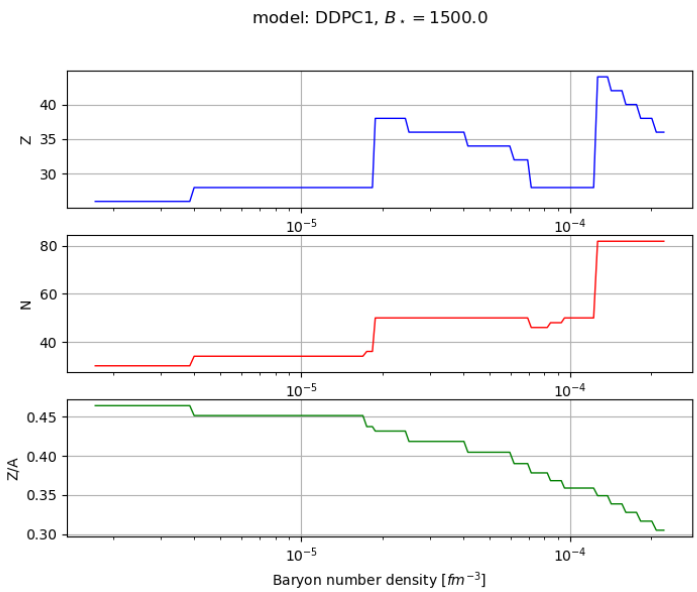

(b)

Figure F.68: The same as Figure F.62, using the DDPC1 model with $B_\star = 1500$

F.8.8 SVMIN

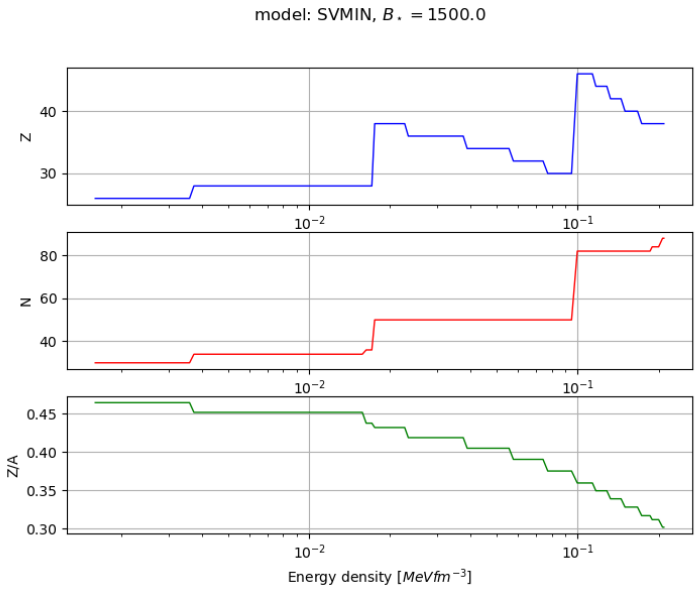

(a)

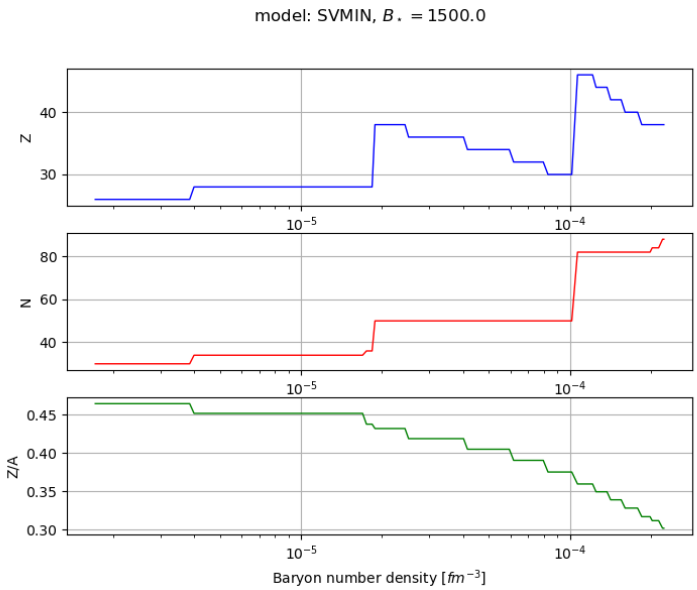

(b)

Figure F.69: The same as Figure F.62, using the SVMIN model with $B_\star = 1500$

F.8.9 UNEDF0

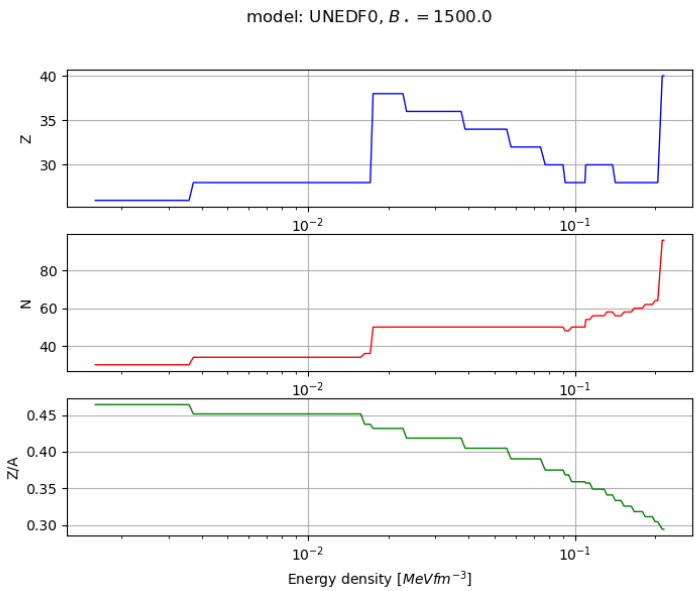

(a)

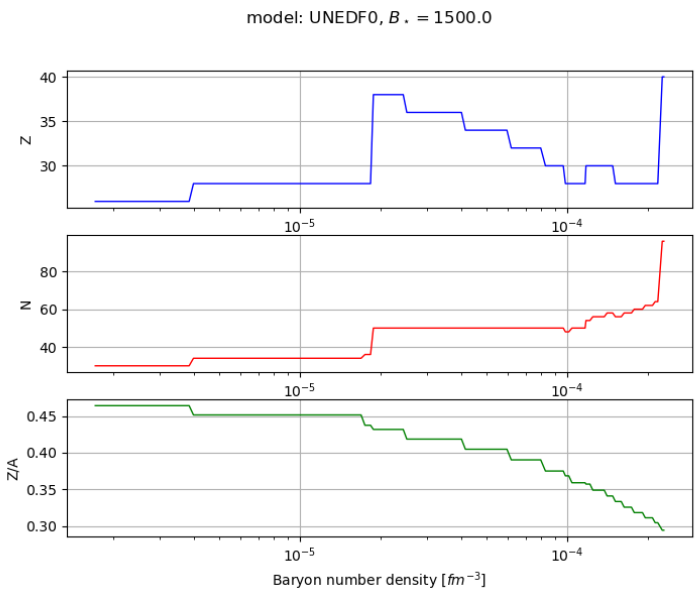

(b)

Figure F.70: The same as Figure F.62, using the UNEDF0 model with $B_\star = 1500$

F.9 M_{cr} for different M and R

F.9.1 SEMF

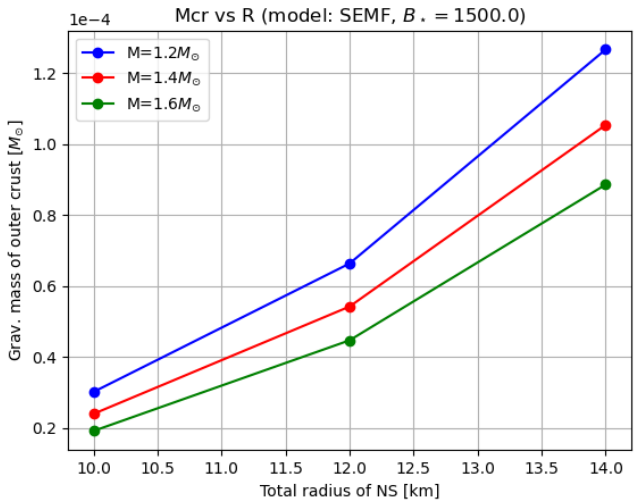

Figure F.71: Mass of outer crust for different masses and radii of NS, using the SEMF model with magnetic field strength $B_\star = 1500$

F.9.2 FRDM2012

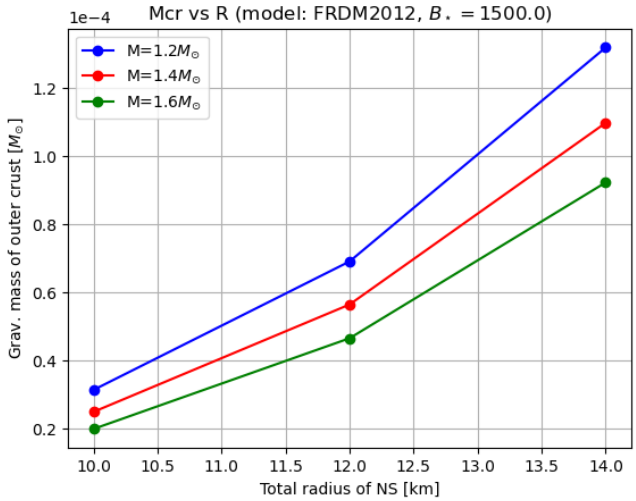

Figure F.72: The same as Figure F.71, using the FRDM2012 model with $B_\star = 1500$

F.9.3 WS4RBF

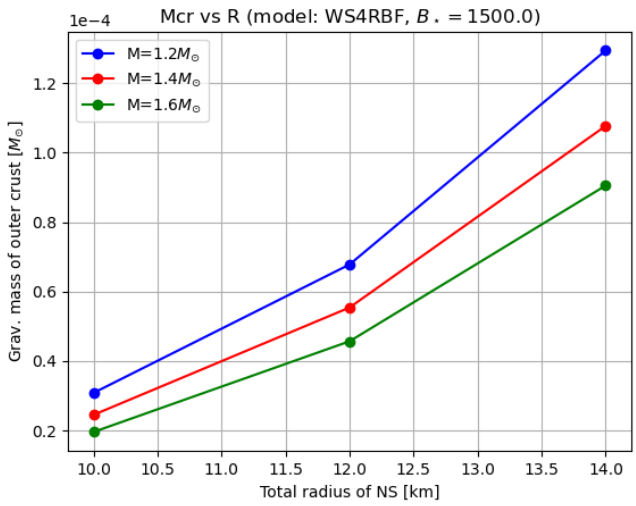

Figure F.73: The same as Figure F.71, using the WS4RBF model with $B_\star = 1500$

F.9.4 BSKG3

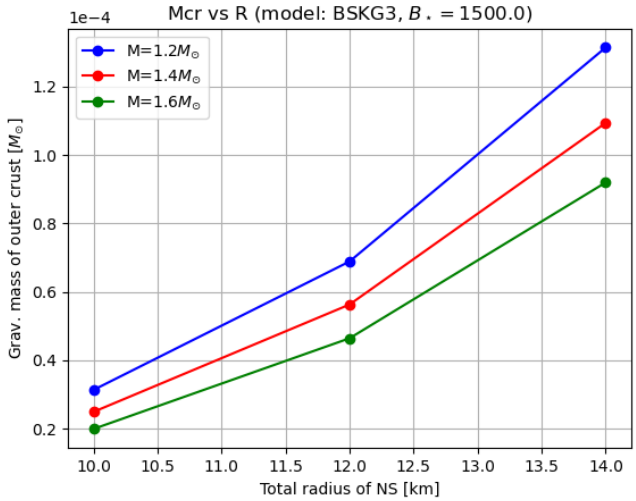

Figure F.74: The same as Figure F.71, using the BSKG3 model with $B_\star = 1500$

F.9.5 HFB31

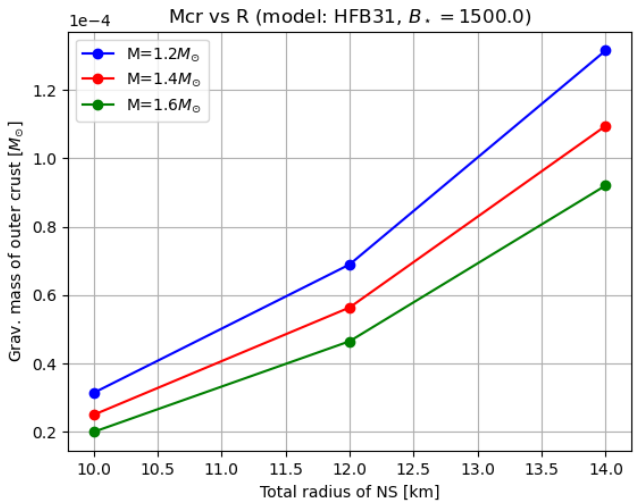

Figure F.75: The same as Figure F.71, using the HFB31 model with $B_\star = 1500$

F.9.6 DDMED

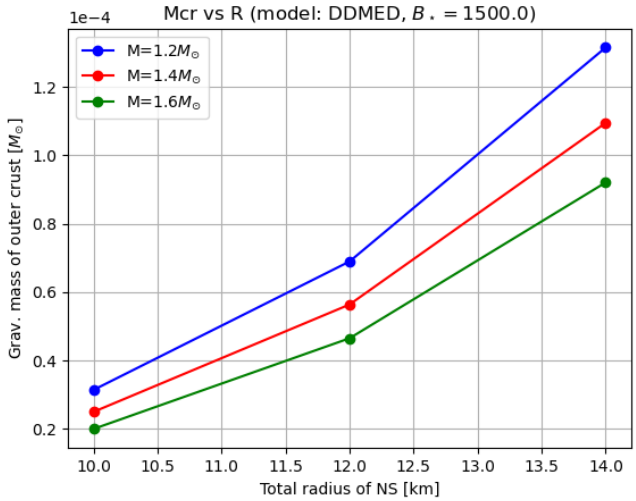

Figure F.76: The same as Figure F.71, using the DDMED model with $B_\star = 1500$

F.9.7 DDPC1

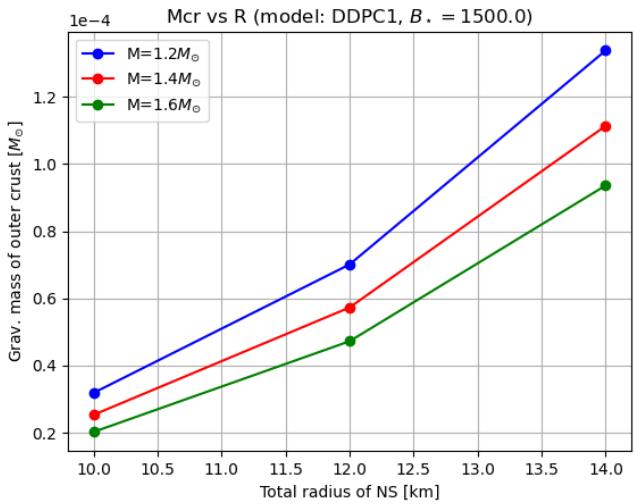

Figure F.77: The same as Figure F.71, using the DDPC1 model with $B_\star = 1500$

F.9.8 SVMIN

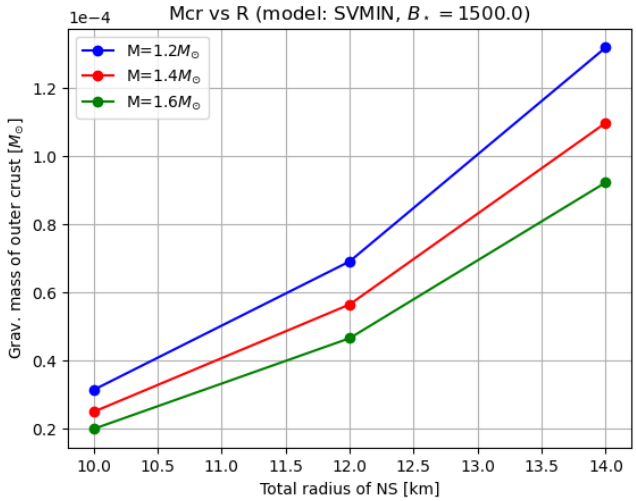

Figure F.78: The same as Figure F.71, using the SVMIN model with $B_\star = 1500$

F.9.9 UNEDF0

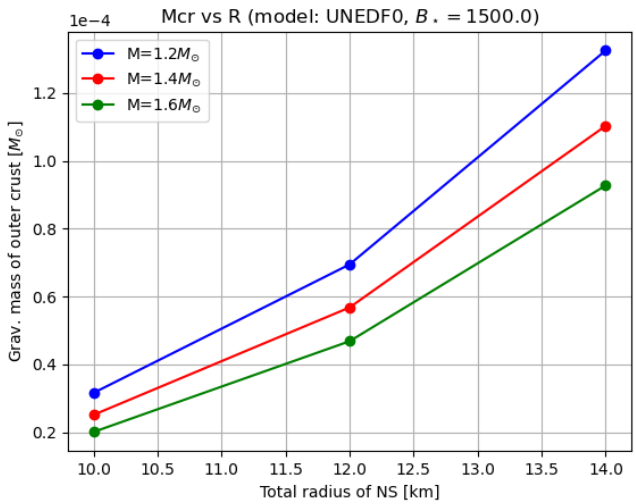

Figure F.79: The same as Figure F.71, using the UNEDF0 model with $B_\star = 1500$

F.10 z_{drip} for different M and R

F.10.1 SEMF

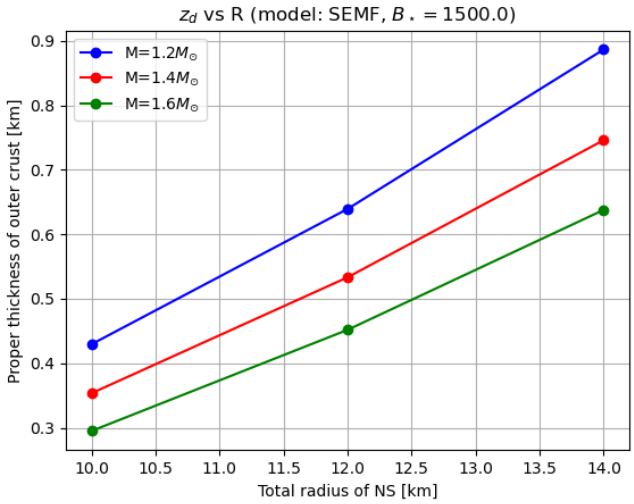

Figure F.80: Proper depth of neutron-drip transition for different masses and radii of NS, using the SEMF model with magnetic field strength $B_\star = 1500$

F.10.2 FRDM2012

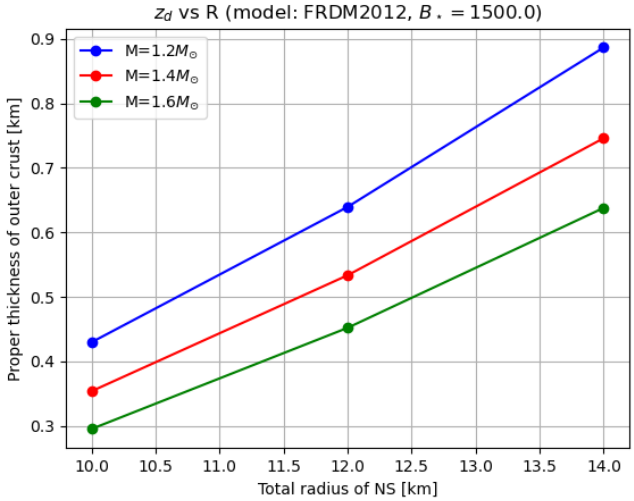

Figure F.81: The same as Figure F.80, using the FRDM2012 model with $B_\star = 1500$

F.10.3 WS4RBF

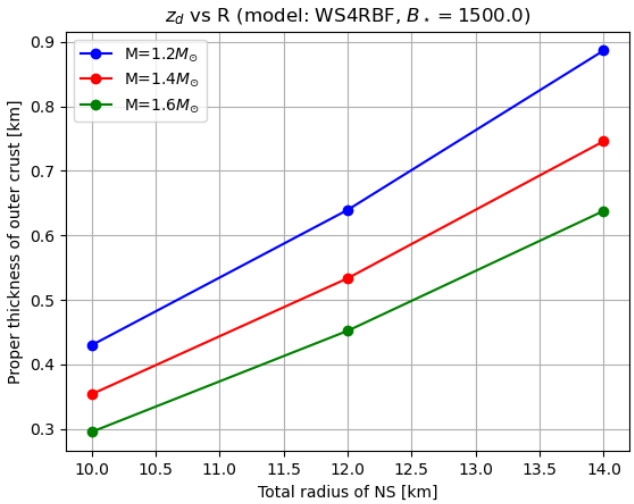

Figure F.82: The same as Figure F.80, using the WS4RBF model with $B_\star = 1500$

F.10.4 BSKG3

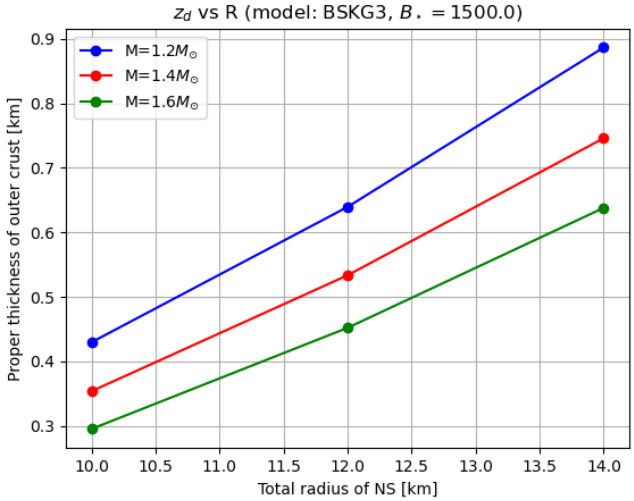

Figure F.83: The same as Figure F.80, using the BSKG3 model with $B_\star = 1500$

F.10.5 HFB31

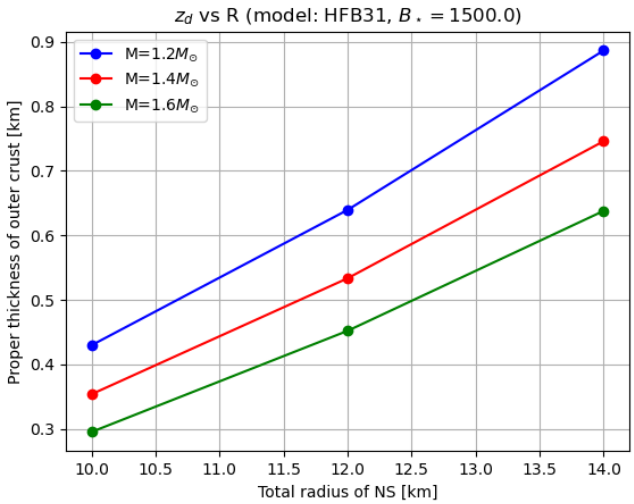

Figure F.84: The same as Figure F.80, using the HFB31 model with $B_\star = 1500$

F.10.6 DDMED

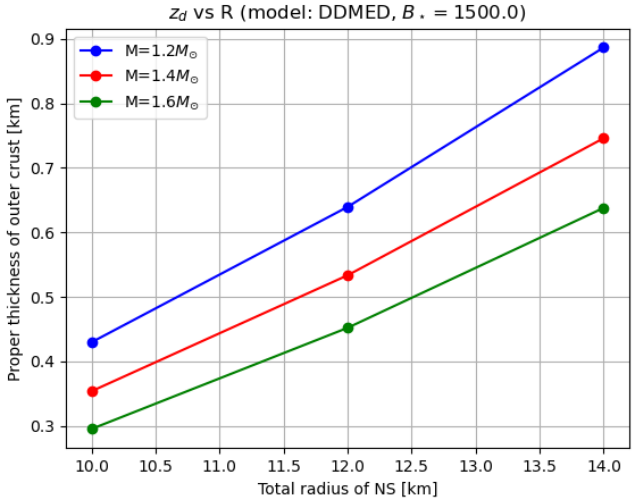

Figure F.85: The same as Figure F.80, using the DDMED model with $B_\star = 1500$

F.10.7 DDPC1

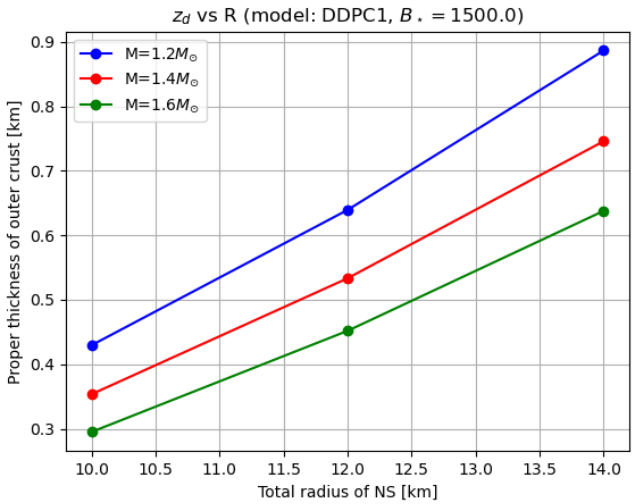

Figure F.86: The same as Figure F.80, using the DDPC1 model with $B_\star = 1500$

F.10.8 SVMIN

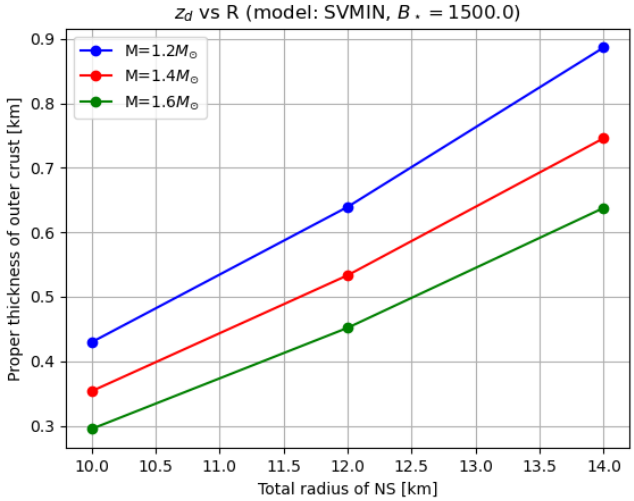

Figure F.87: The same as Figure F.80, using the SVMIN model with $B_\star = 1500$

F.10.9 UNEDF0

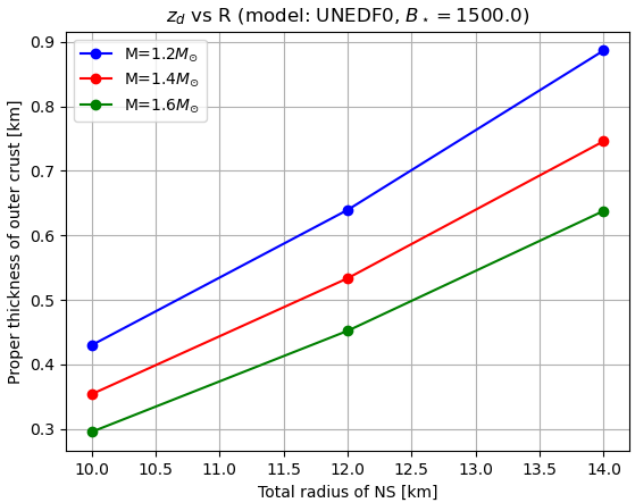

Figure F.88: The same as Figure F.80, using the UNEDF0 model with $B_\star = 1500$

Appendix G

Figures for $B_\star = 2000$

Below are the Figures, like those in Subsections 5.4.3 - 5.4.13, for the models: SEMF, FRDM2012, WS4RBF, BSKG3, HFB31, DDMED, DDPC1, SVMIN and UNEDF0, individually, with magnetic field strength $B_\star = 2000$.

G.1 P vs ϵ or n_b

G.1.1 SEMF

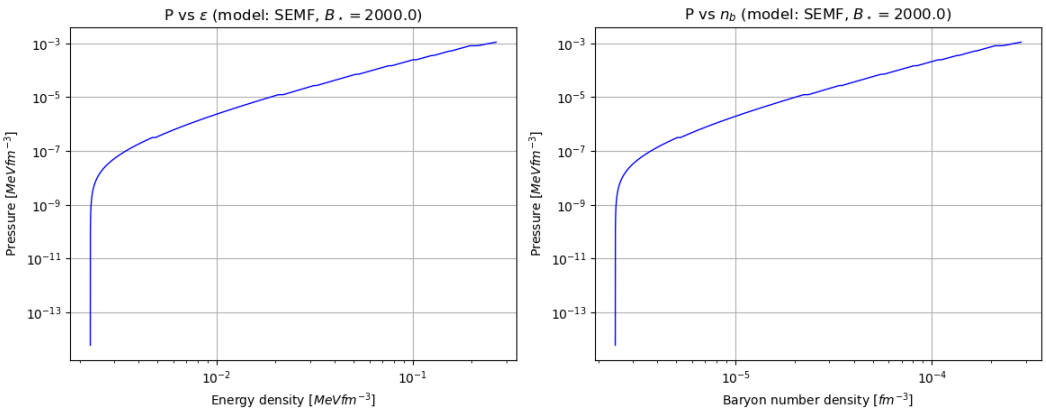

(a) (b)

Figure G.1: Equation of State, (a) pressure as a function of energy density and (b) pressure as a function of baryon number density, using the SEMF model with magnetic field strength $B_\star = 2000$

G.1.2 FRDM2012

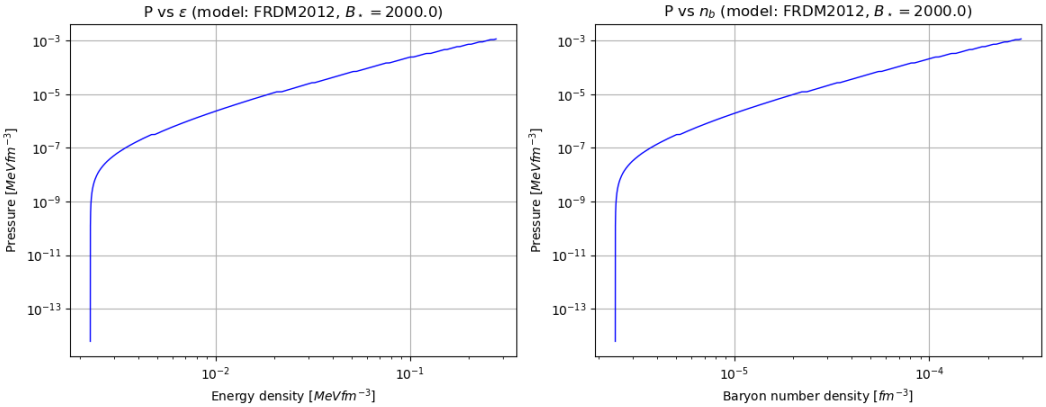

(a) (b)

Figure G.2: The same as Figure G.1, using the FRDM2012 model with $B_\star = 2000$

G.1.3 WS4RBF

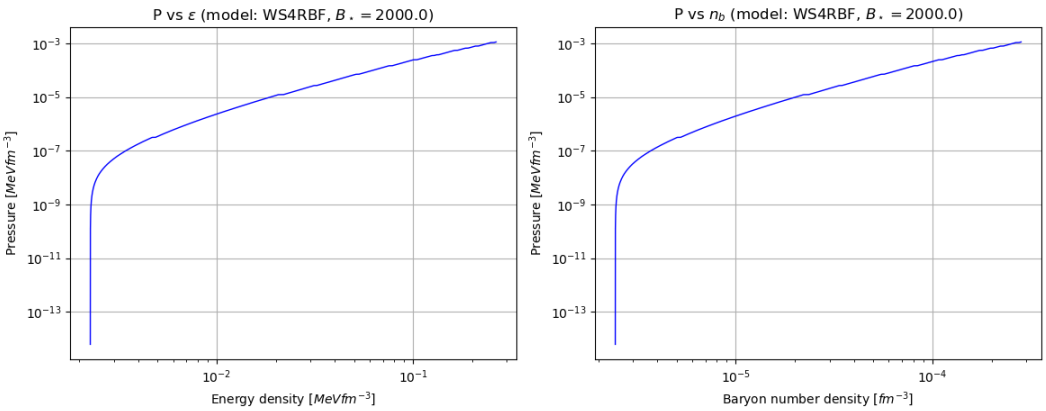

(a) (b)

Figure G.3: The same as Figure G.1, using the WS4RBF model with $B_\star = 2000$

G.1.4 BSKG3

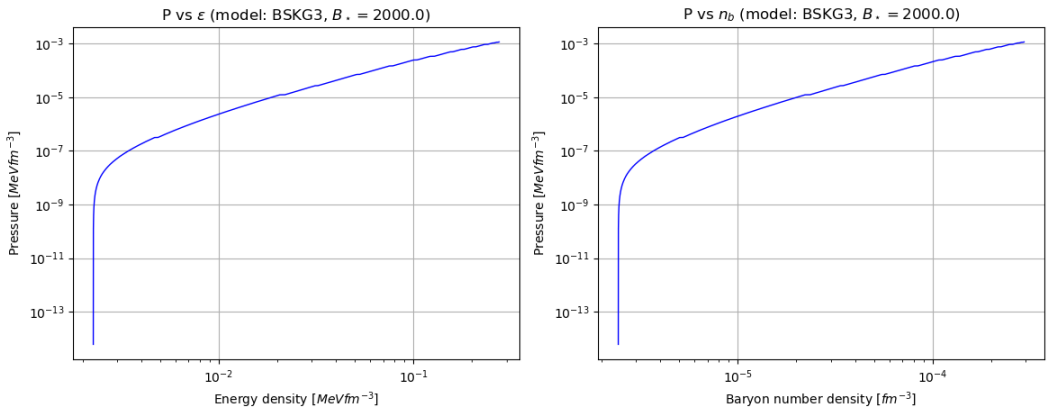

(a) (b)

Figure G.4: The same as Figure G.1, using the BSKG3 model with $B_\star = 2000$

G.1.5 HFB31

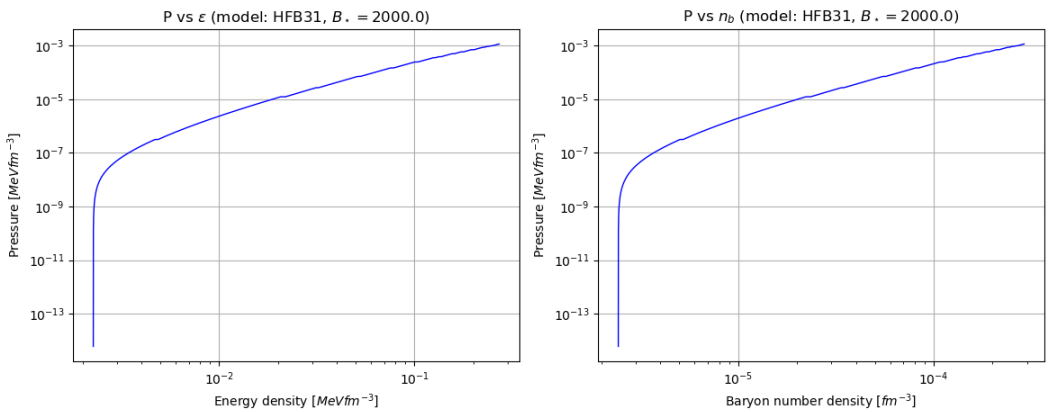

(a) (b)

Figure G.5: The same as Figure G.1, using the HFB31 model with $B_\star = 2000$

G.1.6 DDMED

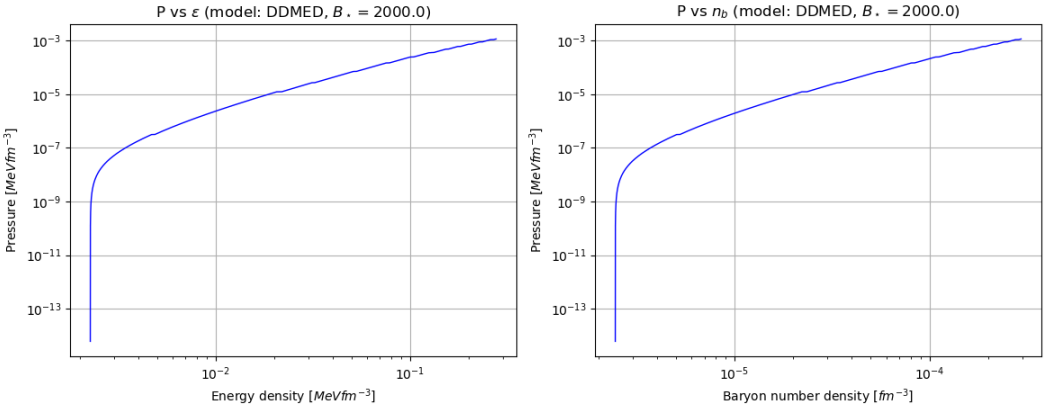

(a) (b)

Figure G.6: The same as Figure G.1, using the DDMED model with $B_\star = 2000$

G.1.7 DDPC1

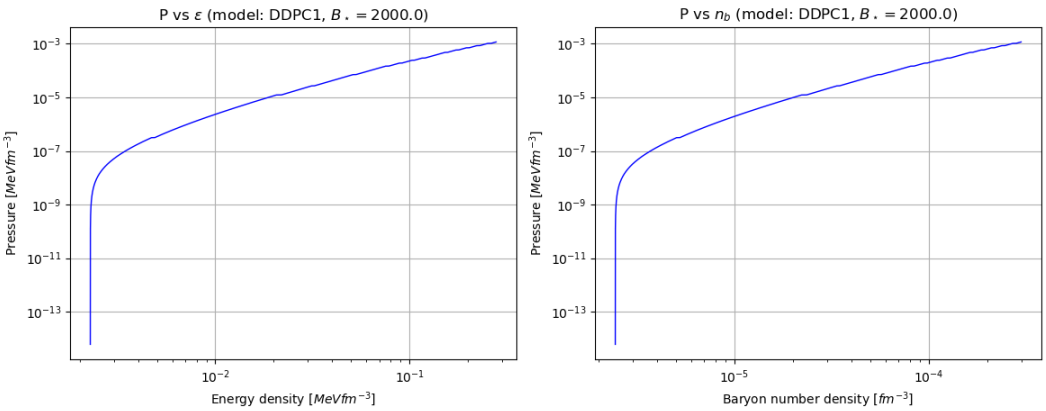

(a) (b)

Figure G.7: The same as Figure G.1, using the DDPC1 model with $B_\star = 2000$

G.1.8 SVMIN

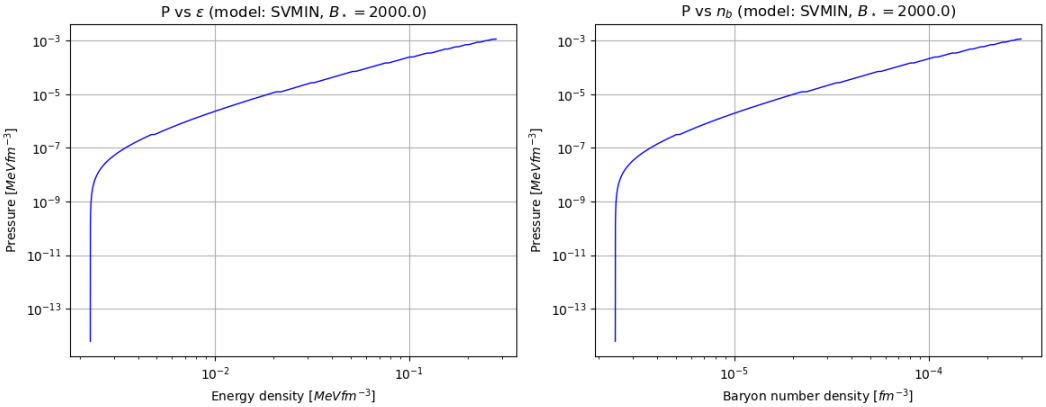

(a) (b)

Figure G.8: The same as Figure G.1, using the SVMIN model with $B_\star = 2000$

G.1.9 UNEDF0

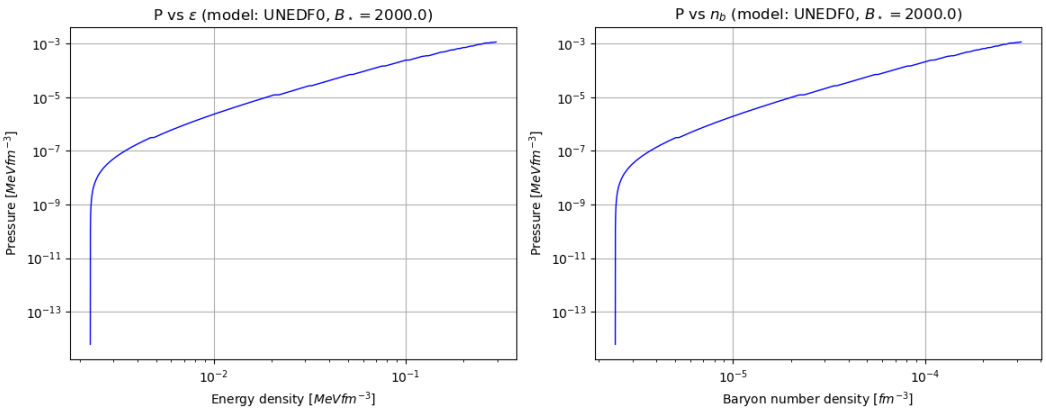

(a) (b)

Figure G.9: The same as Figure G.1, using the UNEDF0 model with $B_\star = 2000$

G.2 Fitting $P = K\epsilon^G$

G.2.1 SEMF

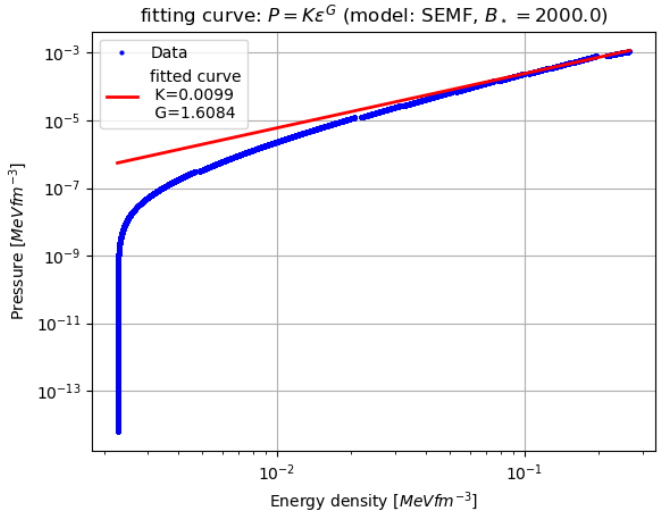

Figure G.10: A polytropic EoS $P = K\epsilon^G$ for fitting, using the SEMF model with magnetic field strength $B_\star = 2000$

G.2.2 FRDM2012

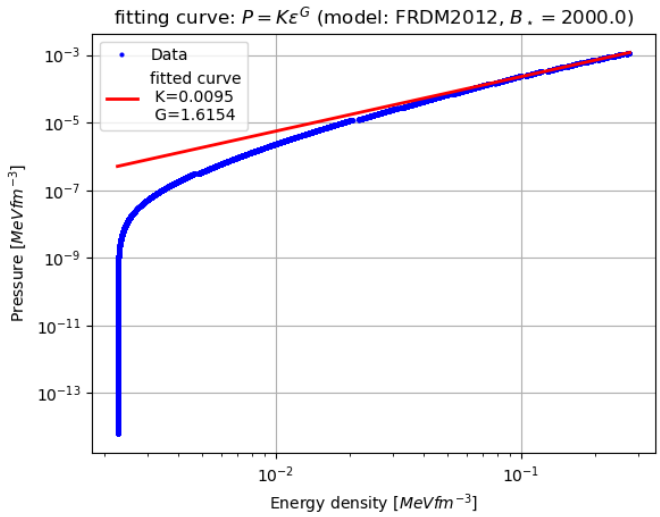

Figure G.11: The same as Figure G.10, using the FRDM2012 model with $B_\star = 2000$

G.2.3 WS4RBF

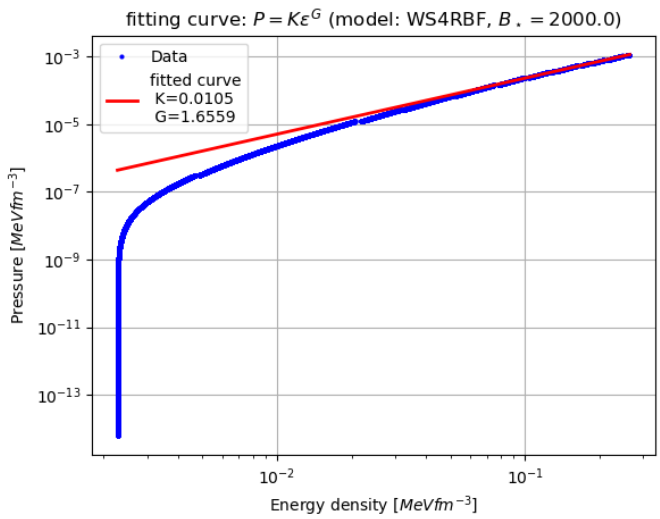

Figure G.12: The same as Figure G.10, using the WS4RBF model with $B_\star = 2000$

G.2.4 BSKG3

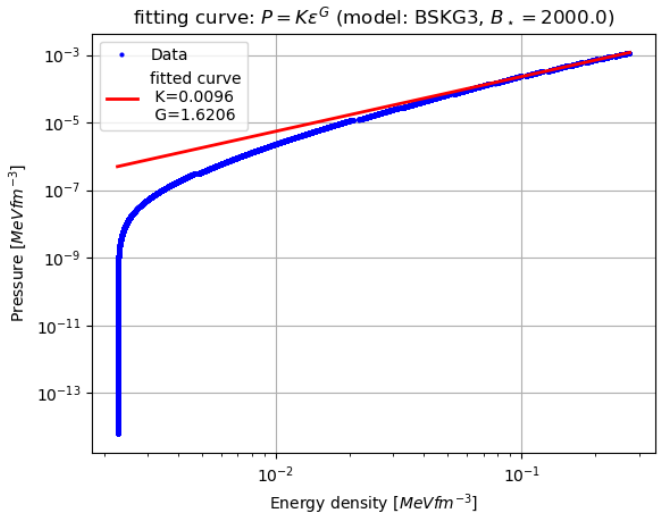

Figure G.13: The same as Figure G.10, using the BSKG3 model with $B_\star = 2000$

G.2.5 HFB31

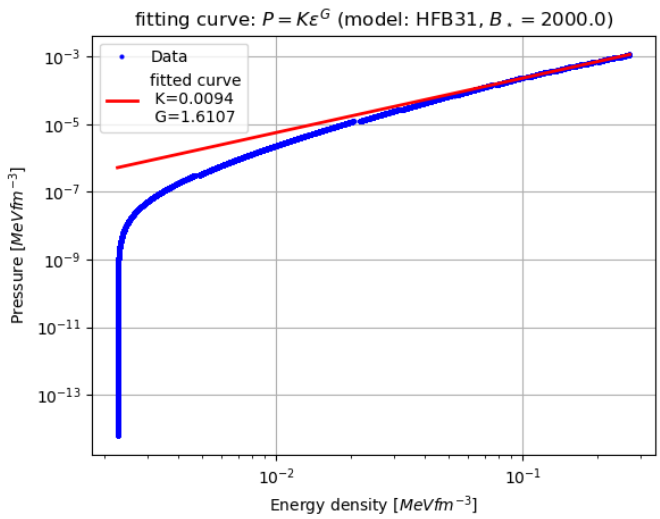

Figure G.14: The same as Figure G.10, using the HFB31 model with $B_\star = 2000$

G.2.6 DDMED

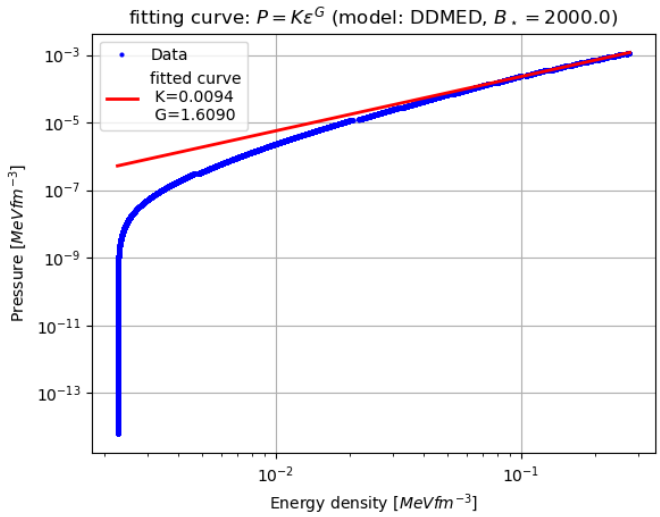

Figure G.15: The same as Figure G.10, using the DDMED model with $B_\star = 2000$

G.2.7 DDPC1

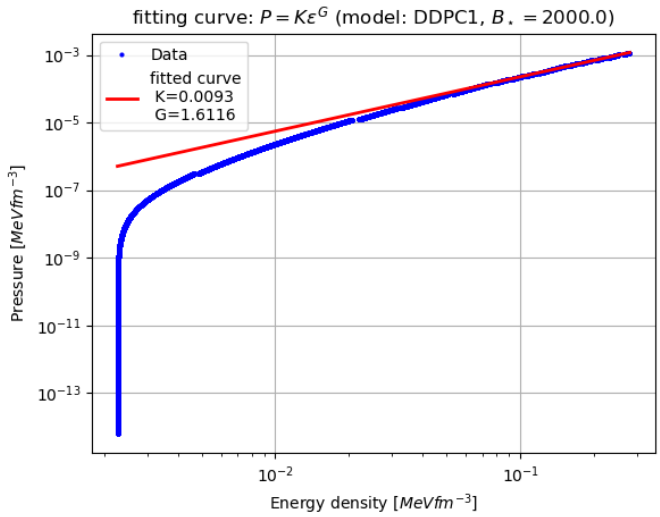

Figure G.16: The same as Figure G.10, using the DDPC1 model with $B_\star = 2000$

G.2.8 SVMIN

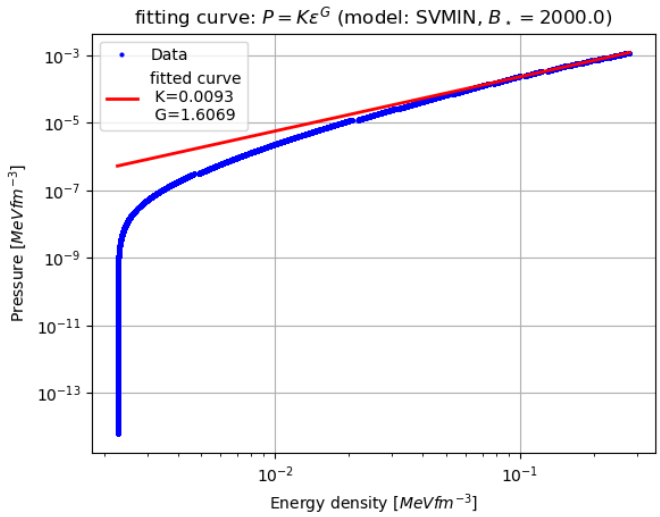

Figure G.17: The same as Figure G.10, using the SVMIN model with $B_\star = 2000$

G.2.9 UNEDF0

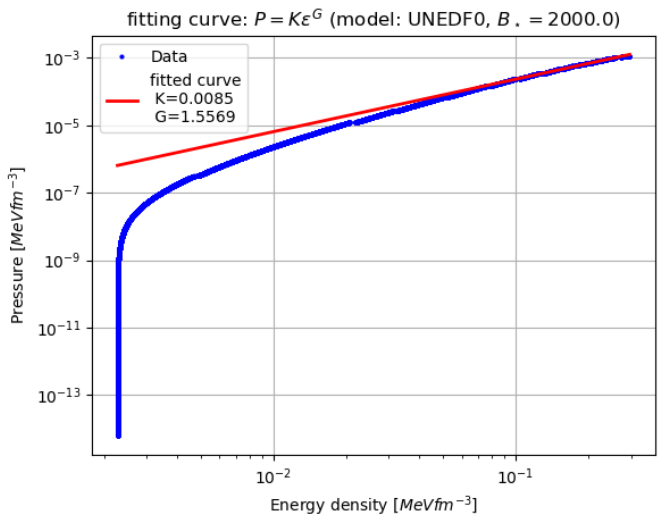

Figure G.18: The same as Figure G.10, using the UNEDF0 model with $B_\star = 2000$

G.3 Γ vs ϵ or n_b

G.3.1 SEMF

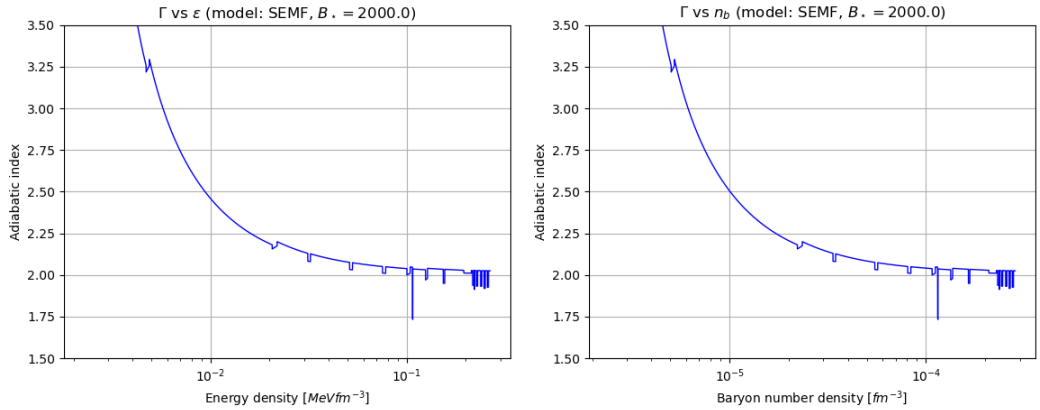

(a) (b)

Figure G.19: Adiabatic index as a function of (a) energy density and of (b) baryon number density, using the SEMF model with magnetic field strength $B_\star = 2000$

G.3.2 FRDM2012

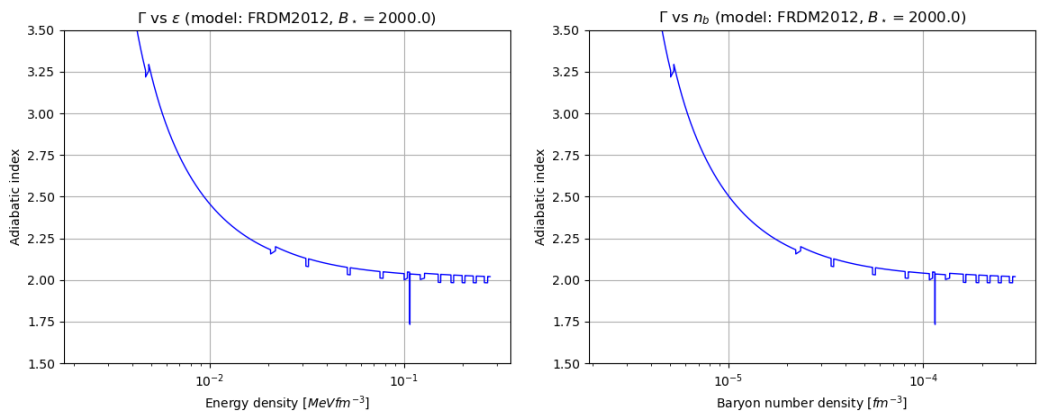

(a) (b)

Figure G.20: The same as Figure G.19, using the FRDM2012 model with $B_\star = 2000$

G.3.3 WS4RBF

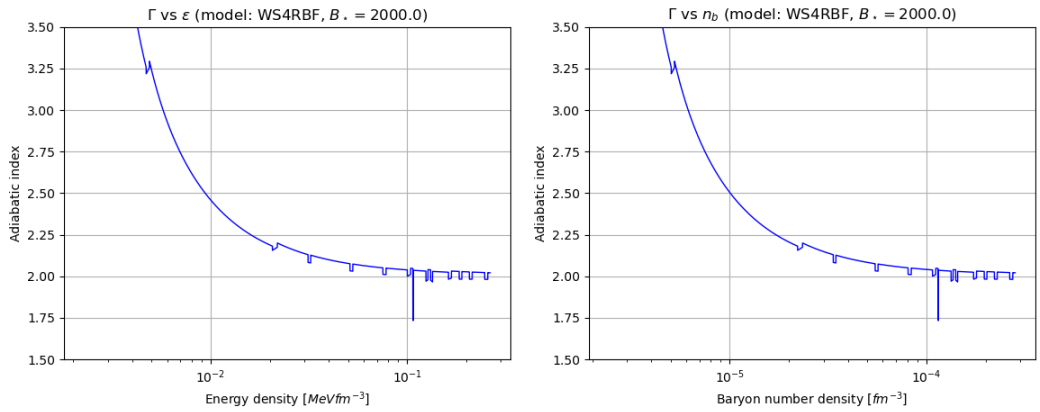

(a) (b)

Figure G.21: The same as Figure G.19, using the WS4RBF model with $B_\star = 2000$

G.3.4 BSKG3

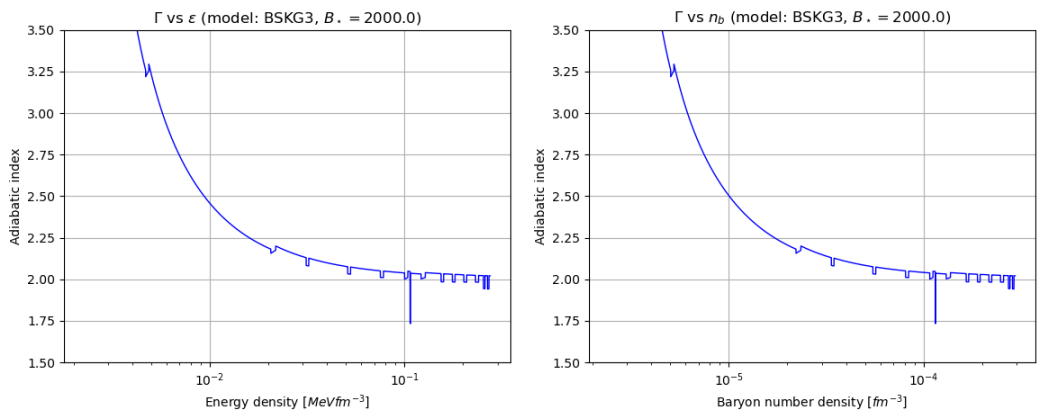

(a) (b)

Figure G.22: The same as Figure G.19, using the BSKG3 model with $B_\star = 2000$

G.3.5 HFB31

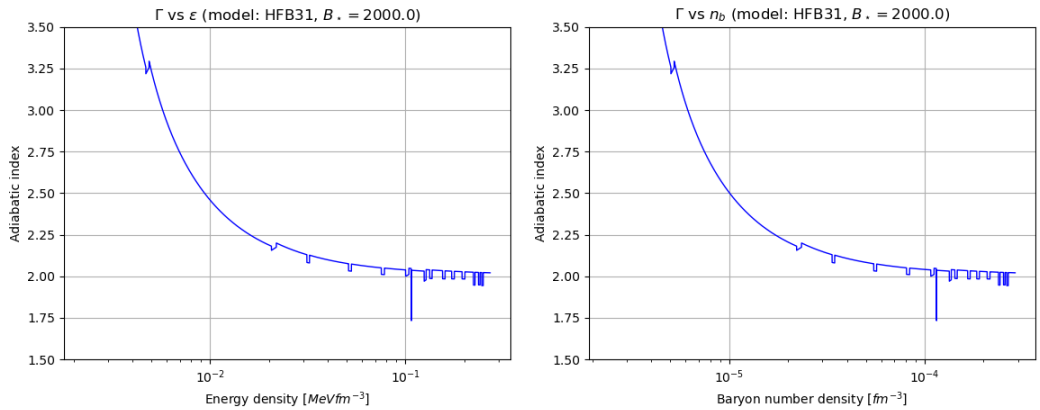

(a) (b)

Figure G.23: The same as Figure G.19, using the HFB31 model with $B_\star = 2000$

G.3.6 DDMED

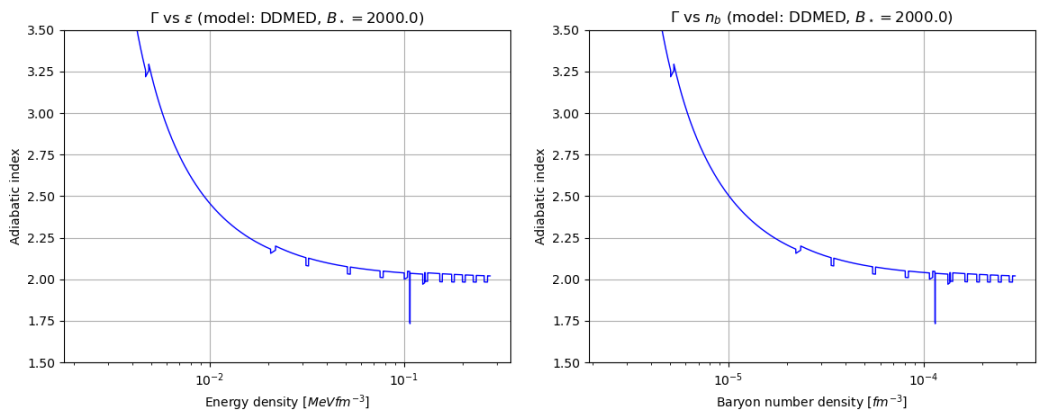

(a) (b)

Figure G.24: The same as Figure G.19, using the DDMED model with $B_\star = 2000$

G.3.7 DDPC1

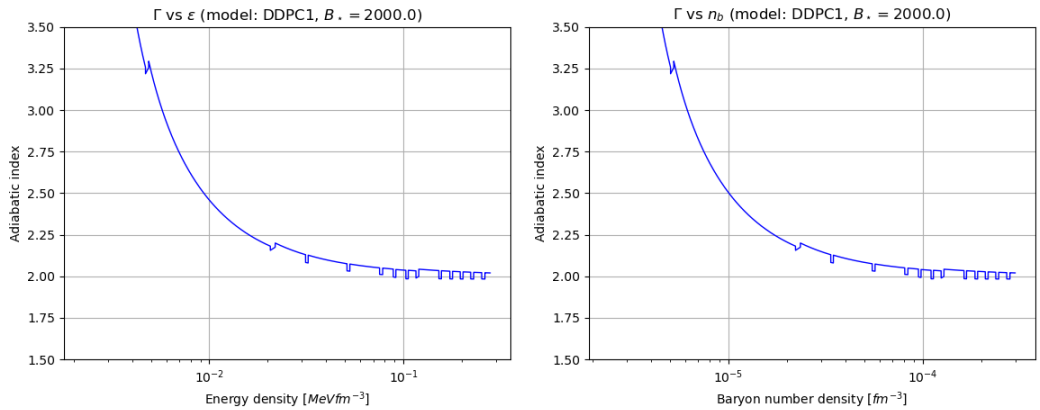

(a) (b)

Figure G.25: The same as Figure G.19, using the DDPC1 model with $B_\star = 2000$

G.3.8 SVMIN

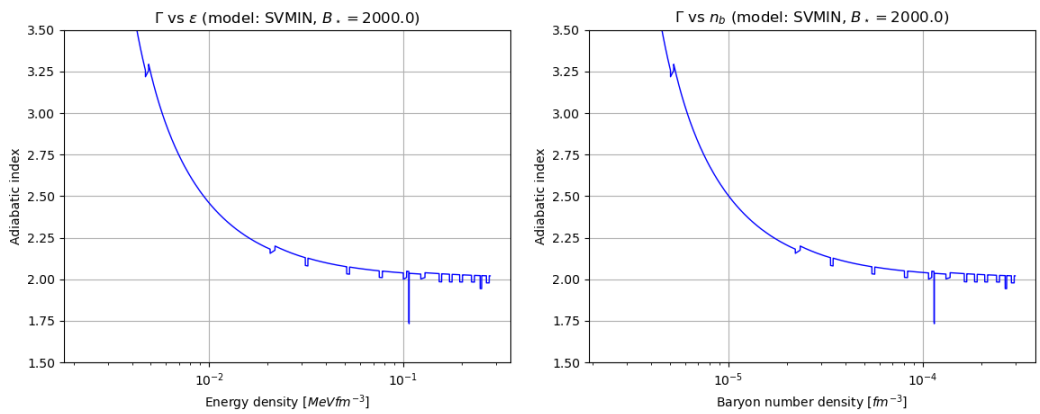

(a) (b)

Figure G.26: The same as Figure G.19, using the SVMIN model with $B_\star = 2000$

G.3.9 UNEDF0

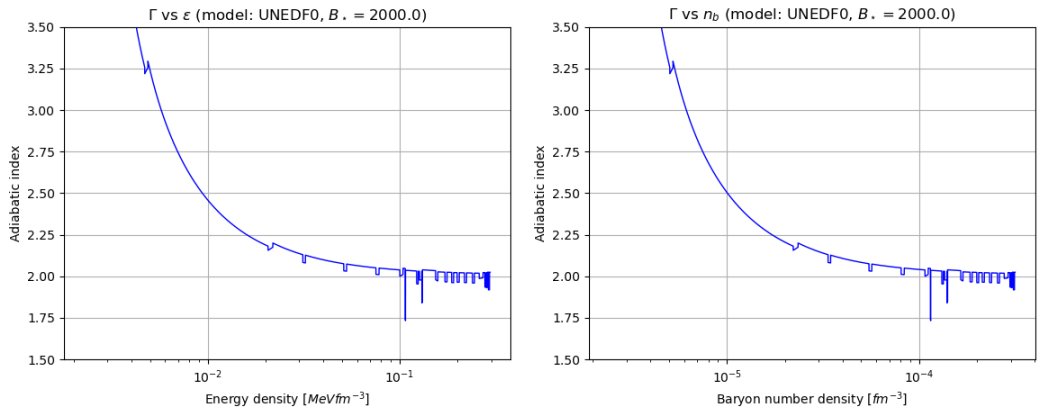

(a) (b)

Figure G.27: The same as Figure G.19, using the UNEDF0 model with $B_\star = 2000$

G.4 c_s vs ϵ or n_b

G.4.1 SEMF

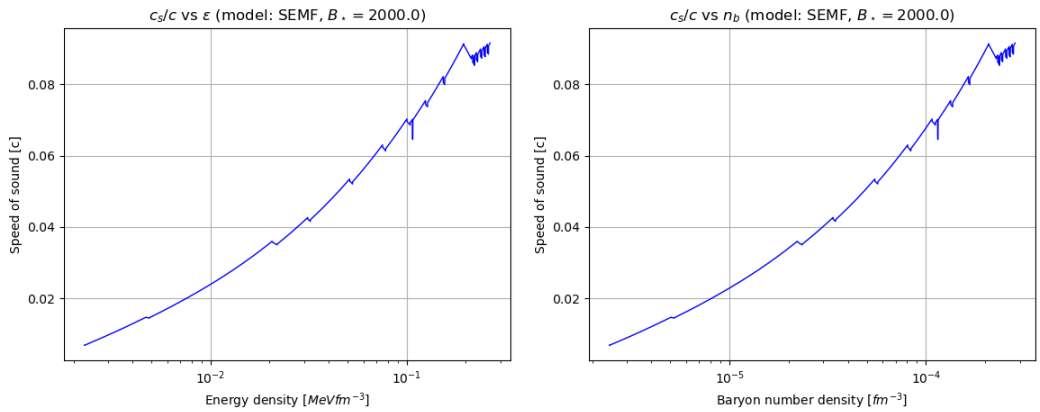

(a) (b)

Figure G.28: Speed of sound as a function of (a) energy density and of (b) baryon number density, using the SEMF model with magnetic field strength $B_\star = 2000$

G.4.2 FRDM2012

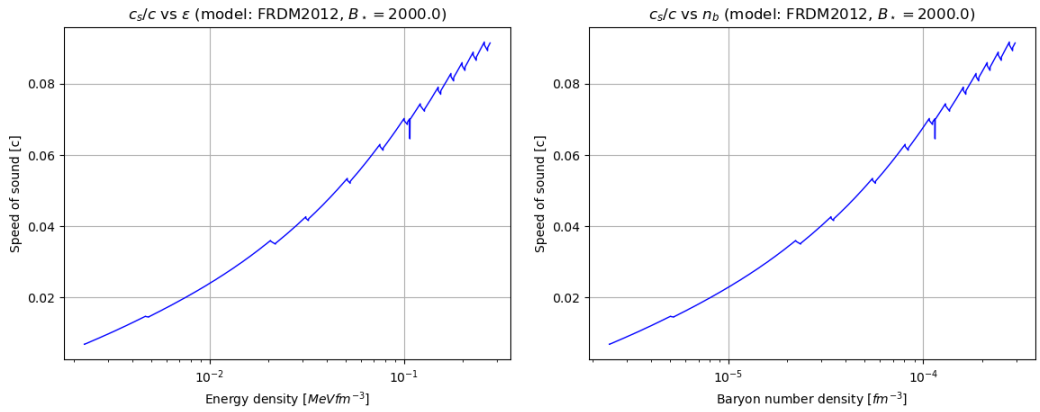

(a) (b)

Figure G.29: The same as Figure G.28, using the FRDM2012 model with $B_\star = 2000$

G.4.3 WS4RBF

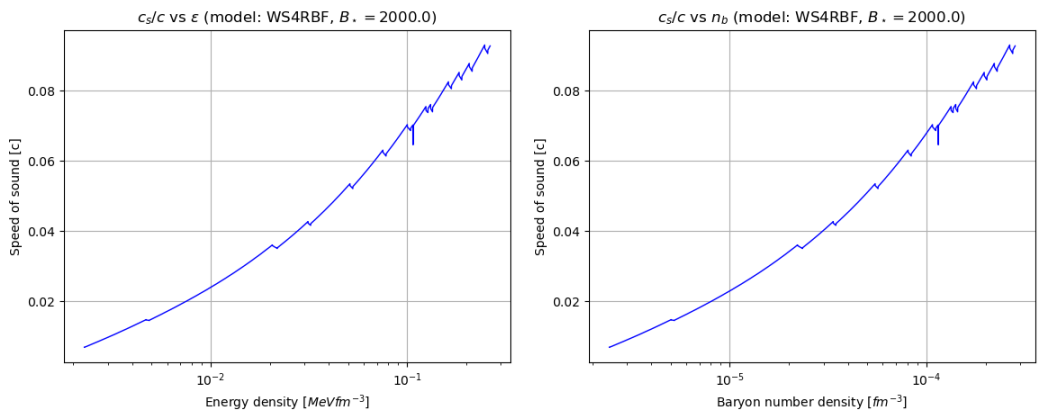

(a) (b)

Figure G.30: The same as Figure G.28, using the WS4RBF model with $B_\star = 2000$

G.4.4 BSKG3

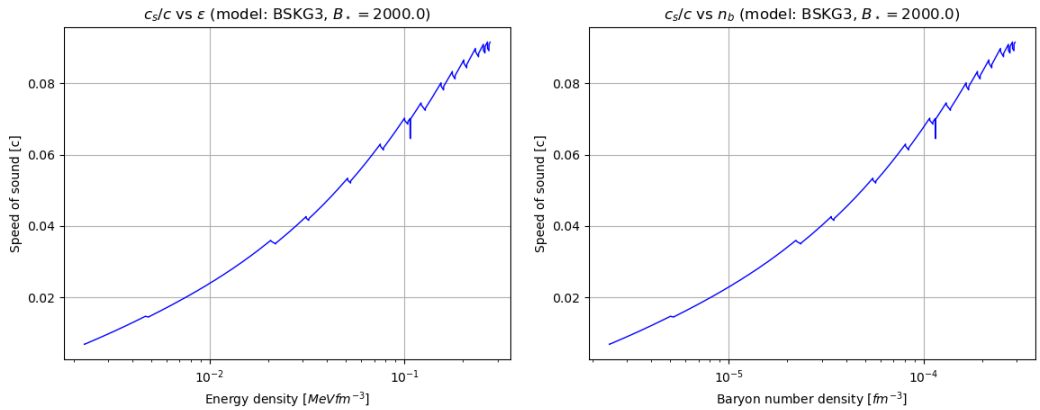

(a) (b)

Figure G.31: The same as Figure G.28, using the BSKG3 model with $B_\star = 2000$

G.4.5 HFB31

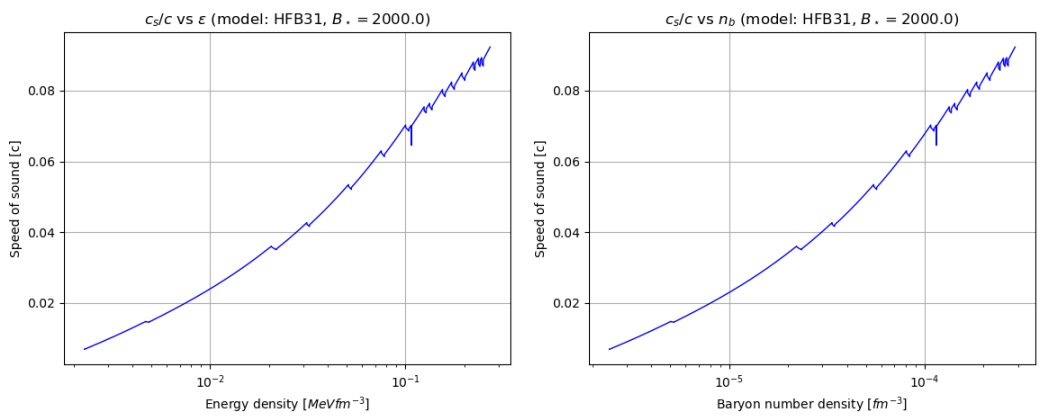

(a) (b)

Figure G.32: The same as Figure G.28, using the HFB31 model with $B_\star = 2000$

G.4.6 DDMED

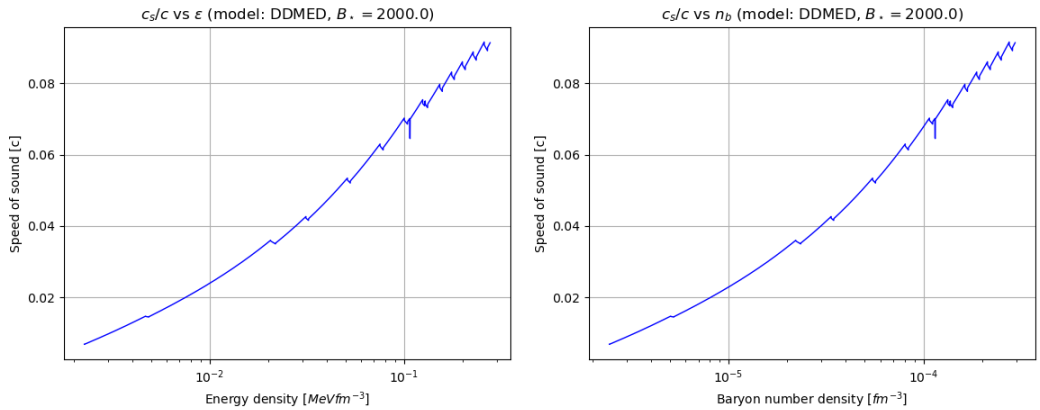

(a) (b)

Figure G.33: The same as Figure G.28, using the DDMED model with $B_\star = 2000$

G.4.7 DDPC1

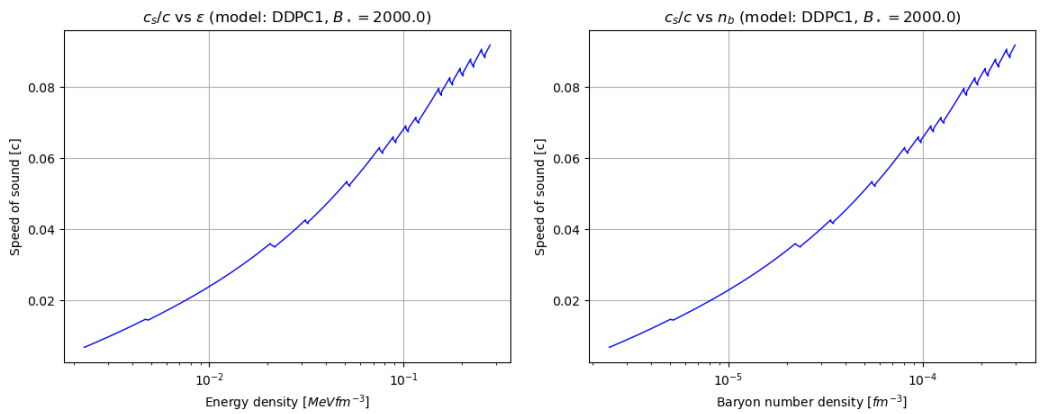

(a) (b)

Figure G.34: The same as Figure G.28, using the DDPC1 model with $B_\star = 2000$

G.4.8 SVMIN

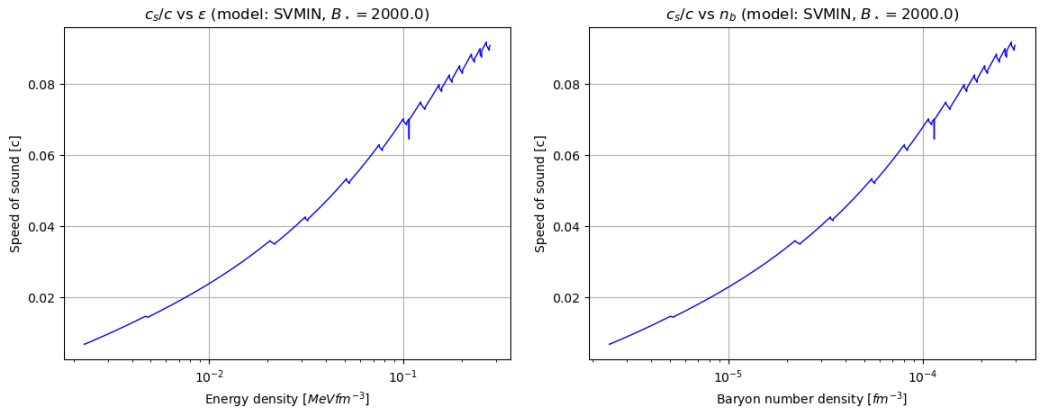

(a) (b)

Figure G.35: The same as Figure G.28, using the SVMIN model with $B_\star = 2000$

G.4.9 UNEDF0

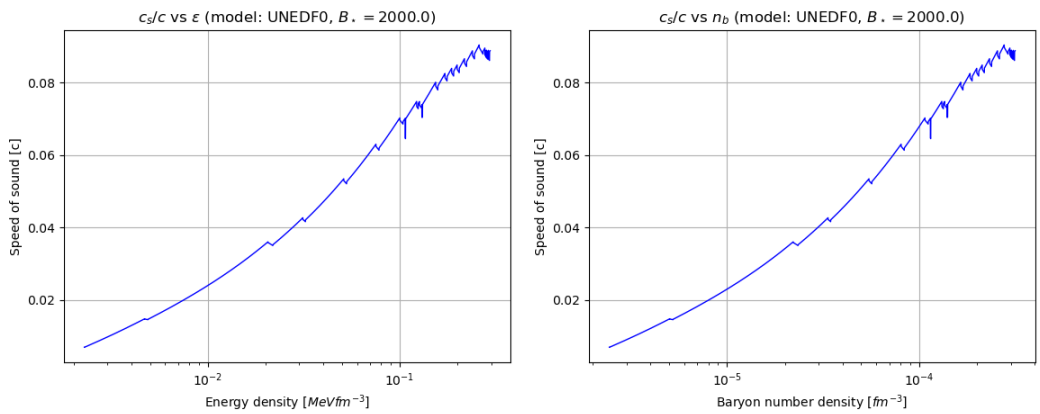

(a) (b)

Figure G.36: The same as Figure G.28, using the UNEDF0 model with $B_\star = 2000$

G.5 K_{mod} vs ϵ or n_b

G.5.1 SEMF

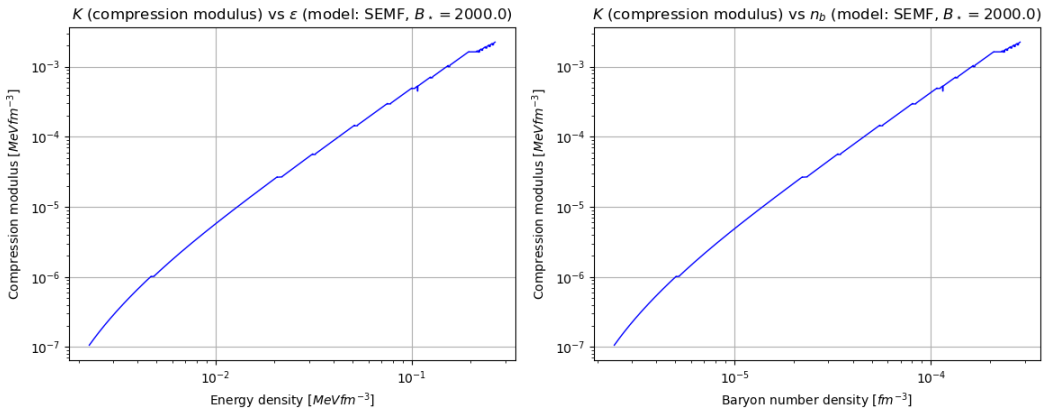

(a) (b)

Figure G.37: Compression modulus as a function of (a) energy density and of (b) baryon number density, using the SEMF model with magnetic field strength $B_\star = 2000$

G.5.2 FRDM2012

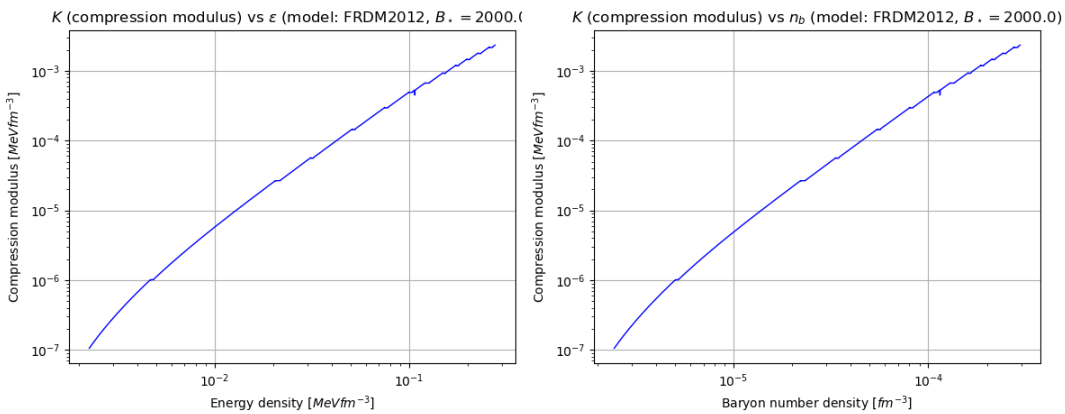

(a) (b)

Figure G.38: The same as Figure G.37, using the FRDM2012 model with $B_\star = 2000$

G.5.3 WS4RBF

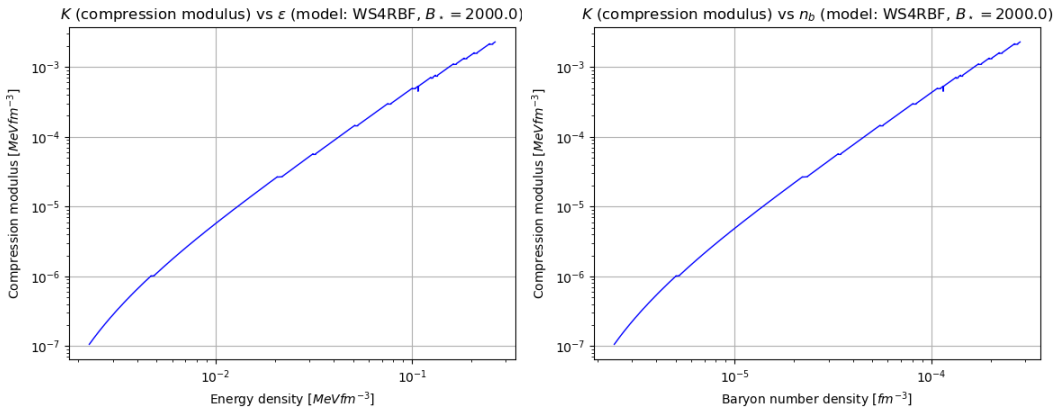

(a) (b)

Figure G.39: The same as Figure G.37, using the WS4RBF model with $B_\star = 2000$

G.5.4 BSKG3

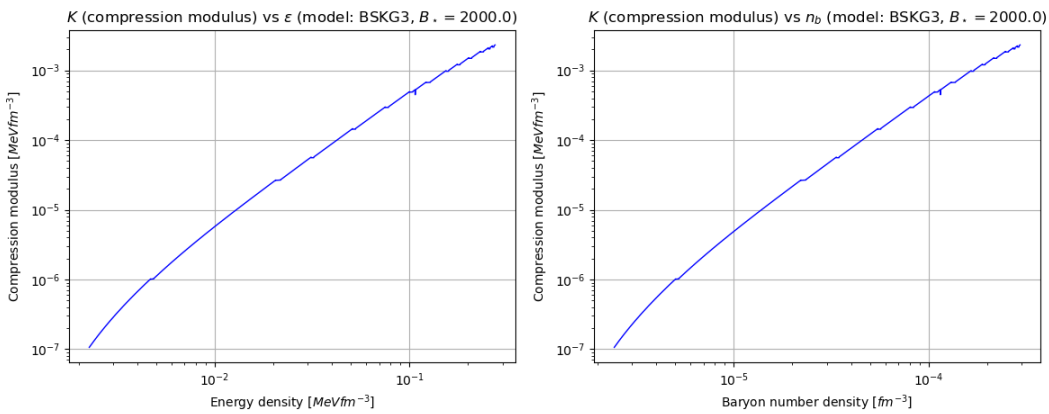

(a) (b)

Figure G.40: The same as Figure G.37, using the BSKG3 model with $B_\star = 2000$

G.5.5 HFB31

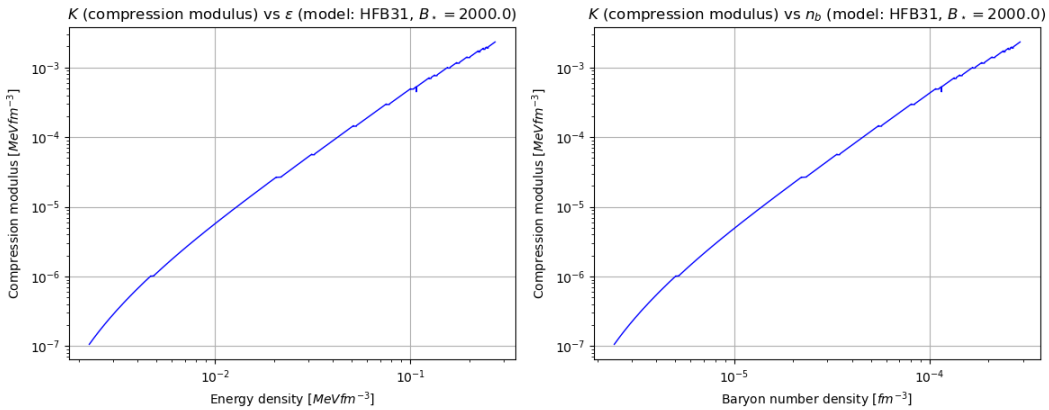

(a) (b)

Figure G.41: The same as Figure G.37, using the HFB31 model with $B_\star = 2000$

G.5.6 DDMED

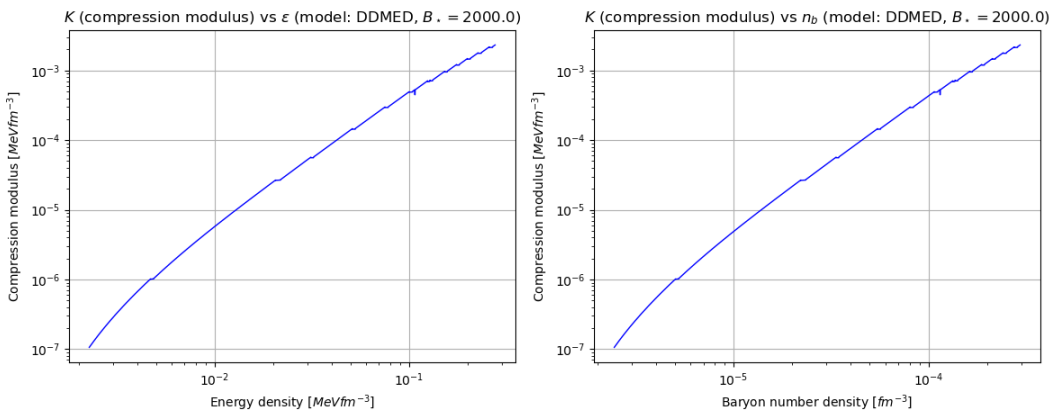

(a) (b)

Figure G.42: The same as Figure G.37, using the DDMED model with $B_\star = 2000$

G.5.7 DDPC1

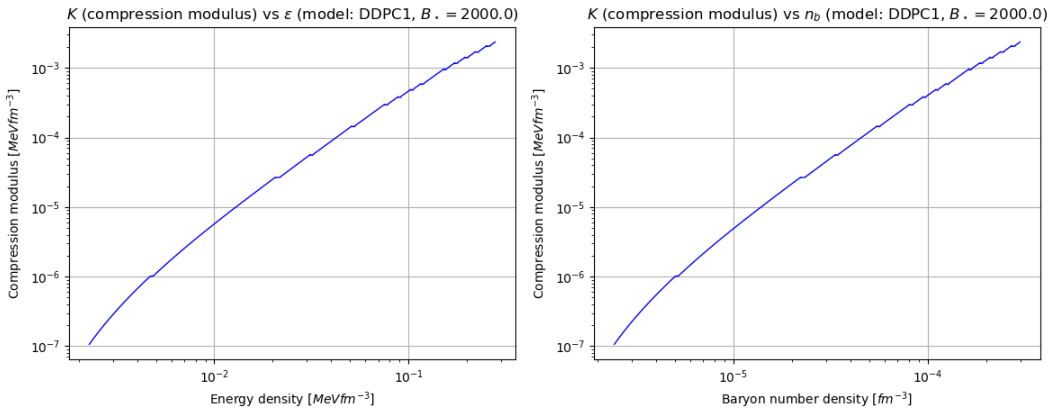

(a) (b)

Figure G.43: The same as Figure G.37, using the DDPC1 model with $B_\star = 2000$

G.5.8 SVMIN

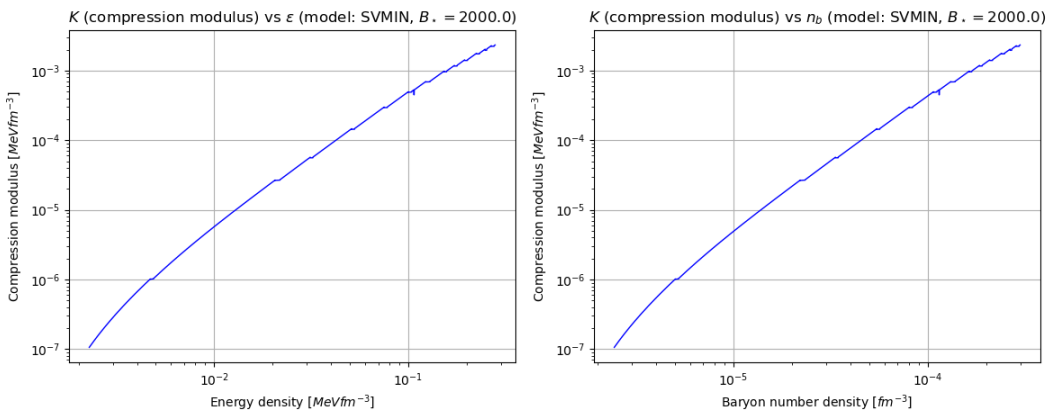

(a) (b)

Figure G.44: The same as Figure G.37, using the SVMIN model with $B_\star = 2000$

G.5.9 UNEDF0

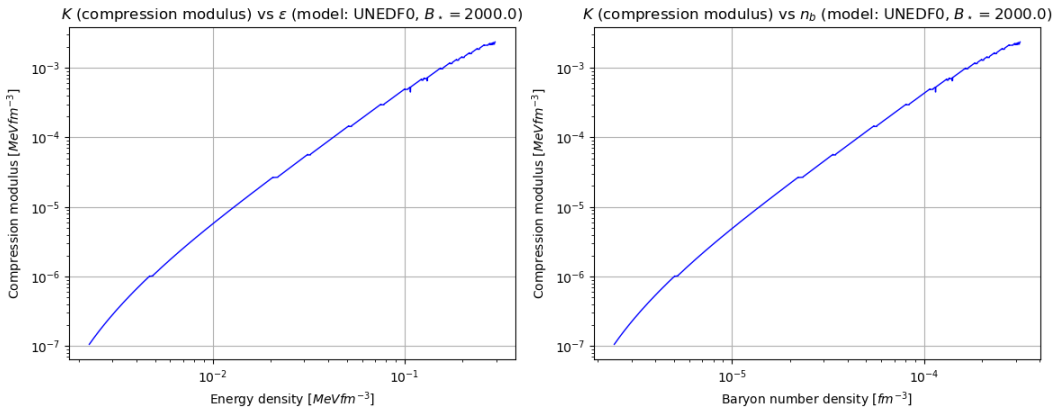

(a) (b)

Figure G.45: The same as Figure G.37, using the UNEDF0 model with $B_\star = 2000$

G.6 S_{mod} vs ϵ or n_b

G.6.1 SEMF

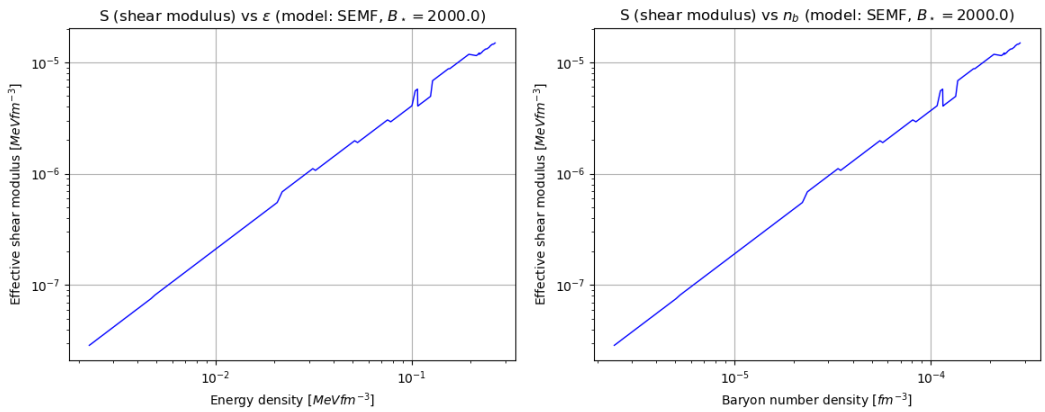

(a) (b)

Figure G.46: Effective shear modulus as a function of (a) energy density and of (b) baryon number density, using the SEMF model with magnetic field strength $B_\star = 2000$

G.6.2 FRDM2012

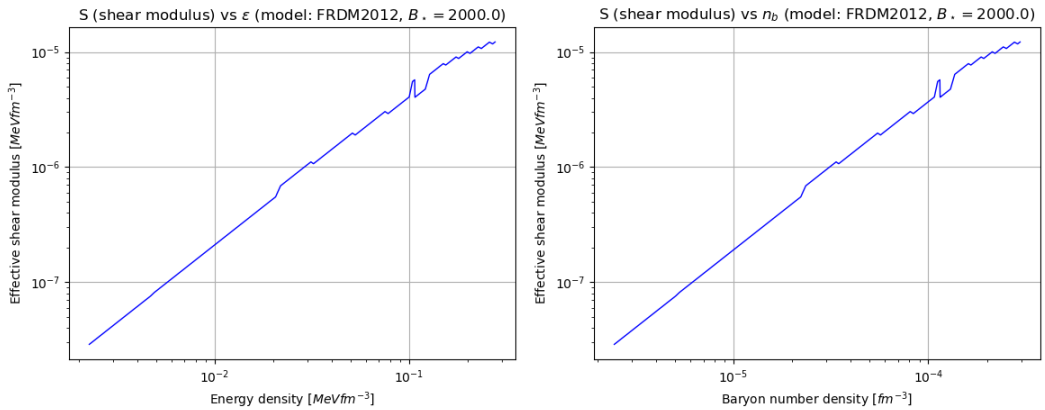

(a) (b)

Figure G.47: The same as Figure G.46, using the FRDM2012 model with $B_\star = 2000$

G.6.3 WS4RBF

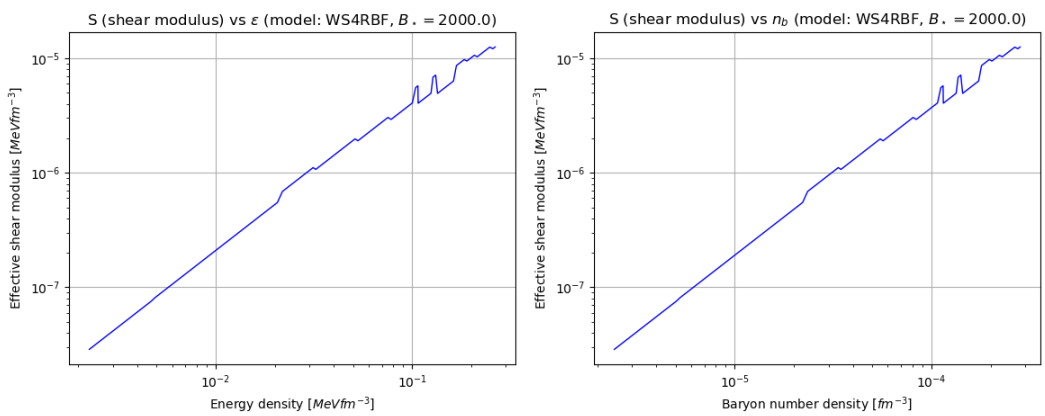

(a) (b)

Figure G.48: The same as Figure G.46, using the WS4RBF model with $B_\star = 2000$

G.6.4 BSKG3

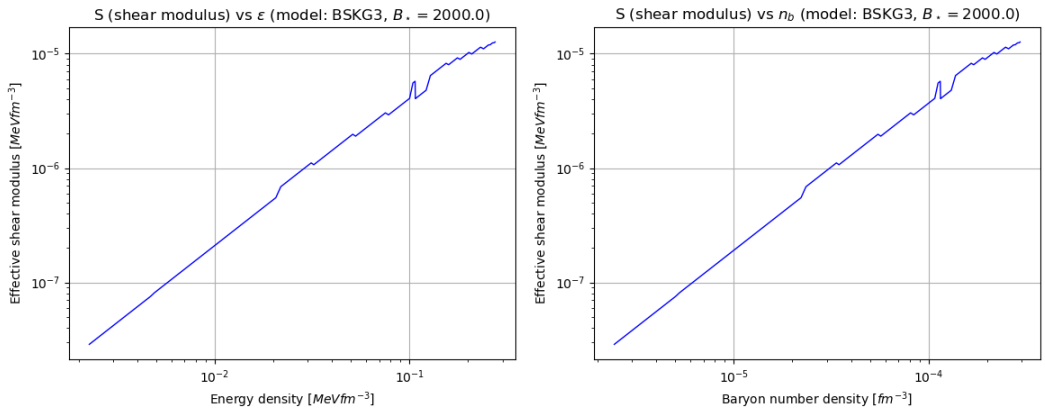

(a) (b)

Figure G.49: The same as Figure G.46, using the BSKG3 model with $B_\star = 2000$

G.6.5 HFB31

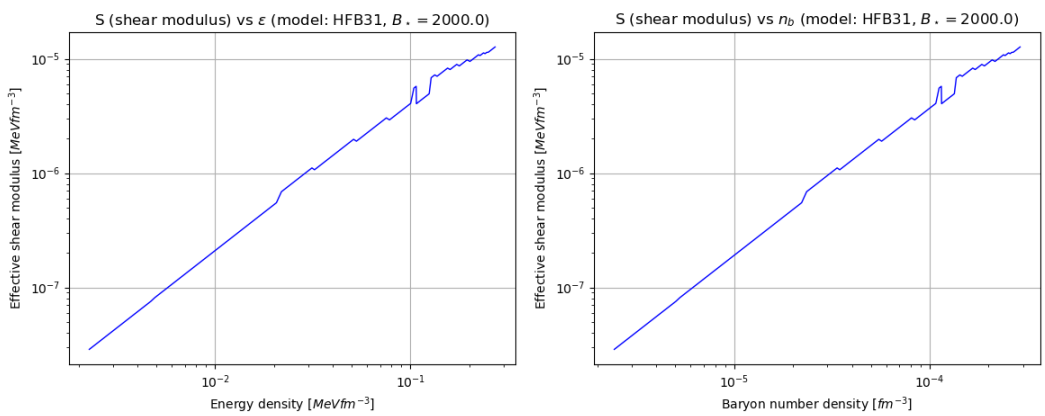

(a) (b)

Figure G.50: The same as Figure G.46, using the HFB31 model with $B_\star = 2000$

G.6.6 DDMED

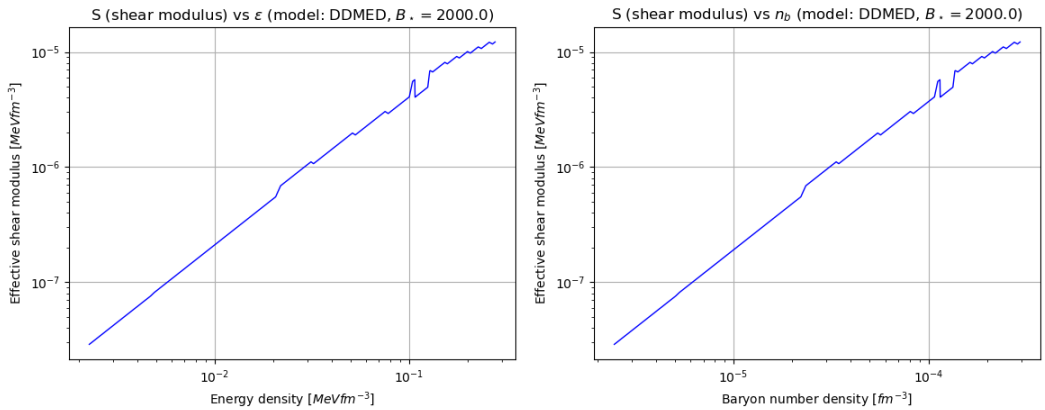

(a) (b)

Figure G.51: The same as Figure G.46, using the DDMED model with $B_\star = 2000$

G.6.7 DDPC1

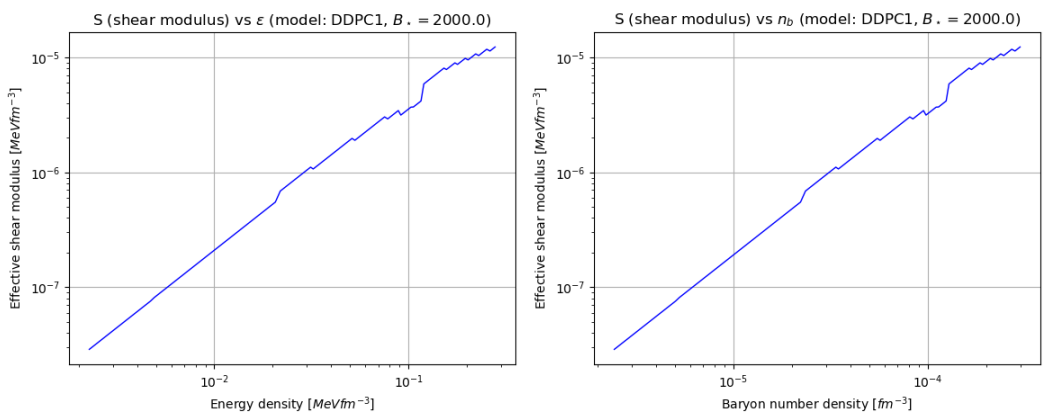

(a) (b)

Figure G.52: The same as Figure G.46, using the DDPC1 model with $B_\star = 2000$

G.6.8 SVMIN

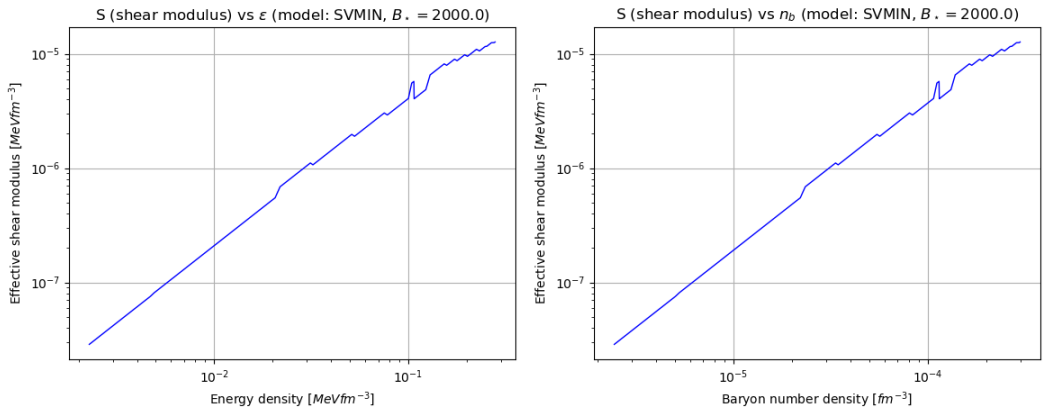

(a) (b)

Figure G.53: The same as Figure G.46, using the SVMIN model with $B_\star = 2000$

G.6.9 UNEDF0

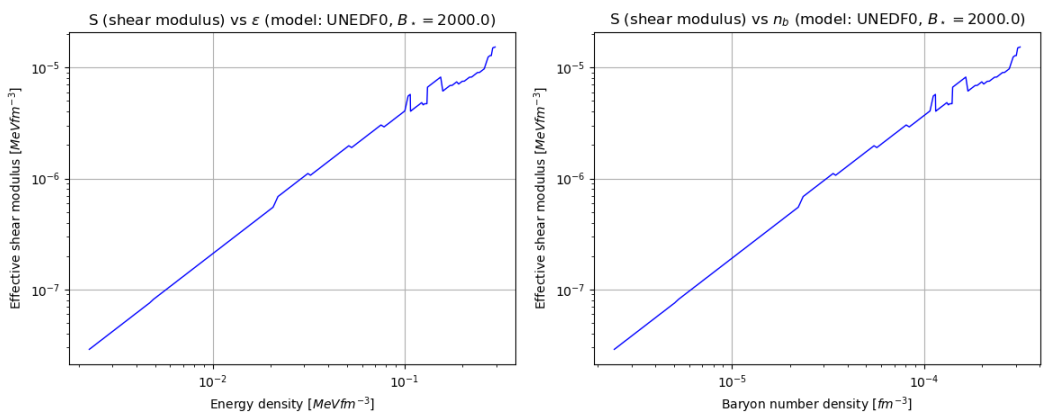

(a) (b)

Figure G.54: The same as Figure G.46, using the UNEDF0 model with $B_\star = 2000$

G.7 S_{mod}/K_{mod} vs ϵ or n_b

G.7.1 SEMF

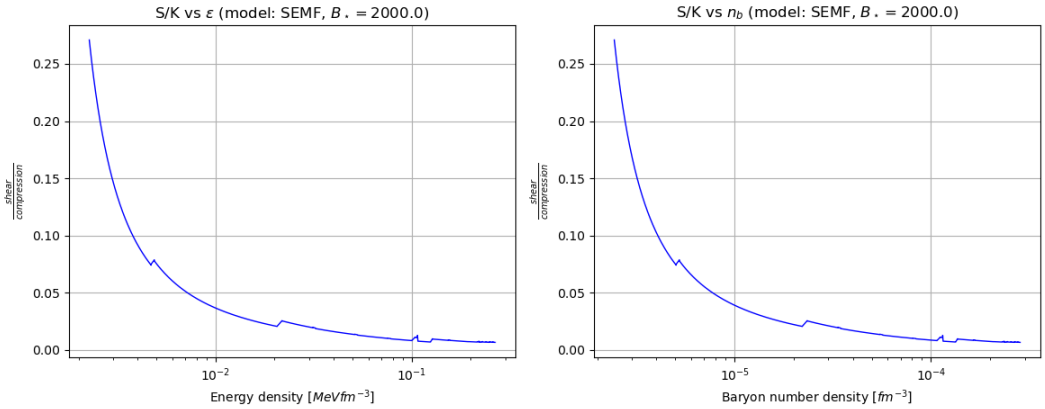

(a) (b)

Figure G.55: Effective shear modulus over compression modulus as a function of (a) energy density and of (b) baryon number density, using the SEMF model with magnetic field strength $B_\star = 2000$

G.7.2 FRDM2012

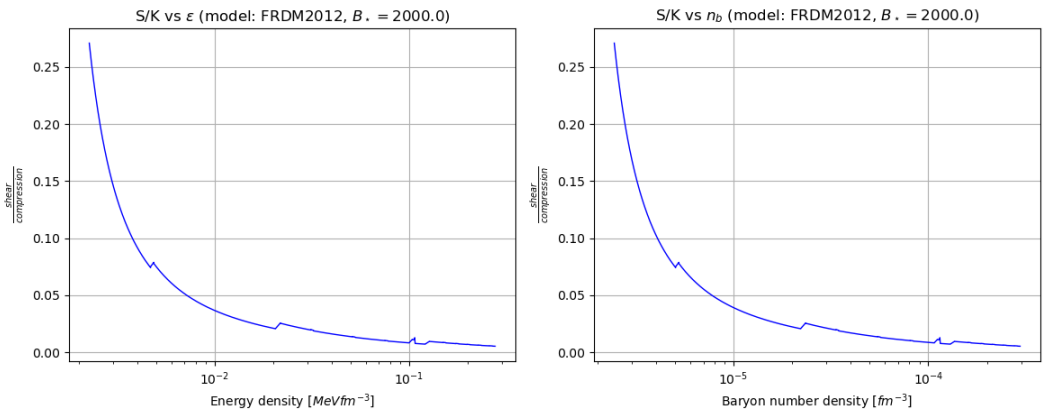

(a) (b)

Figure G.56: The same as Figure G.55, using the FRDM2012 model with $B_\star = 2000$

G.7.3 WS4RBF

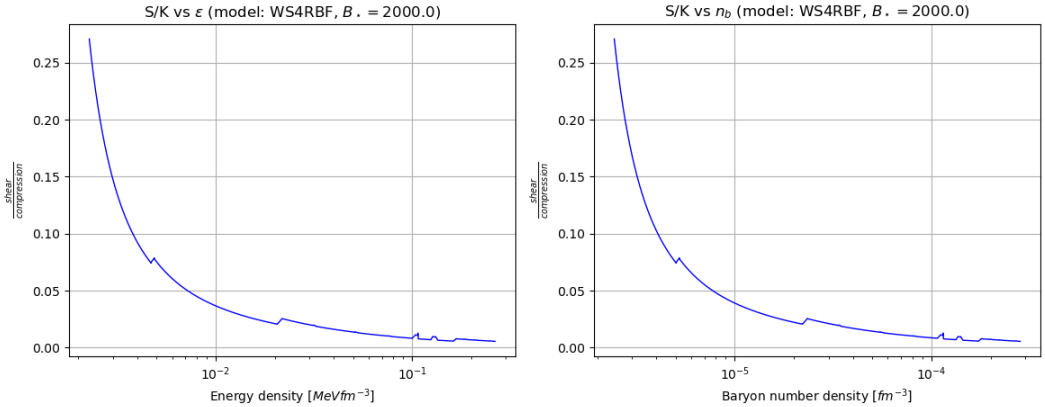

(a) (b)

Figure G.57: The same as Figure G.55, using the WS4RBF model with $B_\star = 2000$

G.7.4 BSKG3

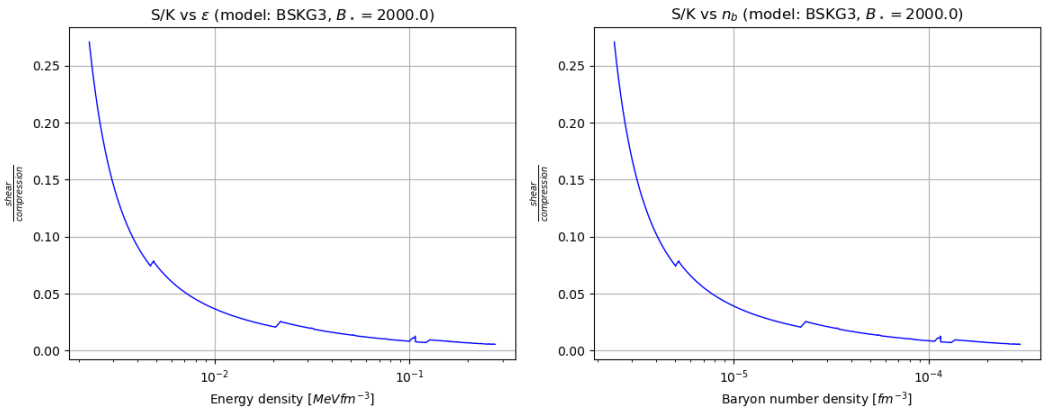

(a) (b)

Figure G.58: The same as Figure G.55, using the BSKG3 model with $B_\star = 2000$

G.7.5 HFB31

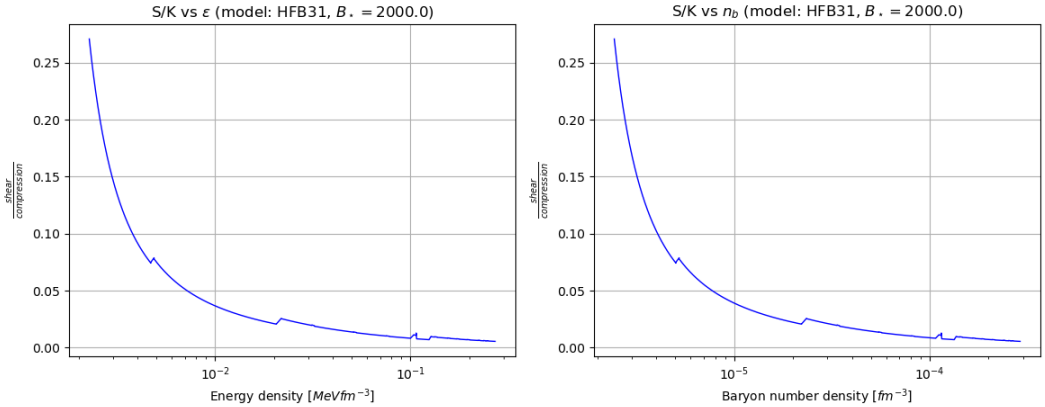

(a) (b)

Figure G.59: The same as Figure G.55, using the HFB31 model with $B_\star = 2000$

G.7.6 DDMED

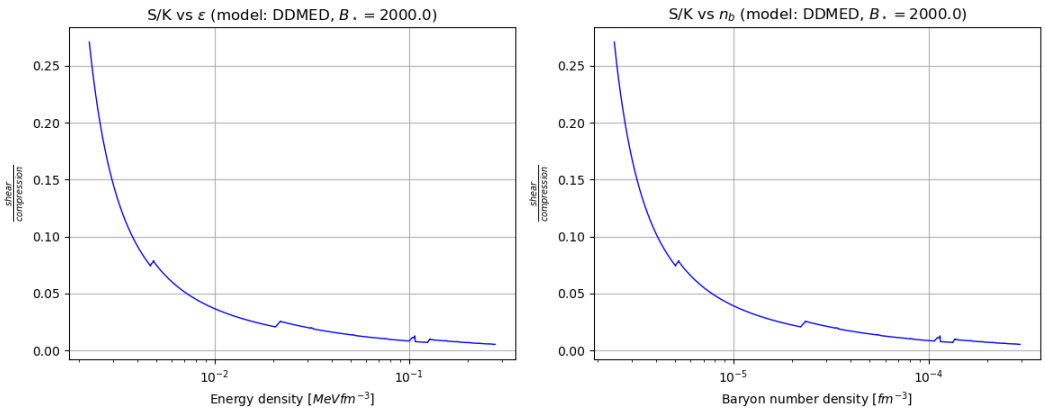

(a) (b)

Figure G.60: The same as Figure G.55, using the DDMED model with $B_\star = 2000$

G.7.7 DDPC1

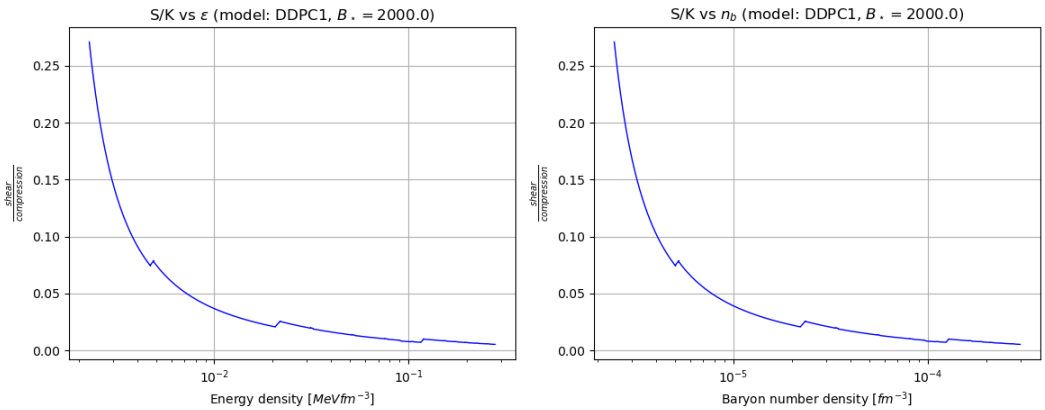

(a) (b)

Figure G.61: The same as Figure G.55, using the DDPC1 model with $B_\star = 2000$

G.7.8 SVMIN

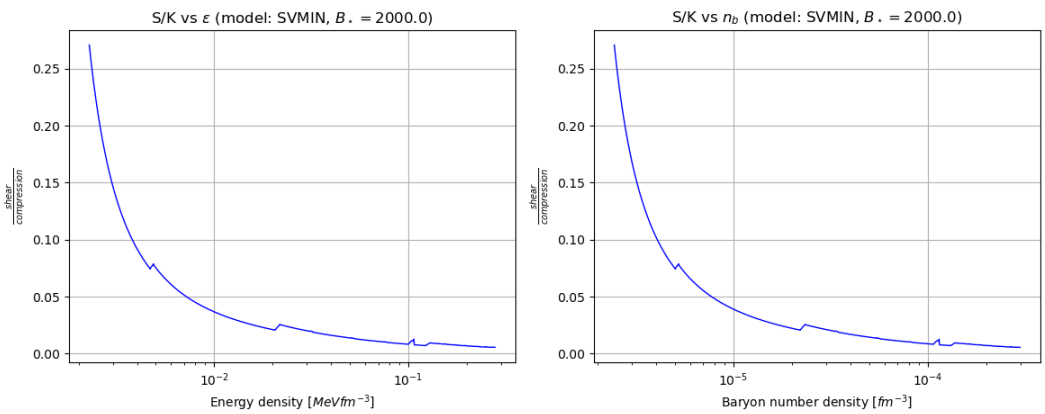

(a) (b)

Figure G.62: The same as Figure G.55, using the SVMIN model with $B_\star = 2000$

G.7.9 UNEDF0

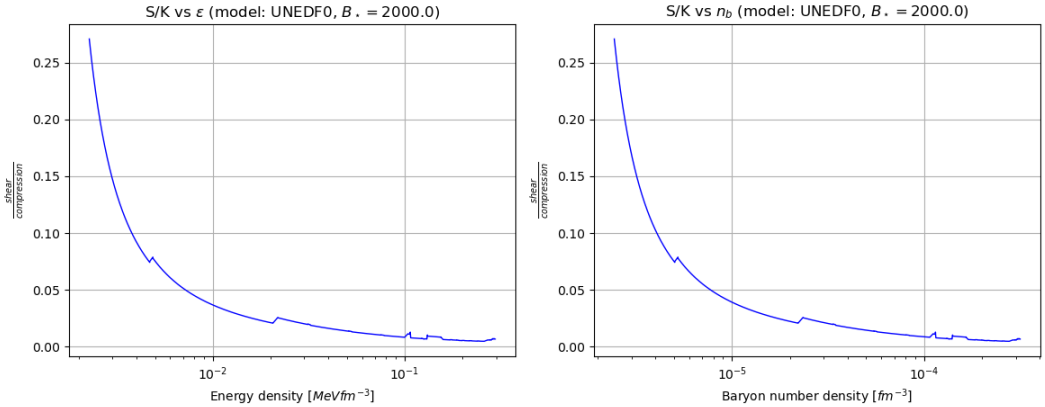

(a) (b)

Figure G.63: The same as Figure G.55, using the UNEDF0 model with $B_\star = 2000$

G.8 Z, N, Z/A vs ϵ or n_b

G.8.1 SEMF

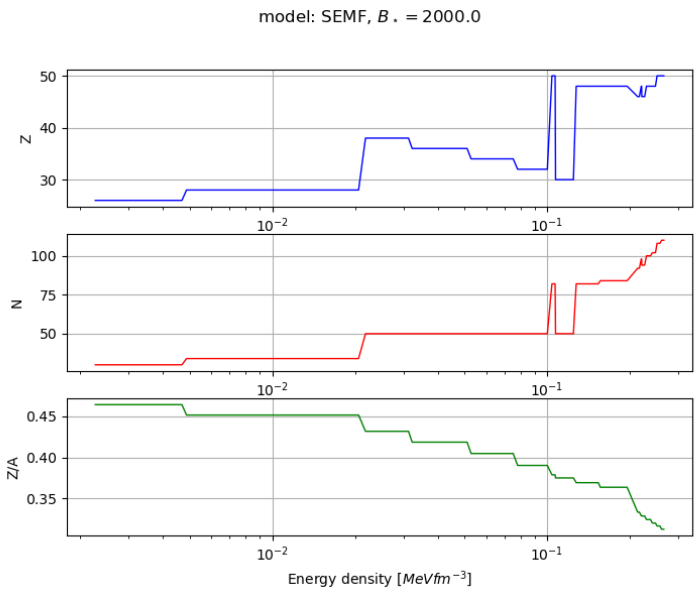

(a)

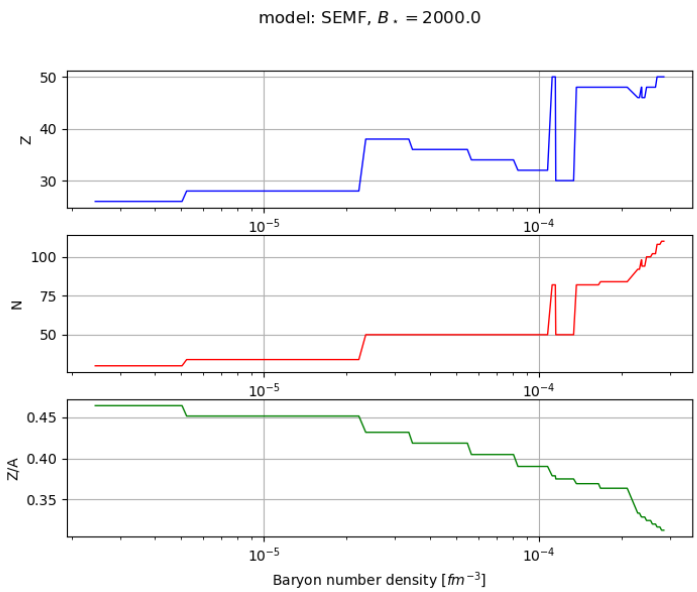

(b)

Figure G.64: Atomic number, neutron number and proton fraction as a function of (a) energy density and of (b) baryon number density, using the SEMF model with magnetic field strength $B_\star = 2000$

G.8.2 FRDM2012

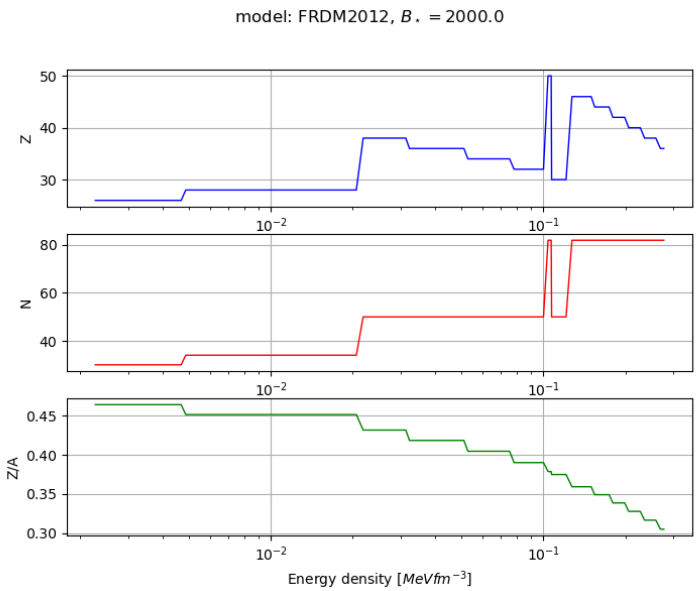

(a)

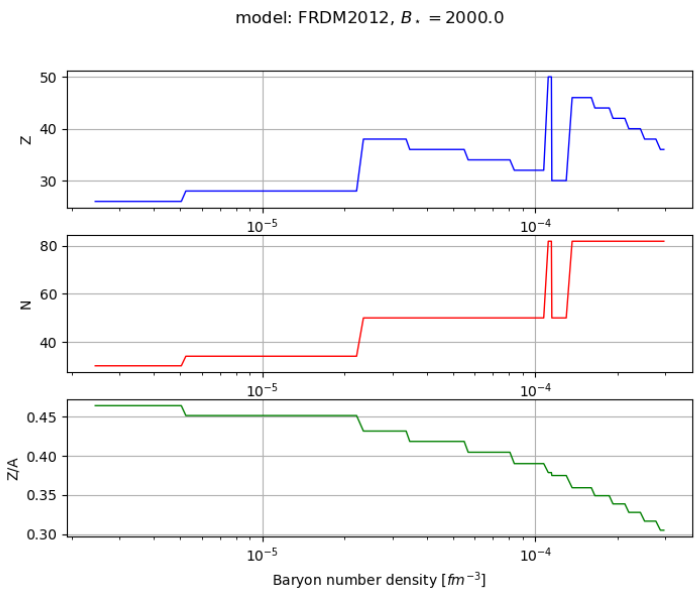

(b)

Figure G.65: The same as Figure G.64, using the FRDM2012 model with $B_\star = 2000$

G.8.3 WS4RBF

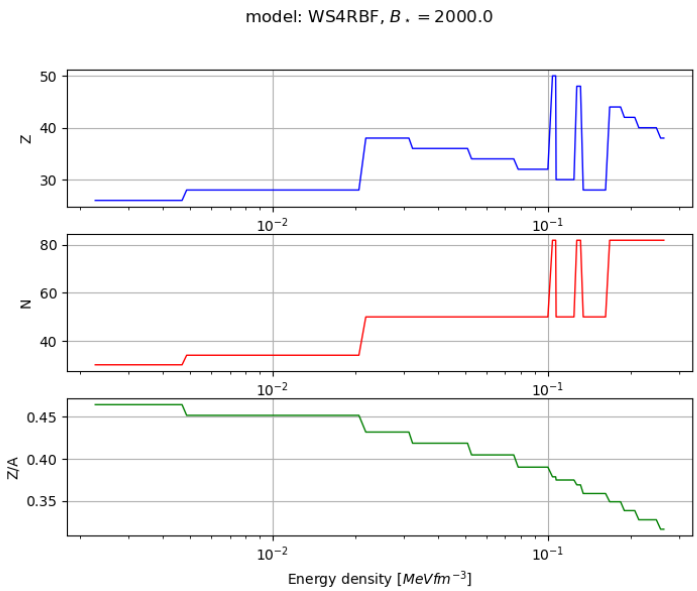

(a)

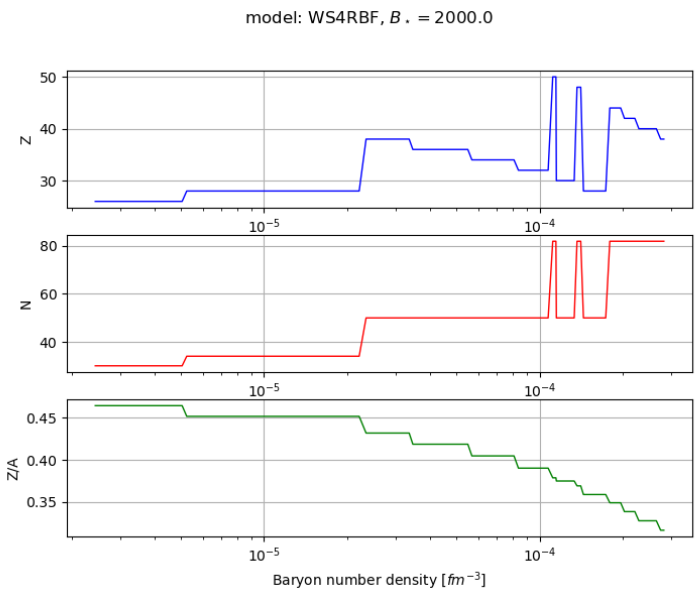

(b)

Figure G.66: The same as Figure G.64, using the WS4RBF model with $B_\star = 2000$

G.8.4 BSKG3

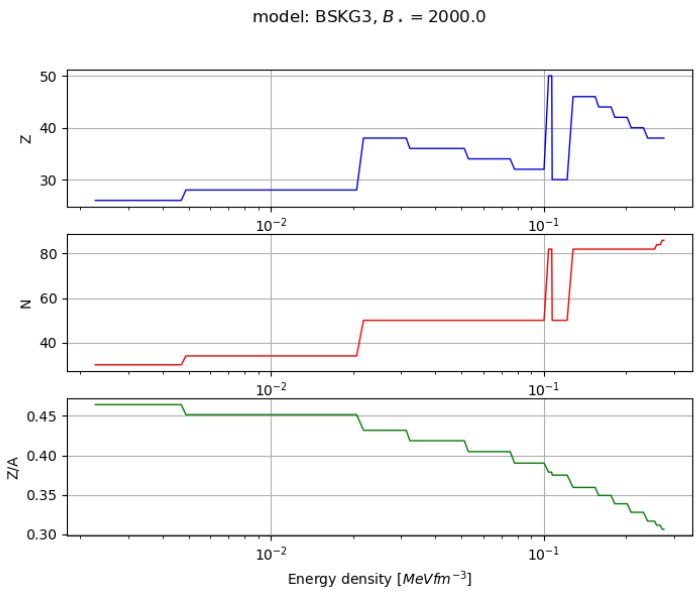

(a)

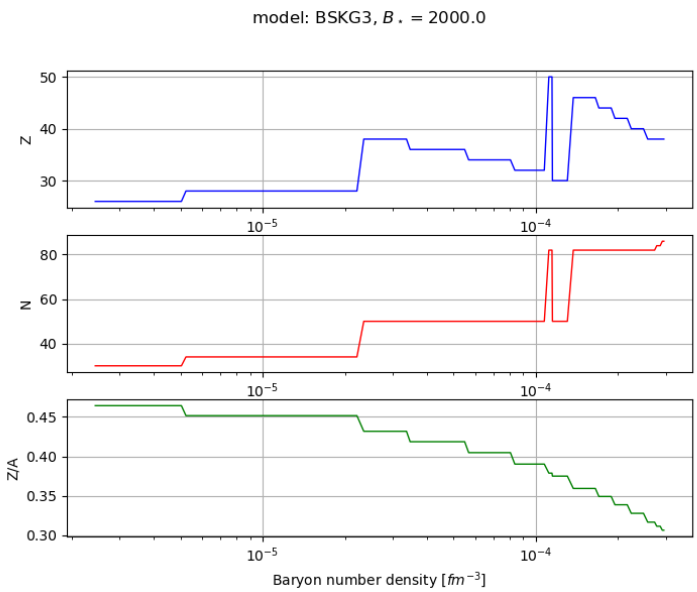

(b)

Figure G.67: The same as Figure G.64, using the BSKG3 model with $B_\star = 2000$

G.8.5 HFB31

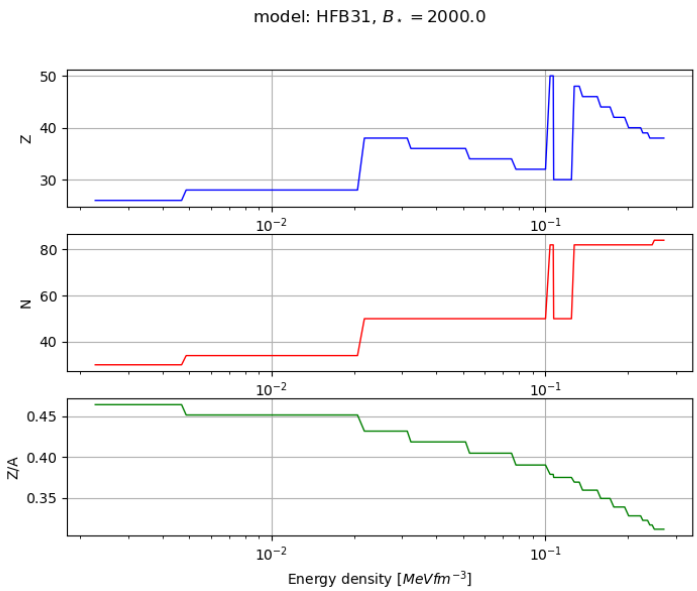

(a)

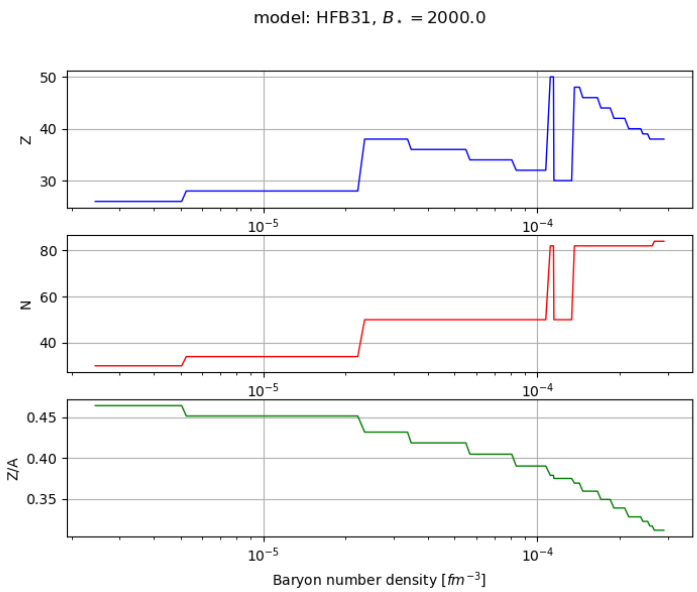

(b)

Figure G.68: The same as Figure G.64, using the HFB31 model with $B_\star = 2000$

G.8.6 DDMED

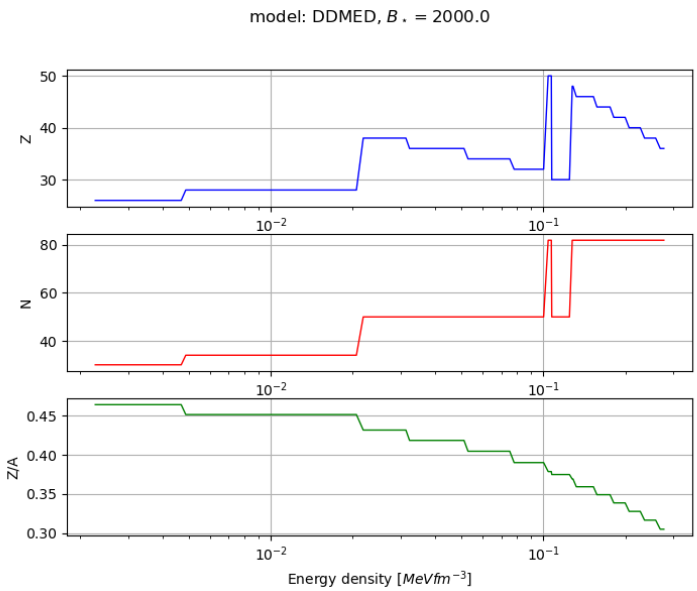

(a)

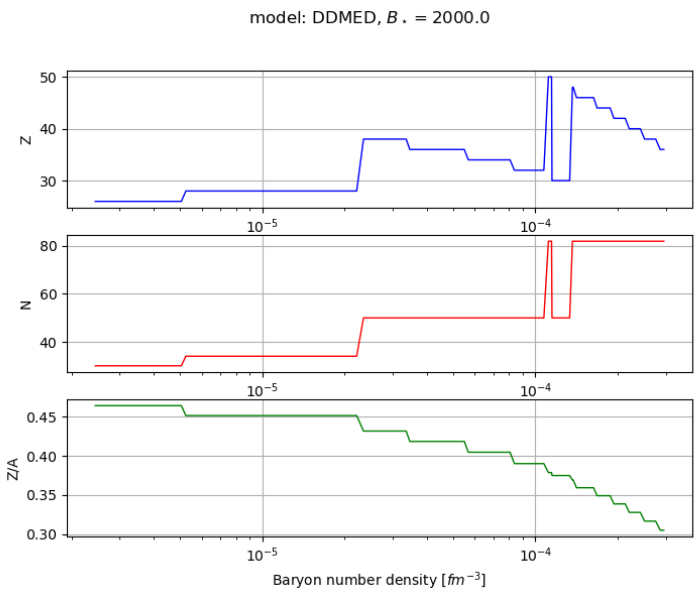

(b)

Figure G.69: The same as Figure G.64, using the DDMED model with $B_\star = 2000$

G.8.7 DDPC1

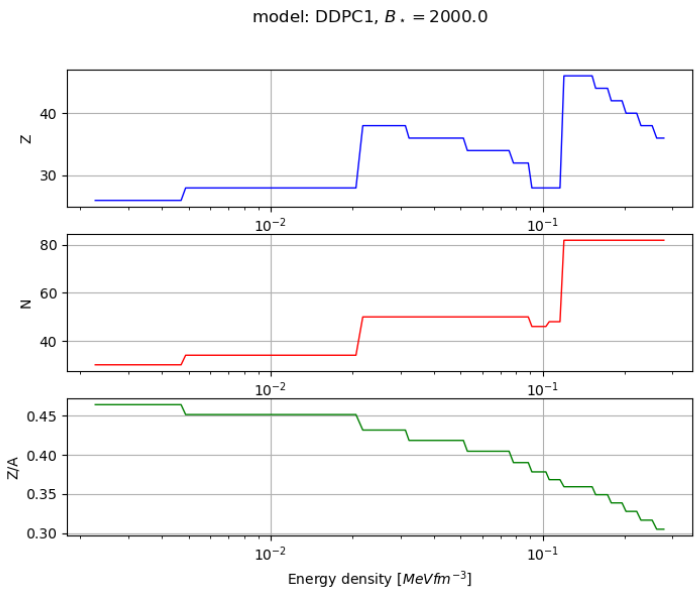

(a)

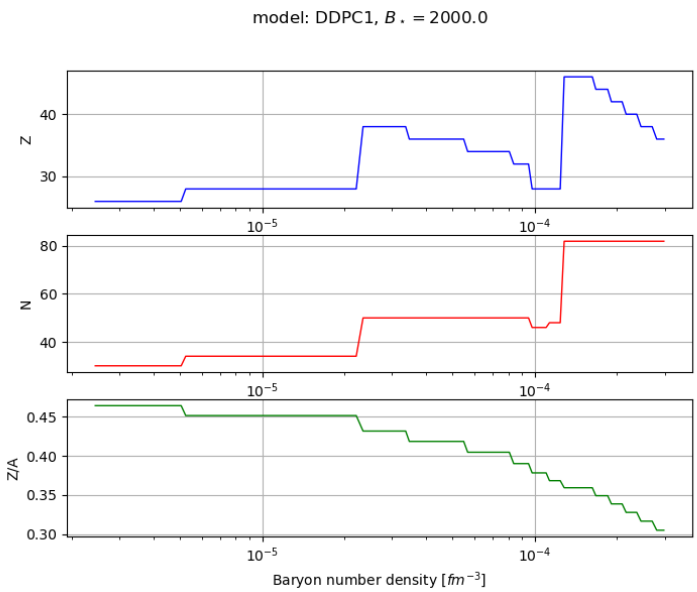

(b)

Figure G.70: The same as Figure G.64, using the DDPC1 model with $B_\star = 2000$

G.8.8 SVMIN

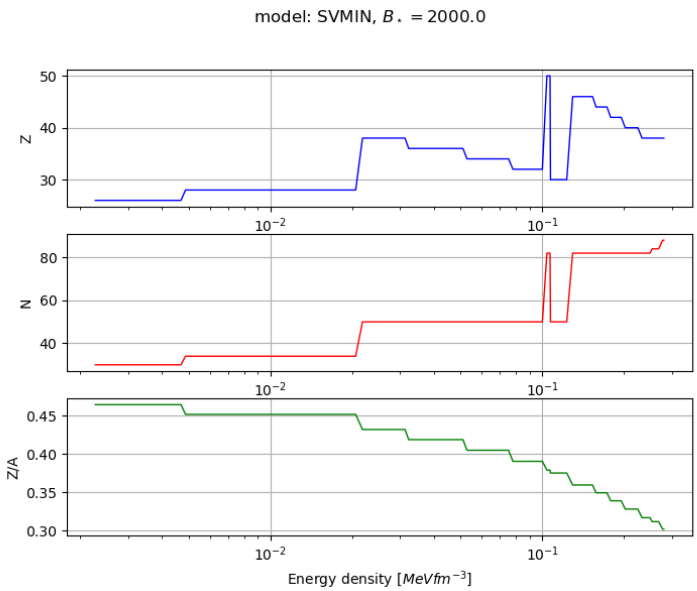

(a)

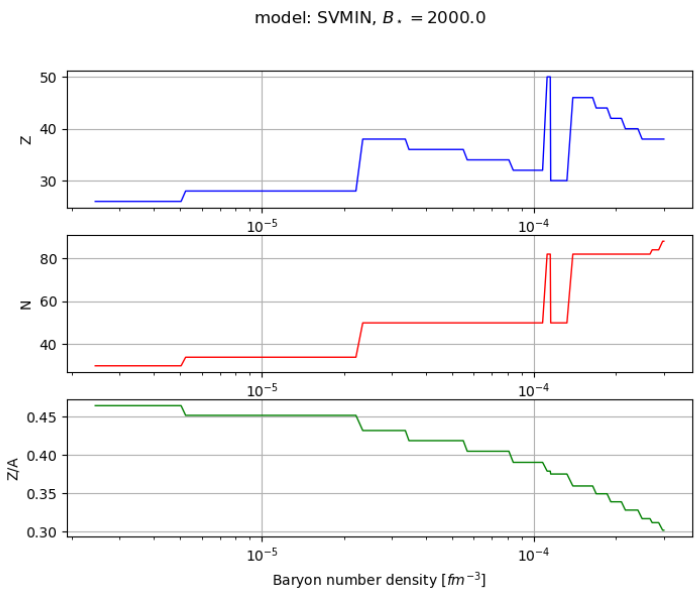

(b)

Figure G.71: The same as Figure G.64, using the SVMIN model with $B_\star = 2000$

G.8.9 UNEDF0

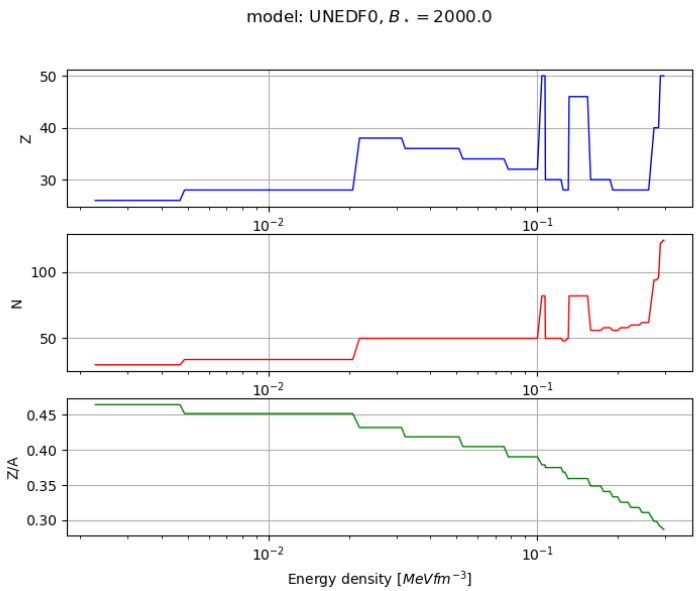

(a)

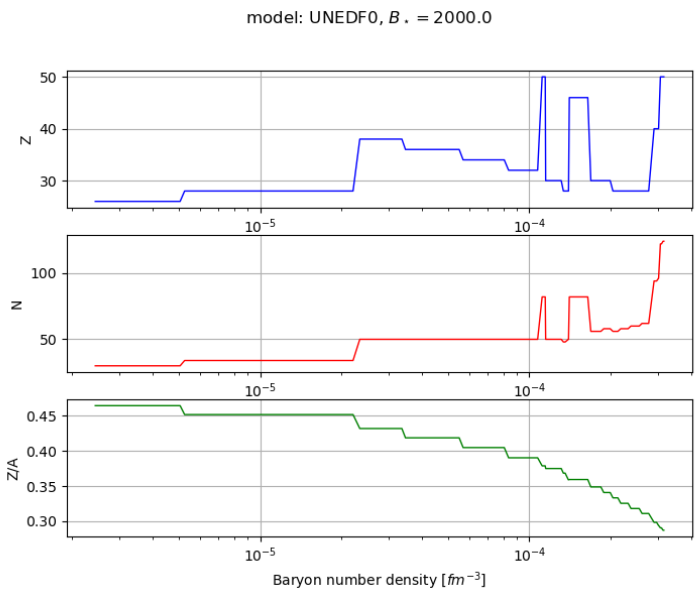

(b)

Figure G.72: The same as Figure G.64, using the UNEDF0 model with $B_\star = 2000$

G.9 M_{cr} for different M and R

G.9.1 SEMF

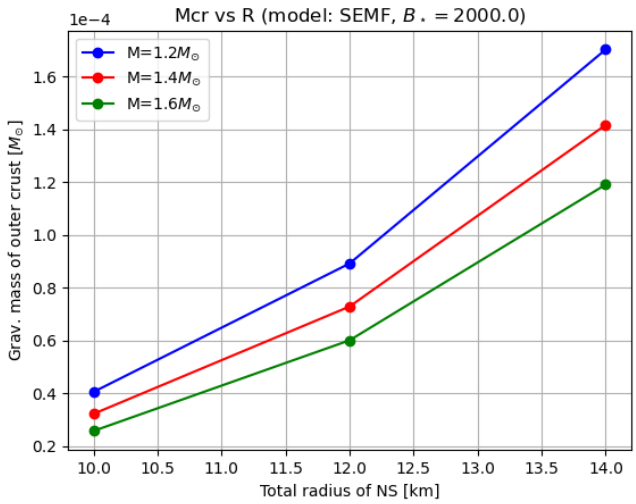

Figure G.73: Mass of outer crust for different masses and radii of NS, using the SEMF model with magnetic field strength $B_\star = 2000$

G.9.2 FRDM2012

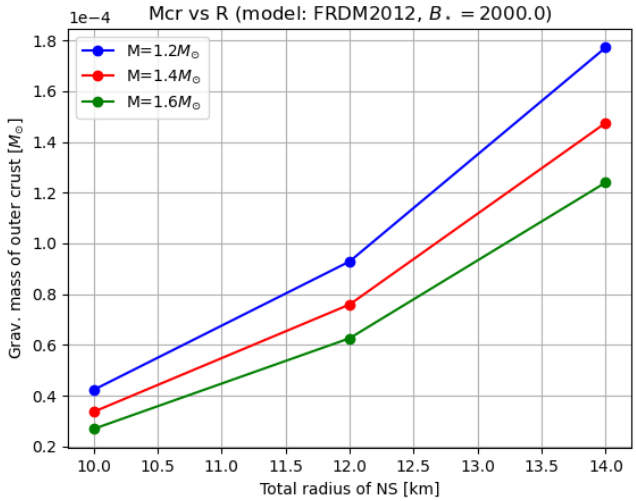

Figure G.74: The same as Figure G.73, using the FRDM2012 model with $B_\star = 2000$

G.9.3 WS4RBF

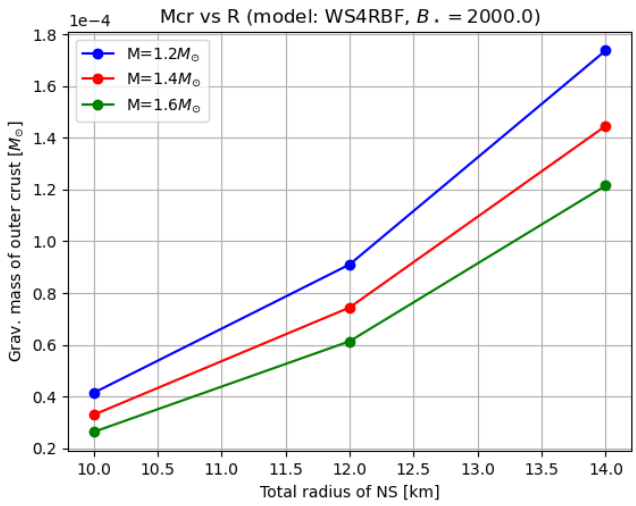

Figure G.75: The same as Figure G.73, using the WS4RBF model with $B_\star = 2000$

G.9.4 BSKG3

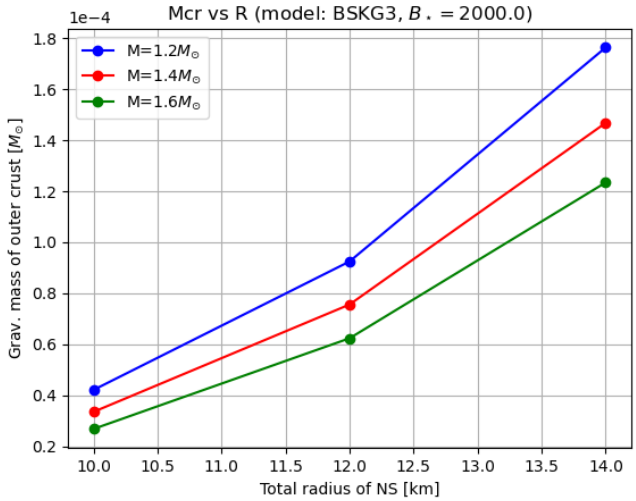

Figure G.76: The same as Figure G.73, using the BSKG3 model with $B_\star = 2000$

G.9.5 HFB31

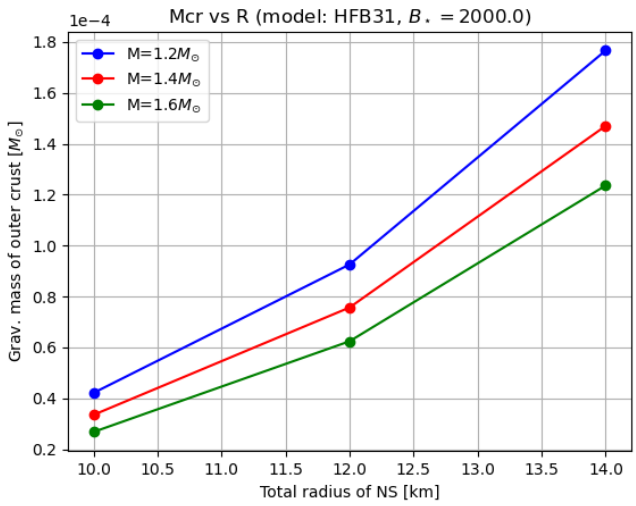

Figure G.77: The same as Figure G.73, using the HFB31 model with $B_\star = 2000$

G.9.6 DDMED

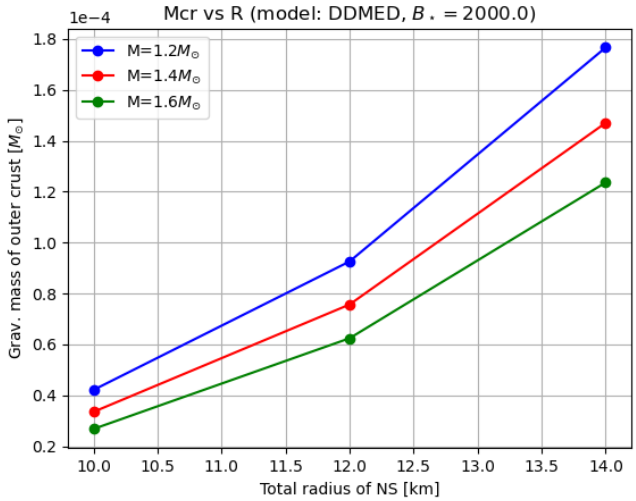

Figure G.78: The same as Figure G.73, using the DDMED model with $B_\star = 2000$

G.9.7 DDPC1

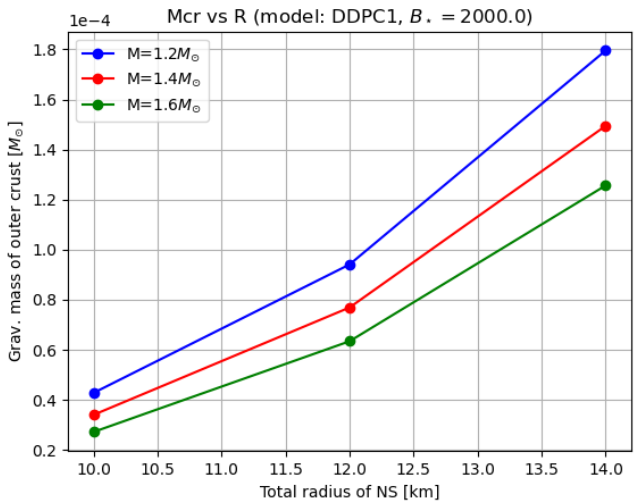

Figure G.79: The same as Figure G.73, using the DDPC1 model with $B_\star = 2000$

G.9.8 SVMIN

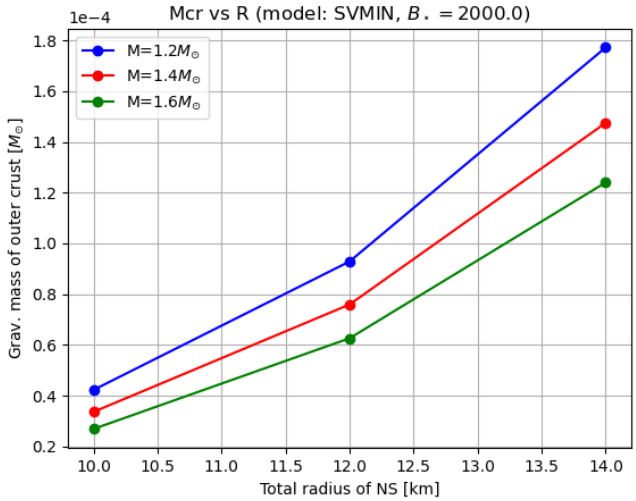

Figure G.80: The same as Figure G.73, using the SVMIN model with $B_\star = 2000$

G.9.9 UNEDF0

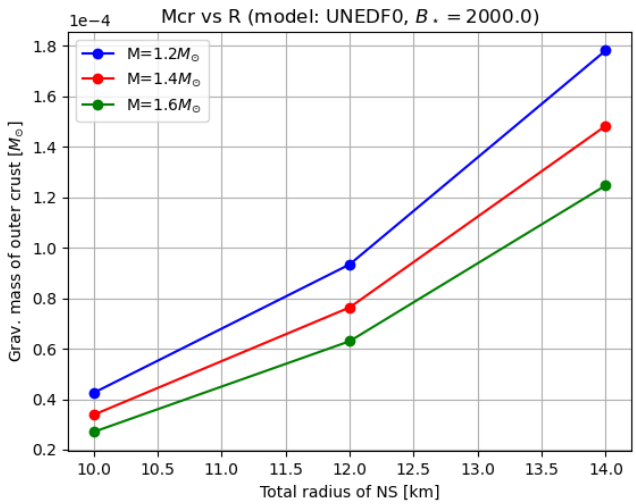

Figure G.81: The same as Figure G.73, using the UNEDF0 model with $B_\star = 2000$

G.10 z_{drip} for different M and R

G.10.1 SEMF

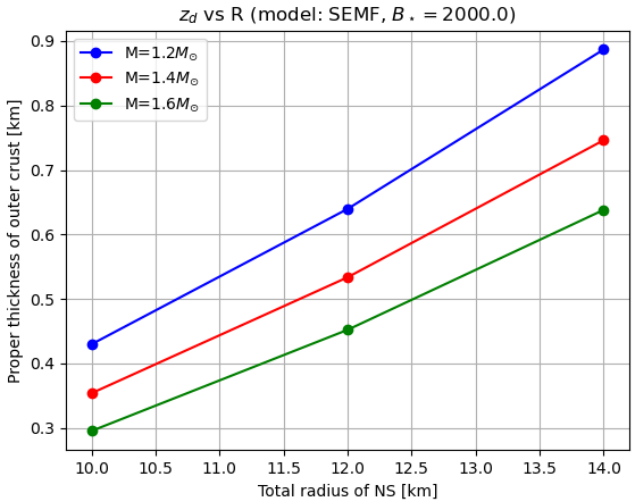

Figure G.82: Proper depth of neutron-drip transition for different masses and radii of NS, using the SEMF model with magnetic field strength $B_\star = 2000$

G.10.2 FRDM2012

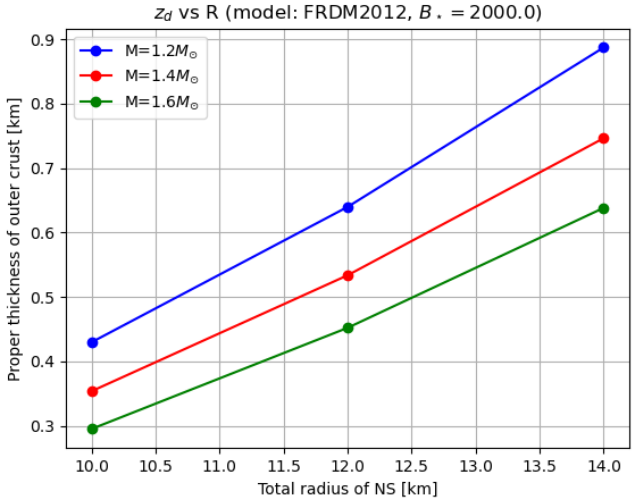

Figure G.83: The same as Figure G.82, using the FRDM2012 model with $B_\star = 2000$

G.10.3 WS4RBF

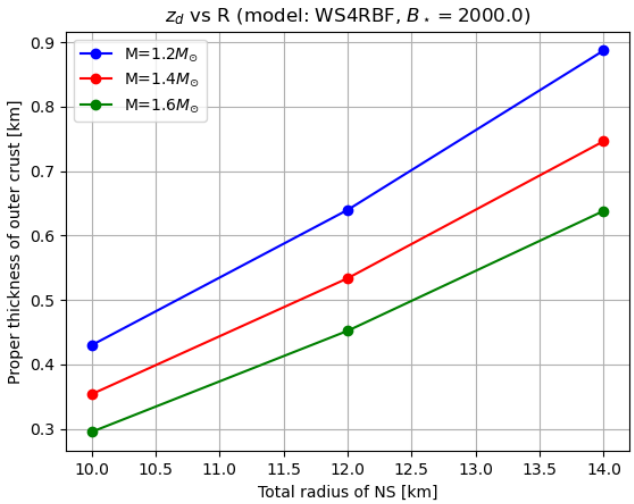

Figure G.84: The same as Figure G.82, using the WS4RBF model with $B_\star = 2000$

G.10.4 BSKG3

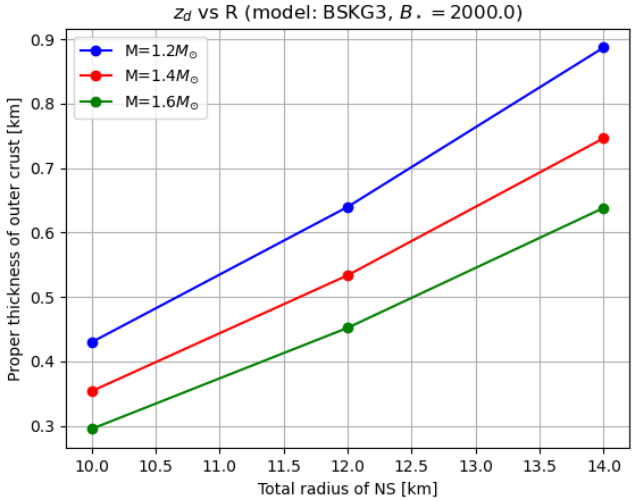

Figure G.85: The same as Figure G.82, using the BSKG3 model with $B_\star = 2000$

G.10.5 HFB31

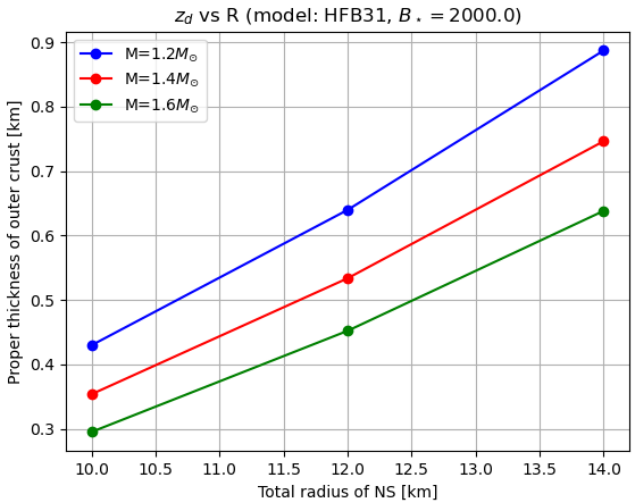

Figure G.86: The same as Figure G.82, using the HFB31 model with $B_\star = 2000$

G.10.6 DDMED

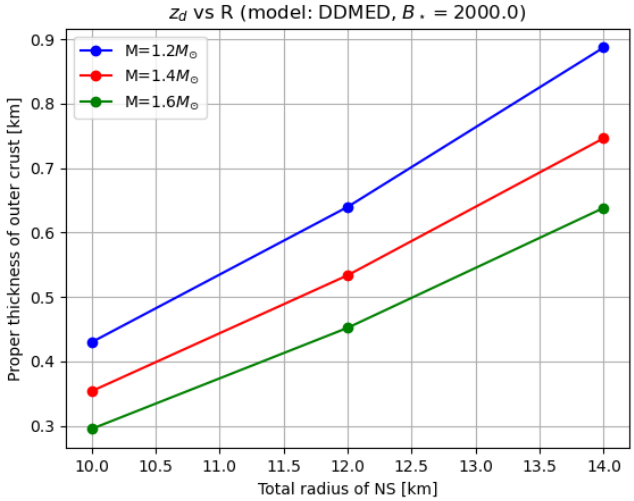

Figure G.87: The same as Figure G.82, using the DDMED model with $B_\star = 2000$

G.10.7 DDPC1

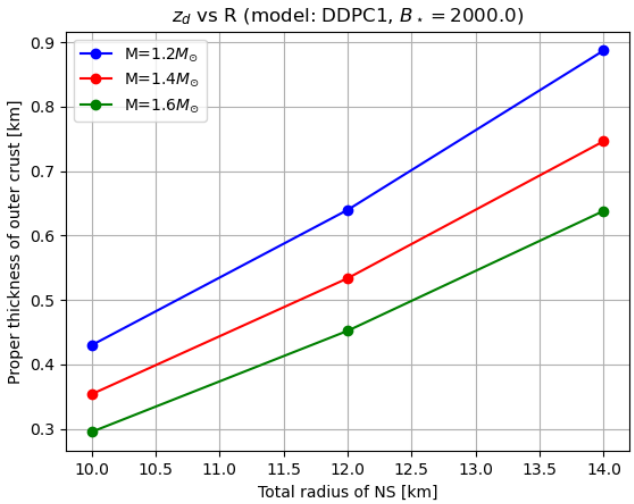

Figure G.88: The same as Figure G.82, using the DDPC1 model with $B_\star = 2000$

G.10.8 SVMIN

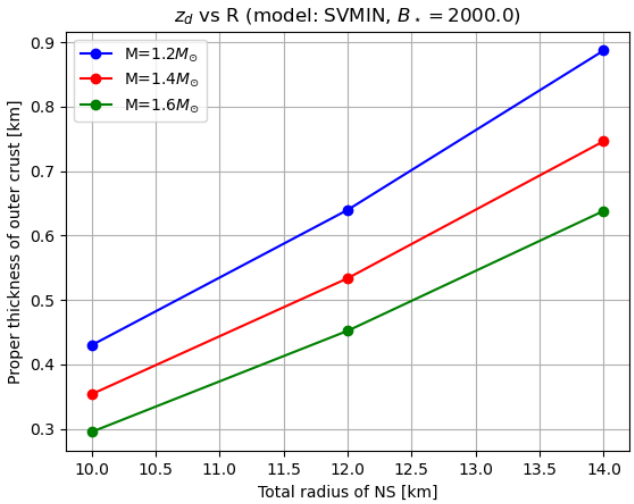

Figure G.89: The same as Figure G.82, using the SVMIN model with $B_\star = 2000$

G.10.9 UNEDF0

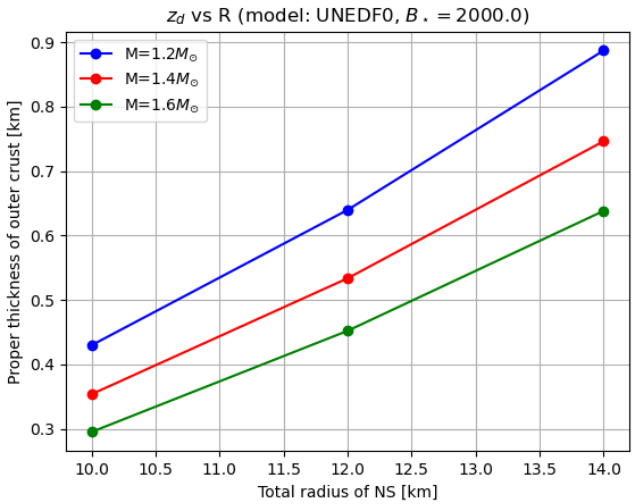

Figure G.90: The same as Figure G.82, using the UNEDF0 model with $B_\star = 2000$

Appendix H

Figures for $B_\star = 2500$

Below are the Figures, like those in Subsections 5.4.3 - 5.4.13, for the models: SEMF, FRDM2012, WS4RBF, BSKG3, HFB31, DDMED, DDPC1, SVMIN and UNEDF0, individually, with magnetic field strength $B_\star = 2500$.

H.1 P vs ϵ or n_b

H.1.1 SEMF

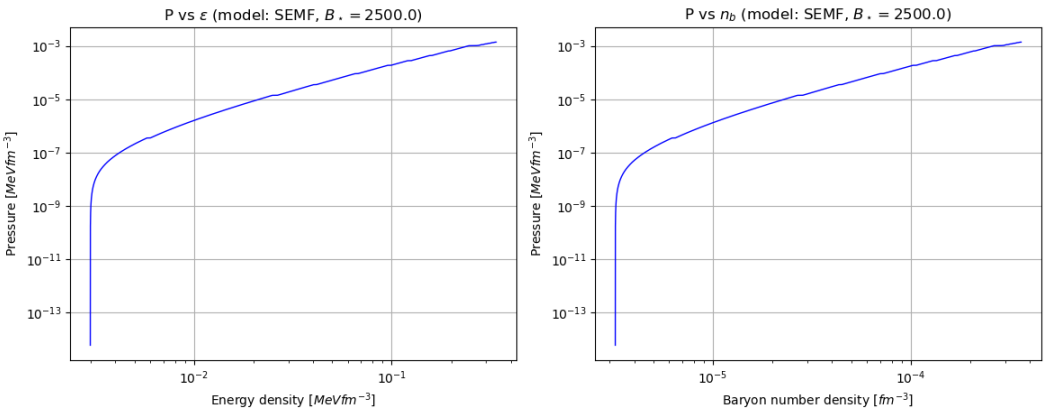

(a) (b)

Figure H.1: Equation of State, (a) pressure as a function of energy density and (b) pressure as a function of baryon number density, using the SEMF model with magnetic field strength $B_\star = 2500$

H.1.2 FRDM2012

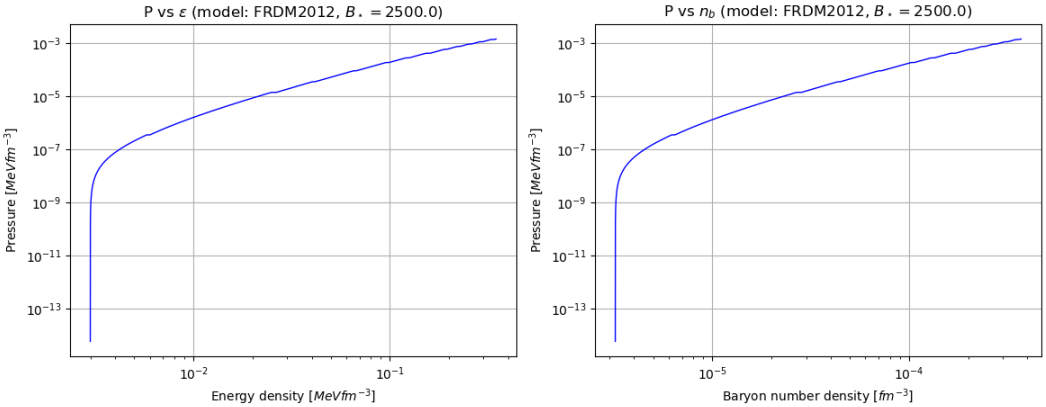

(a) (b)

Figure H.2: The same as Figure H.1, using the FRDM2012 model with $B_\star = 2500$

H.1.3 WS4RBF

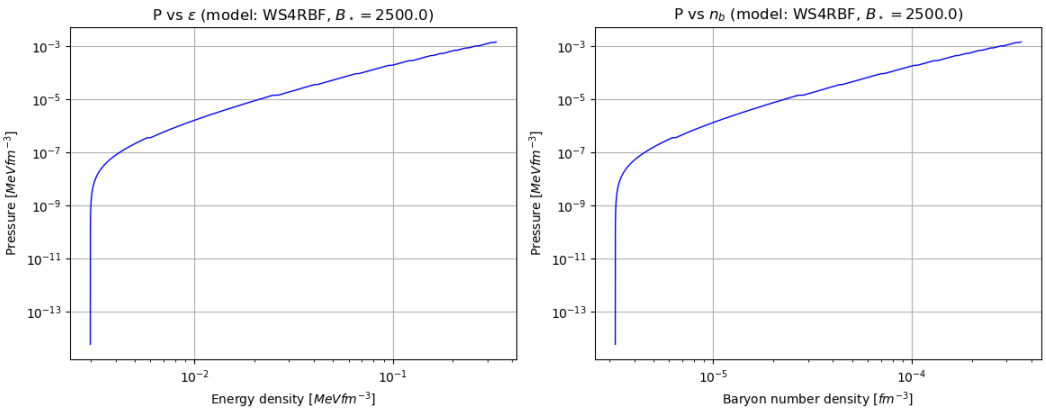

(a) (b)

Figure H.3: The same as Figure H.1, using the WS4RBF model with $B_\star = 2500$

H.1.4 BSKG3

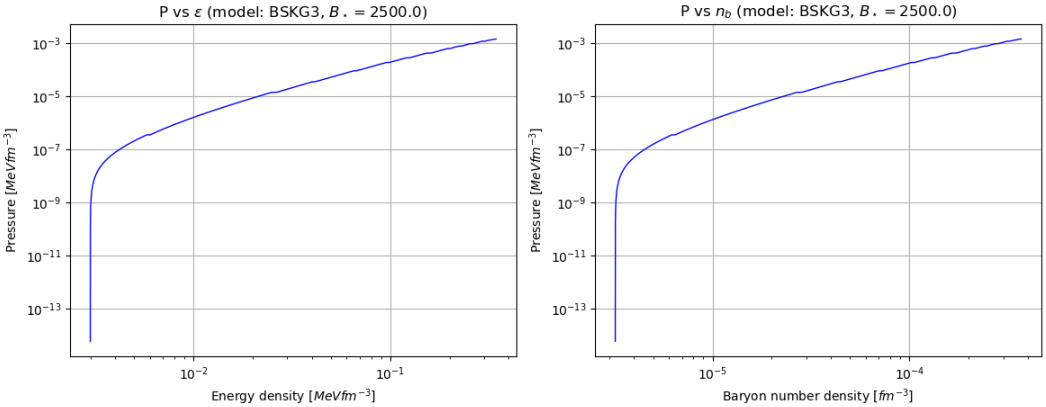

(a) (b)

Figure H.4: The same as Figure H.1, using the BSKG3 model with $B_\star = 2500$

H.1.5 HFB31

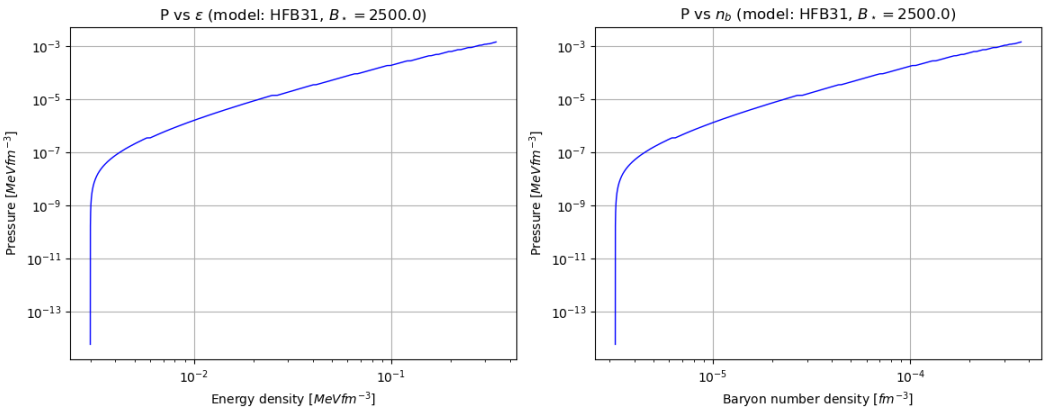

(a) (b)

Figure H.5: The same as Figure H.1, using the HFB31 model with $B_\star = 2500$

H.1.6 DDMED

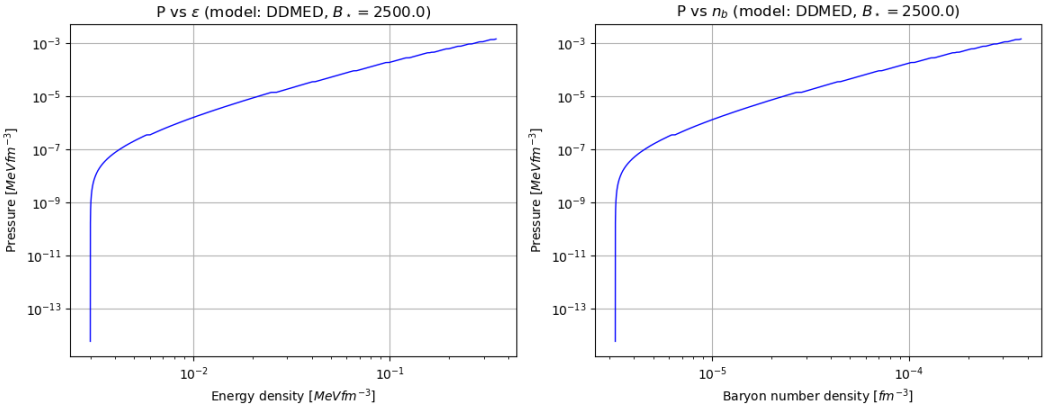

(a) (b)

Figure H.6: The same as Figure H.1, using the DDMED model with $B_\star = 2500$

H.1.7 DDPC1

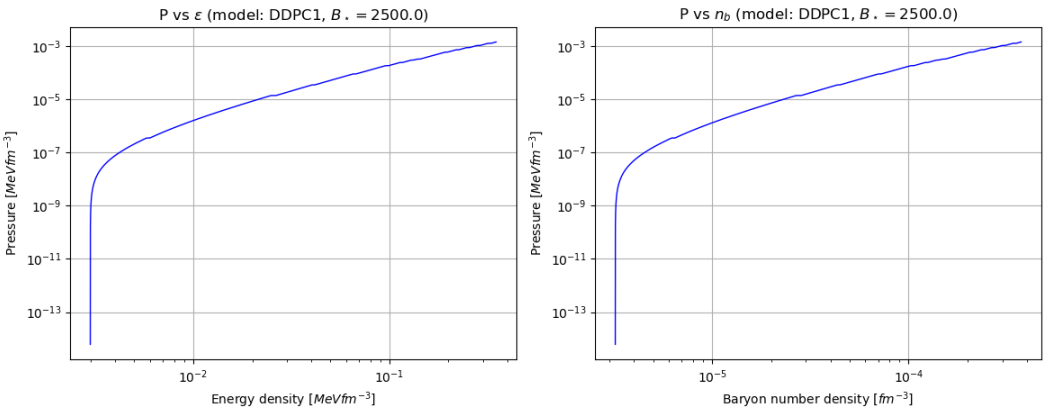

(a) (b)

Figure H.7: The same as Figure H.1, using the DDPC1 model with $B_\star = 2500$

H.1.8 SVMIN

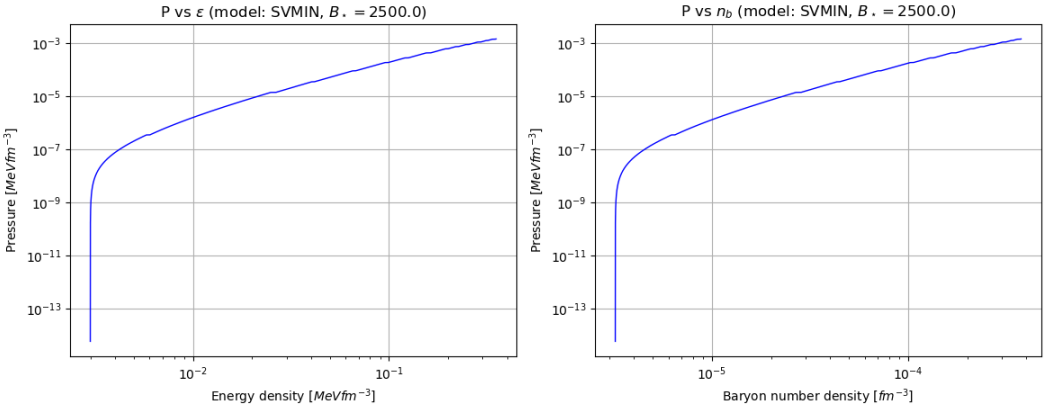

(a) (b)

Figure H.8: The same as Figure H.1, using the SVMIN model with $B_\star = 2500$

H.1.9 UNEDF0

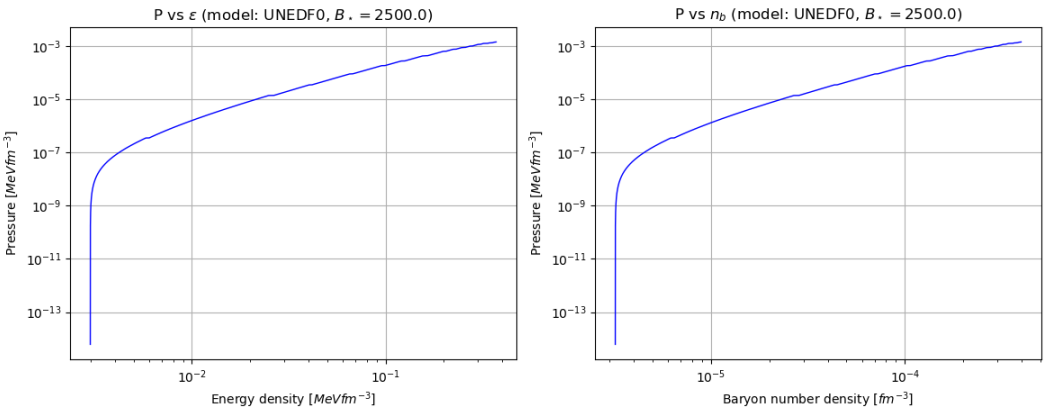

(a) (b)

Figure H.9: The same as Figure H.1, using the UNEDF0 model with $B_\star = 2500$

H.2 Fitting $P = K\epsilon^G$

H.2.1 SEMF

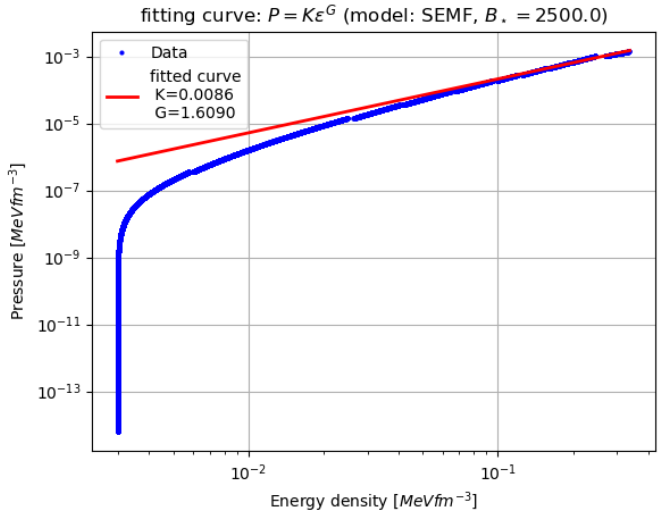

Figure H.10: A polytropic EoS $P = K\epsilon^G$ for fitting, using the SEMF model with magnetic field strength $B_\star = 2500$

H.2.2 FRDM2012

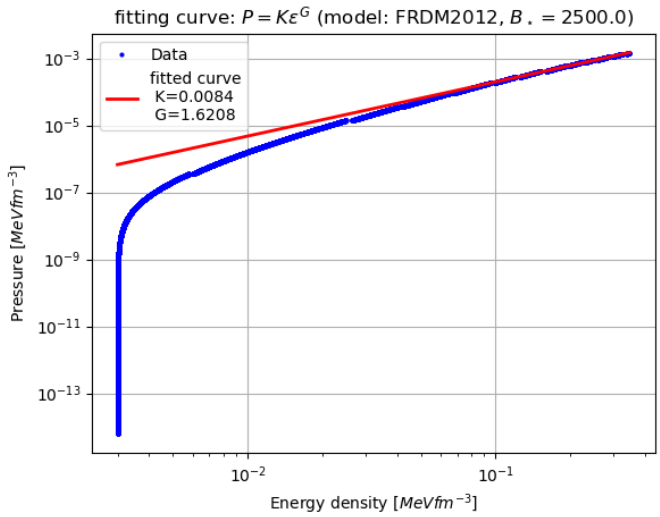

Figure H.11: The same as Figure H.10, using the FRDM2012 model with $B_\star = 2500$

H.2.3 WS4RBF

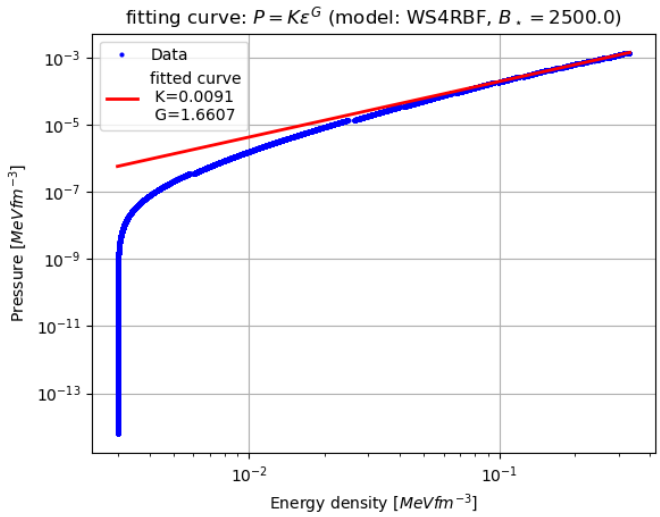

Figure H.12: The same as Figure H.10, using the WS4RBF model with $B_\star = 2500$

H.2.4 BSKG3

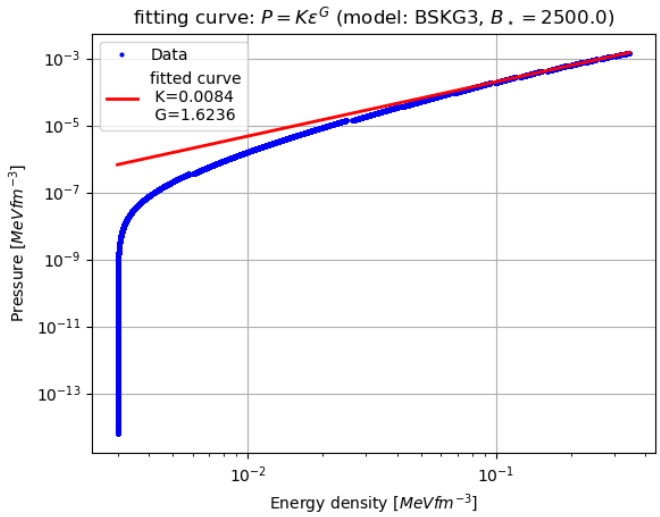

Figure H.13: The same as Figure H.10, using the BSKG3 model with $B_\star = 2500$

H.2.5 HFB31

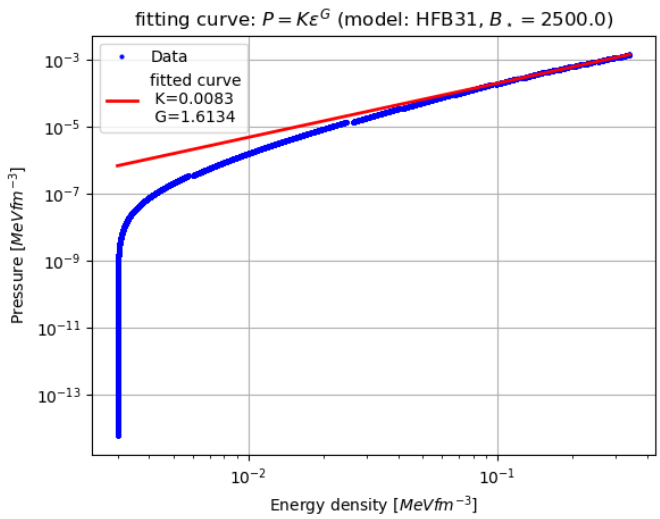

Figure H.14: The same as Figure H.10, using the HFB31 model with $B_\star = 2500$

H.2.6 DDMED

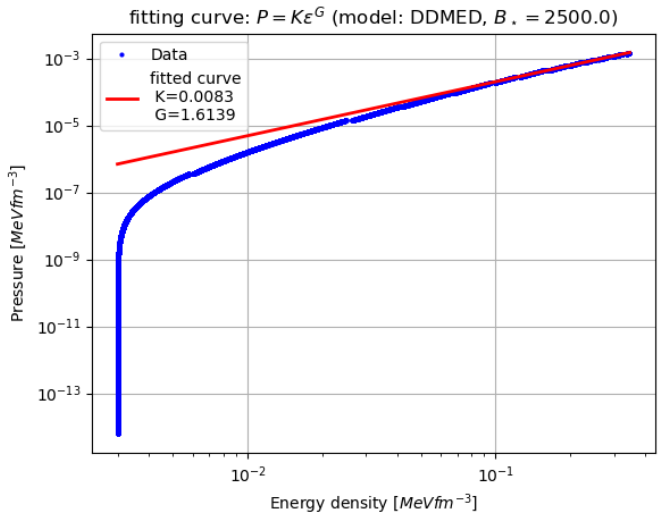

Figure H.15: The same as Figure H.10, using the DDMED model with $B_\star = 2500$

H.2.7 DDPC1

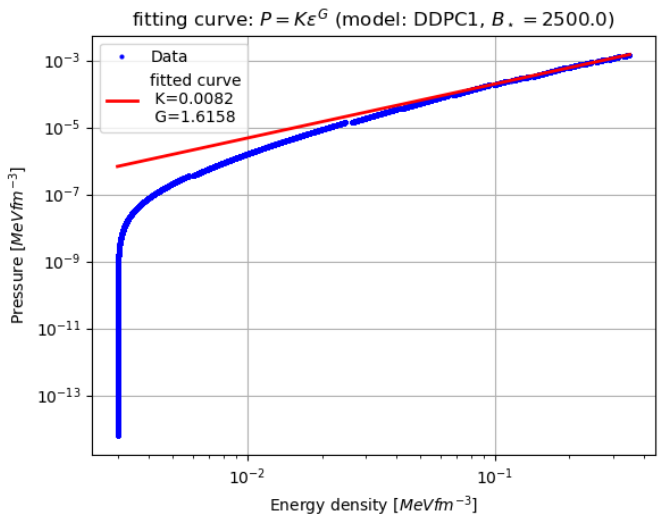

Figure H.16: The same as Figure H.10, using the DDPC1 model with $B_\star = 2500$

H.2.8 SVMIN

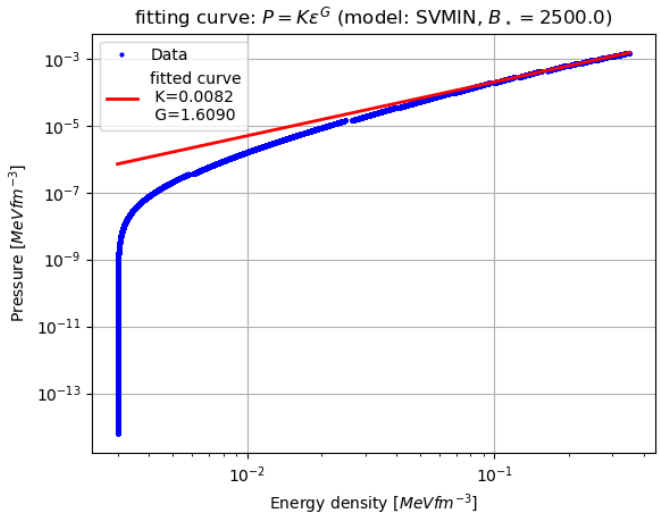

Figure H.17: The same as Figure H.10, using the SVMIN model with $B_\star = 2500$

H.2.9 UNEDF0

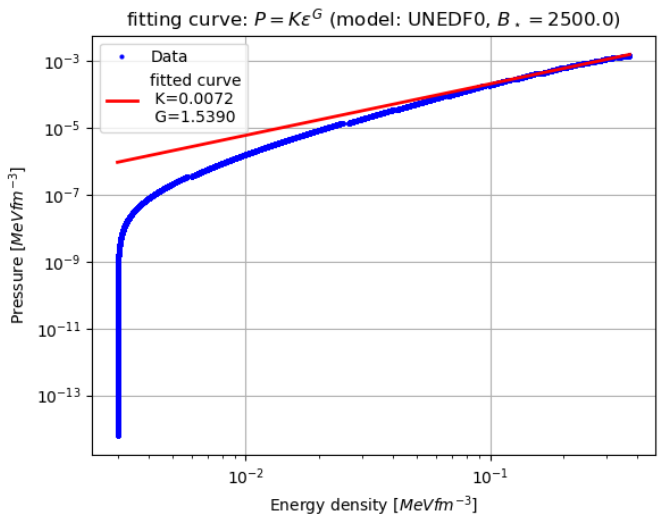

Figure H.18: The same as Figure H.10, using the UNEDF0 model with $B_\star = 2500$

H.3 Γ vs ϵ or n_b

H.3.1 SEMF

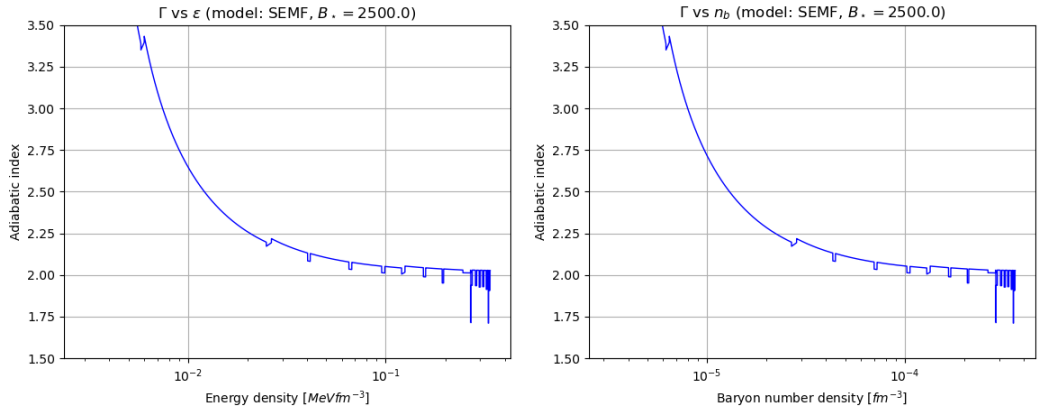

(a) (b)

Figure H.19: Adiabatic index as a function of (a) energy density and of (b) baryon number density, using the SEMF model with magnetic field strength $B_\star = 2500$

H.3.2 FRDM2012

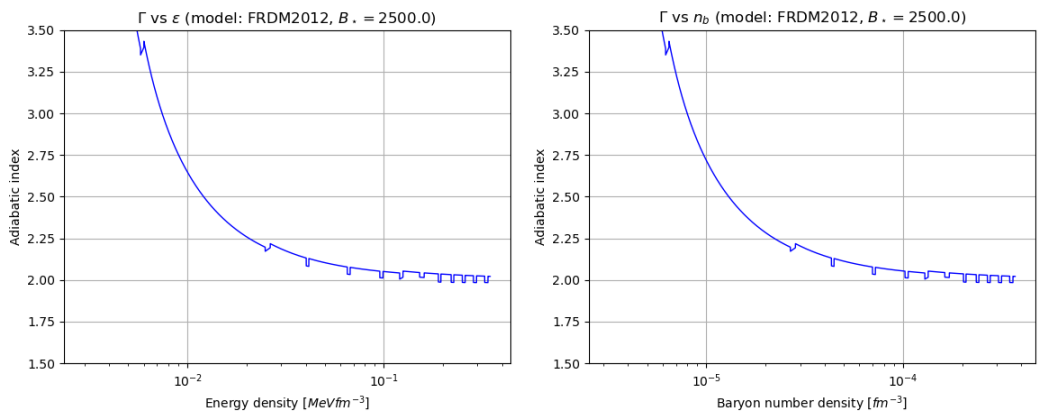

(a) (b)

Figure H.20: The same as Figure H.19, using the FRDM2012 model with $B_\star = 2500$

H.3.3 WS4RBF

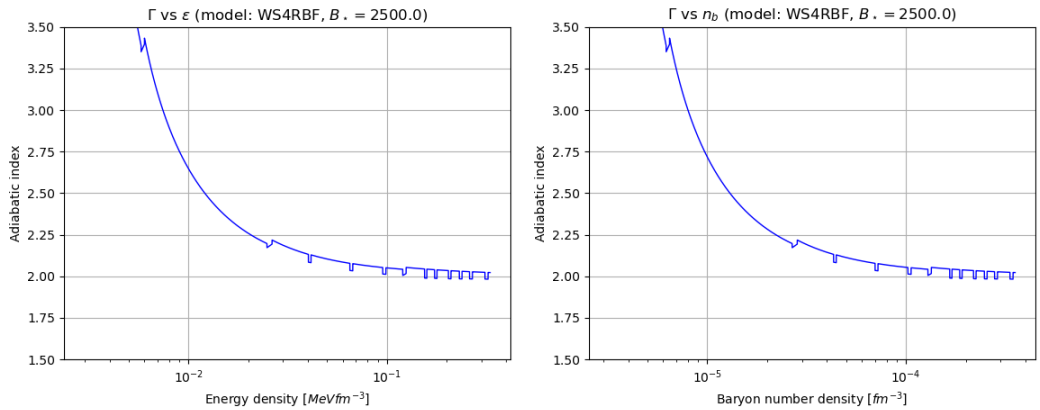

(a) (b)

Figure H.21: The same as Figure H.19, using the WS4RBF model with $B_\star = 2500$

H.3.4 BSKG3

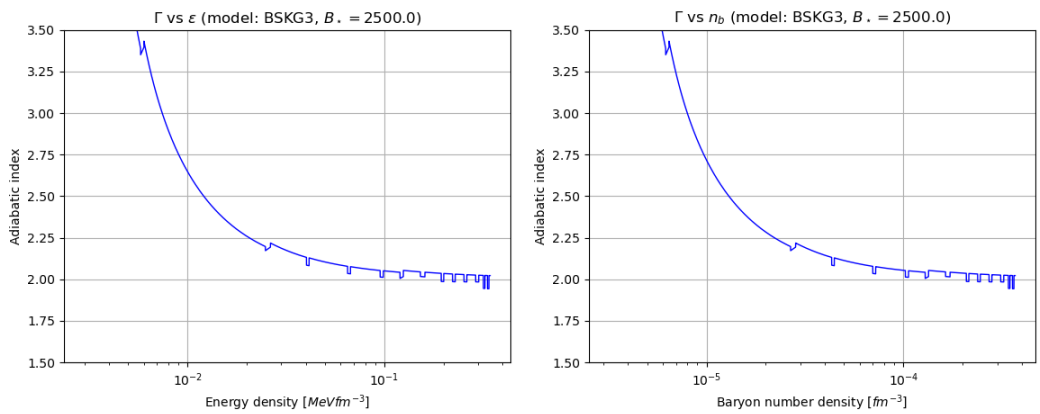

(a) (b)

Figure H.22: The same as Figure H.19, using the BSKG3 model with $B_\star = 2500$

H.3.5 HFB31

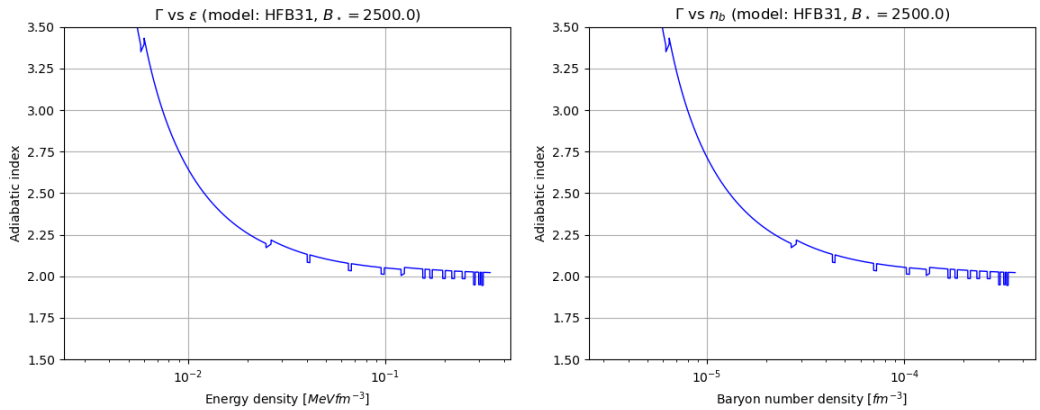

(a) (b)

Figure H.23: The same as Figure H.19, using the HFB31 model with $B_\star = 2500$

H.3.6 DDMED

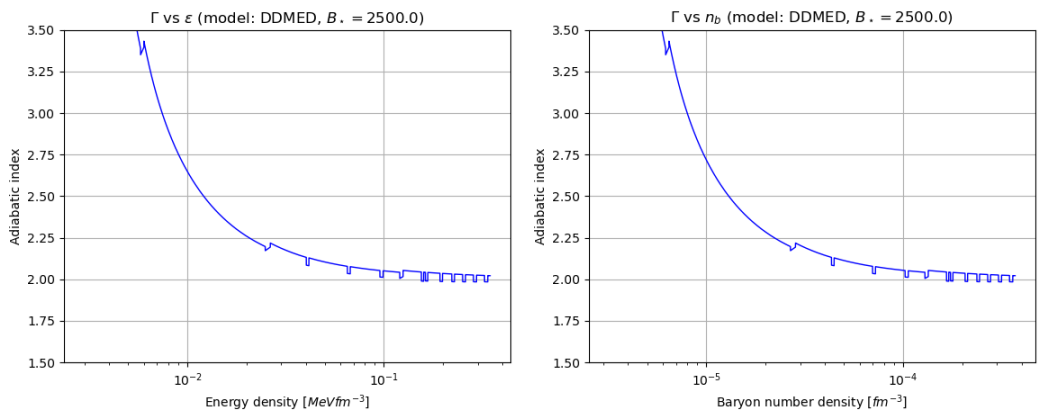

(a) (b)

Figure H.24: The same as Figure H.19, using the DDMED model with $B_\star = 2500$

H.3.7 DDPC1

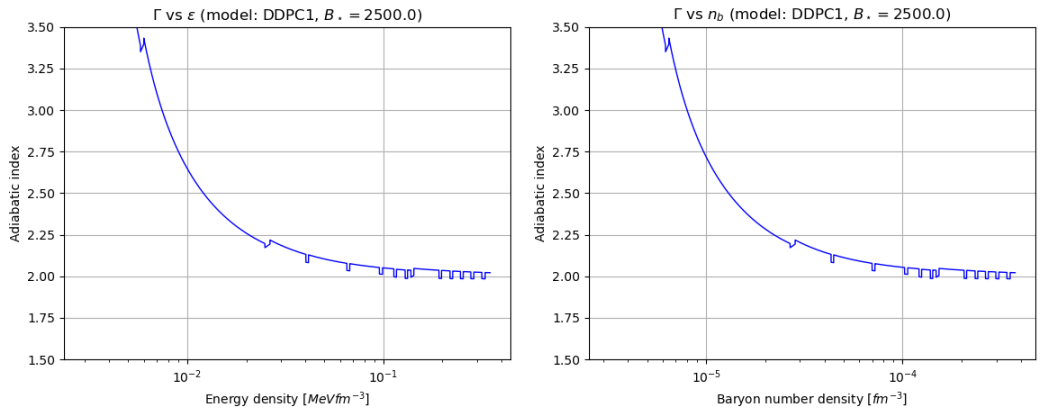

(a) (b)

Figure H.25: The same as Figure H.19, using the DDPC1 model with $B_\star = 2500$

H.3.8 SVMIN

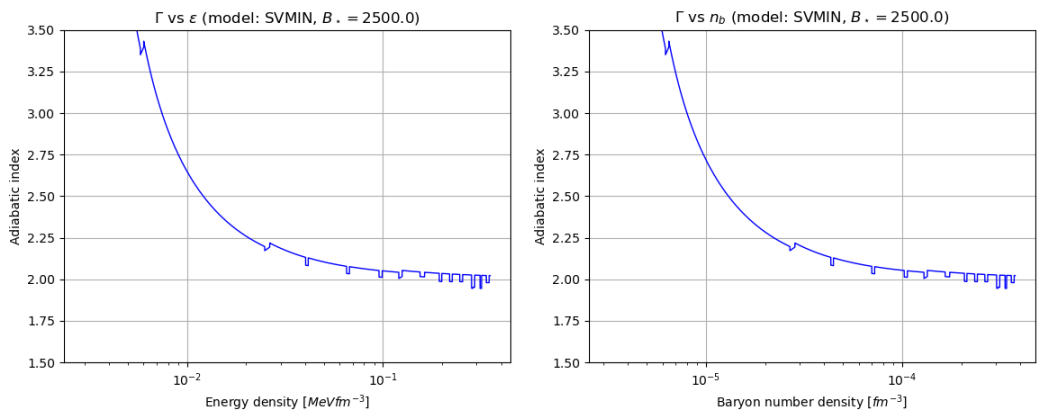

(a) (b)

Figure H.26: The same as Figure H.19, using the SVMIN model with $B_\star = 2500$

H.3.9 UNEDF0

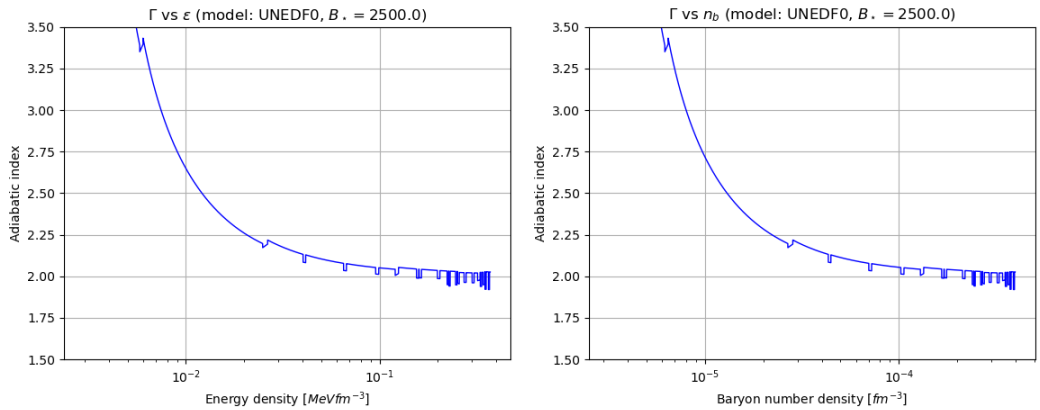

(a) (b)

Figure H.27: The same as Figure H.19, using the UNEDF0 model with $B_\star = 2500$

H.4 c_s vs ϵ or n_b

H.4.1 SEMF

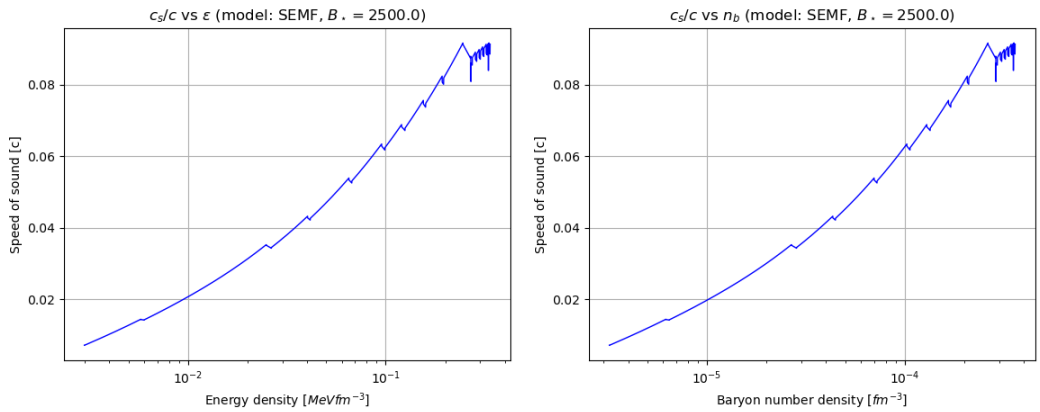

(a) (b)

Figure H.28: Speed of sound as a function of (a) energy density and of (b) baryon number density, using the SEMF model with magnetic field strength $B_\star = 2500$

H.4.2 FRDM2012

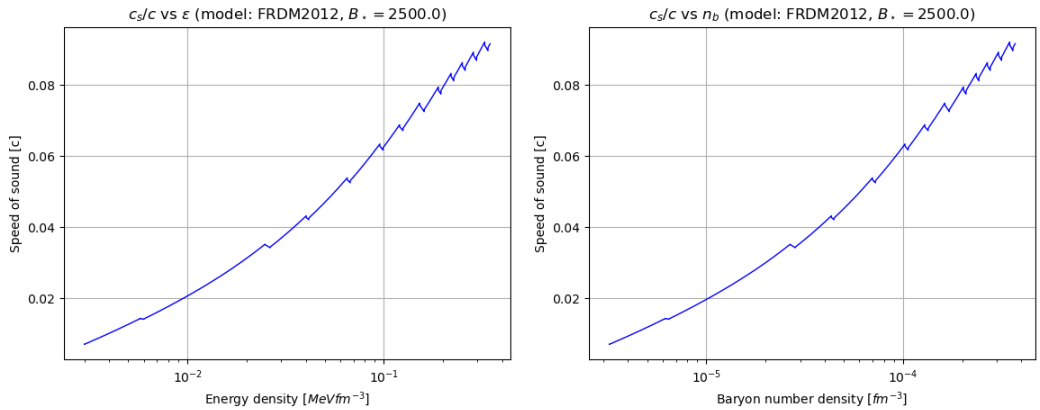

(a) (b)

Figure H.29: The same as Figure H.28, using the FRDM2012 model with $B_\star = 2500$

H.4.3 WS4RBF

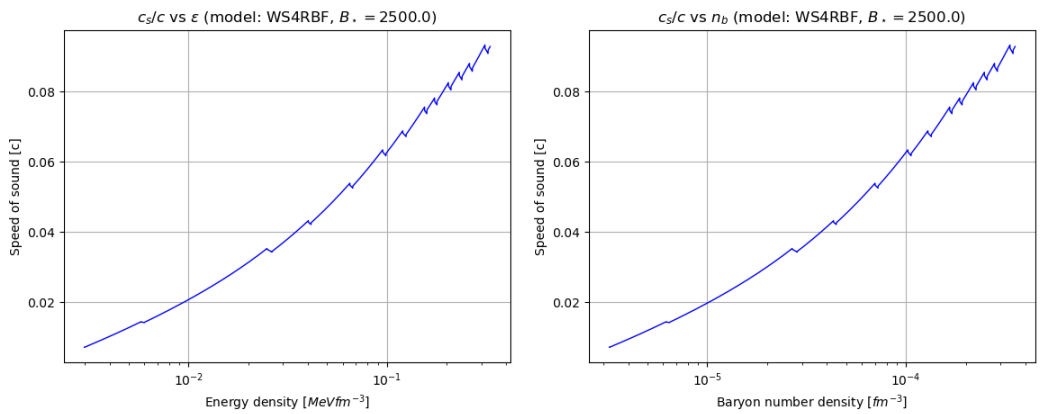

(a) (b)

Figure H.30: The same as Figure H.28, using the WS4RBF model with $B_\star = 2500$

H.4.4 BSKG3

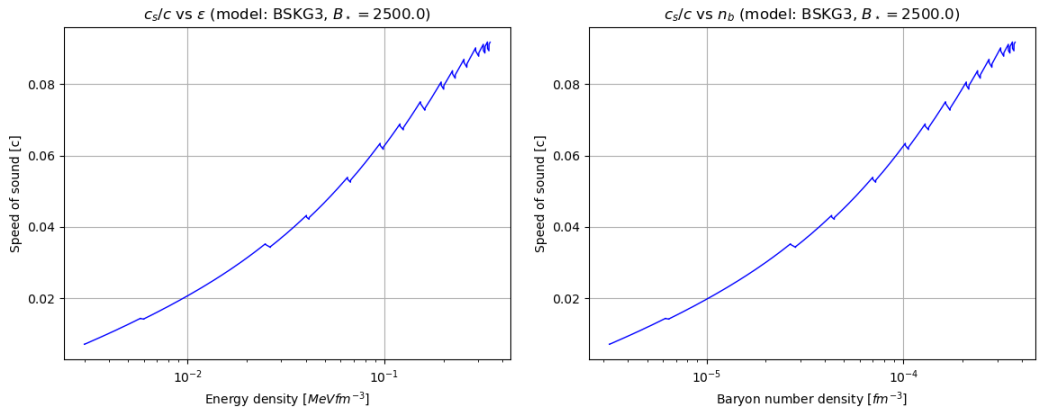

(a) (b)

Figure H.31: The same as Figure H.28, using the BSKG3 model with $B_\star = 2500$

H.4.5 HFB31

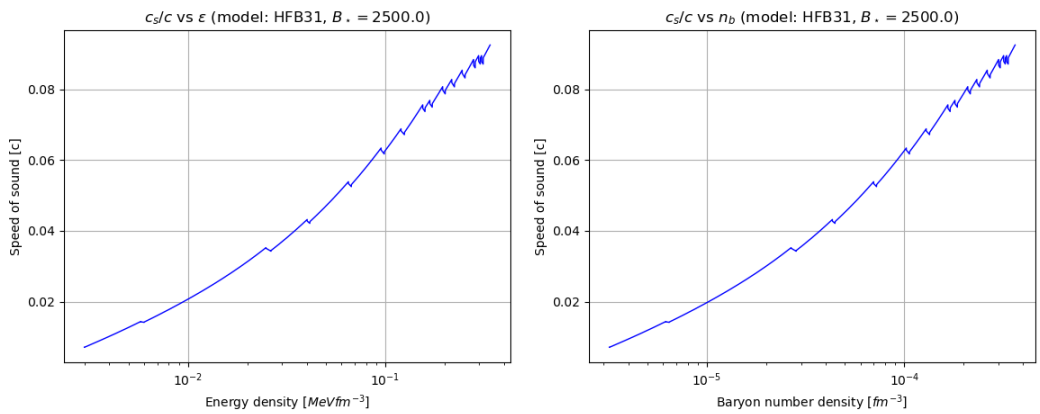

(a) (b)

Figure H.32: The same as Figure H.28, using the HFB31 model with $B_\star = 2500$

H.4.6 DDMED

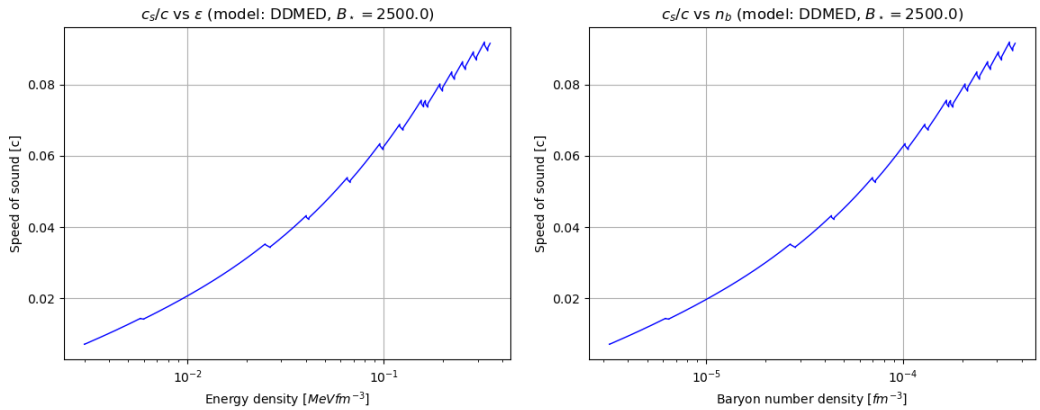

(a) (b)

Figure H.33: The same as Figure H.28, using the DDMED model with $B_\star = 2500$

H.4.7 DDPC1

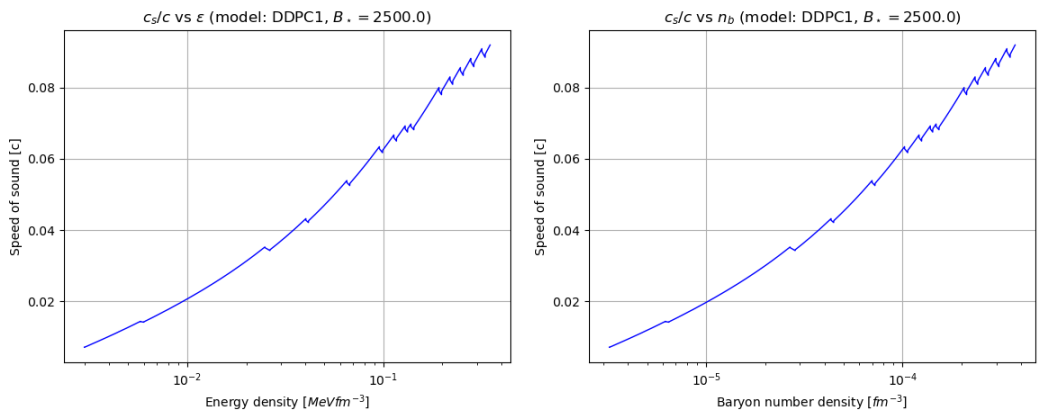

(a) (b)

Figure H.34: The same as Figure H.28, using the DDPC1 model with $B_\star = 2500$

H.4.8 SVMIN

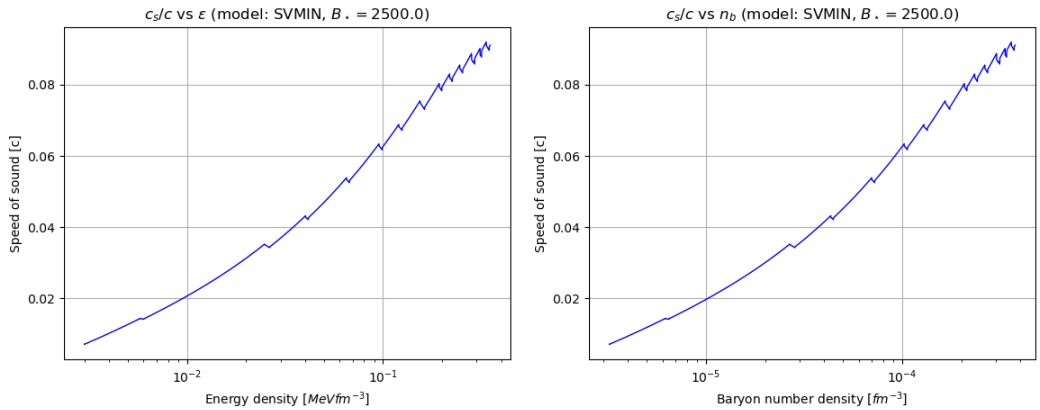

(a) (b)

Figure H.35: The same as Figure H.28, using the SVMIN model with $B_\star = 2500$

H.4.9 UNEDF0

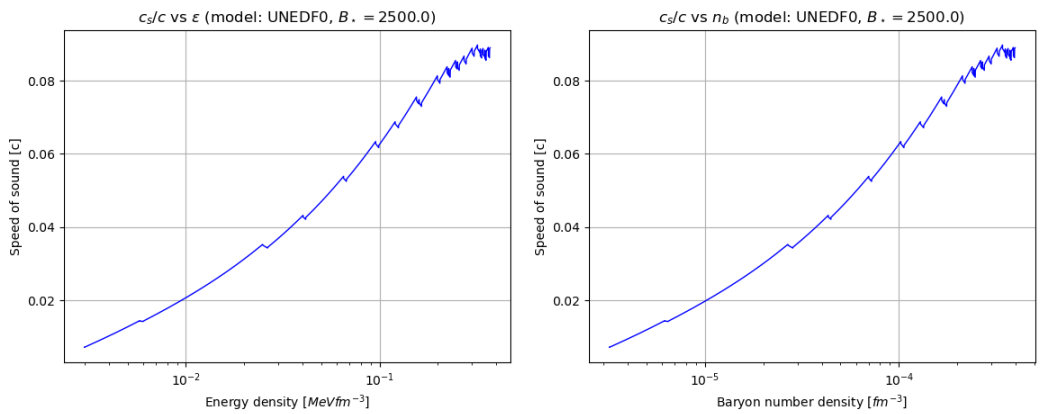

(a) (b)

Figure H.36: The same as Figure H.28, using the UNEDF0 model with $B_\star = 2500$

H.5 K_{mod} vs ϵ or n_b

H.5.1 SEMF

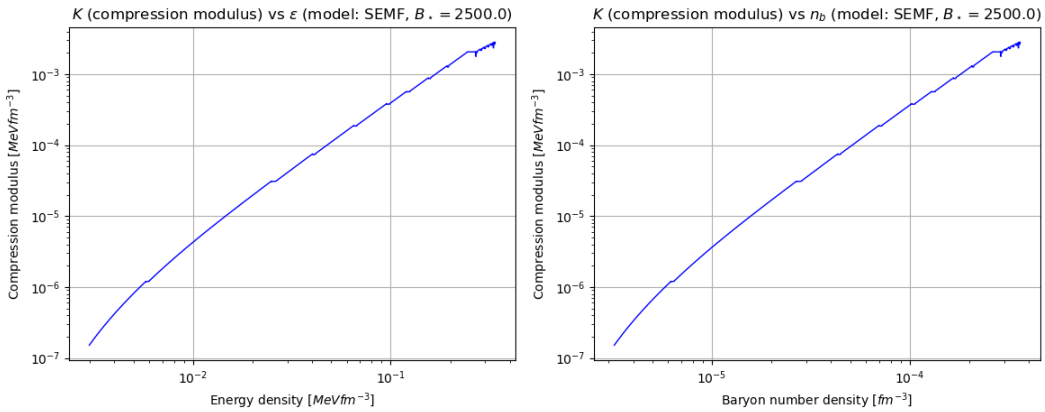

(a) (b)

Figure H.37: Compression modulus as a function of (a) energy density and of (b) baryon number density, using the SEMF model with magnetic field strength $B_\star = 2500$

H.5.2 FRDM2012

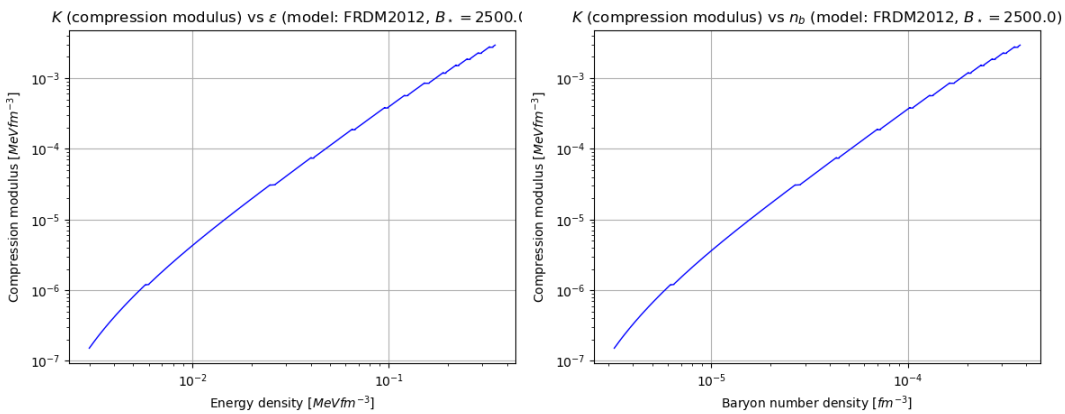

(a) (b)

Figure H.38: The same as Figure H.37, using the FRDM2012 model with $B_\star = 2500$

H.5.3 WS4RBF

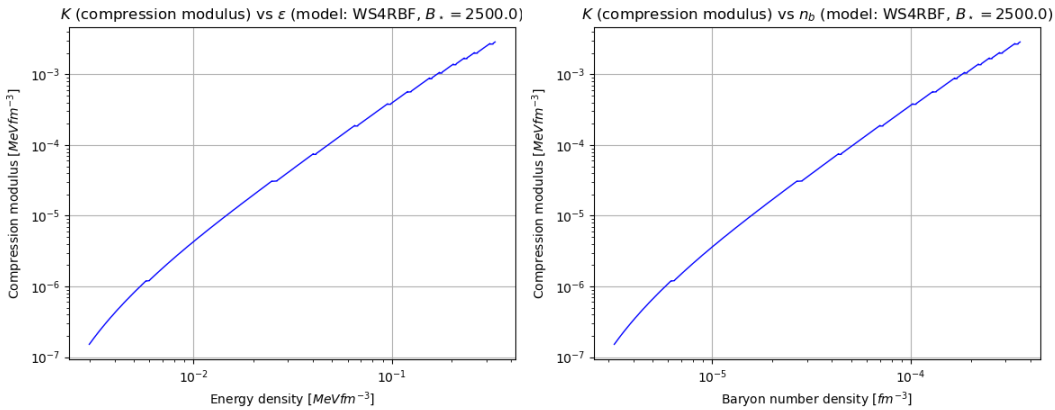

(a) (b)

Figure H.39: The same as Figure H.37, using the WS4RBF model with $B_\star = 2500$

H.5.4 BSKG3

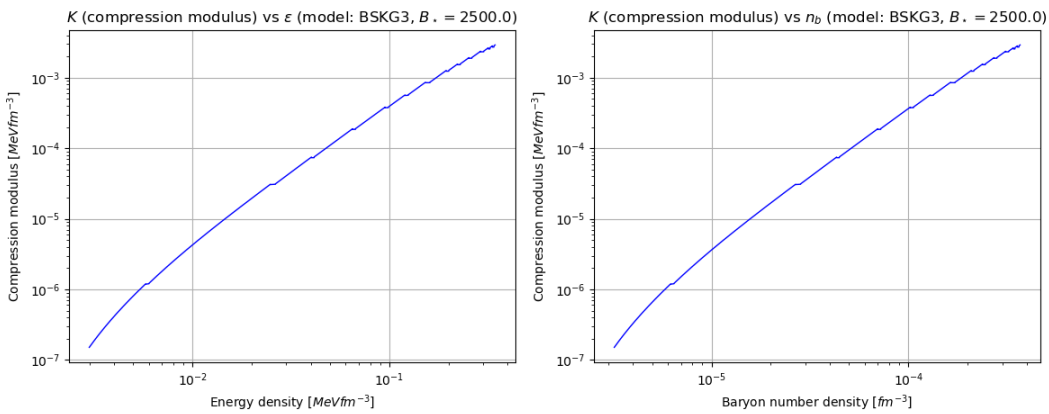

(a) (b)

Figure H.40: The same as Figure H.37, using the BSKG3 model with $B_\star = 2500$

H.5.5 HFB31

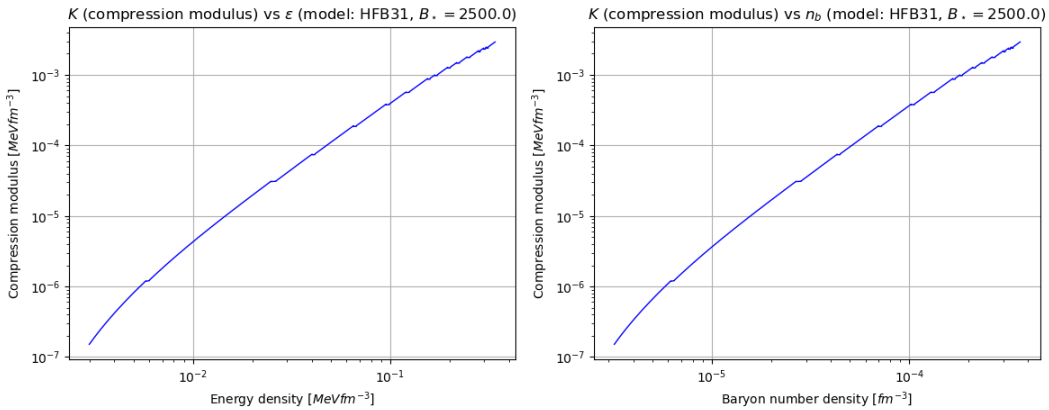

(a) (b)

Figure H.41: The same as Figure H.37, using the HFB31 model with $B_\star = 2500$

H.5.6 DDMED

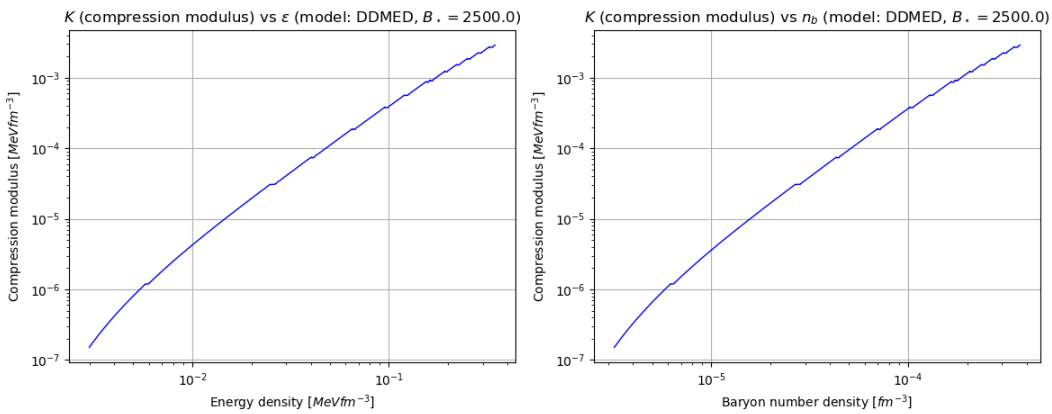

(a) (b)

Figure H.42: The same as Figure H.37, using the DDMED model with $B_\star = 2500$

H.5.7 DDPC1

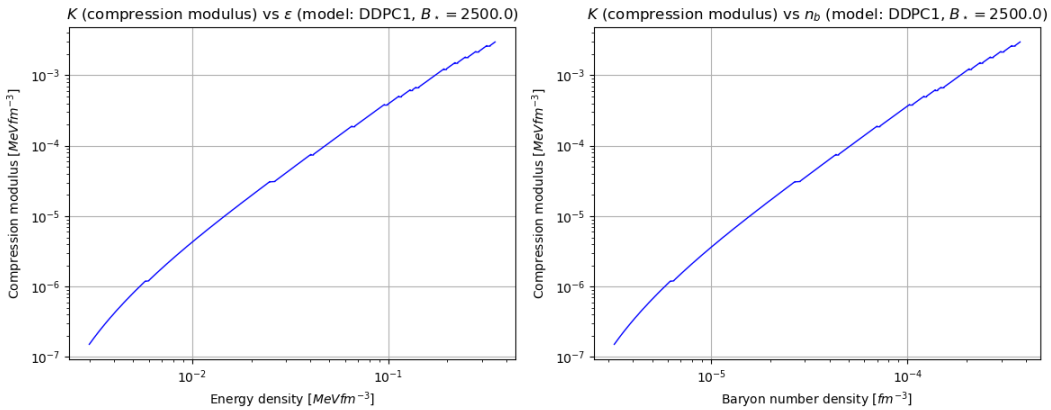

(a) (b)

Figure H.43: The same as Figure H.37, using the DDPC1 model with $B_\star = 2500$

H.5.8 SVMIN

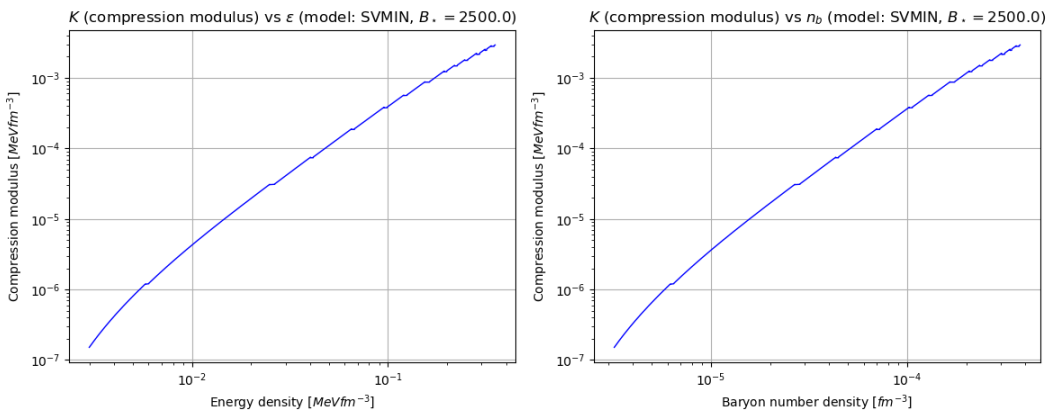

(a) (b)

Figure H.44: The same as Figure H.37, using the SVMIN model with $B_\star = 2500$

H.5.9 UNEDF0

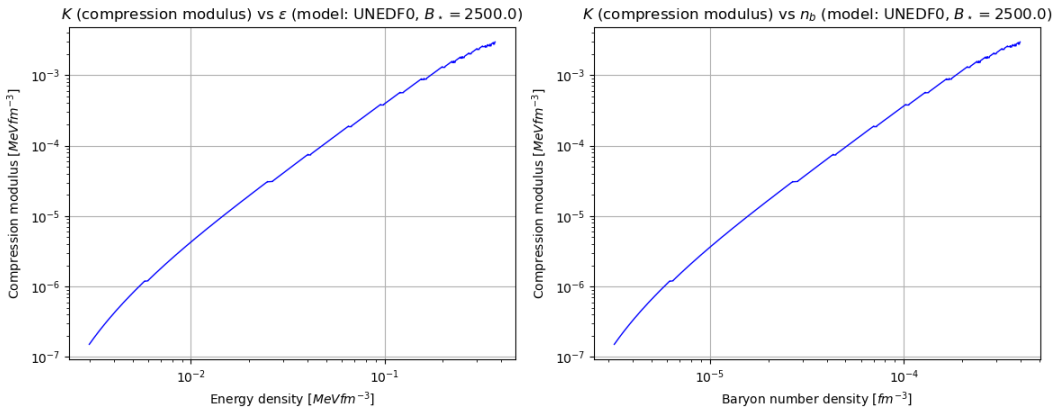

(a) (b)

Figure H.45: The same as Figure H.37, using the UNEDF0 model with $B_\star = 2500$

H.6 S_{mod} vs ϵ or n_b

H.6.1 SEMF

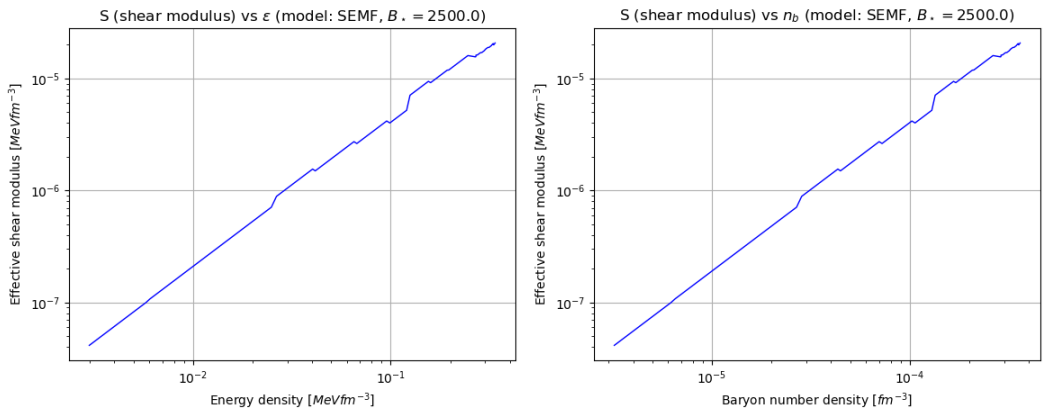

(a) (b)

Figure H.46: Effective shear modulus as a function of (a) energy density and of (b) baryon number density, using the SEMF model with magnetic field strength $B_\star = 2500$

H.6.2 FRDM2012

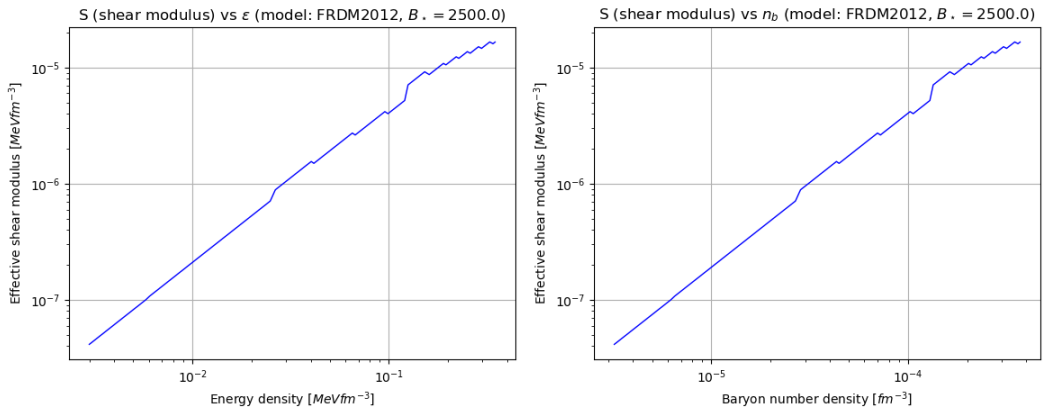

(a) (b)

Figure H.47: The same as Figure H.46, using the FRDM2012 model with $B_\star = 2500$

H.6.3 WS4RBF

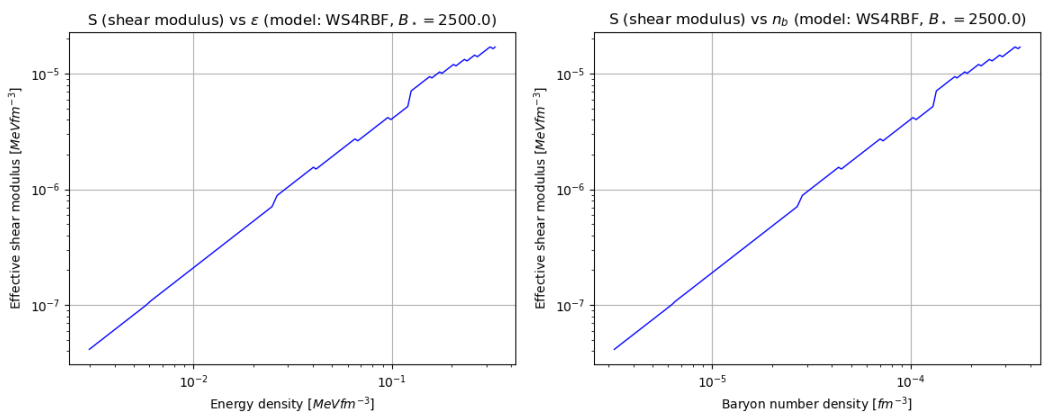

(a) (b)

Figure H.48: The same as Figure H.46, using the WS4RBF model with $B_\star = 2500$

H.6.4 BSKG3

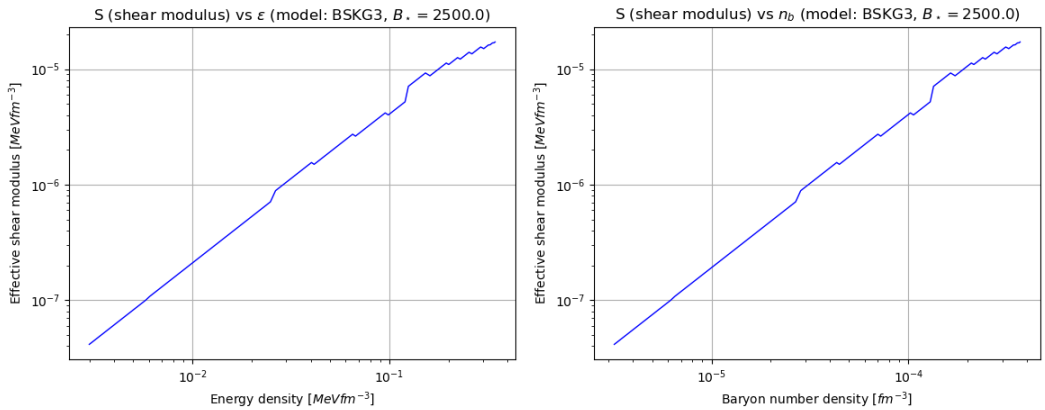

(a) (b)

Figure H.49: The same as Figure H.46, using the BSKG3 model with $B_\star = 2500$

H.6.5 HFB31

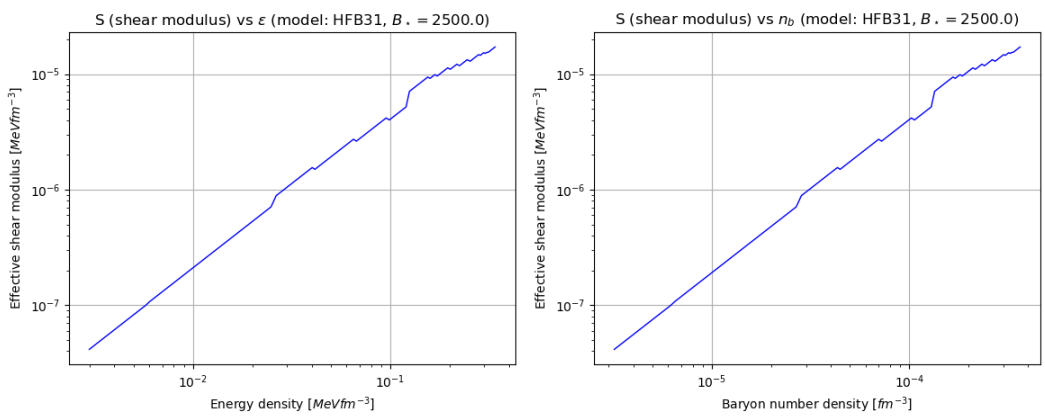

(a) (b)

Figure H.50: The same as Figure H.46, using the HFB31 model with $B_\star = 2500$

H.6.6 DDMED

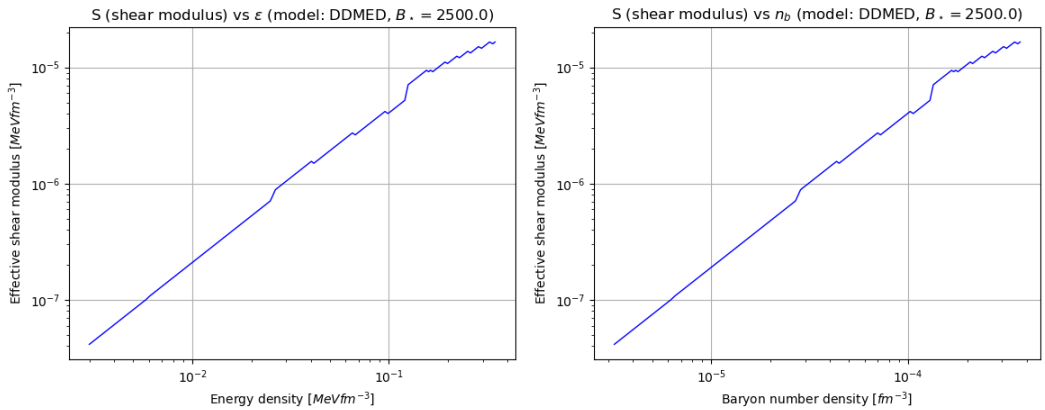

(a) (b)

Figure H.51: The same as Figure H.46, using the DDMED model with $B_\star = 2500$

H.6.7 DDPC1

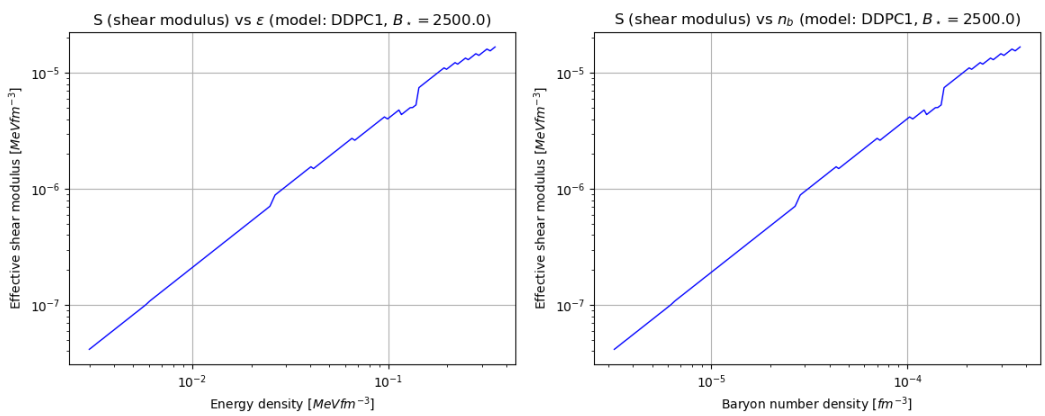

(a) (b)

Figure H.52: The same as Figure H.46, using the DDPC1 model with $B_\star = 2500$

H.6.8 SVMIN

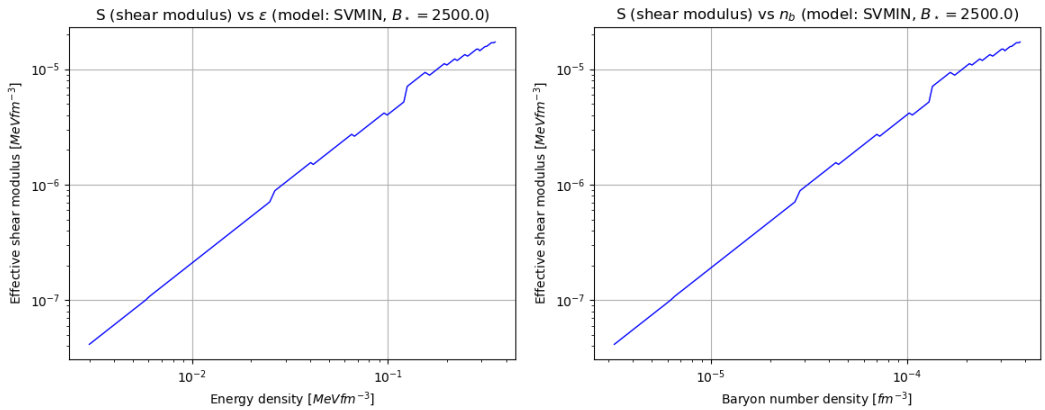

(a) (b)

Figure H.53: The same as Figure H.46, using the SVMIN model with $B_\star = 2500$

H.6.9 UNEDF0

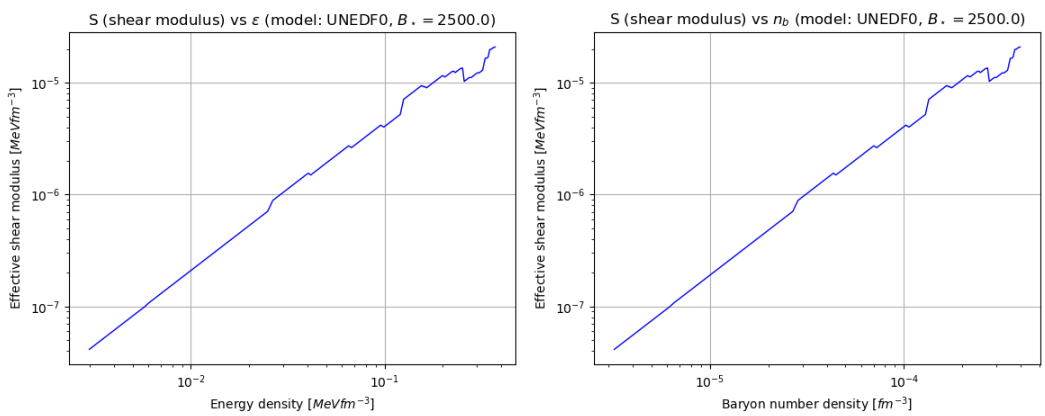

(a) (b)

Figure H.54: The same as Figure H.46, using the UNEDF0 model with $B_\star = 2500$

H.7 S_{mod}/K_{mod} vs ϵ or n_b

H.7.1 SEMF

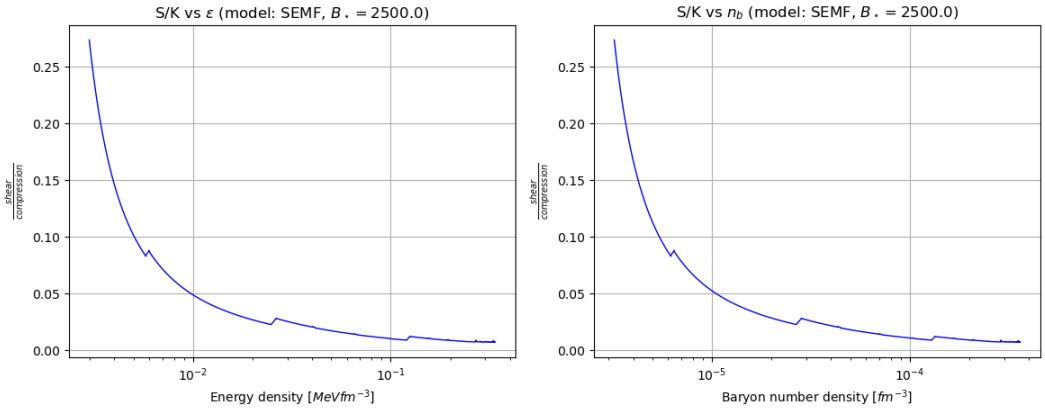

(a) (b)

Figure H.55: Effective shear modulus over compression modulus as a function of (a) energy density and of (b) baryon number density, using the SEMF model with magnetic field strength $B_\star = 2500$

H.7.2 FRDM2012

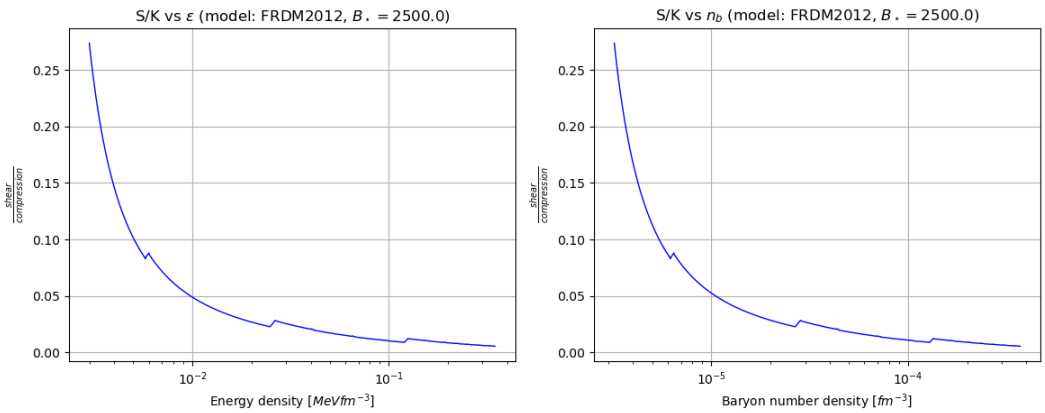

(a) (b)

Figure H.56: The same as Figure H.55, using the FRDM2012 model with $B_\star = 2500$

H.7.3 WS4RBF

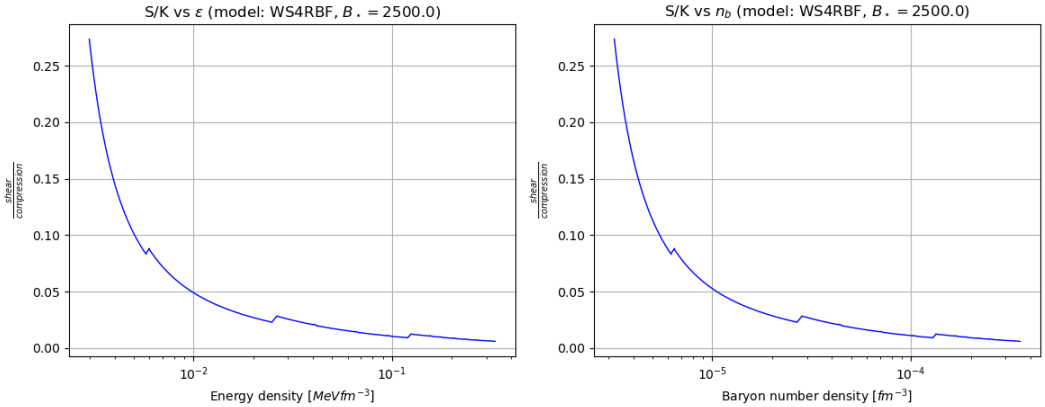

(a) (b)

Figure H.57: The same as Figure H.55, using the WS4RBF model with $B_\star = 2500$

H.7.4 BSKG3

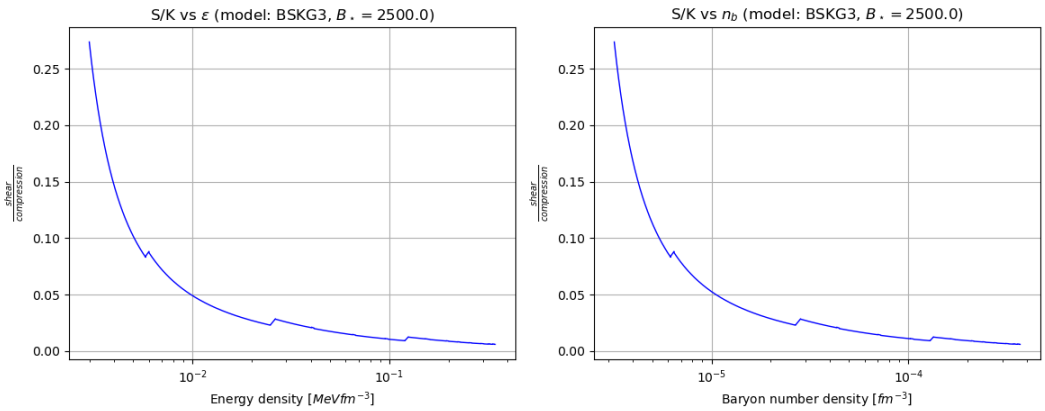

(a) (b)

Figure H.58: The same as Figure H.55, using the BSKG3 model with $B_\star = 2500$

H.7.5 HFB31

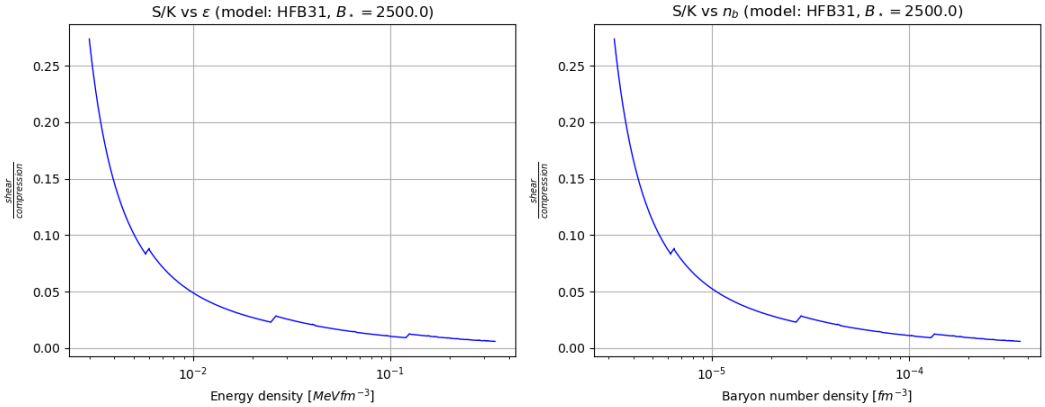

(a) (b)

Figure H.59: The same as Figure H.55, using the HFB31 model with $B_\star = 2500$

H.7.6 DDMED

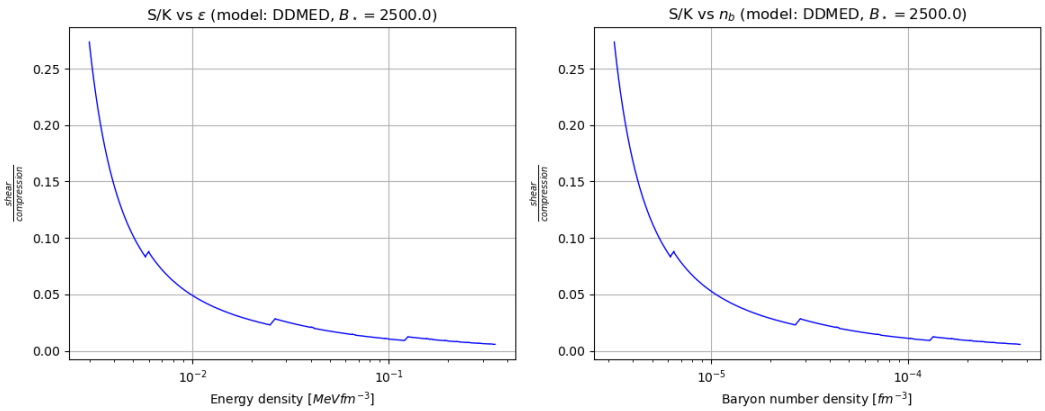

(a) (b)

Figure H.60: The same as Figure H.55, using the DDMED model with $B_\star = 2500$

H.7.7 DDPC1

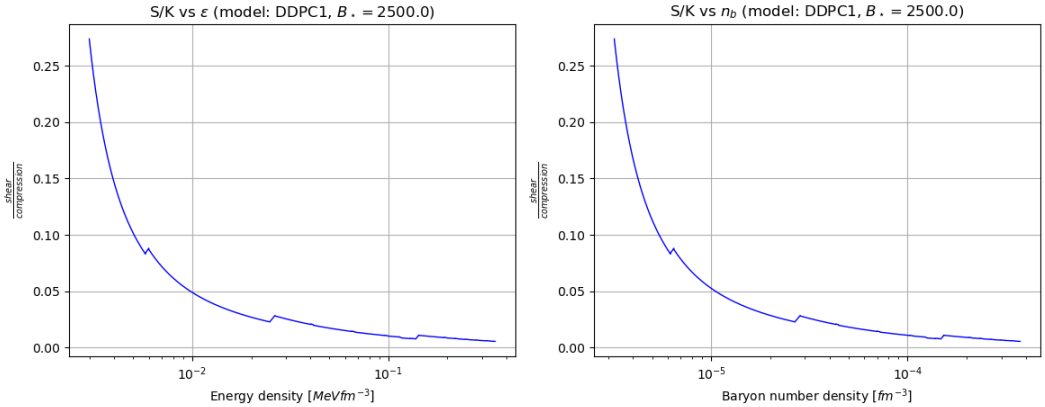

(a) (b)

Figure H.61: The same as Figure H.55, using the DDPC1 model with $B_\star = 2500$

H.7.8 SVMIN

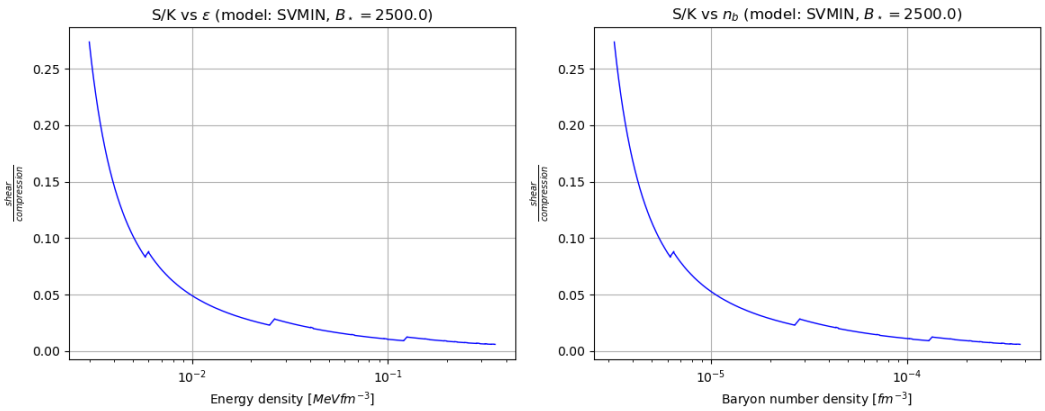

(a) (b)

Figure H.62: The same as Figure H.55, using the SVMIN model with $B_\star = 2500$

H.7.9 UNEDF0

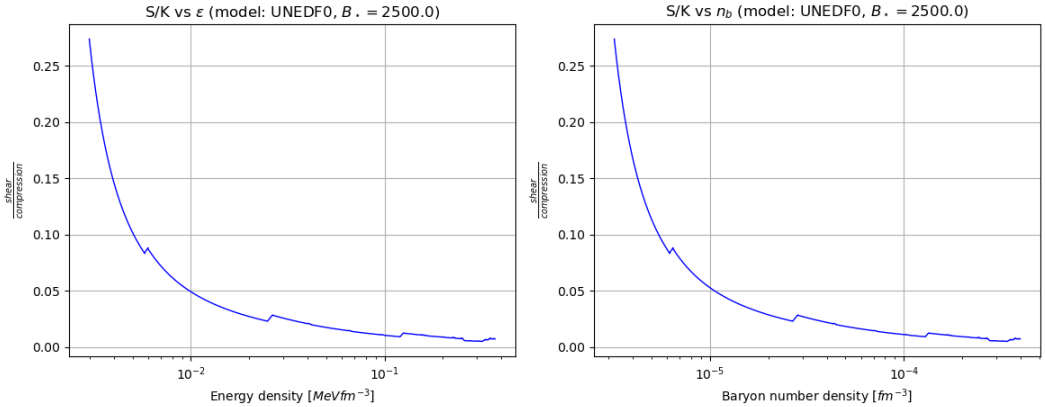

(a) (b)

Figure H.63: The same as Figure H.55, using the UNEDF0 model with $B_\star = 2500$

H.8 Z, N, Z/A vs ϵ or n_b

H.8.1 SEMF

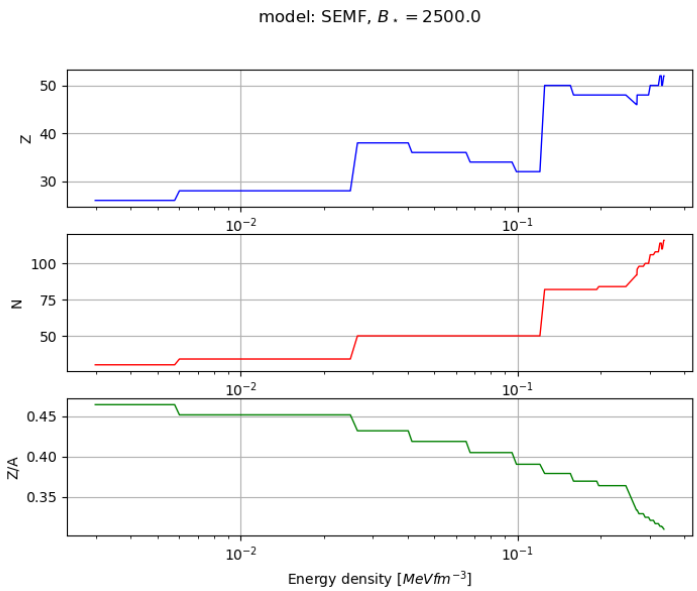

(a)

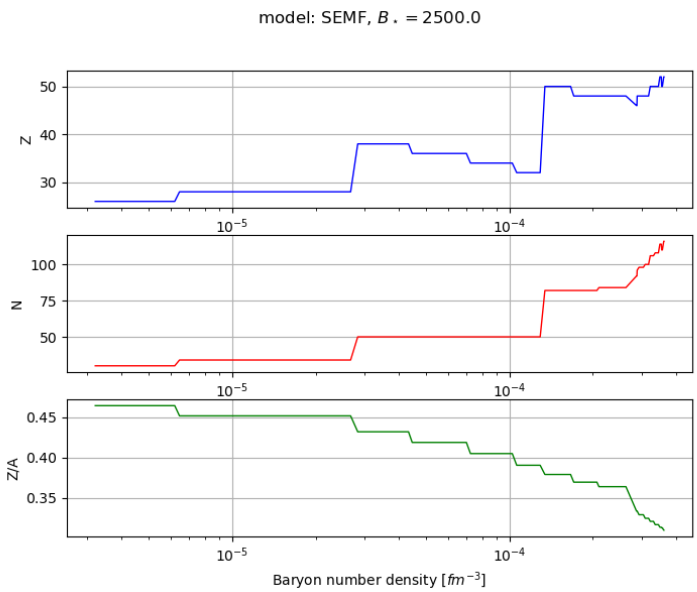

(b)

Figure H.64: Atomic number, neutron number and proton fraction as a function of (a) energy density and of (b) baryon number density, using the SEMF model with magnetic field strength $B_\star = 2500$

H.8.2 FRDM2012

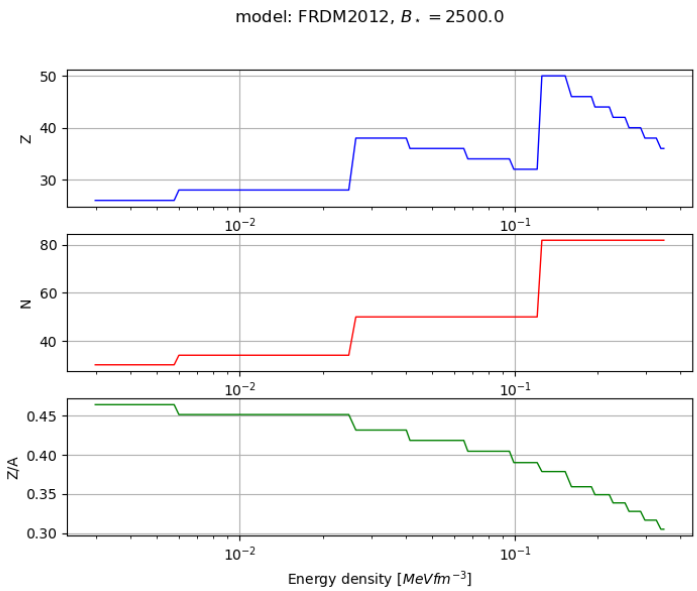

(a)

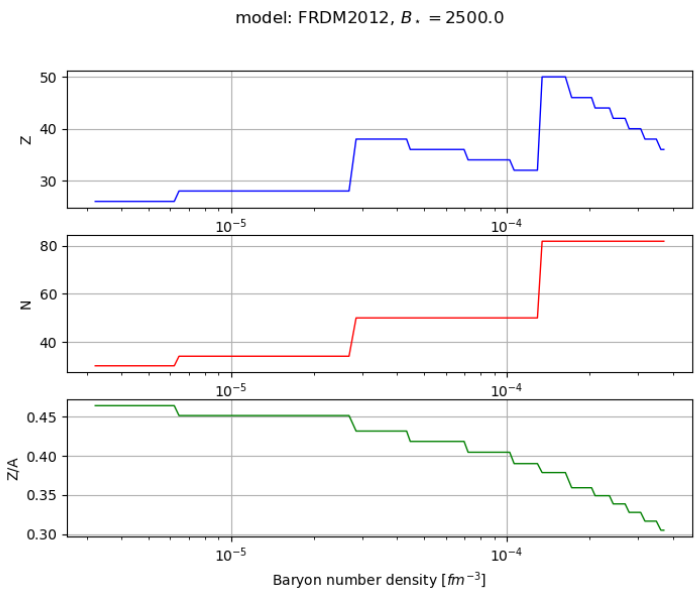

(b)

Figure H.65: The same as Figure H.64, using the FRDM2012 model with $B_\star = 2500$

H.8.3 WS4RBF

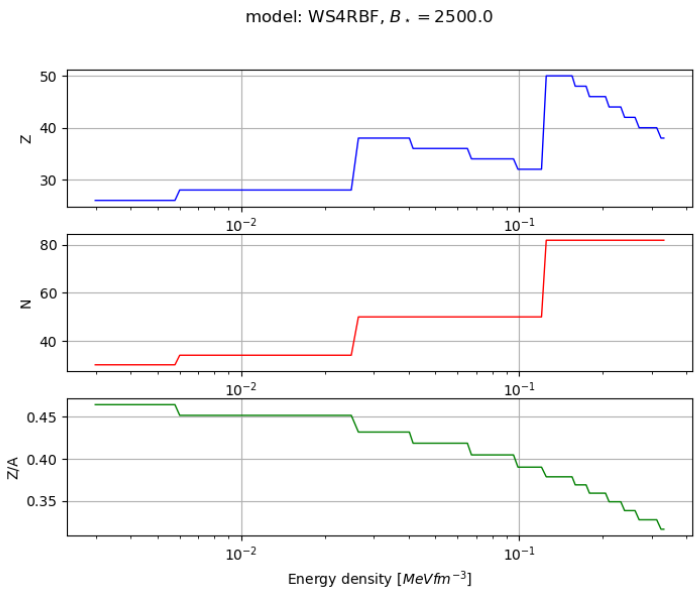

(a)

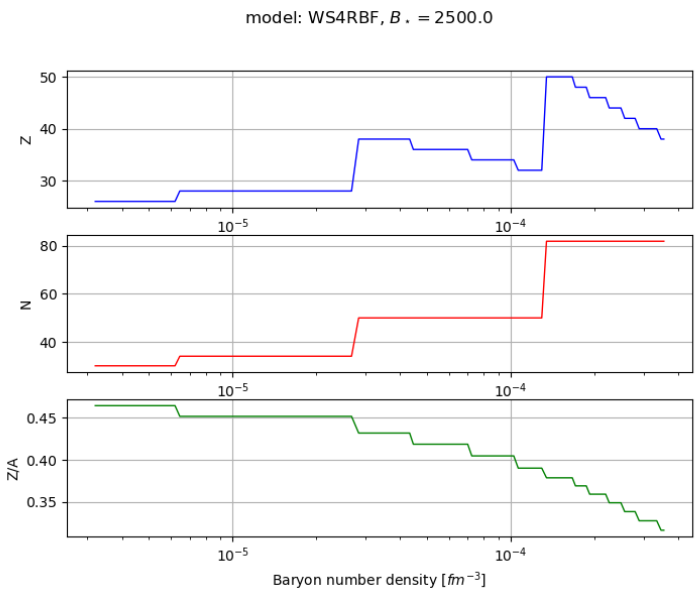

(b)

Figure H.66: The same as Figure H.64, using the WS4RBF model with $B_\star = 2500$

H.8.4 BSKG3

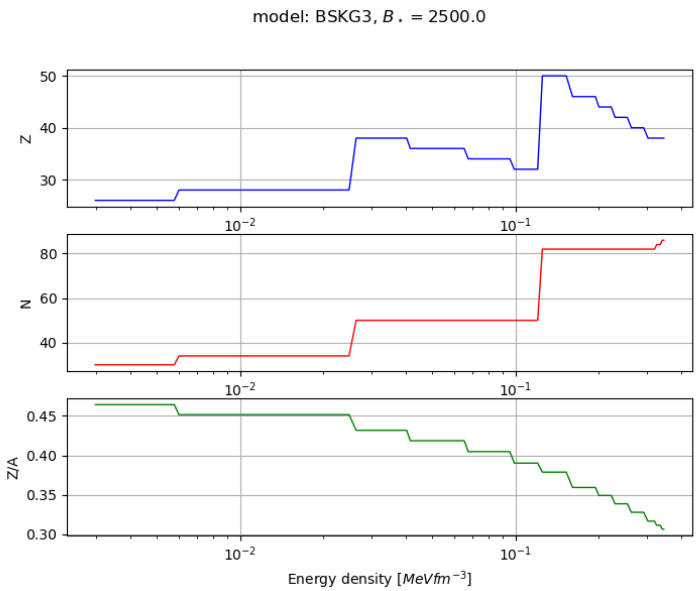

(a)

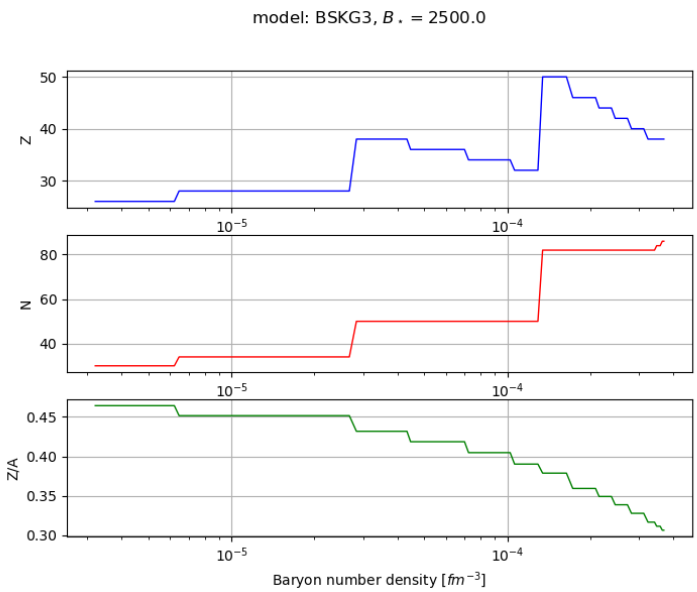

(b)

Figure H.67: The same as Figure H.64, using the BSKG3 model with $B_\star = 2500$

H.8.5 HFB31

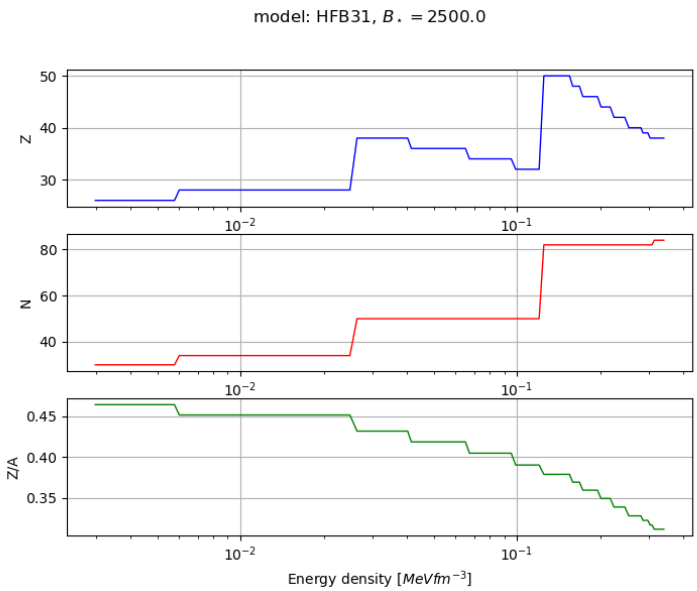

(a)

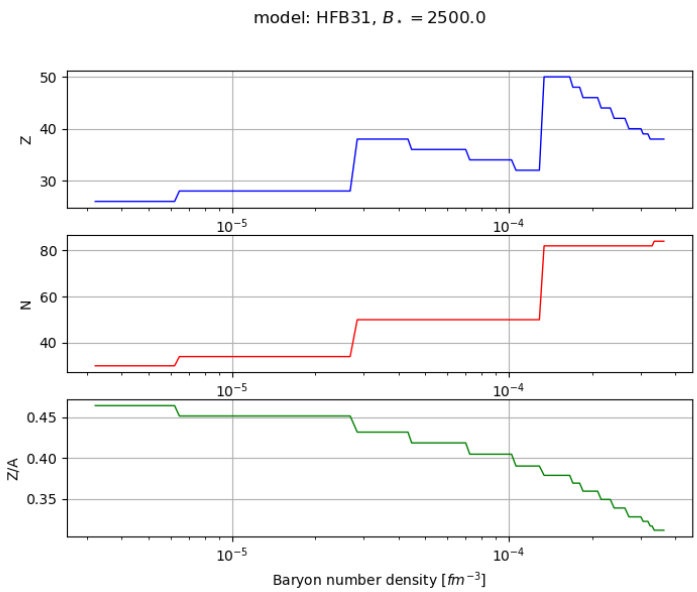

(b)

Figure H.68: The same as Figure H.64, using the HFB31 model with $B_\star = 2500$

H.8.6 DDMED

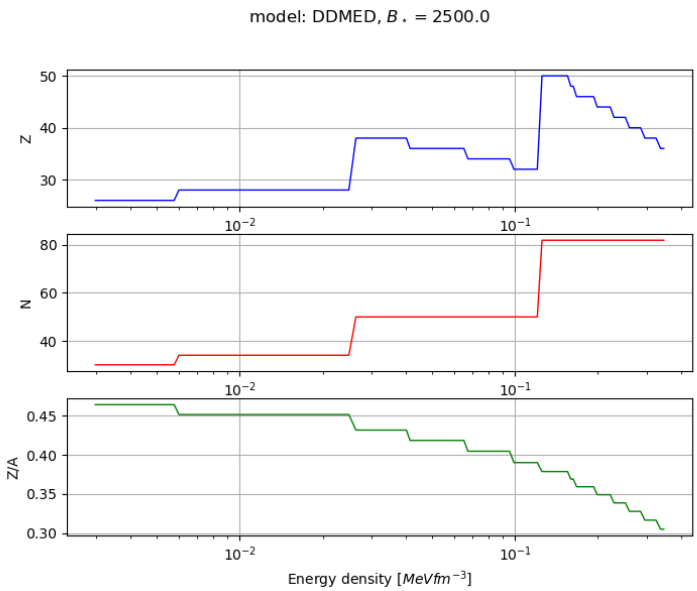

(a)

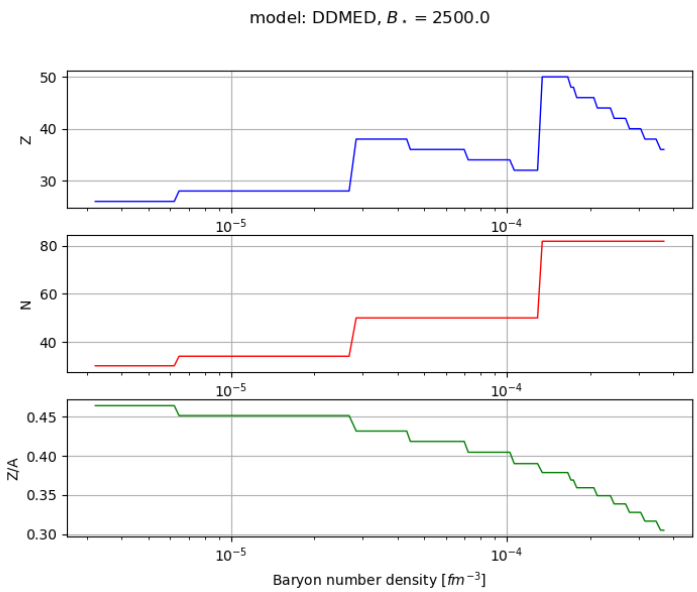

(b)

Figure H.69: The same as Figure H.64, using the DDMED model with $B_\star = 2500$

H.8.7 DDPC1

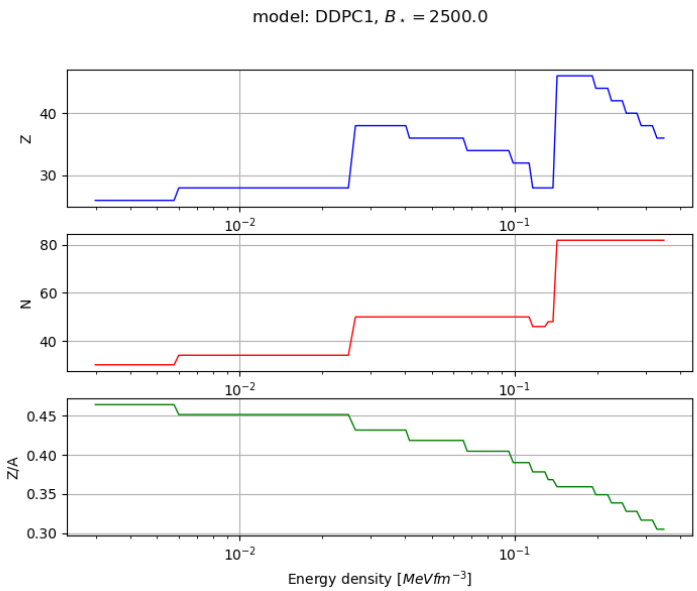

(a)

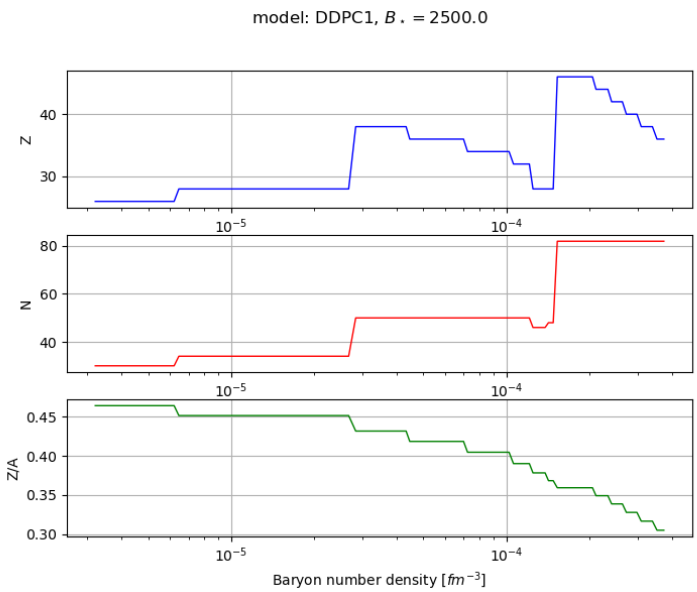

(b)

Figure H.70: The same as Figure H.64, using the DDPC1 model with $B_\star = 2500$

H.8.8 SVMIN

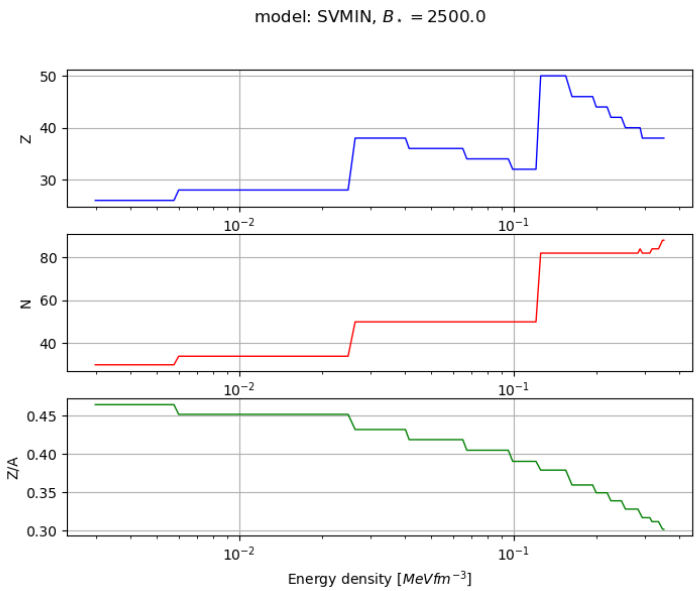

(a)

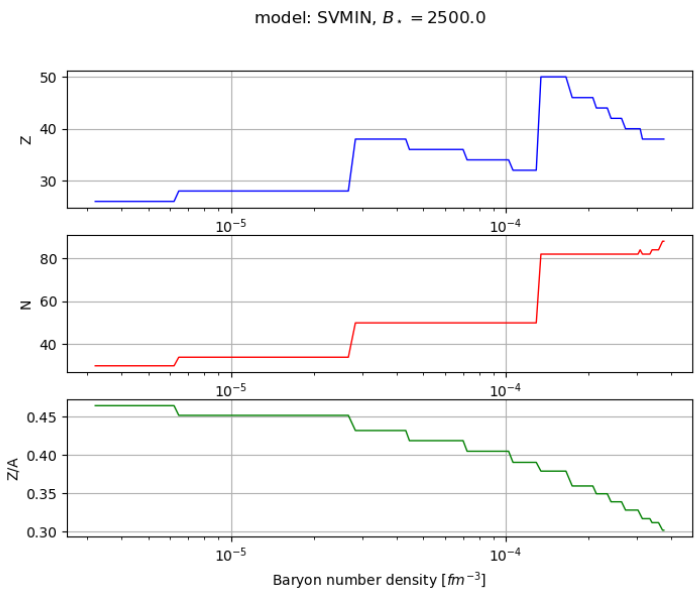

(b)

Figure H.71: The same as Figure H.64, using the SVMIN model with $B_\star = 2500$

H.8.9 UNEDF0

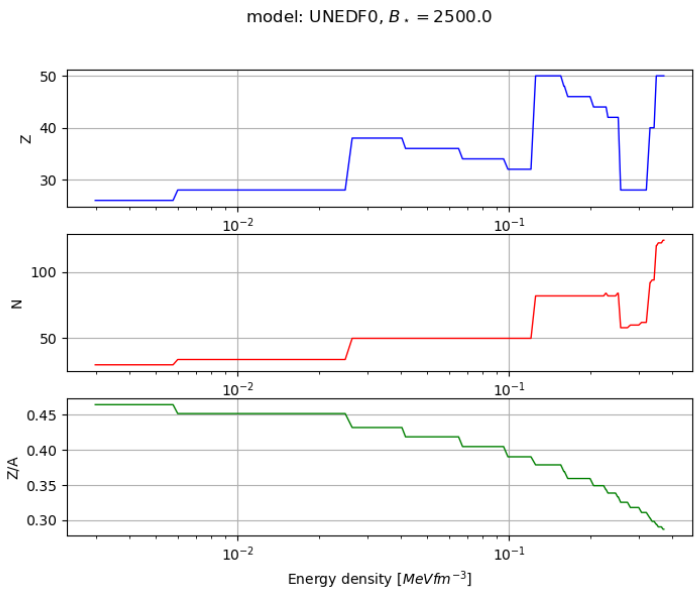

(a)

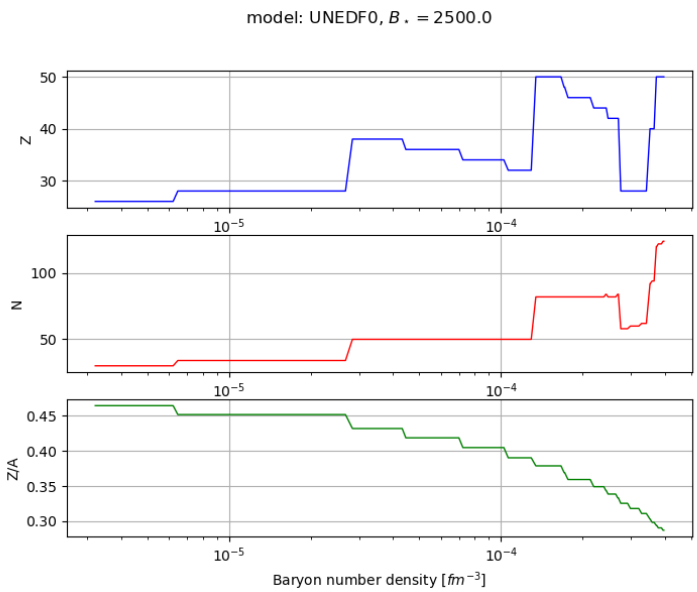

(b)

Figure H.72: The same as Figure H.64, using the UNEDF0 model with $B_\star = 2500$

H.9 M_{cr} for different M and R

H.9.1 SEMF

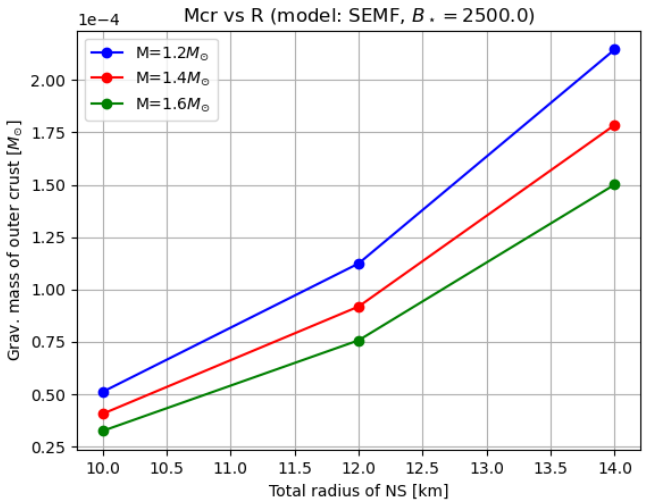

Figure H.73: Mass of outer crust for different masses and radii of NS, using the SEMF model with magnetic field strength $B_\star = 2500$

H.9.2 FRDM2012

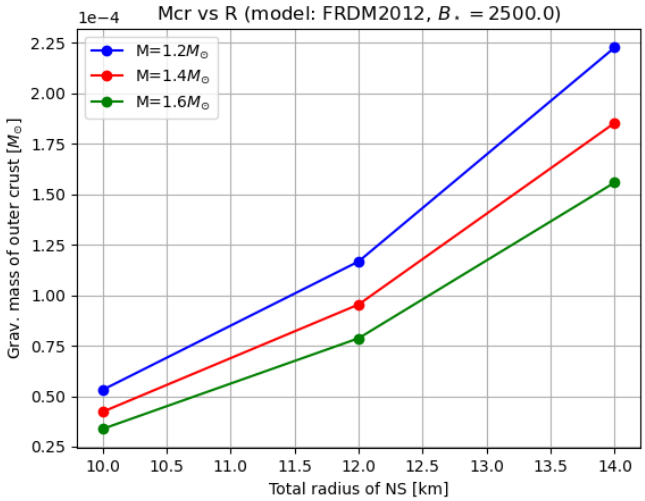

Figure H.74: The same as Figure H.73, using the FRDM2012 model with $B_\star = 2500$

H.9.3 WS4RBF

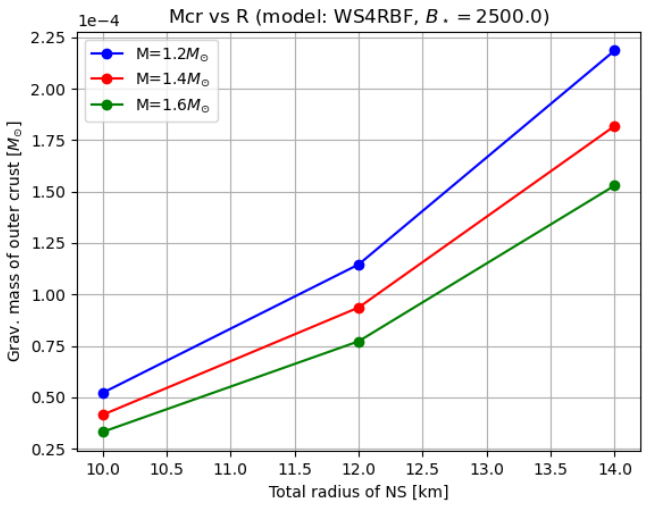

Figure H.75: The same as Figure H.73, using the WS4RBF model with $B_\star = 2500$

H.9.4 BSKG3

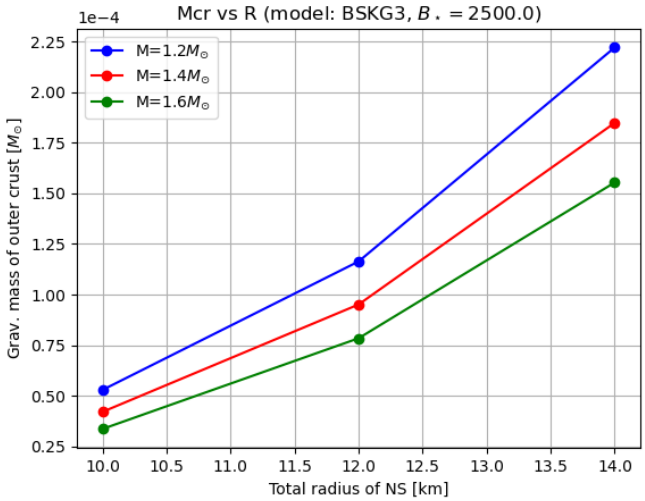

Figure H.76: The same as Figure H.73, using the BSKG3 model with $B_\star = 2500$

H.9.5 HFB31

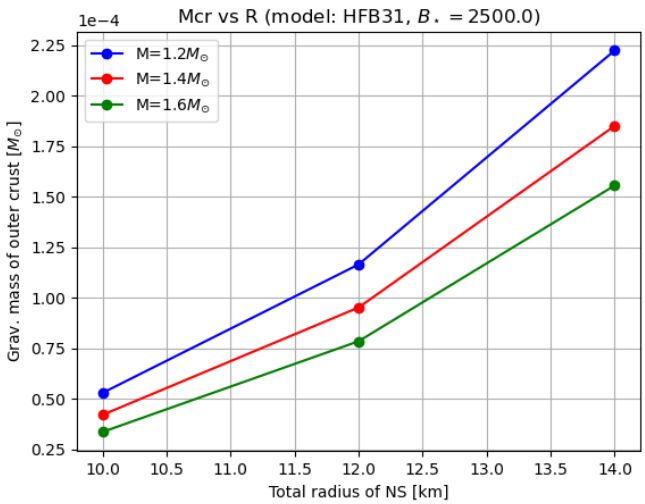

Figure H.77: The same as Figure H.73, using the HFB31 model with $B_\star = 2500$

H.9.6 DDMED

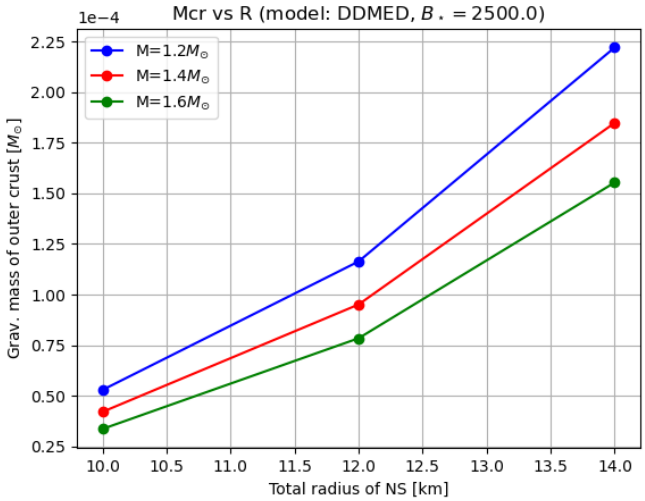

Figure H.78: The same as Figure H.73, using the DDMED model with $B_\star = 2500$

H.9.7 DDPC1

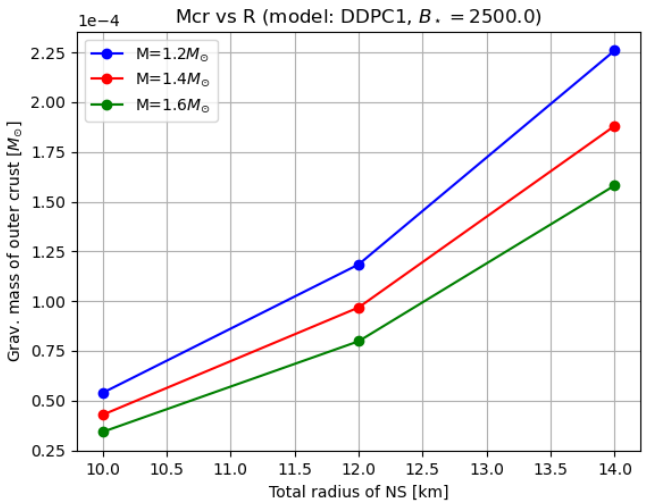

Figure H.79: The same as Figure H.73, using the DDPC1 model with $B_\star = 2500$

H.9.8 SVMIN

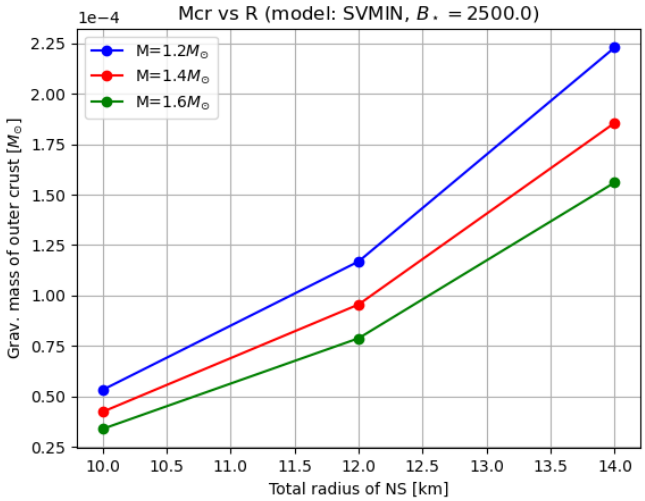

Figure H.80: The same as Figure H.73, using the SVMIN model with $B_\star = 2500$

H.9.9 UNEDF0

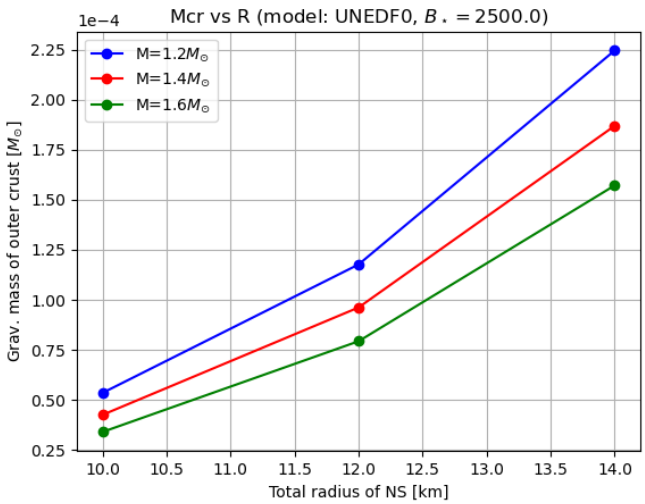

Figure H.81: The same as Figure H.73, using the UNEDF0 model with $B_\star = 2500$

H.10 z_{drip} for different M and R

H.10.1 SEMF

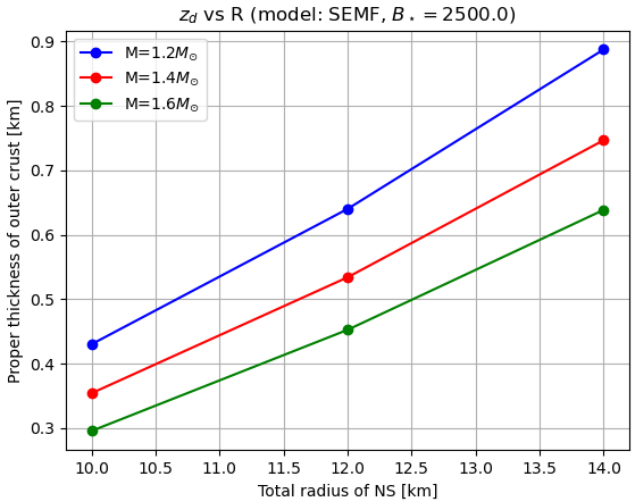

Figure H.82: Proper depth of neutron-drip transition for different masses and radii of NS, using the SEMF model with magnetic field strength $B_\star = 2500$

H.10.2 FRDM2012

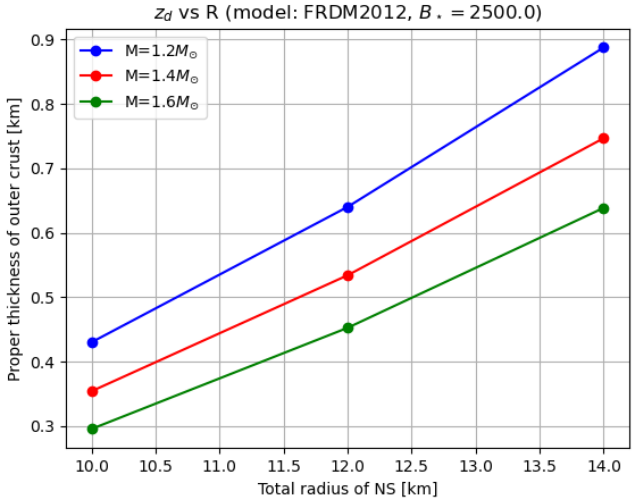

Figure H.83: The same as Figure H.82, using the FRDM2012 model with $B_\star = 2500$

H.10.3 WS4RBF

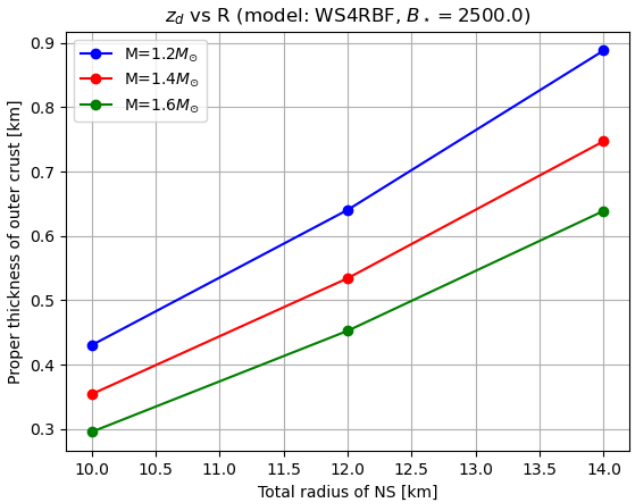

Figure H.84: The same as Figure H.82, using the WS4RBF model with $B_\star = 2500$

H.10.4 BSKG3

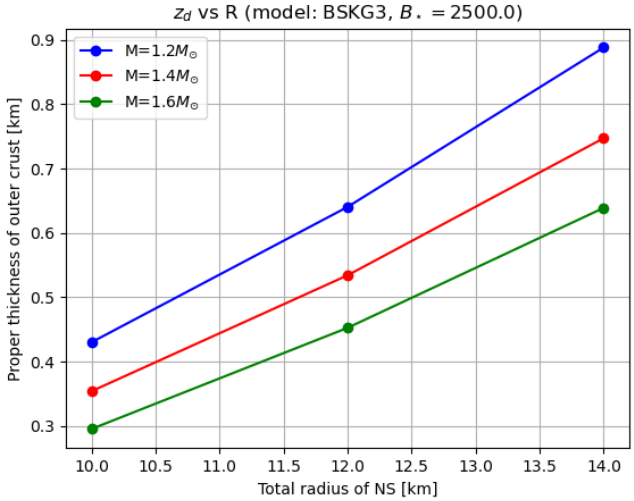

Figure H.85: The same as Figure H.82, using the BSKG3 model with $B_\star = 2500$

H.10.5 HFB31

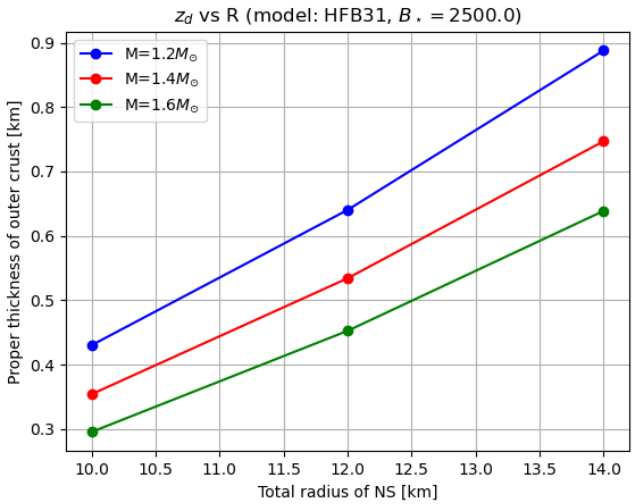

Figure H.86: The same as Figure H.82, using the HFB31 model with $B_\star = 2500$

H.10.6 DDMED

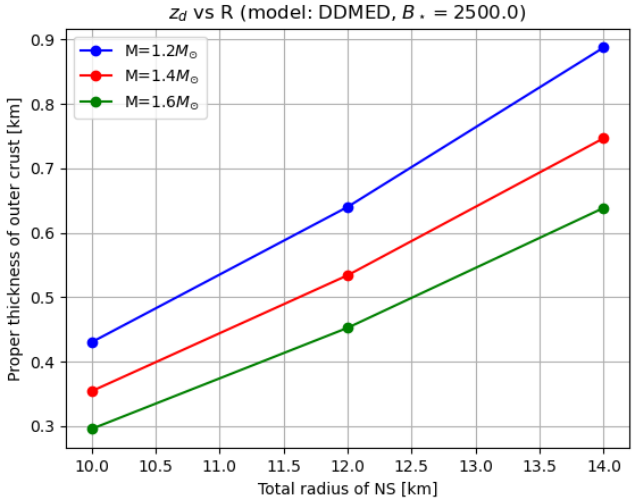

Figure H.87: The same as Figure H.82, using the DDMED model with $B_\star = 2500$

H.10.7 DDPC1

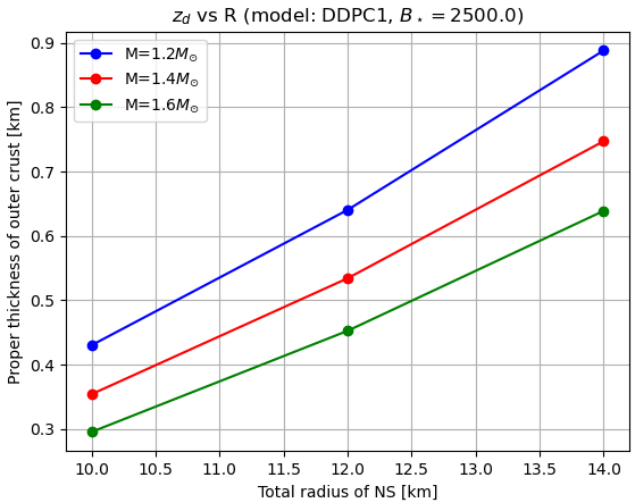

Figure H.88: The same as Figure H.82, using the DDPC1 model with $B_\star = 2500$

H.10.8 SVMIN

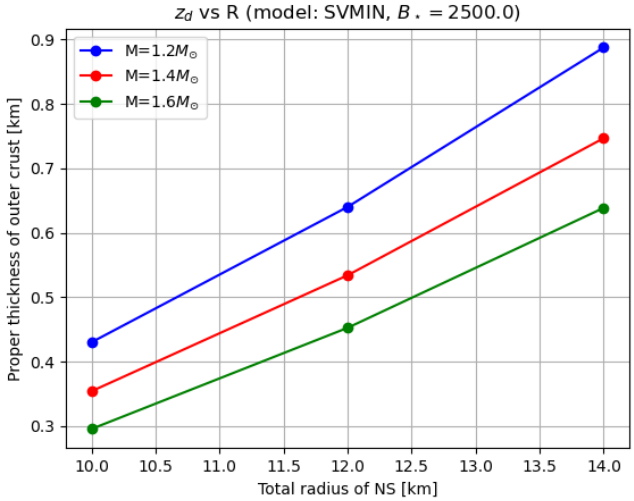

Figure H.89: The same as Figure H.82, using the SVMIN model with $B_\star = 2500$

H.10.9 UNEDF0

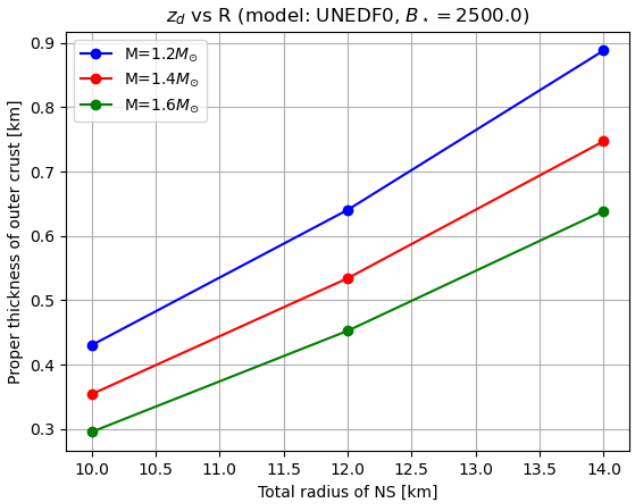

Figure H.90: The same as Figure H.82, using the UNEDF0 model with $B_\star = 2500$

Appendix I

Figures for mixed plots

Below are the Figures, like those in Subsections 5.4.5 - 5.4.13, for the models: WS4RBF, BSKG3, HFB31, DDMED, DDPC1, SVMIN and UNEDF0, and Figures, like those in Subsections 5.8.1 - 5.8.9 for magnetic field strengths $B_\star = 2000, 2500$.

I.1 P vs ϵ or n_b

I.1.1 WS4RBF

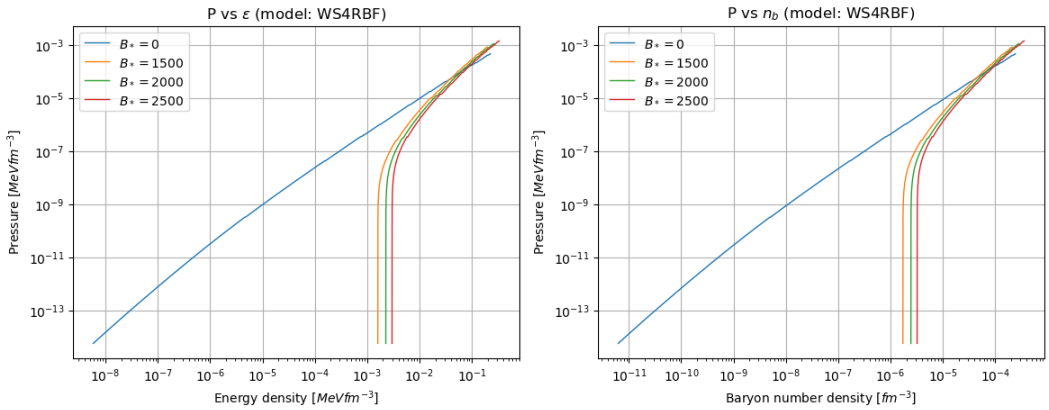

(a) (b)

Figure I.1: The same as Figure 5.5, using the WS4RBF model with different magnetic field strengths $B_\star$

I.1.2 BSKG3

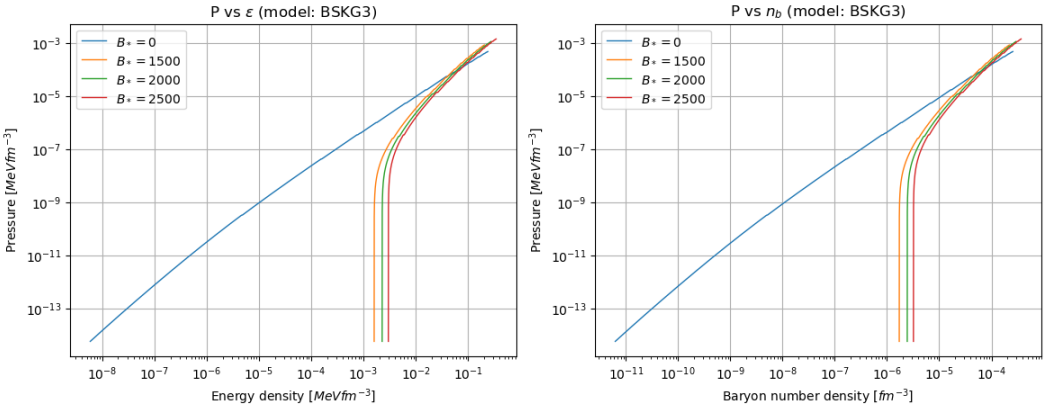

(a) (b)

Figure I.2: The same as Figure 5.5, using the BSKG3 model with different magnetic field strengths $B_\star$

I.1.3 HFB31

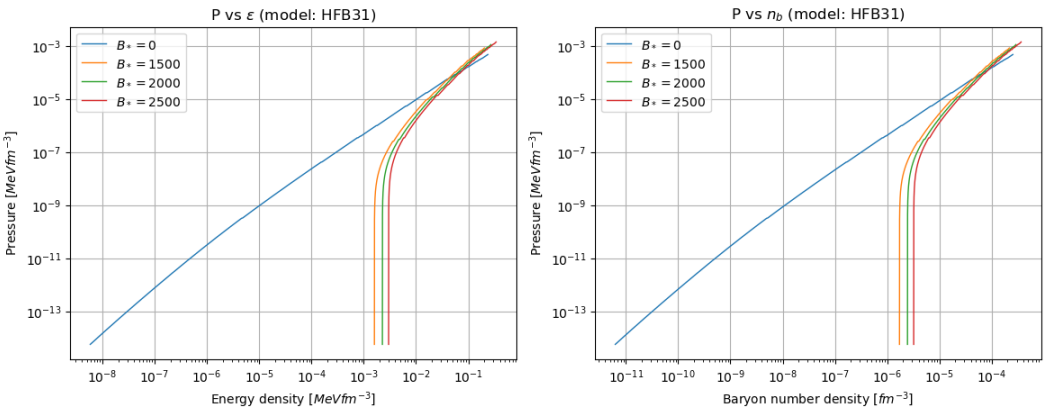

(a) (b)

Figure I.3: The same as Figure 5.5, using the HFB31 model with different magnetic field strengths $B_\star$

I.1.4 DDMED

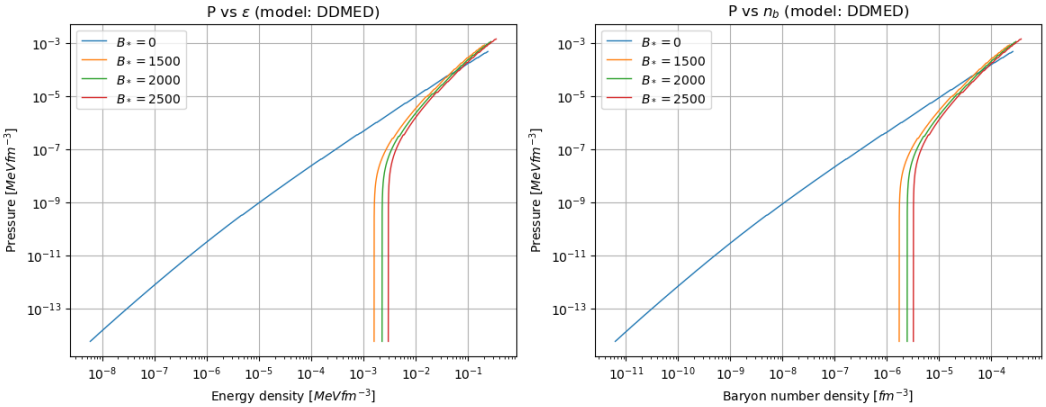

(a) (b)

Figure I.4: The same as Figure 5.5, using the DDMED model with different magnetic field strengths $B_\star$

I.1.5 DDPC1

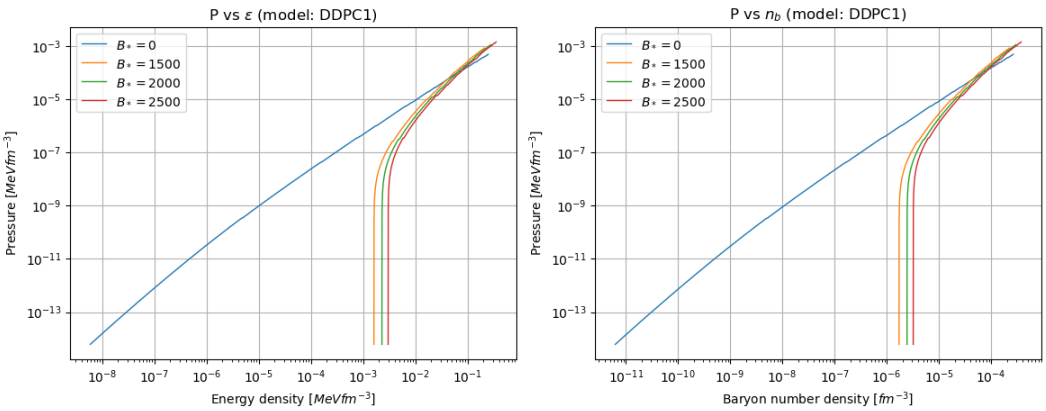

(a) (b)

Figure I.5: The same as Figure 5.5, using the DDPC1 model with different magnetic field strengths $B_\star$

I.1.6 SVMIN

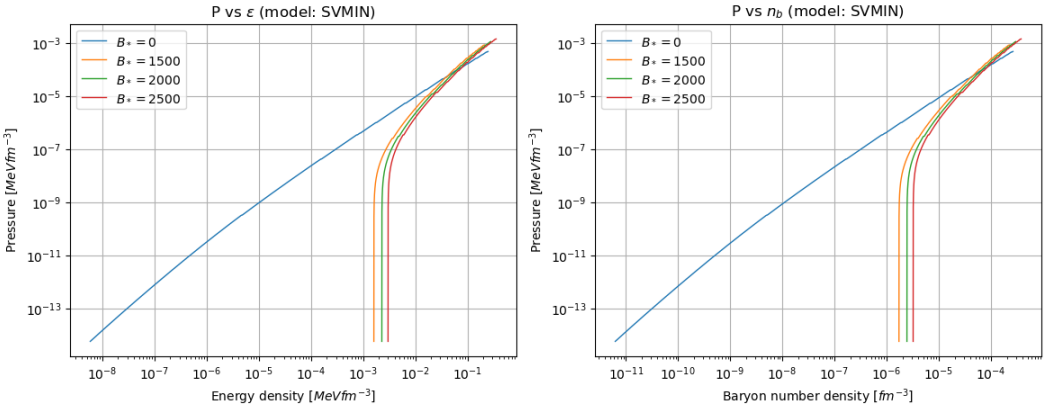

(a) (b)

Figure I.6: The same as Figure 5.5, using the SVMIN model with different magnetic field strengths $B_\star$

I.1.7 UNEDF0

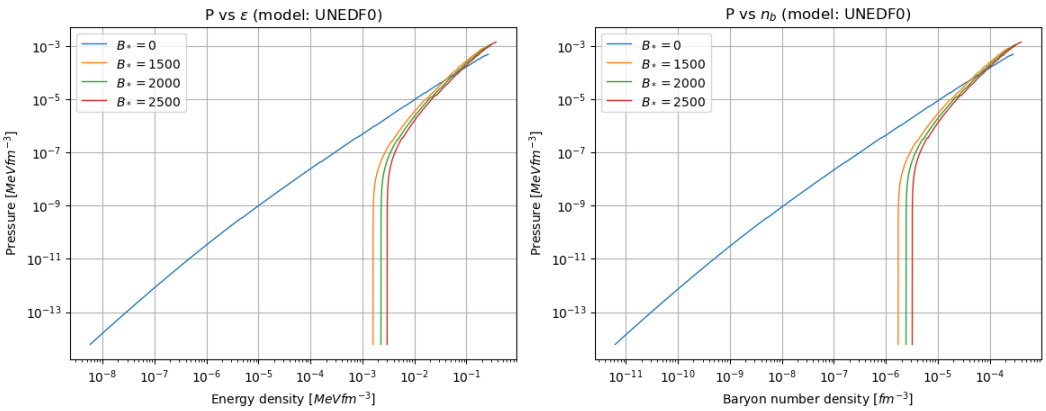

(a) (b)

Figure I.7: The same as Figure 5.5, using the UNEDF0 model with different magnetic field strengths $B_\star$

I.1.8 $B_\star = 2000$

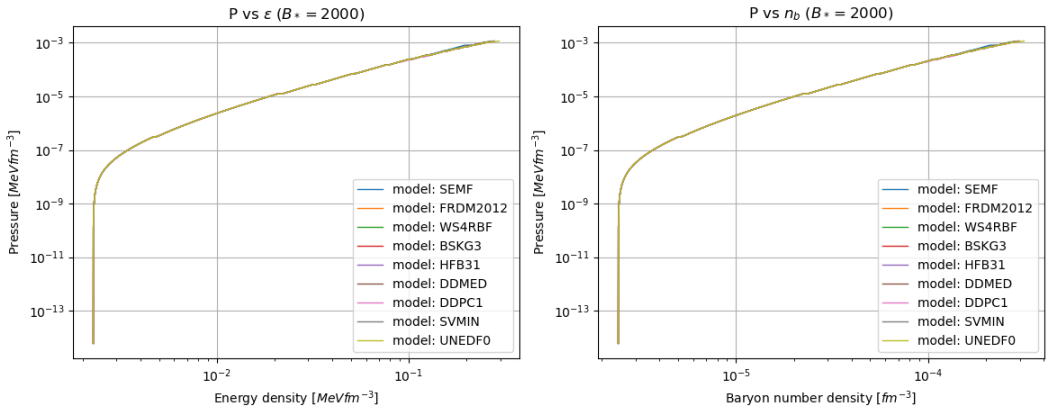

(a) (b)

Figure I.8: The same as Figure 5.24, using different models with magnetic field strength $B_\star = 2000$

I.1.9 $B_\star = 2500$

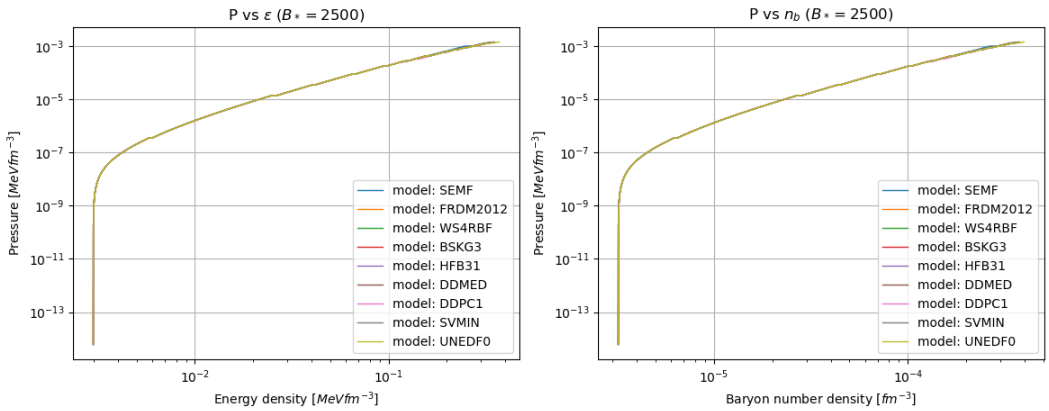

(a) (b)

Figure I.9: The same as Figure 5.24, using different models with magnetic field strength $B_\star = 2500$

I.2 Γ vs ϵ or n_b

I.2.1 WS4RBF

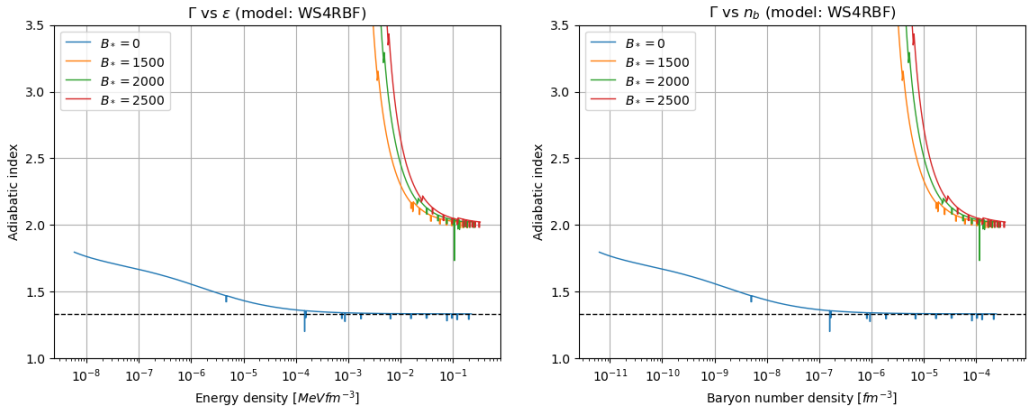

(a) (b)

Figure I.10: The same as Figure 5.7, using the WS4RBF model with different magnetic field strengths $B_\star$

I.2.2 BSKG3

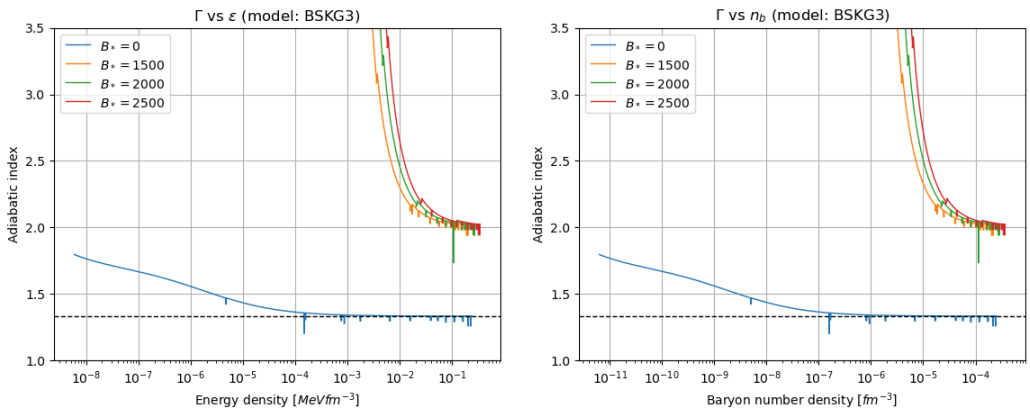

(a) (b)

Figure I.11: The same as Figure 5.7, using the BSKG3 model with different magnetic field strengths $B_\star$

I.2.3 HFB31

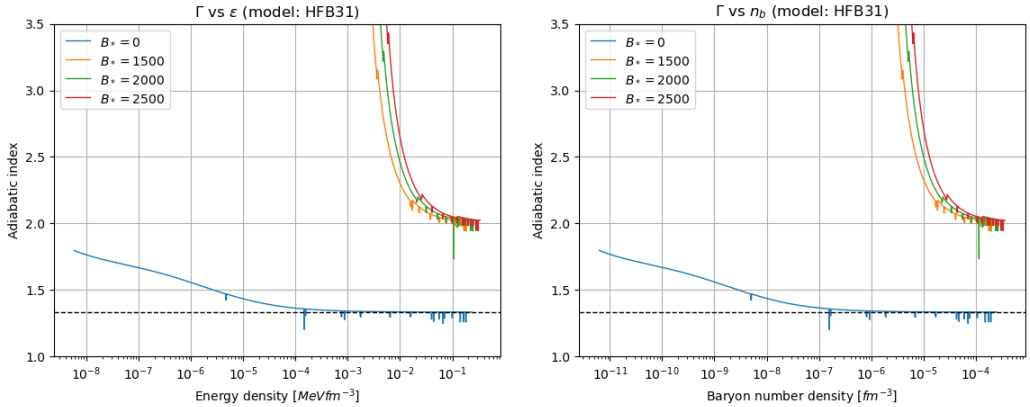

(a) (b)

Figure I.12: The same as Figure 5.7, using the HFB31 model with different magnetic field strengths $B_\star$

I.2.4 DDMED

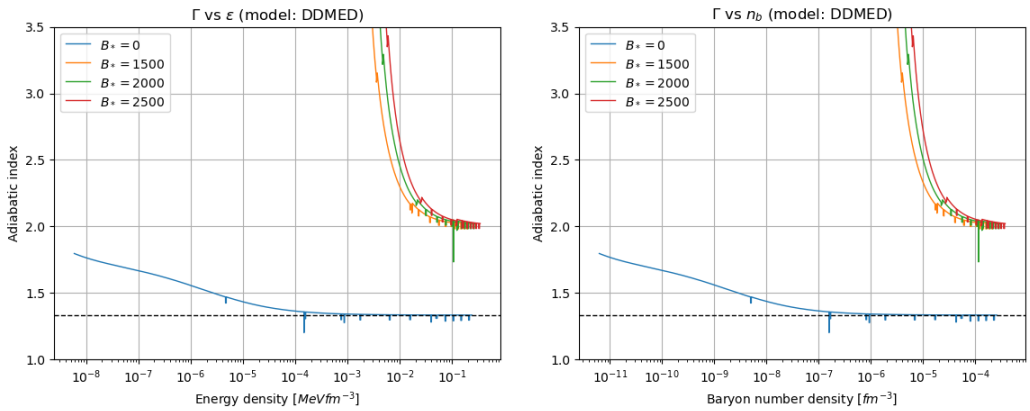

(a) (b)

Figure I.13: The same as Figure 5.7, using the DDMED model with different magnetic field strengths $B_\star$

I.2.5 DDPC1

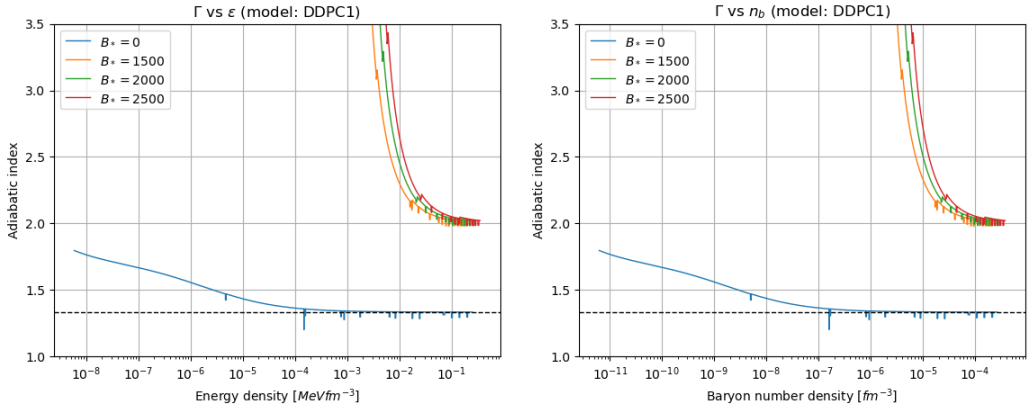

(a) (b)

Figure I.14: The same as Figure 5.7, using the DDPC1 model with different magnetic field strengths $B_\star$

I.2.6 SVMIN

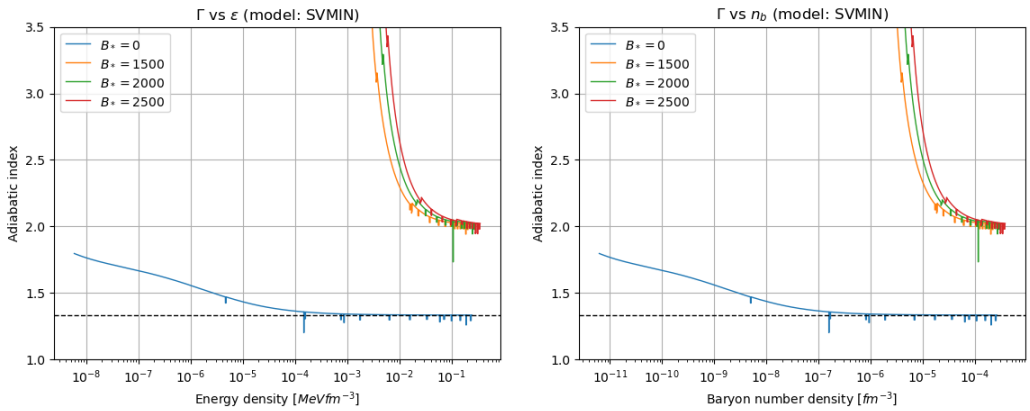

(a) (b)

Figure I.15: The same as Figure 5.7, using the SVMIN model with different magnetic field strengths $B_\star$

I.2.7 UNEDF0

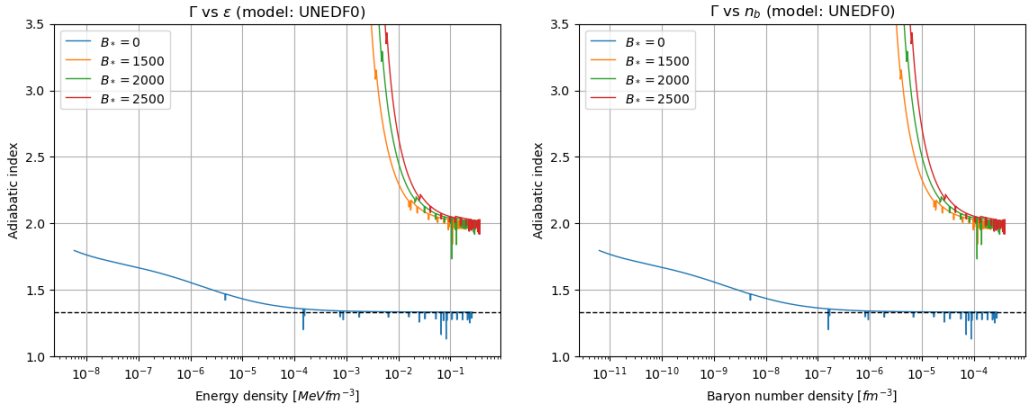

(a) (b)

Figure I.16: The same as Figure 5.7, using the UNEDF0 model with different magnetic field strengths $B_\star$

I.2.8 $B_\star = 2000$

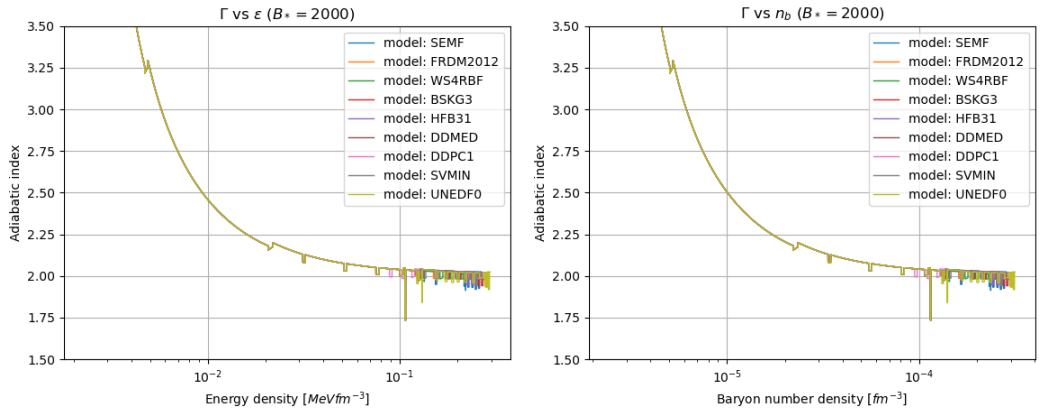

(a) (b)

Figure I.17: The same as Figure 5.26, using different models with magnetic field strength $B_\star = 2000$

I.2.9 $B_\star = 2500$

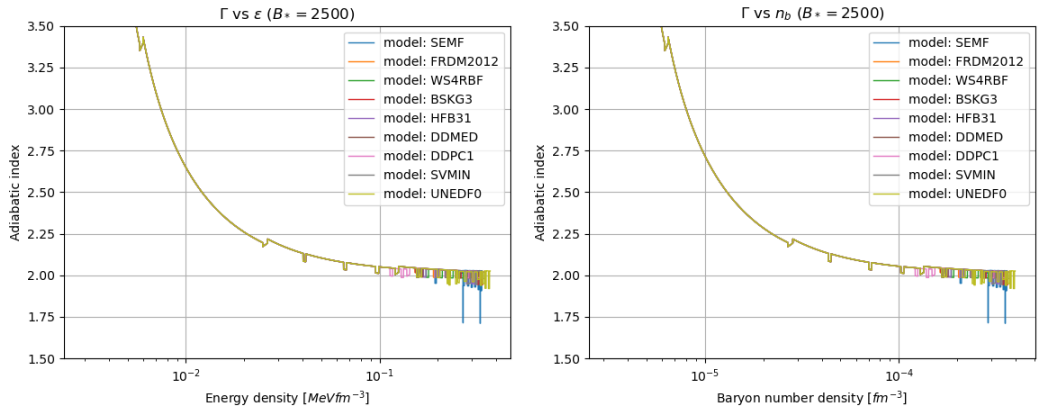

(a) (b)

Figure I.18: The same as Figure 5.26, using different models with magnetic field strength $B_\star = 2500$

I.3 c_s vs ϵ or n_b

I.3.1 WS4RBF

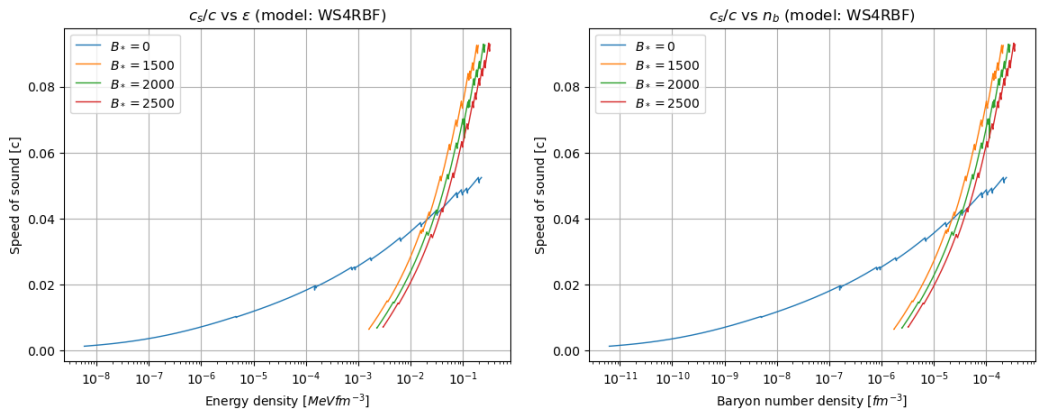

(a) (b)

Figure I.19: The same as Figure 5.9, using the WS4RBF model with different magnetic field strengths $B_\star$

I.3.2 BSKG3

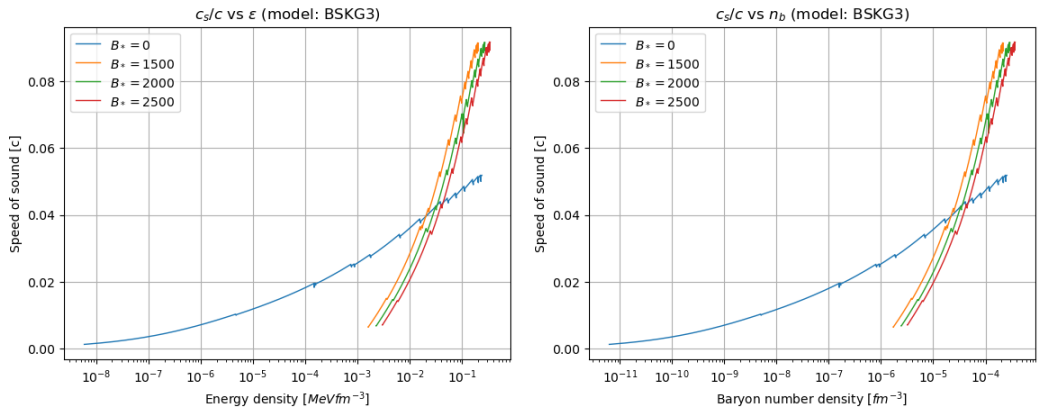

(a) (b)

Figure I.20: The same as Figure 5.9, using the BSKG3 model with different magnetic field strengths $B_\star$

I.3.3 HFB31

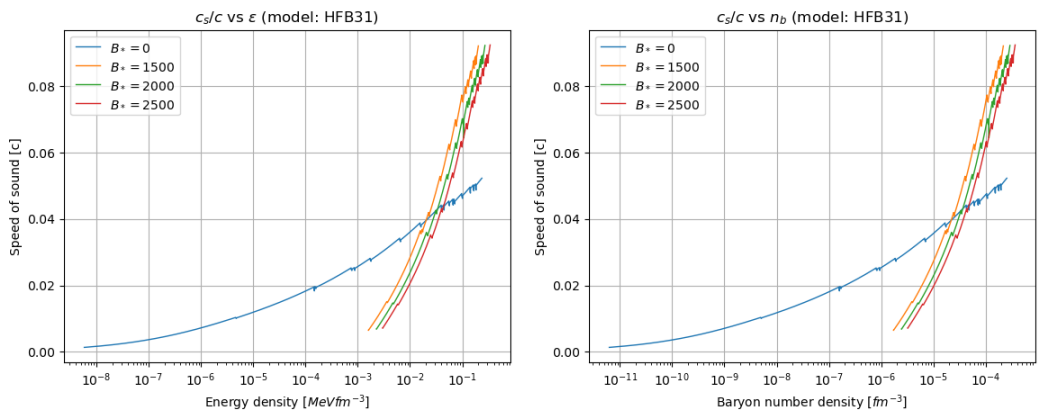

(a) (b)

Figure I.21: The same as Figure 5.9, using the HFB31 model with different magnetic field strengths $B_\star$

I.3.4 DDMED

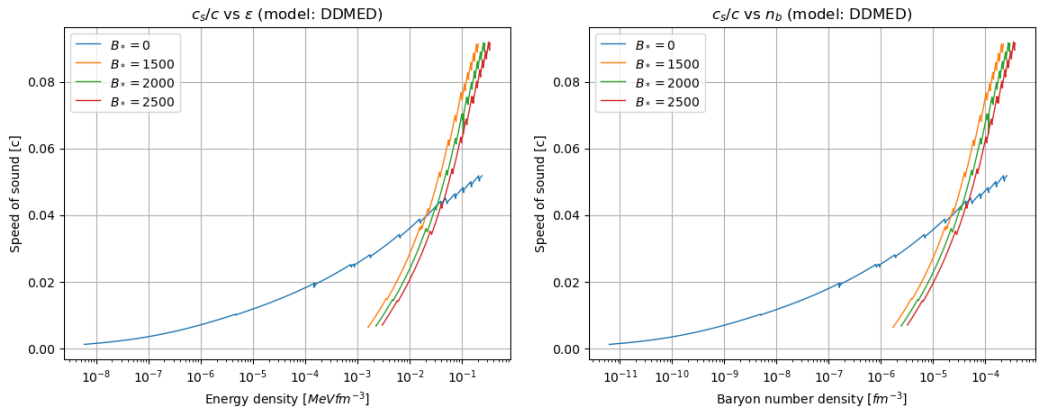

(a) (b)

Figure I.22: The same as Figure 5.9, using the DDMED model with different magnetic field strengths $B_\star$

I.3.5 DDPC1

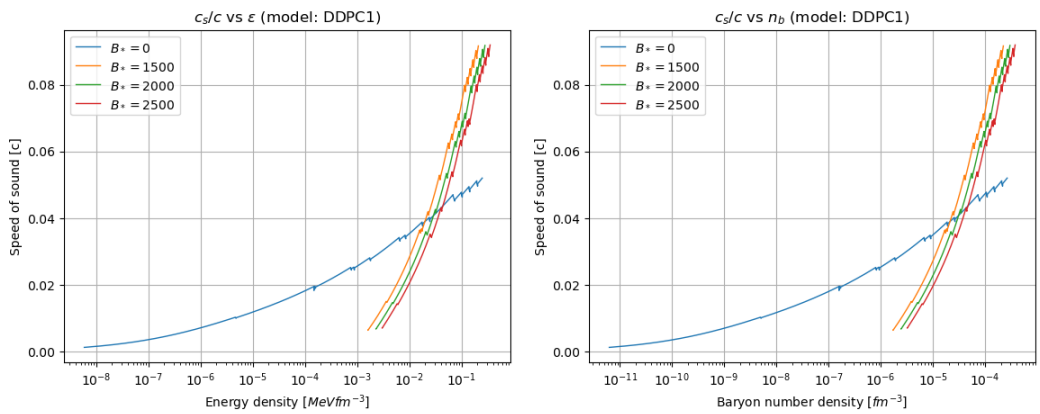

(a) (b)

Figure I.23: The same as Figure 5.9, using the DDPC1 model with different magnetic field strengths $B_\star$

I.3.6 SVMIN

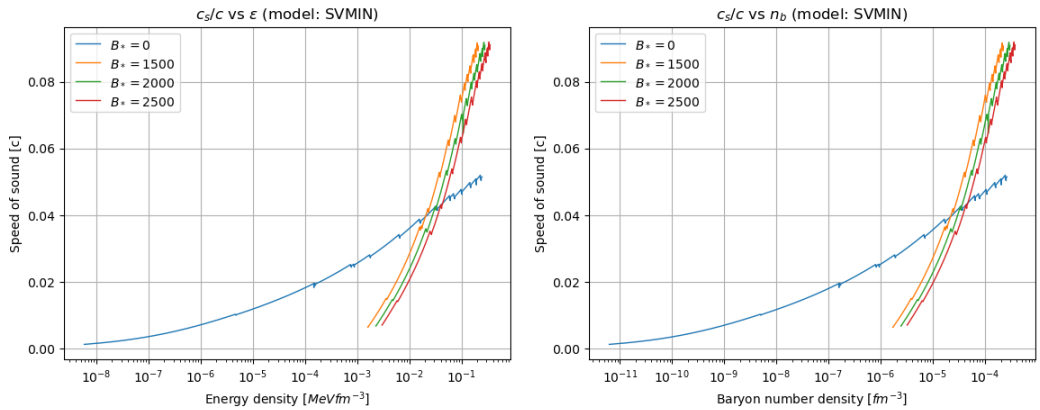

(a) (b)

Figure I.24: The same as Figure 5.9, using the SVMIN model with different magnetic field strengths $B_\star$

I.3.7 UNEDF0

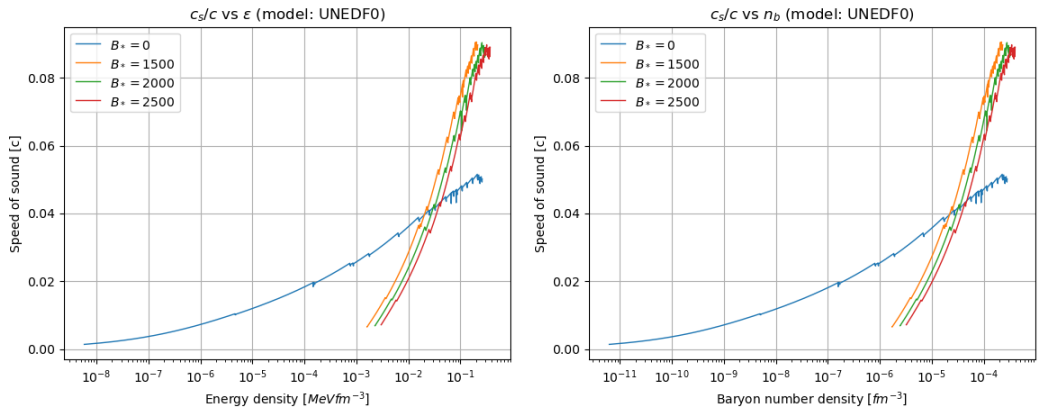

(a) (b)

Figure I.25: The same as Figure 5.9, using the UNEDF0 model with different magnetic field strengths $B_\star$

I.3.8 $B_\star = 2000$

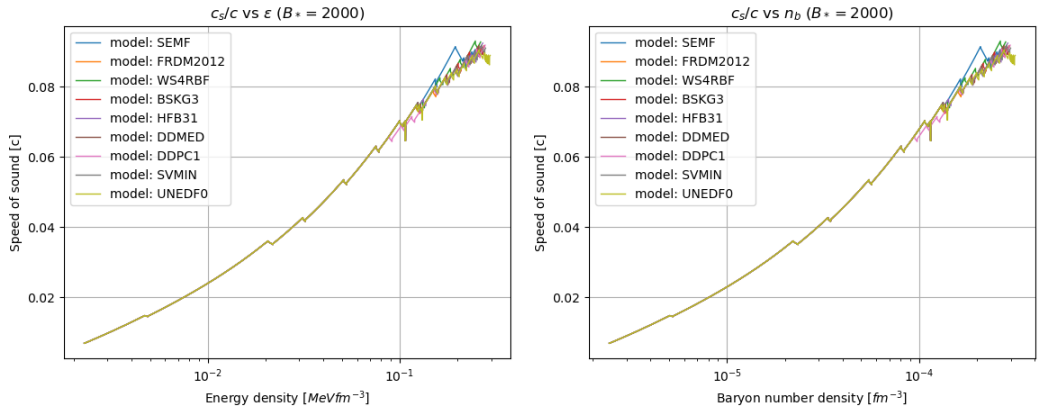

(a) (b)

Figure I.26: The same as Figure 5.28, using different models with magnetic field strength $B_\star = 2000$

I.3.9 $B_\star = 2500$

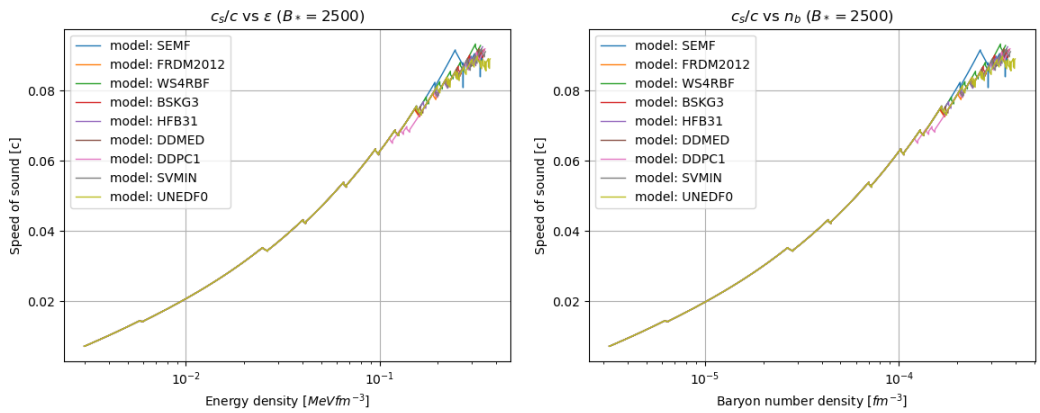

(a) (b)

Figure I.27: The same as Figure 5.28, using different models with magnetic field strength $B_\star = 2500$

I.4 K_{mod} vs ϵ or n_b

I.4.1 WS4RBF

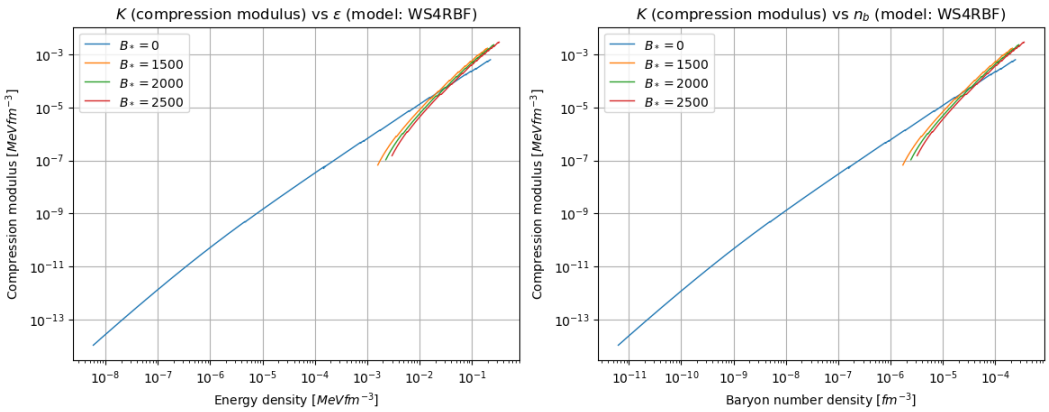

(a) (b)

Figure I.28: The same as Figure 5.11, using the WS4RBF model with different magnetic field strengths $B_\star$

I.4.2 BSKG3

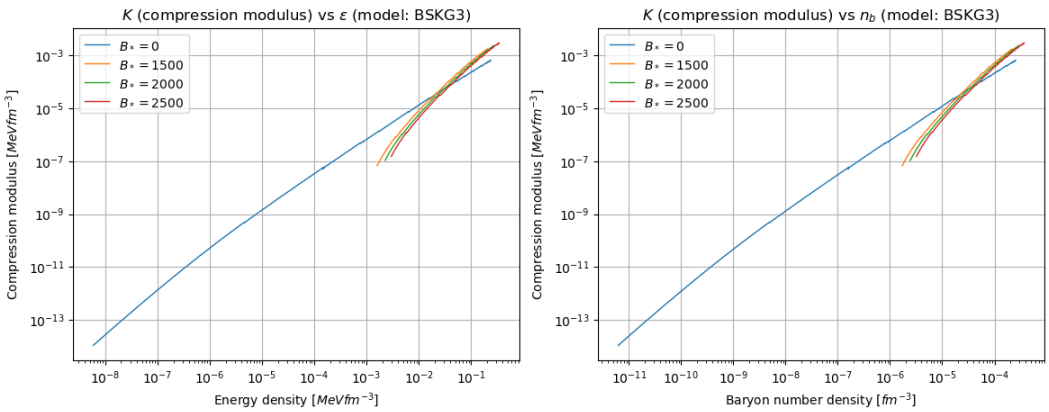

(a) (b)

Figure I.29: The same as Figure 5.11, using the BSKG3 model with different magnetic field strengths $B_\star$

I.4.3 HFB31

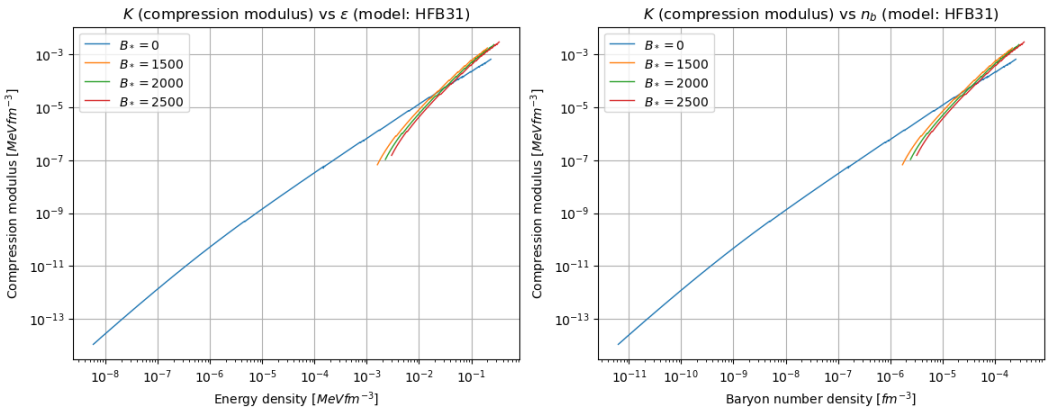

(a) (b)

Figure I.30: The same as Figure 5.11, using the HFB31 model with different magnetic field strengths $B_\star$

I.4.4 DDMED

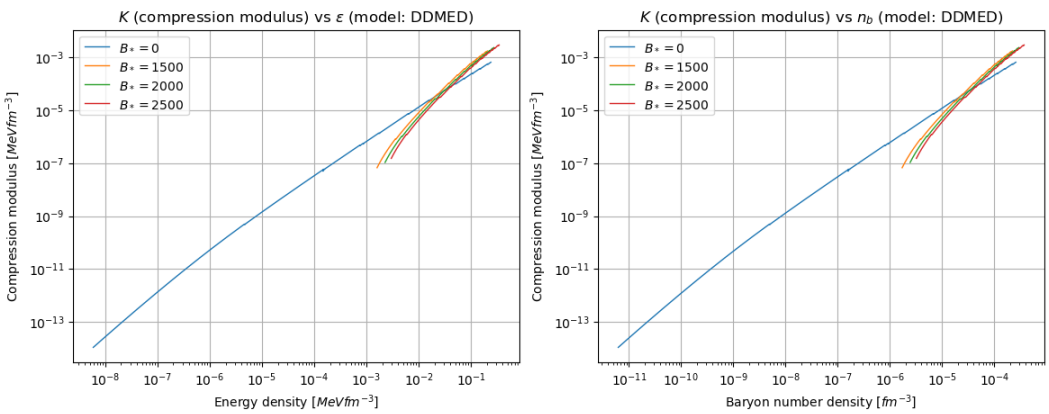

(a) (b)

Figure I.31: The same as Figure 5.11, using the DDMED model with different magnetic field strengths $B_\star$

I.4.5 DDPC1

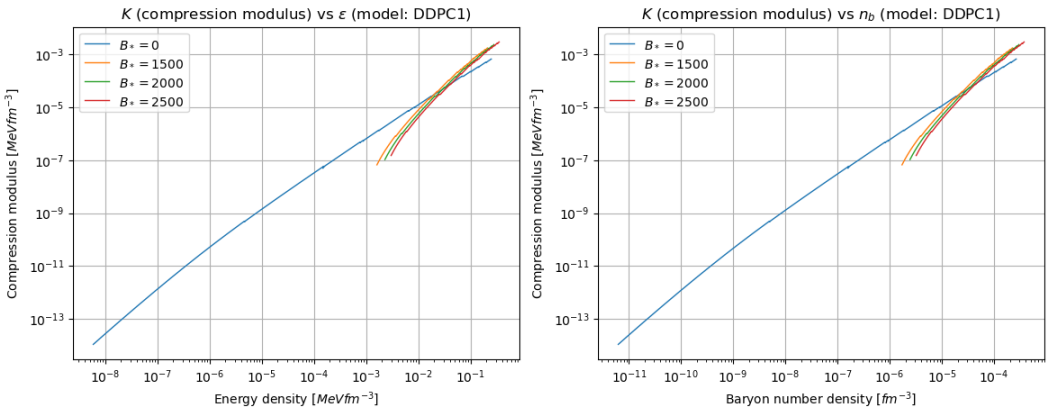

(a) (b)

Figure I.32: The same as Figure 5.11, using the DDPC1 model with different magnetic field strengths $B_\star$

I.4.6 SVMIN

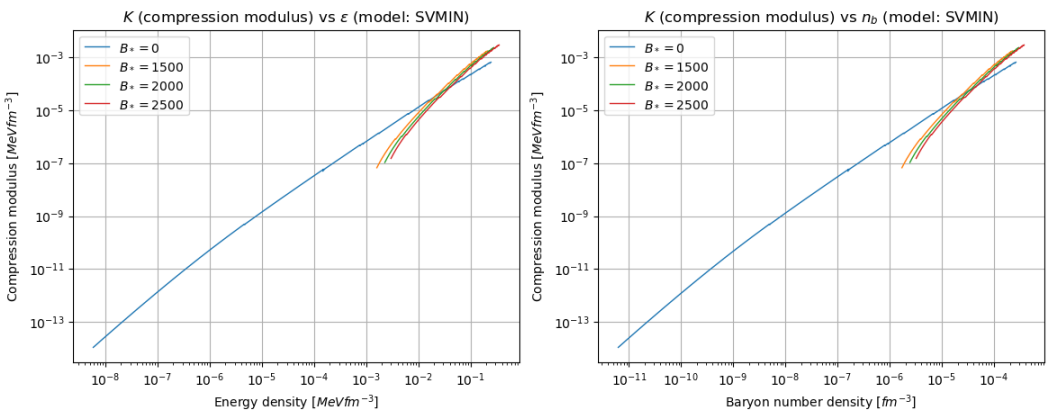

(a) (b)

Figure I.33: The same as Figure 5.11, using the SVMIN model with different magnetic field strengths $B_\star$

I.4.7 UNEDF0

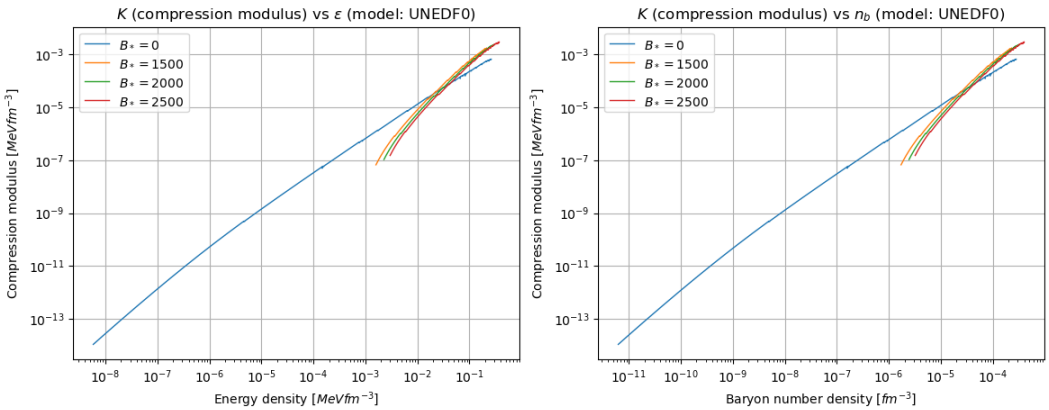

(a) (b)

Figure I.34: The same as Figure 5.11, using the UNEDF0 model with different magnetic field strengths $B_\star$

I.4.8 $B_\star = 2000$

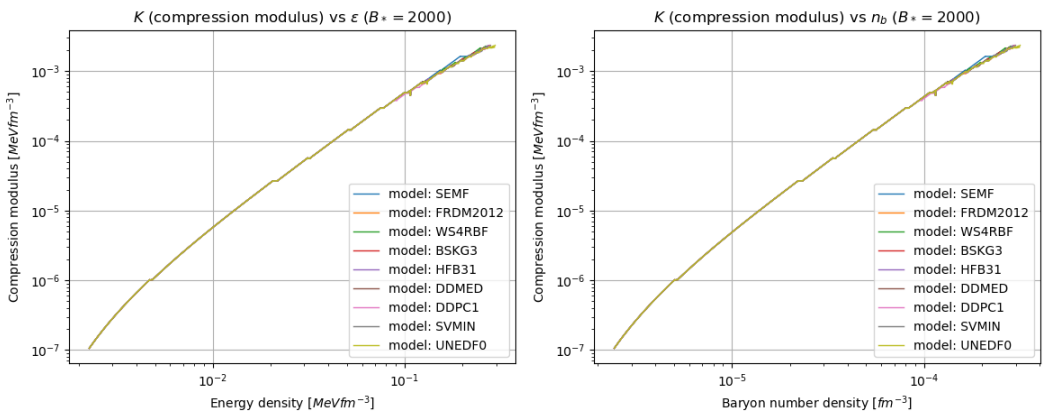

(a) (b)

Figure I.35: The same as Figure 5.30, using different models with magnetic field strength $B_\star = 2000$

I.4.9 $B_\star = 2500$

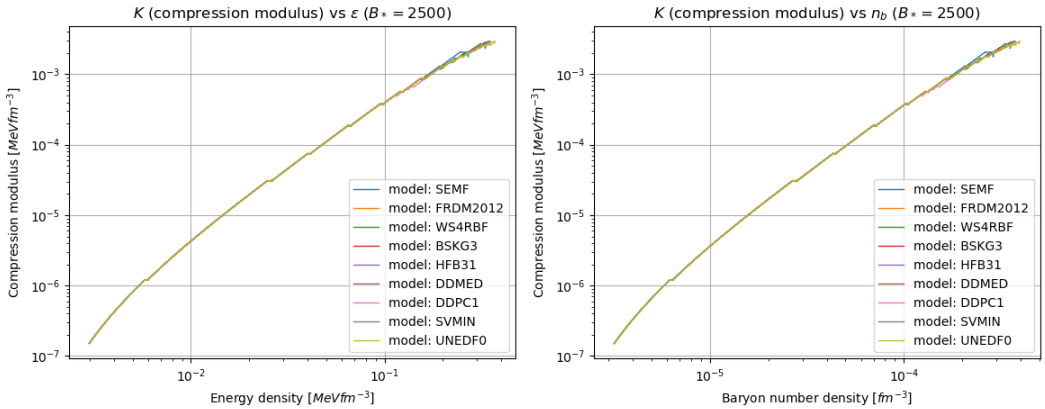

(a) (b)

Figure I.36: The same as Figure 5.30, using different models with magnetic field strength $B_\star = 2500$

I.5 S_{mod} vs ϵ or n_b

I.5.1 WS4RBF

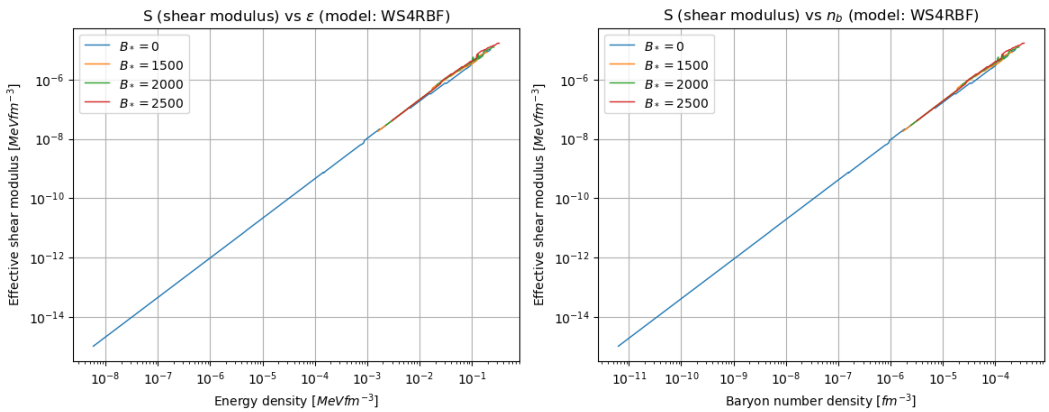

(a) (b)

Figure I.37: The same as Figure 5.13, using the WS4RBF model with different magnetic field strengths $B_\star$

I.5.2 BSKG3

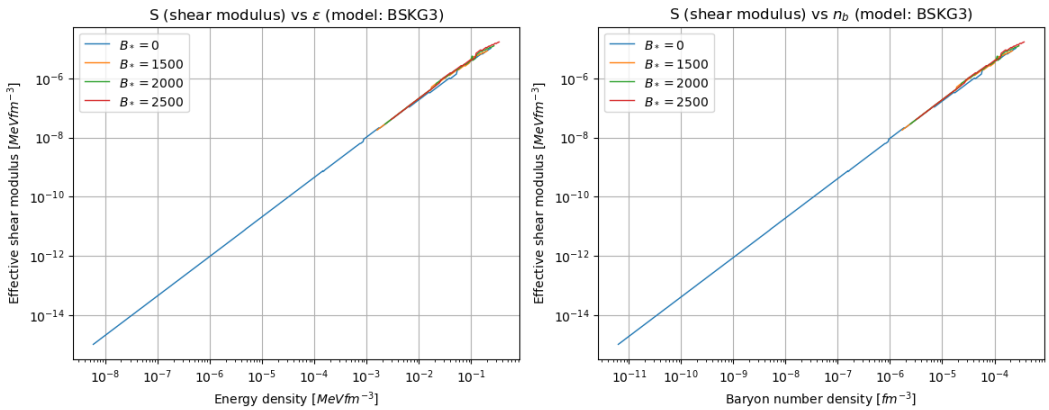

(a) (b)

Figure I.38: The same as Figure 5.13, using the BSKG3 model with different magnetic field strengths $B_\star$

I.5.3 HFB31

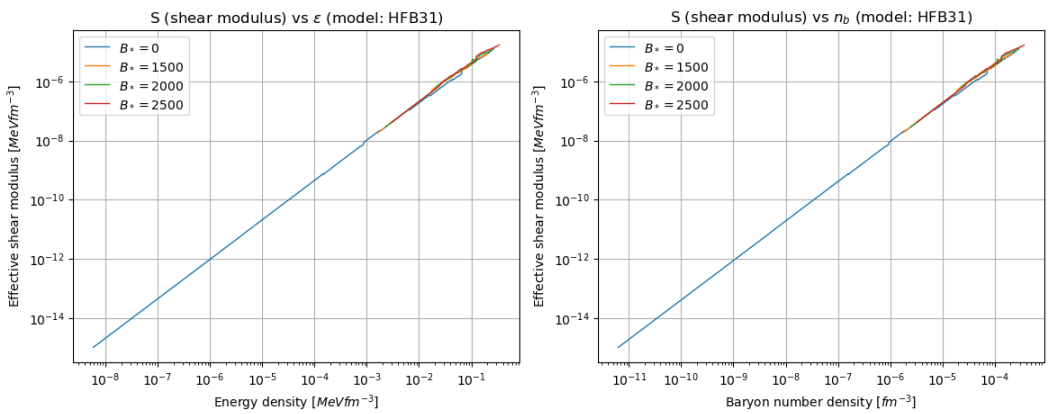

(a) (b)

Figure I.39: The same as Figure 5.13, using the HFB31 model with different magnetic field strengths $B_\star$

I.5.4 DDMED

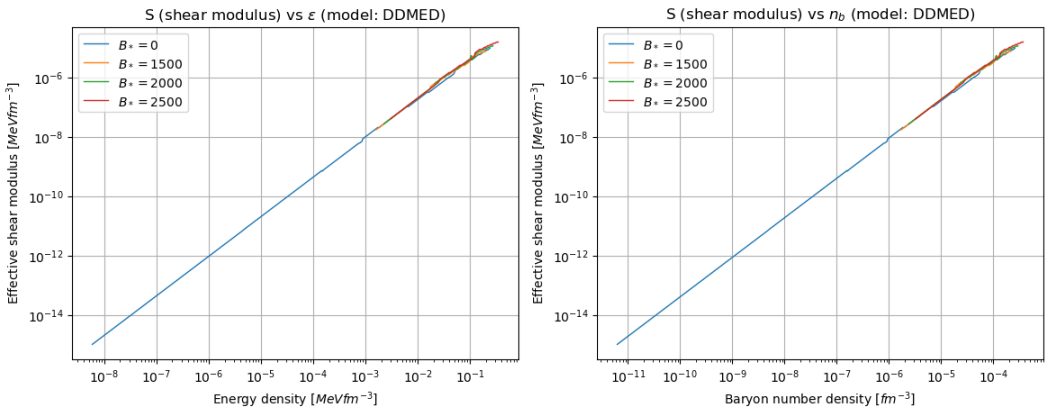

(a) (b)

Figure I.40: The same as Figure 5.13, using the DDMED model with different magnetic field strengths $B_\star$

I.5.5 DDPC1

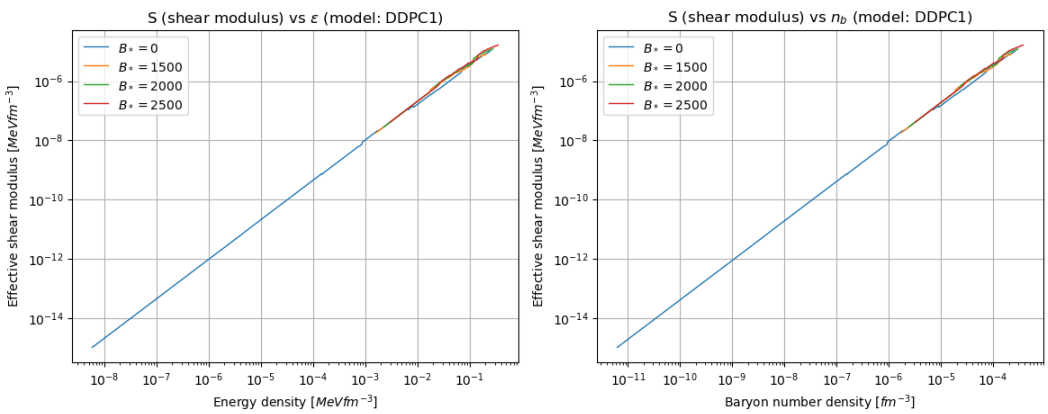

(a) (b)

Figure I.41: The same as Figure 5.13, using the DDPC1 model with different magnetic field strengths $B_\star$

I.5.6 SVMIN

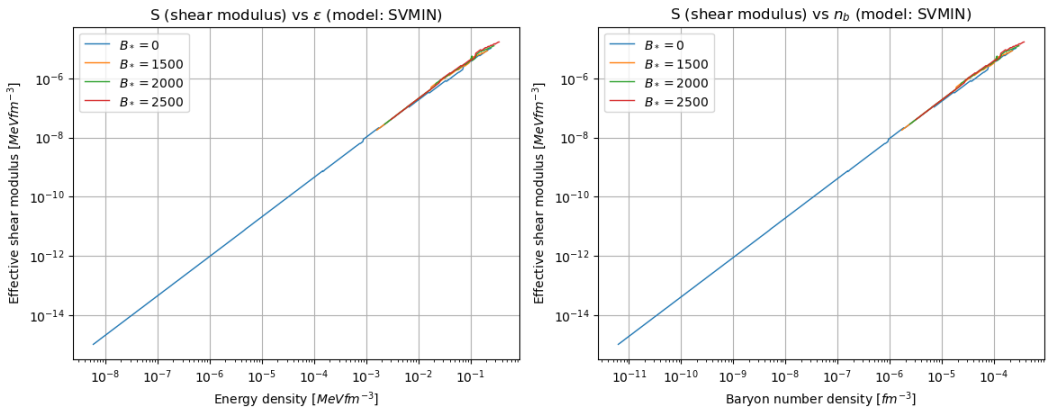

(a) (b)

Figure I.42: The same as Figure 5.13, using the SVMIN model with different magnetic field strengths $B_\star$

I.5.7 UNEDF0

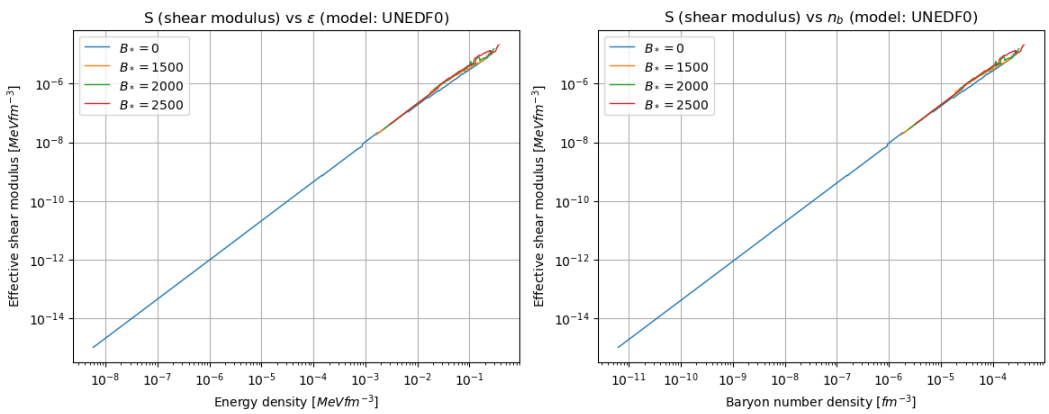

(a) (b)

Figure I.43: The same as Figure 5.13, using the UNEDF0 model with different magnetic field strengths $B_\star$

I.5.8 $B_\star = 2000$

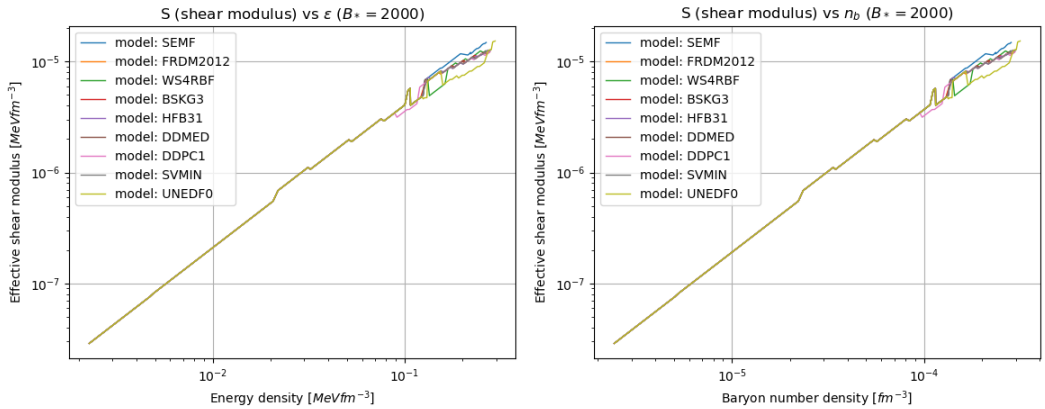

(a) (b)

Figure I.44: The same as Figure 5.32, using different models with magnetic field strength $B_\star = 2000$

I.5.9 $B_\star = 2500$

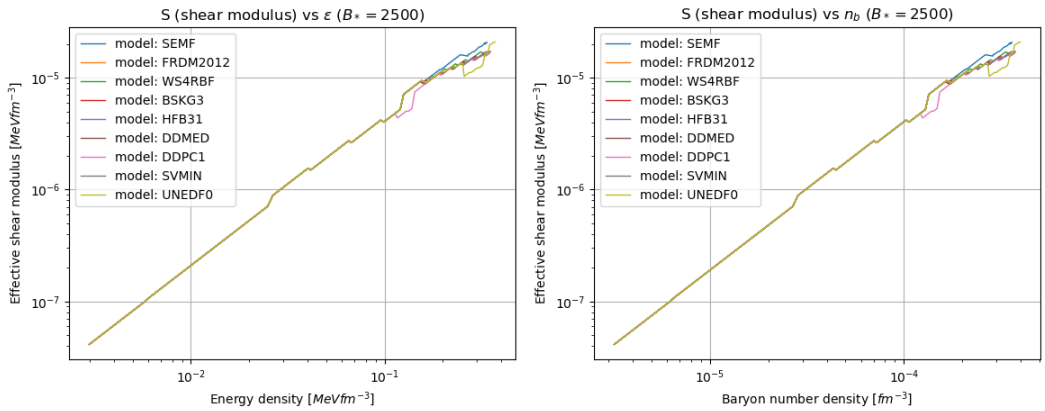

(a) (b)

Figure I.45: The same as Figure 5.32, using different models with magnetic field strength $B_\star = 2500$

I.6 S_{mod}/K_{mod} vs ϵ or n_b

I.6.1 WS4RBF

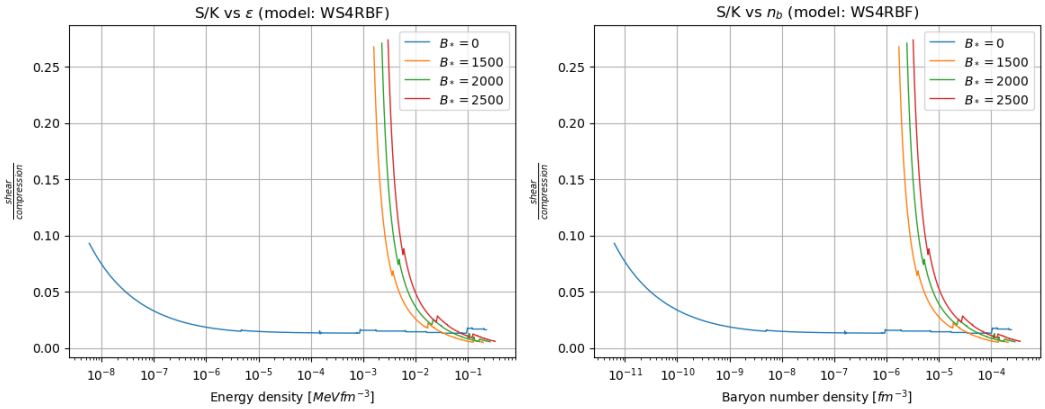

(a) (b)

Figure I.46: The same as Figure 5.15, using the WS4RBF model with different magnetic field strengths $B_\star$

I.6.2 BSKG3

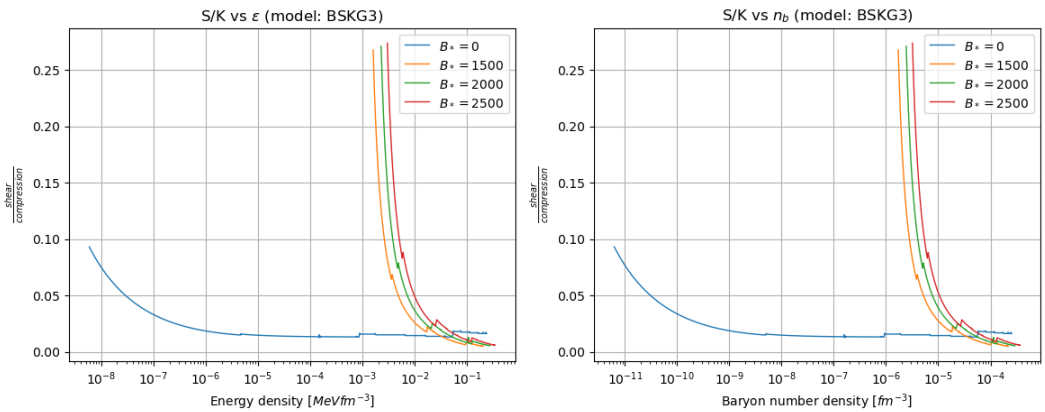

(a) (b)

Figure I.47: The same as Figure 5.15, using the BSKG3 model with different magnetic field strengths $B_\star$

I.6.3 HFB31

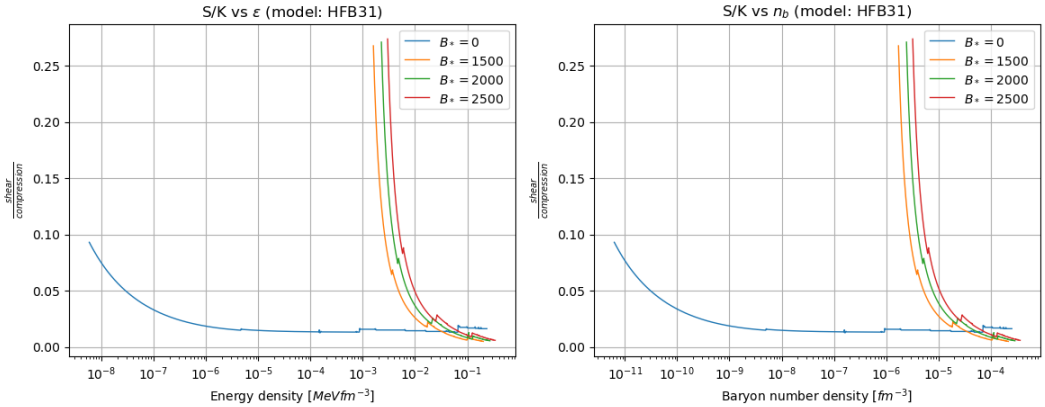

(a) (b)

Figure I.48: The same as Figure 5.15, using the HFB31 model with different magnetic field strengths $B_\star$

I.6.4 DDMED

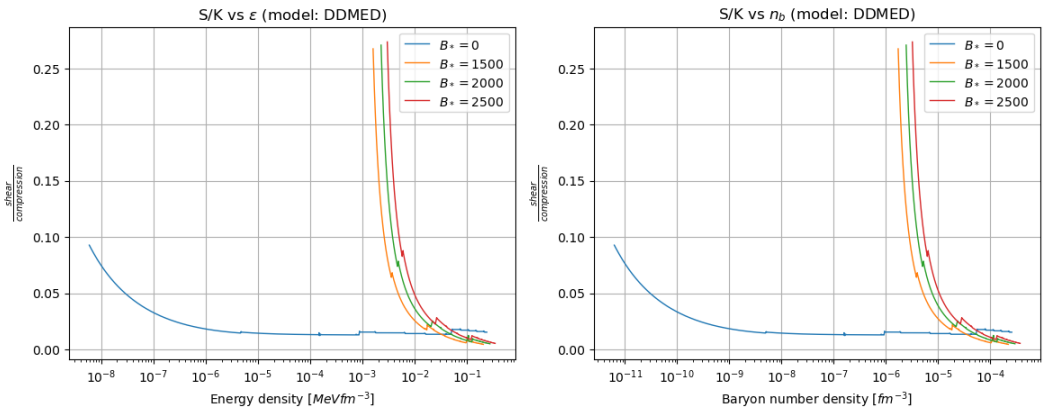

(a) (b)

Figure I.49: The same as Figure 5.15, using the DDMED model with different magnetic field strengths $B_\star$

I.6.5 DDPC1

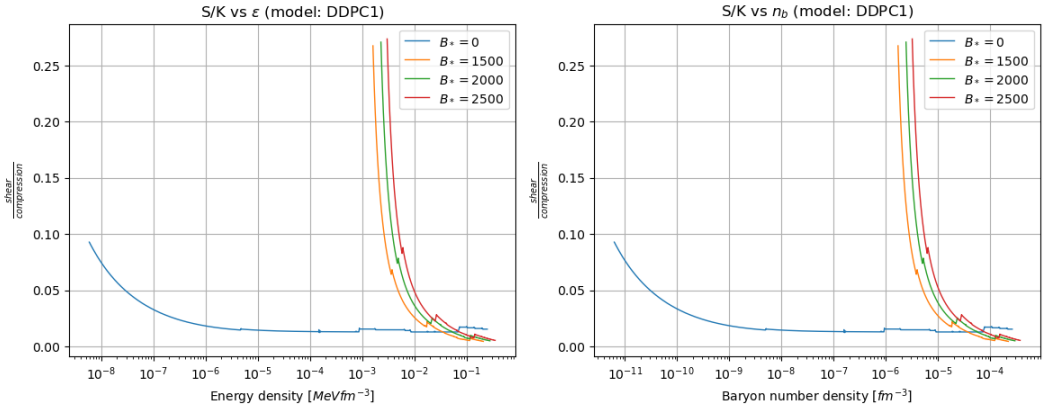

(a) (b)

Figure I.50: The same as Figure 5.15, using the DDPC1 model with different magnetic field strengths $B_\star$

I.6.6 SVMIN

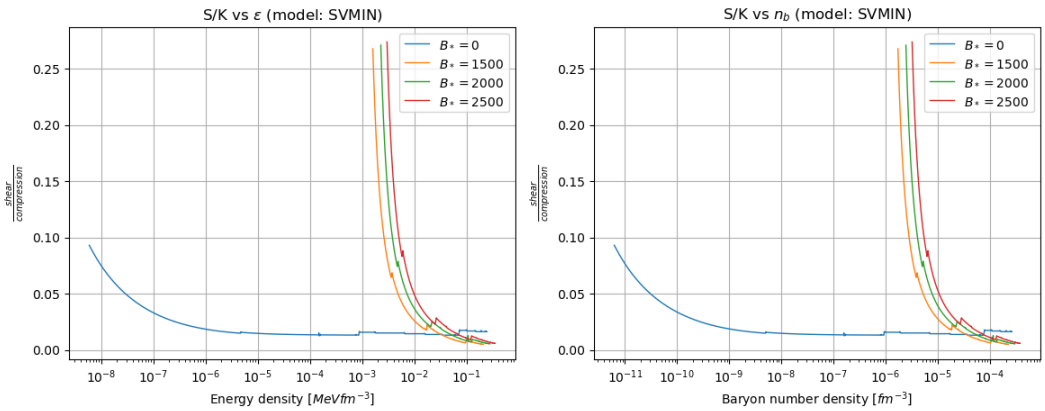

(a) (b)

Figure I.51: The same as Figure 5.15, using the SVMIN model with different magnetic field strengths $B_\star$

I.6.7 UNEDF0

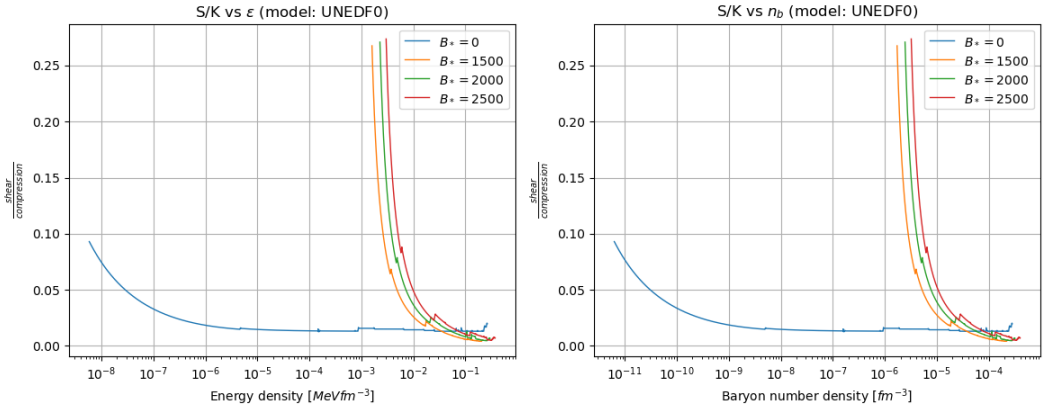

(a) (b)

Figure I.52: The same as Figure 5.15, using the UNEDF0 model with different magnetic field strengths $B_\star$

I.6.8 $B_\star = 2000$

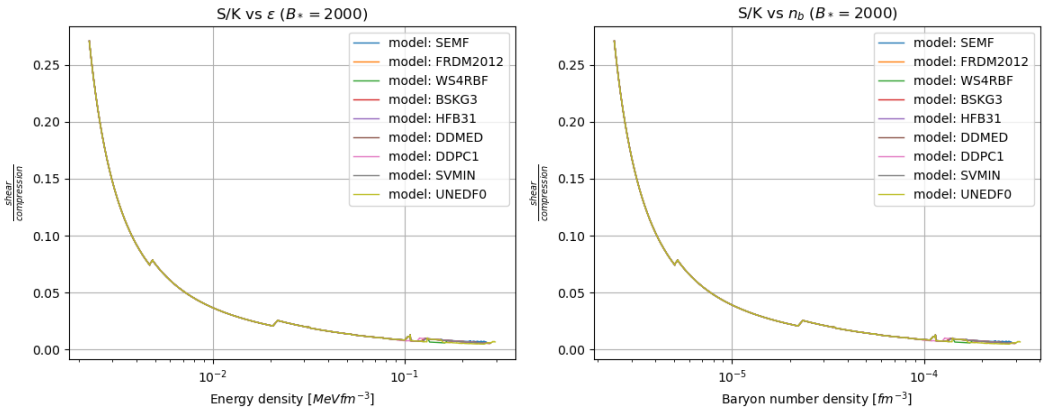

(a) (b)

Figure I.53: The same as Figure 5.34, using different models with magnetic field strength $B_\star = 2000$

I.6.9 $B_\star = 2500$

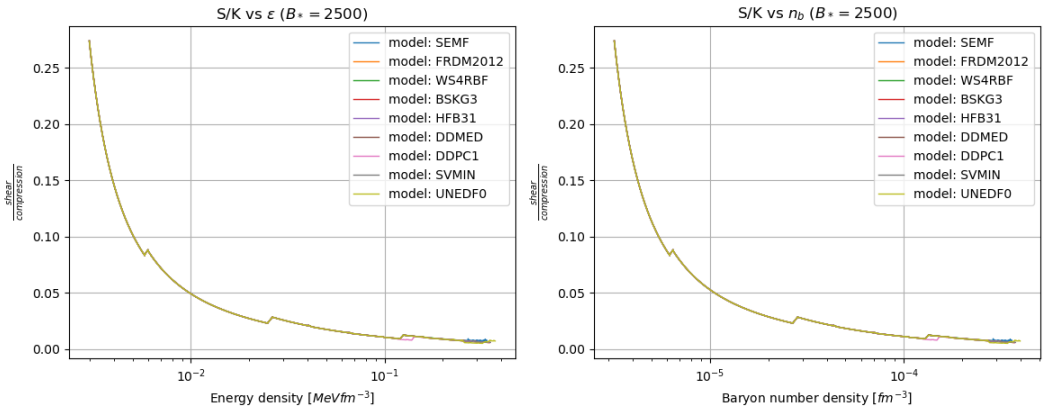

(a) (b)

Figure I.54: The same as Figure 5.34, using different models with magnetic field strength $B_\star = 2500$

I.7 Z, N, Z/A vs ϵ or n_b

I.7.1 WS4RBF

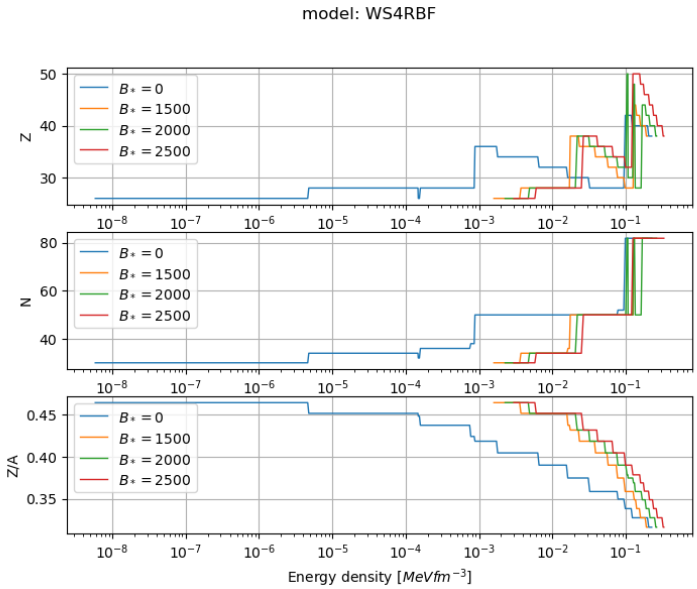

(a)

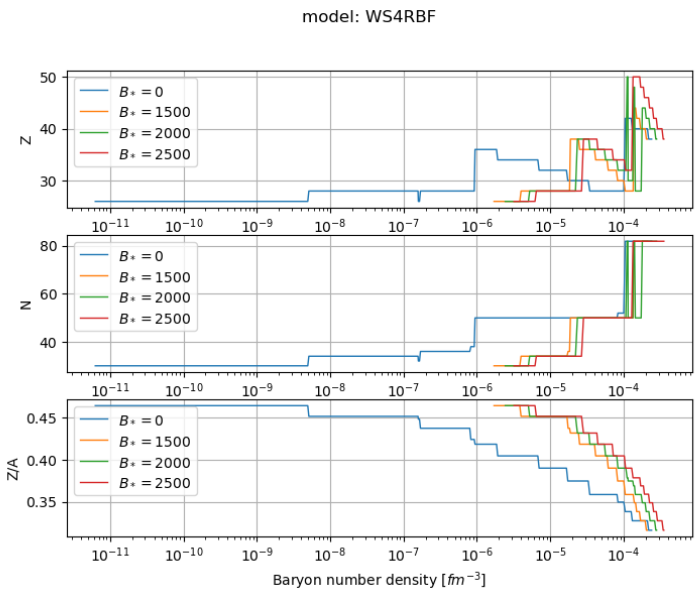

(b)

Figure I.55: The same as Figure 5.17, using the WS4RBF model with different magnetic field strengths $B_\star$

I.7.2 BSKG3

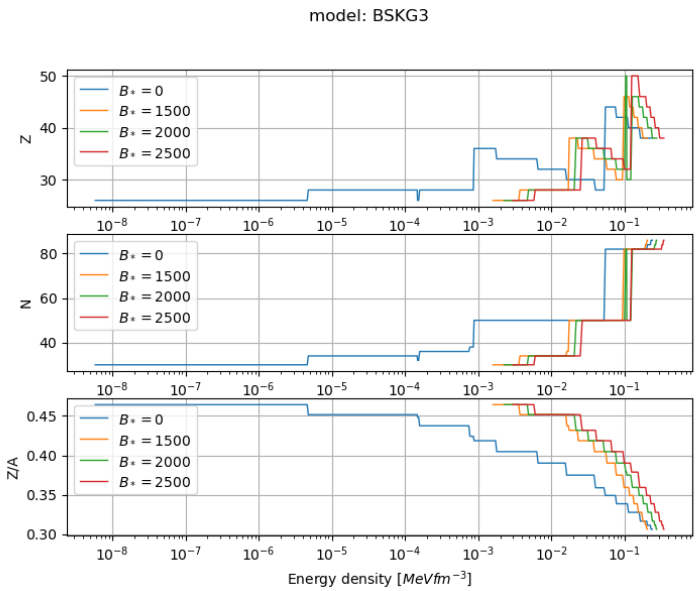

(a)

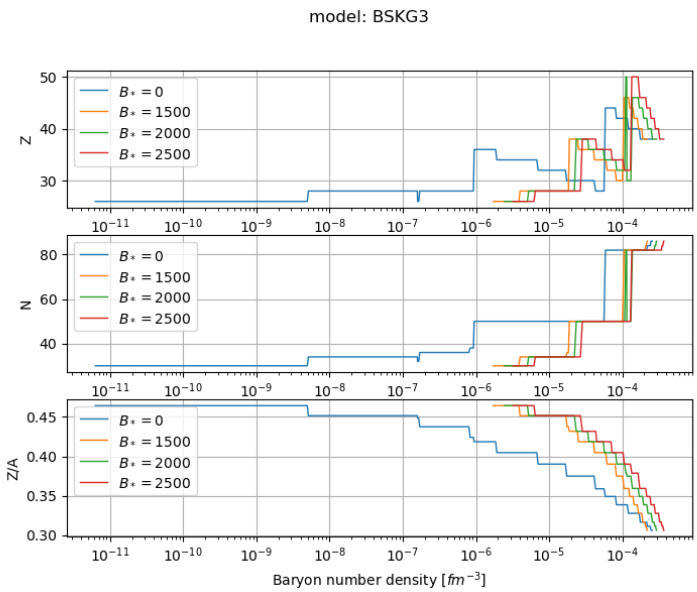

(b)

Figure I.56: The same as Figure 5.17, using the BSKG3 model with different magnetic field strengths $B_\star$

I.7.3 HFB31

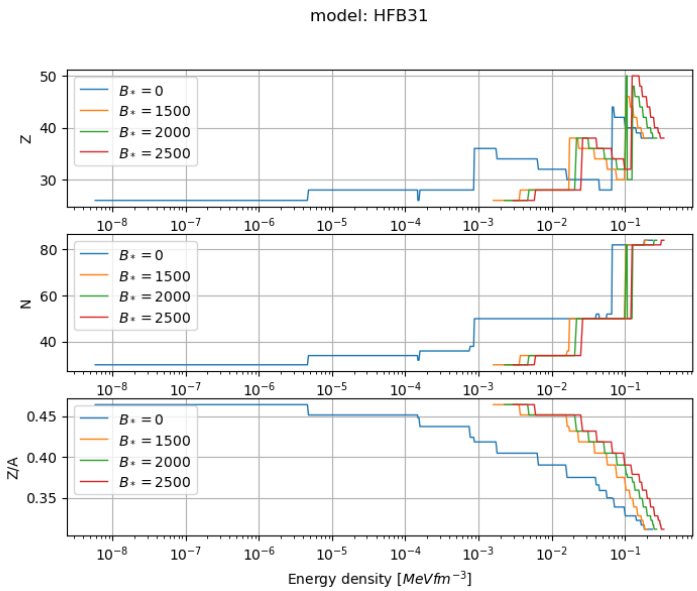

(a)

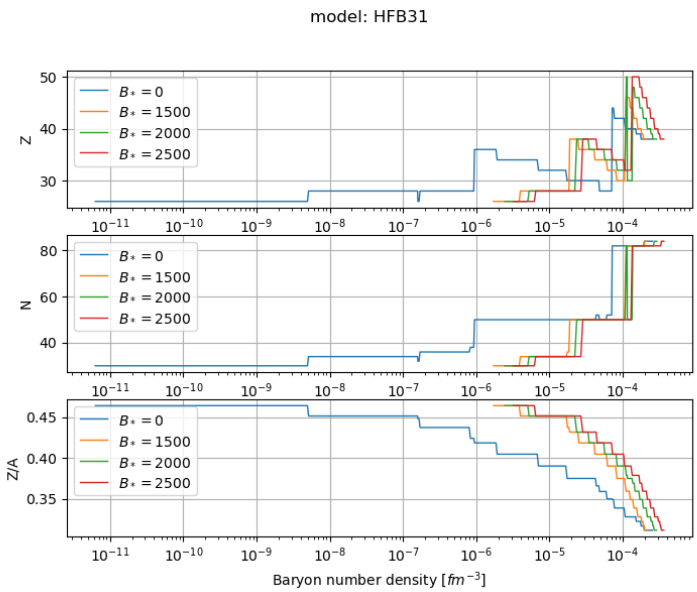

(b)

Figure I.57: The same as Figure 5.17, using the HFB31 model with different magnetic field strengths $B_\star$

I.7.4 DDMED

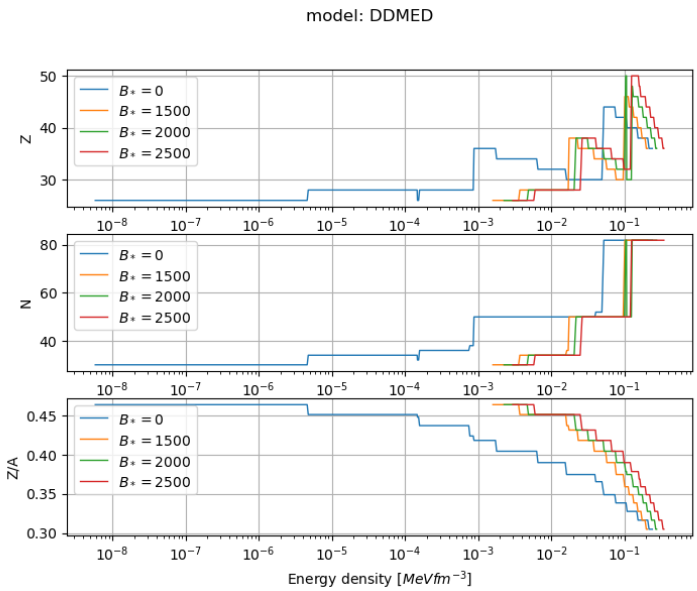

(a)

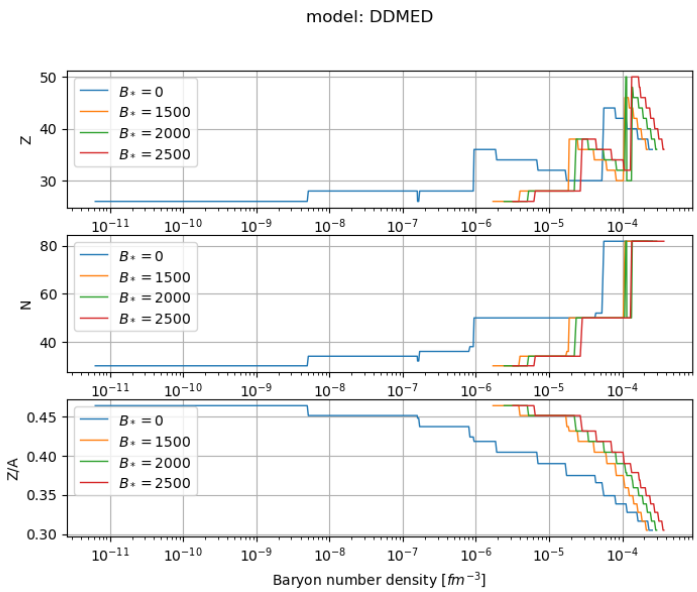

(b)

Figure I.58: The same as Figure 5.17, using the DDMED model with different magnetic field strengths $B_\star$

I.7.5 DDPC1

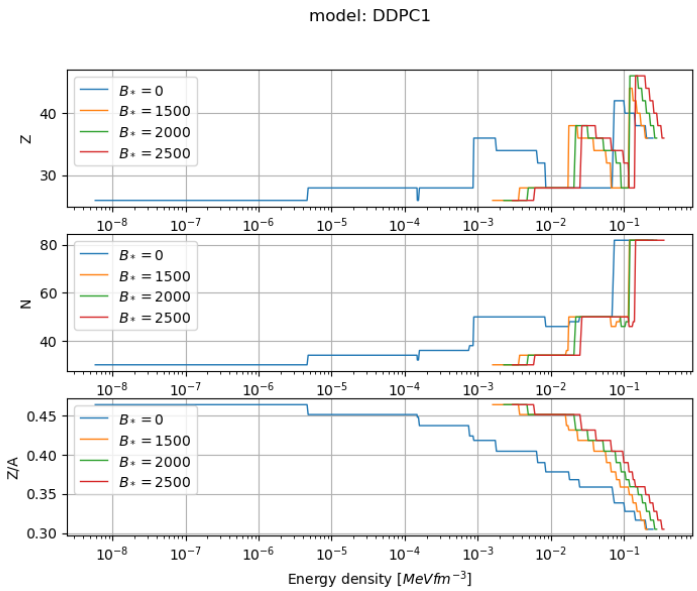

(a)

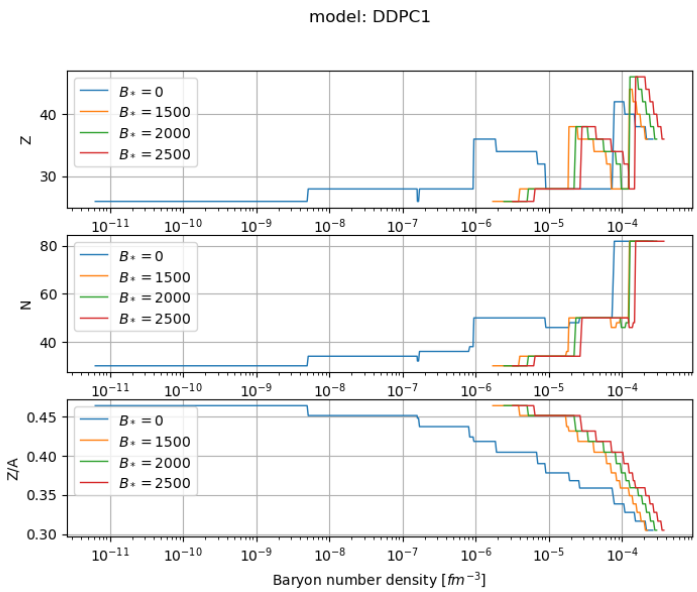

(b)

Figure I.59: The same as Figure 5.17, using the DDPC1 model with different magnetic field strengths $B_\star$

I.7.6 SVMIN

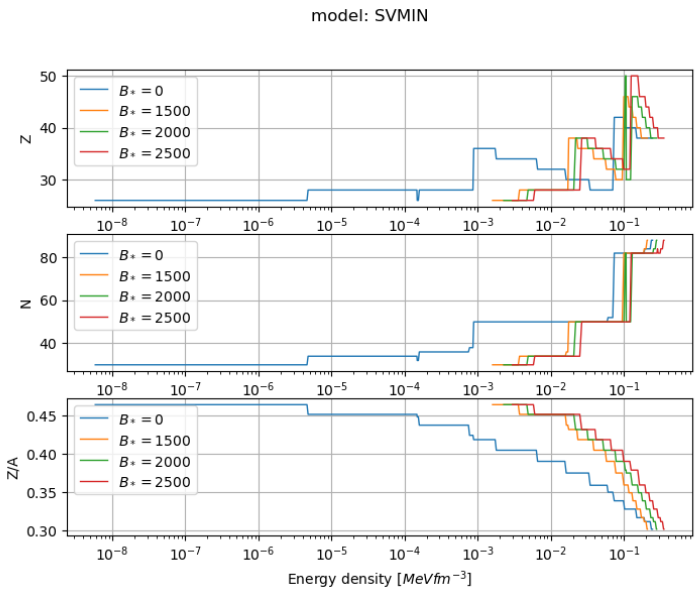

(a)

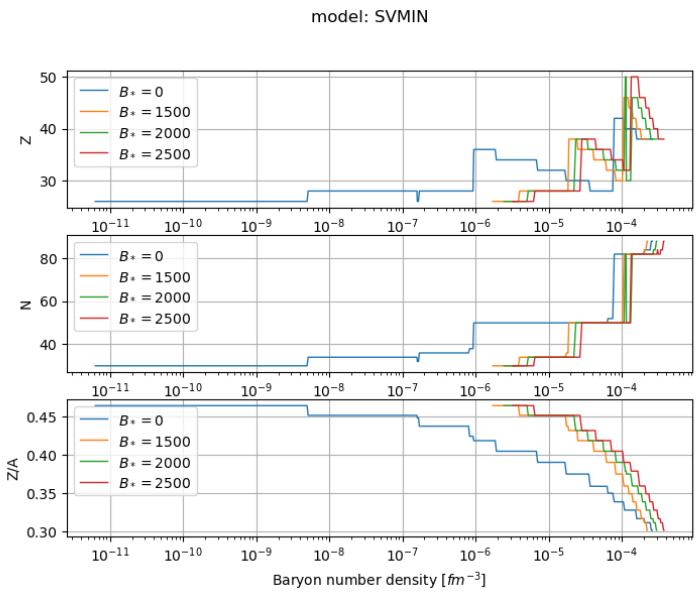

(b)

Figure I.60: The same as Figure 5.17, using the SVMIN model with different magnetic field strengths $B_\star$

I.7.7 UNEDF0

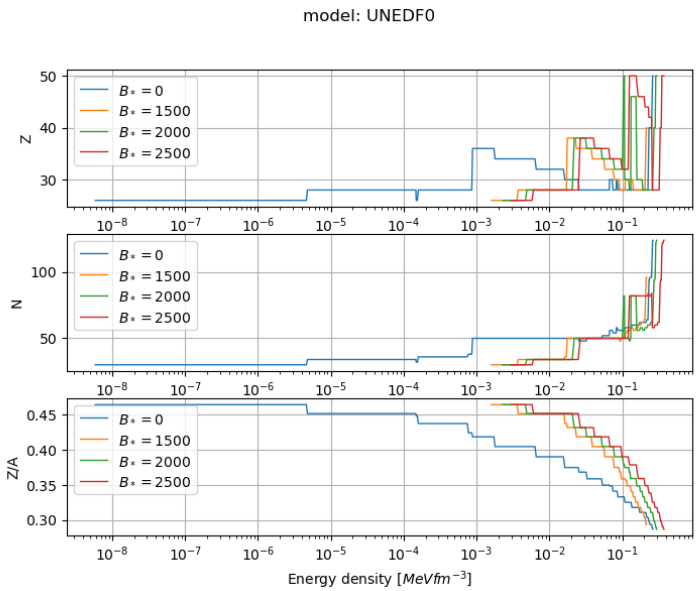

(a)

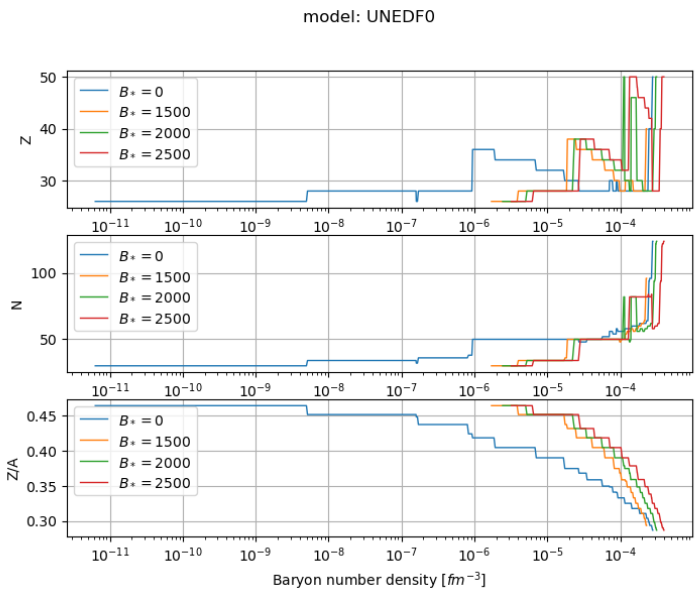

(b)

Figure I.61: The same as Figure 5.17, using the UNEDF0 model with different magnetic field strengths $B_\star$

I.7.8 $B_\star = 2000$

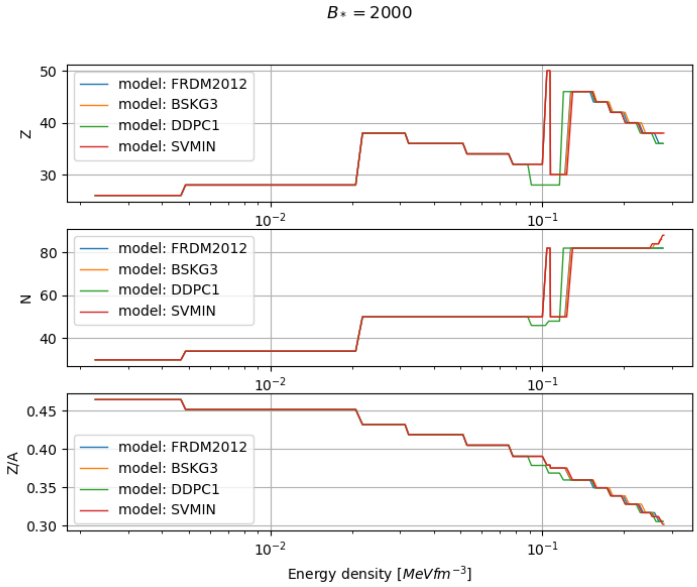

(a)

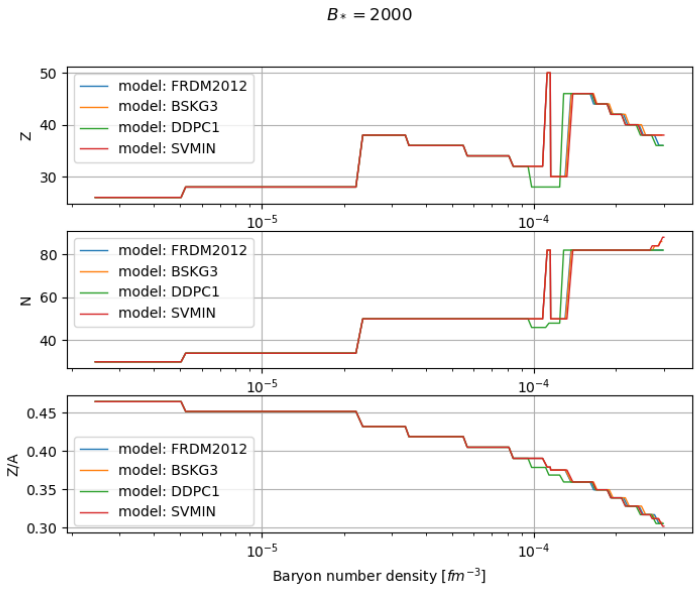

(b)

Figure I.62: The same as Figure 5.36, using different models with magnetic field strength $B_\star = 2000$

I.7.9 $B_\star = 2500$

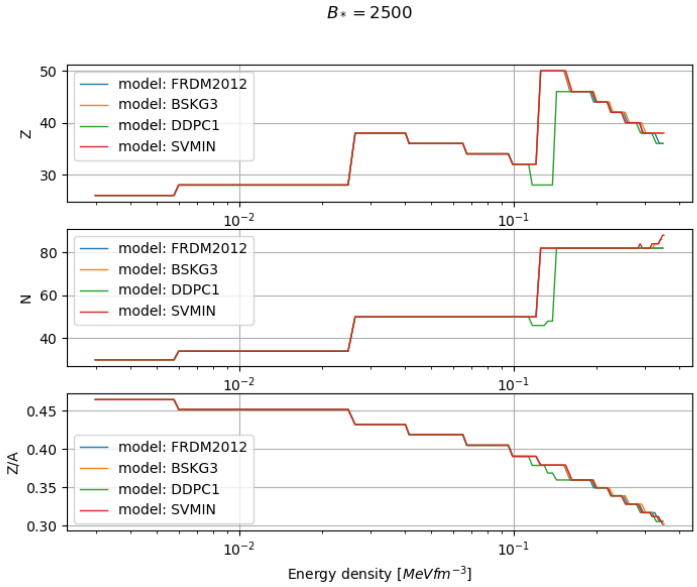

(a)

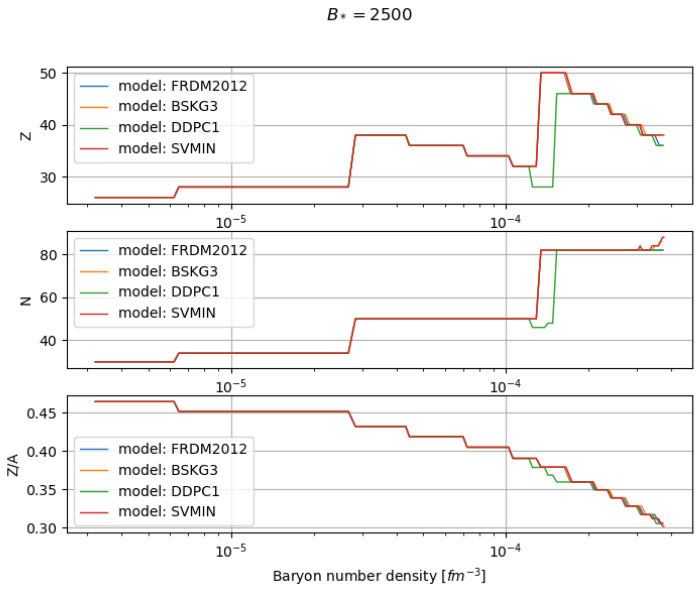

(b)

Figure I.63: The same as Figure 5.36, using different models with magnetic field strength $B_\star = 2500$

I.8 M_{cr} for different M and R

I.8.1 WS4RBF

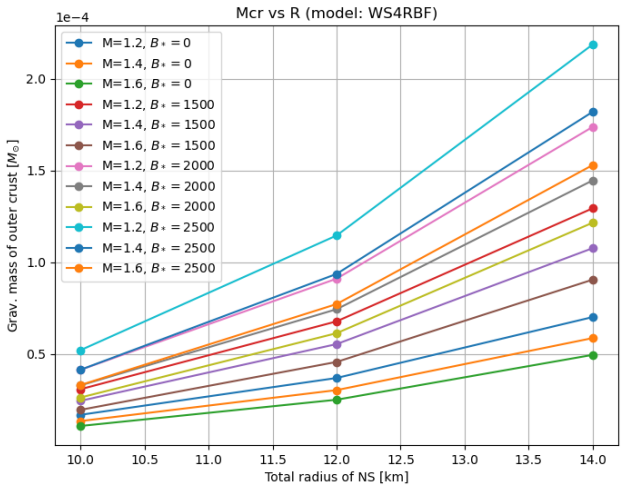

Figure I.64: The same as Figure 5.19, using the WS4RBF model with different magnetic field strengths $B_\star$

I.8.2 BSKG3

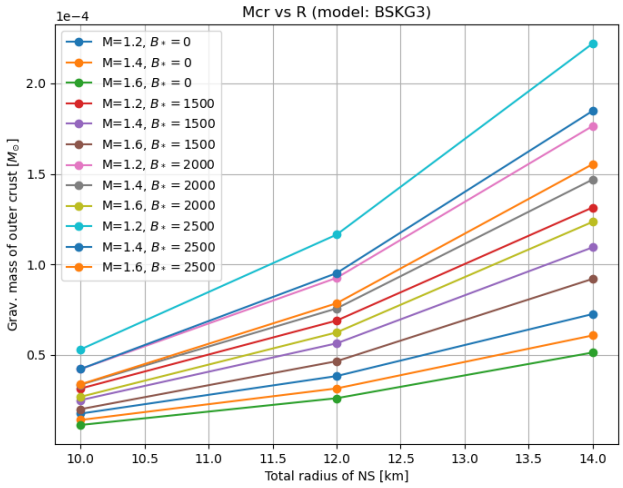

Figure I.65: The same as Figure 5.19, using the BSKG3 model with different magnetic field strengths $B_\star$

I.8.3 HFB31

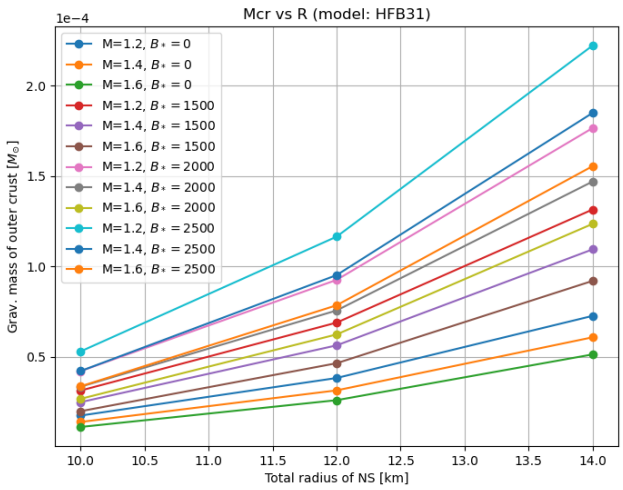

Figure I.66: The same as Figure 5.19, using the HFB31 model with different magnetic field strengths $B_\star$

I.8.4 DDMED

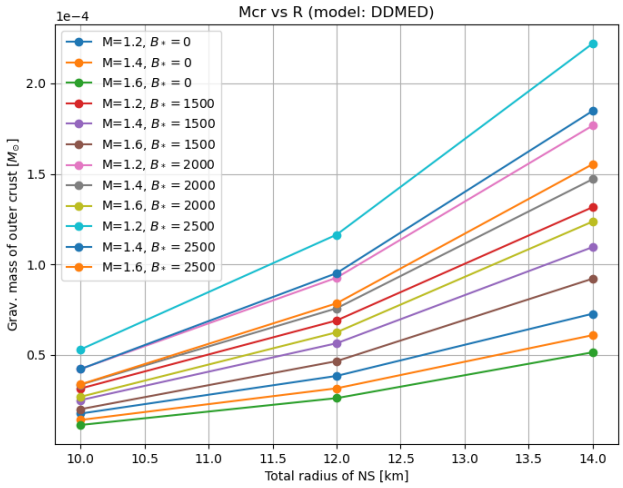

Figure I.67: The same as Figure 5.19, using the DDMED model with different magnetic field strengths $B_\star$

I.8.5 DDPC1

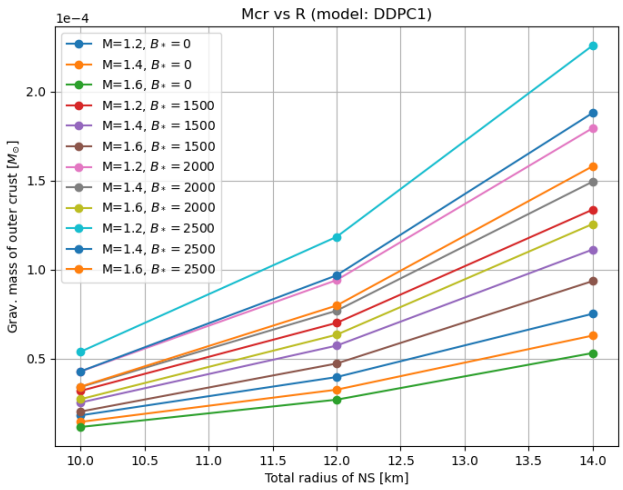

Figure I.68: The same as Figure 5.19, using the DDPC1 model with different magnetic field strengths $B_\star$

I.8.6 SVMIN

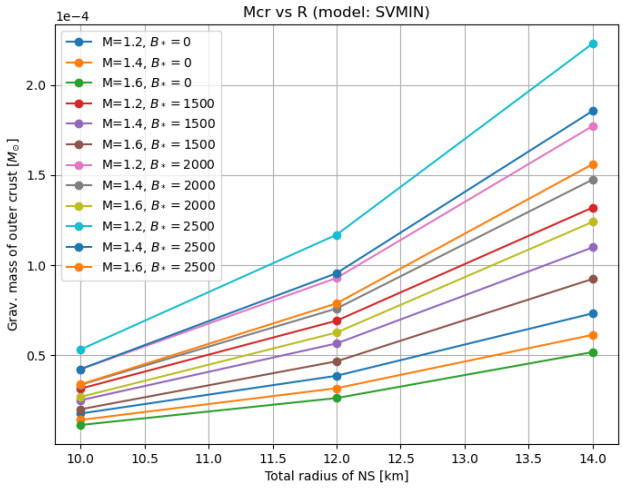

Figure I.69: The same as Figure 5.19, using the SVMIN model with different magnetic field strengths $B_\star$

I.8.7 UNEDF0

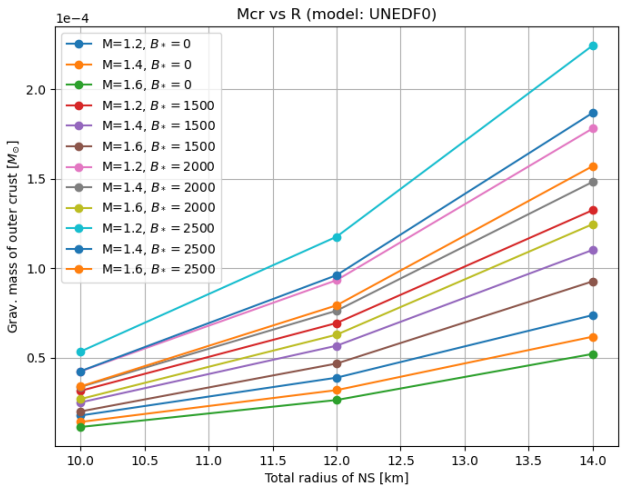

Figure I.70: The same as Figure 5.19, using the UNEDF0 model with different magnetic field strengths $B_\star$

I.8.8 $B_\star = 2000$

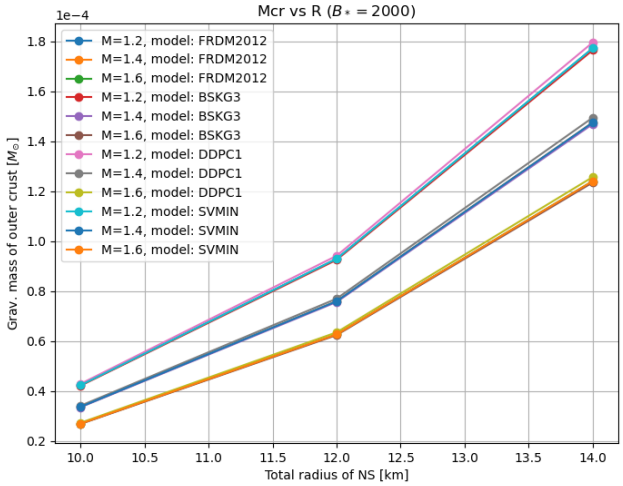

Figure I.71: The same as Figure 5.38, using different models with magnetic field strength $B_\star = 2000$

I.8.9 $B_\star = 2500$

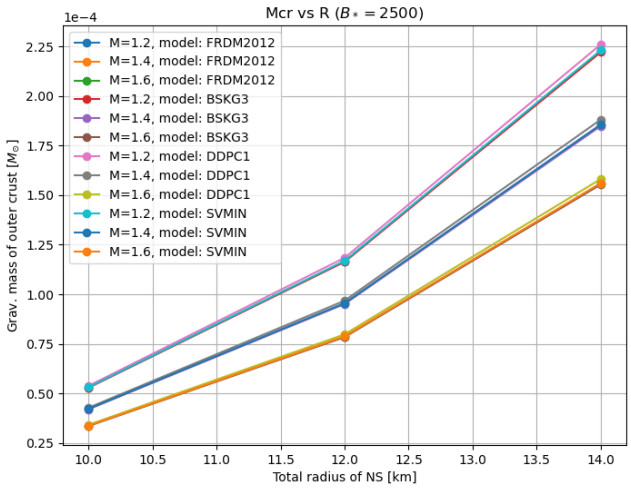

Figure I.72: The same as Figure 5.38, using different models with magnetic field strength $B_\star = 2500$

I.9 z_{drip} for different M and R

I.9.1 WS4RBF

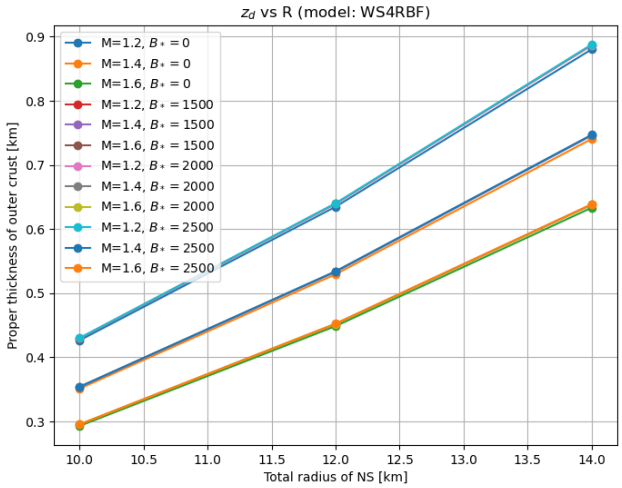

Figure I.73: The same as Figure 5.21, using the WS4RBF model with different magnetic field strengths $B_\star$

I.9.2 BSKG3

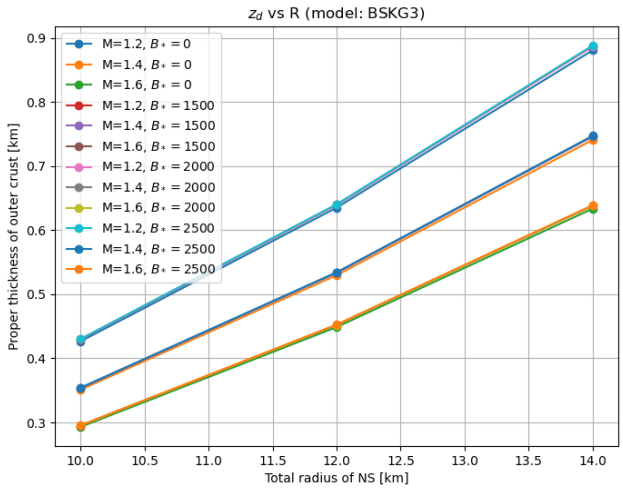

Figure I.74: The same as Figure 5.21, using the BSKG3 model with different magnetic field strengths $B_\star$

I.9.3 HFB31

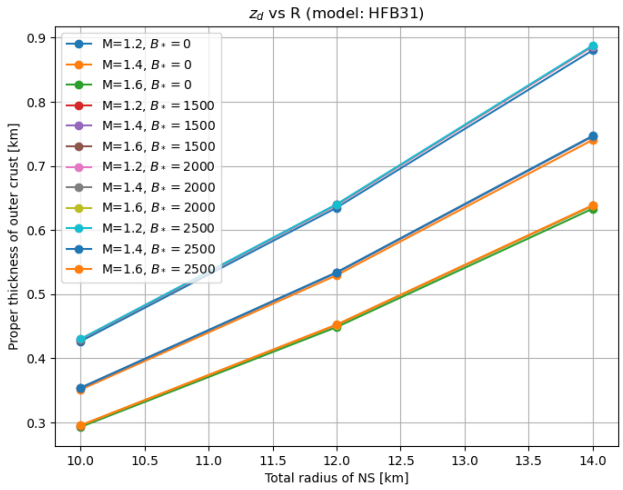

Figure I.75: The same as Figure 5.21, using the HFB31 model with different magnetic field strengths $B_\star$

I.9.4 DDMED

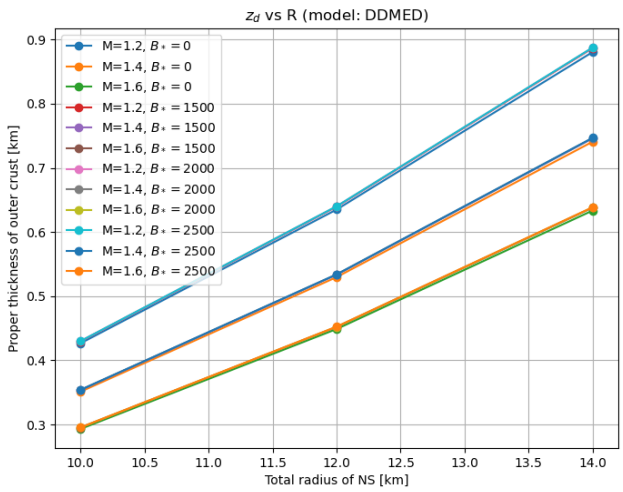

Figure I.76: The same as Figure 5.21, using the DDMED model with different magnetic field strengths $B_\star$

I.9.5 DDPC1

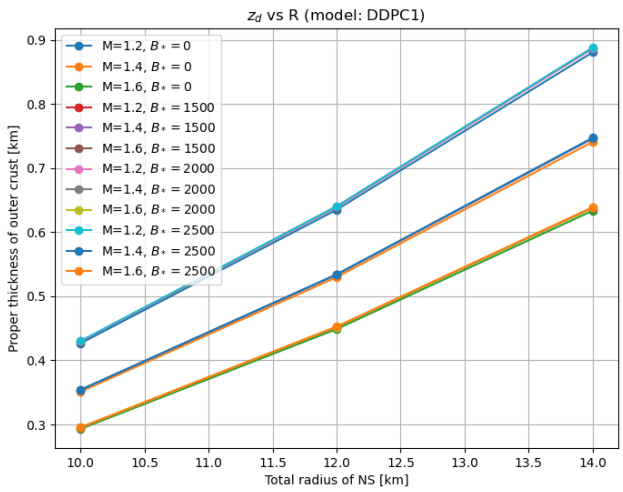

Figure I.77: The same as Figure 5.21, using the DDPC1 model with different magnetic field strengths $B_\star$

I.9.6 SVMIN

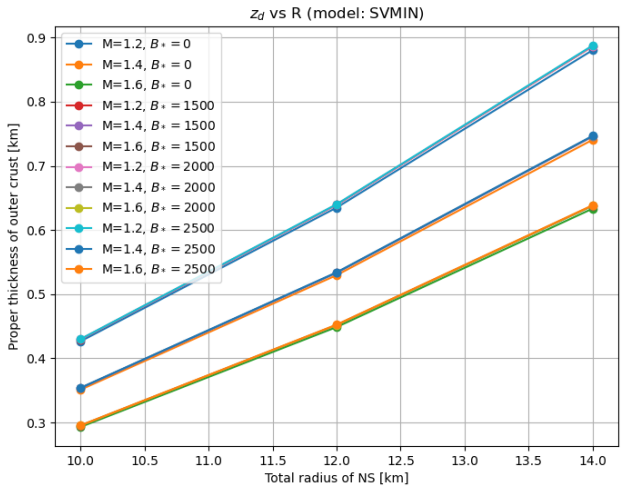

Figure I.78: The same as Figure 5.21, using the SVMIN model with different magnetic field strengths $B_\star$

I.9.7 UNEDF0

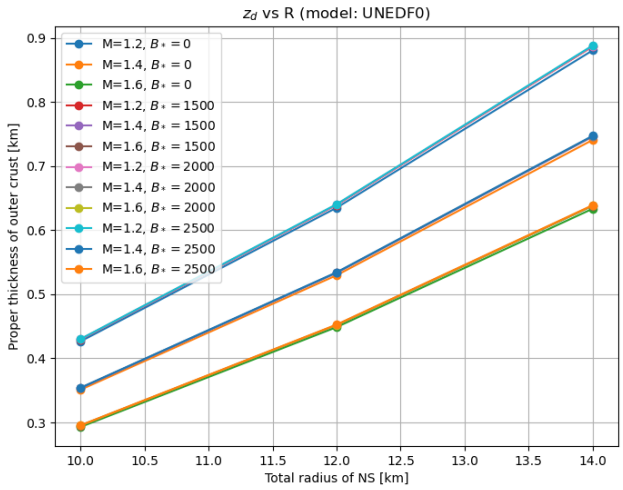

Figure I.79: The same as Figure 5.21, using the UNEDF0 model with different magnetic field strengths $B_\star$

I.9.8 $B_\star = 2000$

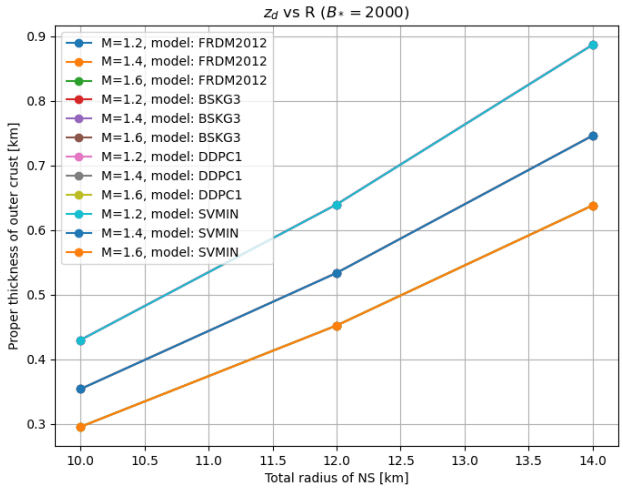

Figure I.80: The same as Figure 5.40, using different models with magnetic field strength $B_\star = 2000$

I.9.9 $B_\star = 2500$

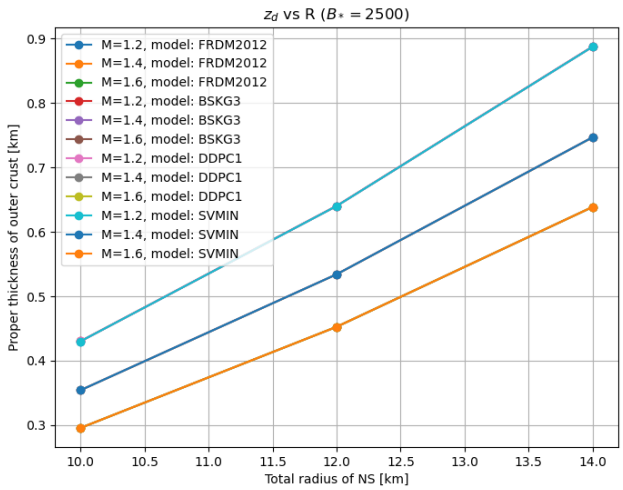

Figure I.81: The same as Figure 5.40, using different models with magnetic field strength $B_\star = 2500$

Appendix J

Code A

Below is the main code, written in *Python 3* programming language, which was used to derive the results of this work. As previously mentioned, the code and data used for this work are available online[1].

```
import numpy as np
import pandas as pd
import scipy as sp
import matplotlib.pyplot as plt
import fortranformat
import time

# parameters of beSEMF
AV, AS, AC, AA, AP=15.777, 18.341, 0.710, 23.211, 11.996
# definition of useful constants
Mn=939.565421 # neutron mass MeV/c**2
Mp=938.272088 # proton mass MeV/c**2
Me=0.510999 # electron mass MeV/c**2
AMU=931.494102 # atomic mass unit MeV/c**2
HBARC=197.326980 # MeVfm
ALPHA=7.297353e-3 # fine structure constant
LAMDAe=386.159268 # reduced electron Compton wavelength fm
K1=Me*LAMDAe**(-3) # MeVfm**(-3)
CM=0.895929255682 # Madelung constant for bcc lattice
# conversion of units
MeV_fm3to_km2=1.3234e-6 # 1MeVfm**(-3)=1.3234e-6 km**(-2)
MeV_c2toMsolar=8.964992783e-61 # 1MeV/c**2=8.964992783e-61
↪  Msolar
```

[1] https://github.com/johnmavr/master-thesis

```

def beSEMF(A,Z):

    '''
    return the nuclear binding energy for SEMF model,
    given mass number A and atomic number Z, in MeV

    '''
    N=A-Z

    be=AV*A-AS*A**(2/3)-AC*Z*(Z-1)*A**(-1/3)-AA*((A-2*Z)**2)/A

    if (Z%2==0) and (N%2==0):
        be=be+AP*A**(-1/2)
    elif (Z%2!=0) and (N%2!=0):
        be=be-AP*A**(-1/2)

    return be

def Sp(A,Z):

    '''
    return the one-proton separation energy

    '''
    return beSEMF(A,Z)-beSEMF(A-1,Z-1)

def S2p(A,Z):

    '''
    return the two-proton separation energy

    '''
    return beSEMF(A,Z)-beSEMF(A-2,Z-2)

def Sn(A,Z):

    '''
    return the one-neutron separation energy

    '''
```

```
    return beSEMF(A,Z)-beSEMF(A-1,Z)

def S2n(A,Z):

    '''
    return the two-neutron separation energy

    '''
    return beSEMF(A,Z)-beSEMF(A-2,Z)

def Bel(Z):

    '''
    return the binding energy of atomic electrons in MeV

    '''
    return 1.44381e-5*Z**(2.39)+1.55468e-12*Z**(5.35)

def WN(A,Z,tabular_form,external=None):

    '''
    return the mass of nucleus in MeV

    '''
    if tabular_form=='semf_be':
        return Z*Mp+(A-Z)*Mn-beSEMF(A,Z)
    elif tabular_form=='be':
        return Z*Mp+(A-Z)*Mn+external # be is tabulated as a negative number, otherwise change here the sign to -
    elif tabular_form=='mass_excess':
        return external+A*AMU-Z*Me+Bel(Z)

def ge(xe):

    '''
    return the nondimensional Fermi energy
    (chemical potential) of electrons ge=mue/(Me*c**2),
    (xe is the nondimensional Fermi momentum xe=peF/(Me*c))

    '''
```

```
    return (xe**2+1)**(1/2)

def mue(ge):

    '''
    return the chemical potential of electrons in MeV

    '''
    return Me*ge

def ne(xe,B):

    '''
    return the number density of electrons in fm**(-3)

    '''
    if B==0:
        return (xe**3)/(3*np.pi**2*LAMDAe**3)
    else:
        return (B*xe)/(2*np.pi**2*LAMDAe**3)

def nb(A,Z,xe,B):

    '''
    return the number density of baryons in fm**(-3)

    '''
    return (A/Z)*ne(xe,B)

def nN(Z,xe,B):

    '''
    return the number density of nuclei in fm**(-3)

    '''
    return ne(xe,B)/Z

def rcell(Z,xe,B):

    '''
    return the Rcell in fm
```

```
    '''
    return (4*np.pi*nN(Z,xe,B)/3)**(-1/3)

def shear(Z,xe,B):

    '''
    return the effective shear modulus in MeVfm**(-3)

    '''
    return 0.1194*nN(Z,xe,B)*Z**2*ALPHA*HBARC/rcell(Z,xe,B)

def f(x,B):

    '''
    function useful for electron energy density

    '''
    if B==0:
        return (1/(8*np.pi**2))*(x*(1+x**2)**(1/2)*(1+2*x**2
        ↪  )-np.log(x+(1+x**2)**(1/2)))
    else:
        return x*(1+x**2)**(1/2)+np.log(x+(1+x**2)**(1/2))

def g(x,B):

    '''
    function useful for electron pressure

    '''
    if B==0:
        return (1/(8*np.pi**2))*(x*(1+x**2)**(1/2)*((2/3)*x*
        ↪  *2-1)+np.log(x+(1+x**2)**(1/2)))
    else:
        return x*(1+x**2)**(1/2)-np.log(x+(1+x**2)**(1/2))

def ee(xe,B):

    '''
    return the energy density of electrons in MeVfm**(-3)

```

```
    '''
    if B==0:
        return K1*f(xe,B)
    else:
        return (K1*B*f(xe,B))/((2*np.pi)**2)

def Pe(xe,B):

    '''
    return the pressure of electrons in MeVfm**(-3)

    '''
    if B==0:
        return K1*g(xe,B)
    else:
        return (K1*B*g(xe,B))/((2*np.pi)**2)

def el(Z,xe,B):

    '''
    return the energy density of lattice in MeVfm**(-3)

    '''
    return -CM*(4*np.pi/3)**(1/3)*Z**(2/3)*ALPHA*HBARC*(ne(x
    ↪  e,B))**(4/3)

def Pl(Z,xe,B):

    '''
    return the pressure of lattice in MeVfm**(-3)

    '''
    return el(Z,xe,B)/3

def Ptot(Z,xe,B):

    '''
    return the total pressure in MeVfm**(-3)

    '''
    return Pe(xe,B)+Pl(Z,xe,B)
```

```python

def etot(A,Z,xe,B,tabular_form,external=None):

    '''
    return the total energy density in MeVfm**(-3)

    '''
    return nN(Z,xe,B)*WN(A,Z,tabular_form,external)+ee(xe,B) +el(Z,xe,B)

def gibbs(A,Z,xe,B,tabular_form,external=None):

    '''
    return Gcell/A (chemical potential of baryons) in MeV

    '''
    return (etot(A,Z,xe,B,tabular_form,external)+Ptot(Z,xe,B ))/nb(A,Z,xe,B)

def funtosolve(xe,Z,Pfix,B):

    '''
    for fixed Z and Pfix, find numerically the xroot
    of this function

    '''
    return Ptot(Z,xe,B)-Pfix

#---------------USER GIVES values---------------------------

model='' # GIVE the name of the nuclear model: 'SEMF' or ...
tabulation='' # GIVE the tabular_form: 'semf_be' or 'be' or 'mass_excess'
Bstar=0 # GIVE a magnetic field in Bcr units (Bcr=4.414e13G): Bstar>1304 or Bstar=0
filename='' # GIVE the filename of the nuclear mass table: 'FRDM2012_table.dat' or ..., or None for SEMF
```

```
extra_tabulation=[] # GIVE what the header of file contains: ('Z','A'], if contains only Z and A in any order) or ('Z','N'], if contains only Z and N in any order) or ('Z','N','A'], if contains only Z, N and A in any order), or None for SEMF
sepform='' # GIVE how the columns are saparated in the file: ' ' or '\\s+' or ',' or ..., or None for SEMF

#-------------------------------------------------------------
# set-up of variables for minimization process
field=(f'{Bstar}').replace(".", "_")

# the endpoint must be bigger than Pdrip~5e-4 MeVfm**(-3) (without magnetic field)
pressinterval=(6.082e-15, 20.0e-4)
numberpoints=18000
presslist=np.logspace(np.log10(pressinterval[0]), np.log10(pressinterval[1]),
                      numberpoints, dtype=np.float64)

Aminlist=np.zeros((numberpoints), dtype=np.int16)
Zminlist=np.zeros((numberpoints), dtype=np.int16)
Nminlist=np.zeros((numberpoints), dtype=np.int16)
xeminlist=np.zeros((numberpoints), dtype=np.float64)
gminlist=np.zeros((numberpoints), dtype=np.float64)
etotminlist=np.zeros((numberpoints), dtype=np.float64)

Zmin_interest=24
Zmax_interest=56
Nmin_interest=24
Nmax_interest=132

reader=fortranformat.FortranRecordReader('(a1,i3,i5,i5,i5,1x,a3,a4,1x,f14.6)')

with open('AME2020_table.dat','r') as fileAME:

    lines=fileAME.readlines()

dfexp=pd.DataFrame(columns=['cc', 'N-Z', 'N', 'Z', 'A', 'el', 'origin', 'mass_excess[keV]'])
```

```

for index in range(1,len(lines)):

    try:
        dfexp.loc[len(dfexp)]=reader.read(lines[index])
    except ValueError as message:
        print(message,'\nIt is not experimentally measured mass\n')
        continue

del lines
dfexp=dfexp.drop(['cc','N-Z','el','origin'], axis=1)
dfexp=dfexp.sort_values(by=['Z','N'])
dfexp_interest=dfexp.query(f'{Zmin_interest}<=Z<={Zmax_interest} and {Nmin_interest}<=N<={Nmax_interest}')
Zexp_array=dfexp_interest['Z'].to_numpy()
Aexp_array=dfexp_interest['A'].to_numpy()
externalexp_array=dfexp_interest['mass_excess[keV]'].to_numpy()
externalexp_array=externalexp_array*10**(-3) # exp. mass excess in MeV

# start of gibbs minimization process
i=0

if (tabulation=='be') or (tabulation=='mass_excess'):

    if extra_tabulation==['Z', 'A']:

        df=pd.read_csv(filename, sep=sepform, header=0, usecols=['Z','A',tabulation])
        df=df.sort_values(by=['Z','A'])
        df['N']=df['A']-df['Z']
        df_interest=df.query(f'{Zmin_interest}<=Z<={Zmax_interest} and {Nmin_interest}<=N<={Nmax_interest}')
        Z_array=df_interest['Z'].to_numpy()
        A_array=df_interest['A'].to_numpy()
        external_array=df_interest[tabulation].to_numpy()

```

```
    elif extra_tabulation==['Z', 'N']:

        df=pd.read_csv(filename, sep=sepform, header=0, usecols=['Z','N',tabulation])
        df=df.sort_values(by=['Z','N'])
        df['A']=df['Z']+df['N']
        df_interest=df.query(f'{Zmin_interest}<=Z<={Zmax_interest} and {Nmin_interest}<=N<={Nmax_interest}')
        Z_array=df_interest['Z'].to_numpy()
        A_array=df_interest['A'].to_numpy()
        external_array=df_interest[tabulation].to_numpy()

    elif extra_tabulation==['Z', 'N', 'A']:

        df=pd.read_csv(filename, sep=sepform, header=0, usecols=['Z','N','A',tabulation])
        df=df.sort_values(by=['Z','N'])
        df_interest=df.query(f'{Zmin_interest}<=Z<={Zmax_interest} and {Nmin_interest}<=N<={Nmax_interest}')
        Z_array=df_interest['Z'].to_numpy()
        A_array=df_interest['A'].to_numpy()
        external_array=df_interest[tabulation].to_numpy()

    delete_list=[]

    for index1 in range(len(external_array)):

        for index2 in range(len(externalexp_array)):

            if (Z_array[index1]==Zexp_array[index2]) and (A_array[index1]==Aexp_array[index2]):

                delete_list.append(index1)

    Z_array=np.delete(Z_array,delete_list)
    A_array=np.delete(A_array,delete_list)
    external_array=np.delete(external_array,delete_list)

    print('Start of gibbs minimization process...\n')
```

```
    start_time=time.time()
    while True:

        Pfix=presslist[i]
        mini=100000.0
        flag=0.0
        ref=True

        for index in range(len(external_array)):

            if Z_array[index]!=Z_array[index-1]:

                xroot=sp.optimize.fsolve(funtosolve, x0=100,
                                         args=(Z_array[index],Pfix,Bstar),
                                         xtol=1e-10)

            flag=gibbs(A_array[index], Z_array[index], xroot, Bstar,
                       tabulation, external_array[index])

            if flag<mini:

                mini=flag
                Amin=A_array[index]
                Zmin=Z_array[index]
                Nmin=A_array[index]-Z_array[index]
                xemin=xroot
                externalmin=external_array[index]
                ref=False

        for index in range(len(externalexp_array)):

            if Zexp_array[index]!=Zexp_array[index-1]:

                xroot=sp.optimize.fsolve(funtosolve, x0=100,
                                         args=(Zexp_array[index],Pfix,Bstar),
                                         xtol=1e-10)

```

```
            flag=gibbs(Aexp_array[index], Zexp_array[index], xroot, Bstar,
                       'mass_excess', externalexp_array[index])

            if flag<mini:

                mini=flag
                Amin=Aexp_array[index]
                Zmin=Zexp_array[index]
                Nmin=Aexp_array[index]-Zexp_array[index]
                xemin=xroot
                externalmin=externalexp_array[index]
                ref=True

        if mini > Mn:
            break

        Aminlist[i]=Amin
        Zminlist[i]=Zmin
        Nminlist[i]=Nmin
        xeminlist[i]=xemin
        gminlist[i]=mini
        if ref==False:
            etotminlist[i]=etot(Amin, Zmin, xemin, Bstar, tabulation, externalmin)
        elif ref==True:
            etotminlist[i]=etot(Amin, Zmin, xemin, Bstar, 'mass_excess', externalmin)

        i=i+1

    end_time=time.time()
    print(f'Execution time for gibbs minimization: {(end_time-start_time):.2f} sec\n')

elif tabulation=='semf_be' :

    Z_array=np.zeros(((Zmax_interest-Zmin_interest+1)*(Nmax_interest-Nmin_interest+1)), dtype=np.int16)
```

```
    A_array=np.zeros(((Zmax_interest-Zmin_interest+1)*(Nmax_interest-Nmin_interest+1)),dtype=np.int16)
    external_array=np.zeros(((Zmax_interest-Zmin_interest+1)*(Nmax_interest-Nmin_interest+1)),dtype=np.float64)
    index=0

    for Z in range(Zmin_interest,Zmax_interest+1):

        for N in range(Nmin_interest,Nmax_interest+1):

            A=Z+N

            if (beSEMF(A, Z)<=0.0) or (Sp(A, Z)<=0.0) or (S2p(A, Z)<=0.0) or (Sn(A, Z)<=0.0) or (S2n(A, Z)<=0.0):
                continue

            Z_array[index]=Z
            A_array[index]=A
            external_array[index]=beSEMF(A, Z)
            index=index+1

    Z_array=Z_array[:index]
    A_array=A_array[:index]
    external_array=external_array[:index]

    delete_list=[]

    for index1 in range(len(external_array)):

        for index2 in range(len(externalexp_array)):

            if (Z_array[index1]==Zexp_array[index2]) and (A_array[index1]==Aexp_array[index2]):

                delete_list.append(index1)

    Z_array=np.delete(Z_array,delete_list)
    A_array=np.delete(A_array,delete_list)
```

```
    external_array=np.delete(external_array,delete_list)

    print('Start of gibbs minimization process...\n')
    start_time=time.time()
    while True:

        Pfix=presslist[i]
        mini=100000.0
        flag=0.0
        ref=True

        for index in range(len(external_array)):

            if Z_array[index]!=Z_array[index-1]:

                xroot=sp.optimize.fsolve(funtosolve, x0=100,
                                         args=(Z_array[index]
                                         ↪  ,Pfix,Bstar),
                                         ↪  xtol=1e-10)

            flag=gibbs(A_array[index], Z_array[index], xroot,
            ↪  Bstar, tabulation)

            if flag<mini:

                mini=flag
                Amin=A_array[index]
                Zmin=Z_array[index]
                Nmin=A_array[index]-Z_array[index]
                xemin=xroot
                ref=False

        for index in range(len(externalexp_array)):

            if Zexp_array[index]!=Zexp_array[index-1]:

                xroot=sp.optimize.fsolve(funtosolve, x0=100,
                                         args=(Zexp_array[ind
                                         ↪  ex],Pfix,Bstar),
                                         ↪  xtol=1e-10)

```

```
            flag=gibbs(Aexp_array[index], Zexp_array[index], xroot, Bstar,
                       'mass_excess', externalexp_array[index])

            if flag<mini:

                mini=flag
                Amin=Aexp_array[index]
                Zmin=Zexp_array[index]
                Nmin=Aexp_array[index]-Zexp_array[index]
                xemin=xroot
                externalmin=externalexp_array[index]
                ref=True

        if mini > Mn:
            break

        Aminlist[i]=Amin
        Zminlist[i]=Zmin
        Nminlist[i]=Nmin
        xeminlist[i]=xemin
        gminlist[i]=mini
        if ref==False:
            etotminlist[i]=etot(Amin, Zmin, xemin, Bstar, tabulation)
        elif ref==True:
            etotminlist[i]=etot(Amin, Zmin, xemin, Bstar, 'mass_excess', externalmin)

        i=i+1

    end_time=time.time()
    print(f'Execution time for gibbs minimization: {(end_time-start_time):.2f} sec\n')

# end of gibbs minimization process
presslist=presslist[:i]
Aminlist=Aminlist[:i]
Zminlist=Zminlist[:i]
Nminlist=Nminlist[:i]
```

```
xeminlist=xeminlist[:i]
gminlist=gminlist[:i]
etotminlist=etotminlist[:i]

mueminlist=mue(ge(xeminlist))
geminlist=ge(xeminlist)
nbminlist=nb(Aminlist, Zminlist, xeminlist, Bstar)
ZoverA=Zminlist/Aminlist
shearlist=shear(Zminlist, xeminlist, Bstar)
gamma=np.gradient(np.log(presslist), np.log(nbminlist))
compression=gamma*presslist
soundspeed=(np.gradient(presslist,etotminlist))**(1/2)

changelist=[]

# find phase transition
for index in range(i-1):

    if (Zminlist[index]!=Zminlist[index+1]) or
    ↪  (Nminlist[index]!=Nminlist[index+1]):

        changelist.append(index)

# min - max values and A, Z, N, Z/A in each layer
pressminmax=np.zeros((len(changelist)+1, 2), dtype=np.float64)
nbminmax=np.zeros((len(changelist)+1, 2), dtype=np.float64)
etotminmax=np.zeros((len(changelist)+1, 2), dtype=np.float64)
mubminmax=np.zeros((len(changelist)+1, 2), dtype=np.float64)
mueminmax=np.zeros((len(changelist)+1, 2), dtype=np.float64)
Alayer=np.zeros((len(changelist)+1, 1), dtype=np.int16)
Zlayer=np.zeros((len(changelist)+1, 1), dtype=np.int16)
Nlayer=np.zeros((len(changelist)+1, 1), dtype=np.int16)
ZoverAlayer=np.zeros((len(changelist)+1, 1), dtype=np.float64)

for index in range(len(changelist)+1):
    if len(changelist)==0:
        pressminmax[index]=[presslist[index],presslist[-1]]
        nbminmax[index]=[nbminlist[index],nbminlist[-1]]
        etotminmax[index]=[etotminlist[index],etotminlist[-1]]
        mubminmax[index]=[gminlist[index],gminlist[-1]]
        mueminmax[index]=[mueminlist[index],mueminlist[-1]]
```

```
        Alayer[index]=Aminlist[index]
        Zlayer[index]=Zminlist[index]
        Nlayer[index]=Nminlist[index]
        ZoverAlayer[index]=ZoverA[index]

    elif index==0:
        pressminmax[index]=[presslist[index],presslist[change
        ↪  list[index]]]
        nbminmax[index]=[nbminlist[index],nbminlist[changelis
        ↪  t[index]]]
        etotminmax[index]=[etotminlist[index],etotminlist[cha
        ↪  ngelist[index]]]
        mubminmax[index]=[gminlist[index],gminlist[changelist
        ↪  [index]]]
        mueminmax[index]=[mueminlist[index],mueminlist[change
        ↪  list[index]]]
        Alayer[index]=Aminlist[index]
        Zlayer[index]=Zminlist[index]
        Nlayer[index]=Nminlist[index]
        ZoverAlayer[index]=ZoverA[index]

    elif index==len(changelist):
        pressminmax[index]=[presslist[changelist[index-1]+1],
        ↪  presslist[-1]]
        nbminmax[index]=[nbminlist[changelist[index-1]+1],nbm
        ↪  inlist[-1]]
        etotminmax[index]=[etotminlist[changelist[index-1]+1]
        ↪  ,etotminlist[-1]]
        mubminmax[index]=[gminlist[changelist[index-1]+1],gmi
        ↪  nlist[-1]]
        mueminmax[index]=[mueminlist[changelist[index-1]+1],m
        ↪  ueminlist[-1]]
        Alayer[index]=Aminlist[changelist[index-1]+1]
        Zlayer[index]=Zminlist[changelist[index-1]+1]
        Nlayer[index]=Nminlist[changelist[index-1]+1]
        ZoverAlayer[index]=ZoverA[changelist[index-1]+1]

    else:
        pressminmax[index]=[presslist[changelist[index-1]+1],
                            presslist[changelist[index]]]
        nbminmax[index]=[nbminlist[changelist[index-1]+1],
```

```
                                nbminlist[changelist[index]]]
        etotminmax[index]=[etotminlist[changelist[index-1]+1],
                                etotminlist[changelist[index]]]
        mubminmax[index]=[gminlist[changelist[index-1]+1],
                                gminlist[changelist[index]]]
        mueminmax[index]=[mueminlist[changelist[index-1]+1],
                                mueminlist[changelist[index]]]
        Alayer[index]=Aminlist[changelist[index-1]+1]
        Zlayer[index]=Zminlist[changelist[index-1]+1]
        Nlayer[index]=Nminlist[changelist[index-1]+1]
        ZoverAlayer[index]=ZoverA[changelist[index-1]+1]

# plots and interpolations of the above data
plt.figure()
plt.loglog(nbminlist, presslist, 'b-', linewidth=1)
plt.grid()
plt.xlabel(r'Baryon number density [$fm^{-3}$]')
plt.ylabel(r'Pressure [$MeVfm^{-3}$]')
plt.title(rf'P vs $n_b$ (model: {model},
↪  $B_\star={Bstar:.1f}$)')
plt.show()
plt.savefig(f'Ptot_vs_nb_m{model}_f{field}.png')

plt.figure()
plt.loglog(etotminlist, presslist, 'b-', linewidth=1)
plt.grid()
plt.xlabel(r'Energy density [$MeVfm^{-3}$]')
plt.ylabel(r'Pressure [$MeVfm^{-3}$]')
plt.title(rf'P vs $\epsilon$ (model: {model},
↪  $B_\star={Bstar:.1f}$)')
plt.show()
plt.savefig(f'Ptot_vs_etot_m{model}_f{field}.png')

plt.figure()
plt.loglog(etotminlist, shearlist, 'b-', linewidth=1)
plt.grid()
plt.xlabel(r'Energy density [$MeVfm^{-3}$]')
plt.ylabel(r'Effective shear modulus [$MeVfm^{-3}$]')
plt.title(rf'S (shear modulus) vs $\epsilon$ (model: {model},
↪  $B_\star={Bstar:.1f}$)')
plt.show()
```

```
plt.savefig(f'S_vs_etot_m{model}_f{field}.png')

plt.figure()
plt.loglog(nbminlist, shearlist, 'b-', linewidth=1)
plt.grid()
plt.xlabel(r'Baryon number density [$fm^{-3}$]')
plt.ylabel(r'Effective shear modulus [$MeVfm^{-3}$]')
plt.title(rf'S (shear modulus) vs $n_b$ (model: {model}, $B_\star={Bstar:.1f}$)')
plt.show()
plt.savefig(f'S_vs_nb_m{model}_f{field}.png')

plt.figure()
plt.semilogx(nbminlist, gamma, 'b-', linewidth=1)
if Bstar>1304:
    plt.ylim(1.5, 3.5)
plt.grid()
plt.xlabel(r'Baryon number density [$fm^{-3}$]')
plt.ylabel(r'Adiabatic index')
plt.title(rf'$\Gamma$ vs $n_b$ (model: {model}, $B_\star={Bstar:.1f}$)')
plt.axhline (y=4/3, color='red', linestyle='--', linewidth=1)
plt.show()
plt.savefig(f'Gamma_vs_nb_m{model}_f{field}.png')

plt.figure()
plt.semilogx(etotminlist, gamma, 'b-', linewidth=1)
if Bstar>1304:
    plt.ylim(1.5, 3.5)
plt.grid()
plt.xlabel(r'Energy density [$MeVfm^{-3}$]')
plt.ylabel(r'Adiabatic index')
plt.title(rf'$\Gamma$ vs $\epsilon$ (model: {model}, $B_\star={Bstar:.1f}$)')
plt.axhline (y=4/3, color='red', linestyle='--', linewidth=1)
plt.show()
plt.savefig(f'Gamma_vs_etot_m{model}_f{field}.png')

plt.figure()
plt.semilogx(nbminlist, soundspeed, 'b-', linewidth=1)
plt.grid()
```

```
plt.xlabel(r'Baryon number density [$fm^{-3}$]')
plt.ylabel(r'Speed of sound [c]')
plt.title(rf'$c_s/c$ vs $n_b$ (model: {model}, $B_\star={Bstar:.1f}$)')
plt.show()
plt.savefig(f'speed_vs_nb_m{model}_f{field}.png')

plt.figure()
plt.semilogx(etotminlist, soundspeed, 'b-', linewidth=1)
plt.grid()
plt.xlabel(r'Energy density [$MeVfm^{-3}$]')
plt.ylabel(r'Speed of sound [c]')
plt.title(rf'$c_s/c$ vs $\epsilon$ (model: {model}, $B_\star={Bstar:.1f}$)')
plt.show()
plt.savefig(f'speed_vs_etot_m{model}_f{field}.png')

plt.figure()
plt.loglog(etotminlist, compression, 'b-', linewidth=1)
plt.grid()
plt.xlabel(r'Energy density [$MeVfm^{-3}$]')
plt.ylabel(r'Compression modulus [$MeVfm^{-3}$]')
plt.title(rf'$K$ (compression modulus) vs $\epsilon$ (model: {model}, $B_\star={Bstar:.1f}$)')
plt.show()
plt.savefig(f'compression_vs_etot_m{model}_f{field}.png')

plt.figure()
plt.loglog(nbminlist, compression, 'b-', linewidth=1)
plt.grid()
plt.xlabel(r'Baryon number density [$fm^{-3}$]')
plt.ylabel(r'Compression modulus [$MeVfm^{-3}$]')
plt.title(rf'$K$ (compression modulus) vs $n_b$ (model: {model}, $B_\star={Bstar:.1f}$)')
plt.show()
plt.savefig(f'compression_vs_nb_m{model}_f{field}.png')

plt.figure()
plt.semilogx(nbminlist, shearlist/compression, 'b-', linewidth=1)
plt.grid()
```

```
plt.xlabel(r'Baryon number density [$fm^{-3}$]')
plt.ylabel(r'$\frac{shear}{compression}$')
plt.title(rf'S/K vs $n_b$ (model: {model},
↪  $B_\star={Bstar:.1f}$)')
plt.show()
plt.savefig(f'SK_vs_nb_m{model}_f{field}.png')

plt.figure()
plt.semilogx(etotminlist, shearlist/compression, 'b-',
↪  linewidth=1)
plt.grid()
plt.xlabel(r'Energy density [$MeVfm^{-3}$]')
plt.ylabel(r'$\frac{shear}{compression}$')
plt.title(rf'S/K vs $\epsilon$ (model: {model},
↪  $B_\star={Bstar:.1f}$)')
plt.show()
plt.savefig(f'SK_vs_etot_m{model}_f{field}.png')

plt.figure(figsize=(8,6))
plt.suptitle(rf'model: {model}, $B_\star={Bstar:.1f}$')
plt.subplot(3,1,1)
plt.semilogx(nbminlist, Zminlist, 'b-', linewidth=1)
plt.grid()
plt.ylabel(r'Z')
plt.subplot(3,1,2)
plt.semilogx(nbminlist, Nminlist, 'r-', linewidth=1)
plt.grid()
plt.ylabel(r'N')
plt.subplot(3,1,3)
plt.semilogx(nbminlist, ZoverA, 'g-', linewidth=1)
plt.grid()
plt.xlabel(r'Baryon number density [$fm^{-3}$]')
plt.ylabel(r'Z/A')
plt.show()
plt.savefig(f'Z_N_ZoverA_vs_nb_m{model}_f{field}.png')

plt.figure(figsize=(8,6))
plt.suptitle(rf'model: {model}, $B_\star={Bstar:.1f}$')
plt.subplot(3,1,1)
plt.semilogx(etotminlist, Zminlist, 'b-', linewidth=1)
plt.grid()
```

```
plt.ylabel(r'Z')
plt.subplot(3,1,2)
plt.semilogx(etotminlist, Nminlist, 'r-', linewidth=1)
plt.grid()
plt.ylabel(r'N')
plt.subplot(3,1,3)
plt.semilogx(etotminlist, ZoverA, 'g-', linewidth=1)
plt.grid()
plt.xlabel(r'Energy density [$MeVfm^{-3}$]')
plt.ylabel(r'Z/A')
plt.show()
plt.savefig(f'Z_N_ZoverA_vs_etot_m{model}_f{field}.png')

# fitting Ptot=Ptot(etot)
def fitfun(x,K,G):

    '''
    a simple polytropic EoS for fitting

    '''
    return K*x**G

parameters=sp.optimize.curve_fit(fitfun, etotminlist, presslist, method='lm')[0]

plt.figure()
plt.loglog(etotminlist, presslist, 'bo', markersize=2, label='Data')
plt.loglog(etotminlist, fitfun(etotminlist, *parameters),
           'r-', linewidth=2, label=f'fitted curve\n K={parameters[0]:.4f}\n G={parameters[1]:.4f}')
plt.grid()
plt.xlabel(r'Energy density [$MeVfm^{-3}$]')
plt.ylabel(r'Pressure [$MeVfm^{-3}$]')
plt.legend()
plt.title(rf'fitting curve: $P=K\epsilon^G$ (model: {model}, $B_\star={Bstar:.1f}$)')
plt.show()
plt.savefig(f'polytropicEOSfit_m{model}_f{field}.png')

```

```
# interpolation Ptot=Ptot(etot)
Ptot_interp=sp.interpolate.interp1d(etotminlist, presslist, kind='linear',
                                    bounds_error=False, fill_value=(presslist[0], presslist[-1]))
etotlistnew=np.logspace(np.log10(etotminlist[0]), np.log10(etotminlist[-1]),
                        25000, dtype=np.float64)
plt.figure()
plt.loglog(etotminlist, presslist, 'bo', markersize=2, label='Data')
plt.loglog(etotlistnew, Ptot_interp(etotlistnew), 'r-', linewidth=2, label='Interpolated function')
plt.grid()
plt.legend()
plt.xlabel(r'Energy density [$MeVfm^{-3}$]')
plt.ylabel(r'Pressure [$MeVfm^{-3}$]')
plt.title(rf'P vs $\epsilon$ (model: {model}, $B_\star={Bstar:.1f}$)')
plt.show()
plt.savefig(f'Interpolated_function_Ptot_interp_m{model}_f{field}.png')

# interpolation etot=etot(Ptot)
etot_interp=sp.interpolate.interp1d(presslist, etotminlist, kind='linear',
                                    bounds_error=False, fill_value=(etotminlist[0], etotminlist[-1]))
presslistnew=np.logspace(np.log10(presslist[0]), np.log10(presslist[-1]),
                         25000, dtype=np.float64)
plt.figure()
plt.loglog(presslist, etotminlist, 'bo', markersize=2, label='Data')
plt.loglog(presslistnew, etot_interp(presslistnew), 'r-', linewidth=2, label='Interpolated function')
plt.grid()
plt.legend()
```

```
plt.xlabel(r'Pressure [$MeVfm^{-3}$]')
plt.ylabel(r'Energy density [$MeVfm^{-3}$]')
plt.title(rf'$\epsilon$ vs P (model: {model}, $B_\star={Bstar:.1f}$)')
plt.show()
plt.savefig(f'Interpolated_function_etot_interp_m{model}_f{field}.png')

# general relativity - TOV equations
# convert units in powers of km (Geometrized unit system)
MSOLARgeom=1.4766 # solar mass in km
presslistgeom=MeV_fm3to_km2*presslist # pressure in km**(-2)
etotminlistgeom=MeV_fm3to_km2*etotminlist # energy density in km**(-2)
etotminmaxgeom=MeV_fm3to_km2*etotminmax

# interpolation etot=etot(Ptot), now in Geometrized unit system
etotgeom_interp=sp.interpolate.interp1d(presslistgeom, etotminlistgeom, kind='linear',
                                        bounds_error=False, fill_value=(etotminlistgeom[0], etotminlistgeom[-1]))

# TOV equations
def dm_dr(r,p):

    return 4*np.pi*r**2*etotgeom_interp(p)

def dp_dr(r,m,p):

    return -(((p+etotgeom_interp(p))*(m+4*np.pi*r**3*p))/(r*(r-2*m)))

# function for baryonic mass
def DMb(r, farg1, farg2):

    return 4*np.pi*r**2*farg1(r)*(1-2*farg2(r)/r)**(-1/2)

```

```
# function for proper depth
def Dz(r, farg):

    return (1-2*farg(r)/r)**(-1/2)

# total grav. mass M in solar mass unit, total radius R in km, h step in km
def tovresults(M, R, choice=False, h=-2e-6, tolerance=1e-15):

    '''
    RK4 method for the solution of TOV equations

    '''
    rlist=np.zeros((int(R/(2*abs(h)))), dtype=np.float64)
    mlist=np.zeros((int(R/(2*abs(h)))), dtype=np.float64)
    plist=np.zeros((int(R/(2*abs(h)))), dtype=np.float64)

    rlist[0]=R
    mlist[0]=M*MSOLARgeom
    plist[0]=presslistgeom[0]

    for j in range(1,len(rlist)):

        k1=h*dm_dr(rlist[j-1], plist[j-1])
        k2=h*dp_dr(rlist[j-1], mlist[j-1], plist[j-1])
        s1=h*dm_dr(rlist[j-1]+h/2, plist[j-1]+k2/2)
        s2=h*dp_dr(rlist[j-1]+h/2, mlist[j-1]+k1/2, plist[j-1]+k2/2)
        l1=h*dm_dr(rlist[j-1]+h/2, plist[j-1]+s2/2)
        l2=h*dp_dr(rlist[j-1]+h/2, mlist[j-1]+s1/2, plist[j-1]+s2/2)
        p1=h*dm_dr(rlist[j-1]+h, plist[j-1]+l2)
        p2=h*dp_dr(rlist[j-1]+h, mlist[j-1]+l1, plist[j-1]+l2)

        mlist[j]=mlist[j-1]+(k1+2*s1+2*l1+p1)/6
        plist[j]=plist[j-1]+(k2+2*s2+2*l2+p2)/6
        rlist[j]=rlist[j-1]+h

        if presslistgeom[-1]-plist[j] < tolerance:
            break

```

```
    mlist=mlist[:j+1]
    plist=plist[:j+1]
    rlist=rlist[:j+1]

    etotlist=etotgeom_interp(plist)

    etotgeomfromr_interp=sp.interpolate.interp1d(rlist, etotlist, kind='linear',
                                                 bounds_error=False, fill_value=(etotlist[-1], etotlist[0]))
    mgeomfromr_interp=sp.interpolate.interp1d(rlist, mlist, kind='linear',
                                              bounds_error=False, fill_value=(mlist[-1], mlist[0]))
    rgeomfrometot_interp=sp.interpolate.interp1d(etotlist, rlist, kind='linear',
                                                 bounds_error=False, fill_value=(rlist[0], rlist[-1]))

    Mcr=(mlist[0]-mlist[-1])/MSOLARgeom # mass of outer crust in solar mass unit
    Mcr_M=Mcr/M # fractional mass of outer crust
    DRcr=rlist[0]-rlist[-1] # coordinate thickness of outer crust in km
```

```
    DRcr_R=DRcr/R # fractional coordinate thickness of outer crust

    # baryonic mass of outer crust in solar mass unit
    Mbcr=(sp.integrate.quad(DMb, rlist[-1], rlist[0], limit=8000,
                            args=(etotgeomfromr_interp, mgeomfromr_interp))[0])/MSOL, ARgeom

    # relative fraction of outer crust's mass due to gravitational binding energy
    gravbe=(Mbcr-Mcr)/(Mcr)

    # proper depth of drip point in km
    zdrip=sp.integrate.quad(Dz, rlist[-1], rlist[0], limit=8000, args=(mgeomfromr_interp))[0]

    # total number of baryons in outer crust
    DN=(Mbcr)/(Mn*MeV_c2toMsolar)

    # now for each layer, defined by etotmin-etotmax
    if choice==True:

        rminmax=np.zeros((len(changelist)+1, 2), dtype=np.float64) # in km
        DRlayer=np.zeros((len(changelist)+1, 1), dtype=np.float64) # in km
        DRlayer_DRcr=np.zeros((len(changelist)+1, 1), dtype=np.float64)
        zlayer=np.zeros((len(changelist)+1, 1), dtype=np.float64) # in km
        zlayer_zdrip=np.zeros((len(changelist)+1, 1), dtype=np.float64)
        Mblayer_Mbcr=np.zeros((len(changelist)+1, 1), dtype=np.float64)
        Mlayer_Mcr=np.zeros((len(changelist)+1, 1), dtype=np.float64)
        Mblayer=np.zeros((len(changelist)+1, 1), dtype=np.float64) # in solar mass unit
```

```
        Mlayer=np.zeros((len(changelist)+1, 1), dtype=np.float64) # in solar mass unit
        DNlayer=np.zeros((len(changelist)+1, 1), dtype=np.float64)
        DNlayer_DN=np.zeros((len(changelist)+1, 1), dtype=np.float64)

        for index in range(len(etotminmaxgeom)):

            rminmax[index]=[rgeomfrometot_interp(etotminmaxgeom[index][1]),
                            rgeomfrometot_interp(etotminmaxgeom[index][0])]
            DRlayer[index]=rminmax[index][1]-rminmax[index][0]
            DRlayer_DRcr[index]=DRlayer[index]/DRcr
            zlayer[index]=sp.integrate.quad(Dz, rminmax[index][0],
                                            rlist[0], limit=8000, args=(mgeomfromr_interp))[0]
            zlayer_zdrip[index]=zlayer[index]/zdrip
            Mblayer[index]=(sp.integrate.quad(DMb, rminmax[index][0],
                                              rminmax[index][1], limit=8000, args=(etotgeomfromr_interp), mgeomfromr_interp))[0])/MSOLARgeom
            Mblayer_Mbcr[index]=Mblayer[index]/Mbcr
            Mlayer[index]=(mgeomfromr_interp(rminmax[index][1])-mgeomfromr_interp(rminmax[index][0]))/MSOLARgeom
            Mlayer_Mcr[index]=Mlayer[index]/Mcr
            DNlayer[index]=(Mblayer[index])/(Mn*MeV_c2toMsolar)
            DNlayer_DN[index]=DNlayer[index]/DN
```

```python

        return rminmax, DRlayer, DRlayer_DRcr, zlayer, zlayer_zdrip, Mblayer, Mblayer_Mbcr, Mlayer, Mlayer_Mcr, DNlayer, DNlayer_DN

    return Mcr, Mcr_M, DRcr, DRcr_R, Mbcr, gravbe, zdrip, DN

# unpack for choice==False, for a typical NS
Mtyp, Rtyp = 1.4, 12.5
Mtyps, Rtyps =  (f'{Mtyp:.2f}').replace(".", "_"), (f'{Rtyp:.2f}').replace(".", "_")

Mcr, Mcr_M, DRcr, DRcr_R, Mbcr, gravbe, zdrip, DN = tovresults(Mtyp, Rtyp)
print(f'nuclear model: {model}\nmagnetic field: {Bstar:.1f} (in critical field unit)\nfor M={Mtyp:.2f} (in solar mass unit) and R={Rtyp:.2f}km:\n\tMcr={Mcr:.3e}\n\tMcr_M={Mcr_M:.3e}\n\tDRcr={DRcr:.3e}\n\tDRcr_R={DRcr_R:.3e}\n\tMbcr={Mbcr:.3e}\n\tgravbe={gravbe:.3e}\n\tzdrip={zdrip:.3e}\n\tDN={DN:.3e}')
# unpack for choice==True, for a typical NS
rminmax, DRlayer, DRlayer_DRcr, zlayer, zlayer_zdrip, Mblayer, Mblayer_Mbcr, Mlayer, Mlayer_Mcr, DNlayer, DNlayer_DN = tovresults(Mtyp, Rtyp, choice=True)

# plots from TOV equations
Mlist=np.array([1.2, 1.4, 1.6])
Rlist=np.array([10.0, 12.0, 14.0])

Mcr1_2=np.zeros(len(Rlist), dtype=np.float64)
Mcr1_4=np.zeros(len(Rlist), dtype=np.float64)
Mcr1_6=np.zeros(len(Rlist), dtype=np.float64)

zdrip1_2=np.zeros(len(Rlist), dtype=np.float64)
zdrip1_4=np.zeros(len(Rlist), dtype=np.float64)
zdrip1_6=np.zeros(len(Rlist), dtype=np.float64)

for index in range(len(Rlist)):

    result=tovresults(Mlist[0], Rlist[index])
    Mcr1_2[index]=result[0]
```

```
    zdrip1_2[index]=result[6]

    result=tovresults(Mlist[1], Rlist[index])
    Mcr1_4[index]=result[0]
    zdrip1_4[index]=result[6]

    result=tovresults(Mlist[2], Rlist[index])
    Mcr1_6[index]=result[0]
    zdrip1_6[index]=result[6]

del result

plt.figure()
plt.plot(Rlist, Mcr1_2, 'o-b', label=r'M=1.2$M_{\odot}$')
plt.plot(Rlist, Mcr1_4, 'o-r', label=r'M=1.4$M_{\odot}$')
plt.plot(Rlist, Mcr1_6, 'o-g', label=r'M=1.6$M_{\odot}$')
plt.ticklabel_format(axis='y', style='sci', scilimits=(0, 0))
plt.grid()
plt.legend()
plt.xlabel(r'Total radius of NS [km]')
plt.ylabel(r'Grav. mass of outer crust [$M_{\odot}$]')
plt.title(rf'Mcr vs R (model: {model},
↪  $B_\star={Bstar:.1f}$)')
plt.show()
plt.savefig(f'Mcr_m{model}_f{field}.png')

plt.figure()
plt.plot(Rlist, zdrip1_2, 'o-b', label=r'M=1.2$M_{\odot}$')
plt.plot(Rlist, zdrip1_4, 'o-r', label=r'M=1.4$M_{\odot}$')
plt.plot(Rlist, zdrip1_6, 'o-g', label=r'M=1.6$M_{\odot}$')
plt.grid()
plt.legend()
plt.xlabel(r'Total radius of NS [km]')
plt.ylabel(r'Proper thickness of outer crust [km]')
plt.title(rf'$z_d$ vs R (model: {model},
↪  $B_\star={Bstar:.1f}$)')
plt.show()
plt.savefig(f'zdrip_m{model}_f{field}.png')

# save useful data arrays as txt files or as .npy files

```

```
def format_column(dataframe, column, fmt):

    '''
    return the desired float format for each column

    '''

    dataframe[column]=dataframe[column].astype(str).apply(lambda x: format(float(x), fmt))

    return dataframe

df1=pd.DataFrame(np.c_[presslist, etotminlist, nbminlist, Aminlist, Zminlist,
                       Nminlist, ZoverA, gminlist, mueminlist, xeminlist, geminlist],
                columns=['Ptot[MeVfm**(-3)]', 'etot[MeVfm**(-3)]',
                         'nb[fm**(-3)]', 'A', 'Z', 'N', 'Z/A', 'mu_b[MeV]',
                         'mu_e[MeV]', 'xe', 'ge'])

df1=format_column(df1,'Ptot[MeVfm**(-3)]','.3e')
df1=format_column(df1,'etot[MeVfm**(-3)]','.3e')
df1=format_column(df1,'nb[fm**(-3)]','.3e')
df1=format_column(df1,'A','.0f')
df1=format_column(df1,'Z','.0f')
df1=format_column(df1,'N','.0f')
df1=format_column(df1,'Z/A','.3f')
df1=format_column(df1,'mu_b[MeV]','.3f')
df1=format_column(df1,'mu_e[MeV]','.3f')
df1=format_column(df1,'xe','.3f')
df1=format_column(df1,'ge','.3f')

df1.to_csv(f'eos_m{model}_f{field}.dat', index=False,
           header=True, sep='\t', na_rep='N/A', mode='w')

df2=pd.DataFrame(np.hstack((pressminmax, etotminmax, nbminmax, Alayer, Zlayer,
```

```
                                Nlayer, ZoverAlayer, mubminmax, mueminmax)),
                    columns=['Pmin[MeVfm**(-3)]', 'Pmax[MeVfm**(-3)]',
                             'etotmin[MeVfm**(-3)]', 'etotmax[MeVfm**(-3)]',
                             'nbmin[fm**(-3)]', 'nbmax[fm**(-3)]',
                             'A', 'Z', 'N', 'Z/A', 'mu_bmin[MeV]', 'mu_bmax[MeV]',
                             'mu_emin[MeV]', 'mu_emax[MeV]'])

df2=format_column(df2,'Pmin[MeVfm**(-3)]','.3e')
df2=format_column(df2,'Pmax[MeVfm**(-3)]','.3e')
df2=format_column(df2,'etotmin[MeVfm**(-3)]','.3e')
df2=format_column(df2,'etotmax[MeVfm**(-3)]','.3e')
df2=format_column(df2,'nbmin[fm**(-3)]','.3e')
df2=format_column(df2,'nbmax[fm**(-3)]','.3e')
df2=format_column(df2,'A','.0f')
df2=format_column(df2,'Z','.0f')
df2=format_column(df2,'N','.0f')
df2=format_column(df2,'Z/A','.3f')
df2=format_column(df2,'mu_bmin[MeV]','.3f')
df2=format_column(df2,'mu_bmax[MeV]','.3f')
df2=format_column(df2,'mu_emin[MeV]','.3f')
df2=format_column(df2,'mu_emax[MeV]','.3f')

df2.to_csv(f'layers_m{model}_f{field}.dat', index=False,
           header=True, sep='\t', na_rep='N/A', mode='w')


df3=pd.DataFrame(np.hstack((rminmax, DRlayer, DRlayer_DRcr, zlayer, zlayer_zdrip, Mblayer, Mblayer_Mbcr, Mlayer, Mlayer_Mcr, DNlayer, DNlayer_DN)),
                 columns=['rmin[km]', 'rmax[km]', 'DRlayer[km]', 'DRlayer_DRcr',
                          'zlayer[km]', 'zlayer_zdrip', 'Mblayer[solarmass]',
                          'Mblayer_Mbcr', 'Mlayer[solarmass]', 'Mlayer_Mcr',
```

```
                                'DNlayer', 'DNlayer_DN'])

df3=format_column(df3,'rmin[km]','.3f')
df3=format_column(df3,'rmax[km]','.3f')
df3=format_column(df3,'DRlayer[km]','.3e')
df3=format_column(df3,'DRlayer_DRcr','.3e')
df3=format_column(df3,'zlayer[km]','.3f')
df3=format_column(df3,'zlayer_zdrip','.3e')
df3=format_column(df3,'Mblayer[solarmass]','.3e')
df3=format_column(df3,'Mblayer_Mbcr','.3e')
df3=format_column(df3,'Mlayer[solarmass]','.3e')
df3=format_column(df3,'Mlayer_Mcr','.3e')
df3=format_column(df3,'DNlayer','.3e')
df3=format_column(df3,'DNlayer_DN','.3e')

df3.to_csv(f'layers_m{model}_f{field}_M{Mtyps}_R{Rtyps}.dat',
    index=False,
            header=True, sep='\t', na_rep='N/A', mode='w')

np.save(f'nbminlist_m{model}_f{field}.npy', nbminlist)
np.save(f'presslist_m{model}_f{field}.npy', presslist)
np.save(f'etotminlist_m{model}_f{field}.npy', etotminlist)
np.save(f'shearlist_m{model}_f{field}.npy', shearlist)
np.save(f'gamma_m{model}_f{field}.npy', gamma)
np.save(f'soundspeed_m{model}_f{field}.npy', soundspeed)
np.save(f'compression_m{model}_f{field}.npy', compression)
np.save(f'Zminlist_m{model}_f{field}.npy', Zminlist)
np.save(f'Nminlist_m{model}_f{field}.npy', Nminlist)
np.save(f'ZoverA_m{model}_f{field}.npy', ZoverA)
np.save(f'Rlist_m{model}_f{field}.npy', Rlist)
np.save(f'Mcr1_2_m{model}_f{field}.npy', Mcr1_2)
np.save(f'Mcr1_4_m{model}_f{field}.npy', Mcr1_4)
np.save(f'Mcr1_6_m{model}_f{field}.npy', Mcr1_6)
np.save(f'zdrip1_2_m{model}_f{field}.npy', zdrip1_2)
np.save(f'zdrip1_4_m{model}_f{field}.npy', zdrip1_4)
np.save(f'zdrip1_6_m{model}_f{field}.npy', zdrip1_6)
```

Appendix K

Code B

Below is an auxiliary code, written in *Python 3* programming language, which was used to create the mixed plots for this work.

```
import numpy as np
import matplotlib.pyplot as plt
import os

# load the .npy files with the saved numpy arrays
# Bstar=0,1500,2000,2500
Bstarlist=[0,1500,2000,2500]
# 'SEMF','FRDM2012','WS4RBF','BSKG3','HFB31','DDMED','DDPC1
↪  ','SVMIN','UNEDF0'
modellist=['SEMF','FRDM2012','WS4RBF','BSKG3','HFB31','DDMED'
↪  ,'DDPC1','SVMIN','UNEDF0']

def keyname(prefix, model, field):

    '''
    return a key of the dictionary data

    '''
    return f'{prefix}_m{model}_f{field}'

data={}

# read the .npy files and assign the value to variables
#having the same name as the filename without
#the extension .npy
```

```
for filename in os.listdir():
    if filename.endswith('.npy'):
        array=np.load(filename)
        key=filename[:-4]
        data[key]=array

del array, filename, key

# plot1
plt.figure()
for m in modellist:
    plt.plot(Bstarlist, [data[keyname('presslist',m,f)][-1] for f in Bstarlist],
                'o-', label=m)
plt.ticklabel_format(axis='y', style='sci', scilimits=(0, 0))
plt.grid()
plt.legend()
plt.xlabel(r'Magnetic field strength $B_{\star}$')
plt.ylabel(r'Pressure at neutron-drip transition [$MeVfm^{-3}$]')
plt.title(r'$P_{drip}$ vs $B_{\star}$')
plt.show()
plt.savefig('Pdrip_vs_Bstar.png')

# plot2, now for the same model, plot for all Bstar
for m in modellist:
    plt.figure()
    for f in Bstarlist:
        plt.loglog(data[keyname('nbminlist',m,f)],
                   data[keyname('presslist',m,f)], '-',
                   linewidth=1, label=rf'$B_*={f}')
    plt.grid()
    plt.legend()
    plt.xlabel(r'Baryon number density [$fm^{-3}$]')
    plt.ylabel(r'Pressure [$MeVfm^{-3}$]')
    plt.title(rf'P vs $n_b$ (model: {m})')
    plt.show()
    plt.savefig(f'Ptot_vs_nb_m{m}.png')

# now for the same Bstar, plot for all models
for f in Bstarlist:
```

```
    plt.figure()
    for m in modellist:
        plt.loglog(data[keyname('nbminlist',m,f)],
                   data[keyname('presslist',m,f)], '-',
                   linewidth=1, label=rf'model: {m}')
    plt.grid()
    plt.legend()
    plt.xlabel(r'Baryon number density [$fm^{-3}$]')
    plt.ylabel(r'Pressure [$MeVfm^{-3}$]')
    plt.title(rf'P vs $n_b$ ($B_*=${f})')
    plt.show()
    plt.savefig(f'Ptot_vs_nb_f{f}.png')

# plot3, now for the same model, plot for all Bstar
for m in modellist:
    plt.figure()
    for f in Bstarlist:
        plt.loglog(data[keyname('etotminlist',m,f)],
                   data[keyname('presslist',m,f)], '-',
                   linewidth=1, label=rf'$B_*=${f}')
    plt.grid()
    plt.legend()
    plt.xlabel(r'Energy density [$MeVfm^{-3}$]')
    plt.ylabel(r'Pressure [$MeVfm^{-3}$]')
    plt.title(rf'P vs $\epsilon$ (model: {m})')
    plt.show()
    plt.savefig(f'Ptot_vs_etot_m{m}.png')

# now for the same Bstar, plot for all models
for f in Bstarlist:
    plt.figure()
    for m in modellist:
        plt.loglog(data[keyname('etotminlist',m,f)],
                   data[keyname('presslist',m,f)], '-',
                   linewidth=1, label=rf'model: {m}')
    plt.grid()
    plt.legend()
    plt.xlabel(r'Energy density [$MeVfm^{-3}$]')
    plt.ylabel(r'Pressure [$MeVfm^{-3}$]')
    plt.title(rf'P vs $\epsilon$ ($B_*=${f})')
    plt.show()
```

```
    plt.savefig(f'Ptot_vs_etot_f{f}.png')

# plot4, now for the same model, plot for all Bstar
for m in modellist:
    plt.figure()
    for f in Bstarlist:
        plt.loglog(data[keyname('etotminlist',m,f)],
                   data[keyname('shearlist',m,f)], '-',
                   linewidth=1, label=rf'$B_*=${f}')
    plt.grid()
    plt.legend()
    plt.xlabel(r'Energy density [$MeVfm^{-3}$]')
    plt.ylabel(r'Effective shear modulus [$MeVfm^{-3}$]')
    plt.title(rf'S (shear modulus) vs $\epsilon$ (model: {m})')
    plt.show()
    plt.savefig(f'S_vs_etot_m{m}.png')

# now for the same Bstar, plot for all models
for f in Bstarlist:
    plt.figure()
    for m in modellist:
        plt.loglog(data[keyname('etotminlist',m,f)],
                   data[keyname('shearlist',m,f)], '-',
                   linewidth=1, label=rf'model: {m}')
    plt.grid()
    plt.legend()
    plt.xlabel(r'Energy density [$MeVfm^{-3}$]')
    plt.ylabel(r'Effective shear modulus [$MeVfm^{-3}$]')
    plt.title(rf'S (shear modulus) vs $\epsilon$ ($B_*=${f})')
    plt.show()
    plt.savefig(f'S_vs_etot_f{f}.png')

# plot5, now for the same model, plot for all Bstar
for m in modellist:
    plt.figure()
    for f in Bstarlist:
        plt.loglog(data[keyname('nbminlist',m,f)],
                   data[keyname('shearlist',m,f)], '-',
                   linewidth=1, label=rf'$B_*=${f}')
    plt.grid()
```

```
    plt.legend()
    plt.xlabel(r'Baryon number density [$fm^{-3}$]')
    plt.ylabel(r'Effective shear modulus [$MeVfm^{-3}$]')
    plt.title(rf'S (shear modulus) vs $n_b$ (model: {m})')
    plt.show()
    plt.savefig(f'S_vs_nb_m{m}.png')

# now for the same Bstar, plot for all models
for f in Bstarlist:
    plt.figure()
    for m in modellist:
        plt.loglog(data[keyname('nbminlist',m,f)],
                   data[keyname('shearlist',m,f)], '-',
                   linewidth=1, label=rf'model: {m}')
    plt.grid()
    plt.legend()
    plt.xlabel(r'Baryon number density [$fm^{-3}$]')
    plt.ylabel(r'Effective shear modulus [$MeVfm^{-3}$]')
    plt.title(rf'S (shear modulus) vs $n_b$ ($B_*=${f})')
    plt.show()
    plt.savefig(f'S_vs_nb_f{f}.png')

# plot6, now for the same model, plot for all Bstar
for m in modellist:
    plt.figure()
    for f in Bstarlist:
        plt.semilogx(data[keyname('nbminlist',m,f)],
                   data[keyname('gamma',m,f)], '-',
                   linewidth=1, label=rf'$B_*=${f}')
        if f>1304:
            plt.ylim(1, 3.5)
    plt.grid()
    plt.axhline (y=4/3, color='black', linestyle='--',
    ↪  linewidth=1)
    plt.legend()
    plt.xlabel(r'Baryon number density [$fm^{-3}$]')
    plt.ylabel(r'Adiabatic index')
    plt.title(rf'$\Gamma$ vs $n_b$ (model: {m})')
    plt.show()
    plt.savefig(f'Gamma_vs_nb_m{m}.png')

```

```
# now for the same Bstar, plot for all models
for f in Bstarlist:
    plt.figure()
    for m in modellist:
        plt.semilogx(data[keyname('nbminlist',m,f)],
                    data[keyname('gamma',m,f)], '-',
                    linewidth=1, label=rf'model: {m}')
        if f>1304:
            plt.ylim(1.5, 3.5)
    plt.grid()
    plt.axhline (y=4/3, color='black', linestyle='--',
    ↪  linewidth=1)
    plt.legend()
    plt.xlabel(r'Baryon number density [$fm^{-3}$]')
    plt.ylabel(r'Adiabatic index')
    plt.title(rf'$\Gamma$ vs $n_b$ ($B_*=${f})')
    plt.show()
    plt.savefig(f'Gamma_vs_nb_f{f}.png')

# plot7, now for the same model, plot for all Bstar
for m in modellist:
    plt.figure()
    for f in Bstarlist:
        plt.semilogx(data[keyname('etotminlist',m,f)],
                    data[keyname('gamma',m,f)], '-',
                    linewidth=1, label=rf'$B_*=${f}')
        if f>1304:
            plt.ylim(1, 3.5)
    plt.grid()
    plt.axhline (y=4/3, color='black', linestyle='--',
    ↪  linewidth=1)
    plt.legend()
    plt.xlabel(r'Energy density [$MeVfm^{-3}$]')
    plt.ylabel(r'Adiabatic index')
    plt.title(rf'$\Gamma$ vs $\epsilon$ (model: {m})')
    plt.show()
    plt.savefig(f'Gamma_vs_etot_m{m}.png')

# now for the same Bstar, plot for all models
for f in Bstarlist:
    plt.figure()
```

```
    for m in modellist:
        plt.semilogx(data[keyname('etotminlist',m,f)],
                    data[keyname('gamma',m,f)], '-',
                    linewidth=1, label=rf'model: {m}')
        if f>1304:
            plt.ylim(1.5, 3.5)
    plt.grid()
    plt.axhline (y=4/3, color='black', linestyle='--',
    ↪  linewidth=1)
    plt.legend()
    plt.xlabel(r'Energy density [$MeVfm^{-3}$]')
    plt.ylabel(r'Adiabatic index')
    plt.title(rf'$\Gamma$ vs $\epsilon$ ($B_*=${f})')
    plt.show()
    plt.savefig(f'Gamma_vs_etot_f{f}.png')

# plot8, now for the same model, plot for all Bstar
for m in modellist:
    plt.figure()
    for f in Bstarlist:
        plt.semilogx(data[keyname('nbminlist',m,f)],
                    data[keyname('soundspeed',m,f)], '-',
                    linewidth=1, label=rf'$B_*=${f}')
    plt.grid()
    plt.legend()
    plt.xlabel(r'Baryon number density [$fm^{-3}$]')
    plt.ylabel(r'Speed of sound [c]')
    plt.title(rf'$c_s/c$ vs $n_b$ (model: {m})')
    plt.show()
    plt.savefig(f'speed_vs_nb_m{m}.png')

# now for the same Bstar, plot for all models
for f in Bstarlist:
    plt.figure()
    for m in modellist:
        plt.semilogx(data[keyname('nbminlist',m,f)],
                    data[keyname('soundspeed',m,f)], '-',
                    linewidth=1, label=rf'model: {m}')
    plt.grid()
    plt.legend()
    plt.xlabel(r'Baryon number density [$fm^{-3}$]')
```

```
    plt.ylabel(r'Speed of sound [c]')
    plt.title(rf'$c_s/c$ vs $n_b$ ($B_*=${f})')
    plt.show()
    plt.savefig(f'speed_vs_nb_f{f}.png')

# plot9, now for the same model, plot for all Bstar
for m in modellist:
    plt.figure()
    for f in Bstarlist:
        plt.semilogx(data[keyname('etotminlist',m,f)],
                     data[keyname('soundspeed',m,f)], '-',
                     linewidth=1, label=rf'$B_*=${f}')
    plt.grid()
    plt.legend()
    plt.xlabel(r'Energy density [$MeVfm^{-3}$]')
    plt.ylabel(r'Speed of sound [c]')
    plt.title(rf'$c_s/c$ vs $\epsilon$ (model: {m})')
    plt.show()
    plt.savefig(f'speed_vs_etot_m{m}.png')

# now for the same Bstar, plot for all models
for f in Bstarlist:
    plt.figure()
    for m in modellist:
        plt.semilogx(data[keyname('etotminlist',m,f)],
                     data[keyname('soundspeed',m,f)], '-',
                     linewidth=1, label=rf'model: {m}')
    plt.grid()
    plt.legend()
    plt.xlabel(r'Energy density [$MeVfm^{-3}$]')
    plt.ylabel(r'Speed of sound [c]')
    plt.title(rf'$c_s/c$ vs $\epsilon$ ($B_*=${f})')
    plt.show()
    plt.savefig(f'speed_vs_etot_f{f}.png')

# plot10, now for the same model, plot for all Bstar
for m in modellist:
    plt.figure()
    for f in Bstarlist:
        plt.loglog(data[keyname('etotminlist',m,f)],
                     data[keyname('compression',m,f)], '-',
```

```
                    linewidth=1, label=rf'$B_*=${f}')
    plt.grid()
    plt.legend()
    plt.xlabel(r'Energy density [$MeVfm^{-3}$]')
    plt.ylabel(r'Compression modulus [$MeVfm^{-3}$]')
    plt.title(rf'$K$ (compression modulus) vs $\epsilon$ (model: {m})')
    plt.show()
    plt.savefig(f'compression_vs_etot_m{m}.png')

# now for the same Bstar, plot for all models
for f in Bstarlist:
    plt.figure()
    for m in modellist:
        plt.loglog(data[keyname('etotminlist',m,f)],
                    data[keyname('compression',m,f)], '-',
                    linewidth=1, label=rf'model: {m}')
    plt.grid()
    plt.legend()
    plt.xlabel(r'Energy density [$MeVfm^{-3}$]')
    plt.ylabel(r'Compression modulus [$MeVfm^{-3}$]')
    plt.title(rf'$K$ (compression modulus) vs $\epsilon$ ($B_*=${f})')
    plt.show()
    plt.savefig(f'compression_vs_etot_f{f}.png')

# plot11, now for the same model, plot for all Bstar
for m in modellist:
    plt.figure()
    for f in Bstarlist:
        plt.loglog(data[keyname('nbminlist',m,f)],
                    data[keyname('compression',m,f)], '-',
                    linewidth=1, label=rf'$B_*=${f}')
    plt.grid()
    plt.legend()
    plt.xlabel(r'Baryon number density [$fm^{-3}$]')
    plt.ylabel(r'Compression modulus [$MeVfm^{-3}$]')
    plt.title(rf'$K$ (compression modulus) vs $n_b$ (model: {m})')
    plt.show()
    plt.savefig(f'compression_vs_nb_m{m}.png')
```

```python

# now for the same Bstar, plot for all models
for f in Bstarlist:
    plt.figure()
    for m in modellist:
        plt.loglog(data[keyname('nbminlist',m,f)],
                   data[keyname('compression',m,f)], '-',
                   linewidth=1, label=rf'model: {m}')
    plt.grid()
    plt.legend()
    plt.xlabel(r'Baryon number density [$fm^{-3}$]')
    plt.ylabel(r'Compression modulus [$MeVfm^{-3}$]')
    plt.title(rf'$K$ (compression modulus) vs $n_b$ ($B_*=${f})')
    plt.show()
    plt.savefig(f'compression_vs_nb_f{f}.png')

# plot12, now for the same model, plot for all Bstar
for m in modellist:
    plt.figure()
    for f in Bstarlist:
        plt.semilogx(data[keyname('nbminlist',m,f)],
                   data[keyname('shearlist',m,f)]/data[keyname('compression',m,f)], '-',
                   linewidth=1, label=rf'$B_*=${f}')
    plt.grid()
    plt.legend()
    plt.xlabel(r'Baryon number density [$fm^{-3}$]')
    plt.ylabel(r'$\frac{shear}{compression}$')
    plt.title(rf'S/K vs $n_b$ (model: {m})')
    plt.show()
    plt.savefig(f'SK_vs_nb_m{m}.png')

# now for the same Bstar, plot for all models
for f in Bstarlist:
    plt.figure()
    for m in modellist:
        plt.semilogx(data[keyname('nbminlist',m,f)],
```

```
                    data[keyname('shearlist',m,f)]/data[keynam
                    ↪  e('compression',m,f)],
                    ↪  '-',
                    linewidth=1, label=rf'model: {m}')
    plt.grid()
    plt.legend()
    plt.xlabel(r'Baryon number density [$fm^{-3}$]')
    plt.ylabel(r'$\frac{shear}{compression}$')
    plt.title(rf'S/K vs $n_b$ ($B_*={f})')
    plt.show()
    plt.savefig(f'SK_vs_nb_f{f}.png')

# plot13, now for the same model, plot for all Bstar
for m in modellist:
    plt.figure()
    for f in Bstarlist:
        plt.semilogx(data[keyname('etotminlist',m,f)],
                    data[keyname('shearlist',m,f)]/data[keynam
                    ↪  e('compression',m,f)],
                    ↪  '-',
                    linewidth=1, label=rf'$B_*={f}')
    plt.grid()
    plt.legend()
    plt.xlabel(r'Energy density [$MeVfm^{-3}$]')
    plt.ylabel(r'$\frac{shear}{compression}$')
    plt.title(rf'S/K vs $\epsilon$ (model: {m})')
    plt.show()
    plt.savefig(f'SK_vs_etot_m{m}.png')

# now for the same Bstar, plot for all models
for f in Bstarlist:
    plt.figure()
    for m in modellist:
        plt.semilogx(data[keyname('etotminlist',m,f)],
                    data[keyname('shearlist',m,f)]/data[keynam
                    ↪  e('compression',m,f)],
                    ↪  '-',
                    linewidth=1, label=rf'model: {m}')
    plt.grid()
    plt.legend()
    plt.xlabel(r'Energy density [$MeVfm^{-3}$]')
```

```
    plt.ylabel(r'$\frac{shear}{compression}$')
    plt.title(rf'S/K vs $\epsilon$ ($B_*={f})')
    plt.show()
    plt.savefig(f'SK_vs_etot_f{f}.png')

# plot14, now for the same model, plot for all Bstar
for m in modellist:
    plt.figure(figsize=(8,6))
    plt.suptitle(rf'model: {m}')
    plt.subplot(3,1,1)
    for f in Bstarlist:
        plt.semilogx(data[keyname('nbminlist',m,f)],
                     data[keyname('Zminlist',m,f)], '-',
                     linewidth=1, label=rf'$B_*={f}')
    plt.ylabel(r'Z')
    plt.grid()
    plt.legend()
    plt.subplot(3,1,2)
    for f in Bstarlist:
        plt.semilogx(data[keyname('nbminlist',m,f)],
                     data[keyname('Nminlist',m,f)], '-',
                     linewidth=1, label=rf'$B_*={f}')
    plt.ylabel(r'N')
    plt.grid()
    plt.legend()
    plt.subplot(3,1,3)
    for f in Bstarlist:
        plt.semilogx(data[keyname('nbminlist',m,f)],
                     data[keyname('ZoverA',m,f)], '-',
                     linewidth=1, label=rf'$B_*={f}')
    plt.xlabel(r'Baryon number density [$fm^{-3}$]')
    plt.ylabel(r'Z/A')
    plt.grid()
    plt.legend()
    plt.show()
    plt.savefig(f'Z_N_ZoverA_vs_nb_m{m}.png')

# now for the same Bstar, plot for all models
for f in Bstarlist:
    plt.figure(figsize=(8,6))
    plt.suptitle(rf'$B_*={f}')
```

```
    plt.subplot(3,1,1)
    for m in modellist:
        plt.semilogx(data[keyname('nbminlist',m,f)],
                     data[keyname('Zminlist',m,f)], '-',
                     linewidth=1, label=rf'model: {m}')
    plt.ylabel(r'Z')
    plt.grid()
    plt.legend()
    plt.subplot(3,1,2)
    for m in modellist:
        plt.semilogx(data[keyname('nbminlist',m,f)],
                     data[keyname('Nminlist',m,f)], '-',
                     linewidth=1, label=rf'model: {m}')
    plt.ylabel(r'N')
    plt.grid()
    plt.legend()
    plt.subplot(3,1,3)
    for m in modellist:
        plt.semilogx(data[keyname('nbminlist',m,f)],
                     data[keyname('ZoverA',m,f)], '-',
                     linewidth=1, label=rf'model: {m}')
    plt.xlabel(r'Baryon number density [$fm^{-3}$]')
    plt.ylabel(r'Z/A')
    plt.grid()
    plt.legend()
    plt.show()
    plt.savefig(f'Z_N_ZoverA_vs_nb_f{f}.png')

# plot15, now for the same model, plot for all Bstar
for m in modellist:
    plt.figure(figsize=(8,6))
    plt.suptitle(rf'model: {m}')
    plt.subplot(3,1,1)
    for f in Bstarlist:
        plt.semilogx(data[keyname('etotminlist',m,f)],
                     data[keyname('Zminlist',m,f)], '-',
                     linewidth=1, label=rf'$B_*=${f}')
    plt.ylabel(r'Z')
    plt.grid()
    plt.legend()
    plt.subplot(3,1,2)
```

```
    for f in Bstarlist:
        plt.semilogx(data[keyname('etotminlist',m,f)],
                     data[keyname('Nminlist',m,f)], '-',
                     linewidth=1, label=rf'$B_*=${f}')
    plt.ylabel(r'N')
    plt.grid()
    plt.legend()
    plt.subplot(3,1,3)
    for f in Bstarlist:
        plt.semilogx(data[keyname('etotminlist',m,f)],
                     data[keyname('ZoverA',m,f)], '-',
                     linewidth=1, label=rf'$B_*=${f}')
    plt.xlabel(r'Energy density [$MeVfm^{-3}$]')
    plt.ylabel(r'Z/A')
    plt.grid()
    plt.legend()
    plt.show()
    plt.savefig(f'Z_N_ZoverA_vs_etot_m{m}.png')

# now for the same Bstar, plot for all models
for f in Bstarlist:
    plt.figure(figsize=(8,6))
    plt.suptitle(rf'$B_*=${f}')
    plt.subplot(3,1,1)
    for m in modellist:
        plt.semilogx(data[keyname('etotminlist',m,f)],
                     data[keyname('Zminlist',m,f)], '-',
                     linewidth=1, label=rf'model: {m}')
    plt.ylabel(r'Z')
    plt.grid()
    plt.legend()
    plt.subplot(3,1,2)
    for m in modellist:
        plt.semilogx(data[keyname('etotminlist',m,f)],
                     data[keyname('Nminlist',m,f)], '-',
                     linewidth=1, label=rf'model: {m}')
    plt.ylabel(r'N')
    plt.grid()
    plt.legend()
    plt.subplot(3,1,3)
    for m in modellist:
```

```
        plt.semilogx(data[keyname('etotminlist',m,f)],
                     data[keyname('ZoverA',m,f)], '-',
                     linewidth=1, label=rf'model: {m}')
    plt.xlabel(r'Energy density [$MeVfm^{-3}$]')
    plt.ylabel(r'Z/A')
    plt.grid()
    plt.legend()
    plt.show()
    plt.savefig(f'Z_N_ZoverA_vs_etot_f{f}.png')

# plot16, now for the same model, plot for all Bstar
for m in modellist:
    plt.figure(figsize=(8,6))
    for f in Bstarlist:
        plt.plot(data[keyname('Rlist',m,f)],
        ↪  data[keyname('Mcr1_2',m,f)],
                     'o-', label=rf'M=1.2, $B_*=${f}')
        plt.plot(data[keyname('Rlist',m,f)],
        ↪  data[keyname('Mcr1_4',m,f)],
                 'o-', label=rf'M=1.4, $B_*=${f}')
        plt.plot(data[keyname('Rlist',m,f)],
        ↪  data[keyname('Mcr1_6',m,f)],
                 'o-', label=rf'M=1.6, $B_*=${f}')
    plt.ticklabel_format(axis='y', style='sci', scilimits=(0,
    ↪  0))
    plt.grid()
    plt.legend()
    plt.xlabel(r'Total radius of NS [km]')
    plt.ylabel(r'Grav. mass of outer crust [$M_{\odot}$]')
    plt.title(rf'Mcr vs R (model: {m})')
    plt.show()
    plt.savefig(f'Mcr_m{m}.png')

# now for the same Bstar, plot for all models
for f in Bstarlist:
    plt.figure(figsize=(8,6))
    for m in modellist:
        plt.plot(data[keyname('Rlist',m,f)],
        ↪  data[keyname('Mcr1_2',m,f)],
                     'o-', label=rf'M=1.2, model: {m}')
```

```
        plt.plot(data[keyname('Rlist',m,f)], data[keyname('Mcr1_4',m,f)],
                 'o-', label=rf'M=1.4, model: {m}')
        plt.plot(data[keyname('Rlist',m,f)], data[keyname('Mcr1_6',m,f)],
                 'o-', label=rf'M=1.6, model: {m}')
    plt.ticklabel_format(axis='y', style='sci', scilimits=(0, 0))
    plt.grid()
    plt.legend()
    plt.xlabel(r'Total radius of NS [km]')
    plt.ylabel(r'Grav. mass of outer crust [$M_{\odot}$]')
    plt.title(rf'Mcr vs R ($B_*=${f})')
    plt.show()
    plt.savefig(f'Mcr_f{f}.png')

# plot17, now for the same model, plot for all Bstar
for m in modellist:
    plt.figure(figsize=(8,6))
    for f in Bstarlist:
        plt.plot(data[keyname('Rlist',m,f)], data[keyname('zdrip1_2',m,f)],
                     'o-', label=rf'M=1.2, $B_*=${f}')
        plt.plot(data[keyname('Rlist',m,f)], data[keyname('zdrip1_4',m,f)],
                 'o-', label=rf'M=1.4, $B_*=${f}')
        plt.plot(data[keyname('Rlist',m,f)], data[keyname('zdrip1_6',m,f)],
                 'o-', label=rf'M=1.6, $B_*=${f}')
    plt.grid()
    plt.legend()
    plt.xlabel(r'Total radius of NS [km]')
    plt.ylabel(r'Proper thickness of outer crust [km]')
    plt.title(rf'$z_d$ vs R (model: {m})')
    plt.show()
    plt.savefig(f'zdrip_m{m}.png')

# now for the same Bstar, plot for all models
for f in Bstarlist:
    plt.figure(figsize=(8,6))
    for m in modellist:
```

```
        plt.plot(data[keyname('Rlist',m,f)],
        ↪  data[keyname('zdrip1_2',m,f)],
                    'o-', label=rf'M=1.2, model: {m}')
        plt.plot(data[keyname('Rlist',m,f)],
        ↪  data[keyname('zdrip1_4',m,f)],
                 'o-', label=rf'M=1.4, model: {m}')
        plt.plot(data[keyname('Rlist',m,f)],
        ↪  data[keyname('zdrip1_6',m,f)],
                 'o-', label=rf'M=1.6, model: {m}')
    plt.grid()
    plt.legend()
    plt.xlabel(r'Total radius of NS [km]')
    plt.ylabel(r'Proper thickness of outer crust [km]')
    plt.title(rf'$z_d$ vs R ($B_*=${f})')
    plt.show()
    plt.savefig(f'zdrip_f{f}.png')
```

Bibliography

[1] J. Schaffner-Bielich, *Compact Star Physics*. Cambridge University Press, 2020.

[2] A. Y. Potekhin, "The physics of neutron stars," *Physics-Uspekhi*, vol. 53, no. 12, p. 1235, 2010.

[3] P. Haensel, A. Potekhin, and D. Yakovlev, *Neutron Stars 1: Equation of State and Structure*. Astrophysics and Space Science Library, Springer New York, 2007.

[4] N. K. Glendenning, *Compact stars: Nuclear physics, particle physics and general relativity*. Springer Science & Business Media, 2012.

[5] R. C. Tolman, "Static solutions of einstein's field equations for spheres of fluid," *Physical Review*, vol. 55, no. 4, p. 364, 1939.

[6] J. R. Oppenheimer and G. M. Volkoff, "On massive neutron cores," *Physical Review*, vol. 55, no. 4, p. 374, 1939.

[7] S. L. Shapiro and S. A. Teukolsky, *Black holes, white dwarfs, and neutron stars: The physics of compact objects*. John Wiley & Sons, 2008.

[8] N. Chamel and P. Haensel, "Physics of neutron star crusts," *Living Reviews in relativity*, vol. 11, pp. 1–182, 2008.

[9] G. Baym, C. Pethick, and P. Sutherland, "The ground state of matter at high densities: equation of state and stellar models," *The Astrophysical Journal*, vol. 170, p. 299, 1971.

[10] S. B. Rüster, M. Hempel, and J. Schaffner-Bielich, "Outer crust of nonaccreting cold neutron stars," *Physical Review C*, vol. 73, no. 3, p. 035804, 2006.

[11] J. Pearson, S. Goriely, and N. Chamel, "Properties of the outer crust of neutron stars from hartree-fock-bogoliubov mass models," *Physical Review C*, vol. 83, no. 6, p. 065810, 2011.

[12] D. Lai and S. L. Shapiro, "Cold equation of state in a strong magnetic field-effects of inverse beta-decay," *The Astrophysical Journal*, vol. 383, pp. 745–751, 1991.

[13] N. Chamel, R. Pavlov, L. Mihailov, C. J. Velchev, Z. K. Stoyanov, Y. Mutafchieva, M. Ivanovich, J. Pearson, and S. Goriely, "Properties of the outer crust of strongly magnetized neutron stars from hartree-fock-bogoliubov atomic mass models," *Physical Review C*, vol. 86, no. 5, p. 055804, 2012.

[14] D. Basilico, D. P. Arteaga, X. Roca-Maza, and G. Colò, "Outer crust of a cold non-accreting magnetar," *Physical Review C*, vol. 92, no. 3, p. 035802, 2015.

[15] D. Lunney, J. Pearson, and C. Thibault, "Recent trends in the determination of nuclear masses," *Reviews of Modern Physics*, vol. 75, no. 3, p. 1021, 2003.

[16] C. Jog and R. Smith, "Mixed lattice phases in cold dense matter," *Astrophysical Journal*, vol. 253, no. 1, pp. 839–841, 1982.

[17] N. Chamel and A. Fantina, "Binary and ternary ionic compounds in the outer crust of a cold nonaccreting neutron star," *Physical Review C*, vol. 94, no. 6, p. 065802, 2016.

[18] S. Goriely, N. Chamel, H.-T. Janka, and J. Pearson, "The decompression of the outer neutron star crust and r-process nucleosynthesis," *Astronomy & astrophysics*, vol. 531, p. A78, 2011.

[19] W. Huang, M. Wang, F. G. Kondev, G. Audi, and S. Naimi, "The ame 2020 atomic mass evaluation (i). evaluation of input data, and adjustment procedures," *Chinese Physics C*, vol. 45, no. 3, p. 030002, 2021.

[20] M. Wang, W. Huang, F. G. Kondev, G. Audi, and S. Naimi, "The ame 2020 atomic mass evaluation (ii). tables, graphs and references," *Chinese Physics C*, vol. 45, no. 3, p. 030003, 2021.

[21] https://www-nds.iaea.org/amdc/.

[22] P. Roy Chowdhury and D. Basu, "Nuclear matter properties with the re-evaluated coefficients of liquid drop model," *Acta Physica Polonica. Series B*, vol. 37, no. 6, pp. 1833–1846, 2006.

[23] P. Möller, A. J. Sierk, T. Ichikawa, and H. Sagawa, "Nuclear ground-state masses and deformations: Frdm (2012)," *Atomic Data and Nuclear Data Tables*, vol. 109, pp. 1–204, 2016.

[24] https://t2.lanl.gov/nis/molleretal/publications/ADNDT-FRDM2012.html.

[25] N. Wang, M. Liu, X. Wu, and J. Meng, "Surface diffuseness correction in global mass formula," *Physics Letters B*, vol. 734, pp. 215–219, 2014.

[26] http://www.imqmd.com/mass/.

[27] G. Grams, W. Ryssens, G. Scamps, S. Goriely, and N. Chamel, "Skyrme-hartree-fock-bogoliubov mass models on a 3d mesh: Iii. from atomic nuclei to neutron stars," *arXiv preprint arXiv:2307.14276*, 2023.

[28] S. Goriely, N. Chamel, and J. Pearson, "Further explorations of skyrme-hartree-fock-bogoliubov mass formulas. xvi. inclusion of self-energy effects in pairing," *Physical Review C*, vol. 93, no. 3, p. 034337, 2016.

[29] http://www.astro.ulb.ac.be/bruslib/nucdata/.

[30] X. Roca-Maza, X. Vinas, M. Centelles, P. Ring, and P. Schuck, "Relativistic mean-field interaction with density-dependent meson-nucleon vertices based on microscopical calculations," *Physical Review C*, vol. 84, no. 5, p. 054309, 2011.

[31] T. Nikšić, D. Vretenar, and P. Ring, "Relativistic nuclear energy density functionals: Adjusting parameters to binding energies," *Physical Review C*, vol. 78, no. 3, p. 034318, 2008.

[32] S. Agbemava, A. Afanasjev, D. Ray, and P. Ring, "Global performance of covariant energy density functionals: Ground state observables of even-even nuclei and the estimate of theoretical uncertainties," *Physical Review C*, vol. 89, no. 5, p. 054320, 2014.

[33] P. Klüpfel, P.-G. Reinhard, T. Bürvenich, and J. Maruhn, "Variations on a theme by skyrme: A systematic study of adjustments of model parameters," *Physical Review C*, vol. 79, no. 3, p. 034310, 2009.

[34] M. Kortelainen, T. Lesinski, J. Moré, W. Nazarewicz, J. Sarich, N. Schunck, M. Stoitsov, and S. Wild, "Nuclear energy density optimization," *Physical Review C*, vol. 82, no. 2, p. 024313, 2010.

[35] A. Afanasjev, S. Agbemava, D. Ray, and P. Ring, "Neutron drip line: Single-particle degrees of freedom and pairing properties as sources of theoretical uncertainties," *Physical Review C*, vol. 91, no. 1, p. 014324, 2015.

[36] A. Afanasjev and S. Agbemava, "Covariant energy density functionals: Nuclear matter constraints and global ground state properties," *Physical Review C*, vol. 93, no. 5, p. 054310, 2016.

[37] J. Erler, N. Birge, M. Kortelainen, W. Nazarewicz, E. Olsen, A. M. Perhac, and M. Stoitsov, "The limits of the nuclear landscape," *Nature*, vol. 486, no. 7404, pp. 509–512, 2012.

[38] https://massexplorer.frib.msu.edu/.